Late Weichselian and Holocene Glacimarine Sedimentation and Environments in Kejser Franz Josephs Fjord and on the Adjacent Continental Margin, East Greenland

Jeffrey Evans
Darwin College

A dissertation submitted for the degree of Doctor of Philosophy
Scott Polar Research Institute,
University of Cambridge

September 1998

DECLARATION

STATEMENT 1

I hereby declare that this work has not been previously accepted in substance for any degree or diploma or other qualification at any other university and is not being concurrently submitted in candidature for any such degree, diploma or other qualification.

Signed [redacted] (Candidate)

Date 30th September 1998

STATEMENT 2

This thesis is the result of my own investigation, except where otherwise stated.

Other sources are acknowledged with explicit references. A bibliography is appended.

Signed [redacted] (Candidate)

Date 30th September 1998

Late Weichselian and Holocene glacimarine sedimentation and environments in Kejser Franz Josephs Fjord and on the adjacent continental margin of East Greenland

Jeffrey Evans

The study outlines the glacimarine sedimentation patterns and processes and environments in the Kejser Franz Josephs Fjord and on the adjacent continental margin of East Greenland during the Late Weichselian and Holocene.

A variety of techniques are adopted in this study in order to address the objectives outlined previously. The study is based on a suite of 8 cores from the, mid to outer region of Kejser Franz Josephs Fjord, and the continental shelf and slope. Core analyses included i) logging (core and x-radiographs), ii) determination of grain size distribution, iceberg rafted debris and physical properties (water content, porosity, grain density), iii) determination of stable oxygen and carbon isotopes, iv) radiocarbon dating, and v) calculation of sedimentation and accumulation rates. Additionally, acoustic data is incorporated into the study to place the sediment cores within a regional context in terms of the sedimentation patterns and processes throughout the study area.

The sedimentary record within the study dates back to the Late Weichselian glaciation. The record is confined to the continental slope and partly the continental shelf. The nature, extent and mechanisms of ice advance during the Late Weichselian glaciation could not be determined in this study. The upper continental slope is characterised by iceberg sedimentation with additional contribution from distal remnants of meltwater outflows escaping from East Greenland, sea ice rafting and pelagic settling. Mass wasting is recognised by the presence of debris flows, which are derived from the rapid and unstable build-up of large volumes of glacigenic sediment. Mass wasting events are intermittent, vary from small to large scale, and are derived from local slope regions. The mid to lower continental slope are characterised by rain out and suspension settling punctuated by intermittent sediment gravity flows. Sea ice conditions during the Late Weichselian are extended resulting in reduced ventilation of ocean surface waters and decreased exchange of CO_2 between the atmosphere and ocean. Sedimentation rates are high in response to the focusing of sedimentation on the continental margin as ice advances to the continental shelf.

The onset of the Late Weichselian deglaciation is dated to occur after 15,250 yr BP. Deglaciation is recognised by a rapid depletion of oxygen isotopes to very light values, indicating the massive discharge of meltwater to the oceans in response to the decay of the Greenland Ice Sheet. The meltwater pulse culminated at 13,020 yr BP on the continental slope and sometime between 10,000-13,010 yr BP on the continental shelf. The subsequent stratification of ocean surface waters leads to the reduced ventilation of ocean surface waters and decreased exchange of CO_2 between the atmosphere and ocean. The presence of significant volumes of iceberg rafted sediments on the continental shelf between 10,000-13,010 yr BP, and pre-13,010 yr BP indicates that mass ice loss from the Greenland Ice Sheet is through iceberg calving. The lower continental slope between 13,020-15,250 yr BP is dominated by repetitive turbidity current activity derived from upper continental slope mass wasting, which reverts to more quiescent rain out and suspension settling after 13,020 yr BP. The exact nature of ice retreat could not be reconstructed in this study.

The Younger Dryas Stadial is poorly represented in the sedimentary record of this study relating to low sedimentation rates and the low resolution of the sedimentary during this interval. Isotopic records indicate extended sea ice conditions over the continental slope, resulting in reduced ventilation of ocean surface waters and decreased exchange of CO_2 between the atmosphere and ocean. The stillstand position of glacier ice during the Younger Dryas is not well constrained in this study.

The onset of the post Younger Dryas deglaciation occurs soon after 10,000 yr BP and is marked by a meltwater pulse that influences the fjord and inner continental shelf. The meltwater discharge culminated at 9,540 yr BP on the inner continental shelf and sometime before 7,440 yr BP in the outer fjord. The meltwaters are produced from the final retreat of the glacier-ice of the Greenland Ice Sheet to present day positions. The presence of laminated mud facies and iceberg rafted debris (sandy mud diamicton and mud with dropstones) indicate that ice mass loss is through both ablation and iceberg calving. The subsequent stratification of ocean surface waters leads to the reduced ventilation of ocean surface waters and decreased exchange of CO_2 between the atmosphere and ocean. Sedimentation and accumulation rates are high in reponse to deglaciation. Deglaciation sequences are recognised from the outer fjord and inner continental shelf, comprising laminated mud facies, diamicton facies, bioturbated mud facies representing increasingly ice distal settings as glacier-ice retreats into the fjord system.

The Holocene is characterised by decreased sea ice conditions leading to increased ventilation of ocean/fjord surface waters and the increased exchange of CO_2 between the atmosphere and fjord/ocean. Sedimentation within the fjord basins is dominated by sediment gravity flows, which transfer sediment from the fjord margins into the deeper basins. Rain out and suspension settling also occurs and dominates sedimentation over bathymetric highs and also occurs within the fjord basins (accounts for the most recent sedimentation). Sedimentation across the continental shelf is prevented by the erosive action of the East Greenland Current. Sedimentation is pronounced within the inner continental shelf basin, which is protected from the East Greenland Current. Sedimentation on the continental slope is composed of rain out and suspension settling deposits with virtually no iceberg rafted debris related to its ice-distal setting.

ACKNOWLEDGEMENTS

First and foremost I would like to thank Professor J.A. Dowdeswell, Institute of Geography and Earth Science, University of Wales, Aberystwyth for giving me the opportunity of undertaking this PhD research, and fieldwork in Greenland and Svalbard. I am particularly grateful for his supervision, support and encouragement. I would also like to thank Dr. Hans Hubberten of the Alfred Wegener Institute, Potsdam, Germany for his supervision and assistance during my time at the Institute, and during the ARK X/2 cruise of the *RV Polarstern* to East Greenland (August-October 1994).

I thank the captain and crew of the *RV Polarstern* for their cooperation and technical assistance during the ARK X/2 expedition. I specifically thank the geoscientists and support staff who participated on this cruise who provided enjoyable company, stimulating discussions and considerable technical assistance: Tania Anders, Michael Diepenbroek, Hannes Grobe, Norbert Lensch, Jens Matthiessen, Frank Niessen, Michael Seebeck, Rüdiger Stein, Johannes Simstich, Christoph Vogt, Antje Völker, and Robert Whittington.

I again thank Hans Hubberten and the Alfred Wegener Institute for providing financial assistance in order to obtain AMS radiocarbon datings. I thank Dr. J. Heinemeier at the AMS radiocarbon dating laboratory, Institute of Physics and Astronomy, Åarhus University, Denmark for preparing samples and performing AMS radiocarbon datings. Gunther Meyer at the Alfred Wegener Institute, Bremerhaven is also acknowledged with thanks for performing the stable oxygen and carbon isotope measurements.

I am indebted to Professor D.K. Fütterer, Dr. H. Hubberten and Dr. R. Stein, for enabling me to use the facilities at the Alfred Wegener Institute, Bremerhaven which I visited twice. I sincerely thank several geoscientists and support staff for their assistance, discussions, and for making my stay enjoyable: Marion Behrends, Dr. Wolfgang Bonn, Rita Frhölking, Dr. Hannes Grobe, Jochen Knies, Dr. Gerhard Kuhn, Dr. Ute Mann, Dr. Jürgen Monk, Dr. Seung -il. Nam, Dr. Frank Niessen, Dr. Dirk Nürnberg, Sabine Roth, Dr. Carsten Schubert, Dr. Rainer Stax, Dr. Rüdiger Stein, and Dr. Monika Wahsner. I especially thank Dr. Christoph Vogt for all his advice and assistance.

My colleague and friend Dr. Seung il Nam is especially thanked for all his guidance, and encouraging comments and suggestions. In particular his contribution to our discussions on the Late Quaternary environmental history of East Greenland is gratefully acknowledged.

This thesis has profited hugely from other work associated with the PONAM (Polar North Atlantic Margins: Late Cenozoic Evolution) Programme. Thanks go to Professor Anders Elverhøi at the department of geology, University of Oslo, Norway for enabling me to participate in the PONAM workshop in Randsvangen, Norway. Thanks also to Professor Svend Funder at the Geological Museum, Copenhagen, Denmark for identification of mollusc faunas (Chapter 4), and informative discussions on the glacial geologic history of East Greenland.

Special thanks to Dr. Robert Whittington for his support and hugely enjoyable company during the ARK X/2 cruise , and for his considerable guidance and supervision of the geophysical work of my PhD. He is also thanked for careful reading of sections of my PhD manuscript. Thanks also to Dr. Martin Siegert at the Institute of Geography and Earth Science, University of Wales, Aberystwyth for useful comments and suggestions on the PhD manuscript.

Many thanks go to the people of Scott Polar Research Institute, University of Cambridge, in particular the secretaries and librarians who were more than helpful. Thanks go to Dr. Victoria Cadman for useful suggestions on the methods of grain size analyses. Very special thanks to friends in Cambridge: Andy Bingham, Mark Brandon, Jackie Bruce, Kim Crosbie and Mark Tadross for much needed entertainment and many laughs.

Heartfelt thanks to Anne Marie Nuttall, Institute of Geography and Earth Science, University of Wales, Aberystwyth for her friendship, technical assistance, generosity, and the occasional game of badminton, during my stay at Aberystwyth.

Finally, this thesis would not have been completed without the considerable love, support and encouragement of my wife Rebecca. Thank you Becca for your warm words of wisdom when I needed them, your continual jollying and robust attitude and your understanding of my rather unusual working practices and hours! Lastly but not least, this thesis would not have been possible without the unwhavering love and support of my mum and dad, and family who have proudly and without question supported me throughout my education.

CONTENTS

2. GLACIMARINE SEDIMENTATION AND ENVIRONMENTS AND THE LATE WEICHSELIAN AND HOLOCENE IN EASTERN GREENLAND

3. DATA SOURCES AND ACQUISITION

5. ACOUSTIC RECORDS OF SEDIMENTATION PATTERNS AND PROCESSES IN KEJSER FRANZ JOSEPHS FJORD AND ON THE EAST GREENLAND CONTINENTAL MARGIN

LIST OF FIGURES

1.6 Oceanographic circulation patterns in the Greenland-Iceland-Norwegian Sea.

1.7 Annual total precipitation (mm) for Greenland. From Ohmura & Reeh (1991).

1.8a&b The geology of (a) Greenland, and (b) East Greenland showing the main geological divisions of the Kejser Franz Josephs Fjord region (study area). Reproduced from Escher & Watt (1976).

1.9 Chronostratigraphy and marine oxygen isotope stratigraphy of the last 30,000 yr BP of the Late Quaternary. Based on Mangerud et al. (1974), Mangerud & Berglund (1978), Martinson et al. (1987), Nam et al. (1995), Nam (1996), and Mangerud et al. (1996).

2.1 System diagram illustrating the sediment sources, processes and environments of deposition making up the complex glacimarine sedimentary environment (from Dowdeswell 1987).

2.2 Hypothetical pattern of debris release for an iceberg calved from outlet glaciers or ice streams, and resulting sea-floor sedimentation rate. The effects of calving, overturning of icebergs and processes of meltwater, mudflow and rockfall activity are shown (from Drewry & Cooper 1981).

2.3 (a) Schematic diagram illustrating the subglacial discharge of meltwater and the development of a turbid surface (overflow) plume. Associated bedload and suspension settling (cyclopsams and cyclopels) sediments are shown (from Powell & Molnia 1989). (b) The variability of subglacial meltwater efflux in response to differences in water/sediment discharge. Associated sediment fan systems are shown (from Powell 1990). Although both (a) and (b) are examples from subglacial drainage they would also apply to glacifluvial/fluvial systems discharging into the marine environment.

2.4 Model for the downslope transition of a slide/slump to a debris flow and finally a turbidity current, controlled by the increasing amount deformation undergone by the sediment during movement. Corresponding core lithologies are shown. This is an example from the Weddell Sea, Antarctica (from Wright & Anderson 1982).

2.5 Summary of the various schemes for subdivision of medium to fine grained turbidites (from Pickering et al. 1989). Two of these schemes are adopted in this study: (i) Bouma (1962) scheme for medium grained turbidites (units Ta-Te), and (ii) Stow & Shanmugam (1980) scheme for fine grained turbidites (units T0-T8).

2.6 Conceptual model of meltwater sedimentation and associated dispersal of sediments by subaqueous mass wasting in Arctic fjord settings (from Gilbert 1983). Meltwaters are derived from subglacial drainage and glacifluvial systems.

2.7 Reconstructed ice margins in Greenland for the Last Glacial Maximum between 16-21,000 yr BP (LGM; green) and at 10 ka (red). Brown areas are major ice free areas and numbers are ice surface altitudes during LGM. The East Greenland region is indicated. From Funder & Hansen (1996).

2.8 Isopach map of unlithified Quaternary sediment thickness in Scoresby Sund and Hall Bredning. The map shows: (i) the Kap Brewster Moraine at the mouth of Scoresby Sund marking the seaward advance of glacier-ice during the Late Weichselian glaciation, and (ii) a major depocentre at the head of Hall Bredning representing ice-proximal sediments deposited from a glacier margin during the Younger Dryas or Milne Land Stadial in East Greenland (10,000 yr BP). From Dowdeswell et al. (1994b).

2.9 Oxygen isotope stratigraphy for the last 30,000 years measured on the planktonic foraminifera N. pachyderma sin. The light oxygen isotope signal indicative of a major meltwater pulse associated with the first stages of deglaciation during the Late Weichselian is shown, with its earliest onset dated at ca. 15,800 yr BP and culmination at ca. 13,200 yr BP.

2.10 Oxygen isotope records showing the timing of the deglacial meltwater signal in the Polar North Atlantic and Labrador Sea. The global eustatic sea level curve based on Fairbanks (1989) is shown. From Dokken et al. (1996).

2.11 Map of the Scoresby Sund region showing (i) a dark zone representing the Kap Brewster moraine at the mouth of Scoresby Sund marking the seaward advance of glacier-ice during the Late Weichselian glaciation (dark zone), (ii) a light grey zone marking the Younger Dryas or Milne Land Stadial moraines (9,500-10,000 yr BP). AMS radiocarbon ages (kyr) associated with deglaciation are indicated in bold, and the circled numbers are altitudes of marine limits (m a.s.l.). From Funder & Hansen (1996).

2.12 The global eustatic sea level curve for the last 18,000 years. From Fairbanks (1989).

2.13 Altitude of postglacial (Late Weichselian to Early Holocene) marine limits (m a.s.l.) in Greenland. The East Greenland region is indicated. From Funder & Hansen (1996).

2.14 Six sedimentological logs from a transect through the Scoresby Sund fjord system and shelf, East Greenland showing the main sedimentary facies deposited since the last deglaciation. AMS radiocarbon dates are shown. From Dowdeswell et al. (1994a).

2.15 Model of sedimentation for the Scoresby Sund fjord system before the onset of the Younger Dryas cooling period. From Marienfeld (1991).

2.16 Model of sedimentation for the Scoresby Sund fjord system during the Younger Dryas cooling period. From Marienfeld (1991).

2.17 Model of sedimentation for the Scoresby Sund fjord system between the end of the Younger Dryas cooling period and the present day. From Marienfeld (1991).

3.1 Schematic diagram/flowchart illustrating the various laboratory processing stages of gravity cores, and the analytical techniques adopted in this study. The results of the methods are indicated, and in combination provide a composite reconstruction of glacimarine sedimentation and environments within Kejser Franz Josephs Fjord and on the adjacent East Greenland continental margin.

4.1 Eight sedimentological logs, taken along a west-east transect parallel to 73° N through the mid to outer Kejser Franz Josephs Fjord system and the adjacent continental shelf and slope (refer to Figure 1.1). Water depths (wd) of the recovered cores are indicated. A sedimentary key listing the lithologies and sedimentary characteristics is provided. The logging of the sedimentary characteristics and the subsequent classification into lithofacies followed the convention set out in Eyles et al. (1983), although it has been modified for this investigation. A key to the nomenclature is provided in Table 4.1. Large and small triangle symbols indicate the relative proportion of clasts in excess of 2 mm in the diamicton.

4.2 X-radiographs illustrating the various sedimentary features associated with lithofacies identified from cores examined in this study.

4.3 X-radiographs illustrating the various sedimentary features associated with lithofacies identified from cores examined in this study.

4.4 X-radiographs illustrating the various sedimentary features associated with lithofacies identified from cores examined in this study.

4.5a&b The down-core and lithofacies variation in the grain-size properties of PS2632, PS2631, and PS2641 recovered along the Kejser Franz Josephs fjord-shelf-slope transect. Grain-size properties include distribution (%) of gravel (black shading), sand (stippled shading), silt (grey shading) and clay (hatched shading), mean grain-size (phi units), sorting (σ), distribution of particles >500 μm (1Φ), and the number of particles >2 mm/cm (IRD). Lithofacies of Figure 4.1 are indicated.

4.6a-d The down-core and lithofacies variation in the grain-size properties of PS2630, PS2629, PS2628 and PS2627 recovered along the Kejser Franz Josephs fjord-shelf-slope transect. Grain-size properties include distribution (%) of gravel (black shading), sand (stippled shading), silt (grey shading) and clay (hatched shading), mean grain-size (phi units), sorting (σ), distribution of particles >500 μm (1Φ), and the number of particles >2 mm/cm (IRD). Lithofacies of Figure 4.1 are indicated.

4.7a-c Distribution of grain size within lithofacies identified from the cores recovered along the west-east transect through the mid to outer Kejser Franz Josephs Fjord and adjacent continental shelf and slope parallel to 73 N. The dotted lines represent the boundary between the clay-silt grades at 9Φ, silt-sand grades at 4Φ, and sand-gravel grades at 0Φ. The plots for each lithofacies represent the grain size determined on a number of samples (n).

4.8a-d Distribution of grain size within lithofacies identified from the cores recovered along the west-east transect through the mid to outer Kejser Franz Josephs Fjord and adjacent continental shelf and slope parallel to 73 N. The dotted lines represent the boundary between the clay-silt grades at 9Φ, silt-sand grades at 4Φ, and sand-gravel grades at 0Φ. The plots for each lithofacies represent the grain size determined on a number of samples (n).

4.9 Coarse particle counts (particles >2 mm/cm), also termed ice rafted debris (IRD), from eight cores, recovered along a west-east transect parallel to 73° N through the mid to outer Kejser Franz Josephs Fjord and adjacent continental shelf and slope (Figure 1.1). The lithofacies illustrated in the sedimentological logs of Figure 4.1 are indicated. For the exact position of the lithofacies boundaries the reader is directed to the sedimentological logs in Figure 4.1.

4.10a-c The down-core and lithofacies variation in the physical properties of PS2632, PS2631 and PS2641 recovered along the Kejser Franz Josephs fjord-shelf-slope transect. Physical properties include wet bulk density (WBD), water content, porosity, and the number of particles >2 mm/cm (IRD). Lithofacies of Figure 4.1 are indicated.

4.11a-d The down-core and lithofacies variation in the physical properties of PS2630, PS2629, PS2628 and PS2627 recovered along the Kejser Franz Josephs fjord-shelf-slope transect. Physical properties include wet bulk density (WBD), water content, porosity, and the number of particles >2 mm/cm (IRD). Lithofacies of Figure 4.1 are indicated.

5.1 Map of Kejser Franz Josephs Fjord and the adjacent continental shelf and slope showing: (a) Ship tracks (dotted lines) of the Polarstern during the ARK X/2 cruise, for which Parasound records are available. Locations of the Parasound records used as examples in Figures 5.2-5.8 are shown. (b) Bathymetry (100 m intervals) based on the Parasound records. a = mid fjord basin, b = mid/outer fjord sill, c = innermost sub-basin of the outer fjord, d = intermediate sub-basin of the outer fjord, e

= outermost sub-basin of the outer fjord, and f = inner shelf basin. The shelf break is at a water depth of about 300 m. The locations of the sediment cores of this study are indicated in both (a) and (b). The study area in relation to Greenland is shown within the insets of both (a) and (b). KFJ = Kejser Franz Josephs Fjord, GF = Geologfjord, NF = Nordfjord, and B = Bontekoe Ø. The map scale is shown in both (a) and (b).

5.2 Parasound record illustrating the acoustic character of units Ia and II. Unit Ia consists of stratified internal (sub sea-floor) reflectors beneath a planar to hummocky sea-floor. Syn-sedimentary faulting is displayed. Unit II consists of a number of sub sea-floor, acoustically massive and transparent, unconformable lense shaped sediment bodies. Both units represent basin fill confined by the bathymetric high of the basin margin. The record is an example from the western margin of a basin within the mid region of Kejser Franz Josephs Fjord located in Figure 5.1. The vertical and horizontal scales (metres) are shown. The former is water depth with depth increments of 20 m.

5.3 Parasound record illustrating the acoustic character of units Ia, II and VII. Units Ia and II are basin fill. Unit Ia consists of stratified internal (sub sea-floor) reflectors beneath a planar sea-floor. Unit II consists of a number of sub sea-floor, acoustically massive and transparent, unconformable lense to elongate shaped sediment bodies. The unit also appears on the bathymetric high adjoining two similar units of adjacent basins. Unit VII consists of parallel, hummocky sea-floor and sub sea-floor reflectors that form a single conformable cover draping the bathymetric high, slope and troughs. The record is an example from adjoining basins within the mid to outer region of Kejser Franz Josephs Fjord located in Figure 5.1. The vertical and horizontal scales (metres) are shown. The former is water depth with depth increments of 20 m.

5.4(A-C) Parasound records illustrating the acoustic units of the upper (A), mid (B) and lower (C) continental slope which are located in Figure 5.1. (A) Unit VI consists of acoustically massive sediment with diffuse to discontinuous internal (sub sea-floor) reflectors. (B) and (C) Unit Ib consists of stratified internal reflectors beneath a planar to hummocky sea-floor. (C) Unit II consists of unconformable wedge shaped sub sea-floor reflectors separating lense shaped sediment bodies. The horizontal sections of the records result from the ship track set at 90° to the slope gradient. Sediment cores PS2629, PS2628 and PS2627 were recovered from the slope, and the lithofacies (refer to Table 4.1 and Fig. 4.1) and locations are shown. The vertical and horizontal scales (metres) are shown. The former is water depth with depth increments of 10 m.

5.5 Parasound record illustrating the acoustic character of units III, VI and VII. Unit III consists of acoustically chaotic to stratified to massive sub sea-floor reflectors beneath a hummocky top-surface reflector. Unit VI consists of acoustically massive sediment with diffuse to discontinuous internal reflectors. Unit VII consists of parallel, hummocky sea-floor and sub sea-floor reflectors that form a single conformable cover draping the deepest region of the basin and bordering margin. The record is obtained from a basin in the outer region of Kejser Franz Josephs Fjord located in Figure 5.1. The

vertical and horizontal scales (metres) are shown. The former is water depth with depth increments of 10 m.

5.6 Parasound record illustrating the acoustic character of unit IV. The unit consists of stratified, parallel and hummocky sea-floor and sub sea-floor reflectors that form a conformable cover draping the bathymetric trough of the basin, and the bathymetric high of the margin. The record is an example from the eastern margin of a basin on the inner continental shelf adjacent to Kejser Franz Josephs Fjord located in Figure 5.1. Sediment core PS2641 was recovered from the lower region of the eastern basin margin, and the lithofacies (Table 4.1 and Fig. 4.1) and location are shown. The vertical and horizontal scales (metres) are shown. The former is water depth with depth increments of 20 m.

5.7(A-C) Parasound records illustrating the acoustic character and irregularity of the sea-floor reflector of sub-units Va and Vb, located in Figure 5.1. (A-C) Sub-unit Va consists of acoustically homogeneous sediment with diffuse sub sea-floor reflectors. (C) Sub-unit Vb consists of acoustically discontinuous to continuous stratified sediment. The intensity of sea-floor reflector irregularities vary between high (A), intermediate (B) and low (C). The irregularities are composed of paired crests and troughs. The intensity of the sea-floor irregularities reflect the degree of scouring by icebergs. The records are examples from the inner (A), mid (B) and outer (C) continental shelf located in Figure 5.1. The vertical and horizontal scales (metres) are shown. The former is water depth with depth increments of 10 m.

5.8 Parasound record illustrating the acoustic character of units II, Va and VII. The western section of the record is dominated by a bathymetric high, thought to reflect underlying bedrock. Unit II consists of unconformable wedge shaped sub sea-floor reflectors separating an elongated lobe shaped sediment body. The unit is thickest in the proximity of the bathymetric high and pinches out eastwards. Unit Va covers the bathymetric high, and consists of acoustically homogeneous sediment with diffuse sub sea-floor reflectors. Unit VII consists of parallel, hummocky sea-floor and sub sea-floor reflectors that form a single conformable cover draping bathymetric highs and troughs. Sediment core PS2630 was recovered close to the bathymetric high, and the lithofacies (Table 4.1 and Fig. 4.1) and location are shown. The record is from the mid continental shelf located in Figure 5.1. The vertical and horizontal scales (metres) are shown. The former is water depth with depth increments of 10 m.

5.9 Map of Kejser Franz Josephs Fjord and the adjacent continental shelf and slope showing the distribution of acoustic units recognised from Parasound records. The study area in relation to Greenland is shown within the inset of Figure 5.1. A key to the symbols representing the acoustic units is provided. The map scale is indicated. The distribution was based on Parasound records obtained along the ship tracks shown in Figure 5.1. Sediment cores of this study are shown.

5.10 Map of Kejser Franz Josephs Fjord and the adjacent continental shelf and slope showing the distribution of seafloor irregularity. Four levels of intensity are recognised: i) High, ii) Intermediate, iii) Low, and iv) Absent. A key to the symbols representing the four levels of intensity is provided. The intensity of irregularity is taken as an index of iceberg scouring. The study area in relation to Greenland is shown within the inset of Figure 5.1. The map scale is indicated. The distribution was based on Parasound records obtained along the ship tracks shown in Figure 5.1. Bathymetric contours are shown and spaced at intervals of 100 metres in the fjord and adjacent continental shelf, and 500 metres on the continental slope.

5.11 Schematic diagram illustrating the relationship of iceberg scouring intensity and water depth within the study area (Fig 5.1a). Iceberg scouring intensity falls within the four classes: (i) high, (ii) intermediate, (iii) low, and (iv) absent. Water depths are in metres (m). A map illustrating the pattern of iceberg scouring intensity within the study area is provided in Figure 5.10.

5.12 Map of Kejser Franz Josephs Fjord and the adjacent continental shelf and slope showing the regional distribution of the main sedimentary processes and environments interpreted from core lithofacies (Chapter 4) and acoustic units recognised from Parasound records. The study area in relation to Greenland is shown within the inset of Figure 5.1. A key to the symbols representing the sedimentary processes and environments is provided. The map scale is indicated. Sediment cores of this study are shown.

6.1 AMS radiocarbon datings (yr BP) in relation to the lithostratigraphy of the sedimentary cores of this study. The cores were taken along a west-east transect parallel to 73° N through the mid to outer Kejser Franz Josephs Fjord system and the adjacent continental shelf and slope (refer to Figure 1.1). Water depths (wd) of the recovered cores are indicated. A sedimentary key listing the lithologies and sedimentary characteristics is provided. A key to the lithofacies nomenclature is provided in Table 4.1.

6.2 Plot of age (kyr) derived from measured and correlated radiocarbon datings against core depth (cm) for cores PS2641, PS2631, PS2630, PS2629, PS2628, and PS2627 recovered along the Kejser Franz Josephs fjord-shelf-slope transect. The closed circles represent AMS/conventional radiocarbon dated samples, and open circles correlated/estimated ages. The question marks refer to core sections in which the timescale is not certain. The chronostratigraphy based on this thesis is indicated.

6.3 Stable oxygen isotope ($\delta^{18}O$) records measured on the planktonic foraminifer *Neogloboquadrina pachyderma* (sin) from cores PS2632, PS2631, PS2641, PS2630, PS2629, PS2628 and PS2627 recovered from the Kejser Franz Josephs Fjord-shelf-slope transect. The oxygen isotopic stage scale is indicated. The dotted lines correlate the oxygen isotopic chronology between the cores. Termination Ia and Ib are shortened to Ia and Ib, respectively, and are indicated by a solid black bar. AMS radiocarbon ages are indicated and provide an absolute chronological

control on the oxygen isotope stratigraphy. The depth of the gravity core PS2629 is corrected by 40 cm by comparing its isotopic record with that of the box core. The box core record is indicated by the open circles.

6.4 Stable carbon isotope ($\delta^{13}C$) records measured on the planktonic foraminifer *Neogloboquadrina pachyderma* (sin) from cores PS2632, PS2631, PS2641, PS2630, PS2629, PS2628 and PS2627 recovered from the Kejser Franz Josephs Fjord-shelf-slope transect. The oxygen isotopic stage scale is indicated. Termination Ia and Ib are shortened to Ia and Ib, respectively, and are indicated by a solid black bar. AMS radiocarbon ages are indicated and provide an absolute chronological control on the carbon isotope stratigraphy. The depth of the gravity core PS2629 is corrected by 40 cm by comparing its isotopic record with that of the box core. The box core record is indicated by the open circles.

6.5a&b Schematic representation of the Stage I (Holocene) $\delta^{18}O$ and $\delta^{13}C$ records of cores PS2631, PS2641, PS2629, PS2628, and PS2627 with respect to their position along the Kejser Franz Josephs Fjord-shelf-slope transect. The average isotopic values associated with each record are indicated by points and the range of values by the bracketing bars.

6.6 Time (kyr) variant mass accumulation rates (g cm^{-2} kyr^{-1}) and stable oxygen and carbon isotope stratigraphy of PS2628 from the mid continental slope. Oxygen isotopic and chronostratigraphical scales are indicated where Termination Ia is shortened to Ia. The lithostratigraphy of PS2628 is shown, and the lithofacies code is provided in Table 4.1. Fm(b-d) is shortened to Fm, SFm(b-d) to SFm, and SFc(m-l) to SFc.

6.7 Time (kyr) variant mass accumulation rates (g cm^{-2} kyr^{-1}) and stable oxygen and carbon isotope stratigraphy of PS2627 from the lower continental slope. Oxygen isotopic and chronostratigraphical scales are indicated where Termination Ia is shortened to Ia. The lithostratigraphy of PS2627 is shown, and the lithofacies code is provided in Table 4.1. SFc(m-l) is shortened to SFc, SFm(b-d) to SFm, and Fm(b-d-sl) to Fm.

6.8 Time (kyr) variant mass accumulation rates (g cm^{-2} kyr^{-1}) and stable oxygen and carbon isotope stratigraphy of PS2630 from the mid continental shelf. Oxygen isotopic and chronostratigraphical scales are indicated where Termination Ia is shortened to Ia, and the Late Weichselian to Late Weich. Rates must be considered minima. The time scale should be used with caution (refer to text for details. The lithostratigraphy of PS2630 is shown, and the lithofacies code is provided in Table 4.1.

6.9 Time (kyr) variant mass accumulation rates (g cm^{-2} kyr^{-1}) and stable oxygen and carbon isotope stratigraphy of PS2629 from the upper continental slope. Oxygen isotopic and chronostratigraphical scales are indicated where Termination Ia is shortened to Ia. The lithostratigraphy of PS2629 is shown, and the lithofacies code is provided in Table 4.1.

6.10 Time (kyr) variant mass accumulation rates (g cm^{-2} kyr^{-1}) and stable oxygen and carbon isotope stratigraphy of PS2631 from the outer region of Kejser Franz Josephs Fjord. Oxygen isotopic and chronostratigraphical scales are indicated where Termination Ib is shortened to Ib. The time scale is not extended below 7,440 yr BP due to poor chronological constraints. The lithostratigraphy of PS2631 is shown, and the lithofacies code is provided in Table 4.1.

6.11 Time (kyr) variant mass accumulation rates (g cm^{-2} kyr^{-1}) and stable oxygen and carbon isotope stratigraphy of PS2641 from the inner continental shelf. Oxygen isotopic and chronostratigraphical scales are indicated where Termination Ib is shortened to Ib. The lithostratigraphy of PS2641 is shown, and the lithofacies code is provided in Table 4.1.

6.12 Linear sedimentation rates (cm kyr^{-1}) calculated for specific periods in the last 25 kyr for cores along the Kejser Franz Josephs Fjord (PS2631) continental shelf (PS2641 and PS2630) continental slope (PS2629, PS2628 and PS2627) transect parallel to approximately 73°N. Termination Ia and Ib are shortened to Ia and Ib, respectively, in the oxygen isotope and chronostratigraphical scales. Note the linear sedimentation rates axis (x-axis) are not to the same scales.

6.13 Bulk accumulation rates (g cm^{-2} kyr^{-1}) calculated for specific periods in the last 25 kyr for cores along the Kejser Franz Josephs Fjord (PS2631) continental shelf (PS2641 and PS2630) continental slope (PS2629, PS2628 and PS2627) transect parallel to approximately 73°N. Termination Ia and Ib are shortened to Ia and Ib, respectively, in the oxygen isotope and chronostratigraphical scales. Note the linear sedimentation rates axis (x-axis) are not to the same scales.

6.14 Coarse fraction (>63 μm) accumulation rates (g cm^{-2} kyr^{-1}) calculated for specific periods in the last 25 kyr for cores along the Kejser Franz Josephs Fjord (PS2631) continental shelf (PS2641 and PS2630) continental slope (PS2629, PS2628 and PS2627) transect parallel to approximately 73°N. Termination Ia and Ib are shortened to Ia and Ib, respectively, in the oxygen isotope and chronostratigraphical scales. Note the linear sedimentation rates axis (x-axis) are not to the same scales.

6.15 Fine fraction (<63 μm) accumulation rates (g cm^{-2} kyr^{-1}) calculated for specific periods in the last 25 kyr for cores along the Kejser Franz Josephs Fjord (PS2631) continental shelf (PS2641 and PS2630) continental slope (PS2629, PS2628 and PS2627) transect parallel to approximately 73°N. Termination Ia and Ib are shortened to Ia and Ib, respectively, in the oxygen isotope and chronostratigraphical scales. Note the linear sedimentation rates axis (x-axis) are not to the same scales.

6.16 Terrigenous matter (>500 μm) accumulation rates (g cm^{-2} kyr^{-1}) calculated for specific periods in the last 25 kyr for cores along the Kejser Franz Josephs Fjord (PS2631) continental shelf (PS2641

and PS2630) continental slope (PS2629, PS2628 and PS2627) transect parallel to approximately 73°N. Termination Ia and Ib are shortened to Ia and Ib, respectively, in the oxygen isotope and chronostratigraphical scales. Note the linear sedimentation rates axis (x-axis) are not to the same scales.

7.1 Sedimentation and environmental model for the East Greenland continental margin adjacent to Kejser Franz Josephs Fjord during the Late Weichselian glaciation. EGC is short for East Greenland Current, and IRD for iceberg rafted debris.

7.2 Sedimentation and environmental model for the East Greenland continental margin adjacent to Kejser Franz Josephs Fjord during the Late Weichselian deglaciation (Termination Ia) of the continental margin. EGC is short for East Greenland Current, and IRD for iceberg rafted debris.

7.3 Sedimentation and environmental model for the outer Kejser Franz Josephs Fjord, Fosters Bugt and adjacent East Greenland continental margin during Early Holocene deglaciation of the Kejser Franz Josephs Fjord system (Termination Ib). EGC is short for East Greenland Current, and IRD for iceberg rafted debris.

7.4 Sedimentation and environmental model for the outer Kejser Franz Josephs Fjord, Fosters Bugt and adjacent East Greenland continental margin associated with the continued deglaciation (Termination Ib) of the Kejser Franz Josephs Fjord system during the Early Holocene. EGC is short for East Greenland Current, and IRD for iceberg rafted debris.

7.5 Sedimentation and environmental model for the East Greenland continental margin adjacent to Kejser Franz Josephs Fjord during the Holocene. EGC is short for East Greenland Current, and IRD for iceberg rafted debris.

7.6 Sedimentation and environmental model for the mid to outer region of Kejser Franz Josephs Fjord during the Holocene period following the deglaciation of the fjord system. IRD is short for iceberg rafted debris.

LIST OF TABLES

5.2 Correlation of core lithofacies (Chapter 4) and acoustic units identified from Parasound records for the Kejser Franz Josephs Fjord - continental shelf - continental slope study area (Fig 1.1). The ordering of the lithofacies/subfacies reflects their downcore sequencing (refer to Fig 4.1 for core depths). In the case of acoustic units Ia/Ib and IV, the individual acoustic layers correlate to the lithofacies/subfacies indicated.

5.3 Summary of the depositional processes of the acoustic units determined from Parasound records obtained along ship tracks from the mid-outer region of the Kejser Franz Josephs Fjord, Fosters Bugt and the adjacent continental shelf and slope (Figure 5,1a). Details include: i) Acoustic units and sub-units, ii) Acoustic unit code, iii) Distribution of the acoustic units, and iv) Processes of deposition indicated by the acoustic units.

6.1 AMS ^{14}C datings of sediment samples from selected intervals within the cores recovered along the Kejser Franz Josephs fjord-shelf-slope transect (Fig 1.1). The table lists the core number, sample depth below seafloor (cmbsf), and uncorrected and corrected (reservoir effect of 550 years) radiocarbon ages. Measurements were performed at the AMS dating laboratory of the Institute of Physics and Astronomy, Aarhus University, Denmark.

6.2 Summary of Stage I $\partial^{18}O$ and $\partial^{13}C$ records from along the Kejser Franz Josephs Fjord-shelf-slope transect.

6.3 Linear sedimentation and mass accumulation rates calculated from cores recovered along the Kejser Franz Josephs fjord-shelf-slope. mass accumulation rates include i) Bulk - BARs, ii) Terrigenous fraction - TARs (>500 µm), iii) Coarse fraction - CARs (>63 µm), and iv) Fine fraction - FARs (<63 µm). The rates listed are minimum, maximum, and average values calculated for the period between the corresponding and previous radiocarbon ages. Numbers in *italics* are: i) estimated/correlated ages discussed in the text, and ii) age of undated lower section of each core determined from the linear timescale (Figure 6.2). ‡ In PS2629, and based on correlation of the oxygen isotope and IRD records between the gravity and box cores, it is determined that the topmost 40 cm are missing from the gravity core and depths are corrected by 40 cm. Numbers in brackets are uncorrected gravity core depths, and the adjacent number is the corrected depth. * No sedimentation rate is calculated between 18,490 - 25,800 yr BP in PS2627 as the latter AMS date was determined on a debris flow unit; at best the rate calculated between 15,330 and 18,490 yr BP is extended to a core depth of 290 cm (i.e. 19753 yr BP) immediately overlying the resedimented section of the core (turbidites and debris flow deposit; Fig 6.1).

LIST OF EQUATIONS

CHAPTER 1

INTRODUCTION AND BACKGROUND

1.1 GENERAL INTRODUCTION AND AIMS OF THE STUDY

Marine sediments in the fjords and on the continental margin of East Greenland record the Late Quaternary environmental history of glacial and interglacial change in East Greenland and the western margin of the Greenland-Norwegian Sea. A thorough investigation of this sedimentary record is important to our understanding of the nature, timing and environmental effects of Late Quaternary glaciations, deglaciations and interglaciations for the East Greenland margin of the Polar North Atlantic. Only a limited number of studies have been performed on the Late Quaternary marine sediments off East Greenland (Section 1.4). This contrasts with the numerous studies off western Svalbard and Norway and in the Barents Sea. This study investigates a new region of the East Greenland margin and, in doing so, contributes further to our understanding of the Late Quaternary environmental history in this region.

The glacimarine/marine sedimentary record, and its relationship to glacial and interglacial environmental change associated with the Late Weichselian and Holocene, is investigated in the mid to outer Kejser Franz Josephs Fjord, and adjacent continental shelf and slope region, East Greenland (73°N; Fig 1.1). A number of objectives are central to this study, and include: (i) to outline the Late Weichselian and Holocene sedimentary facies, and the sedimentation patterns and processes within the Kejser Franz Josephs Fjord and on the adjacent continental shelf and slope using marine geological (sediment cores) and geophysical (acoustic) records, (ii) to outline a chronology for the sediments using absolute and relative dating methods, (iii) to quantitatively define the flux of sediments supplied to the fjord, shelf and slope settings in response to glacial/interglacial climatic change, (iv) to reconstruct the Late Weichselian and Holocene environmental history associated with glacial/interglacial change for this region of East Greenland, and to integrate this within the context of the glacier and climatic fluctuations and palaeoenvironments of East Greenland derived from complementary work.

This study forms part of the European Science Foundation programme on the Late Cenozoic Evolution of the Polar North Atlantic Margins (PONAM). Part of this programme is aimed at reconstructing the Late Quaternary environmental history of East Greenland by investigating and correlating the terrestrial and marine sedimentary records. The study supplements recent geological and geophysical investigations of the Late Quaternary marine record of other fjord and continental margin regions of East Greenland conducted under the PONAM programme (Section 1.4).

Figure 1.1. Location map of East Greenland showing: (i) the core sites (PS2633, PS2632, PS2631, PS2641, PS2630, PS2629, PS2628 and PS2627) of this study (represented as filled triangles) within Kejser Franz Josephs Fjord and on the adjacent continental margin, (ii) the fjord systems of East Greenland, (iii) the outlet glaciers draining the Greenland Ice Sheet (white terrestrial areas). A key to the abbreviated outlet glacier names is provided, and (iv) terrestrial regions not covered by glacial ice (stippled regions). The area covered by the map in relation to Greenland is shown in the inset.

1.2 EAST GREENLAND AND THE STUDY AREA

1.2.1 Greenland

Greenland forms an island with an area of 2,175,600 km^2 (Reeh 1989), and lies to the north east of Canada across the Labrador Sea and to the west of the Greenland, Iceland and Norwegian Seas. Greenland extends from its most northerly point at Kap Morris Jessup (83° 43'N) to its most southerly point at Kap Farvel (59° 45'N), and is characterised by a coastline indented by extensive and branched fjord systems. Approximately 81% of the continent is covered by the Greenland Ice Sheet and associated outlet glaciers (e.g. Reeh 1989; Section 1.2.4). Land areas (bed-rock exposures) are confined to a mountainous coastal zone around the rim of Greenland, covering an area of 408,800 km^2, with a width up to 300 km and an altitude up to 3,700 m (e.g. Funder 1989; Reeh 1989). Greenland is bordered by a continental margin, comprising a continental shelf that attains a maximum width of 300 km off the north east coast of Greenland, and a continental slope that leads down into the deeper abyssal regions of surrounding seas.

1.2.2 Location and description of the study area

The Kejser Franz Josephs Fjord (KFJ) and adjacent continental margin form the focus area for this study (Figs 1.1-1.3). The study area is located in the central region of the eastern margin of Greenland and adjacent continental margin between 73°N and 74°N and 15°W and 28°W (Fig 1.1). The study area borders the western margin of the Greenland Sea. The major fjord systems of Scoresby Sund and Kong Oscars Fjord lie to the south, and Godthaab Golf, Hochstetter Bugten and Dove Bugt to the north of the study area (Fig 1.1).

Kejser Franz Josephs Fjord is relatively long, extending sinuously for approximately 220 km inland from the outer coast (Figs 1.1-1.3). The fjord covers an area of 2,200 km^2. The fjord is relatively narrow and steep in the inner fjord (<10 km wide) and wider in the outer fjord (up to 20 km). The fjord mouth is unsilled (Chapter 5), and the fjord opens out into the embayment of Fosters Bugt (Figs 1.1, 1.2). The island of Bontekoe is situated within Fosters Bugt (Figs 1.1, 1.2). Beyond Fosters Bugt, the continental shelf extends for approximately 110 km to a shelf break with the continental slope leading down into the deeper abyssal regions of the Greenland Sea. The mid to interior region of Kejer Franz Josephs Fjord is fed by the smaller, narrow tributary fjords of Nordfjord, Geologfjord and Isfjord which are about 25 km, 55 km, 40 km, respectively, in length.

The margins of the Kejser Franz Jospehs Fjord, particularly the mid to outer fjord region, together with Nordfjord and Geologfjord, are dissected by numerous glaciofluvial and fluvial systems, with the latter being fed by snow melt and precipitation. Badlanddal and Paralleldal are two such large systems that enter Fosters Bugt and the northern margin of the outer region of the Kejser Franz Josephs Fjord, respectively (Figs 1.2, 1.3). Commonly, river systems occupy formerly ice-filled valleys and form large river plains in low lying areas e.g. Badlanddal in the Hold with Hope region (Figs 1.2, 1.3).

Figure 1.2. Landsat Multispectral Scanner (MSS) image of the Kejser Franz Josephs Fjord and Foster Bugt region showing the tributary fjord system, terrestrial regions, glacifluvial and fluvial drainage systems, and outlet glaciers draining the Greenland Ice Sheet. Placenames of these features are provided. Areas of intense white are snow capped land areas. The boxed areas (A) and (B) correspond to the MSS images in Figure 1.3 (A) & (B). The scale and north orientation of the image is shown. The image should be viewed in a landscape orientation. The image is a composite of two scenes imaged on 14 and 29 August 1987 and is from a mix of MSS bands 2, 3 and 4.

Figure 1.2. Landsat Multispectral Scanner (MSS) image of the Kejser Franz Josephs Fjord and Foster Bugt region showing the tributary fjord system, terrestrial regions, glacifluvial and fluvial drainage systems, and outlet glaciers draining the Greenland Ice Sheet. Placenames of these features are provided. Areas of intense white are snow capped land areas. The boxed areas (A) and (B) correspond to the MSS images in Figure 1.3 (A) & (B). The scale and north orientation of the image is shown. The image should be viewed in a landscape orientation. The image is a composite of two scenes imaged on 14 and 29 August 1987 and is from a mix of MSS bands 2, 3 and 4.

Figure 1.2. Landsat Multispectral Scanner (MSS) image of the Kejser Franz Josephs Fjord and Foster Bugt region showing the tributary fjord system, terrestrial regions, glacifluvial and fluvial drainage systems, and outlet glaciers draining the Greenland Ice Sheet. Placenames of these features are provided. Areas of intense white are snow capped land areas. The boxed areas (A) and (B) correspond to the MSS images in Figure 1.3 (A) & (B). The scale and north orientation of the image is shown. The image should be viewed in a landscape orientation. The image is a composite of two scenes imaged on 14 and 29 August 1987 and is from a mix of MSS bands 2, 3 and 4.

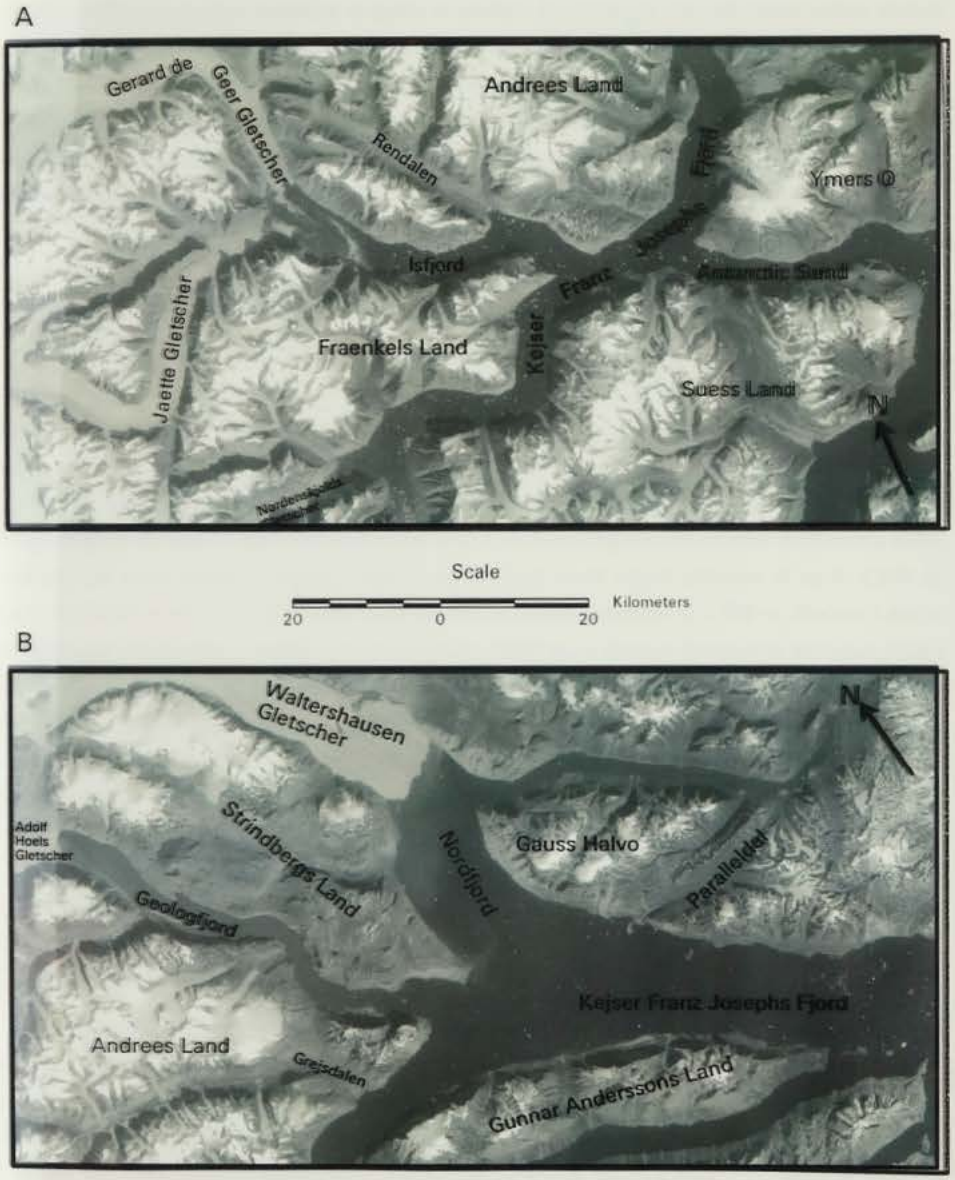

Figure 1.3 A & B. Landsat Multispectral Scanner (MSS) images of the Kejser Franz Josephs Fjord (KFJ) region corresponding to boxes (A) and (B) in Figure 1.2, showing: (i) Numerous icebergs that appear as white specks within the fjord waters. Icebergs decrease from high numbers in the inner region of KFJ Fjord and Isfjord (A) to lower numbers in the mid to outer region of KFJ fjord (B), and (ii) Turbid surface melt and river plumes derived from tidewater glaciers, and glacifluvial and fluvial drainage systems that appear with a cloudy grey tone. The surface plumes have the highest concentrations at the head of KFJ Fjord and Isfjord (A) and throughout Geologfjord and Nordfjord (B), marked by deep cloudy grey tones. The remaining fjord waters, particularly KFJ Fjord, appear with much lighter cloudy grey tones, indicating that surface plumes escape the inner regions of the fjord system and fjord margins, but with markedly lowered concentrations. The scale and north orientation of the images are shown. The scene was imaged on 14 August 1987 and is from MSS band 1.

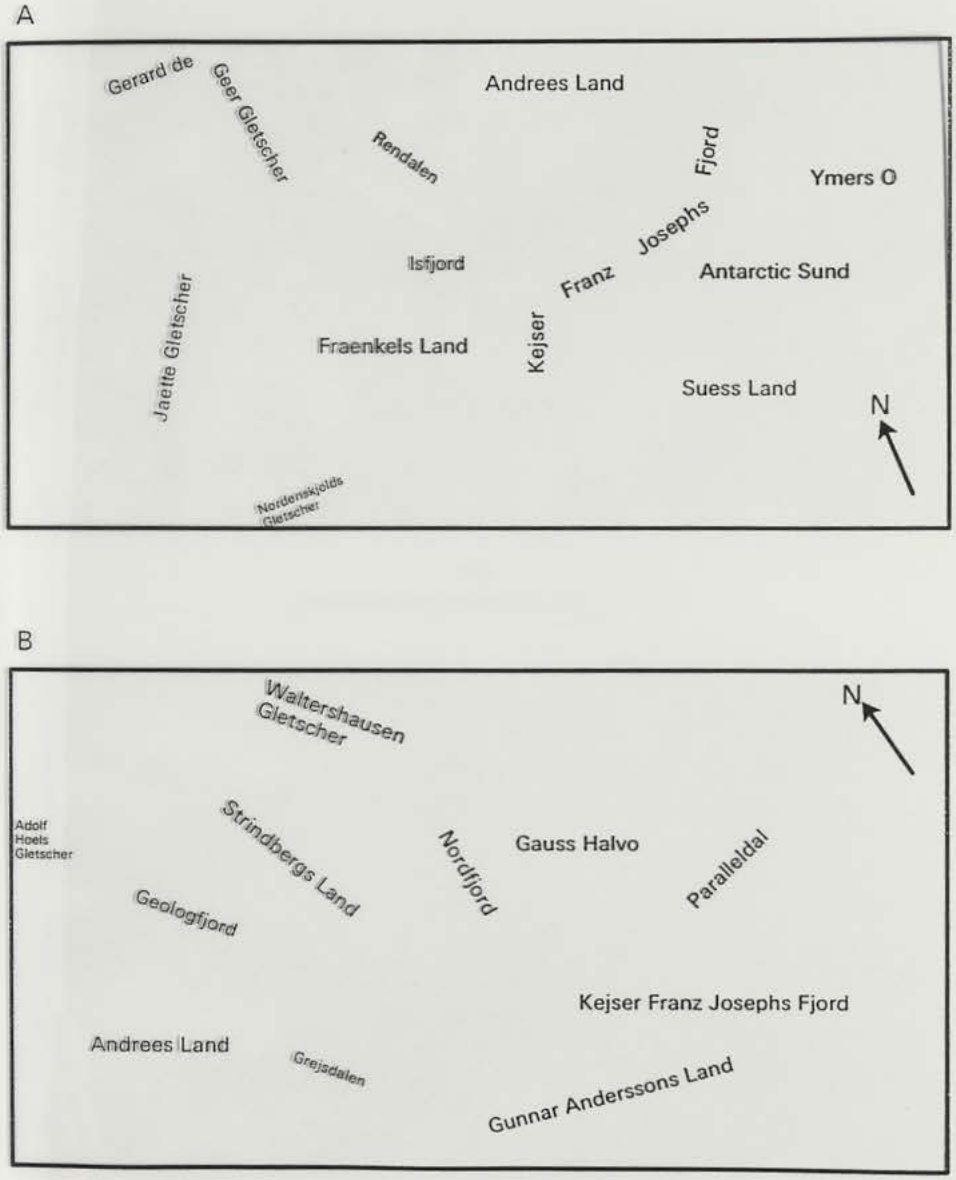

Figure 1.3 A & B. Landsat Multispectral Scanner (MSS) images of the Kejser Franz Josephs Fjord (KFJ) region corresponding to boxes (A) and (B) in Figure 1.2, showing: (i) Numerous icebergs that appear as white specks within the fjord waters. Icebergs decrease from high numbers in the inner region of KFJ Fjord and Isfjord (A) to lower numbers in the mid to outer region of KFJ fjord (B), and (ii) Turbid surface melt and river plumes derived from tidewater glaciers, and glacifluvial and fluvial drainage systems that appear with a cloudy grey tone. The surface plumes have the highest concentrations at the head of KFJ Fjord and Isfjord (A) and throughout Geologfjord and Nordfjord (B), marked by deep cloudy grey tones. The remaining fjord waters, particularly KFJ Fjord, appear with much lighter cloudy grey tones, indicating that surface plumes escape the inner regions of the fjord system and fjord margins, but with markedly lowered concentrations. The scale and north orientation of the images are shown. The scene was imaged on 14 August 1987 and is from MSS band 1.

Scale

20 0 20 Kilometers

Aerial photographs (Geodætisk Institut, July 1973) of the study area show that glaciofluvial/fluvial systems terminate in fjords to produce fjord margin outwash deltas and/or alluvial fans. Aerial photographs and Landsat images show that meltwater/fluvial outflow commonly form surface turbid plumes that extend away from the entry point along the Kejser Franz Josephs Fjord and tributary fjord margin, to more shore-distal locations (Figs 1.2, 1.3). Aerial photographs also show the common presence of subaerial rock-falls/scree that form talus cones along the steep margins of Kejser Franz Josephs Fjord and its tributary fjords.

1.2.3 Topography of the study area

The topography of the interior of the Kejser Franz Josephs Fjord region is dominated by steep mountain peaks and gently undulated high mountain plateaux at 1,500-2,450 m elevations. The mid-outer region of the Kejser Franz Josephs Fjord, Nordfjord and Fosters Bugt, on the other hand, slopes from inland elevations of 1,200 m to areas of coastal lowland that can be fairly extensive. Both regions are incised by numerous glacially-abandoned valleys and cirques (Figs 1.2, 1.3). Higher altitude regions are snow capped all year round (Fig 1.2). Gauss Halvø and Gunnar Anderssons Land, bordering the outer region of Kejser Franz Josephs Fjord, reach inland altitudes of up to 1,680 m. Hold with Hope to the north of Fosters Bugt reaches an inland elevation of 1,500 m. Hudson Land to the north east of Nordfjord reaches elevations up to 2,050 m. A marked increase in elevation occurs towards the interior of the Kejser Franz Josephs Fjord region around Isfjord, Geologfjord and inner-mid Kejser Franz Josephs Fjord (Strindbergs, Andrees and Suess Lands) where elevations are up to 2,450 m. The interior region of Kejser Franz Josephs Fjord is steep walled, reaching high altitudes, and contrasting with the less steep and lower altitude margin of the outer fjord that gives rise to coastal plains.

1.2.4 Glaciology

1.2.4.1 Greenland Ice Sheet and outlet glaciers

Approximately 81% of Greenland is glacierised and is covered by the Greenland Ice Sheet and associated outlet glaciers (Reeh 1989). The Greenland Ice Sheet, with an area of 1,700,000 km^2, accounts for 78%, and is the largest ice sheet in the northern hemisphere. It contains about 7% of the world's fresh water (Reeh 1989). The ice sheet reaches a maximum altitude of 3,205 m. North of Scoresby Sund the coastal and lowland regions are relatively ice-free (Fig 1.1), whereas south of Scoresby Sund the coast is almost totally ice covered due to relatively high precipitation on the southeastern region of Greenland (Hjort 1979; Ohmura & Reeh 1991; Section 1.2.7).

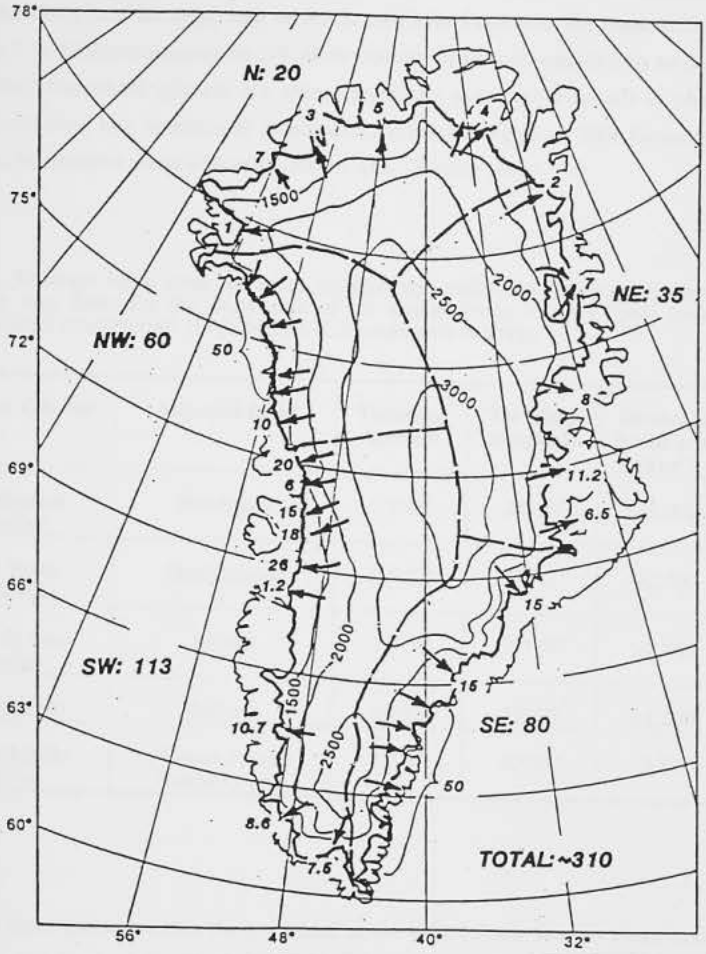

Figure 1.4. Volume of ice discharged from fast flowing outlet glaciers of the Greenland Ice Sheet in the form of icebergs. Small inclined numbers represent the volume of ice in cubic kilometres of water equivalent per year ($km^3\ yr^{-1}$). Large inclined numbers represent the total volume of ice (from Reeh 1985). The study area is indicated.

The interior of the Greenland Ice Sheet is drained through the coastal mountain zone by fast flowing outlet glaciers that terminate mainly at the head of coastal fjords forming tidewater glaciers. A small number of valley glaciers are also present in localised areas. Furthermore, several outlet glaciers also drain local ice caps, such as that at the Geike Plateau on the southern margin of Scoresby Sund (Fig 1.1). Glaciers account for 3% of the ice on Greenland, equating to an area of 65,500 km^2 (Reeh 1989). Greenland glaciers are characteristically polar (cold based) in character (Hambrey 1994). Equilibrium line altitudes of glaciers in the central region of East Greenland, including the study area, lie between about 450 and 1,300 m a.s.l. (Nuttall 1993).

Table 1.1. Drainage basin areas, terminus position and widths for tidewater glaciers, and the fjords into which they drain for the study area of the Kejser Franz Josephs Fjord system, central East Greenland (data from Nuttall 1993; Nuttall & Dowdeswell In Prep).

Tidewater Glacier	Adjacent fjord	Terminus latitude	Terminus longitude	Drainage basin area (km^2)	Terminus width (km)
Walterhausen Gletscher	Nordfjord	73° 48'	24° 10'	>2,000	10.2
Adolf Hoels Gletscher	Geologfjord	73° 57'	25° 47'	>2,400	3.7
Gerard de Geer Gletscher	Isfjord	73° 30'	27° 18'	>1,800	3.3
Jættegletscher	Isfjord	73° 27'	27° 28'	>2,200	2.3
Nordenskjölds Gletscher	Kejser Franz Josephs Fjord	73° 07'	27° 43'	>3,800	2.6

All outlet glaciers within the hinterland of the Kejser Franz Josephs Fjord system terminate at sea level at the head of fjords, forming tidewater glaciers (Figs 1.1-1.3). These tidewater outlet glaciers include: Walterhausen Gletscher, Adolf Hoels Gletscher, Gerard de Geer Gletscher and Jættegletscher, and Nordenskjölds Gletscher draining into Nordfjord, Geologfjord, Isfjord and Kejser Franz Josephs Fjord, respectively (Figs 1.1-1.3). The drainage basin area, terminus width and location of these glaciers are summarised in Table 1.1. The drainage basin area for each of these glacier systems includes both the area of outcropping bedrock and glacial ice. It was not possible to calculate the entire basin area and, therefore, the proportion of glacial ice within the basin area because part of each drainage basin extended outside the satellite imagery (cf. Nuttall & Dowdeswell In Prep). Therefore, basin areas are preceeded by >, indicating that they are minimum areas. The total drainage basin area associated with the glaciers in the study area exceeds 8,400 km^2 (Nuttall & Dowdeswell In Prep) and is, therefore, likely to be an important contributor of sediments to the modern-day fjord

and shelf. Drainage basins to the north of the study area may also contribute to sedimentation on the shelf of the study area as a result of the southward flowing East Greenland Current (Section 1.2.5).

Aerial photographs (Geodætisk Institut July 1973) and Landsat images (August 1987; Figs 1.2, 1.3) show that subglacial meltwater derived from the tidewater glaciers of the study area form surface turbid plumes that extend away to more shore-distal locations of Kejser Franz Josephs Fjord and tributary fjords (Figs 1.2, 1.3).

1.2.4.2 Iceberg calving and drift tracks

Icebergs enter the Kejser Franz Josephs Fjord system from the tidewater glaciers of the Greenland Ice Sheet described in Section 1.2.4.1 and Table 1.1. Reeh (1985) estimates that ca. 8 km^3 of ice is calved into the fjord system annually (Fig 1.4). This compares to ca. 18 km^3 of ice per year for the Scoresby Sund fjord system (70-72°N), and 7 km^3 of icebergs per year for Dove Bugt (75-76°N), which are other major iceberg producing regions of East and Northeast Greenland (Figs 1.1, 1.4). The icebergs calved into the fjords of the study area account for 2-3% of the total iceberg production from Greenland (cf. Reeh 1985).

Iceberg dimensions vary. Dowdeswell et al. (1992, 1993) have documented that tabular icebergs calved from floating termini in the Scoresby Sund fjord system reach dimensions over 100 m, and up to 2,500 m, in length and up to 600 m in thickness, with keel-depths up to and occasionally in excess of 600 m. Smaller icebergs of irregular shape are calved from tidewater glaciers grounded at their margins. These iceberg dimensions are likely for the study area given that ice is also supplied mainly by outlet glaciers.

Satellite images in Figures 1.2-1.3 illustrate the presence of icebergs calved from tidewater glaciers. The drift pattern of icebergs is from the head to the mouth of the fjord system (Figs. 1.2a&b). Fjord bifurcation, bathymetry and currents provide additional complications. Where ice keels are sufficiently shallow with respect to bathymetry, icebergs escape into shelf waters. However, ship-based observations show this number to be minimal (Chapter 5). Icebergs within continental shelf waters follow a southerly drift pattern in response to the East Greenland Current which flows south parallel to the coast (Section 1.2.5). The continental shelf of the study area can also be influenced by icebergs calved from glaciers from further north in East and Northeast Greenland (e.g. Wadhams 1981; Dowdeswell et al. 1993).

1.2.4.3 Sea ice cover

Sea ice forms seasonally within the Kejser Franz Josephs Fjord system. First-year seasonal sea-ice melts during the summer break-up leaving the fjords relatively free of ice (Figs 1.2, 1.3). Landsat imagery of the Scoresby Sund fjord system (Fig 1.1) shows that seasonal sea ice (usually shorefast sea ice) exists for 7-8 months of the year (October-June) with subsequent break-up between June and October (Dowdeswell et al. 1992).

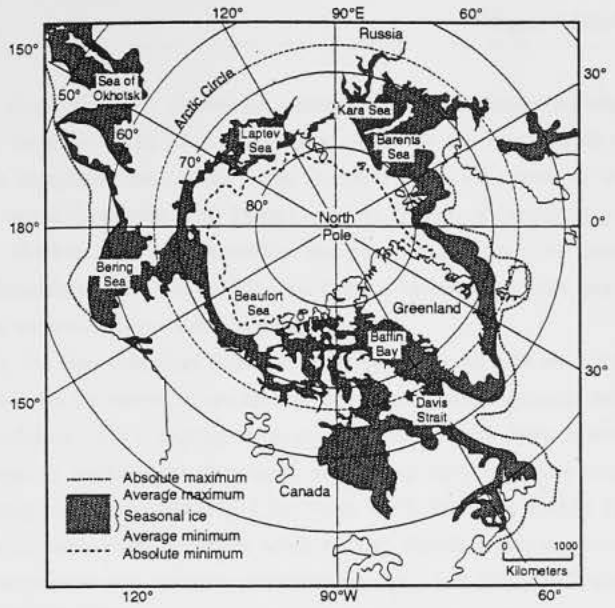

Figure 1.5a. Sea ice limits (1/8-ice) in the East Greenland region and the northern sub-polar and polar oceans. The maximum, minimum and mean sea ice limits are shown. After CIA (1978) and Barry (1989). From Myhre et al. (1995).

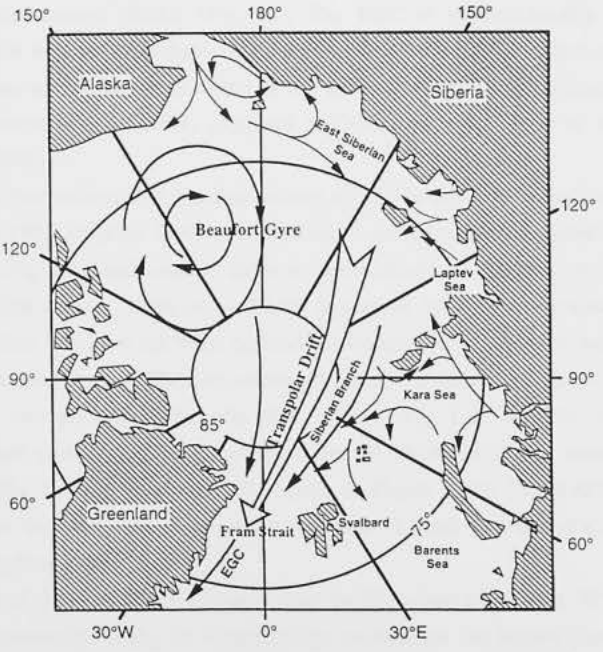

Figure 1.5b. Mean sea-ice drift within the Arctic Ocean and its transport through the Fram Strait and along the East Greenland coast via the East Greenland Current (EGC) (from Nam 1996).

Sea ice along the East Greenland continental margin occurs mainly as pack ice (e.g. Wadhams 1981; Hopkins 1991). This is primarily multi-year sea ice (3 to 10 m thick) originating over the Siberian continental shelf of the Arctic Ocean; This ice exits from the Arctic Ocean through the Fram Strait via the Transpolar Drift Stream and East Greenland Current (Fig 1.5b; Section 1.2.5; Wadhams 1981; Hopkins 1991). Occasionally, this pack ice can enter the fjord system during the summer (e.g. Marienfeld 1991, 1992b). The pack ice is interspersed with quantities of seasonally formed first-year ice which melts during summer months.

Normally, the East Greenland continental margin is covered with sea ice from October to late June, where maximum ice extent occurs during March and minimum extent during September (e.g. Vinje 1977; Wadhams 1981). During mild summers the sea-ice limit retreats north along the continental margin to northeastern Greenland, and during more moderate summers this extent is further south along East Greenland (Fig 1.5a; Vinje 1977; Myhre & Thiede 1995). During winter months the sea-ice limit extends further south to Kap Farvel at the southern tip of Greenland, covering the southeastern and southern continental margin, and across to Iceland (Fig 1.5a; Vinje 1977; Myhre & Thiede 1995).

1.2.5 Oceanography and hydrography

The East Greenland continental margin is dominated by the southward flowing East Greenland Current system (EGC) (Fig 1.6). The EGC is geostrophically constrained to the continental margin of East Greenland (Fig 1.6; Hopkins 1991). The system transports an upper, surface water mass termed the Polar Water (PW), and an underlying water mass termed the Return Atlantic Intermediate Water (RAIW) (Aagaard & Coachman 1968; Swift & Aagaard 1981; Swift 1986; Hopkins 1991).

The cold, low salinity PW (median salinity of 33.7‰ and median temperatures of -1°C: e.g. Swift & Aagaard 1981; Hopkins 1991) is derived and exported southwards from the Arctic Ocean via the Fram Strait (Fig 1.6), and extends down to water depths of 200 m (e.g. Bourke et al. 1987; Hopkins 1991). The warmer, more saline RAIW is derived from (i) a westward directed branch of Atlantic intermediate waters of the West Spitsbergen Current (WSC; Atlantic waters are supplied via the Atlantic/Norwegian Currents flowing northwards along the eastern margin of the Norwegian Sea), which becomes incorporated within the EGC system (Fig 1.6), and (ii) from Polar Atlantic Intermediate Water (submerged WSC) exported out of the Arctic Ocean through the Fram Strait below the PW, (Fig 1.6; e.g. Hopkins 1991; Myhre & Thiede 1995). The RAIW flows at depths of 150-800 m within the EGC, and has a salinity between 34.9 and 35.0‰ and a temperature between 0°C and 2°C (Hopkins 1991).

A branch of the EGC flows eastwards from the Greenland slope at ca. 72° 30'N in response to the bathymetric extensions of the Jan Mayen Ridge, to form the Jan Mayen Current (JMC) (Fig 1.6; e.g. Swift & Aagaard 1981; Hopkins 1991). The Greenland Sea Deep Water (GSDW; temperature of <-1°C, salinity of 34.9‰: Hopkins 1991) underlies the RAIW within the Greenland Sea, and is

volumetrically the most dominant water mass in the western region of the Greenland-Norwegian Sea (Swift 1986). Production of dense, saline bottom waters due to brine expulsion during sea-ice growth (e.g. Midtthun 1985) is thought to occur at places along the East Greenland shelf (Berner & Wefer 1990; Dowdeswell et al. 1996). These waters cascade down the adjacent slope into the deeper basins of the Greenland Sea (Fig 1.6), contributing to the formation of the GSDW.

The water column of the Kejser Franz Josephs Fjord, similar to other East Greenland fjords, comprises three water masses (Swift 1986; Marienfeld 1991, 1992b; Vogt et al. 1995; Syvitski et al. 1996): (i) A warm (0°C-5°C) and low saline (<31‰) surface layer termed the fjord surface water (FSW), produced by spring/summer melting of sea ice and glaciers with heating from Arctic summer insulation. This FSW extends down to a maximum depth of 25 m in Kejser Franz Josephs Fjord, with a thickening towards the fjord head, and can extend, at maximum, out onto the inner shelf to 20-22°W (Vogt et al. 1995). The FSW layer is short-term and exists only during summer months. (ii) Very cold (<0°C), higher salininty (31-34‰) waters extending down to depths of between 200 and 300 m within Kejser Franz Josephs Fjord (Vogt et al. 1995), associated with an inflow of PW of the East Greenland Current from the adjacent continental margin. (iii) Warm (0°C-3°C), high salinity (>34‰) water of the RAIW of the East Greenland Current and Arctic Intermediate Waters (AIW) intruding into deeper regions of the fjord (>300 m).

1.2.6 Bathymetry and sea-floor morphology

A detailed account of the bathymetry and sea-floor morphology of the study area is provided in Section 5.3 as Parasound records of this study were used to compile this information. A brief summary of these data is given at this stage. The Kejser Franz Josephs Fjord reaches maximum water depths of between 500 and 800 m in the inner fjord basin. The mid fjord basin is separated from a series of three sub-basins within the outer fjord by a prominent, shallow sill (60 m below sea level) at the intersection of Kejser Franz Josephs Fjord, Nordfjord and Geologfjord. Water depths range down to ca. 540 m in the basins of the mid and outer Kejser Franz Josephs Fjord. No prominent sill exists at the mouth of Kejser Franz Josephs Fjord. Fosters Bugt is mainly shallow with maximum depths of 340 m associated with small-scale depressions. Water depths across a major proportion of the adjacent continental shelf vary between 280 and 340 m. The inner continental shelf basin forms the deepest part of the continental shelf of up to 520 m. The shallowest region of the continental shelf occurs over a prominent mid continental shelf bathymetric high with water depths of 235 m. The shelf break lies between ca. 280 and 340 m water depth. The continental slope leads down into the deeper regions of the Greenland Sea, and attains a gradient of ca. 4° on the upper continental slope decreasing to 1.4° on the lower continental slope.

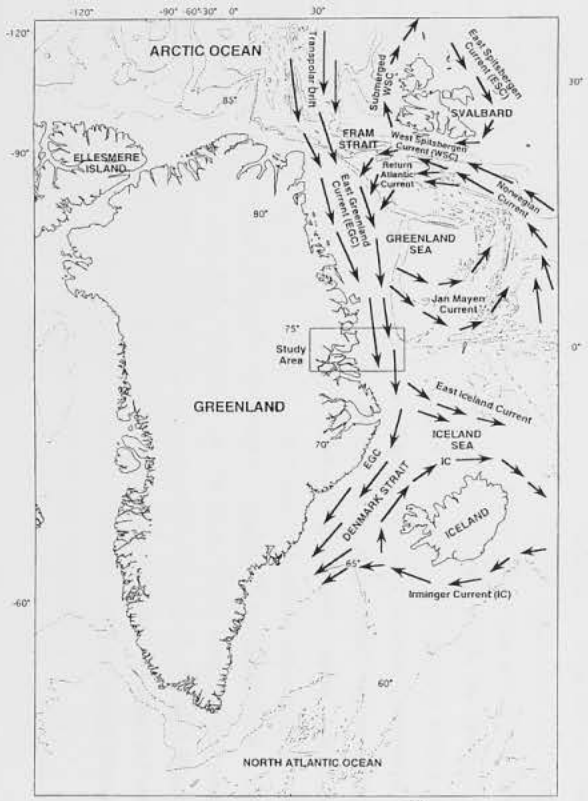

Figure 1.6. Oceanographic circulation patterns in the Greenland-Iceland-Norwegian Sea.

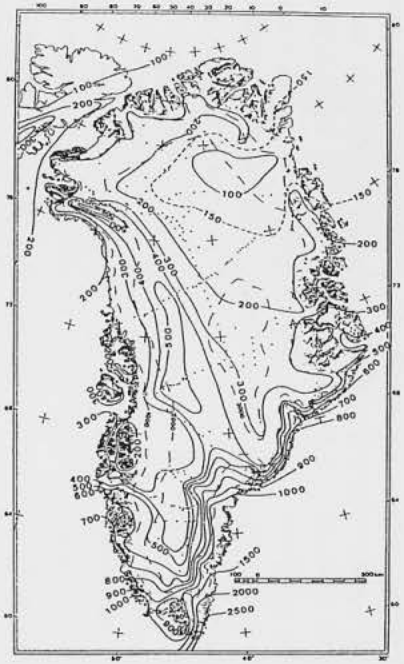

Figure 1.7. Annual total precipitation (mm) for Greenland. From Ohmura & Reeh (1991).

1.2.7 Modern day climate

The climate of East Greenland is generally cold, especially in the coastal regions, due to the influence of the circulation pattern of the polar East Greenland Current, which carries cold, polar water from the Arctic Ocean. Distinct temperature and precipitation gradients occur associated with the oceanic climate at the outer coast and the continental climate closer to the interior of the Greenland Ice Sheet (Hjort 1981; Funder 1989). Mean temperatures for the warmest and coldest months at Scoresby Sund (latitude 70° 25'N) reach values of 3°C and -20°C, respectively, for the period 1969-1979 (Danish Meteorological Institute data in Funder 1989). Annual total precipitation (mm) for Greenland is shown in Figure 1.7. Annual total precipitation, measured at meteorological stations along the East Greenland coast (latitudes 70° 25'N to 74° 18'N), exhibits a northwards decrease in values from 549 mm at Scoresby Sund to 214 mm at Daneborg, with a value of 300 mm close to the study area at Myggbukta, for the period 1951-1980 (Funder 1989; Ohmura & Reeh 1991). This pattern is produced due to the fact that cyclonic centres move northwards along the coast of Southeast and East Greenland and deposit the major part of their precipitation south of Scoresby Sund. They move away from the coast north of Scoresby Sund, where the coastline changes direction and begins to trend north west (Hjort 1979).

1.2.8 Bedrock geology

The geology of Greenland is presented in Figure 1.8a&b, summarised from Haller (1971), Koch and Haller (1971) and Escher and Watt (1976). The coast and fjord hinterland of the interior of Kejser Franz Josephs Fjord and Isfjord and at the head of Geologfjord, inclusive of the Adolf Hoels, Gerard de Geer, Jæette and Nordenskjölds Gletschers and their inland drainage basins, are composed of Precambrian crystalline rocks (gneisses, migmatites and supracrustal and plutonic rock types). Late Precambrian and Early Palaeozoic sandstones, pelites, carbonates and tillites compose the fjord hinterland and coast of Geologfjord, mid Kejser Franz Josephs Fjord, the drainage basin of Walterhausen Gletscher and northern Hudson Land, that were subsequently folded, thrusted, metamorphosed, migmatised and intruded by granite during the Early Silurian Caledonian orogeny. Devonian, Carboniferous and Permian terrestrial sandstones and conglomerates compose the the fjord coast of Nordfjord, the bulk of Hudson Land and Gauss Halvö and Gunnar Anderssons Land bordering Kejser Franz Josephs Fjord. Mesozoic continental and marine-epicontinental sandstone, shale and carbonate rocks compose western Geographical Society Ø bordering Fosters Bugt. Late Mesozoic to Early Tertiary ocean-floor spreading of the Polar North Atlantic was preceded by effusive volcanism producing sheet or plateau basalts across the outer region of Kejser Franz Josephs Fjord, Hold with Hope and Bontekoe Ø. These basalts outcrop and underlie sediments in Fosters Bugt and across the continental shelf. Northwest-southeast and northeast-southwest faults formed during the Mesozoic have determined the location of the fjords of East Greenland.

Figure 1.8 a&b. The geology of (a) Greenland, and (b) East Greenland showing the main geological divisions of the Kejser Franz Josephs Fjord region (study area). Reproduced from Escher & Watt (1976).

1.3 CHRONOLOGY OF THE LAST 30,000 YR BP OF THE LATE QUATERNARY

The chronology of the Late Quaternary is commonly classified and expressed relative to two main time scales: (i) a chronostratigraphical scale, and (ii) a marine oxygen isotope stratigraphical scale. The chronology of boundaries within the time scales are defined by radiocarbon datings for the Late Weichselian and Holocene.

The Late Quaternary is divided into a number of chronostratigraphical subdivisions (cf. Mangerud et al. 1974; Mangerud & Berglund 1978) (Fig 1.9). The Quaternary is divided into the Pleistocene Series and Holocene ~~Series~~ Epochs, where the Holocene/Pleistocene boundary is placed at 10,000 yr BP. The Holocene series is not broken down further into stages. The latter part of the Pleistocene series consists of the Weichselian Stage. This represents the last glacial cycle, during which there were frequent and large amplitude glacial fluctuations. This Stage is subdivided into the Late Weichselian (10,000 to 25,000 yr BP; Fig 1.9), Mid Weichselian (25,000 to 75,000 yr BP; Fig 1.9) and Early Weichselian (75,000 to 115,000 yr BP) Sub-stages. The boundary between the Late Weichselian and Holocene dates at 10,000 yr BP (Fig 1.9). The Last Glacial Maximum associated with the Late Weichselian is dated between 15,000 and 21,000 yr BP in records from the East Greenland margin (e.g. Dowdeswell et al. 1994; Nam et al. 1995; Nam 1996), although the onset of glacial conditions began ca. 25,000 yr BP (e.g. Nam et al. 1995; Nam 1996). The Younger Dryas Stadial (a period of renewed cooling) of the Late Weichselian Sub-stage is dated between 11,000 and 10,000 yr BP (Fig 1.9).

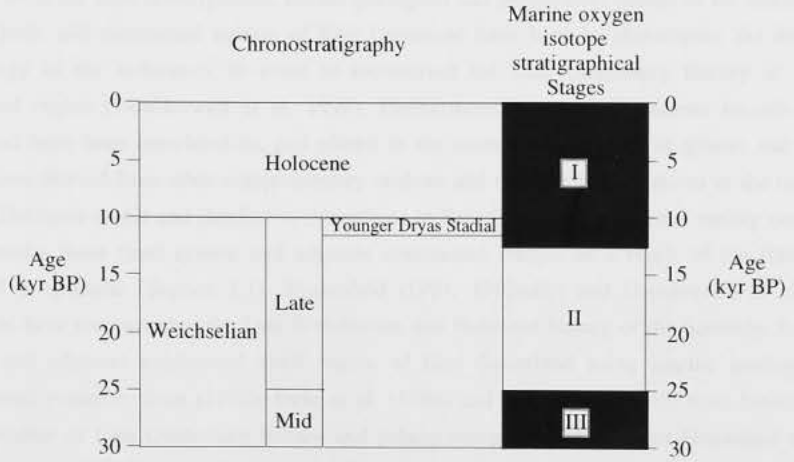

Figure 1.9. Chronostratigraphy and marine oxygen isotope stratigraphy of the last 30,000 yr BP of the Late Quaternary. Based on Mangerud et al. (1974), Mangerud & Berglund (1978), Martinson et al. (1987), Nam et al. (1995), Nam (1996), and Mangerud et al. (1996).

The marine oxygen isotope stratigraphical scale is based on the direct sensitivity of oxygen to temperature and ice volume fluctuations associated with glaciations and interglaciations. The present interglacial is known as Stage I, corresponding in part to the Holocene (Fig 1.9). The last glacial of the Late Weichselian corresponds to Stage II (Fig 1.9). Based on globally representative isotopic records, the Stage II/III boundary dates at ca. 25,000 yr BP (Martinson et al. 1987; Fig 1.9). This corresponds to the Late Weichselian and Mid Weichselian Sub-stage boundary, and is dated similarly by Nam et al. (1995) and Nam (1996) from the East Greenland margin. The Stage I/II boundary is dated from the global isotope records at ca. 12,000 yr BP (Martinson et al. 1987). However, the Stage I/II boundary has been dated and positioned over a range of ages based on other studies in high latitude northern seas, with the oldest dating at 15,800 yr BP (e.g. Zahn et al. 1985; Stein et al. 1994a&b; Nam et al. 1995; Nam 1996; Stein et al. 1996). The boundary in Figure 1.9 is placed at 12,000 yr BP.

1.4 PREVIOUS GLACIMARINE/MARINE GEOLOGICAL INVESTIGATIONS OF THE LATE QUATERNARY HISTORY OF EAST GREENLAND

Previous glacimarine and marine geological investigations into the Late Quaternary history of the fjords and continental margin of East Greenland have been limited. No previous marine-based geological investigations have been performed in the study area. Two fjord systems, Kangerdlugssuaq (68°N) and Scoresby Sund (70°-72°N), and the adjacent continental margin, have formed the main areas of focus for such investigations. Recent geological and geophysical studies of the marine record of the fjords and continental margin of East Greenland have been to characterise the nature and chronology of the sediments, in order to reconstruct the Late Quaternary history of the East Greenland region (Dowdeswell et al. 1994). Furthermore, most of the marine records of East Greenland have been correlated to, and placed in the context of evidence of glacier and climatic fluctuations derived from other complementary onshore and offshore investigations in the region.

The most recent and detailed investigations in East Greenland have been mainly confined to the Scoresby Sund fjord system and adjacent continental margin as a result of the ESF funded PONAM programme (Section 1.1). Marienfeld (1991, 1992a&b) and Dowdeswell et al. (1993, 1994a&b) have reconstructed the Late Weichselian and Holocene history of the Scoresby Sund fjord system and adjacent continental shelf region of East Greenland using marine geological and geophysical evidence. Nam (1996), Stein et al. (1996) and Nam et al. (1995) have broadened the reconstruction of Late Quaternary history and palaeoceanography of the East Greenland region to cover the last 240,000 years using geological evidence from the continental margin between 68°N and 72°N, and at 75°N. More recent studies of the Late Quaternary history of the East and Northeast Greenland continental margin (68°-80°N) have concentrated on determining the large-scale sedimentation patterns and associated processes of deposition using marine geophysical evidence (Dowdeswell et al. 1996, 1997; Mienert et al. 1993, 1995). Detailed investigations of the sedimentary

environment and glacial history of the Kangerdlugssuaq Fjord and continental margin region using glacimarine geological evidence have also been performed and examples include Mienert et al. (1992), Williams (1993), Andrews et al. (1994), Williams et al. (1995) and Syvitski et al. (1996).

1.5 STRUCTURE OF THE THESIS

This thesis is structured into eight chapters in order to address the general aims of the study outlined in Section 1.1:

Chapter 1 has provided a general introduction to the study by outlining (i) the objectives of the study, (ii) a description of East Greenland and the study area, (iii) previous investigations in the East Greenland region, and (iv) a chronology of the last 30,000 yr BP of the Late Quaternary.

Chapter 2 reviews (i) the products, processes and patterns of sedimentation within glacimarine and marine environments of high latitude regions, and (ii) the Late Weichselian and Holocene geological and environmental history of East Greenland and adjacent continental margin.

Chapter 3 introduces the field work and laboratory methodology, with an explanation of the underlying principles used to investigate the objectives of this study. The locations of the cores used in this study are introduced.

Chapter 4 presents the sedimentological characteristics of the cores recovered along the Kejser Franz Josephs Fjord-continental margin transect, with an interpretation of the sedimentary processes producing such sediments.

Chapter 5 presents the Late Quaternary acoustic records of the study area, with subsequent correlation to the sediment cores introduced in Chapter 4. The sedimentation patterns and processes across the study area are then discussed. In addition, analysis of iceberg scours and their associated distribution across the sea-floor is made.

Chapter 6 presents (i) the chronology/chronostratigraphy and oxygen isotope stratigraphy of the cores investigated, (ii) sedimentation and accumulation fluxes of sediments supplied to the fjord, shelf and slope settings. In addition, the palaeoenvironmental implications of the stable isotope records and sediment fluxes are discussed.

Chapter 7 discusses and reconstructs the Late Weichselian and Holocene glacimarine and marine sedimentation and the glacial and environmental history of the study area in the context of the evidence presented in Chapters 4, 5 and 6.

Chapter 8 forms the conclusions to this study.

CHAPTER 2

GLACIMARINE SEDIMENTATION AND ENVIRONMENTS AND THE LATE WEICHSELIAN AND HOLOCENE IN EASTERN GREENLAND

2.1 INTRODUCTION

The aim of this chapter is to set the central themes of the investigation within the environmental context of East Greenland and other high latitude regions. Therefore, the chapter discusses the main processes of glacimarine and marine sedimentation and associated facies common to most high latitude glacier-influenced settings, and presents an overview of the Late Weichselian and Holocene environmental history of East Greenland.

2.2 GLACIMARINE SEDIMENTATION PROCESSES AND FACIES

2.2.1 Introduction

Glacimarine debris can be defined as sediment composed of a mixture of glacigenic detritus (released directly from glaciers or transported subsequently by mass flows, moving fluids or ice-rafting) and marine material deposited more or less contemporaneously (Andrews & Matsch 1983; Dowdeswell 1987; Hambrey 1994). It should be noted that the glacigenic and marine components of glacimarine sediments can be widely variable within this definition. A summary of the glacimarine sedimentary system inclusive of sediment sources, stores, flows and processes is provided in Figure 2.1 (Dowdeswell 1987). More detailed reviews of the processes of glacimarine sedimentation and associated facies are provided in Drewry (1986), Dowdeswell (1987) and Hambrey (1994).

Marine-based sedimentological investigations along East Greenland are limited, and confined mainly to the Scoresby Sund and Kangerdlugssuaq Fjord systems and adjacent continental margins (Section 1.4; e.g. Marienfeld 1991, 1992a,b; Mienert et al. 1992; Dowdeswell et al. 1994a,b, 1996, 1997b; Syvitski et al. 1996). These fjords and the adjacent continental shelf are ice-dominated glacimarine settings in which icebergs produced from fast-flowing outlet glaciers draining the Greenland Ice Sheet dominate the sedimentary regime (Fig 1.4; Reeh 1985; Dowdeswell et al. 1993, 1994a, 1997b; Syvitski et al. 1996). However, the volume of ice calved into the more northerly fjords and shelf settings, including Kejser Franz Josephs Fjord and the continental margin of the study area

(Fig 1.1), is markedly lower (Fig 1.4; Reeh 1985; Dowdeswell et al. 1993). Therefore, it is expected that the supply of iceberg debris and deposition of associated facies will be reduced and, coupled with the narrow and steep sided configuration of the fjord systems, sedimentation from other processes such as meltwater/river outflow and subaqeous mass wasting are likely to be more significant (Chapters 4, 5). This section, therefore, will outline a number of glacimarine and marine sedimentation processes and associated sedimentary facies and products applicable to the East Greenland glacier-influenced setting.

2.2.2 Iceberg rafting and sedimentation

2.2.2.1 Iceberg calving mechanisms and controls

The calving of icebergs occurs when glacier ice becomes detached from a parent ice mass, such as tidewater glaciers, terminating in water (Dowdeswell 1987). A number of mechanisms control iceberg calving at grounded and floating ice fronts, and are reviewed in Dowdeswell (1987) and Warren (1992). In brief, calving mechanisms include: (i) bending creep failure leading to shear rupture (Hughes 1989), (ii) grounding line flexure due to tidal, wave and current vibrational bending (Holdsworth 1985), (iii) hydrostatic imbalance along unsupported ice fronts (Reeh 1968), (iv) vibrational calving linked to cyclical stresses (Holdsworth & Glynn 1978), and (v) creep failure due to lateral spreading.

The flux of icebergs calved from outlet glaciers draining the Greenland Ice Sheet is controlled mainly by the ice flow dynamics and the ice volume of associated drainage basins. Furthermore, the calving speed and, therefore, the flux of icebergs, is related linearly to the depth of water at the fjord head in which the tidewater glacier terminates (Pelto & Warren 1991; Warren 1992).

2.2.2.2 Iceberg sediments and sedimentation

Icebergs are the main mechanism by which glacially derived coarse-grained material can be transported to ice-distal locations the fjords, and adjacent continental shelf and slope of East Greenland. The debris transported by icebergs is inferred to originate mainly from debris-rich ice at the base of the parent glacier (e.g. Drewry 1986; Dowdeswell & Dowdeswell 1989; Dowdeswell et al. 1994a,b). Relatively thick basal debris-rich layers are the most important contributors to iceberg rafting, and such layers have been reported to reach a few metres in thicknesses within icebergs (e.g. Dowdeswell & Dowdeswell 1989). The volume, distribution and character of debris within icebergs is a function of the nature, processes and debris entrainment of the parent glacier (cf. Dowdeswell & Dowdeswell 1989). The debris in icebergs is generally variable in concentration and heterogeneous in grain size, reflecting the basal ice processes of the parent glacier.

The rate of sedimentation from icebergs and the associated spatial distribution of debris across the sea floor and through time are dependent on a number of factors (Syvitski et al. 1987; Dowdeswell & Murray 1990; Hambrey 1994; Syvitski et al. 1996): (i) the distribution and concentration of debris in the parent ice mass, (ii) the rate of iceberg calving and melting, (iii) the

temperature of offshore waters, (iv) the velocity, stability and drift pattern and flux of icebergs, and (v) the number of overturning and fragmentation events. Figure 2.2 presents a hypothetical model for the pattern of debris release for an iceberg calved from outlet glaciers or ice streams, and the resulting sedimentation rate (Drewry & Cooper 1981). Melting and disintegration of icebergs can occur above, at and below the water-line due to solar radiation, wave action and the advection of heat from sea water, particularly during the summer season (Drewry 1986). The rate of iceberg melting is slowed in cold, polar waters (Syvitski et al. 1987; Dowdeswell et al. 1994a). Therefore, the cold East Greenland Current may act to slow the melting rate of icebergs traversing the continental shelf, inhibiting the flux of sediment to the sea floor, and allowing sedimentation within more ice-distal settings.

Iceberg sediments are deposited as either continuous melt-out from the base or steep sides of the melting iceberg or quasi-instantaneous dumping of debris from the iceberg surface during overturn/fragmentation (e.g. Dowdeswell et al. 1994a,b). The resultant characteristics of iceberg sediments vary from isolated dropstones, lenses and clusters to more extensive layers, composed of coarse grains (e.g. Ovenshine 1970; Gilbert 1990; Dowdeswell et al. 1994a,b; Cowan et al. 1997). However, the finer grained rain-out component of iceberg sediments is difficult to distinguish sedimentologically from that originating from meltwater outflows, sea ice and aeolian action (e.g. Syvitski et al. 1996; Cowan et al. 1997; Dowdeswell et al. 1998).

The East Greenland fjords of Kangerdlugssuaq and Scoresby Sund are iceberg dominated glacimarine settings (Marienfeld 1991, 1992a,b; Dowdeswell et al. 1993, 1994a,b; Syvitski et al. 1996). The present interglacial sediments of Scoresby Sund are coarse grained diamictons, reflecting the dominant supply of heterogeneous sediments to the fjord from the large numbers of free drifting icebergs, with a much more limited flux of finer grained sediments from glacifluvial, fluvial and subglacially-derived turbid surface plumes (Section 2.2.4), sea ice (Section 2.2.3) and aeolian processes (Marienfeld 1991, 1992a,b; Dowdeswell et al. 1994a,b). In the Kangerdlugssuaq Fjord system the presence of shorefast sea ice close to the ice margin severely restricts the drift of icebergs through the fjord and, therefore, the sedimentation of most of the iceberg rafted sediment is restricted to the ice-proximal region with finer-grained sediments (Section 2.2.4) dominating the remainder of the fjord system (Syvitski et al. 1996). By contrast, in meltwater dominated settings such as the fjords of SE Alaska and Spitsbergen and the north-eastern Barents Sea (e.g. Elverhøi et al. 1980, 1983; Powell 1981, 1983, 1990; Mackiewicz et al. 1984; Powell & Molnia 1989; Pfirman & Solheim 1989; Sexton et al. 1992; Svendsen et al. 1992, 1996; Cadman 1996), glacifluvial, fluvial and subglacial outflows play a more significant role in sedimentation. The flux of iceberg-derived sediments is greatly subordinate, and probably intermittant in comparison (Syvitski et al. 1996; Dowdeswell et al. 1998). The resulting sediments are predominantly fine-grained, consisting of a limited coarser grained component (gravel and sand grade material) representing iceberg rafted dropstones and sand (e.g. Elverhøi et al. 1980, 1983; Svendsen et al. 1992).

2.2.2.3 Controls on iceberg drift

The pattern of iceberg drift is controlled by fjord geometry, fjord and ocean circulation patterns (currents) and winds associated with storm tracks and Katabatic winds initiated from the influence of ice masses such as the Greenland Ice Sheet (e.g. Hjort 1979; Marienfeld 1991, 1992a,b; Hambrey 1994; Cowan et al. 1997). The icebergs calved from glaciers in eastern and north eastern Greenland that escape the fjord systems are transported to lower latitudes in the southward flowing East Greenland Current (e.g. Wadhams 1981). The drift of icebergs is influenced further by the bathymetry of the sea floor. Where the iceberg keel depth exceeds water depth grounding occurs, inhibiting further drift. At these sites iceberg sedimentation and turbation are more concentrated (Section 2.2.6.1). Iceberg drift is also controlled by the nature and extent of sea ice cover. Multi-year and winter shorefast sea ice (the former is known as sikussak in Greenland) strongly suppress the drift of icebergs, and commonly trap them close to the ice margin (e.g. Dowdeswell 1989; Syvitski et al. 1996; Dowdeswell et al. 1998). Only on the break up of this fast ice will icebergs be released (usually in pulses) to traverse the fjord system. Together with the free-drifting sea ice floes found within the fjords and across the shelf, icebergs are able to drift freely. The subsequent iceberg drift is controlled mainly by the prevailing current system due to their large submarine keels.

2.2.3 Sea-ice processes and sedimentation

2.2.3.1 Sea-ice formation and mechanisms of debris entrainment

Sea ice is an effective medium for the transportation of fine-grained debris originating mainly from shallow offshore regions in water depths <50 m (e.g. Pfirman et al. 1989, 1990; Nürnberg et al. 1994). Coarse debris is incorporated within sea ice mainly through the formation and floatation of anchor ice, where supercooled water is transferred to the sea bed and ice nucleation occurs around coarse sediment grains prior to floatation (Barnes et al. 1982; Osterkamp & Gosink 1984). Fine grained debris is incorporated within sea ice through the formation of frazil ice during freezing of turbid sea water. Water turbulence is induced mainly by autumn and winter season storms which act to resuspend fine, shallow sea bed sediments (Barnes et al. 1982; Osterkamp & Gosink 1984). Additional sediment can accumulate on the surface of sea ice from direct river flow (particularly onto shorefast ice prior to breakup), aeolian input mainly from katabatic winds blowing off the Greenland Ice Sheet and rockfalls from steep fjord walls (e.g. Dowdeswell 1987; Syvitski 1989; Gilbert 1990; Marienfeld 1991, 1992b; Cowan et al. 1997).

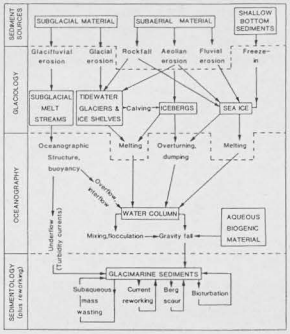

Figure 2.1. System diagram illustrating the sediment sources, processes and environments of deposition making up the complex glacimarine sedimentary environment (from Dowdeswell 1987).

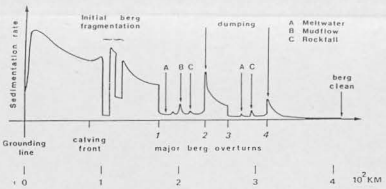

Figure 2.2. Hypothetical pattern of debris release for an iceberg calved from outlet glaciers or ice streams, and resulting sea-floor sedimentation rate. The effects of calving, overturning of icebergs and processes of meltwater, mudflow and rockfall activity are shown (from Drewry & Cooper 1981).

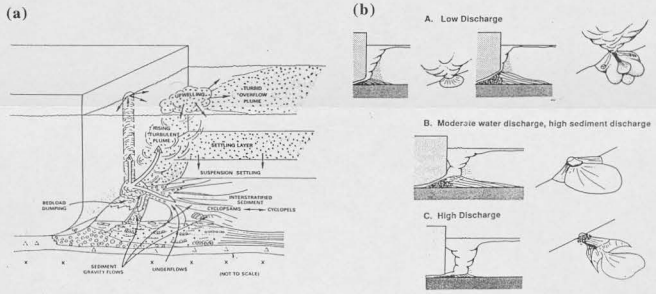

Figure 2.3. **(a)** Schematic diagram illustrating the subglacial discharge of meltwater and the development of a turbid surface (overflow) plume. Associated bedload and suspension settling (cyclopsams and cyclopels) sediments are shown (from Powell & Molnia 1989). **(b)** The variability of subglacial meltwater efflux in response to differences in water/sediment discharge. Associated sediment fan systems are shown (from Powell 1990). Although both (a) and (b) are examples from subglacial drainage they would also apply to glacifluvial/fluvial systems discharging into the marine environment.

2.2.3.2 Sea-ice sediment and sedimentation

The extent of debris-rich sea ice formation, and the subsequent pattern of drift, break up, dispersal and melting controls sea ice sedimentation (Dowdeswell 1987). The drift of sea ice is controlled by ocean currents and winds which act to disperse the entrained debris over wider areas. The melting of sea ice and, therefore, the flux of sediment to the modern-day sea floor is inhibited along the western margin of the Fram Strait due to the influence of the cold East Greenland Current exiting the Arctic Ocean (Hebbeln & Wefer 1991). As the cold East Greenland Current influences the East Greenland continental margin further south (inclusive of the study area), sea ice sediment flux to the sea floor may also be low (e.g. Hebbeln et al. 1998). If the summer ice margin transgresses the continental margin of East Greenland during summer seasons the associated break-up and melting of sea ice will result in the greater flux of sediment to the sea floor (e.g. Hebbeln & Wefer 1991; Hebbeln et al. 1998). Analysis of the sediment character of sea ice within the Eurasian sector of the Arctic Ocean shows that over 80% of sediment grains are finer than 63 μm i.e. silt and clay size (e.g. Pfirman et al. 1989, 1990; Nürnberg et al. 1994). The predominance of fine grained debris indicates that the formation of frazil ice and associated incorporation of resuspended debris in turbid shallow waters contributes the most significant supply of sediment to the sea ice canopy in the Arctic Ocean (cf. Kempema et al. 1989; Pfirman et al. 1989; Nürnberg et al. 1994). The fine grained nature of sea ice sediments is difficult to distinguish from that deposited from icebergs and meltwater outflows.

Within the fjords and on the continental shelf of East Greenland, the incorporation of debris in sea ice through ice floe contact with the sea bed, and anchor and frazil ice formation is restricted because water depths are very high immediately offshore (Dowdeswell et al. 1994a). Furthermore, sea ice sedimentation will only occur within localised regions of the fjords during summer break up, provided the autumn/winter ice cover had come into contact with fluviatile, deltaic, rock fall and/or aeolian sediments along the fjord margins (e.g. Syvitski 1989; Marienfeld 1991, 1992a). It is most likely that the majority of sea ice debris supplied to the East Greenland margin is derived from far-travelled sea ice originating on the extensive, shallow Eurasian Arctic continental shelf and transported in the Transpolar Drift System through the Fram Strait and south in the East Greenland Current (e.g. Pfirman et al. 1989; Berner & Wefer 1990; Hebbeln & Wefer 1991; Baumann et al. 1993; Nürnberg et al. 1994; Dowdeswell et al. 1998; Hebbeln et al. 1998).

2.2.3.3 Sea-ice formation and development of underflows

During winter sea ice formation across the Polar North Atlantic, particularly on the East Greenland shelf, brine is rejected during the freezing of marine waters producing a cold, dense water underflow (Dowdeswell et al. 1996, 1998). The underflows produced during this process commonly sink to and flow across the sea floor of the shelf and cascade down the continental slope (Midttum 1985; Dowdeswell et al. 1996, 1998). These dense underflows can entrain sediment grains, depending on a combination of the nature and grain size of the sea-floor sediment and velocity of the underflow (e.g. Parker 1982). Turbidity currents may be induced on the slope in association with these underflows (Dowdeswell et al. 1998). It is thought that the dense underflows are linked with a series

of large submarine channels within the abyssal Greenland Basin (Mienert et al. 1993, 1995; Dowdeswell et al. 1996, 1998), and fine silt and clay laminations on the Spitsbergen continental slope (Andersen et al. 1996).

2.2.4 Meltwater and fluvial systems and sedimentation

2.2.4.1 Introduction to melt and river waters

Meltwaters and rivers containing variable sediment concentrations in the form of suspension and bedload enter the marine environment within fjords from subglacial drainage below the water line at tidewater glacier margins, from subaerial glacier-fed rivers (glacifluvial origin) and melting of the snow pack on land and subaerial fluvial systems (e.g. Powell 1981, 1983, 1984, 1990; Elverhøi et al. 1983; Mackiewicz et al. 1984; Dowdeswell 1987; Syvitski et al. 1987; Syvitski 1989; Powell & Molnia 1989; Cowan & Powell 1990; Stewart 1991; Dowdeswell et al. 1994a,b; Cowan et al. 1997). Examples of sediment laden melt and river waters discharging into the Kejser Franz Josephs Fjord and tributary fjords system of the study area are shown in Figures 1.2 and 1.3a,b. Regardless of the subglacial, glacifluvial, snow melt or fluvial source, the sediment laden water will behave according to similar controlling parameters discussed in this section.

2.2.4.2 Dynamics of melt and river discharge

The inflowing water takes up a position within the water column, commonly at the surface, where it attains neutral buoyancy and spreads out laterally to form an overflow or turbid surface plume (Figs 1.3a,b, 2.3a) (e.g. Mackiewicz et al. 1984; Syvitski 1989; Powell 1990). The upwelling of the inflow results because fresh water is less dense than the normal-salinity sea water of the fjord. Underflows are uncommon events as suspended sediment concentrations in excess of 30 gl^{-1} are required and are rare occurrences (e.g. Mackiewicz et al. 1984; Dowdeswell 1987; Syvitski 1989; Dowdeswell et al. 1998). If buoyancy dominates the inflow, the surface turbid plume forms immediately on efflux (e.g. Syvitski 1989; Powell 1990). In contrast, if the inflow is dominated by momentum flux, particularly with subglacial discharge, the efflux behaves as a turbulent jet that will change to a plume when momentum forces are exceeded by buoyant forces (Powell 1990). The transition to a plume is driven by the entrainment of ambient marine waters and the loss of jet momentum (Powell 1990). Sediment and water discharge, subglacial tunnel/river channel size and buoyancy forces are additional factors that control the distance to which the jet efflux travels before buoyancy occurs (Fig 2.3b; Powell 1990).

2.2.4.3 Controls on the distribution and behaviour of turbid surface plumes

The discharge of melt and river water into marine settings is greatest during the summer melt season but can continue in limited amounts throughout the year (Dowdeswell 1987; Cowan & Powell 1990; Cowan et al. 1997). The melt and river waters possess variable discharge and suspended debris and bedload concentrations which show diurnal and seasonal fluctuations (Dowdeswell 1987). The

highest bedload and suspended sediment concentrations are associated with the high velocity, turbidity and carrying capacity and competence of peak discharges. Higher discharges are able to maintain sediment grains up to coarser grain sizes within suspension for longer periods and, therefore, to be transported to more distal locations (Fig 2.3b). The suspended sediment concentration, grain size and rates of sedimentation associated with the surface turbid plume decrease exponentially with distance from its efflux due to a decrease in plume turbidity, velocity, competence and carrying capacity (Powell 1981, 1984; Elverhøi et al. 1983; Mackiewicz et al. 1984; Dowdeswell 1987; Syvitski et al. 1987; Cowan et al. 1997). This relationship is controlled by the degree of dispersal and mixing between the plume and ambient sea water, and loss of plume momentum (e.g. Dowdeswell 1987; Syvitski et al. 1987; Powell 1990). The distribution and behaviour of turbid surface plumes is influenced by fluctuations in the location of effluxes, discharge, tidal state and the prevailing wind and currents (Fig 2.3b; e.g. Mackiewicz et al. 1984; Cowan & Powell 1990; Dowdeswell & Cromack 1991; Cowan et al. 1997).

2.2.4.4 Turbid surface plumes and sedimentation

Coarse grained tractional bedload will be deposited proximal to the discharge outlet, producing side entry fluvial and glacifluvial deltas and fans, and tidewater glacier fans (Fig 2.3b) (e.g. Powell 1981, 1983, 1984, 1990; Mackiewicz et al. 1984; Syvitski et al. 1987; Syvitski 1989; Powell & Molnia 1989; Syvitski & Hein 1991; Sexton et al. 1992). The finer grained, suspended sediment is transported within surface turbid plumes to offshore regions distal to the ice front and the fjord margins/ coastline (Figs 1.3a&b, 2.3a&b) (e.g. Elverhøi et al. 1983; Dowdeswell 1987; Syvitski 1989; Powell 1990; Stewart 1991). Sedimentation from the plumes is through the vertical settling of suspended sediment grains (Fig 2.3a).

The carrying capacity and competence of turbid surface plumes varies with annual, diurnal and seasonal fluctuations in discharge, that result in laminated sediment sequences/ facies (e.g. Powell 1981, 1984, 1990; Mackiewicz et al. 1984; Powell & Molnia 1989; Cowan & Powell 1990; Stewart 1991; Cowan et al. 1997). Furthermore, sedimentation from turbid surface plumes can also result in cyclic deposits termed cyclopels and cyclopsams, particularly in the ice-proximal zone, whose distribution can be controlled by the degree of interaction with diurnal tidal currents (Mackiewicz et al. 1984; Dowdeswell 1987; Cowan & Powell 1990; Powell 1990). In ice proximal and/or high energy settings, deposits consist of crudely-laminated coarse sand to silt arranged into couplets termed cyclopsams (Fig 2.3a). In increasingly ice-distal and/or low energy regions, deposits are more thinly laminated fine silt to clay arranged into couplets termed cyclopels (Fig 2.3a). During peak discharge at flood tide cyclopsams occur in ice-proximal locations, whereas peak discharge at ebb tide leads to thinner and more distal laminae (Mackiewicz et al. 1984). At peak discharges cyclopels are deposited in more distal locations from the ice margin beyond the cyclopsam zone, and at lower discharges cyclopels dominate ice-proximal regions.

The massive nature of some meltwater-related sediments results from either rapid sedimentation, limited grain size variation within turbid surface plumes (such as the fine grained

remnants of surface plumes in ice distal locations), and/or no discharge variations on surface plumes (e.g. Elverhøi et al. 1983; Mackiewicz et al. 1984; Cowan et al. 1997). The fine grained sediments found in increasingly ice-distal settings of the outer zone of the inner fjord to outer fjord and continental margin of East Greenland and Svalbard are thought to be related to the very low rate of sedimentation of fine grained sediment from the dispersed remnants of distal melt/river water plumes escaping the fjord system (e.g. Elverhøi et al. 1980, 1983; Elverhøi & Solheim 1983; Dowdeswell et al. 1994a,b).

The suspension settling of clay sized sediments is retarded but settling can be assisted by flocculation (e.g. Syvitski 1989 and Hambrey 1994). Flocculation is the aggregation of clay particles to form larger particles or floccules that settle out from the water column at a higher rate than for very fine clays according to Stoke's Law. Flocculation occurs due to the reduction of clay repulsive forces caused by a rise in temperature or a stronger concentration of electrolytes such as dissolved salts of sea water. Agglomeration (welding of grains by organic matter) and pelletization (ingestion of sedimentary particles by zooplankton and subsequent egestion as faecal pellets) are further processes enhancing the rate of clay sedimentation (e.g. Syvitski 1989; Hambrey 1994).

2.2.5 Biogenic sedimentation

Aqueous benthic and planktonic fauna contribute to sedimentation in glacimarine environments. The flora and fauna of polar seas include siliceous diatoms and radiolaria (biogenic opal), and calcareous nannofossils, molluscs, echinoids, sponges and foraminifera, which form only a small fraction of the total sediment (e.g. Hambrey 1994). The presence of organisms within the water column and on the sea floor, and the preservation of biogenic material, is controlled by the habitat of the surrounding environment (e.g. Drewry 1986; Dowdeswell 1987; Syvitski et al. 1987; Berner & Wefer 1990; Hebbeln & Wefer 1991; Baumann et al. 1993; Hambrey 1994; Nam et al. 1995; Nam 1996).

The most abundant fauna, and hence biogenic flux to sea-floor sediments, occur in environments influenced by upwelling nutrient-rich bottom-waters, low clastic sediment input, stable susbstrate (limited iceberg scouring and sediment mass wasting) and water column settings, warm and open marine hydrographic conditions and/or seasonal to low sea ice cover, predominantly in ice distal regions, such as the continental slope of East Greenland (e.g. Berner & Wefer 1990; Hebbeln & Wefer 1991; Hambrey 1994; Nam et al. 1995; Nam 1996; Dowdeswell et al. 1998). The presence of planktonic and benthic organisms is limited within environments such as the glacier-influenced fjords of East Greenland in response to high sedimentation rates, sea floor instability (iceberg scouring and sediment mass wasting), unfavourable hydrographic conditions (e.g. low salinity waters), and high suspended sediment concentration within the water column that acts to attenuate light needed for photosynthesis (e.g. Görlich et al. 1987; Marienfeld 1991, 1992b; Syvitski et al. 1996).

In the fjords and across the continental margin of East Greenland sea-ice coverage breaks up during the summer season, and in response, biogenic productivity is restricted in bottom and surface

waters. This is because sea ice restricts the supply of organic matter (nutrients) to the sea floor, which are needed to sustain benthic organisms, and the penetration of light needed for photosynthesis within light-dependent organisms within the photic zone (e.g. Berner & Wefer 1990; Hebbeln & Wefer 1991; Marienfeld 1991, 1992a; Williams 1993; Williams et al. 1995; Nam et al. 1995; Nam 1996). The high suspended sediment concentration within the water column of most fjords also results in the attenuation of light needed for photosynthesis (e.g. Görlich et al. 1987; Marienfeld 1992b).

On the East Greenland continental shelf, carbonate production and, hence, bioproductivity of calcareous organisms is restricted by the cold, polar surface water masses of the East Greenland Current. This accounts for the low carbonate content (<10 wt-%) of sediments deposited throughout the Late Weichselian and Holocene (Baumann et al. 1993; Nam et al. 1995; Nam 1996). Additionally, carbonate organisms settling out within the fjords and continental margin of East Greenland are subjected to strong carbonate dissolution and dilution resulting in low biogenic carbonate content (Hebbeln & Wefer 1991; Baumann et al. 1993; Nam et al. 1995; Nam 1996). Dissolution is driven mainly by CO_2 within bottom waters. The CO_2 content along East Greenland is derived from: (i) that dissolved within the very cold polar water masses of the East Greenland Current system, (ii) meltwater stratification and the much restricted oxygen ventilation of bottom waters, and (iii) the high terrestrial derived organic content, particularly of fjord sediments, which decomposes releasing CO_2 into bottom waters (Baumann et al. 1993; Nam et al. 1995; Nam 1996). Carbonate dilution results from the increased supply of terrestrial matter over biogenic material, particularly in the fjords and on the inner continental margin.

2.2.6 Small and large-scale subaqueous mass wasting processes

2.2.6.1 Introduction to subaqueous mass wasting processes

Subaqueous mass wasting processes (mass movements or mass flows) are common reworking agents of sediments within glacimarine environments (e.g. Powell 1981, 1984; Wright & Anderson 1982; Wright et al. 1983; Syvitski 1989; Syvitski & Hein 1991; Hein & Syvitski 1992; Sexton et al. 1992; Syvitski et al. 1996; Dowdeswell et al. 1996, 1997b). Mass wasting can be generated on slopes less than 1°. Mass wasting can operate on both small and large-scales depending upon the driving mechanisms. Downslope-driven sediment flows can be divided into slides, slumps and gravity flows (debris flows and turbidity currents). These processes may form a continuous spectrum according to the increasing amount of deformation undergone by the sediment during movement, where debris flows are an intermediate step between slides and slumps and the development of turbidity currents (Fig 2.4) (e.g. Hampton 1972; Middleton & Hampton 1976; Wright & Anderson 1982; Laberg & Vorren 1995, 1996; Dowdeswell et al. 1997b). The transition from slides/slumps to turbidity currents during a downslope flow event can be initiated by either an increase in flow turbulence due to velocity, water uptake and dilution of the flow, and/or turbulence at the head of the debris flow (Pickering et al. 1989).

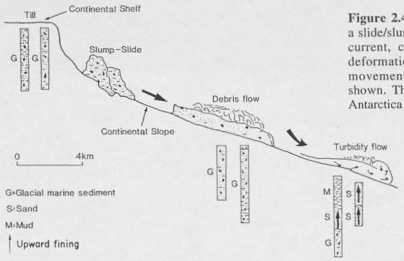

Figure 2.4. Model for the downslope transition of a slide/slump to a debris flow and finally a turbidity current, controlled by the increasing amount of deformation undergone by the sediment during movement. Corresponding core lithologies are shown. This is an example from the Weddell Sea, Antarctica (from Wright & Anderson 1982).

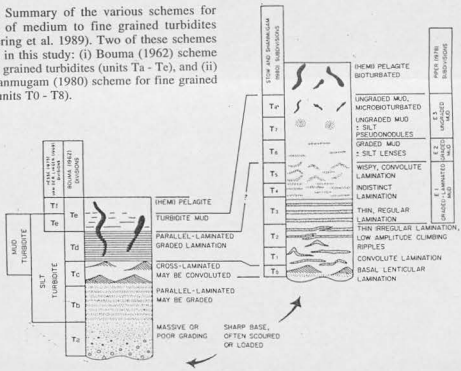

Figure 2.5. Summary of the various schemes for subdivision of medium to fine grained turbidites (from Pickering et al. 1989). Two of these schemes are adopted in this study: (i) Bouma (1962) scheme for medium grained turbidites (units Ta - Te), and (ii) Stow & Shanmugam (1980) scheme for fine grained turbidites (units T0 - T8).

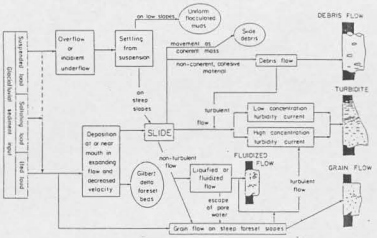

Figure 2.6. Conceptual model of meltwater sedimentation and associated dispersal of sediments by subaqueous mass wasting in Arctic fjord settings (from Gilbert 1983). Meltwaters are derived from subglacial drainage and glacifluvial systems.

2.2.6.2 Slides, slumps, debris flows and turbidity currents

The mechanical behaviour, transport, sediment support mechanisms and sedimentary characteristics for slides, slumps, debris flows and turbidity currents are summarised in Nardin et al. (1979), Pickering et al. (1989) and Stow (1992). The main mass wasting processes are outlined below:

Slides - Shear failure of the sediment mass along discrete shear planes with little internal deformation of the original sedimentary structure; beds are coherent during sliding.

Slumps - Shear failure of the sediment mass accompanied by rotation along discrete shear surfaces with little internal sediment disaggregation; deformation consists of folding, rotation and faulting of the original sedimentary structure.

Debris flows - Particle support during the flow comes from frictional resistance to settling by the fine grained matrix, matrix (clay) cohesion, buoyancy, elevated matrix pore pressure, and dispersive pressure. The larger clasts are supported by the finer matrix and interstitial waters. Flows can behave as either viscous fluids, where the shear is distributed throughout the sediment mass leading to total homogenisation of the internal sedimentary structure (Nardin et al. 1979), or as Bingham-type plastic flow where the flow moves as a rigid plug (the yield strength of the debris is not exceeded) over a basal shear zone without significant internal reorganisation of the sediment mass (e.g. Elverhøi et al. 1997). Sedimentation is normally by rapid, mass emplacement when the strength of the debris exceeds gravitational forces, total shear stress decreases, or as intergranular friction increases.

Turbidity currents - Particle support during the flow is provided by suspension, which is driven by upward directed fluid turbulence. Sediment grains settle out from suspension to produce graded beds. Several schemes have been constructed to represent the ideal bed sequences of the graded sub-divisions (fining upward sequence) within turbidites. The Bouma (1962) scheme is used for medium grained, low/medium concentration flows (Fig 2.5), but is too general for the deposits of low concentration turbidity currents transporting finer grained sediment. Therefore, several other schemes have been developed for fine grained turbidites, and the scheme of Stow & Shanmugam (1980), used in this thesis (Chapter 4), is shown in Figure 2.5. Complete bed sequences of all schemes are uncommon within turbidites but top-absent, base-absent, or middle-absent sequences are common.

Mass wasting are triggered through a number of processes (e.g. Powell 1984; Dowdeswell 1987; Syvitski 1989; Syvitski & Hein 1991; Laberg & Vorren 1995, 1996; Dowdeswell et al. 1996; Elverhøi et al. 1997) that include: (i) small tectonically induced earthquakes, (ii) build-up of excess pore pressure due to rapid sedimentation, (iii) oversteepening of the sediment pile, (iv) accumulation of sediment on unstable slopes or sea-floor, (v) iceberg and sea ice scouring, (vi) tidal and wave loading, and/or (vii) seepage of shallow gas.

2.2.6.3 Subaqeuous mass wasting within fjord settings

Mass wasting occurring in the fjords of SE Alaska and Arctic settings (e.g. East Greenland and Canada) is most prevalent during the Holocene and since the last deglaciation (e.g. Powell 1981, 1983, 1984; Syvitski 1989; Syvitski & Hein 1991; Hein & Syvitski 1992; Dowdeswell et al. 1994b; Syvitski et al. 1996). Figure 2.6 illustrates a conceptual model of mass wasting processes initiated from glacifluvial sediments delivered to an Arctic fjord setting. The ice-proximal regions, and steep sided sills and margins of fjords, are loci for the temporary and unstable storage of high volumes of sediment that rapidly accumulate following their delivery from the adjacent land mass via processes involving: (i) rain out and suspension settling under icebergs, sea ice and subglacial, glacifluvial and fluvial derived outflows and associated turbid surface plumes, (ii) prograding side entry fluvial and glacifluvial deltas and fans, (iii) subglacial-fed fans at tidewater glacier margins, and/or (iv) talus cones derived from subaerial rock falls (e.g. Powell 1981, 1983, 1984; Gilbert 1982, 1983; Syvitski et al. 1987; Syvitski 1989; Syvitski & Hein 1991; Hein & Syvitski 1992; Syvitski et al. 1996). The unstable sediment will be remobilised downslope from topographic highs and unstable sediment depocentres, and redeposited in more stable and deeper fjord basins, via slumps, slides, debris flows and turbidity currents. Subaqueous mass wasting at tidewater glacier margins is also prevalent in more outer fjord locations during glacial stillstands associated with fluctuations in the extent of ice since the Late Weichselian (e.g. Dowdeswell et al. 1994b).

2.2.6.4 Subaqeuous mass wasting on continental slope settings

Mass wasting processes were most prevalent on the East Greenland and other Arctic continental margins during the glacial periods of the Late Pleistocene, when significant volumes of glacier-derived sediment were delivered rapidly in response to increased glacial activity (e.g. Larberg & Vorren 1995, 1996; King et al. 1996; Dowdeswell et al. 1996, 1997b, 1998). Sediment is delivered to the shelf break/continental slope through either glacimarine processes (icebergs, meltwater, sea ice), or direct from fast-flowing outlet glaciers or ice streams. Major submarine fan systems were developed on the Norwegian and Greenland continental slopes in response to such processes, particularly in association with ice streams and fast-flowing outlet glaciers that terminated at or close to the shelf break (e.g. Larberg & Vorren 1995, 1996; Dowdeswell et al. 1996, 1997b, 1998).

One such glacier-fed fan system developed adjacent to Scoresby Sund, East Greenland (Dowdeswell et al. 1996, 1997b). This system was built up through the high and rapid flux of glacier-derived debris. Such sediment is delivered to the continental slope through: (i) deforming sediment layer below rapidly flowing ice channelised within a cross-shelf trough when the ice margin is located close to the shelf break, (ii) glacier-driven sediment-laden bottom currents transported to the the shelf break from an ice margin located towards the mouth of the cross shelf trough, and (iii) iceberg and meltwater processes when the ice margin was located close to the mouth of Scoresby Sund (Alley et al. 1989; Dowdeswell et al. 1996, 1997b). These sediments subsequently underwent successive downslope mass wasting, with debris flow activity on the upper slope and turbidity current activity further down the slope beyond the fan system, where the former provide the main components in the

long-term development of the fan system (Dowdeswell et al. 1996, 1997b). Debris flow activity is confined mainly to the southern two thirds of the Scoresby Sund fan system, indicating the importance of the southerly cross shelf trough, and also the delivery of debris-rich icebergs from full glacial ice masses in the southward flowing East Greenland Current (Dowdeswell et al. 1997b).

The East Greenland continental slope north of 72°N was relatively sediment starved during the Late Weichselian, because the maximum ice sheet margins terminated on the inner shelf (Hjort 1979; Funder 1989; Funder & Hansen 1996) and, subsequently, no submarine fan/channelised systems were developed (Mienert et al. 1993, 1995; Dowdeswell et al. 1996, 1997b). However, localised, smaller-scale resedimentation events are expected to occur along this region of the continental slope, including the study area as this thesis will show, in response to the rapid accumulation of significant volumes of glacimarine-derived sediments (Dowdeswell et al. 1996, 1997b).

2.2.7 Other reworking processes

2.2.7.1 Iceberg and sea ice scouring

Ice scouring occurs when iceberg or sea ice keels come into contact with sea floor sediments (Dowdeswell 1987). The distribution of scouring is controlled by (i) ice volume and dimensions, (ii) ice drift tracks, velocity and drag, (iii) sediment geotechnical properties, and (iv) depth and configuration of the sea floor (e.g. Drewry 1986; Dowdeswell 1987; Dowdeswell et al. 1993). The strength and integrity of ice keels, together with ice forces, must be greater than the resistance to ploughing by sediment in order to sustain ploughing (e.g. Kovacs & Mellor 1974). Ice ceases to move or becomes grounded when the resistance met at the sea floor by the keel becomes greater than the forces moving the ice (e.g. Rearic et al. 1990). Scour marks formed during this process result commonly in a paired tough-crest morphology (e.g. Syvitski et al. 1987; Dowdeswell et al. 1993, 1997a).

The scouring associated with sea ice keels and pressure ridges is restricted to shallower regions along the fjord margins, within embayments and on the continental shelf, because sea ice keels only reach maximum depths of ca. 30 m (e.g. Drewry 1986; Dowdeswell 1987; Hambrey 1994). Therefore, the majority of sea floor scours in deeper water result from icebergs, as their keels can commonly reach much larger dimensions (e.g. Dowdeswell et al. 1992, 1993). The intensity of scouring is inversely proportional to water depth where shallower regions are affected most by iceberg scouring (Dowdeswell et al. 1993). The scouring associated with icebergs commonly leads to turbation or reworking of sea floor sediments (e.g. Dowdeswell et al. 1993). In highly scoured regions, sea floor sediments tend to be totally turbated and the original sediment structure is destroyed. In regions of lower intensity scouring, the sediment structure is partially preserved (e.g. Dowdeswell et al. 1993).

The outer region of the Scoresby Sund fjord system, and the continental shelf of East Greenland, are subject to iceberg scouring (Marienfeld 1991, 1992a,b; Mienert et al. 1992;

Dowdeswell et al. 1992, 1993, 1997a). Iceberg keels are known to reach maximum depths of 550 m within Scoresby Sund (Dowdeswell et al. 1992). Icebergs that escape the fjord systems impinge on the continental shelf, but this influence diminishes to zero once the deeper waters of the continental slope are reached. Not only are the continental shelf regions adjacent to the iceberg producing fjord systems influenced by scouring, but those adjacent to non producing fjords can also be affected by icebergs transported south in the East Greenland Current (Dowdeswell et al. 1993). The iceberg scours have ages that range as far back as the Late Weichselian.

2.2.7.2 Bioturbation

The action of bottom-sediment mixing through the activity of benthic organisms will tend to homogenise the sediment column, and primary sedimentary structures such as bedding will become totally or partially destroyed (e.g. Drewry 1986; Dowdeswell 1987; Hambrey 1994). Bioturbation is indicated by the presence of mottling and burrow structures in core sediments. However, some polychaete burrows called *Chondrites*, do not completely bioturbate the sediment but leave characteristic fine networks of tiny burrows in an otherwise unreworked sediment sequence (Gorsline 1985). Bioturbation is most marked within (i) stable ecological settings that allow rich benthic habitats to develop, such as in the outer fjord and open-marine region of the continental slope or settings distal to sediment sources controlled by optimum conditions of temperature, salinity, water depth and sedimentation rate, and (ii) debris that has accumulated at low sedimentation rates, particularly distal to glacial/river sediment sources (e.g. Gilbert 1982; Drewry 1986; Dowdeswell 1987; Cowan & Powell 1990; Cowan et al. 1997).

2.2.7.3 Current activity

Bottom currents redistribute the finer fraction of non-cohesive glacimarine sediments at critical flow velocities, either leaving behind a lag deposit of mainly gravel/sand, or removing fine grained sediment units (e.g. Berner & Wefer 1990; Mienert et al. 1992; Baumann et al. 1993; Nam 1996; Cadman 1996). Major sedimentary structures such as sand waves/drifts and mega ripples are common in cases of strong currents (e.g. Damuth 1978; Hambrey 1994). Where bottom currents (also termed contour currents) flow parallel to the bathymetric contours of the continental margin, deposits termed contourites may result (e.g. Stow & Lovell 1979; Stow & Holbrook 1984; Stow 1979, 1992).

Bottom currents influence sea floor sediments over shallow banks, fjord sills, and the continental shelf and upper slope of eastern Greenland and western Svalbard (e.g. Funder & Larsen 1989; Marienfeld 1991, 1992b; Mienert et al. 1992; Nam 1996; Cadman 1996). Bottom current activity across the East Greenland continental margin is associated with the East Greenland Current system, particularly in exposed and relatively shallow regions, where the fine grained component of bottom sediments is winnowed to produce sand/gravel enriched lag deposits or hiati i.e. total removal of sediment (Funder & Larsen 1989; Berner & Wefer 1990; Mienert et al. 1992; Baumann et al. 1993; Nam 1996). Current winnowing has been documented to reach depths of 1000 m on the East

Greenland slope adjacent to Kangerdlugssuaq Fjord in relation to the Denmark Strait Overflow (Mienert et al. 1992). The East Greenland Current intrudes into both the Kejser Franz Josephs Fjord and other fjord systems of East Greenland, to depths greater than 300 m (Vogt et al. 1995) and, therefore, probably acts as a major agent actively reworking shallow bank and/or sill bottom sediments. The finer grained sediments winnowed by currents, both in the fjords and on the continental margin, are removed and settle out within deeper basins and/or troughs sheltered from current activity (e.g. Marienfeld 1991, 1992b; Mienert et al. 1992; Cadman 1996). Equally, sediments of basin/trough regions are protected from bottom current activity, and fine grained sediments form a major component of bottom sediment facies (e.g. Mienert et al. 1992).

2.3 EXTENT OF THE GREENLAND ICE SHEET IN EASTERN GREENLAND DURING THE LATE WEICHSELIAN AND HOLOCENE

2.3.1 Introduction

In general, the reconstructed Late Weichselian and Holocene dimensions of the Greenland Ice Sheet and associated glaciers in Eastern Greenland are not well constrained due to limited terrestrial and marine-based geological and geophysical evidence (Section 1.4). However, Late Weichselian and Holocene ice limits have been reconstructed for the East Greenland region based on the terrestrial and marine-based evidence available and, in particular, are reasonably well constrained in the Scoresby Sund region (Fig. 1.1) where recent investigations have been concentrated (cf. Funder 1972a,b; Funder & Hjort 1973; Hjort 1979, 1981; Funder 1989; Marienfeld 1991, 1992a,b; Mienert et al. 1992; Dowdeswell et al. 1994a,b; Lysså & Landvik 1994; Mangerud & Funder 1994; Funder et al. 1994; Hansen et al. 1994; Israelson et al. 1994; Landvik et al. 1994; Ingólfsson et al. 1994; Tveranger et al. 1994; Hubberten et al. 1995; Funder & Hansen 1996). The evidence outlined in these sources has been compiled into a map by Funder & Hansen (1996) showing the reconstructed ice limits and glacial coverage associated with the Last Glacial Maximum (16-21,000 yr BP) and, at 10,000 yr BP for the culmination of the Younger Dryas event (Fig. 2.7).

2.3.2 The Late Weichselian glaciation

The onset of glaciation along the eastern margin of Greenland is only poorly constrained and very little is known about the timing and nature of the onset and early phase of glaciation. The onset of glaciation and the associated eastward advance of the glaciers of the Greenland Ice Sheet started between 25,000 and 28,000 yr BP in response to cooling air temperatures, and culminated during the glacial maximum of the Late Weichselian (Last Glacial Maximum) ca. 15,000-21,000 yr BP (e.g. Dansgaard et al. 1993; Nam et al. 1995; Nam 1996; Stein et al. 1996; Funder & Hansen 1996).

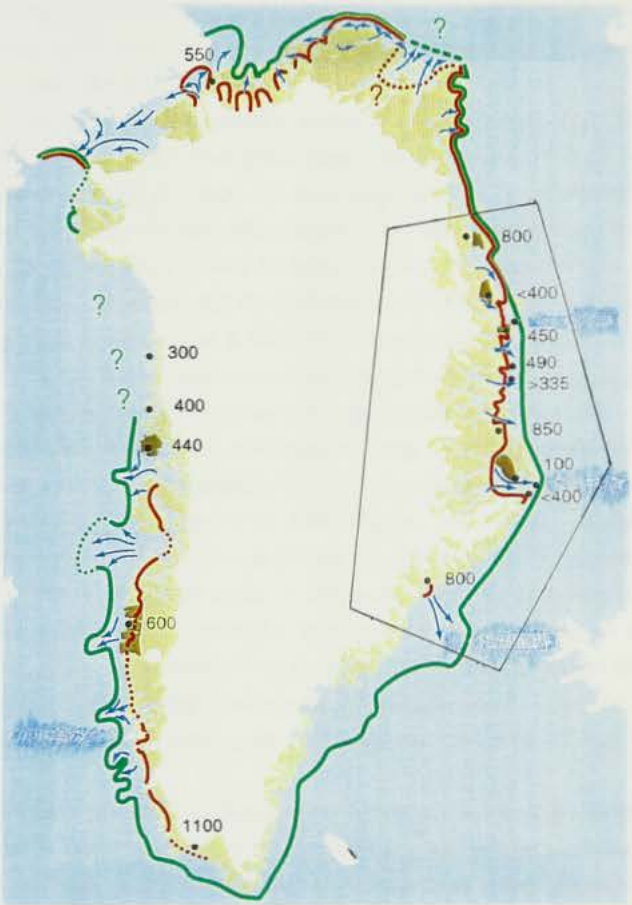

Figure 2.7. Reconstructed ice margins in Greenland for the Last Glacial Maximum between 16-21,000 yr BP (LGM; green) and at 10 ka (red). Brown areas are major ice free areas and numbers are ice surface altitudes during LGM. The East Greenland region is indicated. From Funder & Hansen (1996).

Nam et al. (1995) and Nam (1996) has shown that the timing of the culmination of the LGM can vary in East Greenland. The culmination of the LGM dates at ca. 16,000 yr BP on the continental slope adjacent to Scoresby Sund, and at ca. 15,000 yr BP on the East Greenland continental slope bordering the Denmark Strait and adjacent to Carlsberg Fjord. The LGM is reflected in the increased amounts of iceberg rafted debris and flux of terrigenous sediments on the continental slope (e.g. Nam et al. 1995; Nam 1996; Stein et al. 1996).

Pulses of iceberg rafted debris centred around 29,000, 27-26,000, 23-22,000, 21-20,000, 18-17,000 and 16,000 yr BP on the continental slope between 70 and 75°N are suggested to have resulted from iceberg discharge events on short-term intervals of 1,000-3,000 years, possibly reflecting the repeated, short term and rapid collapse of the Greenland Ice Sheet (Nam 1996; Stein et al. 1996). The frequency of major iceberg discharge, and hence ice sheet collapse, is proposed to be more frequent than those associated with the 5-10,000 year Heinrich events in the North Atlantic (e.g. Heinrich 1988; Bond et al. 1992; Bond & Lotti 1995; Dowdeswell et al. 1995).

The East Greenland coast shows two distinct regions where the nature of glaciation contrasts strongly: south of 68°N the inland ice of the Greenland Ice Sheet expanded a significant distance out onto the continental shelf, reaching the shelf break in some cases; and north of 68°N outlet glaciers occupied the fjords but left adjacent uplands free of ice, and terminated at the mouths of fjords or on the inner shelf (Figs 2.7, 2.8; Hjort 1979, 1981; Funder 1989; Funder & Hansen 1996). It is suggested that this pattern reflects the present day accumulation on the ice sheet (Section 1.2.7; Ohmura & Reeh 1991) where the north is influenced by a dry and cold climate with little accumulation and melting, and the south by more oceanic climate and higher accumulation (e.g. Funder & Hansen 1996). Furthermore, the Greenland and Iceland ice sheets formed a barrier to cyclones tracking northwards through the Denmark Strait, and most of the moisture is precipitated on the southern part of the ice sheet leaving the north relatively starved of moisture (Funder & Hansen 1996).

The glacial limit and ice cover associated with the Late Weichselian glacial maximum is well constrained in the Scoresby Sund region through terrestrial and marine geological and geophysical evidence. During the Late Weichselian glaciation (or Flakkerhuk Stade) grounded outlet glacier ice of the Greenland Ice Sheet advanced to a maximum extent at the fjord mouth, producing the Kap Brewster sedimentary ridge or end moraine (Figs 2.7, 2.8; Dowdeswell et al. 1994b). A high ice-rafted debris content and terrigenous sediment flux is dated to between ca. 15,000 and 19,000 yr BP on the adjacent continental slope (Stein et al. 1993; Nam et al. 1995), and is thought to relate to the proximity of the glacier front at the mouth of the fjord (Nam et al. 1995; Nam 1996). This indicates the probable age for the moraine (Dowdeswell et al. 1994b) but can be extended to 21,000 yr BP in light of more recent work (Nam 1996; Stein et al. 1996). The grounded glacier filling Scoresby Sund was thin, about 400 m thick at the fjord mouth, and covered the northern coastal region of Scoresby Sund up to 200 m a.s.l., depositing glacial till and glaciofluvial sediments along the coast of Jameson Land (Lysså & Landvik 1994; Hansen et al. 1994; Landvik et al. 1994; Ingólfsson et al. 1994; Tveranger et al. 1994; Mangerud & Funder 1994; Funder et al. 1994).

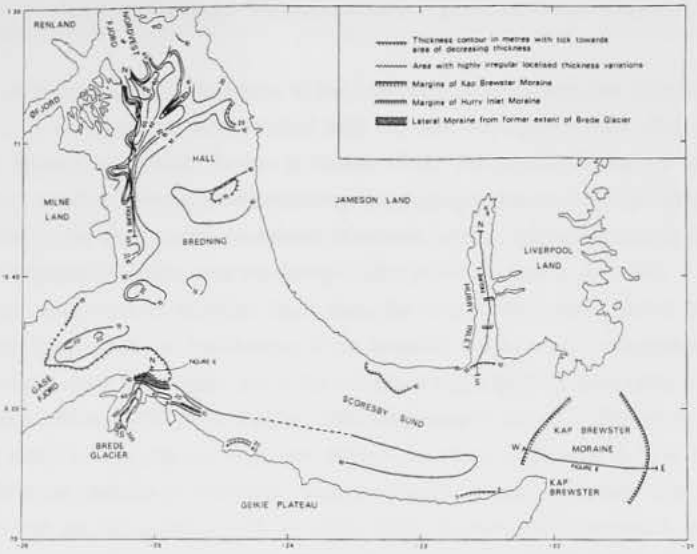

Figure 2.8. Isopach map of unlithified Quaternary sediment thickness in Scoresby Sund and Hall Bredning. The map shows (i) the Kap Brewster Moraine at the mouth of Scoresby Sund marking the seaward advance of glacier-ice during the Late Weichselian glaciation, and (ii) a major depocentre at the head of Hall Bredning representing ice-proximal sediments deposited from a glacier margin during the Younger Dryas or Milne Land Stadial in East Greenland (10,000 yr BP). From Dowdeswell et al. (1994b).

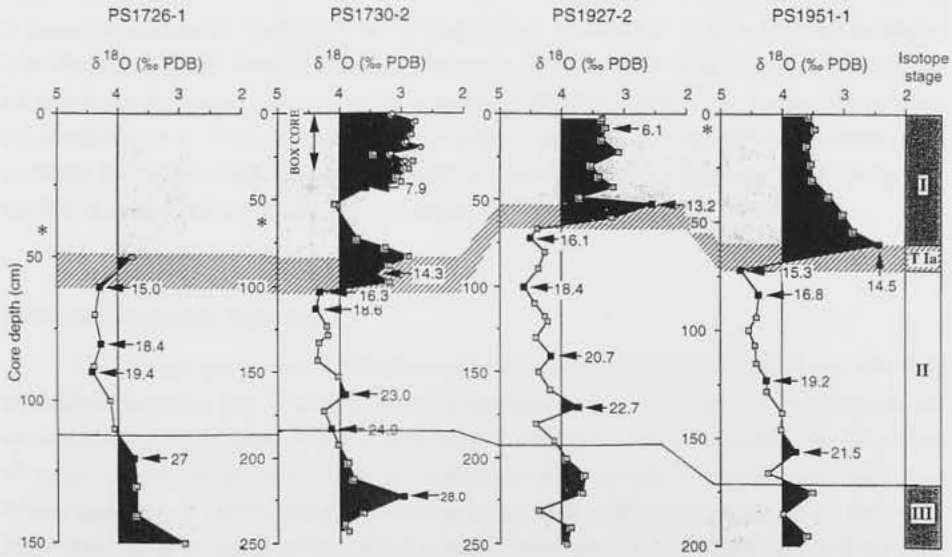

Figure 2.9. Oxygen isotope stratigraphy for the last 30,000 years measured on the planktonic foraminifera *N. pachyderma* sin. The light oxygen isotope signal indicative of a major meltwater pulse associated with the first stages of deglaciation during the Late Weichselian is shown, with its earliest onset dated at ca. 15,800 yr BP and culmination at ca. 13,200 yr BP. AMS ^{14}C ages (kyr) are indicated. Asterisks mark the Vedde ash layer, which is dated at 10,600 yr BP. From Nam (1996).

The ice margin at the culmination of the Late Weichselian glaciation along East Greenland south of 68°N is interpreted to have reached well out onto the adjacent shelf (Fig 2.7; Funder & Larsen 1989; Mienert et al. 1992; Funder & Hansen 1996). The position of the ice margin is based on bathymetric mapping showing push/grounding line moraines and ice-marginal sediments (Funder & Larsen 1989), and from overconsolidated diamicton within sediment cores interpreted to be indicative of subglacial till deposition pre-dating 15,000 yr BP (Mienert et al. 1992).

The ice limit north of Scoresby Sund along the coast of East Greenland is not constrained with any great certainty due to the absence of ice marginal features such as moraines and outwash sediments on land, along the margins and at the mouths of major fjord systems and/or on the adjacent continental shelf (Hjort 1979, 1981; Funder 1989; Hubberten et al. 1995; Funder & Hansen 1996; Jokat unpub data). Instead, the ice limits are derived mainly by extrapolation from ice thicknesses ascertained from the altitudes of weathering limits on coastal mountains, together with the upper limit of till cover and glacial striations (Hjort 1979, 1981; Funder 1989; Funder & Hansen 1996). Therefore, the ice limits reconstructed in this region of East Greenland are not well fixed and are generally considered as minima (Funder & Hansen 1996). Based on available evidence on land, and even with the absence of morainic and ice proximal features on seismic profiles, the glacial maximum ice limit of the Late Weichselian is thought to have extended at least onto the inner continental shelf adjacent to the mouths of Kejser Franz Josephs Fjord, Hochstetter Bugten and Kong Oscars Fjord, but probably not much further (Fig 2.7; Hjort 1979, 1981; Funder 1989; Funder & Hansen 1996). Overconsolidated diamicton, interpreted to represent subglacial till, in the mid region of Hochstetter Bugten and on the adjacent inner shelf at 75°N (Fig 1.1) supports the interpretation of an extension of glacier ice towards the continental shelf during the Late Weichselian (Stein et al. 1993; Hubberten et al. 1995). A morainal feature is present at the mouth of Kong Oscars Fjord, possibly indicating the ice limit at the last glacial maximum of the Late Weichselian but further work is needed to ascertain this (Hubberten et al. 1995). Altitudes of the ice surface during the Last Glacial Maximum have been estimated for the East Greenland margin north of Scoresby Sund and generally vary between 335 and 490 m close to the ice margin (Fig 2.7; Funder 1989; Funder & Hansen 1996).

2.3.3 Late Weichselian deglaciation

The timing, nature and mechanisms of deglaciation in East Greenland are not fully constrained due to the lack of geological and geophysical evidence on land or from the fjords and continental margin. The onset of deglaciation of the Greenland Ice Sheet is dated by the occurrence of a light oxygen isotope signal from the continental slope adjacent to the Scoresby Sund fjord system, beginning ca. 15,800 yr BP and culminating at 13,200 yr BP (Fig 2.9; Nam et al. 1995; Nam 1996). This signal is indicative of a major meltwater pulse thought to be associated with the early disintegration and retreat of the ice sheet and associated glaciers from their maximum extent (Nam et al. 1995; Nam 1996). The timing of the onset of this event may differ along other margins of the ice sheet in East Greenland, as indicated by a younger meltwater signal beginning at 15,300 yr BP from

the East Greenland margin bordering the Denmark Strait south of Scoresby Sund (Fig 2.9; Nam 1996). Meltwater pulses associated with deglaciation around this time are commonly referred to as Termination Ia (e.g. Zahn et al. 1985; Jansen & Veum 1990; Sarnthein et al. 1992; Nam 1996). This signal is several hundred years earlier than the deglaciation signal in the Fram Strait beginning at ca. 15,000 yr BP which relates to the disintegration of the Barents Sea ice sheet (Fig 2.10; Jones & Keigwin 1988).

In general, the onset of deglaciation of ice sheets in other regions bordering the GIN Sea indicated from light oxygen meltwater signals are not synchronous, but are dated between about 15,000 and 13,000 yr BP (Fig 2.10; e.g. Jones & Keigwin 1988; Lehman et al. 1991; Sarnthein et al. 1992; Koc & Jansen 1994; Elverhøi et al. 1995; Hald et al. 1996; Dokken et al. 1996; Hebbeln et al. 1998). Similarly, a major influx of meltwater to the North Atlantic is documented to have occurred between ca. 13,000 and 16,000 yr BP (Ruddiman & MacIntyre 1981). Even though the meltwater signal in East Greenland culminated at 13,200 yr BP (Nam 1996), it may not indicate the end of deglaciation, as this age corresponds closely to the culmination of early deglaciation along the western Svalbard margin after which sediment sequences suggest the continuation of deglaciation and glacier-ice recession with only the occasional corresponding presence of a light oxygen isotope signal (e.g. Jones & Keigwin 1988; Svendsen et al. 1992, 1996; Weinelt 1993; Elverhøi et al. 1995; Dokken et al. 1996; Hebbeln et al. 1998).

Following about 15,300-15,800 yr BP, ice retreated fjordwards and stabilised at topographically favourable positions between around 10,000 to 11,000 yr BP in response to renewed cooling associated with the Younger Dryas or Milne Land Stadial in East Greenland (Funder & Hjort 1973; Hjort 1979, 1981; Funder 1972, 1989; Marienfeld 1991, 1992b; Dowdeswell et al. 1994b; Funder & Hansen 1996). The Younger Dryas (Milne Land Stadial) ice limit at around ca. 10,000 yr BP is well constrained in East Greenland based on ice proximal deposits, moraines, and kame terraces that are in some cases dated (e.g. Funder 1972, 1978; Hjort 1979, 1981; Funder 1989; Dowdeswell et al. 1994b). No evidence is present in East Greenland for the readvance of glaciers associated with the Younger Dryas, suggesting that the climate was too cold and dry for ice growth. This may have possibly been in response to the migration of the Arctic anticyclone over the East Greenland region at this time (Lamb & Woodroffe 1970; Hjort 1979; Funder & Hansen 1996).

It is suggested that the principal mechanism of ice retreat up to 11,000 yr BP in East Greenland was through iceberg calving coincident with, and driven by, a rise in global sea level during this time (Fig 2.13; Fairbanks 1989; Funder & Hansen 1996). Similarly, this mechanism has been invoked for the initial break up of the Barents Sea ice sheet prior to 13,000 yr BP, reflected in the deposition of large amounts of ice-rafted debris on the continental slope west of Svalbard (e.g. Jones & Keigwin 1988; Elverhøi et al. 1995; Andersen et al. 1996; Dokken et al. 1996). Following 13,000 yr BP, melting and iceberg calving have been invoked for ice retreat in Svalbard (e.g. Elverhøi et al. 1995; Andersen et al. 1996; Dokken et al. 1996), and this may also apply to East Greenland.

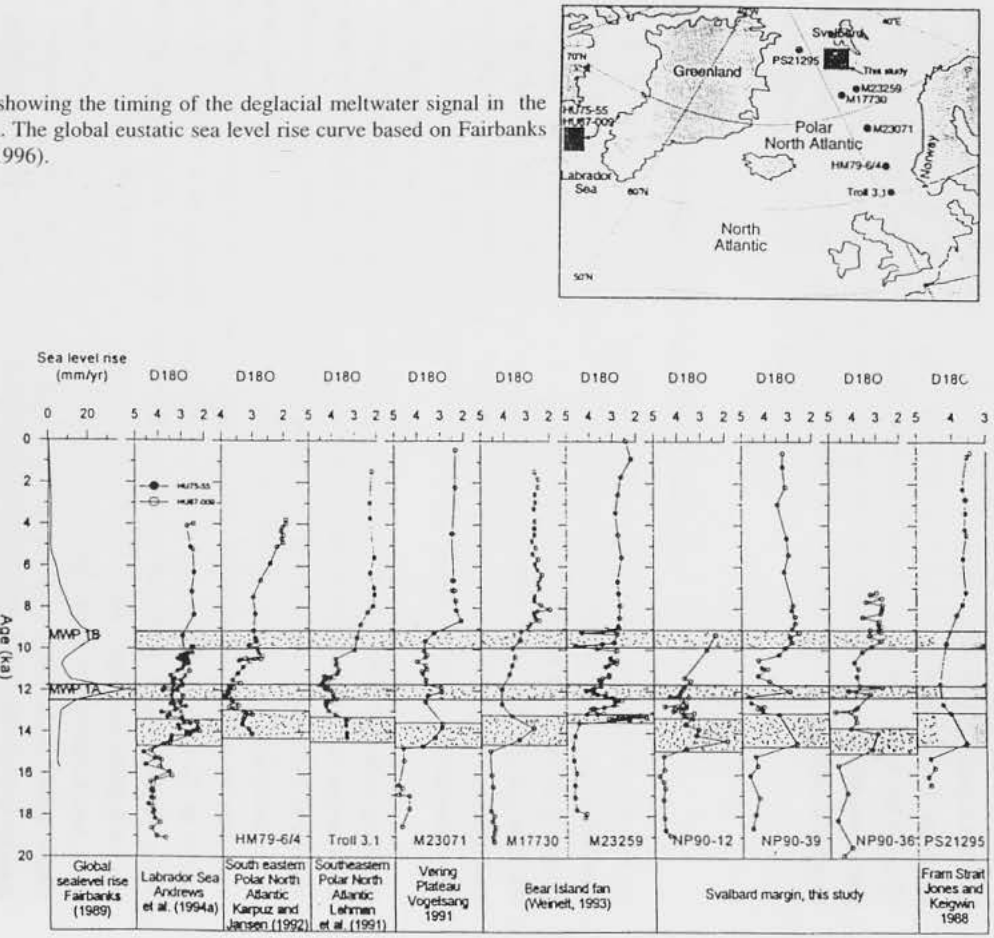

Figure 2.10. Oxygen isotope records showing the timing of the deglacial meltwater signal in the Polar North Atlantic and Labrador Sea. The global eustatic sea level rise curve based on Fairbanks (1989) is shown. From Dokken et al. (1996).

Low resolution sedimentary records from the East Greenland continental margin, coupled with the absence of records from the continental shelf, corresponding to this time are inconclusive in support of the nature and mechanism of ice retreat. However, increased amounts of IRD are documented for the deglaciation period prior to 13,000 yr BP from the continental slope adjacent to Scoresby Sund and further south bordering the Denmark Strait (Nam et al. 1995; Nam 1996; Stein et al. 1996). Increased amounts of IRD also occur on the continental slope adjacent to the Carlsberg/ Kong Oscars Fjords during the period up to the Younger Dryas (Nam 1996). Coarse diamicton containing large amounts of IRD pre-dating the Younger Dryas is also present within the Scoresby Sund fjord system (Marienfeld 1991; Dowdeswell et al. 1994a,b). These observations support iceberg calving, rather than melting, as a mechanism driving glacier-ice recession during deglaciation between the Late Weichselian glaciation and the Younger Dryas.

2.3.4 Younger Dryas or Milne Land Stadial in East Greenland

The Younger Dryas ice limit at 10,000 yr BP in the fjords to the north of Scoresby Sund is positioned in the outer region of Kong Oscars and Kejser Franz Josephs Fjords and in the inner region of Hochstetter Bugten (Figs 1.1, 2.7; e.g. Hjort 1979, 1981; Funder 1989; Funder & Hansen 1996). The retreat of glacier ice from its Late Weichselian maximum extent on the inner continental shelf into the outer fjords shows that the retreat was not as extensive as that in the Scoresby Sund region (Fig 2.7; Funder 1989; Funder & Hansen 1996). The timing, nature and mechanism of this retreat of glacier ice is not well constrained.

In the Scoresby Sund region the Younger Dryas ice limit at about 10,000 yr BP is positioned at the head of Hall Bredning, marked by the presence of a major sediment depocentre interpreted to represent ice-proximal deposits from a glacier margin, and by dated moraine systems at adjacent locations onshore (Figs 2.8, 2.11; Funder & Hjort 1973; Funder 1972, 1978; Dowdeswell et al. 1994b). The glacier ice in Scoresby Sund is inferred to have either retreated through the outer fjord region to the mouths of the inner fjords adjoining Hall Bredning by around 10,000 yr BP, or to have remained grounded within the outer fjord system until an abrupt retreat at about 10,000 yr BP (Björck et al. 1994; Dowdeswell et al. 1994b). Lake evidence on land suggests Scoresby Sund and the coastal zone of Jameson Land may have been covered by ice during this period (Björck et al. 1994). However, the presence of diamictons pre-dating Younger Dryas sediments at around 10,000 yr BP within the outer fjord, interpreted to be deposited through iceberg rafting, indicate that ice must have retreated from the outer fjord system during the period since 15,800 yr BP (Marienfeld 1991, 1992b; Dowdeswell et al. 1994b).

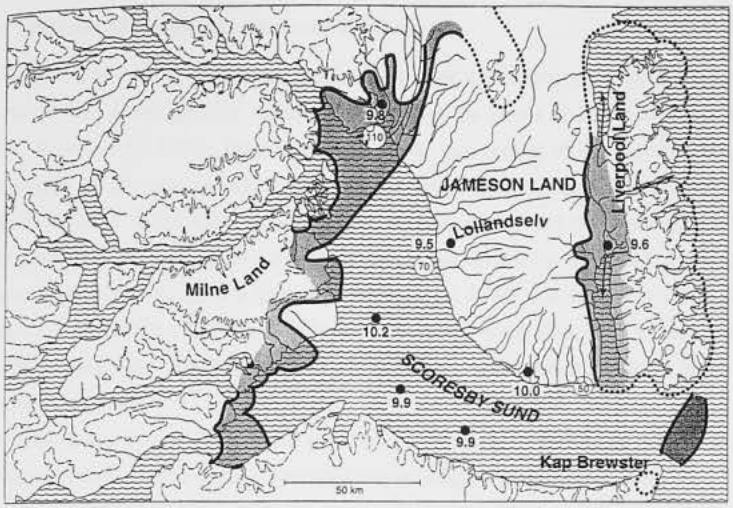

Figure 2.11. Map of the Scoresby Sund region showing (i) a dark zone representing the Kap Brewster moraine at the mouth of Scoresby Sund marking the seaward advance of glacier-ice during the Late Weichselian glaciation (dark zone), (ii) a light grey zone marking the Younger Dryas or Milne Land Stadial moraines (9,500 - 10,000 yr BP). ^{14}C ages (kyr) associated with deglaciation are indicated in bold, and the circled numbers are altitudes of marine limits (m a.s.l.). From Funder & Hansen (1996).

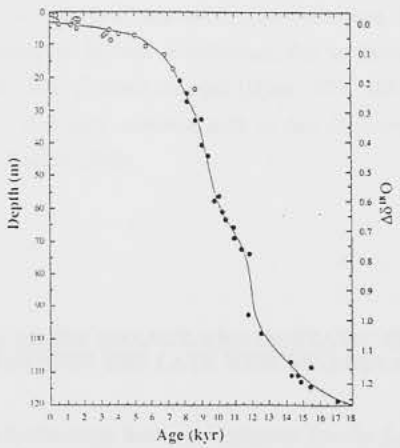

Figure 2.12. The global eustatic sea level curve for the last 18,000 years. From Fairbanks (1989).

2.3.5 Post Younger Dryas deglaciation and Holocene

During the Holocene, following immediately after the Younger Dryas or Milne Land Stadial at ca. 10,000 yr BP, outlet glaciers retreated further into the fjords of East Greenland (Funder 1972, 1978, 1989; Hjort 1979, 1981). Dated moraines show that retreat of ice into the inner fjords may even have began as recently as 9,500 yr BP in the Scoresby Sund and Hochstetter Bugten region (Funder & Hjort 1973; Hjort 1981; Funder 1989). It is suggested that the principal mechanism of ice retreat occurred through both iceberg calving and melting driven by increased Northern Hemisphere summer insolation, which reached a maximum between ca. 8,000 and 10,000 yr BP (COHMAP 1988; Koc & Jansen 1994; Funder & Hansen 1996). The iceberg rafted diamicton immediately post dating 10,000 yr BP in Scoresby Sund (Marienfeld 1991, 1992b; Dowdeswell 1994a,b), supports ice retreat through iceberg calving.

In Hochstetter Bugten, proglacial sediments, consisting of meltwater-derived laminated muds and occasional iceberg rafted debris, directly overlie subglacial till (Stein et al. 1993) within a core positioned close to the 10,000 yr BP ice margin (Hjort 1981; Funder & Hansen 1996). Even though there are no radiocarbon dates from above or within the proglacial sediments, the proximity of the core to the 10,000 yr BP ice margin supports sedimentation during post-10,000 yr BP deglaciation, and ice retreat driven by melting. Meltwater signals associated with the retreat of ice following the Younger Dryas (Termination Ib) are not documented in the oxygen or carbon isotope records from the East Greenland continental slope (e.g. Nam et al. 1995; Nam 1996; Stein et al. 1996). The presence of kame terraces and lateral and terminal moraines within the fjords can be used to date the retreat of glaciers through the fjord. Evidence from the Scoresby Sund region shows that the ice retreated to its present position by ca. 7,000 yr BP (Funder 1978, 1989; Funder & Hansen 1996), which probably also applies to other fjord regions in East Greenland. The retreat of ice varied in rate and was commonly interrupted by periods of stillstand, due to interactions of the glacier with the underlying topography rather than climatic changes (Hjort 1979, 1981; Funder 1978, 1989). During this period, readvance of ice may have occurred such as that occurring just after 9,500 yr BP in the Scoresby Sund region (e.g. Funder 1989).

2.4 RELATIVE SEA LEVEL CHANGE AND ISOSTATIC EMERGENCE IN EAST GREENLAND DURING THE LATE WEICHSELIAN AND HOLOCENE

Global eustatic sea levels have been reconstructed for the Late Weichselian and Holocene from dated coral reef terraces (Fig 2.12; Fairbanks 1989). Global sea level was at its lowest, approximately 121 m below present sea level, during the Last Glacial Maximum centred around 18,000 yr BP (Fig 2.12; Fairbanks 1989). Between 17,100 and 12,500 yr BP sea level rose by around 20 m (Fig 2.12; Fairbanks 1989). At around 12,000 yr BP global sea level rose rapidly by about 24 m in under 1,000 years, correlating to Meltwater Pulse 1A (equating to the latter part of Termination

ı; Fig 2.12; Fairbanks 1989). The rate of sea level rise reached a minimum between 10,500 and 1,000 yr BP, corresponding to the first half of the Younger Dryas, but the rate of sea level rose etween 10,000 and 10,500 yr BP in the latter part of the Younger Dryas (Fig 2.12; Fairbanks 1989). he rise in sea level culminated around 9,500 yr BP with a rapid rise of about 28 m correlating to eltwater pulse IB (Termination Ib; Fig 2.12; Fairbanks 1989). The rate of sea level rise stabilised fter 7-8,000 yr BP increasing gradually to the present day (Fig 2.12; Fairbanks 1989).

Global eustatic sea level documented since the Late Weichselian is countered somewhat in laciated regions by residual isostatic depression related to glacier-ice loading during the Last Glacial Maximum and by isostatic uplift or emergence following the glacial unloading during deglaciation nd the Holocene. The rate of isostatic depression cannot be quantified for the Late Weichselian laciation. The rate of isostatic uplift or emergence in East Greenland relative to present day sea level following deglaciation can be ascertained using marine limits based on dated fossiliferous marine delta surfaces, shorelines, or erosional fossil cliffs (Funder 1989; Funder & Hansen 1996). Figure 2.13 shows the distribution and altitudes of marine limits in Greenland assocated with the Late Weichselian-Early Holocene uplift (Funder & Hansen 1996).

The marine limits were formed immediately after deglaciation in East Greenland. Uplift or emergence along East Greenland began at 10,000 to 11,000 yr BP following the onset of rapid deglaciation from the fjord region (Funder 1989; Funder & Hansen 1996). Late Weichselian - Early Holocene maximum uplift correspond to regions around the 10,000 yr BP ice margin (Section 2.3.3), reflecting melting and unloading of ice from these areas during deglaciation (Funder & Hansen 1996). Marine limits reach maxima of up to 135 m around the head of Hall Bredning in the Scoresby Sund region and 80-120 m a.s.l. in the mid to outer regions of Kong Oscars and Kejser Franz Josephs Fjords. This reflects maximum uplift for these regions of East Greenland (Fig 2.13; Funder & Hansen 1996). The lowest marine limits, of 40-80 m a.s.l., correspond to the lowest uplift occurred outside the 10,000 yr BP ice margin in the outer coastal regions of East Greenland, and the majority of the fjords to the north of 73°N (Fig 2.13; Funder & Hansen 1996). The age of the marine limits become younger and lower towards the outer coasts of East Greenland away from the 10,000 yr BP ice margin. Therefore, the rate of uplift must be lower for the coastal regions than around the 10,000 yr BP ice margin. An average rate of uplift of 3.7 cm $^{14}Cyr^{-1}$ occurs at the 10,000 yr BP ice limit in Scoresby Sund following 9,750 yr BP, decreasing to a rate of 2.4 cm $^{14}Cyr^{-1}$ outside this ice margin in western Jameson Land following 9,500 yr BP (Funder & Hansen 1996).

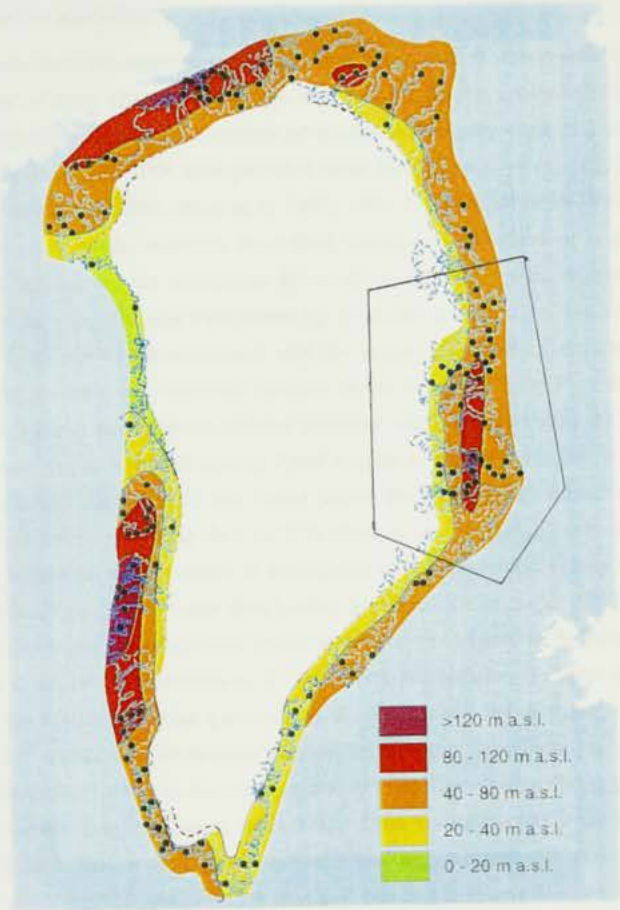

Figure 2.13. Altitude of postglacial (Late Weichselian to Early Holocene) marine limits (m a.s.l.) in Greenland. The East Greenland region is indicated. From Funder & Hansen (1996).

2.5 SEDIMENTATION PATTERNS, PROCESSES AND ENVIRONMENTS IN EAST GREENLAND DURING THE LATE WEICHSELIAN AND HOLOCENE

2.5.1 Late Weichselian glaciation

Late Weichselian sedimentation patterns, processes and environments in the fjords and continental margin of East Greenland are not well known due to limited sedimentological and geophysical investigations. However, a number of studies in Scoresby Sund and across the adjacent continental margin between 68-71°N have provided some detail for this period (e.g. Dowdeswell et al. 1994b; Nam et al. 1995; Nam 1996; Stein et al. 1993, 1996; Dowdeswell et al. 1996, 1997b).

As demonstrated for the Scoresby Sund fjord system (e.g. Dowdeswell et al. 1994a,b, 1998), it is highly likely that during ice occupation of the fjords and inner shelf of East Greenland pre-existing sediments are removed and transported by grounded glacier ice to the continental margin. Direct deposition from glacier ice associated with the glacial maximum of the Late Weichselian, is documented by the presence of a terminal moraine at the mouth of Scoresby Sund (Section 2.3.2; Dowdeswell et al. 1994b) and overconsolidated diamictic sediment pre-dating 15,000 yr BP on the continental shelf adjacent to Kangerdlugssuaq Fjord thought to represent subglacial till (Mienert et al. 1992). Overconsolidated diamicton is also found within the mid region of Hochstetter Bugten and close to the adjacent inner continental shelf at 75°N (Stein et al. 1993; Hubberten et al. 1995). This is interpreted to be subglacial till deposited in association with glacier ice that had advanced onto the inner continental shelf during the Late Weichselian glaciation (Stein et al. 1993; Hubberten et al. 1995). However, there are no dates from above or within these units to provide an exact age for deposition (Stein et al. 1993; Hubberten et al. 1995). The till close to the inner shelf was probably deposited during the Late Weichselian glaciation as the 16-21,000 yr BP ice margin lay fairly close to this region. The till further into Hochstetter Bugten, on the other hand, was probably influenced by glacier ice up until 10,000 yr BP, as the ice margin at this time lay close to this region (Section 2.5.2).

The continental margin adjacent to Scoresby Sund is dominated by the Scoresby Sund fan system (Section 2.2.6.5; Dowdeswell et al. 1996, 1997b). The main acitivity on the fan system during the Weichselian was confined mostly to the southern two thirds mainly in the form of debris flows (Dowdeswell et al. 1997b). However, the absence of a definitive chronological control makes it difficult to distinguish whether the debris flow activity occurred during the Late Weichselian glaciation in response to cross shelf transport from the ice margin at the mouth of Scoresby Sund, or earlier in the Weichselian when the ice margin may have extended to the shelf break, enabling sediment to be delivered directly to the continental slope (Dowdeswell et al. 1997b).

Sediments of Late Weichselian glaciation age from the continental slope corresponding to the northern third of the Scoresby Sund fan system comprise hemipelagic mud and sandy mud, with variable but high quantities of iceberg rafted debris (Nam et al. 1995; Nam 1996; Dowdeswell et al. 1997b). These sediments indicate that the fan system in this region was relatively inactive during the Late Weichselian (Dowdeswell et al. 1997b). Sediments of a similar composition are also distributed widely across the East Greenland continental slope bordering the Denmark Strait and adjacent to

Carlsberg and Kong Oscars Fjords, beyond the southern and northern limit of the Scoresby Sund fan system, respectively, (Nam et al. 1995; Nam 1996; Dowdeswell et al. 1997b). The hemipelagic and iceberg rafted sediments along the East Greenland continental margin are deposited at high sedimentation (5-17 cm kyr^{-1}) and accumulation (up to 20 g cm^{-2} kyr^{-1}) rates throughout the Late Weichselian glaciation, reaching maximum values during the glacial maximum at 16-21,000 yr BP (Nam et al. 1995; Nam 1996; Stein et al. 1996). The high iceberg rafted debris and flux of sediment delivered to the East Greenland continental slope occurs in response to the focusing of glacial and glacimarine sedimentation on the continental margin due to the advance of glacier-ice to the fjord mouths/inner continental shelf during the Late Weichselian (e.g. Nam et al. 1995; Nam 1996; Stein et al. 1993, 1996). The amount of iceberg rafted debris in hemipelagic sediments on the lower continental slope are greatly reduced in comparison to their counterparts further up the continental slope (Nam et al. 1995; Nam 1996). This distribution reflects the reduced number of icebergs reaching the lower continental slope due to its more distal position with respect to the ice margin in East Greenland, and the southward flowing East Greenland Current that confines the majority of icebergs to the continental shelf and upper regions of the continental slope (e.g. Nam 1996; Dowdeswell et al. 1997b). The fluctuations in the amount of iceberg rafted debris within the hemipelagic sediments of the East Greenland continental slope are interpreted to indicate the repeated collapse of the Greenland Ice Sheet on timescales of 1,000-3,000 years (Section 2.3.2; Nam 1996; Stein et al. 1996). However, a much simpler explanation for the fluctuations in the iceberg rafted debris content may relate to the sporadic supply of icebergs common within ice-distal settings such as the continental slope and/or the influence of the southward flowing East Greenland Current that may have confined icebergs discharged from the ice margin in East Greenland to the continental shelf and upper continental slope.

GLORIA side-scan sonar images along East Greenland reveal that only limited quantities of sediment were transported to the continental slope north of 72°N during the Late Quaternary. This is probably the result of the failure of ice to extend across the broad (up to 250 km) Northeast Greenland continental shelf during the Weichselian (Mienert et al. 1993, 1995; Dowdeswell et al. 1996). Therefore, it is possible to suggest that the Northeast Greenland continental margin during the Late Weichselian glaciation may have been dominated by hemipelagic sedimentation with a significant contribution through enhanced iceberg and meltwater activity, similar to that for the East Greenland continental margin south of 72°N (e.g. Stein et al. 1993; Nam et al. 1995; Nam 1996). However, downslope mass wasting on relatively small-scales cannot be discounted as a possible sediment transport mechanism north of 72°N in East Greenland.

2.5.2 Late Weichselian deglaciation and Younger Dryas

Sedimentation patterns, processes and environments have not been elucidated for the continental shelf and majority of the fjords of East Greenland during the deglacial period between the Late Weichselian glaciation and the Holocene. This relates mainly to the limited number of

recovered sediment cores, and a lack of any chronological control within such sediments. Therefore, our understanding of the sedimentation and environmental history associated with glacier-ice recession during this period is very limited.

Low resolution records are available from the continental slope, which becomes increasingly more ice-distal during this time in response to the continued retreat of the glacier-ice margin from the inner continental shelf/ fjord mouths (e.g. Funder & Hansen 1996). Sedimentary records from the continental slope adjacent to Scoresby Sund and further south bordering the Denmark Strait show increased amounts of IRD within mud facies for the deglaciation period pre-dating 13,000 yr BP (Nam et al. 1995; Nam 1996; Stein et al. 1996). Increased amounts of IRD also occur within mud facies on the continental margin adjacent to the Carlsberg/ Kong Oscars Fjords for the period up to the Younger Dryas (Nam 1996). These sediments were deposited at a rate of 4.6-13.6 cm kyr^{-1}, much higher than the following Holocene period, indicating a higher flux of sediments in response to the deglaciation and invigorated processes of sedimentation (Nam et al. 1995; Nam 1996). The records reveal that hemipelagic and iceberg sedimentation dominate these ice-distal settings and that the icebergs are probably derived in association with the early retreat phase of the Greenland Ice Sheet (e.g. Stein et al. 1996). The flux of IRD to the continental slope is probably impeded by the southward flowing East Greenland Current which may have confined icebergs to the continental shelf (e.g. Nam 1996).

Even though investigations are limited in East Greenland, geological and geophysical evidence from the Scoresby Sund fjord system provides some understanding of the sedimentation patterns and processes that occur in response to the recession of glacier ice since the Younger Dryas, although sedimentation pre-dating the Younger Dryas can also be discerned (Marienfeld 1991, 1992a; Dowdeswell et al. 1994a,b). The retreat of glacier ice through the outer region of the Scoresby Sund fjord system is indicated by the presence of iceberg rafted diamicton facies pre-dating the Younger Dryas (Figs 2.14, 2.15), showing that the recession of ice was controlled by iceberg calving (Marienfeld 1991, 1992a; Dowdeswell et al. 1994a,b). During the Younger Dryas period (around 10,000 yr BP), the presence of a semi-permanent shorefast sea-ice cover prevented icebergs from traversing the fjord system with subsequent suppression of iceberg sedimentation (Figs 2.14, 2.16; Marienfeld 1991, 1992a; Dowdeswell et al. 1994a,b). This enables the smaller input of meltwater-derived fine grained sediments normally obscured by the much larger supply from icebergs, to dominate sedimentation within the fjord, with the subsequent deposition of a laminated mud facies (Figs 2.14, 2.16; Marienfeld 1991, 1992a; Dowdeswell et al. 1994a,b). In locations close to the Younger Dryas glacier-ice margin at the head of Hall Bredning, acoustically stratified sediments organised into a major depocentre, are interpreted to be ice-proximal sediments derived through meltwater processes and/or subaqueous mass wasting events driven by downslope currents and failure of ice-proximal sediments (Fig 2.8; Dowdeswell et al. 1994b).

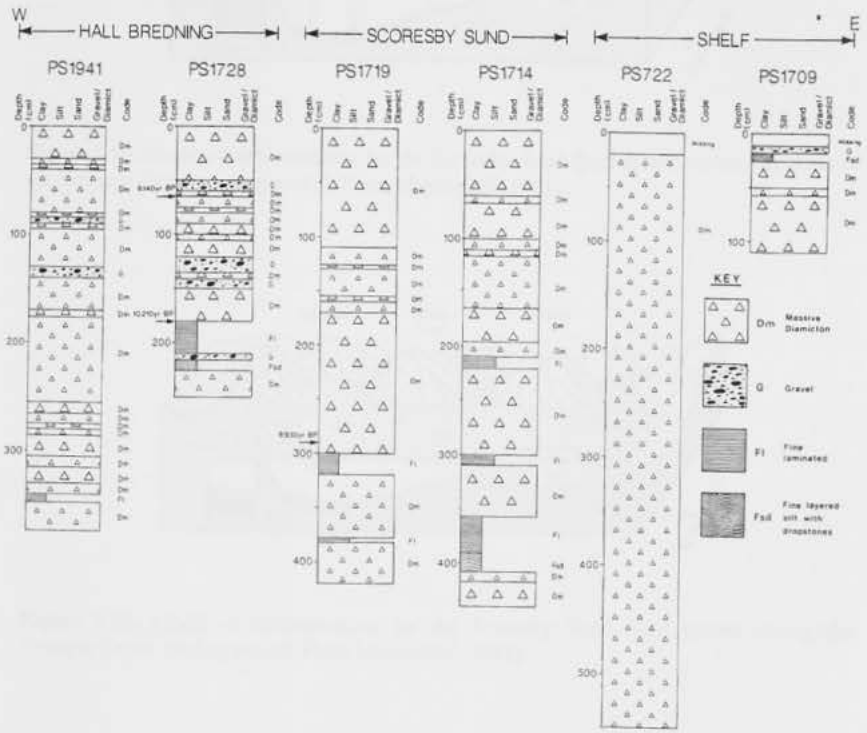

Figure 2.14. Six sedimentological logs from a transect through the outer Scoresby Sund fjord system and shelf, East Greenland showing the main sedimentary facies deposited since the last deglaciation. AMS radiocarbon dates are shown. From Dowdeswell et al. (1994a).

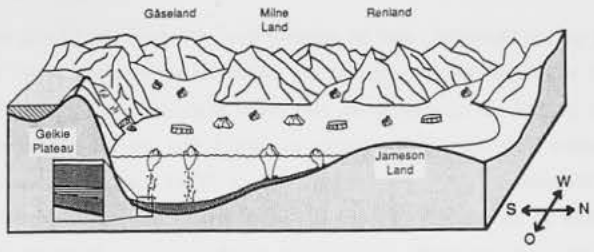

Figure 2.15. Model of sedimentation for the Scoresby Sund fjord system before the onset of the Younger Dryas cooling period. From Marienfeld (1991).

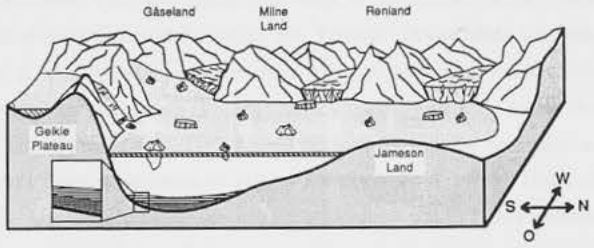

Figure 2.16. Model of sedimentation for the Scoresby Sund fjord system during the Younger Dryas cooling period. From Marienfeld (1991).

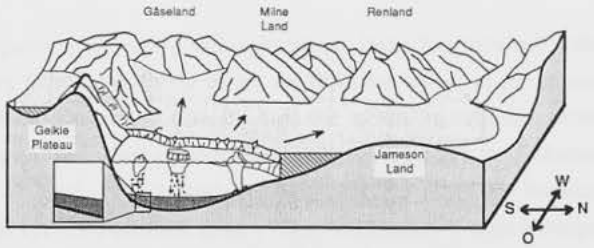

Figure 2.17. Model of sedimentation for the Scoresby Sund fjord system between the end of the Younger Dryas cooling period and the present day. From Marienfeld (1991).

2.5.3 Post Younger Dryas deglaciation

The removal of glacier ice from the fjord systems of East Greenland during the deglaciation following the Younger Dryas and into the Holocene, allowed glacimarine deposition to re-commence. In the Scoresby Sund fjord system, Holocene sediments are dominated by iceberg rafted diamicton facies indicating the continued calving and drifting of icebergs during the final retreat of glacier ice to present-day positions at around 7,000 yr BP (Figs 2.14, 2.17; Marienfeld 1991, 1992a; Dowdeswell et al. 1994a,b). A core recovered from the inner to mid region of Hochstetter Bugten comprises a complete deglacial sequence (Stein et al. 1993). However, the exact timing of the sequence cannot be established as there are no radiocarbon datings (Stein et al. 1993). Even so, the sequence probably represents deposition following the Younger Dryas as the core is located close to the position of the ice margin at this time (Section 2.5.2; cf Funder & Hansen 1996). At the base of the core is an overconsolidated diamicton, interpreted to be a subglacial till. This till was probably influenced by glacier-ice up until Younger Dryas times, after which the ice retreated fjordwards. A sequence of mainly laminated mud and occasional beds of diamicton facies overlies this till, and probably represents the deglacial period following the Younger Dryas when ice retreated to present-day positions (Stein et al. 1993). The dominance of laminated mud facies (Stein et al. 1993) indicates the dominance of sedimentation from meltwater-related processes rather than from icebergs during deglaciation. The diamicton facies, which are not known to be overconsolidated, were interpreted to result from slight readvances of glacier ice (Stein et al. 1993). However, the diamicton could equally have been deposited in association with icebergs or debris flows initiated from the rapid and unstable accumulation of sediment, both produced as a result of the retreating ice (e.g. Powell 1981, 1983; Dowdeswell et al. 1994b). The deglacial sequence is overlain by massive mud, and this change represents the progressive shift from ice proximal to ice distal conditions as ice retreated further into the fjord and Holocene sedimentation began (e.g. Svendsen et al. 1992).

2.5.4 Holocene

Continued deposition of iceberg rafted diamicton facies has occurred within the ice-distal setting of the Scoresby Sund fjord system during the Holocene and up to the present-day (Fig 2.14; Dowdeswell et al. 1994a). This results from the high rate of iceberg discharge currently observed in the Scoresby Sund region, and which probably has occurred throughout the Holocene (Fig 1.4; Reeh 1985; Dowdeswell et al. 1992, 1993, 1994a). Sedimentation to produce this diamicton occurred at a mean rate of 0.1-0.3 m kyr^{-1} (Dowdeswell et al. 1994a). Sedimentation from icebergs dominates over that from meltwater/fluvial outflows, which are in any case very limited and confined mainly to the coastal margins in Scoresby Sund (Dowdeswell et al. 1994a,b).

Iceberg-related sedimentation and the production of diamicton facies is not likely to occur in East Greenland fjord systems where the discharge of icebergs is low (Fig 1.4). The Hochstetter Bugten region is one such fjord system (Fig 1.4; Reeh 1985), and Holocene sediments comprise mainly mud facies and low amounts of iceberg rafted debris (Stein et al. 1993; Hubberten 1995;

Hubberten et al. 1995) reflecting the low drift of icebergs. Sedimentation through glaciofluvial/ fluvial/ subglacial discharge-related processes dominates this fjord setting.

A brief analysis of high resolution acoustic records from the outer region of Kejser Franz Josephs Fjord shows ponded acoustic facies within fjord basins and conformable acoustic facies draping the underlying topography (Niessen & Whittington 1997a; Whittington & Niessen 1997). Holocene sedimentation within this fjord is intepreted to result mainly from subaqueous mass wasting (debris flows and turbidity currents) and vertical settling of iceberg and meltwater plume sediments (Niessen & Whittington 1997a; Whittington & Niessen 1997). This clearly contrasts with the sedimentation patterns and processes in the iceberg-dominated Scoresby Sund fjord system (cf. Dowdeswell et al. 1994a,b).

Holocene sediments from the continental shelf adjacent to the Scoresby Sund region and Carlsberg/ Kong Oscars Fjord comprise sediments with high amounts of iceberg rafted debris that in some cases form diamicton facies (e.g. Marienfeld 1991; Dowdeswell et al. 1994a; Nam 1996). This indicates that a significant number of icebergs escape the fjord systems of East Greenland and drift across the ice-distal continental shelf to contribute to sedimentation. The relatively high amount of iceberg rafted debris within these sediments has also been interpreted to result from the winnowing of fine-grained sediment by the East Greenland Current (e.g. Funder & Larsen 1989; Mienert et al. 1992; Nam 1996).

Holocene sediments from the continental slope of East Greenland comprise mainly hemipelagic mud facies with an insignificant amount of iceberg rafted debris, deposited at a slow sedimentation rate of 1-5 cm kyr^{-1} (Nam et al. 1995; Nam 1996). The low flux of sediments to the East Greenland continental margin occurs due to: (i) the ice-distal position, if not open-marine setting, of the continental margin with respect to glacier ice within the fjords of East Greenland, and (ii) the focusing of sedimentation in the fjord systems of East Greenland in response to glacier ice positioned within the inner fjord region. The very low amount of iceberg rafted debris indicate that the supply and drift of icebergs is low in response to the ice-distal, if not more open-marine setting of the continental slope, which only a few far travelled icebergs reach (Nam et al. 1995; Nam 1996). This is influenced further by the southward flowing East Greenland Current which acts to confine icebergs to the continental shelf following their escape from East Greenland fjord systems (Dowdeswell et al. 1992; Nam 1996).

2.6 OCEANOGRAPHY AND SEA ICE COVER IN EAST GREENLAND DURING THE LATE WEICHSELIAN AND HOLOCENE

2.6.1 Late Weichselian glaciation

A permanent or year round (perennial) sea ice cover has been suggested for the Greenland-Iceland-Norwegian Sea throughout the entire glacial period of the Late Weichselian (e.g. CLIMAP 1976; Kellogg 1976, 1980; Kellogg et al. 1980). More recent work has challenged this

reconstruction. Isotopic records indicate that the continental margin of East Greenland was also covered by extended sea ice during the Late Weichselian glaciation (Nam et al. 1995; Nam 1996). During the period 21,000 to 25,000 yr BP, the East Greenland continental margin experienced a perennial sea ice cover, as indicated by a low biogenic carbonate content, and reduced iceberg rafted debris indicative of suppressed iceberg drift (Nam 1996). During the Last Glacial Maximum following 21,000 yr BP, the extended sea ice cover in East Greenland experienced at least some seasonally ice free conditions (Nam et al. 1995; Nam 1996). This is suggested by high accumulation rates of marine organic matter, high carbonate content and the presence of planktonic foraminifera from the East Greenland continental slope that indicate some surface water bioproductivity. Seasonally ice free water conditions have also been reconstructed for the Fram Strait during the Late Weichselian glaciation between 14,500 to 19,500 yr BP (Last Glacial Maximum) and 22,500 to 27,000 yr BP (Hebbeln et al. 1994; Hebbeln & Wefer 1997).

Isotopic values from the western margin of the Greenland Sea are much lighter compared to those from other regions of the Greenland and Norwegian Seas (Kellogg 1976, 1980; Kellogg et al. 1978; Jones & Keigwin 1988; Baumann et al. 1993; Nam 1996). This is interpreted to reflect the influence of cold, low-saline Arctic waters that are transported along the East Greenland continental margin in the East Greenland Current from the Arctic Ocean via the Fram Strait (Nam 1996). Two meltwater events are dated between 21,500 and 23,000 yr BP in East Greenland, indicative of localised glacier melting on land (Nam 1996). Light oxygen and carbon isotope records are documented from the continental margin south of Scoresby Sund, indicating major but localised discharge of meltwater from a proposed glacier-ice margin on the continental shelf during the Last Glacial Maximum (Nam 1996). The light carbon isotopes indicate that the meltwater contributed to stratification of ocean waters in this region causing a reduction in the ventilation of surface waters and the associated reduced exchange of CO_2 between the atmosphere and ocean (Nam 1996).

The isotope records of planktonic and benthic foraminiferas suggest that the extended sea ice cover may have prevented deep water formation along the East Greenland continental slope, and in the Greenland Sea during the Late Weichselian glaciation (Nam 1996). However, the presence of heavy carbon isotopes together with an increase in the carbonate content on the lower regions of the East Greenland continental slope, suggests that regional deep water formation may have occurred during isotope stage 2.2 (17,900-19,200 yr BP; Nam 1996).

2.6.2 Late Weichselian deglaciation and Younger Dryas

The onset of deglaciation, or Termination Ia, during the Late Weichselian is indicated by a light oxygen and carbon isotope signal beginning at ca. 15,800 yr BP on the continental slope adjacent to Scoresby Sund and at 15,300 yr BP on the East Greenland continental slope bordering the Denmark Strait and Carlsberg Fjord (Fig 2.9; e.g. Nam et al. 1995; Nam 1996). The signals are indicative of massive meltwater production associated with the early and rapid disintegration of the Greenland Ice Sheet (Nam et al. 1995; Nam 1996). The light oxygen isotope signal culminates at

13,200 yr BP, indicating the end of either the meltwater event, or the influence of meltwaters as the retreating ice sheet becomes more distal to the continental margin (Nam et al. 1995; Nam 1996).

The shift in oxygen isotope values during the transition from the Last Glacial Maximum exceeds the 1.3‰ value calculated for the glacial-interglacial ice volume effect (e.g. Chappell & Shackleton 1986; Labeyrie et al. 1987; Mix 1987; Jansen & Veum 1990; Nam et al. 1995; Nam 1996). The oxygen isotope excess documented from the East Greenland continental margin is thought not to be temperature related, because modern-day surface waters are close to freezing point; a situation similar to that predicted for the Late Weichselian glaciation (Hopkins et al. 1991; Nam 1996). Instead the excess is thought to be the result of a decrease in surface-water salinity related to a large influx of isotopically light freshwater to the ocean linked to: (i) the melting of the Greenland Ice Sheet and discharged icebergs, and (ii) the increased inflow of low-saline Arctic waters transported from the Eurasian Basin of the Arctic Ocean to the Fram Strait via the Transpolar Drift system, and along the East Greenland margin within the East Greenland Current. The low saline waters are derived from the Siberian rivers and meltwaters discharged into the Eurasian Basin of the Arctic Ocean associated with the deglaciation of the Eurasian Arctic ice sheets following 15,700 yr BP (Stein et al. 1994a,b; Nam et al. 1995; Nam 1996). The largest excess in oxygen isotope values occurs across the East Greenland continental slope bordering the Denmark Strait, indicating the most extensive production of meltwater as a result of the proximity of the ice margin to the continental slope, and/or large numbers of icebergs that may undergo melting (Nam 1996).

The large discharge of meltwaters lead to a capping or stratification of ocean waters in this region causing reduced ventilation of ocean surface waters and the associated reduced exchange of CO_2 between the atmosphere and ocean (Nam 1996). Additionally, the meltwaters may have led to a widespread stratification between surface and deeper waters in East Greenland, prohibiting deep-water formation within the Greenland Sea (Nam 1996). Reduced production of North Atlantic Deep Waters (NADW) has also been documented in the North Atlantic during the Late Weichselian deglaciation (e.g. Jansen & Veum 1990). The influence of sea ice on the stratification between surface and deeper waters along the East Greenland continental margin has not been ascertained because the sea ice cover for this period has not been reconstructed. However, it has been suggested that heavier carbon isotopes indicate seasonally fluctuating ice-free conditions across the East Greenland continental margin between the culmination of the meltwater event at 13,200 yr BP and the Younger Dryas (Nam 1996).

In general there is very little evidence of the Younger Dryas (10-11,000 yr BP) in the Greenland Sea (e.g. Baumann et al. 1993; Nam et al. 1995). This is probably related to the short length of the Younger Dryas and associated low sedimentation rates (Nam 1996). However, the Younger Dryas is documented from the East Greenland continental margin adjacent to Scoresby Sund (Nam 1996). Heavy oxygen and light carbon isotopes indicate a period of extended sea ice cover in East Greenland (Nam 1996), similar to that reconstructed for the Scoresby Sund fjord system (Marienfeld 1991, 1992a; Dowdeswell et al. 1994a,b). However, an increase in marine organic

carbon indicative of increased surface water bioproductivity suggests at least some seasonally sea ice free conditions prevailed at the time (Nam 1996).

2.6.3 Post Younger Dryas deglaciation and Holocene

The deglaciation following the Younger Dryas is not well documented along the East Greenland continental margin, although a meltwater signal dated at 8,000 yr BP from the continental slope adjacent to Scoresby Sund may indicate this period (e.g. Nam 1996). The modern-day surface water circulation and polar front system within the Greenland Sea was established at 6,100-7,400 yr BP (Nam 1996). Throughout the Holocene, the inner continental shelf of East Greenland (south of 72°N) is characterised by lighter oxygen and carbon isotope records than in comparison to the outer regions of the continental margin, showing that the influence of meltwaters are most intensive in regions more proximal to melt/river waters produced from fluvial, glacifluvial and subglacial systems draining into the fjords of East Greenland (Nam 1996).

Heavy carbon isotopes and high amounts of organic carbon within sediments indicates that surface waters have been well ventilated (high exchange of CO_2 between ocean and atmosphere) and that more seasonal (greatly reduced, more open water) sea ice conditions have prevailed in East Greenland and the western Greenland Sea throughout the Holocene (Baumann et al. 1993; Stein et al. 1993; Nam et al. 1995; Nam 1996). These conditions enable increased surface water bioproductivity, which is highest over the continental slope (Nam et al. 1995; Nam 1996). Bioproductivity within the fjords is restricted to a much greater extent due to the unfavourable hydrographic conditions and the relatively high suspended sediment concentrations within the water column (e.g. Marienfeld 1991, 1992a,b). An absence of biogenic carbonate within Holocene sediments across the East Greenland continental margin results from strong dissolution at the sea floor due mainly to the cold polar waters of the East Greenland Current, and increased flux of organic carbon which result in high CO_2 content in bottom waters (Baumann et al. 1993; Nam 1996).

CHAPTER 3

DATA SOURCES AND ACQUISITION

3.1 INTRODUCTION

A number of analytical methods are employed to investigate a suite of sediment cores recovered from the East Greenland study area (Chapter 1) during the cruise of the German research vessel RV *Polarstern* in 1994 (ARK X/2; cf. Hubberten 1995) (Table 3.1; Fig 1.1). Additional acoustic data collected along the ship cruise tracks (Fig 5.1a) were included in this study to aid this investigation. These methods are outlined in this chapter. All methods were adopted with the specific aim of providing a broad but complementary sedimentological, geophysical and environmental investigation into glacimarine sedimentation patterns, processes and environments during the Late Weichselian and Holocene for the mid to outer Kejser Franz Josephs Fjord and adjacent East Greenland continental margin (Fig 1.1).

3.2 CORE LOCATION AND SAMPLING METHODOLOGY

3.2.1 Core locations

Cores of this study were intentionally recovered from specific locations to establish a record of Late Weichselian and Holocene sediments within mid fjord, continental shelf and continental slope settings. A total of 8 gravity cores and 1 box core from the Kejser Franz Josephs Fjord-continental shelf-continental slope transect were investigated in this study. The exact position, environmental setting and water depth from which the cores were recovered is summarised in Table 3.1, and their geographical positions in relation to East Greenland are illustrated in Figure 1.1. The physiography of the sea-floor in the region of the core locations was ascertained using the acoustic data of the Parasound 3.5 kHz system (Section 3.6) presented in Chapter 5. Cores PS2627 (SL), PS2628 (SL) and PS2629 (SL and GKG) were recovered from the lower, mid and upper continental slope, respectively. Core PS2630 was recovered adjacent to the eastern margin of a bathymetric high on the mid continental shelf, and core PS2641 from the eastern margin close to the centre of a basin on the inner continental shelf (Chapter 5). Cores PS2631 and PS2632 were recovered from the outermost and innermost sub-basins, respectively, of the outer region of Kejser Franz Josephs Fjord. Core PS2633 was recovered from the margin of the mid fjord basin of the Kejser Franz Josephs Fjord (Chapter 5).

3.2.2 Field sampling

Field sediment sampling was performed using gravity and box coring methods. In brief, the gravity corer consists of a cylinderical barrel of 12 cm diameter and variable length (fitted in 5 m sections) with an attached core catcher, and provides the most extensive geological record of sea-floor sediments. The box core consists of a square barrel of dimensions 0.5 m x 0.5 m x 0.5 m providing undisturbed sea-floor surface sediments used to correct for those lost by the gravity coring.

Table 3.1. An inventory of the sedimentary cores investigated in this study. Details include, i) core number (gravity and box core are symbolised by SL and GKG, respectively), ii) environmental setting/location of the core site, where KFJ Fjord represents Kejser Franz Josephs Fjord, iii) core length (cm), iv) investigated core length (cm), v) latitude (N) and longitude (W), and vi) water depth (m) (sea-surface to sea-floor) from which the core was recovered.

Core No.	Environmental Setting/Location	Core Length (cm)	Investigated core length (cm)	Latitude (N)	Longitude (W)	Water depth (m)
PS2627-SL	Lower continental slope	414	414	73° 07.40'	15° 40.85'	2009
PS2628-SL	Mid continental slope	235	235	73° 09.79'	15° 57.98'	1694
PS2629-SL	Upper continental slope	214	214	73° 09.52'	16° 28.96'	850
PS2629-GKG		056	056	73° 09.52'	16° 28.96'	850
PS2630-SL	Mid continental shelf	302	302	73° 09.52'	18° 04.06'	287
PS2641-SL	Inner continental shelf (inner shelf basin)	700	700	73° 09.34'	19° 28.93'	469
PS2631-SL	Outer KFJ Fjord (outermost sub-basin)	725	725	73° 10.67'	22° 11.04'	430
PS2632-SL	Outer KFJ Fjord (innermost sub-basin)	258	258	73° 24.40'	23° 38.00'	505
PS2633-SL	Mid KFJ Fjord (mid fjord basin)	585	585	73° 28.82'	24° 36.84'	283

The positions of the core locations were selected based on the geophysical Krupp-Atlas Parasound acoustic profiling system, and bathymetrical Hydrosweep mapping system (cf. Grant & Schreiber 1990). Navigation, and the exact latitude and longitude of the core locations were based on processed GPS and satellite data. Both methods enabled core sites to be selected in order to sample the various sedimentary environments represented within the study area. Further use of the Parasound acoustic data is made in this study (Chapter 5) and a broader description of the system is provided in Section 3.7.

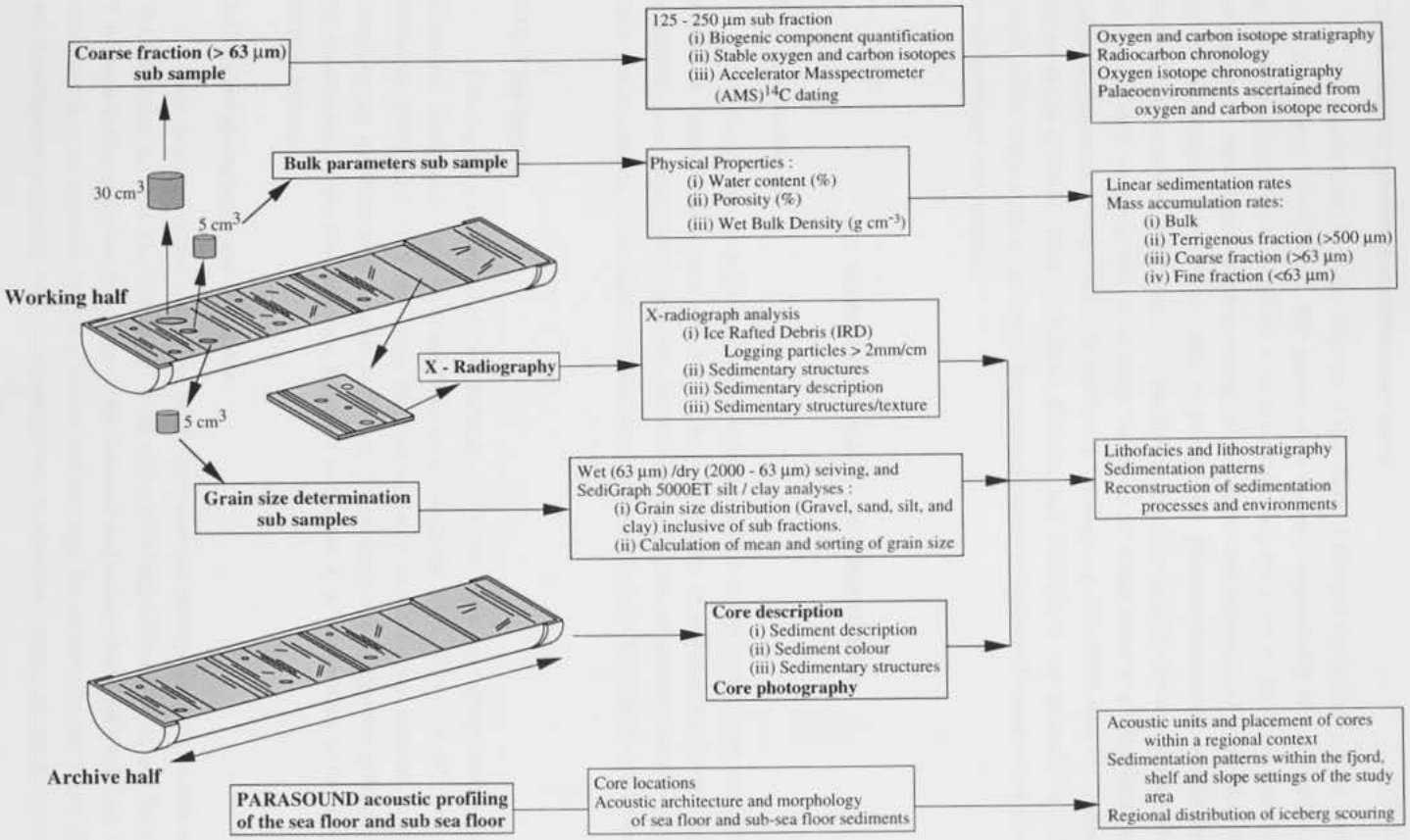

Figure 3.1. Schematic diagram/flowchart illustrating the various laboratory processing stages of gravity cores, and the analytical techniques adopted in this study. The results of the methods are indicated, and in combination provide a composite reconstruction of glacimarine sedimentation and environments within Kejser Franz Josephs Fjord and on the adjacent East Greenland continental margin.

3.2.3 Laboratory processing of sedimentary cores

The gravity cores form the majority of this study. Additional but limited use are made of the box cores, notably PS2629-GKG. The gravity cores are split longitudinally into two halves (archive and working halves), and an additional 1 cm thick slab along the entire length of the core. Figure 3.1 summarises the laboratory processing strategy of this author and the analytical techniques adopted to analyse the sediment samples in order to provide the palaeoenvironmental and chronological parameters used in this investigation. A number of sediment samples (termed sub samples) were taken from each sampling interval at every 10-20 cm or where there is a lithological or colour change. Problems arise with frequently alternating lithology e.g. associated with the laminated and couplet facies (PS2633, PS2631, PS2641, PS2628, and PS2627). It was generally impossible to sample within single laminae and obtain the required amount of sediment for analysis so a composite sampling strategy was adopted.

3.3 SEDIMENTOLOGICAL METHODOLOGY

3.3.1 Introduction

The complementary sedimentological methods outlined in this section were adopted in order to provide comprehensive data sets for: i) the construction of sedimentary facies, and ii) the reconstruction of depositional processes influencing glacimarine sedimentary environments of the study area in response to the climatic fluctuations throughout the Late Weichselian and Holocene.

3.3.2 Core logging

Core logging encompassed two methods: (i) Visual core description performed by the *Shipboard Geological Party* on board *Polarstern* during the ARK X/2 cruise (cf. Stein et al. in Hubberten 1995), and (ii) X-radiograph description. Based on the logging methods, a number of lithofacies are identified from the core sediments. The methods and background principles used in the classification of the lithofacies are discussed in Chapter 4. A brief outline of the core logging methods follows.

3.3.2.1 Core photography and description

Prior to sampling, the two halves of the split core are photographed to provide a detailed visual record of the core. The archive half of the split core is logged visually to include the following: i) sediment colour classified according to the "Munsell soil colour chart" (Munsell Ltd. 1954), ii) classification of the sediment type by grain size and lithology, iii) sediment texture (types of grading, and bioturbation), iv) sedimentary structures (lenses, laminations, ripples, dropstone structures e.g.

clusters, lenses and layers), and organic spots/ lenses, and v) biogenic material. In addition, smear slides are investigated for grain size and sediment composition.

3.3.2.2 X - radiography and description

The use of X - radiographs is based on the original work developed by Hamblin (1962). The x-radiographs reveal very discrete sedimentary microfabrics, contrast sediments composed of differing grain sizes, sedimentary structures, bioturbation and organic material, and particles >2 mm (interpreted as Ice Rafted Debris) not normally identified by visual description. The 1 cm thick sediment slabs produced during the core opening are split up into 25 cm lengths. The sediment slabs were placed on x-ray film within a Hewlett Packard cabinet x-ray system with the tube voltage set to 40 KV. The sediments are exposed to the x-ray radiation for 3-6 minutes dependent upon the sediment nature (grain size and mineralogy).

3.3.3 Grain size determination

Grain size analyses were performed on 5 cm^3 sub samples (Fig 3.1) from a variety of representative sedimentary facies along the East Greenland continental margin. There is no single measurement technique allowing the determination of clay, silt, sand and gravel grades. Therefore, a combination of methods, involving seiving and use of a SediGraph, were adopted for the analysis of these grades. Seiving was used to analyse sand and gravel grades and the SediGraph for silt and clay grades split at 63 µm (4Φ). Grain size can be expressed relative to two scales, microns (µm) and phi (Φ), where both are interchangeable using a conversion table (cf. Tucker 1988).

3.3.3.1 Sample Preparation

The wet sediment sub-samples were air dried in the laboratory, and the dried bulk sediment weighed. The bulk sediment is dispersed in 0.05% sodium hexometaphosphate (Calgon) solution using ca. 20 ml per 1 gram of sediment. The sediment - Calgon solution was agitated for twenty four hours, and further dispersed using an ultrasonic bath for upto 5 minutes. Following this the sediment - Calgon solution was wet seived at 63 µm (4Φ) to separate the sand and gravel from the silt and clay grades.

3.3.3.2 Sieving Technique

The gravel and sand (coarse) fractions obtained from the wet sieving described in Section 3.3.3.1 are washed with water to remove the Calgon, and dried in an oven at approximately 50°C. The bulk coarse fraction is weighed and dry seived by hand into 63-125 µm (4-3Φ), 125-250 µm (3-2Φ), 250-500 µm (2-1Φ), 500-1000 µm (1-0Φ), 1000-2000 µm (0- -1Φ), and >2000 µm (> -1Φ) sub-fractions. The sub-fraction sizes were specifically chosen for consistency with that quoted in the

literature. The sediment obtained within each sub-fraction are weighed, and totalled to obtain the both the sand and gravel and the composite weights. The gravel and sand and associated sub fractions are expressed as a weight based percentages (%) relative to the original bulk sediment weight. Furthermore, the bulk silt and clay weight based percentage (%) is calculated using the weight differential between the bulk sediment and coarse fraction weights.

3.3.3.3 SediGraph Technique

Grain size grades <63 μm (4Φ) were determined from sediment samples using a Micromeritics SediGraph (model 5000ET) at the University of Wales, Aberystwyth. Micromeritics (1984), Stein (1985), Singer et al. (1988), and Jones et al. (1988) provide summaries on the operation and output of the SediGraph system. The machine determines, through the attenuation of x-rays, the concentration of particles (Mass-%) coarser than the operator chosen spherical diameters of 63 μm (4Φ), 31 μm (5Φ), 16 μm (6Φ), 8 μm (7Φ), 4 μm (8Φ), 2 μm (9Φ) remaining at decreasing sedimentaton depths in a suspension filled cell as a function of time. This assumes that particle settling obeys Stoke's law. The particle concentration <2 μm approximates to the difference between the cumulative mass concentration (Mass-%) of the chosen grades and the assumed total concentration (100%).

The SediGraph provides rapid and accurate determination at a high sampling rate of the percentage mass distribution of grain sizes between 100 μm (3.25Φ) and 0.1 μm (13Φ). However, the grades < 1 μm (10Φ) are not analysed in this study as the clay particles below this size rarely obey Stoke's Law of particle settling resulting in inaccurate grain size determination. Measurements are documented to be perfomed with a precision of +/-1% per sample (Micromeritics 1984).

Measurement with the SediGraph is performed on the fine grained fraction. No pre-treatment of this fraction was performed as the organic matter content was not significant enough to disturb measurements, and the carbonate content forms a significant proportion of the bulk sample which needed to be ascertained. The weight of the fine fraction was calculated following the removal and weighing of the coarse fraction (Section 3.3.3.2). Therefore, it was possible to determine whether the fine grained sediment fraction (< 63 μm) - Calgon solution needed to be diluted further with Calgon solution to the optimum concentration of 25-40 ml for every 1 gram of sediment. This concentration is necessary for accurate analysis (Stein 1985). The silt and clay and their associated sub fractions are converted from mass modal percentages determined by the SediGraph to weight based percentages using the bulk silt and clay weight percentage calculated in Section 3.3.3.2.

3.3.3.4 Manipulation of grain size data

The grain size distribution is expressed as a weight based percentage (%) and grouped into gravel (>2000 μm), sand (>63 μm), silt (>2 μm), and clay (<2 μm) fractions. These are further divided into sub fractions described in Sections 3.3.3.1-3.3.3.3. This data is plotted as down core variations and with lithofacies. The grain size intervals can be expressed as either Φ (phi) or μm (microns). Both notations are expressed in this study. The sediment distribution is described in terms

of the graphic mean, and inclusive standard deviation (σ_1) and associated sorting following the graphical method described in Folk (1954) and Folk and Ward (1957). The formulae and descriptive scales of this method are shown in Equations 3.1 and 3.2. This method adopts the phi notation but can be converted to microns (cf. Tucker 1988).

(a) Graphic mean - Mz (from Folk 1954; Folk & Ward 1957):

$$Mz = \frac{\Phi_{16} + \Phi_{50} + \Phi_{84}}{3} \qquad \text{(Eq. 3.1)}$$

(b) Inclusive graphic standard deviation - σ_1 (from Folk 1954; Folk & Ward 1957):

$$\sigma_1 = \frac{\Phi_{84} - \Phi_{16}}{4} + \frac{\Phi_{84} - \Phi_{16}}{6.6} \qquad \text{(Eq. 3.2)}$$

Where:

< 0.35	Very well sorted
0.35 - 0.50 Φ	Well sorted
0.50 - 0.71 Φ	Moderately well sorted
0.71 - 1.00 Φ	Moderately sorted
1.00 - 2.00 Φ	Poorly sorted
2.00 - 4.00 Φ	Very poorly sorted
> 4.00 Φ	Extremely poorly sorted

3.3.4 Number of particles >2 mm/cm, and weight percent of sediment >500 μm (Iceberg Rafted Debris - IRD)

The fraction of sediment >500 μm (0.5 mm) in size within glacimarine lithofacies are considered to be a clear indicator of direct sedimentation of ice rafted debris (Grobe 1987; Elverhøi et al. 1995). This ice index system can only be applied to sediment with significant confidence beyond regions most proximal to the ice front, and other points of efflux, where sediment particles >500 μm in size could not be transported in meltwater and fluvial plumes discharged into the marine environment. Additionally, the ice index is not applicable to sediment >500 μm deposited by subaqueous mass wasting processes, even though the original sediments may have been derived through ice rafting. A contribution of gravel and sand sized particles from sea ice processes is negligible as the majority of sediment rafted within ice floes are predominantly fine grained i.e. <63 μm (e.g. Pfirmann et al. 1989, 1990; Wollenburg 1991; Nürnberg et al. 1994). Therefore, the fraction of sediment >500 μm in size within glacimarine sediments is taken as an indicator of iceberg rafting and sedimentation within the geographical location of the core, and termed **I**ceberg **R**afted **D**ebris (IRD).

Two methods are used to measure the iceberg rafted debris content of sediments: the number of particles >2 mm/cm and the weight percent of sediment >500 µm (cf. Grobe 1987; Elverhøi et al. 1995). The method of determining the number of particles >2 mm/cm described by Grobe (1987) is adopted as it provides the most rapid and representative iceberg index system. The particles >2 mm are counted for each centimetre increment of sediment with depth. As the x-radiograph dimensions are 1 cm thickness by 10 cm core width, and the count thickness is 1 cm, the IRD analysis is a measure of grains >2 mm per 10 cm^3 of sediment. The IRD values are smoothed by a five point moving average. IRD measurements were performed by *Hannes Grobe* (unpubl data) of the *Alfred Wegener Institute*, Bremerhaven, Germany, and permission was granted for my application and interpretation of the data in this study. The x-radiograph method is of insufficient resolution to accurately gauge sediment grains <2 mm in size. Instead, the distribution of sediment >500 µm in size is based on the weight percent of sediment >500 µm (0.5 mm) determined using the SediGraph and sieving techniques (Section 3.3.3).

Iceberg rafted sediments are heterogeneous, and comprise grain sizes <500 µm in size but this component is difficult to distinguish with any confidence, as other simultaneously occurring processes can contribute to this finer grained fraction. Therefore, it must be noted that the IRD index adopted in this study does not reflect the total amount of sediment carried by icebergs but only the identifiable coarse grained component. It follows though, that this index is a sufficient representation of the relative amount of iceberg rafted material in time and space.

The amount of iceberg rafted debris within glacimarine sediments is determined in this investigation, as it can be used to reconstruct iceberg activity and sedimentation within the glacier-influenced East Greenland study area for the Late Weichselian and Holocene period. Furthermore, the amount of iceberg rafted debris has wider implications, as it is an indicator of the rate of iceberg calving and supply to the marine environment, and reflects former ice mass behaviour (variations in ice extent and dynamics) in reponse to Late Quaternary climatic change.

3.4 SEDIMENT PHYSICAL PROPERTIES METHODOLOGY

3.4.1 Water Content (%)

The sub samples taken for bulk parameter analysis are freeze-dried for 24 hours, and then vacuum dried in a Lyovac GT 2 ~~dessication~~ dessiccation system for a further 24 hours. The sediment and bottle weight are ascertained before and after drying with the difference in weight between the two representing the water content weight (g). The water content weight is expressed as a percentage relative to the original wet sediment weight using Equation 3.3. All weights are expressed in grammes (g).

$$\text{Water content (\%)} = \frac{\text{Wet sediment weight} \times \text{Dry sediment weight}}{\text{Wet sediment weight}} \times 100 \qquad \text{(Eq. 3.3)}$$

3.4.2 Porosity (%) and Wet Bulk Density (g cm^{-3})

The porosity (%) and wet bulk density (g cm^{-3}) are calculated using the water content (%) derived in Section 3.4.1 and grain density (Gd). Sediment grain density (Gd), following milling to obtain a homogeneous powder, is calculated using a Micromeritics Accupyc 1330 pycnometer (takes approximately 20 minutes per sample). The wet bulk density is adopted as the water content (%) was originally expressed relative to the wet sediment weight. Both parameters are calculated using Equations 3.4 and 3.5 presented in Nam (1996) based on the work of Gealy (1971) and Hamilton (1971):

$$\text{Porosity (\%)} = 100 \times \frac{(WC \times 100 / (96.5 \times 1.024))}{((100 - WC) / Gd - WC \times 3.5 / (96.5 \times 2.1) + WC \times 100 / (96.5 \times 1.024))} \qquad \text{(Eq. 3.4)}$$

$$\text{Wet bulk density (gcm}^{-3}\text{)} = \frac{100}{((100 - WC) / Gd - WC \times 3.5 / (96.5 \times 2.1) + WC \times 100 / (96.5 \times 1.024))} \qquad \text{(Eq. 3.5)}$$

where WC = Water content (%); Gd = Grain density; 96.5 = proportion of water (%) in seawater; 1.024 = porewater density (g cm^{-3}) at a laboratory temperature of 23°C and a salinity of 35‰; 3.5 = proportion of salt (%) in seawater; and 2.1 = density (g cm^{-3}) of salt.

3.5 CHRONOLOGICAL AND STABLE ISOTOPE METHODOLOGY

3.5.1 Introduction

Accurate dating techniques are essential to this study as they provide a chronological control on the palaeoenvironments reconstructed within Kejser Franz Josephs Fjord and adjacent continental margin. Two methods have been adopted with the aim of constructing a chronology for each core:

- The first method derives a relative chronostratigraphy through the measurement of stable oxygen and carbon isotopes within foraminifera, and the subsequent construction of an oxygen isotope stratigraphy. This is based on the principle that stable oxygen isotopes are directly sensitive to

Late Quaternary climatic change (Emiliani, 1955) and, therefore, commonly used as a chronostratigraphical method in palaeoenvironmental studies.

- The second method involves AMS radiocarbon (^{14}C) dating. This method provides an absolute chronological control on the stable oxygen isotope stratigraphy and associated palaeoenvironmental implications of the stable isotopes. Coupled with the linear sedimentation rates (Section 3.6.1), the radiocarbon dates are used to construct a linear timescale for each core.

The stable oxygen and carbon isotope records determined on foraminifera also yield important Late Weichselian and Holocene palaeoclimatic and palaeoenvironmental implications for the study area. These include the reconstruction of marine and terrestrial bioproductivity, sea-ice cover, meltwater discharge events associated with the melting of ice masses and the associated salinity changes within seawater, variations in the exchange of CO_2 between atmosphere and ocean surface waters, and ice sheet volume change.

3.5.2 Sample preparation: coarse fraction separation and analysis

Stable isotope and radiocarbon analyses are undertaken on the planktonic foraminifera species *Neogloboquadrina pachyderma sin.*, and a number of bivalvia and gastropoda species. *N. pachyderma* is used as it has a widespread distribution throughout the high latitude regions during both glacial and interglacial periods. The individual forams are obtained from the $30cm^3$ sub-samples (Fig 3.1). The sub-samples are wet seived at 63 µm and the gravel and sand fraction (>63 µm) retrieved for coarse fraction analyses. The gravel and sand fractions are dry seived for ca. ten minutes into sub-fraction sizes of 63-125 µm, 125-250 µm, 250-500 µm, 500-1000 µm, 1000-2000 µm, >2000 µm using a Jürgens ATM sonic stacked sifter.

3.5.3 Stable isotope technique

The stable oxygen and carbon isotope method involves the measurement of the $^{18}O/^{16}O$ ($\delta^{18}O$) and $^{13}C/^{12}C$ ($\delta^{13}C$) isotope ratios of foraminifera shell carbonate using a Masspectrometer. Samples were prepared using the method outlined in Section 3.5.3.1, measured using a Masspectrometer (Section 3.2.3.2) and the expression of the results are discussed in Section 3.2.3.3.

3.5.3.1 Sample preparation

For each sub-sample, stable isotope analyses were based on 8-30 specimens of the planktonic foraminifera *Neogloboquadrina pachyderma sin.* The foraminifera were picked from the 125-250 µm sub-fraction (Section 3.5.2) using a binocular microscope. The 125-250 µm sub-fraction size adopted is consistent with that described in the scientific literature and is kept constant throughout the measurement as stable isotope fractionation is size dependent, even when crystallisation occurs in the same water (Savin and Douglas, 1973).

3.5.3.2 Stable isotope measurement

Measurements were performed on a Finnigan MAT 251 Masspectrometer at the Alfred Wegener Institut, Bremerhaven, Germany. The reader is directed to Craig (1957), Mooks and Grootes (1973), and Siegenthaler and Eicher (1986) for a more extensive description of this method. Prior to the isotopic measurements the carbonate is purified of organic impurities using either chemical oxidants (KClO, NaClO, H_2O_2) or roasting to 450°C in a helium medium, as they yield organic derived vapours with masses similar to that of CO_2. The purified carbonate is then reacted with phosphoric acid, and the $^{18}O/^{16}O$ ($\delta^{18}O$) and $^{13}C/^{12}C$ ($\delta^{13}C$) ratios of the released CO_2 are measured.

3.5.3.3 Expression of stable isotope data

The stable isotope ratios are expressed as the departure from the isotopic composition of an arbitary standard i.e. Equation 3.6. This involves the calibration to the PDB scale (Pee Dee Belemnite from a North Carolina formation) using the National Bureau of Standards (NBS-20).

$$\partial^{18}O = \frac{(^{18}O/^{16}O)_{sample} - (^{18}O/^{16}O)_{standard}}{(^{18}O/^{16}O)_{standard}} \times 1000 \qquad \text{(Eq. 3.6)}$$

where $\partial^{18}O$ is the isotopic difference of oxygen expressed in per mille or parts per 1000 (‰ PDB). For the carbon isotopic composition the notation adopts $\partial^{13}C$ and $^{13}C/^{12}C$ in Equation 3.6 (Craig, 1957).

3.5.4 Radiocarbon dating

The AMS (Accelerated Mass Spectrometer) method was adopted as it enables the measurement of very small quantities of carbonate (40-50 mg C), characteristic of samples in this study. The radiocarbon datings were performed at the AMS Laboratory, Institute of Physics and Astronomy, University of Aarhus, Denmark.

3.5.4.1 Principles and methodology of radiocarbon dating

In brief, the method involves the measurement of the radiocarbon concentration within foraminifera, gastropoda and bivalvia carbonate using an accelerator masspectrometer (AMS). A detailed account of the Accelerator Masspectrometer (AMS) and radiocarbon dating is provided by Geyh and Schleicher (1990), Hedges (1981), Mook (1984), and Gove et al. (1987). The radiocarbon determined within carbonate, similar to the other stable carbon isotopes, are assimilated from the atmosphere-ocean system during shell secretion, and is assumed to cease after death. Therefore, the radiocarbon age is ascertained through comparison of the measured proportion of ^{14}C to other

carbon isotopes (^{12}C and ^{13}C) in the sample, to that of an uncontaminated standard of zero age. A half life of 5568 yrs for the decay of ^{14}C to ^{14}N within a closed system is assumed, whereby the proportion of radiocarbon within the sample is converted into a radiocarbon age.

The majority of the AMS radiocarbon datings were performed on 2000-3000 specimens of non-reworked planktonic foraminifera *Neogloboquadrina pachyderma sin.* The foraminifera were picked from the 125-250 µm sub-fraction (Section 3.5.2) of each sample with the aid of a binocular microscope. In PS2631 and PS2641, additional datings were performed on shells of gastropoda, and bivalvia species. As only individual specimens per sample were measured, the size of the sub-fraction from which they were removed is not important. It is assumed, based on the host lithofacies and intact nature of the shells, that the carbonate used in the datings were in-situ and not reworked. An inventory of the sample points and corresponding mono-carbonate of various species of foraminifera, gastropoda, and bivalvia used in this study are listed in Table 3.2.

Table 3.2. An inventory of the planktonic foraminifera, gastropoda and bivalvia samples used for AMS ^{14}C dating. N. pachyderma is short for *Neogloboquadrina pachyderma* sin. Sample depth is measured in cm below seafloor (cmbsf).

Core No.	Depth (cmbsf)	Planktonic Foraminifera	Gastropoda Species	Bivalvia Species
PS2631	99		*Buccinum hydrophanum*	
	390			*Thyasira gouldi*
PS2641	375			*Bathyarca glacialis*
	413			*Bathyarca glacialis*
	535			*Bathyarca glacialis*
	554			*Bathyarca glacialis*
	565			*Portlandia fraterna*
	585			*Portlandia fraterna*
PS2630	180	*N. pachyderma*		
PS2629	70	*N. pachyderma*		
	130	*N. pachyderma*		
PS2628	30	*N. pachyderma*		
	150	*N. pachyderma*		
	210	*N. pachyderma*		
PS2627	20	*N. pachyderma*		
	220	*N. pachyderma*		
	270	*N. pachyderma*		
	330	*N. pachyderma*		

3.5.4.2 Manipulation and expression of radiocarbon data

Routine AMS radiocarbon age determinations of samples from the study area attain variable precisions listed in Tables 6.1 & 6.2. The calculated ^{14}C ages are corrected for natural isotopic fractionation using the $\partial^{13}C$ value measured from the sample, and carbon reservoir effects (related to

the Arctic sea ice coverage and oceanic circulation and deep water formation influencing the exchange and equilibrium of CO_2 and, hence ^{14}C, between the ocean and atmosphere) to account for the apparent differences in radiocarbon between the atmosphere and ocean water that do not reflect the actual period in which the organism lived (Stuiver and Polach 1977; Bradley 1985; Geyh and Schleicher 1990; Nielsen et al. 1995). The ocean reservoir age for coastal regions of East Greenland is calculated at ca. 550 years (Hjort 1973; Heinemeier pers comm.) and subtracted from the conventional ^{14}C age to obtain the reservoir corrected age (^{14}C age BP).

Dates obtained from the radiocarbon method are not calender years (cal yr) as dendrochronological studies show that the atmospheric ^{14}C concentration has varied throughout the recent past, and has not been constant as originally assumed. Damon et al. (1978) provide a summary on the causes of radiocarbon fluctuations to which the reader is directed. Instead the ages are reported in conventional radiocarbon year BP (^{14}C age BP where BP represents "before present" and is taken to be 1950) in accordance with international convention (Stuiver and Polach 1977; Heinemeier pers comm.). Radiocarbon ages can be converted to calender years using the calibration data of Stuiver and long and references therein (1993), and the calibration program of Stuiver and Reimer (1993) for the last ca. 19000 ^{14}C yr BP (22000 cal yr). However, the conversion is not followed in this study as radiocarbon ages (^{14}C age BP) are commonly adopted throughout palaeoenvironmental studies from high latitude regions and are, therefore, adopted here for direct comparisons.

3.6 SEDIMENTATION AND ACCUMULATION RATES

3.6.1 Introduction

Linear sedimentation and mass accumulation rates were calculated in order to determine: i) the flux of sediment and individual components delivered to fjord, shelf and slope settings, and ii) the variation in the fluxes of these settings in response to the climatic change during the Late Weichselian and Holocene.

3.6.2 Calculation of linear sedimentation rates (cm kyr^{-1})

Linear sedimentation rates are defined as the thickness of sediment inclusive of the water content deposited in a unit length of time. The length of time is calculated using the chronological scale derived from the measured, correlated and inferred AMS ^{14}C radiocarbon dates, and oxygen isotope stratigraphy presented in chapter 6. The sedimentation rate can be expressed using Equation 3.7:

$$LSR = ST / Age \qquad \text{(Eq. 3.7)}$$

where LSR = linear sedimentation rate (cm kyr^{-1}), ST = sediment thickness (cm), Age = AMS ^{14}C radiocarbon dating (kyr BP). The linear sedimentation rate is expressed as cm kyr^{-1} or cm 1000 yr^{-1}.

3.6.3 Calculation of mass accumulation rates (g cm^{-2} kyr^{-1})

The mass accumulation rate represents the mass of sediment accumulated in a unit area of the seafloor per unit length of time (expressed as g cm^{-2} kyr^{-1}) and corrected for the water content using the porosity (%) and wet bulk density parameters (discussed in Sections 3.4, 4.5). A number of component accumulation rates can be calculated and include: (i) bulk accumulation rate, (ii) <63 µm (fine fraction) accumulation rate, (iii) >63 µm (coarse fraction) accumulation rate, and (iv) terrigenous component (>500 µm) accumulation rate. Bulk accumulation rates (BAR) were calculated according to Van Andel (1975) using Equation 3.8:

$$BAR = LSR \times (WBD - 1.026 \times (PO / 100)) \qquad \text{(Eq. 3.8)}$$

where LSR = linear sedimentation rate in cm Kyr^{-1}, WBD = wet bulk density in gcm^{-3}, and PO = porosity (%).

In addition, the mass accumulation rate of various sediment components (MAR_X) are calculated according to the equation set out in Nam et al (1995) and listed as Equation 3.9:

$$MAR_X = (P_X / 100) \times BAR \qquad \text{(Eq. 3.9)}$$

where x denotes the sediment component, P_X = sediment component (%), BAR = mass accumulation rate calculated in Equation 3.8.

3.7 GEOPHYSICAL METHODOLOGY

3.7.1 Introduction

The geophysical method is based solely on the Krupp-Atlas Parasound acoustic profiling system (Krupp Atlas Elecktronik GmbH, Bremen). The system enabled a thorough investigation of the acoustic architecture of the upper sedimentary record for the entire study area. Acoustic data collected from a series of transects through Kejser Franz Josephs Fjord, and across the continental margin parallel to ca. 73°N (Fig 5.1) during the ARK X/2 cruise (Niessen & Whittington 1995; Niessen unpubl. data), are included in this study. The application and interpretation of the acoustic data to this study is essential for a number of related reasons: (i) to aid the investigation of the lithofacies and associated processes of deposition interpreted from the sedimentary record, (ii) to place the cores within a regional context, and (iii) to describe seafloor characteristics such as iceberg scouring. The application and results of the Parasound data are presented in Chapter 5.

3.7.2 Parasound acoustic profiling system

A detailed account of the Krupp-Atlas Parasound acoustic profiling system is provided in Grant and Schreiber (1990) on which the description of this section is based. The system was mounted on the hull of *RV Polarstern* and in continual operation throughout the ARK X/2 cruise. Therefore, Parasound data were collected along all ship cruise tracks (Fig 5.1). Exact positions along the transect were determined with the Global Positioning System (GPS).

3.7.2.1 Principles of the Parasound profiling system

The Parasound acoustic system adopts the parametric principle by which it simultaneously emits two primary signals of different frequencies. The first primary signal has a frequency of 18 kHz, and the second primary signal of a frequency that varies between 20.5 and 23.5 kHz. The frequency of the primary signals were specifically set such that the non-linear interaction generated a secondary signal or beam with a frequency of 4 kHz that equates to the difference in the frequency between the two primary signals. The high primary frequencies enable a pulse of short length to be radiated. The resultant beam is used as the bottom and sub-bottom profiler, and has a width of 4° that in turn produces a footprint diameter of 7% of the water depth compared to 35% for a 3.5 kHz profiling system. Parasound data are converted from two way travel time to water depth and unlithified sediment thickness using a velocity of 1500 ms^{-1} for true sound wave travel through the water column.

3.7.2.2 Advantages and limitations of the Parasound profiling system

The configuration of the Parasound system (described in Sub-section 3.6.2.1) enables the beam to penetrate upto 100 m of the sediment column with a vertical resolution of ca. 0.3 m. Either maximum penetration or maximum vertical (or depth) resolution can be selected by varying the second primary frequency and pulse length (Kuhn and Weber 1993). Greater depth resolution is achieved with a combination of short pulse length and low secondary frequency.

The smaller footprint diameter of the Parasound system increases the spatial resolution vertically and laterally, and reduces diffraction patterns in the acoustic records (Kuhn and Weber 1993; Dowdeswell et al. 1993, 1997a). This allows the detection of seafloor characteristics, and sub-seafloor sedimentary morphology with greater resolution and much more straightforward and accurate, than with the use of a conventional 3.5 kHz system (Kuhn and Weber 1993; Dowdeswell et al. 1993, 1997a).

A major limitation of the Parasound system, is that only very weak bottom signals are reflected back to the ship in regions of steep topography resulting in poorly defined, or even an absence of bottom and sub-bottom reflectors within the acoustic records (Kuhn and Weber 1993).

CHAPTER 4

LITHOSTRATIGRAPHY AND GLACIMARINE SEDIMENTARY PROCESSES IN KEJSER FRANZ JOSEPHS FJORD AND ON THE EAST GREENLAND CONTINENTAL MARGIN

4.1 INTRODUCTION

The identification and analysis of lithofacies from sediment cores in high latitude regions, is an important research objective for the reconstruction of patterns and processes of deposition in glacimarine sedimentary environments (e.g. Powell 1981, 1983, 1984; Molnia 1983; Powell & Molnia 1989; Henrich et al. 1989; Henrich 1990; Hein et al. 1990; Dowdeswell et al. 1994a). Lithofacies are distinctive sedimentary units deposited by specific processes and environments (Reading & Levell 1996). The facies variation within a core is referred to as the lithostratigraphy and represents a sequence of events at that site through time. The major lithofacies of high latitude seas possess distinct sedimentary attributes that reflect the variation in the process of deposition. These processes were sensitive to Late Quaternary climate change and, therefore, the lithostratigraphy documents the impact of climate change during this period.

This chapter reconstructs the sedimentary processes and environments along the East Greenland continental margin that occur in response to Late Quaternary climate change. This work addressess subsequent objectives that encompass the reconstruction of ice extent and dynamics associated with the major ice sheets (most notably the Greenland Ice Sheet), icebergs and sea ice, with time (Chapter 7). A number of sedimentological methods are used in order to address these objective. The objectives of this chapter includes:

- to introduce the classification scheme used to identify lithofacies from the logged sedimentology of each core.
- to present the sedimentology and lithostratigraphy of the eight cores along the Kejser Franz Josephs Fjord (PS2633, PS2632, and PS2631), continental shelf (PS2641 and PS2630), and continental slope (PS2629, PS2628, and PS2627) transect (Fig 1.1), with emphasis on the description, distribution and thickness of each identified lithofacies.
- to present the downcore and lithofacies variations of grain size distribution, number of particles >2 mm/cm (IRD), wet bulk density, porosity, and water content. No grain size or physical properties analyses were performed on PS2633. It was the original intention to restrict the study to cores from the outer fjord and continental margin region. However, PS2633 was subsequently

included in the study as it yielded important additional sedimentological data for the mid fjord region supportive of the interpretations made for the outer fjord. The sedimentological and x-radiograph logging of PS2633 was sufficient for this purpose.

- to interprete the identified lithofacies and sedimentological data with regards the sedimentary environments and associated depositional processes that they represent. Place a preliminary chronology on these interpretations in terms of Late Quaternary climate change.

4.2 CORE LOGGING AND LITHOFACIES IDENTIFICATION

4.2.1 Principles and method of core logging

The sediments of sectioned gravity cores recovered along the Kejser Franz Josephs fjord-shelf -slope transect (Fig 1.1) were logged sedimentologically and, additionally, from x-radiographs (Section 3.3). Grain size analyses were performed on these cores for additional, quantitative sedimentological detail (Section 4.4). Both logging techniques follow the method set out in Eyles et al. (1983) and, with the aid of the grain-size distribution, a number of lithofacies were identified. The classification scheme of Eyles et al. (1983) was modified for this thesis in order to most effectively represent the sedimentary characteristics encountered within the cores. The modified scheme is outlined in Table 4.1.

The classification scheme allows the description of diamict, gravel, sand, and fine-grained sediments determined from the logging and grain size measurements. Additionally, sedimentary characteristics, such as the laminated to massive to couplet nature, upper and lower boundaries, grading, loading, dropstones, bioturbation, were described quantitatively. It is important to note several points concerning the scheme:

- Diamicton is adopted as a descriptive, non-genetic term for poorly sorted admixtures of boulder to clay grain sizes, regardless of origin (Eyles et al., 1983; Cadman, 1996). It follows that the units possessing occasional and dispersed clasts (>0.5 mm) within a predominantly fine grained matrix (<0.5 mm) are described as fine grained sediments (muds) with dropstones, rather than as diamicton. Occasionally, however, the term 'diamict' is used with a genetic connotation within the scheme; in relation to their sedimentary characteristics and acoustic architecture (Chapter 5), some diamicton are interpreted as resedimented, and subsequently denoted as Dmm(r).
- Couplets of sand to silt rich and clay rich units, SFc(m-l), are distiniguished from laminates within the scheme. The couplets possess sedimentary characteristics that require a separate designation from laminations. The individual units are rhythmically intercalated and grouped into couplets with each unit characterised by an exclusive well defined nature.
- Following the lithological classification, the massive, laminated or bioturbated structure of the sediments are used as primary classification parameters provided they are the predominating sedimentary characteristics. In the case of bioturbation, if the laminated, massive or graded

structure of a sedimentary unit is the dominant characteristic then it becomes a subordinate classification parameter. Similarly for the sandy mud couplets, SFc(m-l), the massive to laminated structure becomes the subordinate classification characteristic to the couplet nature.

- The code 'F' denotes 'fine grained' and corresponds to 'mud' quoted in the general description of the lithofacies and Table 4.1. This term further groups together the silt and clay particle sub-fraction sizes.

Table 4.1. Facies code for the classification scheme used in the identification of lithofacies, modified from Eyles et al. (1983).

Facies code	Lithofacies type	Sedimentary characteristics
D	Diamicton	
Dmm		massive, matrix supported
Dmm(r)		massive, matrix supported
GS	Gravelly Sand	
GSng		normal grading
S	Sand	
Sm		massive
Sm(d)		massive, with dropstones
FS	Muddy (Fine grained) Sand; Mud is subordinate	
FSng		normal grading
SF	Sandy Muds (Fine grained); Sand is subordinate	
SFng		normal grading
SFm		massive
SFm(d)		massive with dropstones
SFc		couplets composing sand/silt rich and clay rich
SFc(m-l)		units couplet units are composed of a massive to laminated structure
F	Muds (Fine grained)	
Fm		massive
Fb		bioturbated (most prominent structure)
Fl		laminated (parallel, cross, wavey and lensed)
F----(d)		(massive/laminated/bioturbated), with dropstones
F----(b)		(massive/laminated), with bioturbation
F----(len/l)		(massive/laminated), with sandy lenses or layers

4.2.2 Identification of Lithofacies

Preliminary sedimentary facies were identified from the changes in sediment lithology, structure, boundaries and colour, logged sequentially down-core. The facies were further delineated

into more precise lithofacies using core x-radiographs and grain size distribution determined on selective but representative sediment samples. More detailed sediment characteristics including: i) sediment lithology and grain size (although only qualitatively), ii) sedimentary structures, iii) sedimentary boundaries, iv) sedimentary clasts >2 mm in size interpreted as dropstones or iceberg rafted debris, and v) the nature and intensity of bioturbation, were logged from x-radiographs .

The scheme adopted allows the non-genetic identification of lithofacies. This is important because lithofacies are rarely exclusive to one environment. Therefore, individual facies should not be used as sole indicators of a particular sedimentary process. Instead facies should be compared with overlying and underlying and laterally associated facies, together with their lateral continuity and the nature of their boundary in order to facilitate the interpretation of depositional systems.

4.3 CORE SEDIMENTOLOGY AND LITHOSTRATIGRAPHY

4.3.1 Introduction

The lithostratigraphy of the logged cores from the Kejser Franz Josephs fjord-shelf-slope transect (Fig 1.1) are presented. Emphasis is placed on a general description of lithofacies identified from the cores, and their associated distribution and thickness. The results of the grain size analyses and determination of the number of particles >2mm/cm provide additional parameters used in the identification of lithofacies. The results of analyses are discussed in Sections 4.4 and 4.5. A comparison of the sedimentary sequence in the uppermost section of the gravity core and corresponding box core was made at each core site. This revealed that the surface sediments of only the gravity core, PS2629, were lost during coring. To compensate, the addition of 40 cm of surface sediment was made to the top of this gravity core. The lithostratigraphy of each core along the sample transect is shown in the logs of Figure 4.1. A complete summary of all recorded lithofacies characteristics is provided in Table 4.2.

4.3.2 Diamicton (lithofacies Dmm)

General description of the lithofacies: The lithofacies is subdivided into three subfacies relating to the sedimentary characteristics and grain size distribution (Section 4.4): i) Sandy mud diamicton (Dmm), ii) Sandy diamicton (Dmm), and iii) Resedimented sandy mud diamicton (Dmm[r]). In general, the diamicton has consistent characteristics between all three subfacies. The lithofacies comprises a very to extremely poorly sorted, massive, non stratified and matrix supported diamicton (Dmm). The particle size distribution consists of a gravel-sand-mud (silt and clay) admixture. The concentration and size range of the gravel clasts tends to be well mixed within the supporting matrix. The size and distribution of the gravels are expressed by the size and distribution of the triangles in the lithostratigraphical logs of Figure 4.1. However, the size of the triangles should not be interpreted in

terms of absolute sizes but rather as relative indicators of the distribution of large (>10 mm) and small (<10 mm) clasts. Typically, the gravels vary from predominantly dispersed to occasional clustering and thin layerings (<5 mm thick). The gravels comprise both rock fragments and sediment pellets or mud balls, where the latter consists of a mixture of subglacial to marine muds and rock fragments frozen together within a mud cement (Goldschmidt 1992, 1994). The two are distinguished using their appearance on x-radiographs, where sediment pellets appear grey, and rock grains black.

Distribution and thickness of the subfacies: The sandy mud diamicton subfacies (Section 4.3.2.1) is distributed within PS2641 (inner shelf), PS2630 (mid shelf) and PS2629 (upper slope) (Figure 4.1). The subfacies attains a minimum thickness of 28 cm in the lowermost section of PS2641; 174 cm in the uppermost section of PS2630; and 189 cm in PS2629 separated into two units of 51 cm and 138 cm in the uppermost and lowermost section of the core, respectively, by a massive sandy mud facies (SFm[d]) between a core depth of 65-79 cm. The sandy diamicton facies (Section 4.3.2.2) is found exclusively between 0-20 cm in the uppermost section of PS2630 (mid shelf). The resedimented sandy mud diamicton subfacies (Section 4.3.2.3) is identified within PS2630 (mid shelf), PS2628 (mid slope) and PS2627 (lower slope). The subfacies attains a minimum thickness of 117 cm in the lowermost section of PS2630; ca. 7 cm between core depths 168-175 cm in PS2628; <3 cm between core depths 231-233 cm, 240-243 cm, 248-250 cm, 251-254 cm, 262-265 cm and 274-276 cm in PS2627; and a minimum thickness of 88 cm in the lowermost section of PS2627.

4.3.2.1 Sandy mud diamicton (subfacies Dmm)

Description: X-radiographs of this subfacies are presented in Figures 4.2a,b. The colour of this subfacies varies from dark greyish brown (10YR 4/2-2.5Y 4/2) to dark olive grey (5Y 3/2) in PS2629, dark olive grey (5Y 3/2) to olive grey (5Y 4/2) in PS2630, and dark grey (5Y 4/1) in PS2641. The particle size distribution consists of a gravel-sand-mud (clay and silt) admixture where the matrix is dominated by a sandy mud component. The size of the gravels ranges up to 140 mm in PS2629, 100mm in PS2630, and 5mm in PS2631 and PS2641 (Figs 4.2a, b). The upper and lower boundaries with adjacent lithofacies (predominantly massive or laminated muds) vary from gradational in PS2629 and PS2631 to sharp in PS2630 and PS2641 (Figs 4.2b, 4.3b). Bioturbation, evident as burrows and mottling is virtually absent, but reaches approximately 10% intensity in PS2629. The estimated concentration of biogenic material, comprising foraminifers and nannofossils, remains below 5 grain-% content in all cases.

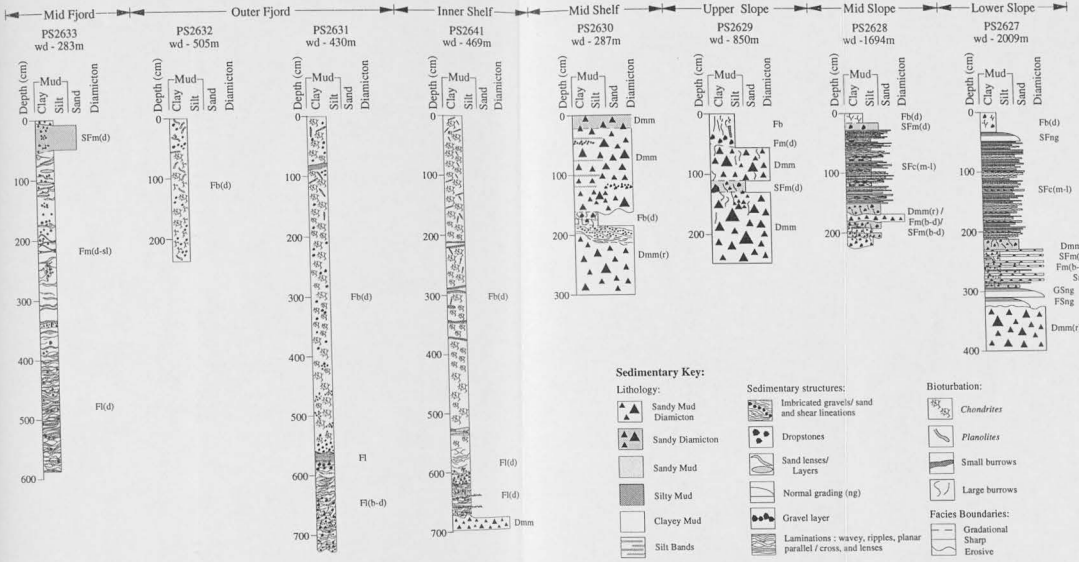

Figure 4.1. Eight sedimentological logs, taken along a west-east transect parallel to 73° N through the mid to outer Kejser Franz Josephs Fjord system and the adjacent continental shelf and slope (refer to Figure 1.1). Water depths (wd) of the recovered cores are indicated. A sedimentary key listing the lithologies and sedimentary characteristics is provided. The logging of the sedimentary characteristics and the subsequent classification into lithofacies followed the conventions set out in Eyles et al. (1983), although it has been modified for this investigation. A key to the nomenclature is provided in Table 4.1. Large and small triangle symbols indicate the relative proportion of clasts in excess of 2 mm in the diamicton.

Lithofacies	Subfacies	Code	Distribution	Thickness range (cm)	Colour	Sedimentary characteristics	Range in the number of particles > 2 mm/ cm	Sorting	Standard deviation σ_I (Φ)	Graphic mean grain size range (Φ)	Gravel (%) range	Sand (%) range	Silt (%) range	Clay (%) range
Diamicton	Sandy Mud Diamicton	Dmm	Shelf, Upper slope	28 cm (PS2641) 174 cm (PS2630); 51 cm and 138 cm (PS2629)	Very dark to dark olive grey to olive grey to dark greyish brown	Massive; Non-stratified; Gravels mainly dispersed but also partly layered and clustered within a sandy mud supporting matrix. <5 grain-% biogenic content; Weak bioturbation (appears as narrow and small burrows) but restricted to the facies in PS2629 (upper slope).	3 - 16	Extremely poorly sorted	4.52 - 5.13	6.02 - 8.03	0 - 9.46	20.11 - 42.91	25.77 - 31.73	28.16 - 39.68
	Sandy Diamicton	Dmm	Mid shelf	20 cm (PS2630)	Dark olive grey	Massive; Gravels well dispersed and supported within a sand matrix; Unbioturbated; <5 grain-% biogenic content.	3 - 8	Very poorly sorted to extremely poorly sorted	3.58 - 4.62	4.06 - 4.65	2.78 - 13.43	49.32 - 62.99	19.03 - 20.08	15.19 - 17.17
	Resedimented Sandy Mud Diamicton	Dmm(r)	Mid shelf, Lower slope	2 - 3 cm and ca. 88 cm (PS2627); 1 cm (PS2628); ca. 117 cm (PS2630)	Dark olive grey to dark grey to dark reddish grey	Gravels widely dispersed in a sandy mud supporting matrix; Upper section of the facies in PS2630 exhibits minor clast and matrix foliation; Ungraded; Boundaries in PS2627 are well defined and is representative of scouring; The boundaries are occasionally peppered by droppstones; Unbioturbated; <1 grain-% biogenic content.	2 - 15	Extremely poorly sorted	4.41 - 5.19	6.83 - 7.97	0.85 - 8.51	18.05 - 38.60	22.34 - 38.01	33.28 - 40.33
Normally Graded Gravel - Sand - Mud	Normally Graded Sandy mud	SFsg	Lower slope	5 cm	Brown	Strong normal grading; Well defined lower boundary representing scouring; Exhibits loose Bouma unit Tb, Tc and Te where Tb is parallel laminated, Tc is wavey to cross laminated and Te is massive.	0 - 1	Very poorly sorted	3.60	6.63	0	35.46	36.97	27.58
	Normally Graded Gravelly Sand	GSsg	Lower slope	14 cm	Brown	Strong normal grading; Well defined lower boundary representing scouring; Exhibits clear Bouma unit Ta, Tb and Tc where Tb is parallel laminated and Tc is wavey laminated.	0 - 6	Very poorly sorted	3.11	3.26	2.71	77.07	9.22	11.00
	Normally Graded Muddy Sand	FSsg	Lower slope	7 cm	Dark greyish brown	Strong normal grading; Well defined lower boundary representing scouring; Exhibits loose Bouma units Tc and Te where Tc is parallel to wavey laminated and Te is massive.	0 - 1	Poorly sorted	1.90	3.06	0.78	81.98	10.98	6.26
Massive sand		Sm(d)	Mid fjord, lower slope	0 - 1 cm (PS2627) 25 cm (PS2633)	Dark grey	Massive to weakly graded. Minor gravels penetrate into upper boundaries; Exhibits Bouma unit Ta with a massive nature; Well defined to occasionally diffuse boundaries.	0	No data	No data	No data	No data	No data	No data	No data
Massive sandy mud with dropstones		SFm(d)	Upper to Lower slope	25 cm (PS2633) 16 cm (PS2620) 9 - 18 cm (PS2628) 1 - 17 cm (PS2627)	Dark greyish brown to dark olive grey to olive grey to grey	Massive; Ungraded; Dropstones are mainly dispersed but do exhibit occasional clustering; Minor sand lenses and concentrations; >15 % biogenic content; Weak to moderate bioturbation (appearing as narrow and small burrows). Gradational to well defined boundaries.	0 - 15	Very poorly sorted to extremely poorly sorted	3.82 - 4.59	8.55 - 9.37	0 - 3.73	8.91 - 14.30	30.39 - 48.00	39.00 - 55.51
Sandy mud Couplets		SFc(m-l)	Mid to Lower slope	104 cm (PS2628) 180 cm (PS2627) Individual couplets < 2.8 cm; Upper unit (clay rich mud) < 2 cm and lower unit (silt - sand rich mud) < 0.8 cm	Dark greyish brown to Brown to dark grey	Facies units are organized into couplets and, therefore, exhibit abrupt normal grading across the units; The couplets consist of a lower unit of massive to planar, wavey and cross laminated (occasional ripple structures) silt to sand rich mud that grades abruptly across a sharp boundary into an upper unit of massive to parallel and wavey laminated clay rich mud; Both units are typically layered but the lower unit can be lensed; Occasional water escape structures disrupt the couplets; The silt - sand lenses are commonly cross bedded; Both units exhibit well defined boundaries; The lower boundary of the lower unit is typically sharp and wavey representative of scouring; The couplets exhibit Bouma & Shanmugam units Tc to Te and possibly up to Tf; Occasional bioturbation in top restricted and appears as small burrows.	0 - 2	Very poorly sorted	2.93 - 3.68	8.37 - 10.87	0	0 - 9.21	34.10 - 47.34	43.46 - 65.90
Laminated mud with dropstones/ bioturbation		Fl(b-d)	Mid to outer fjord, Inner shelf	49 cm (PS2641) ca. 149 cm (PS2631) ca. 206cm (PS2633) Laminae < 0.12 cm and laminae cycle < 0.12 cm (PS2641); Laminae <0.35 cm and laminae cycle <0.42 cm (PS2631 and PS2633)	Grey to dark grey to olive grey to dark brown	Mainly laminated although massive subunits occationally occur in PS2631 and PS2633; Occasional gravel layers occur in PS2641; Laminations include parallel (PS2641), wavey to parallel (PS2641, PS2631 and PS2633) forms; Lenses are most common in PS2633 and PS2631. In general the laminations and lenses possess diffuse boundaries but on occasion develop well defined forms; Laminations are composed of silt rich mud and clay rich mud and occasional sand rich mud alternations; Minor dropstones exhibit dispersed and clustered patterns; Bioturbation varies from weak (PS2641 and PS2633) to strong (PS2631) resulting in destruction of the laminations and occasional mottling. Some structures in PS2633 and PS2631 are difficult to differentiate between syn-sedimentary and coring induced fauling or primary laminations.	0 - 8	Very poorly sorted	2.47 - 3.30	9.93 - 11.2	0 - 1.15	0.28 - 5.05	20.6 - 35.37	59.59 - 79.4
Homogeneous Mud	Massive mud with dropstones/ sand lenses	Fm(d-sl)	Mid shelf, Upper to Lower slope	334 cm (PS2633 20 cm (PS2628) 4 - 15 cm (PS2627)	Dark greyish brown to dark olive grey to olive	Massive; Rare discontinuous and weak laminations and silt bands; Ungraded; Abundant dispersed dropstones; Sand lenses and layers; >10 grain-% biogenic content; Weak to moderate bioturbation appearing as narrow and small burrows, and minor mottling.	0 - 8	Very poorly sorted	3.20 - 3.55	9.65 - 10.32	0	1.95 - 7.76	29.75 - 35.61	56.64 - 64.39
	Bioturbated mud with dropstones	Fb(d)	Mid and outer fjord, Inner shelf, upper to lower slope	258 cm (PS2632) 558 cm (PS2631) 600 cm (PS2641) 11 cm (PS2630) 40 cm (PS2629) 20 cm (PS2628) 34 cm (PS2627)	Dark grey to olive brown to olive grey to dark brown to dark olive grey to dark greyish brown	Massive with almost to rare structure; Minor dispersed and clustered dropstones; Sand lenses and layers are common in PS2633 and less so in PS2631 and PS2641; Organic rich spots and layers present in PS2631 and PS2641; Weak to very strong bioturbation comprising predominantly *chondrites* and very occasional *planolites* burrow types, occasional borings (PS2632, PS2631, PS2641, PS2629, PS2628, and PS2627) and unidentified types (PS2631, PS2641 and PS2630). The *chondrites* form a sparse (PS2629, PS2628 and PS2627) to dense/ very dense (PS2633, PS2632, PS2631 and PS2641) network of burrows. Sediments are mottled (particularly in PS2630) due to burrowing. Burrows are flecked with iron sulphide in PS2631 and PS2641; <30 grain-% biogenic content in fjord inner shelf cores and >30 grain-% in slope cores. Common bivalvia and gastropoda shells, and fish bones in PS2631 and PS2641.	0 - 9	Poorly sorted to very poorly sorted	1.47 - 3.99	7.88 - 10.2	0 - 0.19	1.05 - 8.81	32.07 - 50.01	15.6 - 64.12

Table 4.2. Summary of the lithofacies characteristics determined from cores recovered along the Kejser Franz Josephs fjord-continental shelf-continental slope transect (Fig. 1.1). Details of characteristics include: i) Lithofacies type, ii) Lithofacies code (modified after Eyles et al. 1983), iii) Distribution along the sample transect, iv) Thickness range (cm), v) Colour, vi) Sedimentary structures, vii) Number of particles >2 mm/cm (commonly referred to as Ice Rafted Debris), viii) Graphic standard deviation range and associated sorting (after Folk and Ward, 1957), ix) Graphic mean grain size range quoted in units of phi (Φ) (after Folk and Ward, 1957), and x) Percentage distribution of gravel, sand, silt and clay particles; certain lithofacies were too thin to obtain enough sediment sample for analyses, including the massive sand facies - Sm(d), and the individual units of the Sandy mud couplet facies - SFc(m-l) and laminae of the laminated mud facies Fl(d).

4.3.2.2 Sandy diamicton (subfacies Dmm)

Description: The colour of this subfacies varies from dark greyish brown (10YR 4/2-2.5Y 4/2) to dark olive grey (5Y 3/2) in PS2629, dark olive grey (5Y 3/2) to olive grey (5Y 4/2) in PS2630, and dark grey (5Y 4/1) in PS2641. The particle size distribution consists of a gravel-sand-mud (clay and silt) admixture where the supporting matrix is dominated by the sand component. The size of the gravels ranges up to 100 mm. The lower boundary with the underlying sandy mud diamicton facies is gradational. In general, bioturbation is absent. The estimated concentration of biogenic material, comprising foraminifers and nannofossils, remains below 5 grain-% content.

4.3.2.3 Resedimented sandy mud diamicton (subfacies Dmm[r])

Description: X-radiographs of this subfacies are presented in Figures 4.2c,d. The colour of this subfacies varies from dark olive grey (5Y 3/2) in PS2630 to dark grey (5Y 4/1-5Y 3/1) and dark reddish grey (5YR 4/2) in PS2627 to dark reddish grey (5YR 4/2) and dark olive grey (5Y 4/2) in PS2628. The particle size distribution is dominated by an admixture of gravels within a sandy mud matrix. The nature of the gravels is very similar to that described Section 4.3.2.1. The facies exhibits no internal organisation, where gravels are, on the whole, well dispersed. However, the uppermost 20 cm of the lowermost diamicton unit (below a core depth of 190 cm) in PS2630 exhibits strong imbrication of the gravel, and shear lineations within the fine grained matrix (Fig 4.2c). The diamicton in the lower continental slope core, PS2627, form discrete and well defined units (Fig 4.2d). In all cores, the lower and upper boundaries with adjacent lithofacies, where visible, are well defined and sharp (Figs 4.2c,d). These sedimentary characteristics are interpreted as a product of resedimentation. The size of the gravels range up to 90 mm in PS2630, 9 mm in PS2628 and 30 mm in PS2627. The estimated concentration of biogenic material, comprising foraminifers and nannofossils, remains below 1 grain-% content in all cases.

4.3.3 Normally graded gravel - sand - mud (lithofacies G-S-Fng)

General description of lithofacies: This lithofacies comprises three subfacies consisting of poorly to very poorly sorted and normal graded units: i) SFng - sandy mud (sand grading to mud), ii) GSng - gravelly sand (gravelly sand grading to sandy mud), and iii) FSng - muddy sand (sand grading to mud). Due to the nature of the sediment, x-radiographs were difficult to ascertain and, therefore, the determination of facies characteristics are based on sedimentological logging.

Distribution and thickness of subfacies: The distribution of the lithofacies is restricted to the lower continental slope (PS2627) of the Kejser Franz Josephs fjord-shelf-slope transect (Fig 4.1). The lithofacies is distributed at three stratigraphic positions in PS2627. The uppermost unit, SFng (core depth of 34-38 cm), attains a thickness of 5 cm. The other units of GSng (core depths of 292-306 cm) and FSng (core depths of 306-313 cm) form adjacent units within the sedimentary sequence, attaining thicknesses of 14 cm and 7 cm, respectively.

4.3.3.1 Normally graded sandy mud (subfacies SFng)

Description: The subfacies comprises very poorly sorted, normally graded sandy mud (subfacies SFng). The colour of the lithofacies varies from brown (10YR 4/3) to dark greyish brown (2.5Y 4/2). The subfacies comprises a lowermost unit of massive sand that grades into massive mud (silt and clay). Parallel to cross and wavey laminations are observed in the latter unit. The lowermost unit possesses a sharp lower boundary.

4.3.3.2 Normally graded gravelly sand (subfacies GSng)

Description: The subfacies is composed of very poorly sorted, normal graded gravelly sand (subfacies GSng). The colour of the lithofacies varies from brown (10YR 4/3) to dark greyish brown (2.5Y 4/2). The subfacies comprises a lowermost unit of massive gravelly sand to sand that grades into parallel laminated sand and then wavey laminated sand. The lowermost unit possesses a sharp lower boundary.

4.3.3.3 Normally graded muddy sand (subfacies FSng)

Description: The lithofacies comprises poorly sorted, normal graded muddy sand (subfacies FSng). The colour of the lithofacies varies from brown (10YR 4/3) to dark greyish brown (2.5Y 4/2). The subfacies comprises a lowermost unit of massive sand that grades into laminated sand and then mud. Parallel laminations and overlying irregular whispy to cross laminated forms are observed in the sand. The lowermost unit possesses a sharp lower boundary.

4.3.4 Massive sandy mud (lithofacies SFm[b-d])

Description: X-radiograph of this lithofacies is presented in Figure 4.3a. The lithofacies comprises very to extremely poorly sorted, non-graded, massive sandy mud (SFm[b-d]). The colour varies from dark greyish brown (2.5Y 4/2) in PS2629, olive to olive grey (5Y 4/2) in PS2628, dark greyish brown (10YR 4/2-2.5Y 4/2) to dark olive grey (5Y 3/2) in PS2627. The sand concentrates into patches and lenses in rare places. The lithofacies comprises abundant and widely dispersed gravels whose nature is similar to that described in Section 4.3.2. The size of the gravels ranges up to 12 mm in PS2629, 7 mm in PS2628, and 5 mm in PS2627. The upper and lower boundaries of the lithofacies are typically sharp to gradational in PS2628 and PS2627, and gradational with the over and underlying sandy mud diamicton facies in PS2629. Additionally, the boundaries are occasionally peppered with gravels. Bioturbation, evident as burrows and mottling, is weak in PS2627 but moderate in PS2628 where it reaches concentrations of up to 20%. The estimated concentration of biogenic material, comprising foraminifers and nannofossils, reaches ca. 20 grain-%, and occasionally upto 50 grain-%.

Figure 4.2. X-radiographs illustrating the various sedimentary features associated with lithofacies identified from cores examined in this study. Lithofacies include:

a) Sandy mud diamicton (Dmm) in PS2629 (upper continental slope). Gravel clasts are well dispersed within a sandy mud supporting matrix.

b) Sandy mud diamicton (Dmm) overlying bioturbated mud with dropstones (Fb[d]) in PS2630 (mid continental shelf). Gravel clasts vary from dispersed to clustered. White areas represent gravels that were removed during the splitting of the core (Chapter 3). The diamicton changes, via a semi-gradational boundary, into the underlying bioturbated mud (Fb[d]). The bioturbated mud (Fb[d]) comprises gravels representative of dropstones, and bioturbation results in the mottling of the facies.

c) Bioturbated mud (Fb[d]) overlying resedimented sandy mud diamicton (Dmm[r]) in PS2630 (mid continental shelf). The boundary between the two facies is semi-gradational. The upper section of the resedimented sandy mud diamicton is characterised by shear lineations within the matrix and imbrication of gravel clasts. The main unit consists of dispersed gravel clasts.

d) Resedimented sandy mud diamicton (Dmm[r]) interbedded with massive mud with dropstones (Fm[d]) in PS2627 (lower continental slope). The resedimented sandy mud diamicton is characterised by sharp upper and lower boundaries, penetrated by occasional gravel clasts, and dispersed gravel clasts. The massive bioturbated mud comprises occasional dispersed gravel clasts representative of dropstones, and bioturbation which appear as burrows and mottling.

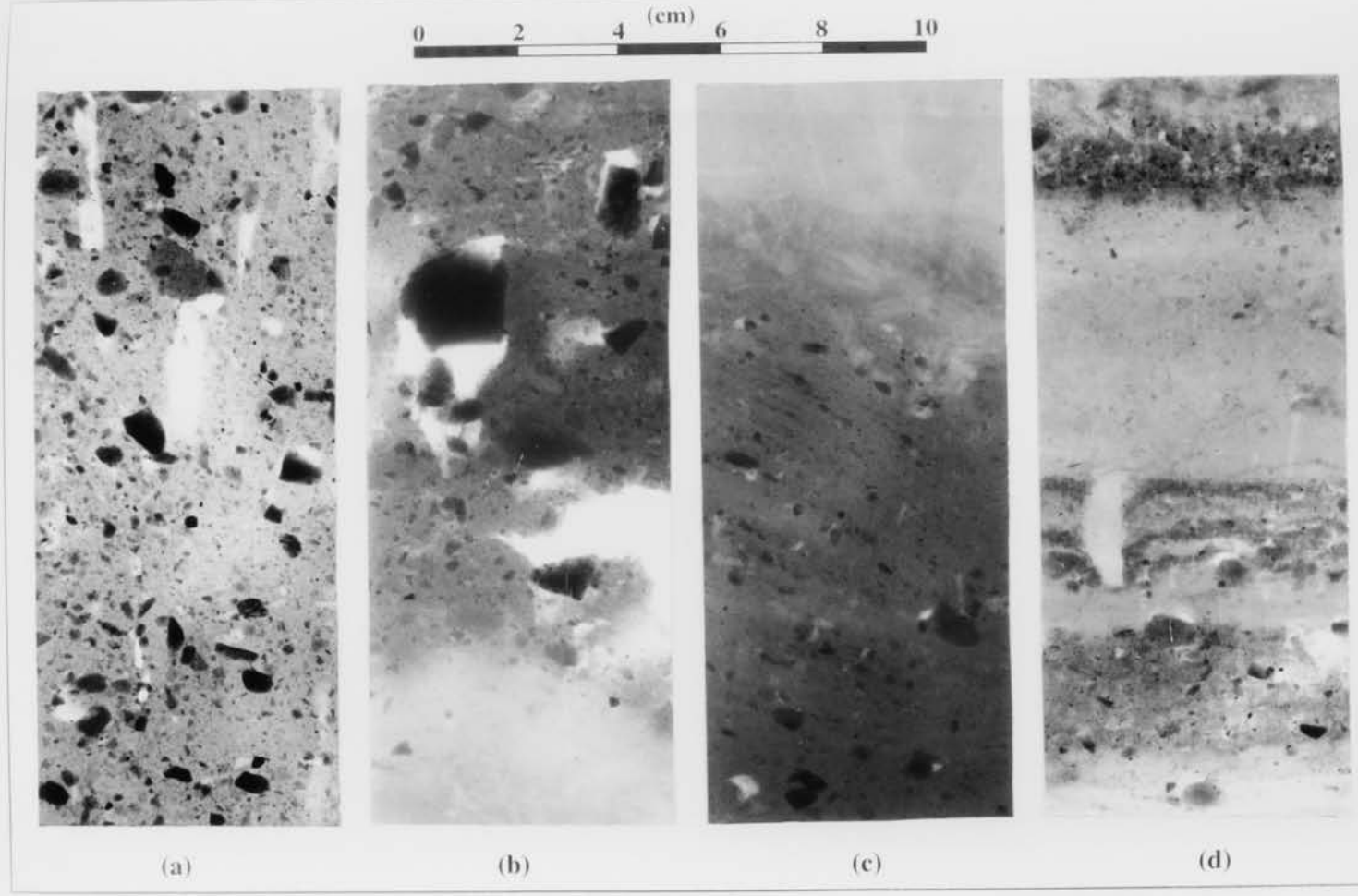
0
2
4
(cm)
6
8
10
(a)
(b)
(c)
(d)

Figure 4.3. X-radiographs illustrating the various sedimentary features associated with lithofacies identified from cores examined in this study. Lithofacies include:

a) Sandy mud with dropstones (SFm[b-d]) in PS2628 (lower continental slope). The massive sandy mud comprises dispersed gravel clasts representative of dropstones, and bioturbation which appears as burrows.

b) Laminated mud (Fl[d]) overlying sandy mud diamicton (Dmm) in PS2641 (inner continental shelf). Laminations are composed of alternating silt rich mud and clay rich mud. They vary from parallel to whispy, continuous to discontinuous, and possess gradational boundaries. The boundary between both facies is wavey and sharp. The sandy mud diamicton comprises dispersed gravel clasts representative of dropstones. Large structures are either fault induced through coring, or syn-sedimentary deformation.

c) Laminated mud (Fl[d]) in PS2631 (outer fjord). Laminations are composed of alternating silt rich mud and clay rich mud, vary from parallel to whispy to wavey, continuous to discontinuous, and possess gradational boundaries. Strong bioturbation has destroyed much of the sedimentary structures leaving the sediment mottled. Gravel clasts represent dropstones. Large structures are either fault induced through coring, or syn-sedimentary deformation.

d) Laminated mud (Fl[d]) in PS2633 (mid fjord). Laminations are composed of alternating silt rich mud and clay rich mud, vary from parallel to wavey to lensed, continuous to discontinuous, and possess gradational to semi-gradational to sharp boundaries. Massive units are occasionally present. Gravel clasts represent dropstones. Large structures are either fault induced through coring, or syn-sedimentary deformation.

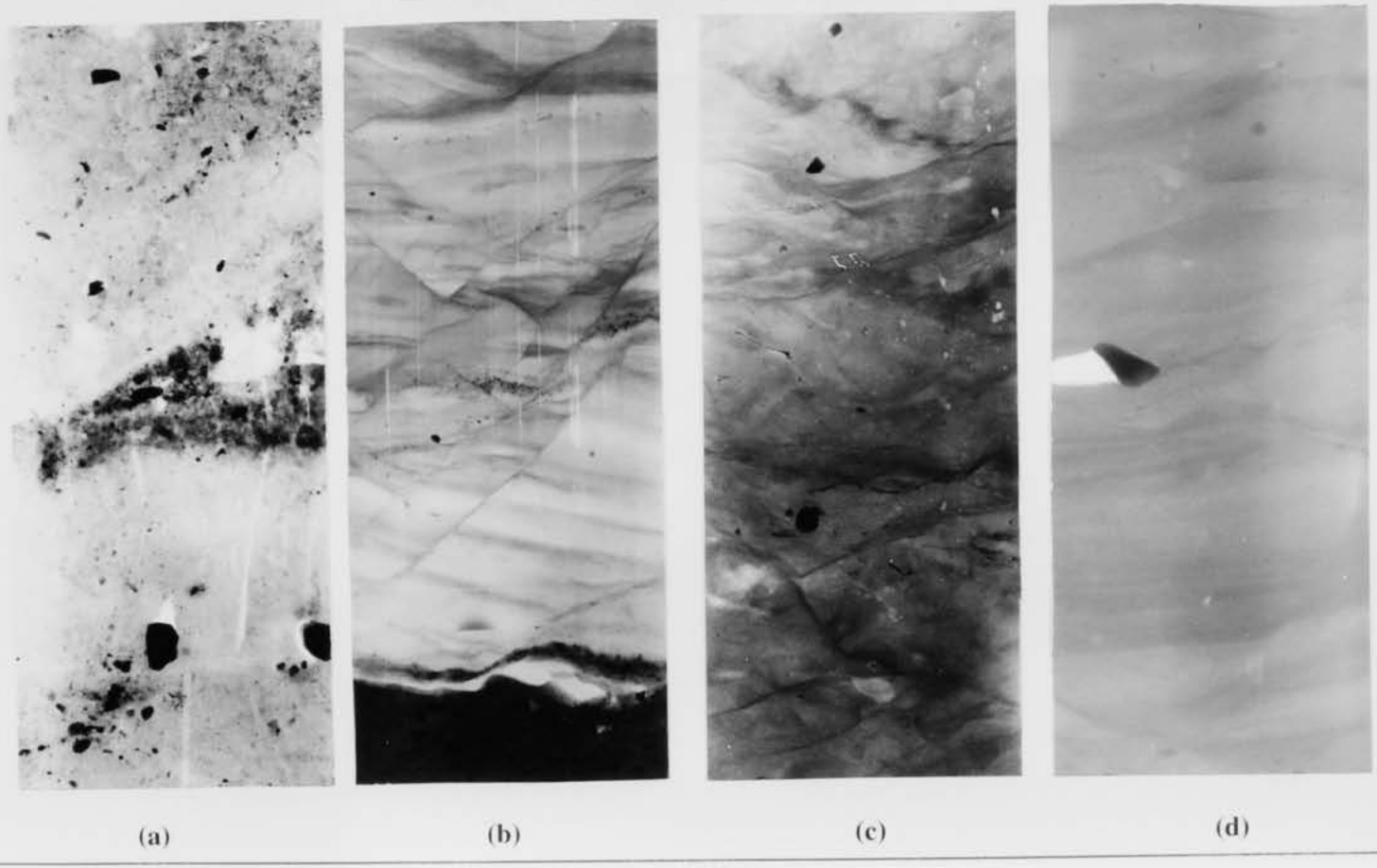
0
2
4
(cm)
6
8
10
(a)
(b)
(c)
(d)

Figure 4.4. X-radiographs illustrating the various sedimentary features associated with lithofacies identified from cores examined in this study. Lithofacies include:

a & b) Sandy mud couplets (SFc[m-l]) in PS2627 (lower continental slope). The facies comprises rhythmically intercalated sandy mud units organised into couplets. Consists of a lower unit of lensed to layered, homogeneous to mainly parallel and cross laminated sand to silt rich mud, and an upper unit of layered, predominantly homogeneous to occasionally parallel laminated clay rich mud. The units together display a fining upwards sequence. The lower boundary of the lower unit is sharp and wavey typical of scouring, and other boundaries are sharp and wavey to parallel. Laminations represent subtle changes in silt or sand grades in the upper unit, and silt rich mud and clay rich mud in the lower unit. Lenses are commonly infilled with cross bedded sands. Water escape structures are present in (b), and are directed upwards, representative of loading.

c & d) Bioturbated mud (Fb[d]) in PS2631 and PS2641 (outer fjord to inner continental shelf). The facies is massive and comprises intense bioturbation, appearing as a dense network of tiny burrows produced by polychaetes and termed *Chondrites*. These burrows are typically infilled with iron sulphide and appear as black flecks. The large structure to the top of (c) is a large unidentified burrow. The intermediate sized burrows, vertically aligned, are *Planolites*.

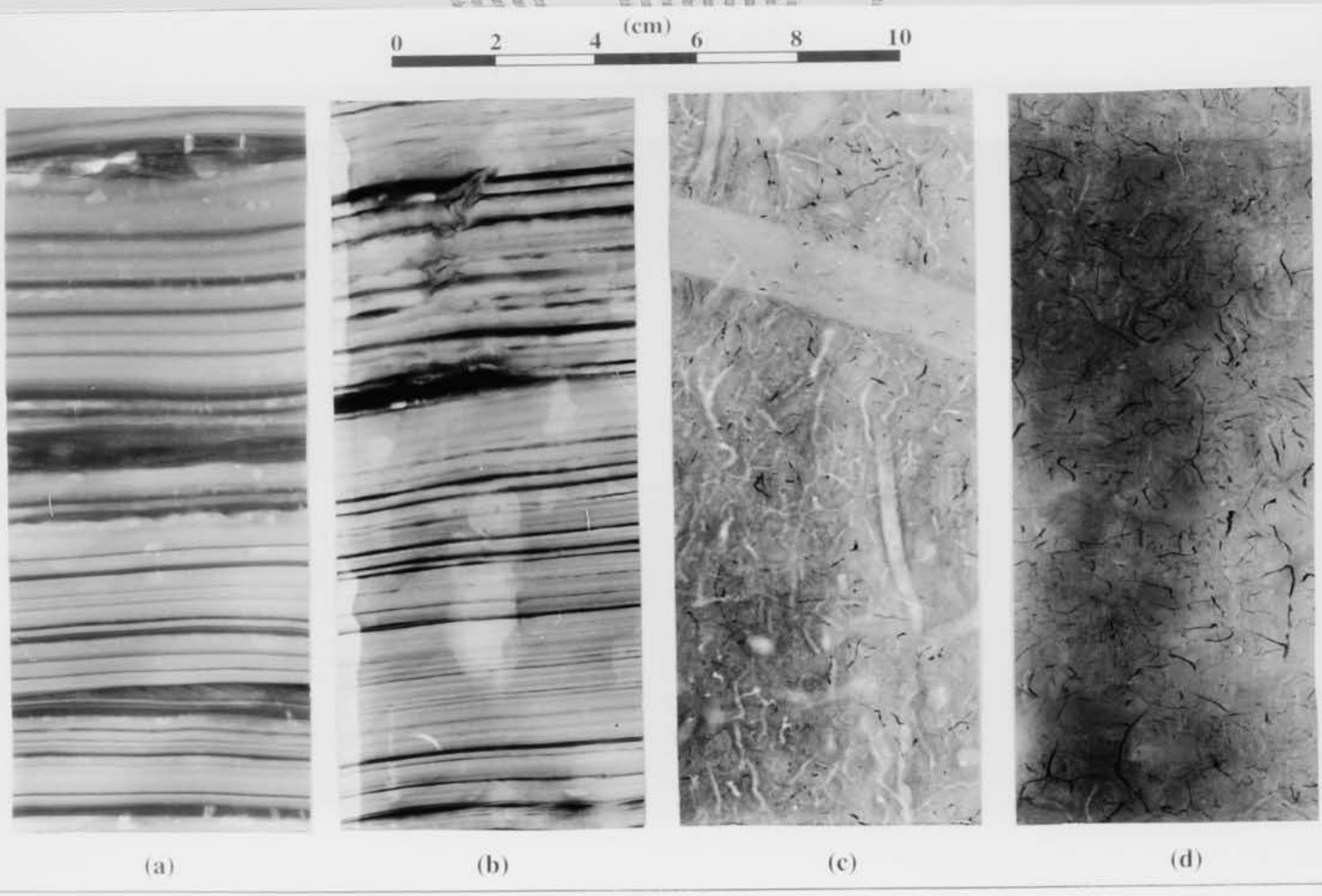
0
2
4
(cm)
6
8
10
(a)
(b)
(c)
(d)

Distribution and thickness: The distribution of the lithofacies is restricted to the mid and lower continental slope of the Kejser Franz Josephs fjord-shelf-slope transect (Fig 4.1). The lithofacies attains thicknesses of up to 18 cm occurring as units between core depths of 40-54 cm and 106-122 cm in PS2629, 20-31 cm, 140-168 cm, 176-194 cm, and 198-215 cm in PS2628 (mid slope), and 214-231 cm, 250-251 cm, 258-262 cm and 288-292 cm within PS2627 (lower slope).

4.3.5 Sandy mud (fine grained) couplets (lithofacies SFc[m-l])

Description: X-radiographs of this subfacies are presented in Figures 4.4a,b. The lithofacies comprises numerous rhythmically intercalated, very poorly sorted, sandy mud units organised into couplets. The colour of the lithofacies varies from brown (10YR 4/3) to dark grey (10YR 4/1) in PS2627, and dark greyish brown (10YR 4/2) to dark grey (10YR 4/1) in PS2628. The couplet consists of a lower unit of lensed to layered, homogeneous to mainly parallel and cross laminated sand to silt rich mud, and an upper unit of layered, predominantly homogeneous to occasionally parallel laminated clay rich mud (Figs 4.4a,b). Organised into couplets, the units represent a fining upward sequence. The laminae in the upper unit vary from discontinuous to continuous, regular to irregular, and horizontal to wavy (Figs 4.4a,b). In the upper unit, laminae are mainly laterally continuous and horizontal (Figs 4.4a,b). Laminations in the lower unit are recognised through subtle textural (grain size) changes in silt or sand grades. The upper unit laminations are alternations of silt rich mud laminae and clay rich mud laminae. Individual laminations are <2 mm thick (Figs 4.4a,b). The laminations occasionally exhibit climbing ripple morphology in PS2628. Typically, the lower unit ranges up to a maximum thickness of 8 mm, and 20 mm for the upper unit (Figs 4.4a,b). The lower unit is commonly lensed, thinning laterally into layers (Figs 4.4a,b). The lenses comprise cross bedded laminations. Occasionally, the units are punctured by water escape structures comprising upward directed wispy sediment (Fig 4.4b). The upper and lower boundaries of each unit within the couplet are, in general, well defined and sharp (Figs 4.4a,b). The lower boundary of the lower unit is typically wavey (Figs 4.4a,b). The upper unit is occasionally bioturbated exhibiting burrows that originate from the upper boundary.

Distribution and thickness: The distribution of the lithofacies is restricted to the mid and lower continental slope of the Kejser Franz Josephs fjord-shelf-slope transect (Fig 4.1). The lithofacies is present between core depths of 31 and 140 cm (thickness of 109 cm) in PS2628 (mid continental slope), and 38 and 214 cm (thickness of 176 cm) in PS2627 (lower continental slope).

4.3.6 Laminated mud (lithofacies Fl[d])

Description: X-radiographs of this lithofacies are presented in Figures 4.3b,c,d. The lithofacies comprises very poorly sorted, finely laminated muds (Fl[d]). The colour of the lithofacies varies from grey (5Y 5/1) to dark grey (5Y 4/1) in PS2633, grey (5Y 5/1) to olive grey (5Y 5/2) to dark

grey (5Y 4/1) in PS2631, and dark brown (10YR 4/3) to grey (5Y 5/1) in PS2641. The laminated sediments are composed predominantly of alternating layers of medium silt to clay rich mud in PS2633, PS2631 and PS2641, additional sand in PS2631 and PS2633, and limited gravel in PS2641.

In PS2641 the laminae are well defined, and vary from mainly parallel to wispy, regular to irregular, continuous to semi-continuous, and possess diffuse boundaries (Fig 4.3b). In PS2633 and PS2631, the laminae are predominantly diffuse, wavey to wispy to parallel occasionally developing into lenses, regular to mainly irregular, continuous to semi-continuous, and possess predominantly diffuse (gradational) to occasionally well defined boundaries (Fig 4.3c,d). In PS2633, the laminae occasionally grade or change into interspersed massive mud units. However, the laminae in PS2631 are disturbed by intense bioturbation (>50% of the sediment) whereby mottling greatly reduces the clarity of their appearance (Fig 4.3c). It is difficult to gauge the thicknesses of the individual laminae and intercalation cycle (coarse-fine cycle) due to the diffuse nature of the laminations. However, in PS2641 the individual laminae and intercalation cycles attain thicknesses of up to 12 mm each (Fig 4.3b). In PS2633 and PS2631, the individual laminae and intercalation cycles attain thicknesses of up to 35 mm and 42 mm, respectively, (Fig 4.3c,d).

Throughout all cores, the laminations are disturbed by sub-horizontal fault structures interpreted to result from either syn-sedimentary processes, or the action of coring. However, it is very difficult to ascertain the precise origin of these structures. In PS2641 the structures have a regular distribution and orientation exhibiting concave to straight inclined forms, which are typically aligned, resulting in rotation of sections within the unit (Fig 4.3b). In PS2631, the nature and orientation of the structures is dominated by irregular, wavey to straight forms (Fig 4.3c). Furthermore, in PS2631 and PS2633, macro-scale cross laminated structures are present. They are interpreted to be related to the deformation structures and not primary depositional features.

Gravel-sized clasts are present but not very common within the lithofacies. In general, the gravels vary from well dispersed to occasional clustering in all of the cores. However, the gravels in PS2641 form occasional layering. In PS2631, gravel and sand are well dispersed and more abundant and occasionally form units with gradational boundaries. The size of the gravels range up to a maximum size of 12 mm.

Distribution and thickness: The distribution of the lithofacies is restricted to the inner region of the Kejser Franz Josephs fjord-shelf-slope transect (Fig 4.1). The lithofacies forms the lowermost unit in both PS2633 (core depths 385-585 cm) and PS2631 (558-710 cm), and between 623-672 cm in PS2641. The unit attains minimum thicknesses of 149 cm in PS2631, and 200 cm in PS2633, and an absolute thickness of 49 cm in PS2641.

4.3.7 Homogeneous mud (lithofacies F[d])

General description of the lithofacies: The lithofacies comprises poorly to very poorly sorted, non graded, mud with variable amounts of gravel sized dropstones (F[d]). The mud facies is divided into

two subfacies; visually massive (Fm) and visually bioturbated (Fb). Both subfacies are readily distinguished by x-radiography. Even though both subfacies exhibit bioturbation, the type and percentage are used as a classification characteristic. The subfacies are outlined in the following sub sections.

Distribution and thickness of subfacies: The lithofacies is widely distributed along the Kejser Franz Josephs fjord-shelf-slope transect (Fig 4.1). The massive mud subfacies (Fm[d]) attain thicknesses of up to 334 cm, and occur between 51-385 cm in PS2633, 215-235 cm in PS2628, and 234-239 cm, 243-248 cm, 265-274 and 276-288 cm in PS2627. The bioturbated mud (Fb[d]) subfacies, in general, forms the uppermost unit in all cores except for PS2630 (mid continental shelf). The thickness varies from 34 cm in PS2627, 20 cm in PS2628, 40 cm in PS2629, 600 cm in PS2641, 558 cm in PS2631, and 258 cm in PS2632. In PS2630 the subfacies attains a thickness of 11 cm between core depths of 174-185 cm.

4.3.7.1 Massive mud with dropstones (subfacies Fm[d])

Description: X-radiograph of this subfacies is presented in Figure 4.2d. The lithofacies comprises very poorly sorted massive muds (Fm[d]). The colour of the lithofacies varies from grey to dark grey (5Y 5/1-5Y 4/1) in PS2633, dark greyish brown (10YR 4/2-2.5Y 4/2) to dark olive grey (5Y 3/2) in PS2627, and olive to olive grey (5Y 4/2) in PS2628. In addition, discontinuous silt bands and weak laminations are occasionally present, and attain thicknesses of up to 3 mm. Also in PS2633, sand lenses and layers are common, ranging up to 10 mm thick and possessing diffuse boundaries. The layers are most common between core depths of 212-340 cm. The lithofacies comprises variable amounts of gravels that are both widely dispersed, and concentrated into lenses and layers (Fig 4.2d). The general size of the gravels range up to 11 mm in PS2627, 10 mm in PS2628, and 4 mm in PS2630. The upper and lower boundaries of the lithofacies vary between gradational in PS2629 and PS2628 to sharp in PS2630 and PS2627, and is dependent upon the over and underlying facies. Bioturbation is present but subordinate to the massive nature. Typically, the bioturbation varies between very weak (<5% concentration) in PS2627, to weak (5-10% concentration) in PS2628, PS2629, and PS2630. Commonly, the bioturbation leaves the sediment mottled with burrow structures partially exhibited. The estimated concentration of biogenic material, comprising foraminifers and nannofossils, remains over 10 grain-% content in all cores.

4.3.7.2 Bioturbated mud with dropstones (subfacies Fb[d])

Description: X-radiographs of this subfacies are presented in Figures 4.4c,d. The lithofacies comprises poorly to very poorly sorted bioturbated muds (Fb[d]). The colour of the lithofacies varies from olive brown (2.5Y 4/3) to olive grey (10YR 4/1) in PS2632, dark brown (10YR 4/3) to dark grey (5Y 4/1) to dark olive grey (5Y 3/2) in PS2631, olive grey (5Y 4/2) in PS2630, dark olive grey 5Y 3/2) in PS2641, dark brown (10YR 4/3) in PS2629, and dark greyish brown (10YR 4/2) to dark brown (10YR 3/3) in PS2628 and PS2627. The lithofacies comprises variable amounts of gravels. In

more detail, the amount of gravel varies from rare in PS2627, PS2628, PS2629, PS2630 and PS2641, to more common in PS2631, PS2632 and PS2633. The gravels vary between mainly widely dispersed, to occasionally clustered. The size of the gravels range up to 11 mm in PS2633, 12 mm in PS2632, 11 mm in PS2631, 5 mm in PS2641, 4mm (although one gravel clast of up to 25mm is recorded) in PS2629, 5 mm in PS2628, and 5mm in PS2627.

Bioturbation is the predominant characteristic of the lithofacies, and may have destroyed any original sedimentary structures. However, weak laminations and sand lenses are occasionally present, particularly in PS2631 and PS2641. The concentration of the bioturbation varies from intense (>50%) in PS2632, PS2631 and PS2641, to moderate to weak (10-30%) in PS2630, PS2628, and PS2627. The lithofacies appears mottled, and heavily burrowed where the latter comprise a dense (50-70%) to very dense (>70%) network of individual burrows in PS2632, PS2631 and PS2641 (Fig 4.4c,d). The density of the burrows is less in PS2629, PS2628 and PS2627, where concentrations reach values of upto 25%. The burrows comprise: (i) predominantly narrow, dendritic and single to multi branched forms consistent with *Chondrites* (Fig 4.4c,d; e.g. Frey & Pemberton 1885; Marienfeld 1991, 1992a,b; Eyles et al. 1992; Andersen et al. 1995), (ii) very occasional large, vertically aligned, unlined forms distinct from the surrounding sediment and consistent with *Planolites* (Fig 4.4c; e.g. Pemberton & Frey 1982; Marienfeld 1991, 1992a,b; Eyles et al. 1992) and unidentified worm burrows and tubes. Commonly, the *Chondrites* are weakly to moderately pyritised, appearing black in x-radiographs (Fig 4.4c,d; e.g. Marienfeld 1991, 1992b). In PS2630, the bioturbation appears as mottling, although unidentified burrows are observed.

Table 4.3. Bivalvia and gastropoda species identified within lithofacies Fb(d) of PS2631 (outer Fjord), and PS2641 (inner continental shelf).

Macrofossils	Core number	Core depth (cm)
Bivalvia species		
Thyasira gouldi (Philippia)	PS2631	390
Bathyarca glacialis (Gray)	PS2641	413, 535, 554
Nucula tenuis (Bush)	PS2641	535
Portlandia fraterna (Verrill & Bush)	PS2641	565
		585
Gastropoda species		
Buccinum hydrophanum (Hancock)	PS2631	98 - 100
Buccinum finmarkium (verkruzen)	PS2631	98 - 100

In PS2631 and PS2641, black spots and horizons are present throughout the lithofacies representing organic rich sections. Black spots vary from common (40-230 cm in PS2631; 0-64 cm, 82-256 cm; 272-325 cm, 474-510 cm and 580-619 cm in PS2641) to abundant (490-558 cm in

PS2631; 64-82 cm, 256-272 cm, 325-474 cm and 510-580 cm in PS2641). Black layers (2.5Y 2/1) are less common and occur between 96-101 cm in PS2631 and 210 cm, 230-231 cm and 286 cm in PS2641. The estimated concentration of biogenic material, comprising foraminifers and nannofossils, remains <25 grain-% content in PS2631 and PS2641 and >30 grain-% in PS2630, PS2629, PS2628 and PS2627. In addition, several species of gastropoda and bivalvia were identified in PS2633, PS2632, PS2631 and PS2641 (Table 4.3).

4.3.8 Massive sand (Lithofacies Sm[d])

Description: The lithofacies comprises poorly sorted, weakly graded and structureless sand to silty sand, and appears dark grey (5Y 4/1) in colour. Minor gravels are present in PS2633, and vary from predominantly widely dispersed to occasionally clustered. The size of the gravels range up to 3 mm. The gravels consist wholly of rock fragments representing dropstones. In PS2627 the gravels tend to be very rare but protrude into the upper and lower boundaries when present. The lower and upper boundaries of the lithofacies are mainly diffuse, although occasionally well defined. The bioturbation of the lithofacies is absent as there is no biogenic content.

Distribution and thickness: The distribution of the lithofacies is restricted to PS2633 and PS2627 of the Kejser Franz Josephs fjord-shelf-slope transect (Figure 4.1). The lithofacies attains a thickness of 46 cm between a core depth of 5-51 cm in PS2633. In PS2627, the facies forms several discrete units of <3 cm thickness between 223-226 cm, 247-249 cm, 258-260 cm, and 290-291 cm.

4.4 GRAIN SIZE DISTRIBUTION

4.4.1 Introduction

The determination of the grain size distribution provides additional sedimentological detail important to the identification of lithofacies. This section will present the grain size distribution of each lithofacies. Measurements were performed on representative samples from the entire range of lithofacies. Some lithofacies (massive to bioturbated muds Fm-b(d) in PS2631 and PS2641) were distributed over considerable thicknesses, but their general homogeneity made it necessary for only a relatively small number of samples to be taken in order to represent the general grain size distribution. In the case of the laminated mud Fl(d) and sandy mud couplet SFc(m-l) facies, only composite samples could be obtained as the individual couplet units and laminae were too thin for enough sediment to be generated for the determination of the grain size distribution.

The fraction of sediment >500 µm in size within glacimarine lithofacies is considered an indicator of iceberg rafting and sedimentation, and termed iceberg rafted debris (IRD; cf. Section 3.3.4; Elverhøi et al. 1995). This iceberg index system can only be applied to sediment with

significant confidence beyond regions most proximal to the ice front, and other points of efflux, where sediment >500 μm could not be transported in meltwater and fluvial plumes discharged into the marine environment. The iceberg index is not applicable to sediment >500 μm in lithofacies deposited by subaqueous mass wasting processes, even though the original sediments may have derived through iceberg rafting. The weight percent of sediment >500 μm is displayed as downcore data in Figures 4.5 and 4.6.

The grain size distribution of the gravel, sand, silt and clay grades together with the graphic mean grain size and degree of sorting (inclusive of standard deviation) within each lithofacies are summarised in Table 4.2 and displayed as downcore data in Figures 4.5 and 4.6. The grain size distribution is further subdivided into whole phi intervals and displayed as lithofacies data in Figures 4.7 and 4.8. These illustrate the grain size distribution determined on all samples from each lithofacies. The grain size distribution corresponds to that within whole number phi intervals (e.g. 1-2 Φ or 500-250 μm) and determined as the distribution coarser than the corresponding phi class.

4.4.2 Diamicton (lithofacies Dmm)

The grain size of the resedimented sandy mud diamicton (Dmm[r]) comprises up to 9% gravel, <39% sand, <38% silt and <40% clay with a graphic mean grain size of 6.8-8.0 Φ and exhibits an extremely poor degree of sorting (Figs 4.6a,c,d). The sandy mud diamicton (Dmm) comprises upto 10% gravel, <43% sand, <32% silt and <40% clay with a graphic mean grain size of 6.0-8.0 Φ, and exhibits an extremely poor degree of sorting (Figs 4.5b, 4.6a,b). The sandy mud diamicton in PS2629 possesses a greater sand content (typically >30%) than that of the subfacies in PS2630 (typically <30%) (Fig 4.7a). In both subfacies, a significant proportion of the sand is distributed between 2-4 Φ (250-63 μm) where the distribution can reach maximum values of 16% within individual phi classes (Fig 4.7a). The proportion of the particles within grades >1 Φ (>500 μm) ranges up to 16% (Fig 4.7a). The sandy diamicton displays a much coarser grain size distribution centred around a graphic mean of 4.1-4.7 Φ (Fig 4.6a). The grain size comprises up to 13% gravel, <63% sand, <20% silt and <17% clay, and displays a very poor to extremely poor degree of sorting (Fig 4.6a). A significant proportion of the sand is distributed between 1-4 Φ (250-63 μm), where values reach a maximum of 30% within the individual phi classes (Fig 4.7a). The proportion of particles within grades >1 Φ (>500 μm) ranges up to 25% (Fig 4.7a).

4.4.3 Normally graded gravel - sand - mud (lithofacies G-S-Fng)

Grain size determination were performed on composite sediment samples encompassing the whole lithofacies thickness. The grain size of the normally graded sandy mud subfacies comprises 36% sand, 37% silt and 28% clay, with a graphic mean grain size of 6.6 Φ and a very poor degree of sorting (Fig 4.6d).

a) **PS2631**

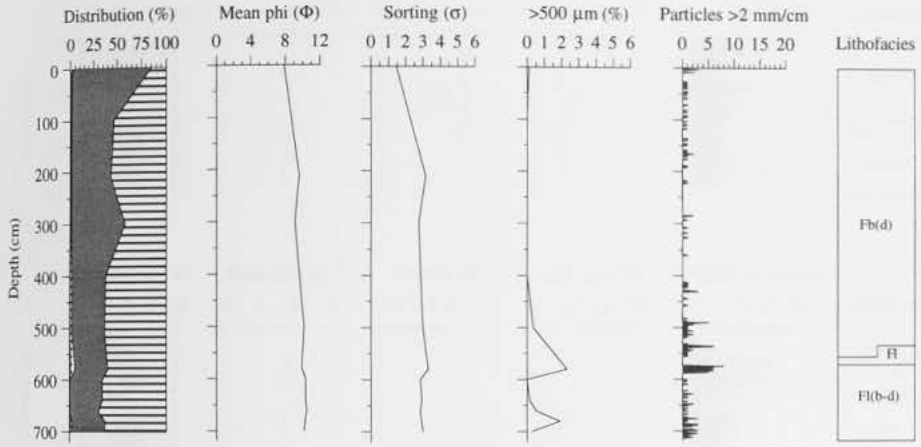

b) **PS2641**

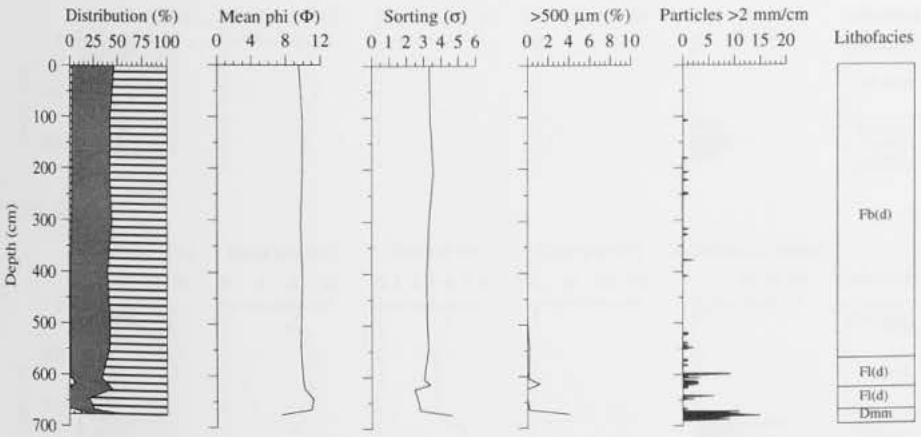

Figure 4.5a-b. The down-core and lithofacies variation in the grain-size properties of PS2632, PS2631, and PS2641 recovered along the Kejser Franz Joseph fjord-shelf-slope transect. Grain-size properties include distribution (%) of gravel (black shading), sand (stippled shading), silt (grey shading) and clay (hatched shading), mean grain-size (phi units), sorting (σ), distribution of particles >500 µm (1 Φ), and the number of particles >2 mm/cm (IRD). Lithofacies of Figure 4.1 are indicated.

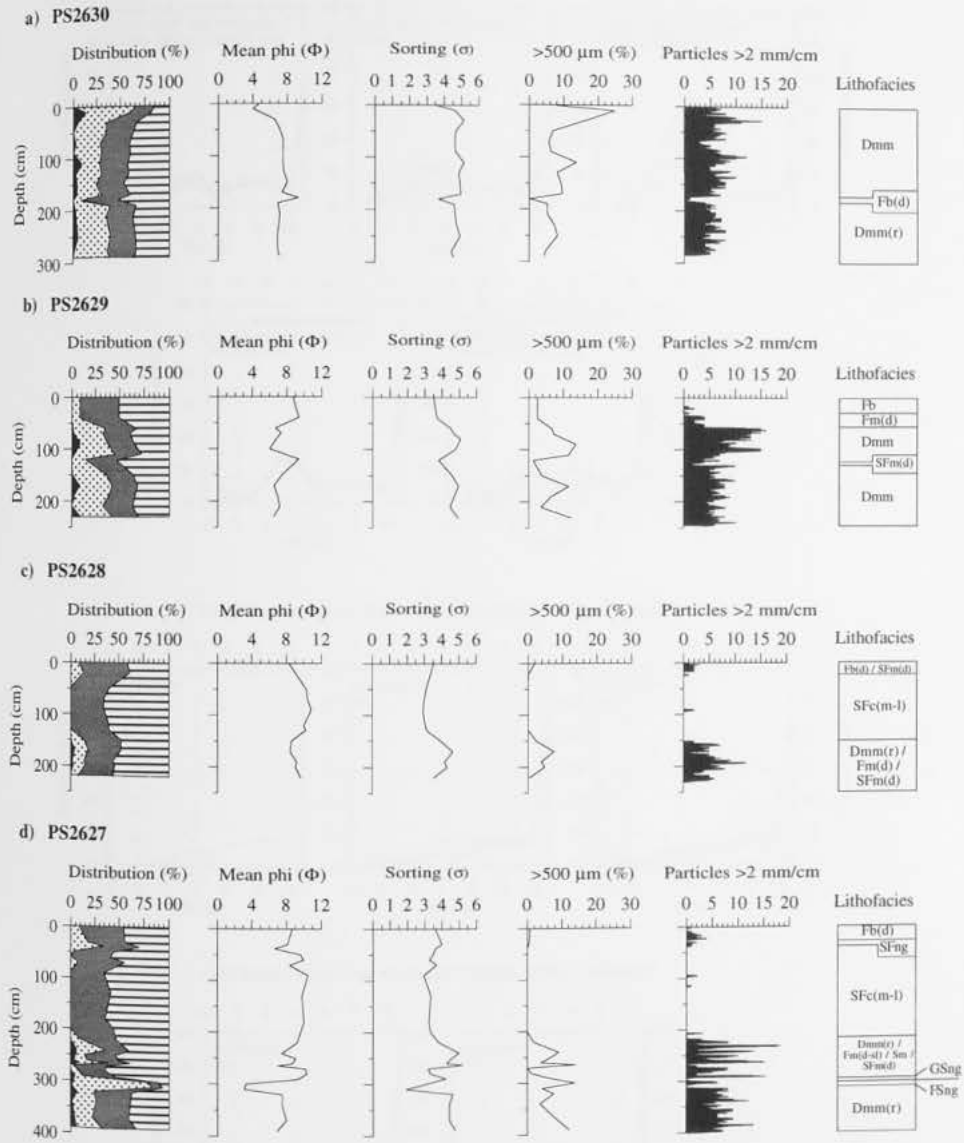

Figure 4.6a-d. The down-core and lithofacies variation in the grain-size properties of PS2630, PS2629, PS2628, and PS2627 recovered along the Kejser Franz Joseph fjord-shelf-slope transect. Grain-size properties include distribution (%) of gravel (black shading), sand (stippled shading), silt (grey shading) and clay (hatched shading) fractions, mean grain-size (phi units), sorting (σ), distribution of particles >500 µm (1 Φ) in size, and the number of particles >2 mm/ cm (IRD). Lithofacies of Figure 4.1 are indicated.

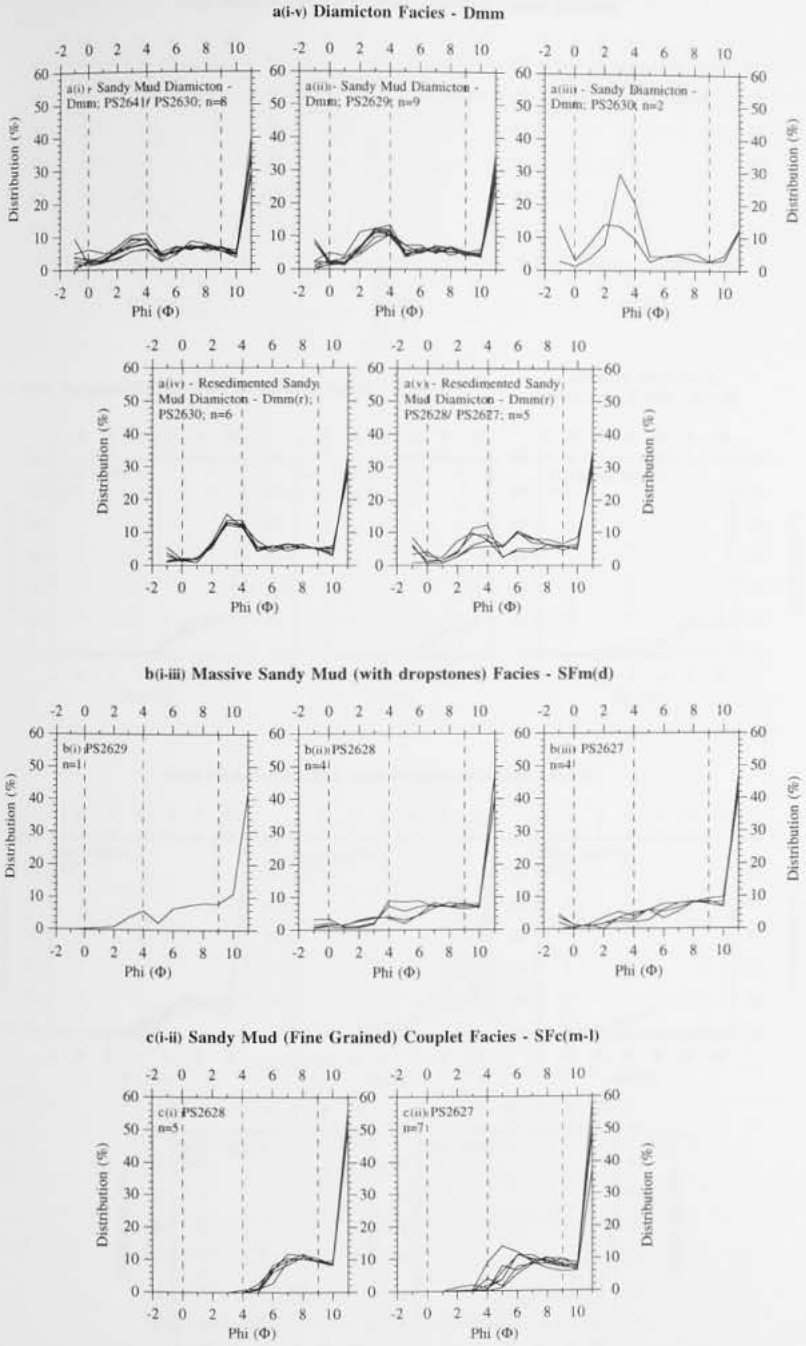

Figure 4.7a-c. Distribution of grain size within lithofacies identified from the cores recovered along the west-east transect through the mid to outer Kejser Franz Josephs Fjord and adjacent continental shelf and slope parallel to 73° N. The dotted lines represent the boundary between the clay-silt grades at 9 Φ, silt-sand grades at 4 Φ, and sand-gravel grades at 0 Φ. The plots for each lithofacies represent the grain size determined on a number of samples (n).

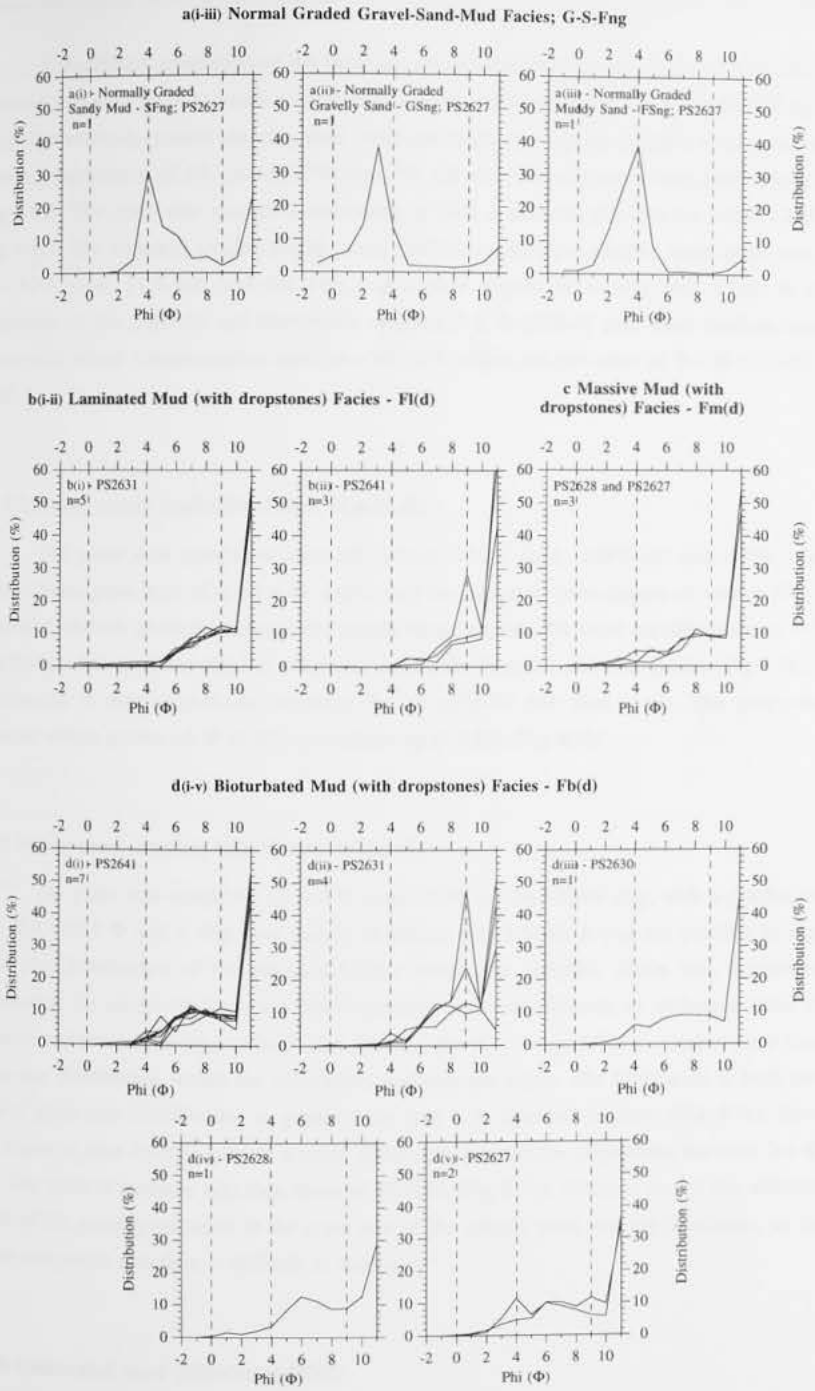

Figure 4.8a-d. Distribution of grain size within lithofacies identified from the cores recovered along the west-east transect through the mid to outer Kejser Franz Josephs Fjord and adjacent continental shelf and slope parallel to 73° N. The dotted lines represent the boundary between the clay-silt grades at 9 Φ, silt-sand grades at 4 Φ, and sand-gravel grades at 0 Φ. The plots for each lithofacies represent the grain size determined on a number of samples (n).

A significant proportion of the particles are distributed between 3-6 Φ (125-16 μm: fine sand to coarse silt) where values reach a maximum of 31% within the phi class of 3-4 Φ (125-63 μm) (Fig 4.8a). The normally graded gravelly sand subfacies displays a coarser graphic mean grain size of 3.3 Φ with a distribution of 3% gravel, 77% sand, 9% silt and 11% clay and a very poor degree of sorting (Fig 4.6d). The grain size reaches a maximum of 38% within the phi interval 2-3 Φ (250-125 μm) (Fig 4.8a). The normally graded muddy sand subfacies exhibits a graphic mean grain size of 3.1 Φ with 82% sand, 11% silt and 6% clay and a poor degree of sorting (Fig 4.6d). A significant proportion of the particles are distributed between 2-5 Φ (250-32 μm: fine/ medium sand to very coarse silt) where values reach a maximum of 39% within the phi class of 3-4 Φ (125-63 μm) (Fig 4.8a).

4.4.4 Massive sandy mud (lithofacies SFm[b-d])

The grain size comprises upto 4% gravel, <14% sand, <48% silt and <56% clay, with a graphic mean grain size of 8.6-9.4 Φ, and a very to extremely poor degree of sorting (Fig 4.6b,c,d). In general, the silt grade throughout the sample range appears the most variable between 4-7 Φ (63-8 μm: fine sand to medium silt) but consistent within the finer silt and clay grades (Fig 4.7b). The sand distribution is most significant between 2-4 Φ (250-63 μm: fine sand). The proportion of the particles within grades >1 Φ (>500 μm) ranges up to 6.8% (Fig 4.7b).

4.4.5 Sandy mud couplets (lithofacies SFc[m-l])

The grain size comprises up to 9% sand, <47% silt and <66% clay, with a graphic mean grain size of 8.4-10.9 Φ and a very poor degree of sorting (Fig 4.6c,d). It was not possible to ascertain the grain size distribution of the individual units within the couplets. Grain size determination was undertaken on composite samples encompassing variable mixtures of sediment from individual couplets and their associated units. It also follows that it is not possible to ascertain any trends in the grain size distribution within the lithofacies, and between cores. The lithofacies in both cores reveal similar grain size distributions in grades finer than 6 Φ (fine silt to clay) (Fig 4.7c). However, the lithofacies in core PS2627 reveals a more significant distribution of particles between 2-6 Φ (250-16 μm: fine sand to medium silt) than those of PS2628 (Fig 4.7c). Whether or not this difference is the result of the primary variation in the grain size of the couplet units and the lithofacies, or the product of the composite sampling is difficult to ascertain.

4.4.6 Laminated mud (lithofacies Fl[d])

The grain size comprises up to 1% gravel, <5% sand, <35% silt and <79% clay, with a graphic mean grain size of 9.9-11 Φ and a very poor degree of sorting (Figs 4.5a,b). It was not possible to

ascertain the grain size distribution of the individual laminae. Therefore, grain size determination was only possible on composite samples which encompassed variable mixtures of sediment from the coarse and fine grained laminae. Figure 4.8b illustrates that the grain size distribution is relatively more variable between samples from PS2641 but less so in PS2631. The lithofacies in both cores reveal a predominance of particles with grades finer than 8 Φ (4 μm: very fine silt) (Fig 4.8b). However, the lithofacies in core PS2631 reveals a greater percentage of particles coarser than 8 Φ (4 μm: very fine silt) (Fig 4.8b). Sand and gravel grades between -1 to 4 Φ (>2000-63 μm: gravel to fine sand) are documented in PS2631 but not in PS2641 (Fig 4.8b). Whether or not these differences are a result of the primary variation in the grain size of the individual laminae and lithofacies, or the product of the composite sampling, is not clear.

4.4.7 Homogeneous (massive to bioturbated) mud with dropstones (lithofacies Fm-b[d])

The grain size of the bioturbated mud subfacies comprises <9% sand, <50% silt and <64% clay, with a graphic mean grain size of 7.9-10.2 Φ, and a very poor to poor degree of sorting (Figs 4.5, 4.6). Marked variability is documented in the grain size distribution of this subfacies between cores, and of individual samples. In PS2641 and PS2631, a significant proportion of particles are in grades finer than 7 Φ (8 μm: medium silt to clay) (Fig 4.8d). Furthermore, the low proportion of particles in grades between 2-7 Φ (250-8 μm: fine sand to medium silt) is much greater in PS2641 than that of PS2631 (Fig 4.8d). In PS2630, PS2628, and PS2627, particles are concentrated mainly in the grades finer than 6 Φ (16 μm: coarse silt to clay) (Fig 4.8d). The grain size of the massive mud subfacies comprises <8% sand, <36% silt and <64% clay, with a graphic mean grain size of 9.7-10.3 Φ and a very poor degree of sorting (Fig 4.6c,d). In both PS2628 and PS2627, the lithofacies reveal a significant distribution of the grains in grades finer than 6 Φ (16 μm: medium silt to clay) but grades coarser than 6 Φ are present (Fig 4.8c). The proportion of particles within grades >1 Φ (>500 μm) is virtually negligible (<0.5%) in PS2628 and PS2627 (Fig 4.8c).

4.4.8 Massive Sand (Sm[d])

The grain size distribution was not determined on samples from the massive sand facies. The facies is distributed in very thin units (<1 cm) and, therefore, not enough sediment was available for grain size measurement.

4.5 DOWNCORE AND LITHOFACIES DISTRIBUTION OF PARTICLES >2 mm/cm

4.5.1 Introduction

Particles >2 mm/cm in glacimarine lithofacies is considered an indicator of iceberg rafting and sedimentation, and termed iceberg rafted debris (IRD; cf. Section 3.3.4; Grobe 1987). The contribution of debris >2 mm/cm from sea ice rafting is negligible as ice floes consist predominantly of fine grained sediment i.e. <63 μm (cf. Section 3.3.4; Pfirman et al. 1989, 1990; Wollenburg 1993; Nürnberg et al. 1994). The iceberg index is not applicable to particles >2 mm/cm in lithofacies deposited by subaqueous mass wasting processes, even though the original sediments may have been derived through iceberg rafting. The distribution of particles >2 mm/cm was determined in each of the cores recovered along the Kejser Franz Josephs fjord-shelf-slope transect. The method adopted for determining the amount of particles >2 mm/ cm is discussed in Section 3.3.4.

This section documents the downcore and lithofacies distribution of particles >2 mm/cm for each of the cores of the study area. The downcore distribution of particles >2 mm/cm in each core are illustrated in Figures 4.5, 4.6 and 4.9, and summarised in Table 4.2. The implications of the distribution of particles >2 mm/cm will be discussed in association with the interpretation of lithofacies in Section 4.7.

4.5.2 Continental slope

The uppermost 153 cm of sediment in PS2628 and 218 cm in PS2627 are characterised by an absence of particles >2 mm/cm. This corresponds to the massive mud and sandy mud couplet facies in PS2627 and PS2628 (Figs 4.1, 4.6, 4.9). However, occasional particles are documented in the uppermost 30 cm of sediment of both cores. The lowermost 153 cm of sediment in PS2628, and that between 218-290 cm in PS2627, are characterised by an abrupt increase in values that reach up to 18 particles/ cm >2 mm in size. The distribution in these sections of core exhibit pronounced high amplitude fluctuations which correspond to the resedimented sandy mud diamicton, sandy mud, and massive mud facies (Figs 4.1, 4.6, 4.9). Below a depth of 310 cm in PS2627, the sediment is characterised by a less variable number of particles >2 mm/cm that range up to 13, and correspond to the resedimented sandy mud diamicton (Figs 4.1, 4.6, 4.9). Below a depth of 58 cm in PS2629, values range up to 16 particles/ cm >2 mm, and exhibit pronounced fluctuations. The highest number of particles >2 mm/cm occur between 56-126 cm which corresponds to the upper sandy mud diamicton facies (Figs 4.1, 4.6, 4.9). Marked peaks in the number of particles >2 mm/cm occur at core depths between 48-81 cm, 96-103 cm, 131 cm, 159 cm, and 240 cm. A marked decrease in values to 3 particles/ cm >2 mm in size occurs between core depths 126-130 cm, and correspond to the sandy mud facies (Figs 4.1, 4.6, 4.9).

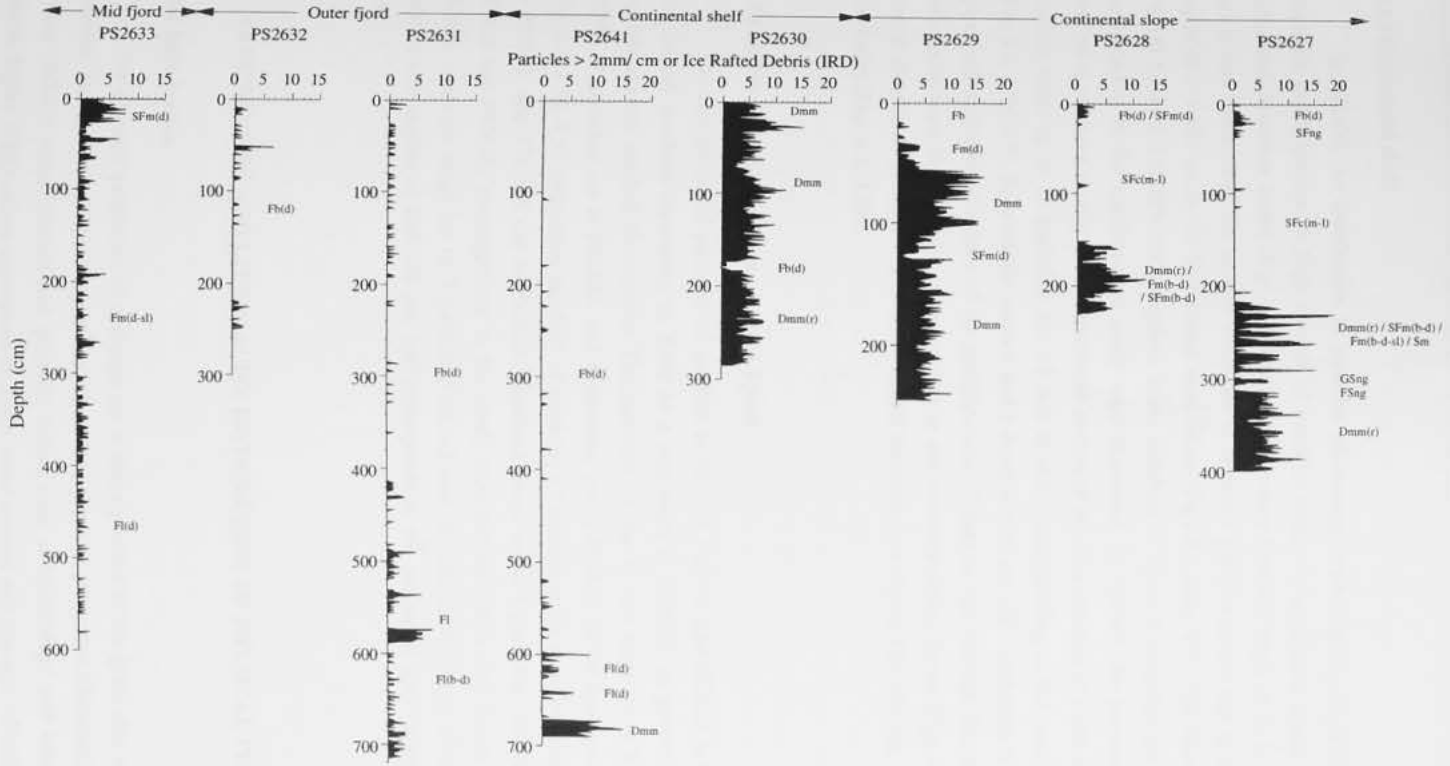

Figure 4.9. Coarse particle counts (particles >2 mm/cm), also termed ice rafted debris (IRD), from eight cores, recovered along a west-east transect parallel to 73° N through the mid to outer Kejser Franz Josephs Fjord system and adjacent continental shelf and slope (Figure 1.1). The lithofacies illustrated in the sedimentological logs of Figure 4.1 are indicated. For the exact position of the lithofacies boundaries the reader is directed to the sedimentological logs in Figure 4.1.

4.5.3 Continental shelf

In PS2630, the distribution of particles >2 mm/cm exhibits strong fluctuations of moderate amplitude and frequency. A high number of particles occurs between core depths 0-173 cm in the sandy mud diamicton facies (Figs 4.1, 4.6a, 4.9). Numbers typically range up to 15 particles/ cm >2 mm in size. Conversely, the number decreases to around 1 particle/ cm >2 mm in size between core depths of 174-182 cm in the bioturbated mud facies (Figs 4.1, 4.6a, 4.9). The lowermost section of PS2630 between 182-285 cm comprises lower numbers of up to 8 particles/ cm >2 mm in size, corresponding to the resedimented sandy mud diamicton. In PS2641, the number of particles >2 mm/ cm is restricted mainly to the lowermost section of the core between 671-689 cm. At this depth, numbers range up to 15 particles/ cm >2 mm in size, corresponding to the sandy mud diamicton (Figs 4.1, 4.5b, 4.9). Between the surface and a depth of 620 cm, the distribution of particles is very sparse and restricted to values of <2 particles/ cm >2 mm in size (though this increases up to 9 particles between 600-620cm), corresponding to the bioturbated mud facies (Figs 4.1, 4.5b, 4.9). A general absence of particles >2 mm/cm occurs between core depths 625-671 cm, in the laminated mud facies (Figs 4.1, 4.5b).

4.5.4 Mid to outer Kejser Franz Josephs Fjord

The distribution of particles >2 mm/cm in PS2633, PS2632 and PS2631 is relatively sparse, with overall numbers increasing up fjord to a maximum in PS2633. In general, the number of particles exhibits marked fluctuations. The numbers >2 mm in size range up to 5 particles/ cm in PS2631, 7 particles/ cm in PS2632, and 4 particles/ cm in PS2633, in the homogeneous mud facies (Fig. 4.1, 4.5a, 4.9). Maximum numbers of particles >2 mm/cm occur between core depths 0-48 cm in PS2633, and 574-588 cm in PS2631. Numbers range up to 8 particles/ cm >2 mm in size in PS2633 and PS2631, corresponding to the sandy mud and laminated mud facies, respectively. In PS2631, numbers range up to 3 particles/ cm >2 mm in size, exhibiting a common distribution between core depths of 600-710 cm, and corresponds to the laminated mud facies (Fig. 4.1, 4.5a, 4.9).

4.6 DOWNCORE AND LITHOFACIES DISTRIBUTION OF PHYSICAL PROPERTIES

4.6.1 Introduction

The physical properties of sediment are a direct product of the grain size and nature of the sediment, and the processes of deposition. Therefore, physical properties characterised by wet bulk density (WBD), water content and porosity reflect core sedimentology and lithofacies type. In general, higher WBD values correspond to lower water content and porosity reflecting coarser grain size of sediments and/ or greater consolidation of sediment (Keller et al. 1979). In contrast, lower

WBD values correspond to higher water content and porosity reflecting finer grain size of sediments and/or normal consolidation of sediment (Keller et al. 1979). The physical properties are included in this study as (i) they provide additional lithofacies data that aid the interpretation of the processes of deposition (Section 4.7), and (ii) they are used in the calculations of mass accumulation rates (Section 6.7). The methods adopted in determining these parameters are discussed in Section 3.4. This section outlines the downcore and lithofacies variations of the water content (%), porosity (%) and wet bulk density (g cm^{-3}). The downcore variations in the physical properties are illustrated in Figures 4.10 and 4.11.

4.6.2 Continental slope

The bioturbated mud facies in the uppermost sediment of each core are characterised by low WBD (<1.9 g cm^{-3}), and high porosity (<77%) and water content (<54%). Within the sandy mud couplet facies of PS2627 and PS2628, the WBD remains low (<1.8 g cm^{-3}), and the porosity (<71%) and water content (<46%) decrease to low values. Furthermore, the water content and porosity decreases, and the WBD increases down facies in PS2627. Higher maximum porosity and water content values occur within PS2628, and lower minimum WBD values occur between 30 cm and ca. 110 cm in PS2628. At the base of PS2628 (below 150 cm) and between 214-290 cm in PS2627, the WBD (1.6-1.9 g cm^{-3}), porosity (48-66%) and water content (25-41%) are variable and correspond to resedimented muddy sand diamicton, sandy mud and massive mud facies. An abrupt increase in the WBD (2.3-2.6 g cm^{-3}), and decrease in the porosity (<30%) and water content (<13%) occurs between 290-310 cm which corresponds to the normal graded muddy sand and gravelly sand subfacies. Within the resedimented sandy mud diamicton at the base of PS2627, the WBD are high (2.0-2.4 g cm^{-3}), and the porosity (<43%) and water content (<22%) low. Similarly for the sandy mud diamicton throughout PS2629, the WBD are high (1.7-2.4 g cm^{-3}), and the porosity (<47%) and water content (<25%) low. The WBD attain low values (1.6-1.7 g cm^{-3}) and the porosity (<64%) and water content (<39%) to high values at a core depth of 120-130 cm, which corresponds to a sandy mud facies.

4.6.3 Continental shelf

The sandy mud diamicton in PS2630 is characterised by high WBD (up to 2.2 g cm^{-3}), and low porosity (<54%) and water content (<29%). The sandy diamicton forming the top 20 cm of PS2630 reveal high WBD (2.3-2.4 g cm^{-3}), and low porosity (20%) and water content (8%). The resedimented sandy mud diamicton in the lowermost 190 cm of PS2630 is characterised by high WBD (2.1-2.3 g cm^{-3}), and low porosity (<41%) and water content (<20%). At a depth of 180-190 cm the bioturbated mud facies comprises the lowest WBD (1.78 g cm^{-3}), and the highest porosity (56%) and water content (31%) in the core.

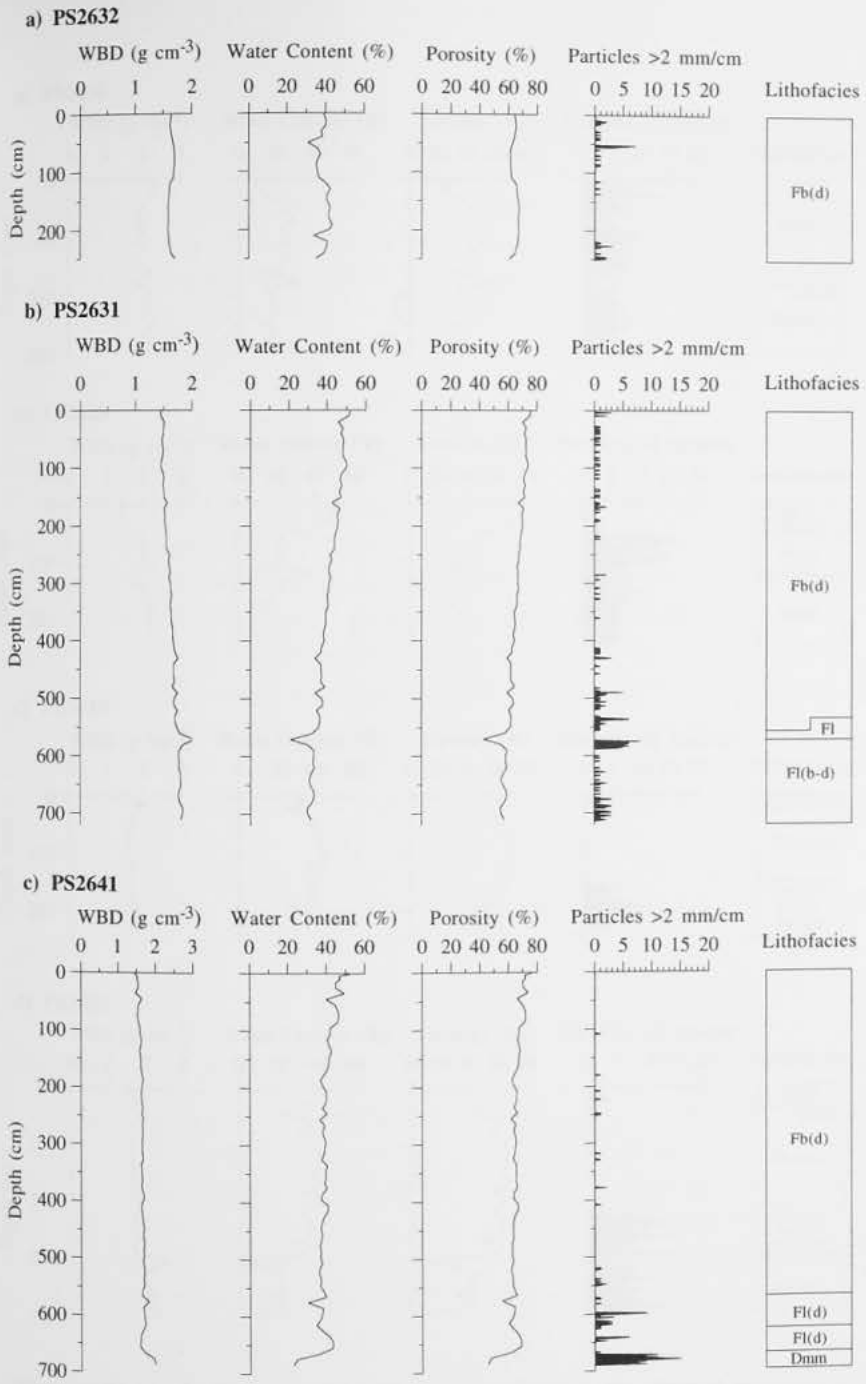

Figure 4.10a-c. The down-core and lithofacies variation in the physical properties of PS2632, PS2631, and PS2641 recovered along the Kejser Franz Joseph fjord-shelf-slope transect. Physical properties include wet bulk density (WBD), water content, porosity, and the number of particles >2 mm/cm (IRD). Lithofacies of Figure 4.1 are indicated.

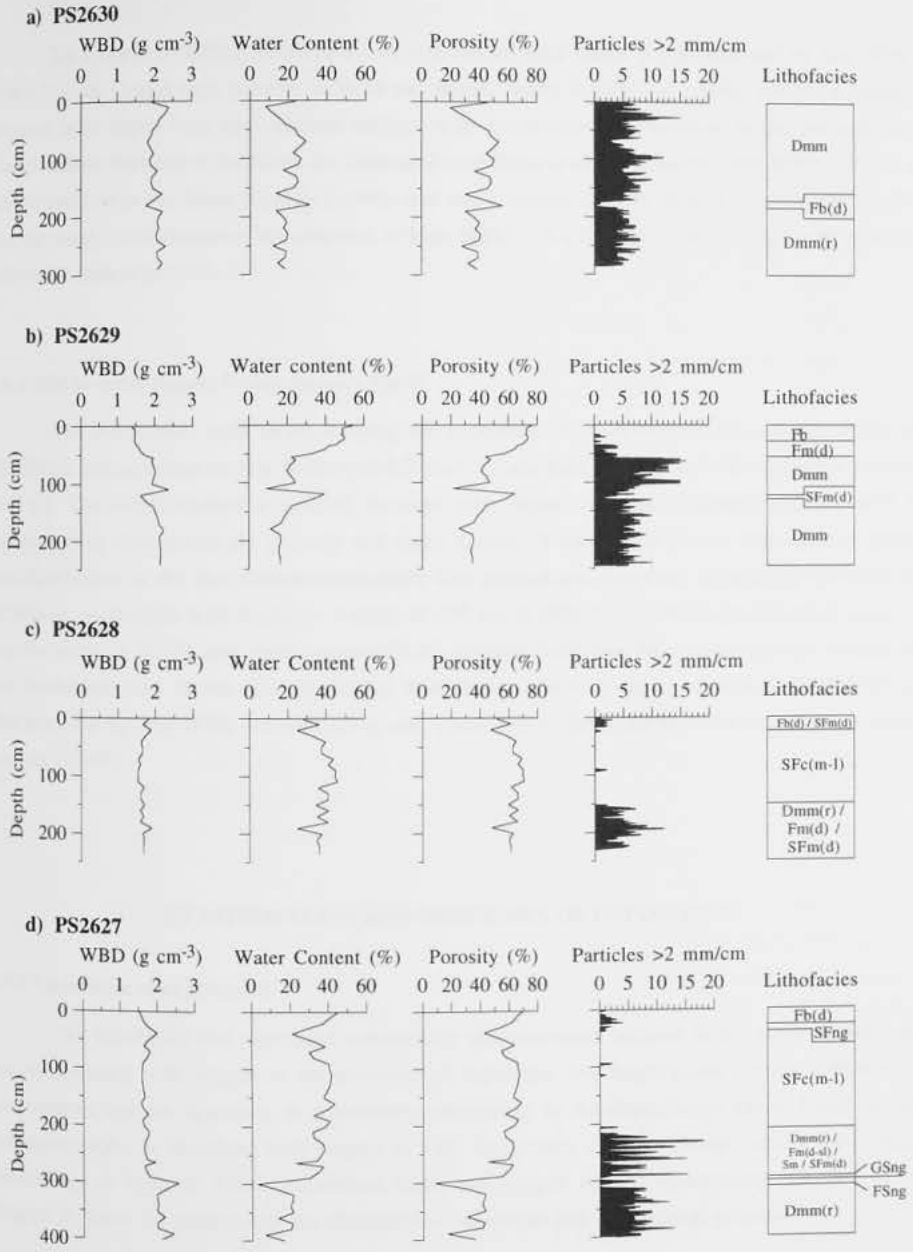

Figure 4.11a-d. The down-core and lithofacies variation in the physical properties of PS2630, PS2629, PS2628, and PS2627 recovered along the Kejser Franz Joseph fjord-shelf-slope transect. Physical properties include wet bulk density (WBD), water content, porosity, and the number of particles >2 mm/cm (IRD). Lithofacies of Figure 4.1 are indicated.

To a depth of 625cm in PS2641, the bioturbated mud facies is characterised by low WBD (1.4-1.7 g cm^{-3}), and high porosity (<76%) and water content (<52%). The WBD reveals a gradual increase with depth from the sediment surface, with a corresponding decrease in the porosity and water content. Between 625-675cm, the laminated mud facies is characterised by low WBD (1.6-1.7 g cm^{-3}), and low to moderate porosity (<69%) and water content (<43%). Below a core depth of 675 cm, the sandy mud diamicton is composed of high WBD (1.9-2.0 g cm^{-3}), and low porosity (<48%) and water content (<24%).

4.6.4 Mid to outer Kejser Franz Josephs Fjord

The bioturbated mud facies forming the uppermost 550 cm of PS2631, and the whole of PS2632, is characterised by low WBD (1.4-1.7 g cm^{-3}), and high porosity (<76%) and water content (<52%). The WBD reveals a gradual increase with depth from the sediment surface, with a corresponding decrease in the porosity and water content. These trends are not explained by grain size distribution as the core remains consistently fine grained and, therefore, is probably the result of increasing compaction with depth. At a depth of 570 cm in PS2631, the WBD increase (2.0 g cm^{-3}), and the porosity (43%) and water content (21%) decrease reflecting the coarser grained content of the laminated mud facies. The laminated mud facies below a depth of 580cm in PS2631 is characterised by low WBD (around 1.8 g cm^{-3}) and low to moderate porosity (<59%) and water content (<33%).

4.7 LITHOFACIES AND PROCESSES OF DEPOSITION

4.7.1 Lithofacies interpretation

The lithofacies and associated sedimentary characteristics outlined in the previous Sections are interpretated with respect to the processes of deposition and implications for the sedimentary environment and ice dynamics. A preliminary chronology of the depositional events based on the lithostratigraphy is discussed with respect to Late Quaternary climatic change, and a more exact chronology in light of AMS radiocarbon dates and oxygen isotope stratigraphy (Chapter 6) in Chapter 7. Table 4.4 summarises the characteristic lithofacies and depositional processes.

4.7.2 Diamicton (lithofacies Dmm)

Diamicton facies occurring within glacier-influenced marine settings are interpreted to have originated from (i) subglacial deposition, (ii) iceberg rafting, and (iii) subaqueous mass wasting.

Therefore, besides the sedimentary characteristics, diamicton thickness, lateral continuity, and contacts and association with overlying and underlying facies are important features used in identifying the process of deposition (Dowdeswell et al. 1994a). Commonly, acoustic records are used together with cores, to establish the thickness and lateral continuity, and these are introduced in Chapter 5. However, the sedimentary characteristics described above are sufficient to identify the processes of deposition resulting in this facies.

4.7.2.1 Resedimented sandy mud diamicton (subfacies Dmm[r])

This lithofacies is found in PS2630, PS2628 and PS2627, where it is associated with the sandy mud and massive mud facies of PS2628 and PS2627 on the mid and lower continental slope, respectively. Core PS2630 is located in the lee of a bathymetric high on the mid continental shelf (Sections 3.2.1, 5.3.3). The well defined upper and lower contacts with neighbouring facies representative of erosion, the occasional imbrication of gravel and shear lineations within the finer sediment grades, dispersed gravels, non bioturbation, and occurrence on or proximal to slopes imply an origin through subaqueous mass-flows (cf. Cook 1979; Nardin et al. 1979; Wright & Anderson 1982; Wright et al. 1983; Anderson et al. 1983; Hill 1984; Pickering et al. 1989; Yoon et al. 1991; Laberg & Vorren 1995, 1996). The high number of particles >2 mm/cm and the distribution of particles >500 μm suggest that iceberg rafting was the original process of deposition as it is the only reasonable process for transporting coarse sediments into glacier distal zones of the continental shelf and slope. The mass-flows result from sediment instability and failure, triggered through mechanisms that involve the build up of excess pore fluid pressure in rapidly accumulating glacigenic deposits, sedimentational and tectonic oversteepening of the sediment pile, iceberg turbation, and/or earthquake activity (Syvitski 1989; Laberg & Vorren 1995; Dowdeswell et al. 1996; King et al. 1996; Elverhøi et al. 1997).

The uppermost section of the lowermost diamicton in PS2630 on the mid continental shelf, reveals strong imbrication of gravels and shear lineations within the supporting matrix, indicative of shearing within the flow (Nardin et al. 1979). As the main part of the sediment is totally homogeneous, it is more likely the facies was emplaced by a debris flow rather than sliding/slumping, as internal organisation and structure is expected from the latter processes (cf. Cook 1979; Nardin et al. 1979; Hill 1984; Yoon et al. 1991; Stow 1992). The minor flow/shear structures observed in this facies would be explained by the debris flow (cf. Nardin et al. 1979). An origin from debris flow is supported by further evidence from acoustic records (Sections 5.7.3, 5.9.3).

The numerous diamicton units on the slope (PS2628 and PS2627) are composed mainly of widely dispersed gravels exhibiting no internal organisation suggestive of debris flow emplacement. It is unlikely the facies is a direct product of iceberg rafting as (i) the facies is confined to distinctive units bordered by sharp boundaries typical of intense erosion and, (ii) its disimilarity to neighbouring sandy mud facies (Section 4.7.2.3) in which iceberg rafting is a major contributing process.

Lithofacies	Subfacies	Depositional Processes
Diamicton	Resedimented sandy mud diamicton	Subaqueous mass wasting derived from debris flows.
	Sandy mud diamicton	Rain out and quasi-instantaneous dumping of debris from continuous supply of melting and overturning icebergs. Silt and clay grades derived from: i) slow suspension settling of debris of meltwater origin; ii) settling of iceberg and sea ice rafted debris; iii) suspension settling of pelagic debris.
	Sandy diamicton	Original process of deposition similar to that described for the sandy mud diamicton. Post depositional modification occurs whereby the silt and clay grades are winnowed through the activity of the East Greenland Current on the shelf leaving a sandy diamicton lag.
Normal graded gravel-sand-mud	Sandy mud	Low concentration turbidity current.
	Gravelly mud	
	Muddy sand	
Massive sand		Low concentration turbidity current.
Massive sandy mud with dropstones		Rain out and suspension settling sedimentation within ice distal glacimarine settings. Composed of gravel and sand grades introduced through an enhanced but fluctuating supply of icebergs, and silt and clay grades supplied through: i) slow suspension settling of fine material of meltwater origin. Dominates fjord sedimentation; ii) settling of pelagic debris (biogenic and lithic). Dominates slope sedimentation; iii) settling of iceberg and sea ice rafted debris; iv) redeposition of sea-floor sediments reworked through the activity of bottom currents at the shelf break and on the slope.
Sandy mud couplets		Periodic, low concentration distal turbidity currents.
Laminated mud		Ice distal sedimentation from the suspension settling from surface turbid meltwater plumes. Laminations result from periodic, non-rhythmic fluctuations in meltwater/ sediment discharge and tidal - wind dynamics. In the outer fjord/ inner shelf, sedimentation is contemporaneous with the deposition of gravel and sand from icebergs, and settling of pelagic debris. Iceberg sedimentation increases towards the mid region of the fjord.
Homogeneous mud	Massive mud with dropstones	Rain out and suspension settling sedimentation within ice distal glacimarine settings. Composed of gravel and sand grades introduced through a reduced but fluctuating supply of icebergs, and silt and clay grades derived through: i) slow suspension settling of fine material of meltwater origin. Dominates fjord sedimentation related to the proximity of meltwater outflows; ii) settling of pelagic debris (biogenic and lithic). Dominates slope sedimentation reflecting open marine conditions; iii) settling of iceberg and sea ice rafted debris; iv) redeposition of sea-floor sediments reworked through the activity of bottom currents. Iceberg sedimentation is at a maximum within the mid fjord setting.
	Bioturbated mud with dropstones	Rain out and suspension settling sedimentation within ice distal settings. Composed of gravel and sand grades introduced through occasional supply of icebergs which reveals a gradual increase towards the mid fjord reflecting proximity to tidewater glaciers. Silt and clay grades derived through: i) slow suspension settling of fine material of meltwater origin. Dominates fjord and inner shelf sedimentation, and less so on the slope; ii) settling of pelagic debris (biogenic and lithic). Dominates slope sedimentation and decreases across the shelf and into the fjord; iii) redeposition of sea-floor sediments reworked through the activity of bottom currents. Thought to be most active within mid/ outer fjord and on the inner shelf in relation to the presence of basins. *Chondrites* and flecking by iron sulphides may reflect bottom water anoxia in the mid/ outer fjord and on the inner shelf.

Table 4.4. Characteristic lithofacies and depositional processes from the west-east transect through the mid to outer region of Kejser Franz Josephs Fjord and the adjacent continental shelf and slope parallel to 73°N.

On the upper slope, the sandy mud diamictons of PS2629 are interpreted to originate from mainly iceberg rafting (Section 4.7.2.2) as opposed to subaqueous mass wasting. This is based on (i) the presence of gradational boundaries with a sandy mud facies (Section 4.7.2.3) separating the diamicton into two units, (ii) partial bioturbated nature, (iii) occasional clusters and lenses of gravels, and (iv) stratigraphically sequenced radiocarbon dates (Chapter 6). However, subsequent mass-flows may have taken place in relation to the gradient of the upper slope, with the retention of the original sedimentary structure. The non-deformation of the original sediment texture is possible within deposits of slides/slumps (cf. Nardin et al. 1979; Pickering et al. 1989; King et al. 1996), and debris flows that behave with Bingham-type fluid properties (Elverhøi et al. 1997). It is not possible to interpret whether mass-flows have occurred based solely on the sedimentary record. As a result, acoustic records are the only means of resolving the exact origin. Therefore, the origin of this facies will be discussed further in Sections 5.7.7 and 5.9.2 in light of evidence obtained from acoustic records from the upper continental slope.

4.7.2.2 Sandy mud diamicton (subfacies Dmm)

The unconsolidated nature, wide range of grain sizes comprising a large number of particles >2 mm/cm and distribution of particles >500 µm, associated sedimentary characteristics and unbroken foram shells imply an origin from iceberg rafting (e.g. Gilbert 1982, 1990; Marienfeld 1991, 1992a,b; Dowdeswell et al. 1994a,b; Cowan et al. 1997). Therefore, the number of particles >2 mm/cm and distribution of particles >500 µm is an index of iceberg rafting (IRD). It is unlikely that these relatively coarse grain sizes are obtained through sea ice rafting as sediments in ice floes are predominantly fine grained (<63 µm; e.g. Pfirman et al. 1989, 1990; Wollenburg 1991; Nürnberg et al. 1994). In general, the grain size of debris within icebergs is heterogeneous (gravel to clay; Dowdeswell & Dowdeswell 1989) as the material is derived from debris rich ice at the base of outlet glaciers draining into the marine environment (Drewry 1986; Dowdeswell 1987). Therefore, icebergs contribute the full range of grain sizes. The identification of isolated lenses and layers of gravel and sand throughout the diamicton in PS2630 and PS2629 supports an origin from iceberg rafting. Such structures are likely to have resulted from iceberg overturn and quasi-instantaneous dumping of sediment on the iceberg surface (Gilbert 1990; Dowdeswell et al. 1994a). A significant proportion of the gravel and sand grades are well dispersed and interpreted to result from the rain out of debris released from melting icebergs as they drift over the shelf and slope (Gilbert 1990; Dowdeswell et al., 1994a,b).

Assuming the modern day ice influenced marine environment can be used as an analogue, the sediment grades <63 µm can also be contributed through a number of processes. First, the fine grained sediment rafted within sea ice transported from the shallow Russian shelf region of the Arctic Ocean in the Transpolar Drift and East Greenland Current systems (Section 2.2.2; Pfirman et al. 1989, 1990; Wollenburg 1993; Nürnberg et al. 1994) contributes to sedimentation on the northeastern and eastern Greenland continental margin (Hebbeln and Wefer 1991; Baumann et al. 1993; Hebbeln et al. 1998; Dowdeswell et al. 1998). Therefore, sedimentation from sea ice could

apply to the study area. If this is the case, then sedimentation is most likely to occur during periods when the sea ice cover breaks up. Sea-ice rafting of locally derived fine grained sediment is insignificant as water depths within the fjords and continental margin are too deep for bottom sediments to become entrained within sea ice during formation (Section 2.2.2; Dowdeswell et al. 1994a). Second, the slow suspension settling of fine grained sediment derived from turbid surface melt/fluvial water plumes, and that introduced to the ambient water column from the dispersed remnants of melt/fluvial water outflows contributes to sedimentation within ice proximal and ice distal settings (e.g. Elverhøi & Solheim 1983; Dowdeswell et al. 1994a,b). Third, the vertical settling of biogenic debris contributes to sedimentation but is limited to only <1 grain-% content, resulting from dilution by abundant terrigenous derived sediments.

Further modification of the deposited sediment may result through the activity of bottom currents. Bottom currents associated with the East Greenland Current (Section 1.2.5) are known to have winnowed the finer fraction of sediments on the upper continental slope adjacent to the Kangerdlugssuaq Fjord (65°N) in East Greenland resulting in the gravel and sand content exceeding 30% (Mienert et al. 1992). Therefore, it is possible that the high distribution of gravel and sand (>30%) in the sandy mud diamicton of PS2629 on the upper continental slope of the study area may have resulted from the winnowing the fine grained component by bottom currents associated with the East Greenland Current. The gravel and sand content on the continental shelf (PS2630) is slightly lower (ca. 30%) which is surprising as the East Greenland Current is very active over this region (e.g. Funder & Larsen 1989; Mienert et al. 1992; Baumann et al. 1993; Nam 1996). If current winnowing of the fine grained component has indeed occurred, the contrast in the coarse sediment content may result from differences in either the current velocity or sedimentation rates between the core sites. The rate of dispersal or winnowing of fine sediment through bottom current activity is more effective with reduced sedimentation rates (e.g. Gorsline 1984). The difference in coarse grades between PS2629 and PS2630 may reflect a lower sediment supply rate on the continental slope. However, there is a possibility that the close proximity of PS2630 to a bathymetric high (Sections 3.2.1, 5.3.3) and other continental shelf irregularities, and possible fluctuations in the current direction, may have combined to shield the core site from bottom current activity during the deposition of the facies.

4.7.2.3 Sandy diamicton (subfacies Dmm)

This lithofacies is restricted to the uppermost section of PS2630 on the mid continental shelf. The high concentration of gravel and sand grades (>61%) and a mean grain size of ca. 4 Φ in the upper 30 cm of PS2630 on the continental shelf are attributed to the activity of strong bottom currents following deposition (e.g. Stow & Holbrook 1984; McCave 1985; Mienert et al. 1992; Baumann et al. 1993; Cadman 1996). The bottom current is ascribed to the strong East Greenland Current flowing southward across the continental shelf (Section 1.2.5), which similarly affecting deposits in neighbouring continental shelf regions (Funder & Larsen 1989; Mienert et al. 1992; Baumann et al. 1993; Nam 1996). The bottom current has resulted in the winnowing of the finer sediment grades (<63 μm) leaving the coarser grades to form a gravel-sand enriched diamicton (lag

deposit). This facies grades into the underlying sandy mud diamicton (Section above) and, therefore, it is likely that the original sediments were deposited through the processes outlined in Section 4.7.2.2. The underlying sandy mud diamicton comprises >65% fine grades, which suggest that current winnowing in comparison, was subordinate during, and subsequent to, deposition. This would only be likely if: (i) the sedimentation rate of the facies was sufficiently high to reduce the rate of dispersal or winnowing (e.g. Gorsline 1984), (ii) the current velocity was reduced, and/or (iii) the influence of the adjacent bedrock outlier and other continental shelf irregularities combined with current direction was such that bottom current activity was reduced. This further suggests that the winnowing of the sandy mud diamicton was either post depositional, or was contemporaneous with the final stages of deposition by which the prevailing situation changed.

4.7.3 Massive sandy mud with dropstones (lithofacies SFm[d])

The facies is interpreted to reflect sedimentation from the rain out and suspension settling of particles through the water column. The progressive and slow sedimentation associated with this process is reflected in the low to moderate bioturbation of the facies. The presence of moderate concentration of gravel and sand grades, the high number of particles >2 mm/cm and distribution of particles >500 μm imply sedimentation from the rain out of IRD during the drift, and subsequent melting of icebergs (Section 4.7.2.2). The lower gravel and sand concentration would indicate that the supply of icebergs was less than that associated with the deposition of the sandy mud diamicton (Section 4.7.2.2). On the slope, the moderate concentration of biogenic particles (>15 grain-%) and a fine grain component in excess of 65% imply that the deposition of the terrigenous component is concomittant with the steady settling of pelagic debris. The pelagic component comprises biogenic (carbonate and siliceous microrganisms) and non-biogenic particles. No data concerning the biogenic content are available for PS2633. Fine material is probably contributed through iceberg rafting associated with the melt out of the terrigeneous debris. Additionally, there is the possibility that the deposition of sea-ice rafted debris, derived and transported from the Arctic Ocean (Section 4.7.2.2), may have accompanied iceberg sedimentation. Sedimentation of fine grades from sea ice is likely to be of little significance within the fjord, and will only result from ice that has come into contact with sediments along the fjord margins (Syvitski 1989). Fine-grained sediment can be further derived from the slow suspension settling of particles from meltwater outflows. This is interpreted to dominate sedimentation in the mid fjord core PS2633. Sedimentation from the slow suspension settling of debris introduced to the ambient water column from the dispersed remnants of meltwater outflows reaching ice-distal, continental margin settings (e.g. Elverhøi & Solheim 1983; Dowdeswell et al. 1994a) is thought likely to influence the continental slope of the study area (Section 4.7.8.2). The redeposition of sea-floor sediment resuspended by the activity of bottom currents at the shelf break or on the slope is also a possibility (e.g. Cadman 1996).

4.7.4 Normally graded gravel - sand - mud (lithofacies G-S-Fng)

The normal grading, sharp base, and massive to cross, planar and wavey laminated subunits of the three subfacies are interpretated as originating from low concentration turbidity currents (Pickering et al., 1989; Stow, 1992). The Bouma sequence (Bouma, 1962) is a good model (Section 2.2.6.2) for classifying medium grained turbidites deposited from low-concentration turbidity currents. The normal graded sandy mud subfacies (SFng) displays Bouma units Tc and Te. The normal graded gravelly sand subfacies (GSng) displays Bouma units Ta, Tb and Tc. The normal graded muddy sands subfacies (FSng) displays Bouma units Tb, Tc and Te. The lowermost unit in all the subfacies displays a sharp lower boundary characteristic of erosion by turbidity currents. Further interpretations can be made from the units whereby unit Ta is indicative of rapid deposition from the high concentration head of the flow; Tb to Tc mark the deposition associated with the transition from upper to lower flow regime within the increasingly diluting body and tail of the flow; and Te marks the deposition from the low density tail of the turbidity current coupled with hemipelagic sedimentation (Pickering et al. 1989). The turbidity currents may have been derived from further up the continental slope due to sediment instability and subsequent failure initiated through processes outlined in Section 4.7.2.1.

4.7.5 Massive sand (lithofacies Sm)

The lithofacies is restricted to the lower slope core PS2627. The presence of the massive to weakly graded nature, the well defined upper and lower contacts with neighbouring facies, the distribution on the slope and no iceberg rafted sediment implies an origin subaqueous mass wasting, probably from low concentration turbidity currents (Pickering et al. 1989; Stow 1992). The facies displays Bouma unit Ta, which is indicative of rapid deposition from the high concentration head of the flow. The implications for initiation of the depositional mode are discussed more thoroughly in Section 4.7.2.1.

4.7.6 Sandy mud couplets (lithofacies SFc[m-l])

The lithofacies is restricted to the mid (PS2628) and lower (PS2627) slope. Based on the general sedimentary characteristics of this lithofacies two processes of deposition can be considered: i) episodic low concentration, fine grained turbidity currents, and ii) persistent contour (bottom) currents. However, it is commonly difficult to distinguish turbidites and contourites. Stow and Lovell (1979), Stow (1979, 1992), related references in Stow and Piper (1984) and Yoon and Chough (1993), have summarised associated defining characteristics. In more detail, the normal grading of the composite sand/silt lower unit and clay upper unit, bioturbation restricted to the upper part of the upper unit, water escape structures characteristic of sudden loading, well defined upper and lower

boundaries, climbing ripples, continuous and regular laminae, and cross laminated lenses all suggest deposition from fine grained turbidity currents (e.g. Piper 1978; Stow & Lovell 1979; Stow & Shanmugam 1980; Hill 1984; Yoon et al. 1991). The turbidity currents were derived further up the continental slope due to episodic sediment instability and small-scale mass failures (Section 5.9.2). This could be initiated through the processes outlined in Section 4.7.2.2. Further evidence against a contourite origin is provided by seismic profiles across the region which fail to find acoustic hyperbolae (acoustically wavey) characteristic of non-migrating/migrating sediment waves produced by contour currents (Damuth 1978).

The Bouma sequence (Bouma 1962) used to classify medium grained turbidites is an inappropriate model. Therefore, the scheme of Stow and Shanmugam (1980) for subdividing fine grained turbidites is followed. The couplet units are consistent with subdivisions T0 to T6 and possibly up to T8. However, the complete sequence is not observed in any one couplet. The sand of the lower unit was deposited from the main body of the turbidity current, and the fines of the lower and upper unit settle rapidly from the cloud of suspended fines during the waning stages of the current. The cross laminations within the lower unit are produced from traction related processes and the low flow regime (Stow & Shanmugam 1980). The regular laminations of both units are attributed to the shear sorting of silt and clay flocs near the base of the flow and subsequent settling through the viscous sublayer (Stow and Bowen 1980), or to the repeated disturbance of shear stresses in the viscous sublayer of the flow which induce periodic suppression of burst and sweep motions (Hesse & Chough 1980).

The low and occasional content of planktonic foraminifers with whole shells may imply primary deposition through pelagic settling rather than reworking by turbidity currents. If indeed, this is the case, then the biogenic debris could settle contemporaneously with the deposition of suspended fines within the cloud of the turbidity current, and/or during the quiescent periods between the emplacement of individual couplets. This would result in deposition within the upper unit of individual couplets and/or in specific layers between couplets. However, it is not possible to determine which stratigraphic level the shells were obtained from as only a composite sampling strategy could be used on the thin sub-units of this facies. Therefore, it is difficult to determine whether the shells were deposited by pelagic settling or from reworking by turbidity currents.

4.7.7 Laminated mud (lithofacies Fl[d])

This lithofacies comprises intensely laminated muds distributed towards the lower sections of cores from the inner continental shelf (PS2641), outer fjord (PS2631) and mid fjord (PS2633). The lamination morphology (parallel, wispy, wavey, lenticular) vary between cores (Section 4.3.6) but are related to the same process of deposition. The laminations within PS2631 and PS2633 develop into massive muds. The fine grained nature of the mud facies, and the variable laminated forms, coupled with diffuse upper and lower boundaries, imply that the facies was deposited through the suspension settling of silt, clay and sand particles from turbid surface meltwater plumes (e.g. Powell 1981, 1983;

Elverhøi et al. 1983; Mackiewicz et al. 1984; Powell & Molnia 1989; Syvitski 1989; Cowan et al. 1997). Such meltwater plumes are derived from subglacial drainage of tidewater glaciers and subaerial glaciofluvial/fluvial systems (Syvitski et al. 1987). The laminations are attributed to periodic, though non-rhythmic fluctuation in the discharge and hence carrying capacity and competence of turbid surface plumes issuing from its point of efflux (e.g. Powell 1981, 1983; Elverhøi et al. 1983; Mackiewicz et al. 1984; Powell & Molnia 1989; Dowdeswell & Cromack 1991). Additionally, the influence of the tidal and wind state can lead to variability in the dynamics of the plume reflected in sedimentation (Mackiewicz et al. 1984; Cowan & Powell 1990; Dowdeswell & Cromack 1991). The fine grained nature of the mud facies implies that deposition from plumes occurred within a low energy environment in an ice distal zone as coarser sediments are typical of the more ice proximal zone (e.g. Elverhøi et al. 1983; Mackiewicz et al. 1984; Syvitski et al. 1987). However, the presence of sandy laminae in PS2633 implies a greater carrying capacity and competence of the meltwater plumes associated with a higher energy environment and probably a more ice proximal setting (e.g. Cowan et al. 1997). The sand units possess diffuse lower boundaries and dispersed gravel grades, and, coupled with their association with adjacent parallel, wavey and whispy, discontinuous laminae, suggests that deposition is associated with sedimentation from meltwater plumes contemporaneous with iceberg sedimentation rather than underflows (turbidity currents).

It was discussed in Section 4.4.6 that the difference in grain size of the lithofacies between PS2631 and PS2641 is possibly an artefact of the composite nature of the samples. However, it is also possible that there is a real difference in the grain size of the facies between the two cores. If the difference in grain size is real then it is possible the layers in PS2631 compose coarser grades (medium silt to gravel). X-radiographs reveal that the gravel and sand grades form occasional dispersed to isolated lenses in PS2633 and PS2631, which are typical of iceberg rafting (Section 4.7.2.2). This is reflected in the number of particles >2 mm/cm, and the distribution of particles >500 µm, both of which are an index of iceberg rafted debris (IRD). Therefore, it is interpreted that iceberg rafting, though limited, is contemporaneous with meltwater sedimentation within the fjord (PS2633 and PS2631) but decreases on the inner continental shelf (PS2641).

4.7.8 Homogeneous mud with dropstones (lithofacies F[d])

4.7.8.1 Massive mud with dropstones (subfacies Fm[d])

This lithofacies is distributed within the deeper sections of PS2633 (mid fjord) and PS2629, PS2628 and PS2627 (continental slope). The facies is interpreted to reflect sedimentation from the rain out and suspension settling of terrestrial and marine derived particles through the water column. The presence of low concentrations of gravel and sand grades, low number of particles >2 mm/cm, and little sediment >500 µm implies that a small component of sediment is derived from the rain out of iceberg rafted debris (IRD) during the drift and subsequent melting of icebergs (Section 4.7.2.2). The much lowered gravel and sand concentration in comparison to the closely associated massive

sandy mud facies (Section 4.7.3) is interpreted to reflect a reduced supply of icebergs during the deposition of this facies. The higher concentration of coarser sediment within clusters, lenses and dispersed patterns within the mid fjord (PS2633) reflects the relative proximity of tidewater glaciers and the greater supply of rafted debris through icebergs. On the continental slope, the moderate concentration of biogenic particles (>10 grain-%) and a fine grained component in excess of 90% implies that the deposition of the terrigenous material is contemporaneous with the steady settling of pelagic (biogenic) debris. No data concerning the biogenic content are available for PS2633. Additionally, fine particles are probably contributed through iceberg and sea-ice rafting (Sections 4.7.2.2 and 4.7.3). Sedimentation of fine material from sea-ice is likely to be of little significance within the fjord and will only result from ice that has come into contact with sediments along the fjord margins (Syvitski, 1989). Mud is also assumed to be derived from the slow suspension settling of fine grained material from meltwater/fluvial outflows. This form of sedimentation is interpreted to dominate the mid fjord core PS2633, and this process is discussed further in Section 4.7.8.2. Sedimentation from the slow suspension settling of debris introduced to the ambient water column from the dispersed remnants of meltwater outflows reaching ice-distal, continental margin settings (e.g. Elverhøi & Solheim 1983; Dowdeswell et al. 1994a) is thought likely to influence the continental slope of the study area (Section 4.7.8.2). The redeposition of sea-floor sediment resuspended by the activity of bottom currents at the continental shelf break or on the continental slope is also a possibility (e.g. Cadman 1996).

4.7.8.2 Bioturbated mud with dropstones (subfacies Fb[d])

The facies is distributed within the uppermost section of the majority of cores and also somewhat deeper in PS2630. The unconsolidated, homogeneous fine silt-clay rich (>90%) mud, with intense to weak bioturbation, and low to high biogenic content reflects sedimentation from the rain out and suspension settling of particles through the water column within an ice distal setting (fjord and inner shelf) to a predominantly marine setting on the continental slope. The extensive thickness of the facies in the fjord and inner continental shelf cores reflects the proximity of the fjord margins and the greater source of sediment, as opposed to the distal pelagic dominated system of the deep sea. The facies is composed of pelagic debris, reflected in the variable biogenic content. The biogenic composition varies from <25 grain-% in the fjord and on the inner continental shelf (PS2632, PS2631 and PS2641) to >30 grain-% on the mid continental shelf and slope (PS2630, PS2629, PS2628 and PS2627) indicating favourable, open-ocean water, more sea-ice free conditions of the latter as opposed to the less favourable, freshwater influenced fjord and inner continental shelf regions of the former. Furthermore, dilution by the high flux of terrestrial derived material, and low carbonate production coupled with high carbonate dissolution associated with the cold polar waters of the East Greenland Current may explain the lower biogenic flux on the inner continental shelf and in the fjords (e.g. Baumann et al. 1993; Nam et al. 1995; Nam 1996).

Within the fjord and on the inner continental shelf, sedimentation is dominated by terrestrial sediment derived from the proximal continental hinterland. This is reflected in the high organic

content (black layers and spots) which, in turn, controls the relatively high content of bioturbation. The intense bioturbation of sediments may have destroyed any primary sedimentary structures. However, the bioturbation is composed of a network of tiny burrows *(Chondrites)* that may not actually completely bioturbate the sediment (e.g. Gorsline 1984), suggesting that the original structure was massive. The slow suspension settling of fine grained sediment introduced to the water column through turbid surface meltwater plumes is interpreted to be the main source of sediment to the fjord (e.g. Powell 1981, 1983; Elverhøi et al. 1983; Mackiewicz et al. 1984; Syvitski 1989; Powell & Molnia 1989; Dowdeswell et al. 1994a; Cowan et al. 1997). The plumes are derived from subglacial drainage of tidewater glaciers, glaciofluvial systems fed by glaciers and snow melt, and fluvial systems.

Aerial photographs and Landsat images reveal surface turbid meltwater/fluvial plume activity within the present day fjord system (Chapter 1; Figs 1.1-1.3). The surface turbid plumes are derived from numerous snow-melt and precipitation-fed river systems (e.g. Promenadedal, Paralleldal and Badlanddal) draining the margins of the mid to outer region of Nordfjord, Kejser Franz Josephs Fjord and Fosters Bugt, and from subglacial drainage of tidewater glaciers in the most proximal tributary fjords of Nordfjord and Geologfjord (Chapter 1; Figs 1.1-1.3). The surface turbid plumes are observed to distribute themselves down-fjord or close to the fjord margins following their efflux (Fig 1.2, 1.3). These surface turbid plumes and dispersed remnants of such outflows are assumed to escape from the tributary fjords and fjord margins (Figs 1.2, 1.3), and influence the mid to outer fjord core sites of PS2631, PS2632 and PS2633 throughout the deposition of the bioturbated mud facies. The dispersed remnants of these outflow plumes are assumed to escape the fjord system (e.g. Elverhøi et al. 1983; Mackiewicz et al. 1984), and significantly influence the core site of PS2641 on the inner continental shelf. Similarly, part of the finer grained component of sediments within the continental slope cores (PS2629, PS2628 and PS2627) is thought to originate from the slow suspension settling of fine material introduced to the ambient water column from the dispersed remnants of meltwater outflows reaching the ice distal setting of the slope (e.g. Elverhøi & Solheim 1983; Dowdeswell et al 1994a). The occasional presence of dispersed to clustered gravel and sand grades reflected in the particles >2mm/ cm and distribution of particles >500 μm, indicates that sedimentation from iceberg rafting is contemporaneous with meltwater deposition. Furthermore, the marked increase of such material from the inner continental shelf to the mid fjord reflects the increasing proximity of the tidewater glaciers at the head of the fjord system, and the stronger influence from icebergs calved from these glacier-ice margins.

This lithofacies is observed in the topmost section of the majority of cores of this study. Core, PS2630 on the mid continental shelf is an exception to this observation. Instead, the facies is only observed in the mid section of the core. The absence of the facies in the topmost section of the core is interpreted to reflect the erosive activity of the East Greenland Current, which has acted to either winnow sea-floor sediments or prevent the deposition of sediment (e.g. Funder & Larsen 1989; Mienert et al. 1992; Baumann et al. 1993; Nam 1996). The presence of the facies in the mid section of the core, as opposed to its absence at the top of the core, can be explained by a number of

possibilities, where: i) accumulation of the sediment occurred at a sufficient rate where it could not be effectively dispersed by the East Greenland Current (e.g. Gorsline 1984), ii) the velocity of the East Greenland Current was much lower during deposition, and iii) a combination of bedrock shoals/ continental shelf irregularities such as the bathymetric high proximal to the core site (Sections 3.2.1, 5.3.3), and variations in current direction may have sheltered the core site from bottom current activity, allowing unhindered deposition. The absence of the facies at the top of PS2630 must have resulted from subsequent changes in these factors, which altered the environment in such a way that it became inducive for intense current winnowing. The facies attains a significant thickness (600 cm) in PS2641 on the inner continental shelf. This is thought to reflect the location of the core within a basin (Sections 3.2.1, 5.3.3). The basin topography acts to pond sediment, allowing the unhindered settling of sediment from surface turbid melt/river water plumes, that introduced to the water column from the dispersed remnants of melt/river water outflows, and/or that transported within the East Greenland Current after being resuspended from neighbouring shallow continental shelf regions (Mienert et al. 1992). Furthermore, the basin shelters seafloor sediments from winnowing by the East Greenland Current. The resuspension of sediment in shallow sill and marginal regions and subsequent redeposition in deeper basins is expected within the fjord (e.g. Syvitski & Hein 1991; Marienfeld 1992b). The main mechanism driving this process is thought to be bottom current activity, which is supported by the observation that continental shelf waters of the East Greenland Current intrude Kejser Franz Josephs Fjord to depths >300 m (Section 1.2.5; Vogt et al. 1995).

4.7.9 Bioturbation and sedimentary environmental implications

As discussed in Section 4.3.7.2 the trace burrows composing the bioturbated mud (Fb[d]) facies in the uppermost section of most cores along the transect are predominantly consistent with *Chondrites* type (e.g. Marienfeld 1991, 1992a,b; Eyles et al. 1992; Andersen et al. 1995). *Chondrites* are feeding traces emplaced deep within sediment by polychaete (Simpson 1957; Häntzschel 1975). The burrow type forms a very dense network in PS2632, PS2631 and PS2641 with a more sparse concentration within PS2633, PS2629, PS2628 and PS2627. The distribution reflects the higher organic content within sediments of the fjord and inner shelf due to the proximity of the Greenland continent, on which the burrowing polychaete can feed. The burrowers are associated with the interstitial/sediment environment in the anoxic (oxygen-poor) region of the sediment column. Their presence would indicate that during the deposition of the facies, the core sites were influenced by anoxic interstitial waters even though bottom waters could have been oxic, or bottom waters close to the sea floor were oxygen starved (Bromley & Ekdale 1984; Ekdale et al. 1984).

In PS2632, PS2631 and PS2641, the *Chondrites* burrow systems are flecked with iron sulphide (Section 4.3.7.2) produced within sulphidic conditions (e.g. Marienfeld 1991, 1992b). The sulphide is precipitated through the bacterial reduction of sea-water sulphate during decomposition of organic matter (Goldhaber & Kaplan 1974). The organic matter can be derived from the host sediment and/or from the burrowing organism (e.g. Thomsen & Vorren 1985). The whole process

proceeds under anoxic conditions when the dissolved oxygen of interstitial and/or bottom sea water has been consumed. No acidic and oxygen concentrations have been measured from bottom waters within the study area. Therefore, it is not known whether present day bottom conditions are oxic or anoxic, which would have provided a contemporaneous control for the environment prevailing during the deposition of the bioturbated mud, and the production of the *Chondrites* and iron sulphides. The core sites are located within deep basins of the outer fjord and inner continental shelf, confined by steep sills or margins. These could possibly act to inhibit or reduce bottom water ventilation by restricting the circulation of oxic waters, which results in the stagnation of bottom waters and anoxia (Syvitski et al. 1987; Andersen et al. 1995; Cadman 1996). Equally the presence of sulphide may simply have resulted due to the anoxic levels commonly found in deeper parts of the sediment column even though bottom waters are totally or partially oxic.

4.8 PRELIMINARY CHRONOLOGY OF DEPOSITIONAL PROCESSES

A preliminary chronology for the deposition of the lithofacies can be attempted based on the processes of sedimentation coupled with the facies distribution within sediment cores. This will be adjusted in Chapter 7 in light of the chronology presented and discussed in Chapter 6. The sedimentary record for the cores probably dates at maximum back to the Late Weichselian glaciation. The bioturbated mud facies (PS2632, PS2631, PS2641, PS2629, PS2628 and PS2627) and massive mud facies (PS2633) are distributed in the uppermost section of the cores. This, coupled with their predominantly fine grained nature, implies they represent Holocene sedimentation where the effects of ice are least.

In the mid fjord to inner continental shelf cores PS2633, PS2631 and PS2641, this facies is underlain by laminated mud facies and suggests sedimentation associated with the later stages of the Late Weichselian deglaciation. Furthermore, the sandy mud diamicton facies underlying the laminated mud facies in PS2641 would probably also correspond to the Late Weichselian deglaciation. The Late Weichselian deglaciation is likely to be represented by the massive mud facies in the upper slope core PS2629 and normal graded sandy mud and sandy mud couplet facies in the mid to lower continental slope cores PS2628 and PS2627. These facies are relatively poor in coarse grained glacigenic debris (ice rafted debris and distribution of particles >500 μm) making sedimentation during the Late Weichselian glaciation unlikely.

Sedimentation associated with the Late Weichselian glaciation is inferred for facies with an enhanced coarse grained, glacigenic derived debris content (ice rafted debris and distribution of particles >500 μm). The sandy mud diamicton, sandy diamicton and resedimented sandy mud diamicton subfacies in the shelf core PS2630 are not overlain by finer grained sediments typical of the Holocene along the transect. Therefore, it is difficult to determine whether these subfacies represent either Late Weichselian deglaciation or glaciation. The coarse grained facies on the slope are interpreted as being sedimented during the Late Weichselian glaciation as this is the only period

that could feasibly generate the processes necessary to deliver coarse sediments to the slope. These sediments include the sandy mud diamicton and sandy mud facies of the continental slope cores PS2629, PS2628 and PS2627. The close association of these facies with the massive mud, massive sand and resedimented sandy mud diamicton facies within the mid to lower continental slope cores PS2628 and PS2627, would similarly imply that sedimentation occurred during the Late Weichselian glaciation. Below this unit, the normal graded gravelly sand and muddy sand subfacies underlain by the resedimented sandy mud diamicton subfacies in the lower slope core PS2627, can at best be interpreted as representing Late Weichselian full glacial conditions.

4.9 SUMMARY

This chapter has presented the sedimentology and lithostratigraphy of the eight cores comprising the Kejser Franz Josephs Fjord-shelf-slope transect through the identification and distribution of seven lithofacies and five subfacies. The downcore and lithofacies variations of grain size distribution, number of particles >2 mm/cm and weight percent of sediment >500 μm (0.5 mm; Ice Rafted Debris), and physical properties (water content, porosity and wet bulk density) are also presented. A summary of the main sedimentological characteristics of each lithofacies and subfacies are summarised in Table 4.2. The lithofacies and subfacies and associated sedimentological properties were interpreted in terms of the sedimentary depositional processes and environments, and are summarised in Table 4.4.

CHAPTER 5

ACOUSTIC RECORDS OF SEDIMENTATION PATTERNS AND PROCESSES IN KEJSER FRANZ JOSEPHS FJORD AND ON THE EAST GREENLAND CONTINENTAL MARGIN

5.1 INTRODUCTION

The close relationship between acoustic character and sedimentary composition, structure and associated depositional processes/environments enables acoustic records to be used as an essential tool in the investigation of Late Quaternary glacimarine sedimentation patterns and processes (e.g. Damuth 1978; Elverhøi et al. 1983; Dowdeswell et al. 1994, 1996, 1997b; Laberg & Vorren 1995, 1996; King et al. 1996). Although sediment cores provide ground truthing of sea-floor sediment composition and facies, it is not known how representative the associated environmental reconstructions are in relation to the whole region. Therefore, acoustic records are essential to such studies as they place the cores within a regional context. A combination of sediment cores and acoustic records provides a more complete investigation into the glacimarine sedimentation patterns and processes occurring in response to glacial-interglacial climatic fluctuations. This approach is adopted here.

The lithostratigraphy and associated sedimentary processes/environments obtained from cores recovered from the study area were discussed in Chapter 4. This chapter is concerned with the description and analysis of acoustic records. The objectives outlined below will be addressed using the acoustic records collected from a series of transects along the axis of the mid-outer region of the Kejser Franz Josephs Fjord, and across the adjacent East Greenland continental margin (Fig 5.1a). The objectives of this chapter are to:

- Describe the acoustic character and distribution of acoustic units representative of the range of sedimentary facies comprising the unlithified Late Weichselian and Holocene sediments of the study area.
- Correlate the lithostratigraphy of each core with the acoustic units.
- Interpret the sedimentary processes and environments associated with each acoustic unit based on ground truthing of sea-floor sediments using the sediment cores discussed in Chapter 4, and information published in the scientific literature.
- Interpret the sea-floor characteristics and, in particular, investigate iceberg scouring throughout the study area.

- Place the lithostratigraphy of each core within a regional context through a discussion of the regional sedimentation patterns and processes interpreted from both the cores and acoustic records of the study area. Relate the sedimentation patterns and processes to a preliminary but broad chronology, and to glacial-interglacial climatic fluctuations.

A further objective addressed in this chapter is the compilation of a bathymetric map for the study area based on the Parasound records as other data sources were not available for this thesis. This objective provides the bathymetric data necessary for all aspects of this study, and is referred to extensively throughout other sections of the thesis.

5.2 GEOPHYSICAL DATA ACQUISITION

The acoustic data of this study were acquired using a hull mounted Parasound profiling system (cf. Grant & Schreiber 1990). The main principles and methodology of the Parasound system were introduced in Section 3.8. Additional seismic data from air gun reflection profiling systems are only available for the Fosters Bugt region (Fig 5.1), as sea ice conditions were too heavy to allow the safe operation of the equipment along the majority of the transects. However, only preliminary air gun results (Jokat unpub data; Jokat et al. 1995; Whittington 1995) were available for this thesis, and these results will be referred to where necessary. The Parasound acoustic system and associated data are suffice for addressing the objectives of this study. This is because air gun systems only provide additional information concerning the identification of the bedrock-sediment interface, and the measurement of total sediment thickness above the underlying bedrock in regions of thick Quaternary deposits (Dowdeswell et al. 1994).

5.3 BATHYMETRY AND PHYSIOGRAPHY OF THE STUDY AREA

5.3.1 Introduction

The bathymetry of the mid-outer region of the Kejser Franz Josephs Fjord, Fosters Bugt and adjacent continental shelf and slope was compiled from water depth data obtained directly from the Parasound records of this study. This is possible as the two-way travel time data of the Parasound system was converted to water depths (Section 3.7). The bathymetry and physiography for the area are described in this section, and a bathymetric map together with the location of cores of this study is presented in Figure 5.1b.

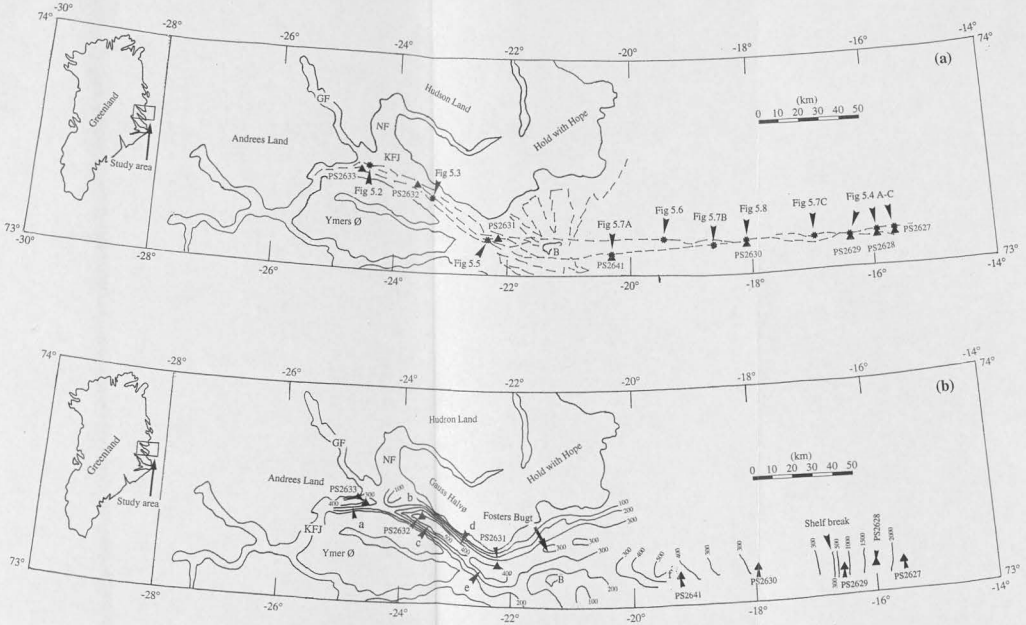

Figure 5.1. Map of Kejser Franz Josephs Fjord and the adjacent continental shelf and slope showing: (a) Ship tracks (dotted lines) of the Polarstern during the ARK X/2 cruise, for which Parasound records are available. Locations of the Parasound records used as examples in Figures 5.2-5.8 are shown. (b) Bathymetry (100 m intervals) based on the Parasound records. a = mid fjord basin, b = mid/outer fjord sill, c = innermost sub-basin of the outer fjord, d = intermediate sub-basin of the outer fjord, e = outermost sub-basin of the outer fjord, and f = inner shelf basin. The shelf break is at a water depth of about 300 m. The locations of the sediment cores of this study are indicated in both (a) and (b). The study area in relation to Greenland is shown within the insets of both (a) and (b). KFJ = Kejser Franz Josephs Fjord, GF = Geologfjord, NF = Nordfjord, and B = Bontekoe Ø. The map scale is shown in both (a) and (b).

5.3.2 Continental slope

The continental slope extends from the shelf break (73° 09' N, 16° 54' W) at a water depth of 280-300 m to the mid-lower slope at 2100 m (Fig 5.1b). The slope gradient gradually decreases from the upper continental slope (4.4°) to the mid-lower continental slope (1.4°). The sea-floor is generally planar but occasional hummocks are observed in the lower region of the upper continental slope and the mid continental slope regions (Fig 5.4A-C).

5.3.3 Continental shelf

The continental shelf between the shelf break and the mid continental shelf (73° 09' N, 18° 06' W) is composed of frequent, small-scale sediment-covered irregularities which probably reflect underlying bedrock hummocks. Water depths in this region vary between 280-340 m. A prominent bathymetric high (Fig 5.8) exists on the mid continental shelf and extends from an eastern margin at 73° 09' N, 18° 06' W to a western margin at ca. 73° 09' N, 18° 31' W. The eastern margin of the bathymetric high attains a slope gradient of between 1.6-3.3° (Fig 5.8), and the water depth at the base of this slope is 300-310 m (Figs 5.1b, 5.8). The sea-floor on the bathymetric high is at a water depth of 235 m and increases to 275 m at the western margin. The inner continental shelf is characterised by a basin ca. 50 km in length (Fig 5.1b), and whose eastern margin grades into the western margin of the bathymetric high. At its deepest, the basin attains a depth of 520 m. The basin is characterised by a gently hummocked eastern margin (Fig 5.6), and an irregular western margin comprising V-shaped depressions incised to depths of up to 20 m. The irregularities are thought to reflect underlying bedrock. The western margin of the basin merges with the inner continental shelf plateau that slopes up towards the east of Bontekoe Ø. Water depths reach up to 300 m in this region (Fig 5.1b).

5.3.4 Mid-Outer Kejser Franz Josephs Fjord and Fosters Bugt

The water depths within Fosters Bugt reach up to 360 m, though the bathymetry is poorly constrained to the south of Bontekoe Ø due to lower density of seismic coverage (Fig 5.1a). The deepest region is located in the central region to the north of Bontekoe Ø bounded by slopes leading away from Bontekoe Ø, southern Hold with Hope and eastern Gauss Halvø (Fig 5.1b). The deeper regions of the Bugt are centred within small-scale depressions. The outer fjord is characterised by three sub-basins bounded by steep margins (Fig 5.1b): i) an outermost sub-basin with water depths up to 450 m, ii) an intermediate sub-basin with water depths between 410-480 m, and iii) an innermost sub-basin with water depths between 500-540 m. The two innermost sub-basins are separated by a sill reaching a water depth of up to 480 m (Fig 5.3), but no prominent sill marks the transition into the outermost sub-basin. An abrupt change occurs in the water depth at the transition between Fosters Bugt and the outer sub-basin of the outer fjord. This is not marked by a prominent

sill but, instead, a steep slope adjoining the broad sea-floor to the west, south and north of Bontekoe Ø (up to 340 m) and the deeper region of the outer fjord (ca. 450 m). The southern margin of the outer fjord is composed mainly shallow water of irregular depth with numerous small-scale basins bordered by bathymetric highs. At the intersection between Kejser Franz Josephs fjord, Nordfjord and Geologfjord, in the mid/outer fjord (Fig 5.1b) is dominated by a prominent sill reaching a minimum water depth of 60 m. The sill separates the innermost sub-basin of the outer fjord from the mid fjord basin with water depths between 320-480 m (Fig 5.1b).

5.4 DESCRIPTION OF ACOUSTIC UNITS

5.4.1 Introduction and classification of acoustic units

Eight acoustic units and associated sea-floor characteristics are identified from Parasound acoustic data collected along the ship tracks of this study (Fig 5.1a; Section 5.2). The acoustic facies are described in this section, illustrated in the Parasound records of Figures 5.2-5.8, and summarised in Table 5.1. Reflectors marking the interface between bedrock and Quaternary sediments, and occasionally the lower surface of acoustic units are not evident in many sections of the Parasound records due either to the extensive sediment thickness or poor acoustic return. The acoustic units are defined mainly on the basis of differences in acoustic character between units using the scheme of Damuth (1975, 1978) which, in-turn, has been modified by Elverhøi et al. (1983), Yoon et al. (1991), Kuhn & Weber (1993), Melles & Kuhn (1993) and Dowdeswell et al. (1993, 1994b). Acoustic characters include clarity, prolongation (distinct, semi-prolonged and prolonged) and continuity (continuous, discontinuous and point) of sea-floor and sub-sea floor reflectors, the degree of transparency and internal character between reflectors, the morphology of the sea-floor reflector, and the geometry/ morphology of the acoustic unit. The acoustic transparency refers to the intensity of the grey tone between reflectors and is divided into classes of transparent, semi-transparent and opaque.

5.4.2 Acoustic unit I - acoustically stratified sediment

The main characteristics of this acoustic unit are summarised in Table 5.1 and illustrated in Figures 5.2, 5.3 and 5.4(B,C). The unit is characterised by a continuous, distinct, sharp sea-floor reflector exhibiting a mainly planar to occasional small scale hummocky morphology. Internal or sub-sea floor reflectors are multiple, parallel with the sea-floor reflector, distinct, sharp, continuous for tens/hundreds of kilometres, and up to several metres thick. The reflectors are separated by acoustically transparent or opaque sediment. Occasionally, the internal reflectors wedge laterally to form lobes. The reflector representing the bottom-surface of this unit is present in only limited sections of the Parasound records and takes a sharp to diffuse and irregular to planar morphology.

Within the fjord, the continuity of the stratification is occasionally disrupted by numerous vertically aligned and parallel dislocations which form a hummocky or folded appearance to the sea-floor and internal reflectors (Fig. 5.2). The unit can be sub-divided into two units based on general morphology:

- Sub-unit Ia - basin infill where reflectors are ponded within basins bordered by bathymetric highs (Figs 5.2 & 5.3).
- Sub-unit Ib - reflectors are confined to the slope (Fig 5.4B&C) whose general morphology is not well constrained due to poor seismic coverage.

5.4.3 Acoustic unit II - acoustically homogeneous sediment exhibiting lobed/ elongate morphology

The main characteristics of this acoustic unit are summarised in Table 5.1 and illustrated in Figures 5.2, 5.3 and 5.4(C). The unit is composed of distinct and sharp sub-seafloor reflectors that produce sediment features with mainly unconformable, small/large scale, lobed to elongate morphologies. These features extend from kilometres to tens of kilometres in length, and up to ca. 30 m thick. Both align parallel to the downslope direction, or at the base of slopes in the fjord, and on the shelf and slope. A large number of the lobes do not exhibit lateral margin reflectors, but instead grade into the neighbouring acoustic unit. In contrast, the unit on the slope is composed of unconformable, wedge shaped sea-floor/sub-seafloor reflectors, separating elongated sediment features. The top and bottom surfaces of all bodies vary from planar to irregular, and are separated by an acoustically homogeneous and transparent unit composed of a small number of point diffractions. On the slope the bodies can appear close to the sea-floor, resulting in an occasionally hummocked morphology.

5.4.4 Acoustic unit III - acoustically heterogeneous sediment with a hummocky top-surface reflector

The main characteristics of this acoustic unit are summarised in Table 5.1 and illustrated in Figure 5.5. The unit is acoustically transparent/ semi-transparent, and composed of a distinct to semi-prolonged, sharp, hummocky top-surface reflector. The bottom-surface reflector is not observed on the acoustic records. Internal reflectors are present within the unit and vary throughout, resulting in a number of characteristics: i) incoherent, irregular, diffuse to sharp reflectors providing an acoustically chaotic appearance, ii) discontinuous (continuous over distances up to tens of kilometres), parallel to sub-parallel, sharp to diffuse stratified reflectors, and iii) acoustically massive with multiple point diffractions.

Acoustic Unit	Acoustic Sub-Units	Code	Distribution	Description
Acoustically stratified sediment	Basin infill	Unit Ia	Mid/outer fjord Fosters Bugt	Planar to occasional hummocky sea-floor reflector underlain by multiple, parallel internal (sub sea-floor) reflectors. All reflectors are distinct and sharp, and continuous over lengths of up to ten's of kilometres. Reflectors are separated by acoustically transparent to opaque sediment. Internal reflectors occasionally wedge laterally to form lobes. The morphology varies between basin (ponded) infill deposits (sub-unit Ia) and slope deposits (sub-unit Ib). Stratification of sub-unit Ia is occasionally disrupted by multiple, vertically aligned dislocations or syn-sedimentary faults.
	Slope deposits	Unit Ib	Midlower continental slope	
Acoustically homogeneous sediment exhibiting lobed/ elongate morphology		Unit II	Mid/outer fjord Mid continental shelf Mid/lower continental slope	Distinct sub sea-floor reflectors separating unconformable, lobed to elongate sediment bodies. A large number of the bodies do not exhibit lateral margin reflectors but grade into neighbouring acoustic units. On the slope, the elongate bodies separate unconformable wedge shaped sub sea-floor reflectors. In both cases the sediment bodies are acoustically homogeneous (massive) with a transparent nature and have a low number of point diffractions characteristic of low internal backscattering. Sediment bodies extend up to ten's of kilometres in length, up to 30 m in thickness.
Acoustically heterogeneous sediment with a hummocky top-surface reflector		Unit III	Outer fjord	Transparent to semi-transparent unit overlain by a distinct to semi-prolonged, hummocky top-surface reflector. The unit varies between (i) acoustically chaotic (incoherent reflectors), (ii) acoustically stratified with weak, discontinuous, parallel to sub-parallel sub sea-floor reflectors, and (iii) acoustically massive with multiple point diffractions characteristic of high internal backscattering.
Acoustically stratified sediment exhibiting conformable sea-floor and internal reflectors		Unit IV	Outer fjord Inner continental shelf	Acoustically stratified sediment consisting of multiple, parallel sea-floor and internal (sub sea-floor) reflectors that are conformable over bathymetric highs and within intervening basins. Sea-floor and internal reflectors are parallel, continuous over ten's of kilometres, distinct and sharp to diffuse in character. All reflectors display a mainly hummocky morphology. The reflectors are separated by acoustically transparent to semi-transparent sediment.
Acoustically homogeneous to stratified sediment with an irregular sea-floor reflector	Acoustically homogeneous	Unit Va	Mid/outer fjord Fosters Bugt Continental shelf	Acoustic unit is characterised by a very irregular sea-floor reflector. Diffraction hyperbolae are occasionally observed. The irregularity is composed of roughness elements that comprise crests and troughs of varying intensities: (i) High intensity comprising a poorly defined, discontinuous to continuous sea-floor reflector, (ii) Intermediate intensity comprising a more distinct, irregular sea-floor reflector where crest morphology is increasingly more separated, and (iii) Low intensity comprising a continuous, distinct sea-floor reflector where crest-trough morphology is separated by extensive planar regions. The internal acoustic nature varies between (i) homogeneous sediment characterised by diffuse signal return associated with high to intermediate intensity (sub-unit Va), and (ii) stratified sediment consisting of continuous to discontinuous internal reflectors associated with intermediate to low intensity (sub-unit Vb). The stratified nature is consistent with acoustic units Ia, IV and VII.
	Acoustically stratified	Unit Vb	Fosters Bugt Outer continental shelf	
Acoustically semi-penetrable sediment with a distinct to semi-prolonged sea-floor reflector		Unit VI	Upper continental slope	Acoustic unit is characterised by a continuous, distinct to semi-prolonged planar to occasional hummocky sea-floor reflector. The internal acoustic character is homogeneous and mainly semi-transparent to opaque. Internal (sub sea-floor) reflections are diffuse and shallow-based with multiple point diffractions indicating high energy backscattering related to small-scale inhomogeneities. There are occasional weak, discontinuous stratified internal reflectors.
Acoustically massive sediment forming a conformable unit		Unit VII	Outer fjord Mid/outer continental shelf	Acoustically transparent to opaque and massive sediment consisting of a parallel, continuous, distinct and sharp sea-floor and sub sea-floor reflector and occasional internal reflectors displaying a planar to hummocky morphology. The reflectors form a single unit conformable over bathymetric highs and within intervening basins and sea-floor depressions.
Acoustically homogeneous sediment with an irregular-hummocky top-surface sub sea-floor reflector		Unit VIII	Mid/outer continental shelf	Acoustically homogeneous and transparent to semi-transparent sediment consisting of continuous, distinct and sharp irregular to hummocky top-surface, internal (sub sea-floor) reflector. The multiple, internal point diffractions indicate high energy backscattering related to small-scale inhomogeneities. A discontinuous bottom-surface reflector is occasionally present and appears with an irregular to hummocky morphology.

Table 5.1. Summary of the characteristics of the acoustic units determined from Parasound records obtained along ship tracks from the mid-outer region of the Kejser Franz Josephs Fjord, Fosters Bugt and the adjacent continental shelf and slope (Figure 5.1a). Details include: i) Acoustic units and sub-units, ii) Acoustic unit code, iii) Distribution of the acoustic units, and iv) Description of the main characteristics of the acoustic units.

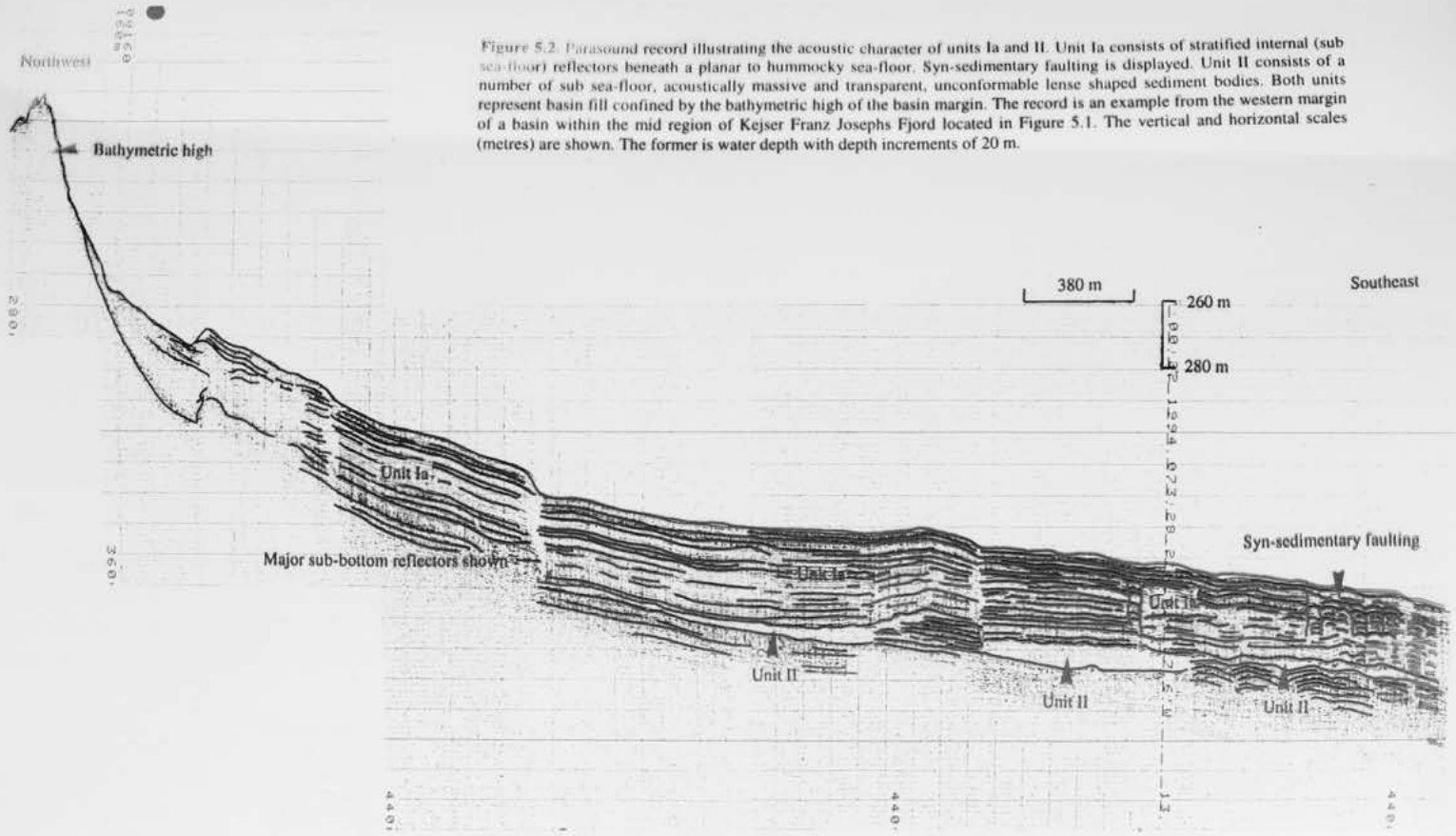

Figure 5.2. Parasound record illustrating the acoustic character of units Ia and II. Unit Ia consists of stratified internal (sub sea-floor) reflectors beneath a planar to hummocky sea-floor. Syn-sedimentary faulting is displayed. Unit II consists of a number of sub sea-floor, acoustically massive and transparent, unconformable lense shaped sediment bodies. Both units represent basin fill confined by the bathymetric high of the basin margin. The record is an example from the western margin of a basin within the mid region of Kejser Franz Josephs Fjord located in Figure 5.1. The vertical and horizontal scales (metres) are shown. The former is water depth with depth increments of 20 m.

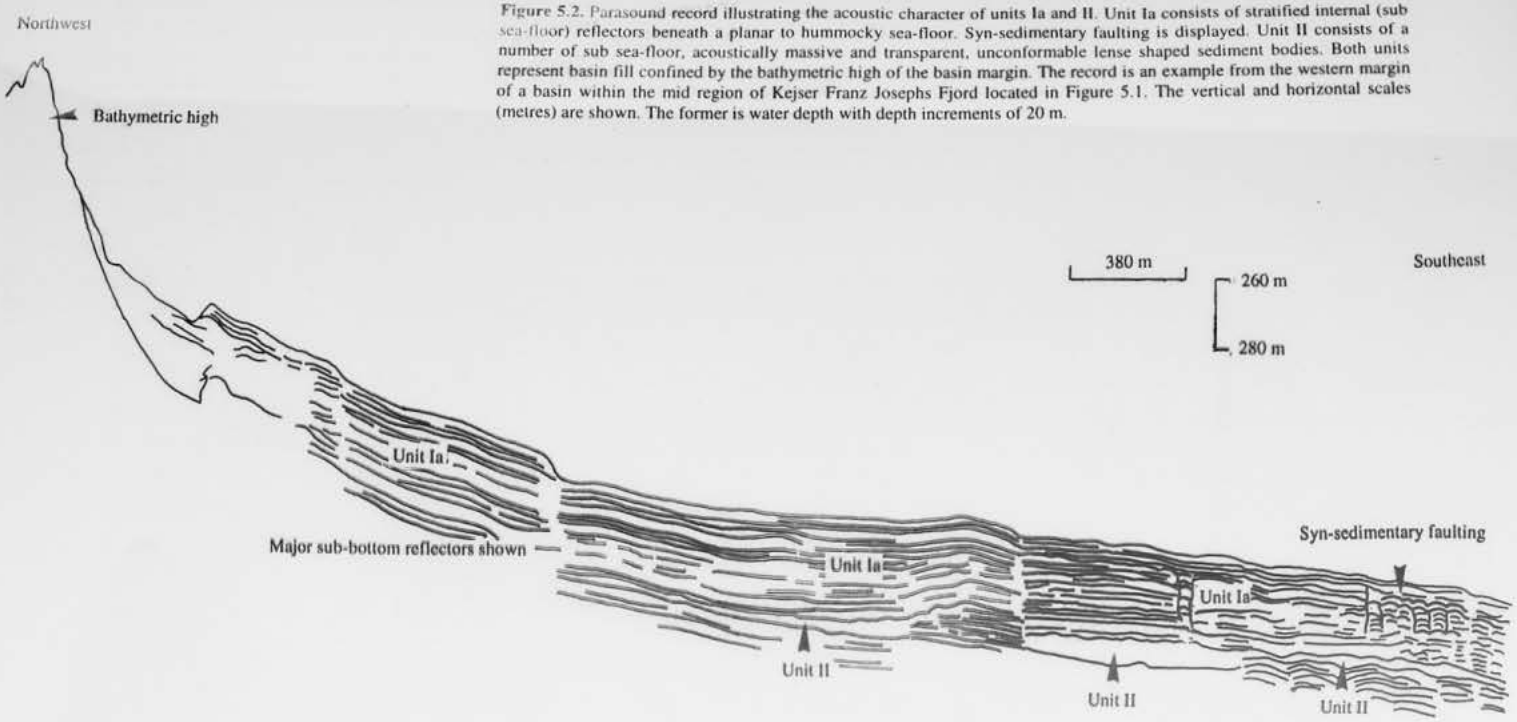

Figure 5.2. Parasound record illustrating the acoustic character of units Ia and II. Unit Ia consists of stratified internal (sub sea-floor) reflectors beneath a planar to hummocky sea-floor. Syn-sedimentary faulting is displayed. Unit II consists of a number of sub sea-floor, acoustically massive and transparent, unconformable lense shaped sediment bodies. Both units represent basin fill confined by the bathymetric high of the basin margin. The record is an example from the western margin of a basin within the mid region of Kejser Franz Josephs Fjord located in Figure 5.1. The vertical and horizontal scales (metres) are shown. The former is water depth with depth increments of 20 m.

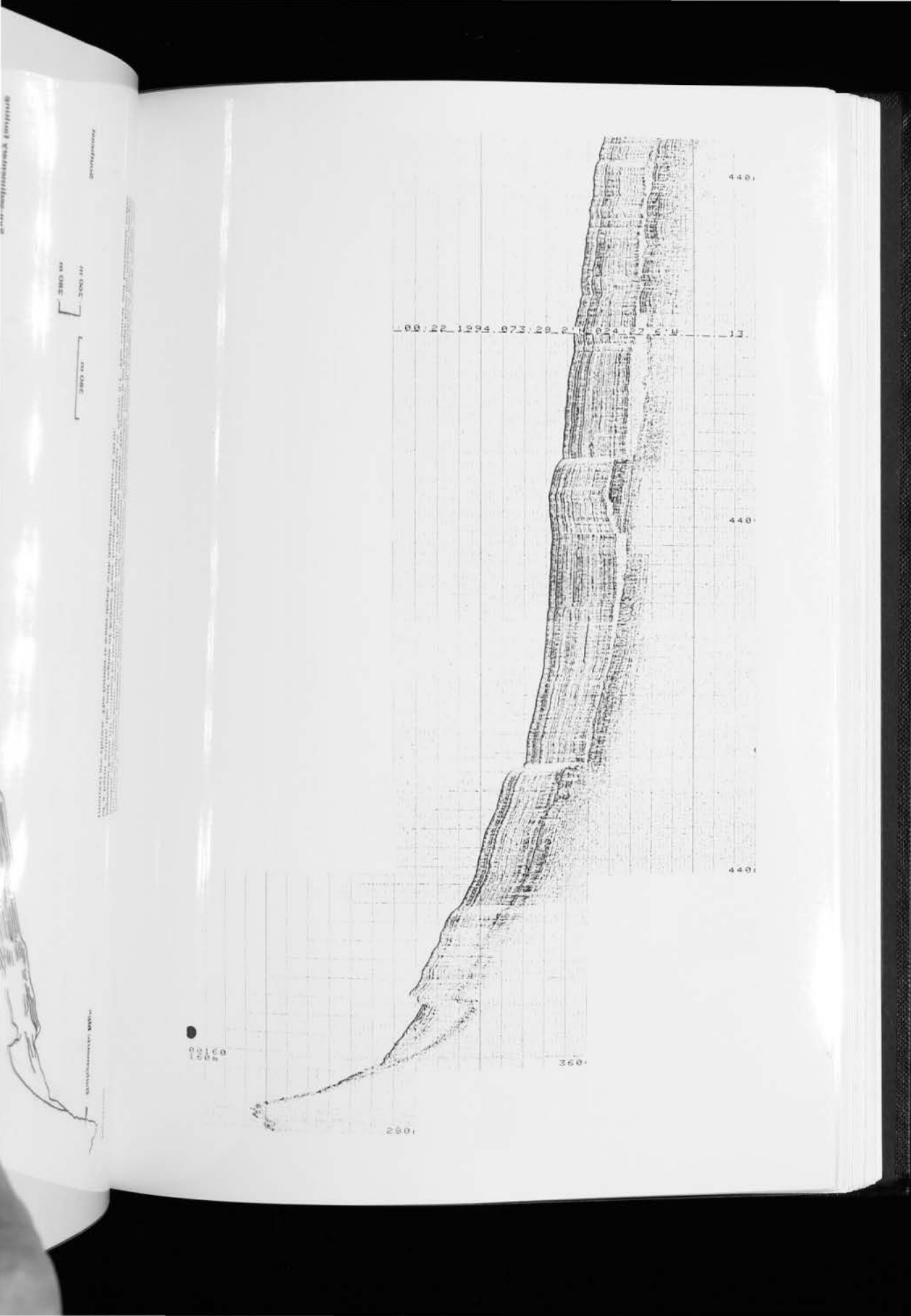
440
440
440
360
280

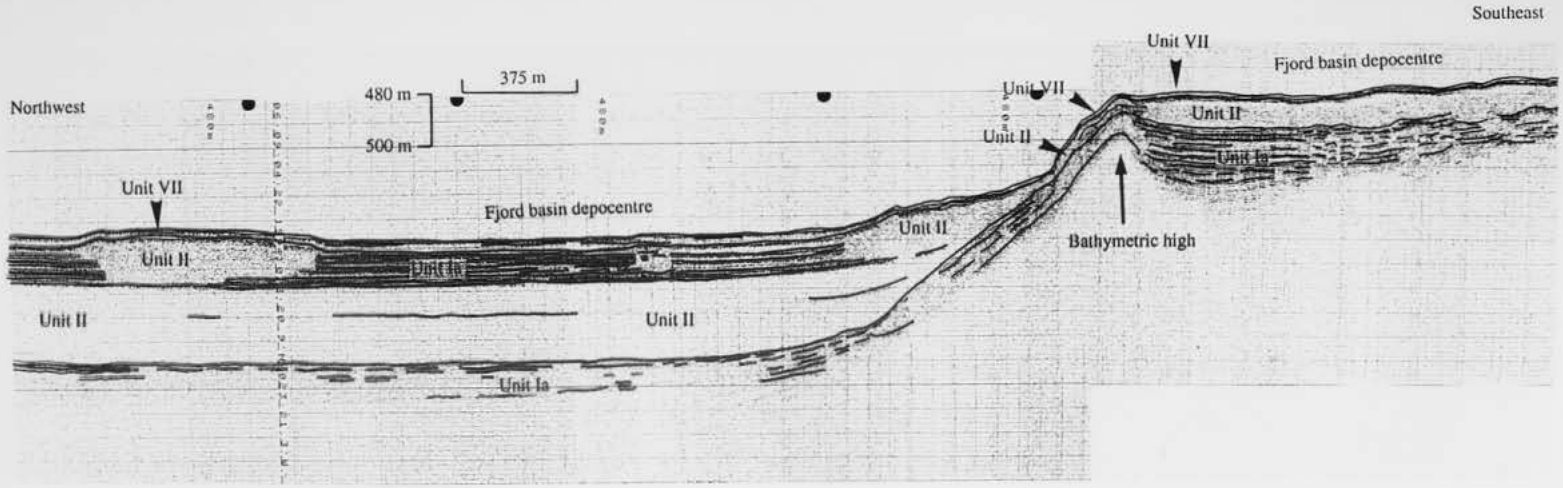

Figure 5.3. Parasound record illustrating the acoustic character of units Ia, II and VII. Units Ia and II are basin fill. Unit Ia consists of stratified internal (sub sea-floor) reflectors beneath a planar sea-floor. Unit II consists of a number of sub sea-floor, acoustically massive and transparent, unconformable lense to elongate shaped sediment bodies. The unit also appears on the bathymetric high adjoining two similar units of adjacent basins. Unit VII consists of parallel, hummocky sea-floor and sub sea-floor reflectors that form a single conformable cover draping the bathymetric high, slope and troughs. The record is an example from adjoining basins within the mid to outer region of Kejser Franz Josephs Fjord located in Figure 5.1. The vertical and horizontal scales (metres) are shown. The former is water depth with depth increments of 20 m.

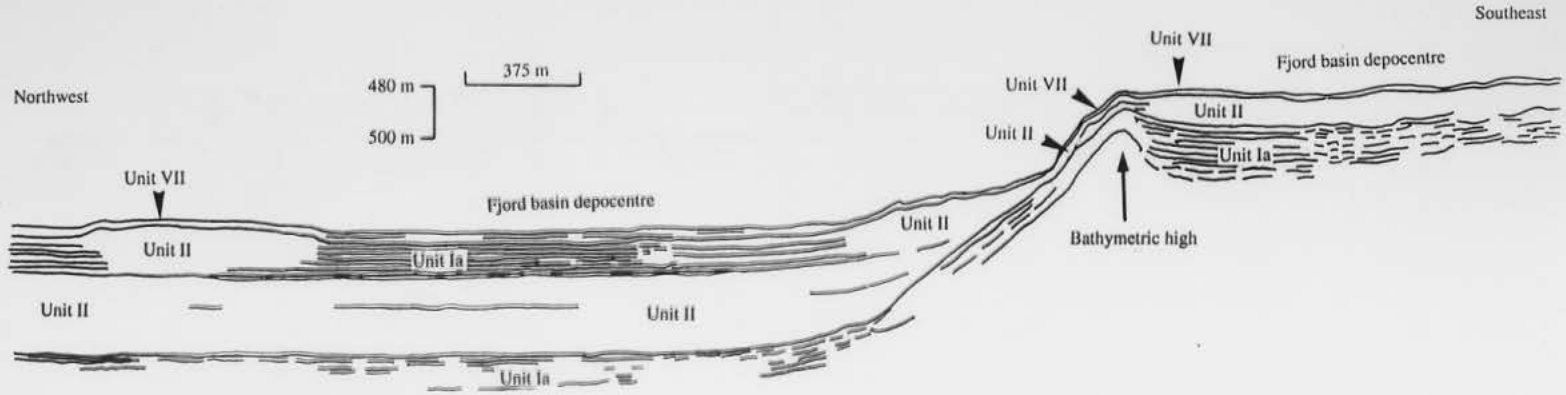

Figure 5.3. Parasound record illustrating the acoustic character of units Ia, II and VII. Units Ia and II are basin fill. Unit Ia consists of stratified internal (sub sea-floor) reflectors beneath a planar sea-floor. Unit II consists of a number of sub sea-floor, acoustically massive and transparent, unconformable lense to elongate shaped sediment bodies. The unit also appears on the bathymetric high adjoining two similar units of adjacent basins. Unit VII consists of parallel, hummocky sea-floor and sub sea-floor reflectors that form a single conformable cover draping the bathymetric high, slope and troughs. The record is an example from adjoining basins within the mid to outer region of Kejser Franz Josephs Fjord located in Figure 5.1. The vertical and horizontal scales (metres) are shown. The former is water depth with depth increments of 20 m.

400m
400m
400m

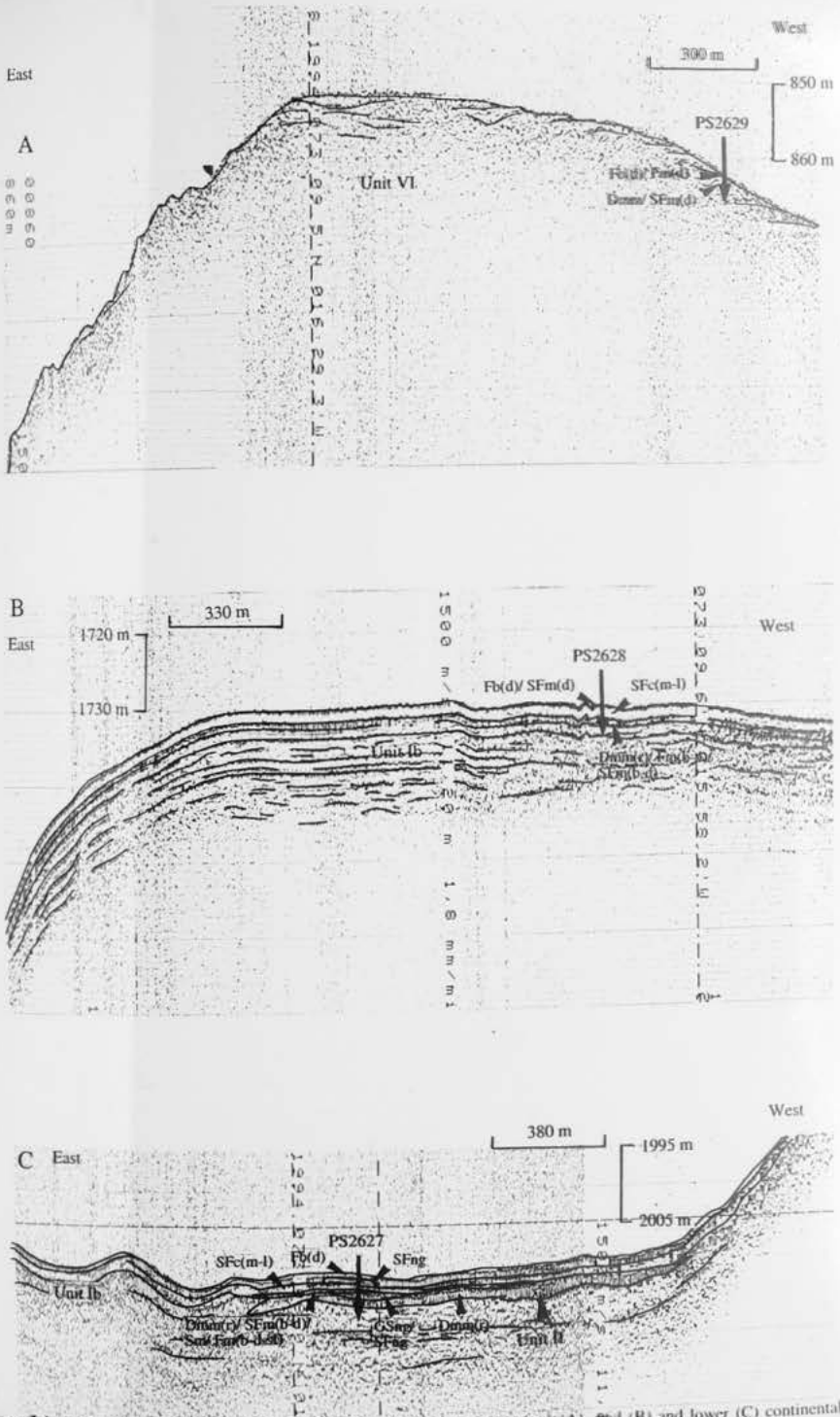

Figure 5.4 (A-C). Parasound records illustrating the acoustic units of the upper (A), and (B) and lower (C) continental slope which are located in Figure 5.1. (A) Unit VI consists of acoustically massive sediment with diffuse to discontinuous internal (sub sea-floor) reflectors. (B) and (C) Unit Ib consists of stratified internal reflectors beneath a planar to hummocky sea-floor. (C) Unit II consists of unconformable wedge shaped sub sea-floor reflectors separating lense shaped sediment bodies. The horizontal sections of the records result from the ship track set at 90° to the slope gradient. Sediment cores PS2629, PS2628 and PS2627 were recovered from the slope, and the lithofacies refer to Table 4.1 and Fig. 4.11 and locations are shown. The vertical and horizontal scales (metres) are shown. The former is water depth with depth increments of 10 m.

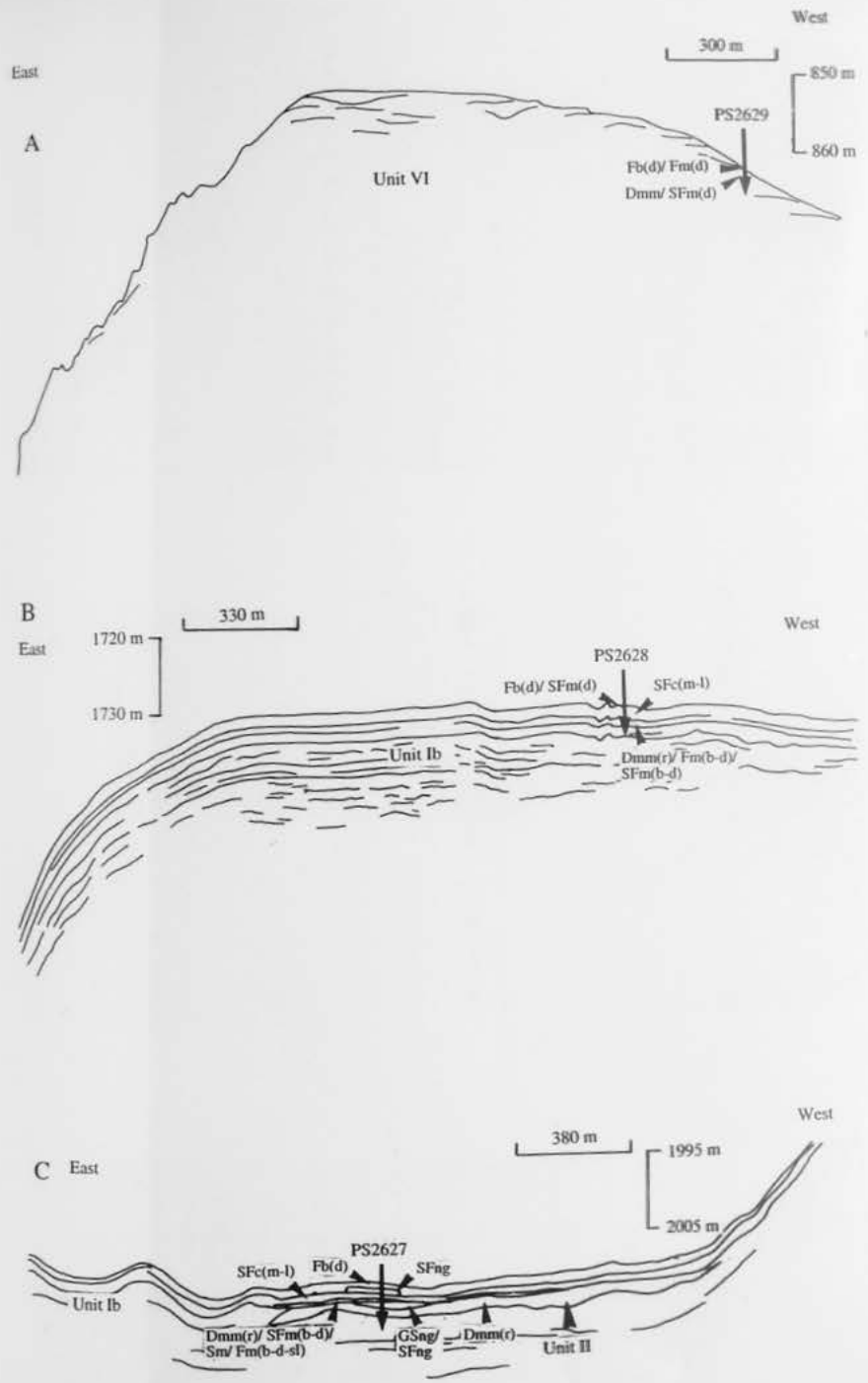

Figure 5.4 (A-C). Parasound records illustrating the acoustic units of the upper (A), mid (B) and lower (C) continental slope which are located in Figure 5.1. (A) Unit VI consists of acoustically massive sediment with diffuse to discontinuous internal (sub sea-floor) reflectors. (B) and (C) Unit Ib consists of stratified internal reflectors beneath a planar to hummocky sea-floor. (C) Unit II consists of unconformable wedge shaped sub sea-floor reflectors separating lense shaped sediment bodies. The horizontal sections of the records result from the ship track set at 90° to the slope gradient. Sediment cores PS2629, PS2628 and PS2627 were recovered from the slope, and the lithofacies (refer to Table 4.1 and Fig. 4.1) and locations are shown. The vertical and horizontal scales (metres) are shown. The former is water depth with depth increments of 10 m.

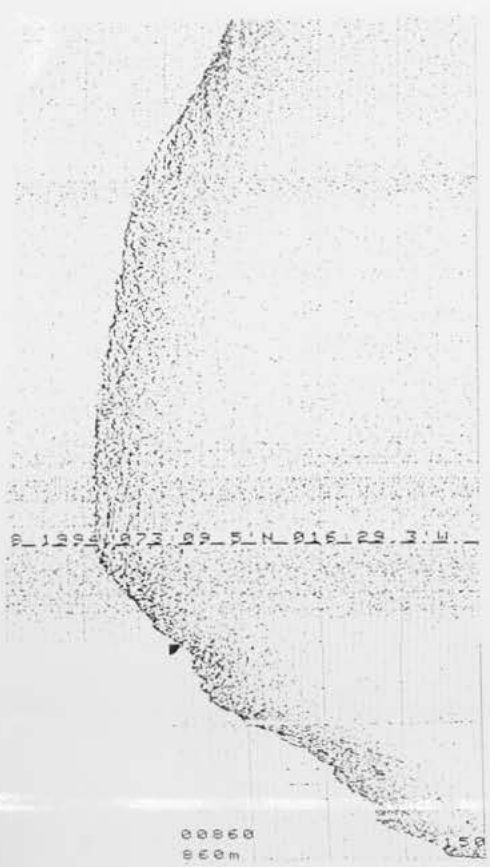

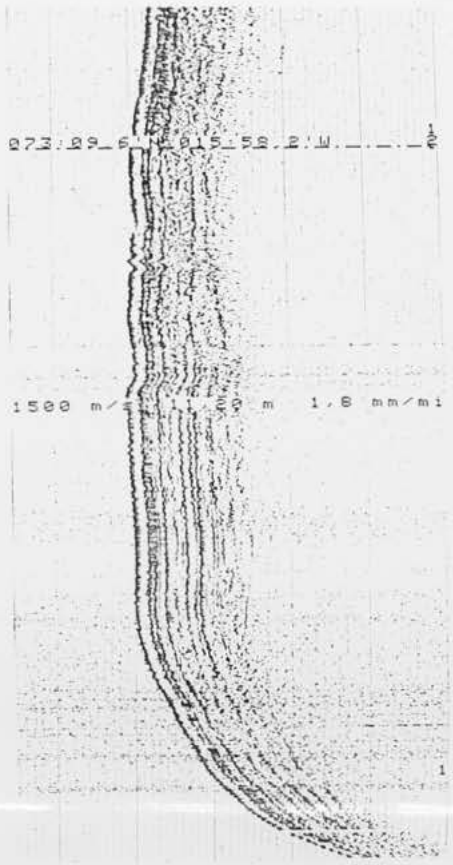

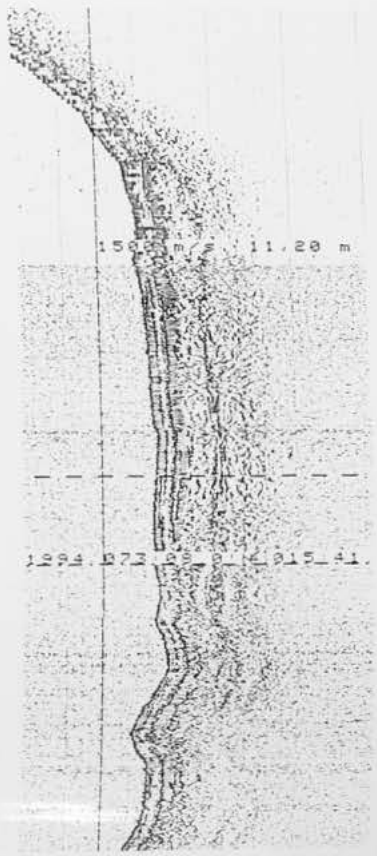

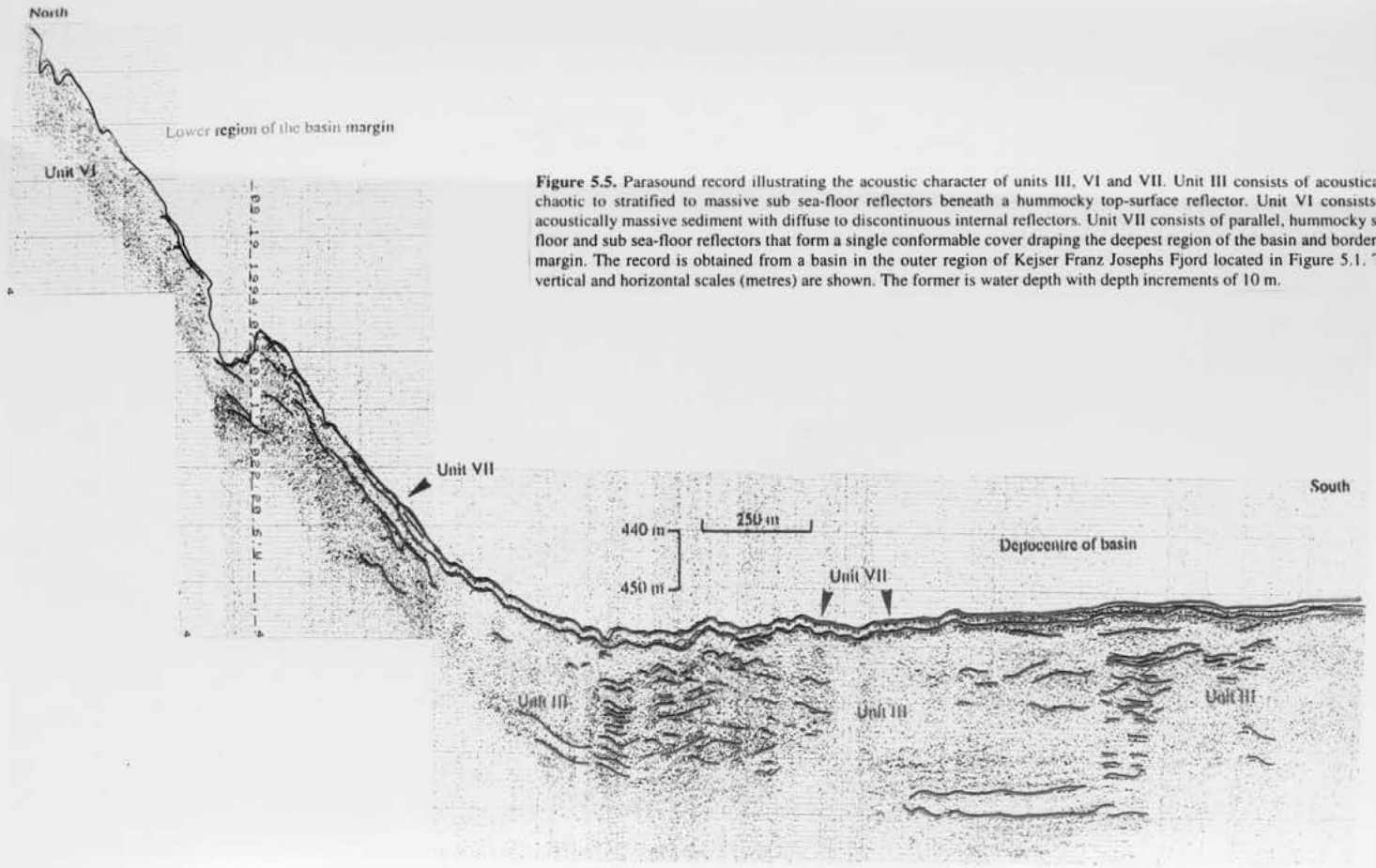

Figure 5.5. Parasound record illustrating the acoustic character of units III, VI and VII. Unit III consists of acoustically chaotic to stratified to massive sub sea-floor reflectors beneath a hummocky top-surface reflector. Unit VI consists of acoustically massive sediment with diffuse to discontinuous internal reflectors. Unit VII consists of parallel, hummocky sea-floor and sub sea-floor reflectors that form a single conformable cover draping the deepest region of the basin and bordering margin. The record is obtained from a basin in the outer region of Kejser Franz Josephs Fjord located in Figure 5.1. The vertical and horizontal scales (metres) are shown. The former is water depth with depth increments of 10 m.

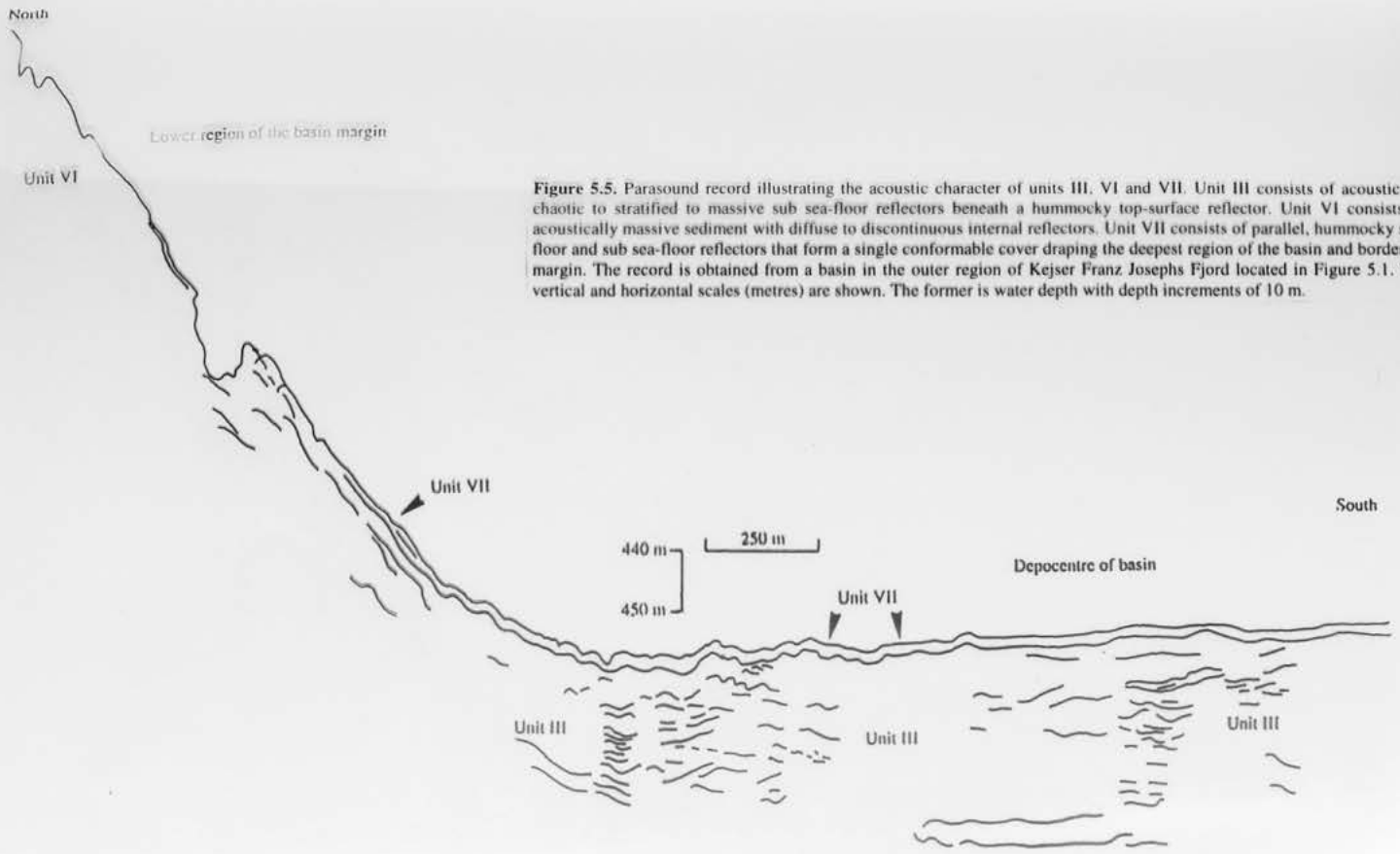

Figure 5.5. Parasound record illustrating the acoustic character of units III, VI and VII. Unit III consists of acoustically chaotic to stratified to massive sub sea-floor reflectors beneath a hummocky top-surface reflector. Unit VI consists of acoustically massive sediment with diffuse to discontinuous internal reflectors. Unit VII consists of parallel, hummocky sea-floor and sub sea-floor reflectors that form a single conformable cover draping the deepest region of the basin and bordering margin. The record is obtained from a basin in the outer region of Kejser Franz Josephs Fjord located in Figure 5.1. The vertical and horizontal scales (metres) are shown. The former is water depth with depth increments of 10 m.

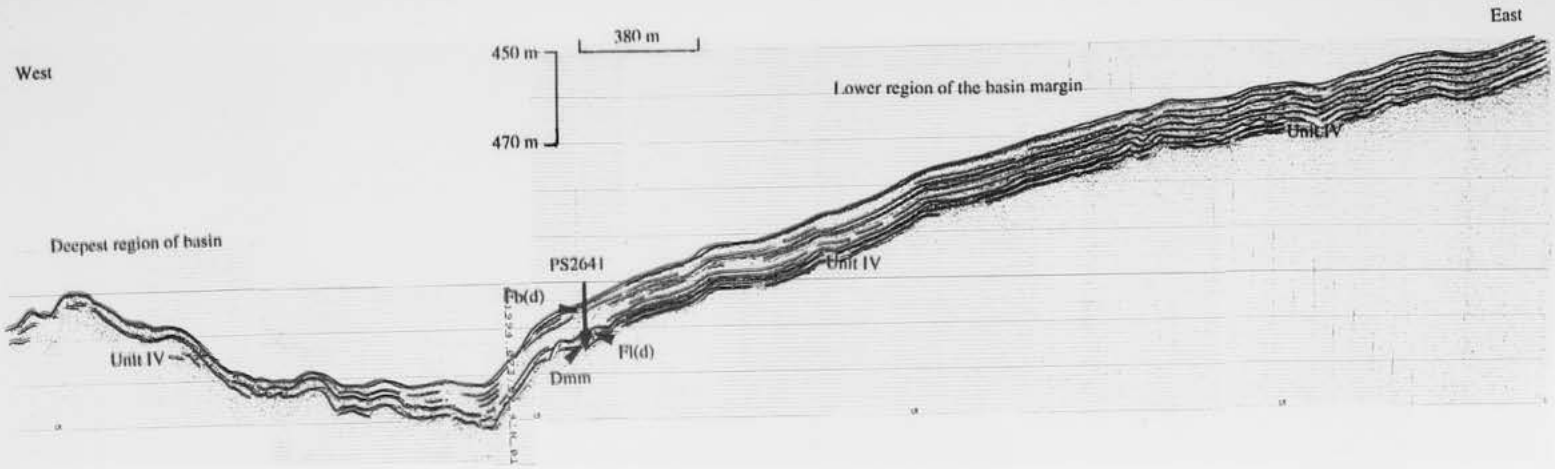

Figure 5.6. Parasound record illustrating the acoustic character of unit IV. The unit consists of stratified, parallel and hummocky sea-floor and sub sea-floor reflectors that form a conformable cover draping the bathymetric trough of the basin, and the bathymetric high of the margin. The record is an example from the eastern margin of a basin on the inner continental shelf adjacent to Kejser Franz Josephs Fjord located in Figure 5.1. Sediment core PS2641 was recovered from the lower region of the eastern basin margin, and the lithofacies (Table 4.1 and Fig. 4.1) and location are shown. The vertical and horizontal scales (metres) are shown. The former is water depth with depth increments of 20 m.

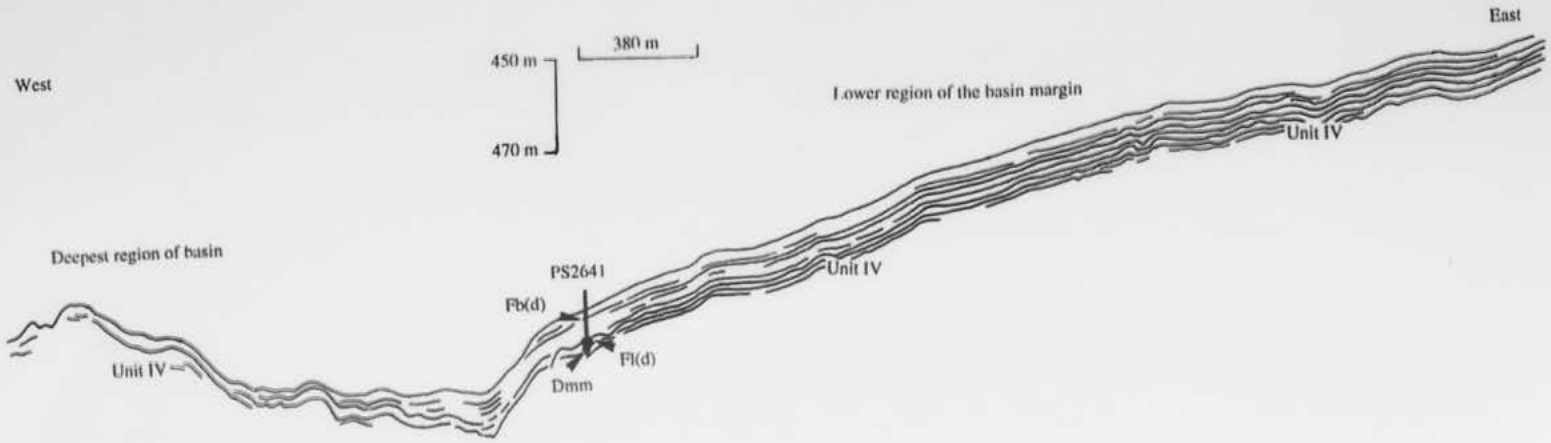

Figure 5.6. Parasound record illustrating the acoustic character of unit IV. The unit consists of stratified, parallel and hummocky sea-floor and sub sea-floor reflectors that form a conformable cover draping the bathymetric trough of the basin, and the bathymetric high of the margin. The record is an example from the eastern margin of a basin on the inner continental shelf adjacent to Kejser Franz Josephs Fjord located in Figure 5.1. Sediment core PS2641 was recovered from the lower region of the eastern basin margin, and the lithofacies (Table 4.1 and Fig. 4.1) and location are shown. The vertical and horizontal scales (metres) are shown. The former is water depth with depth increments of 20 m.

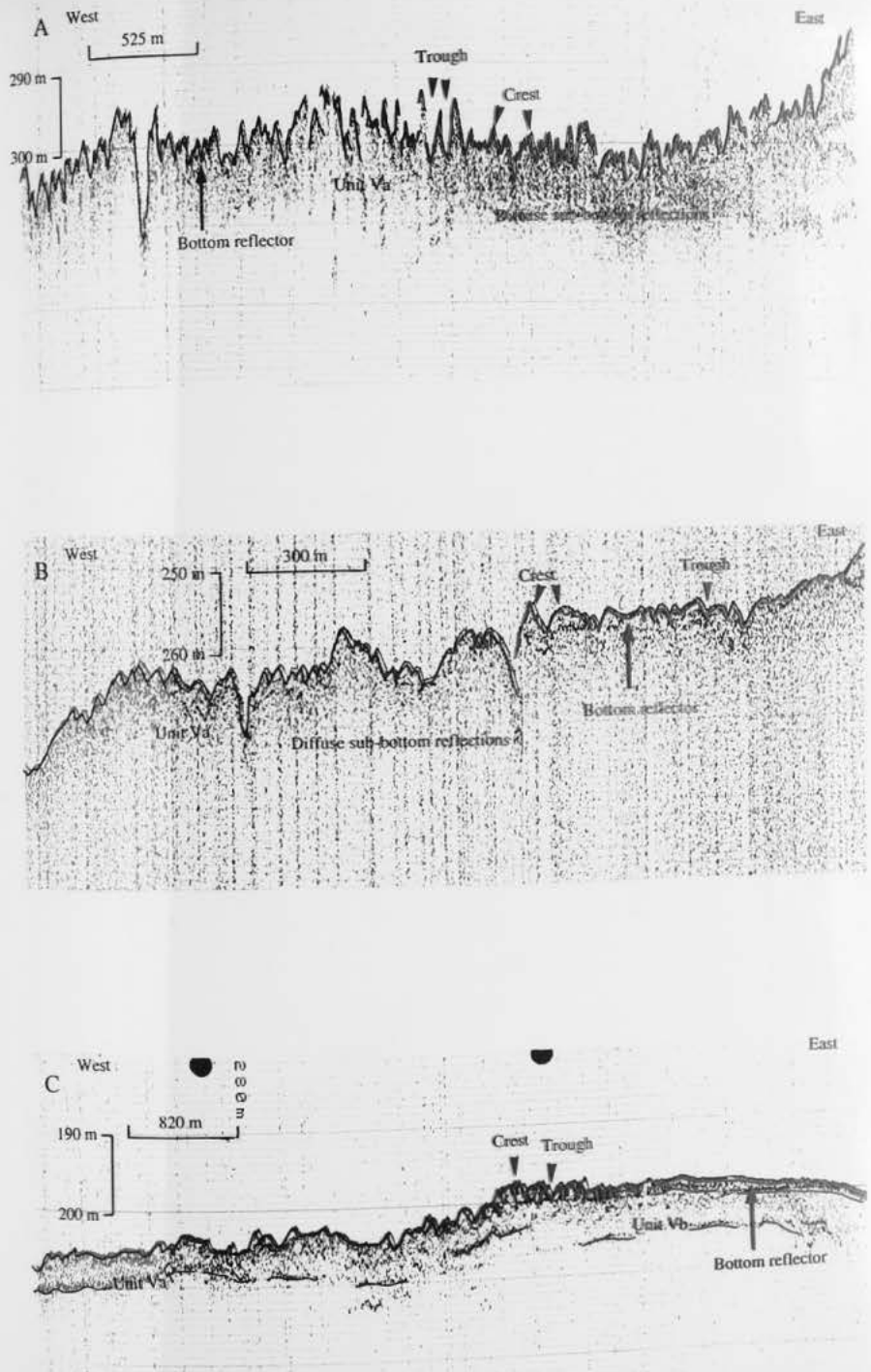

Figure 5.7 (A-C). Parasound records illustrating the acoustic character and irregularity of the sea-floor reflector of sub-units Va and Vb, located in Figure 5.1. (A-C) Sub-unit Va consists of acoustically homogeneous sediment with diffuse sub sea-floor reflectors. (C) Sub-unit Vb consists of acoustically discontinuous to continuous stratified sediment. The intensity of sea-floor reflector irregularities vary between high (A), intermediate (B) and low (C). The irregularities are composed of paired crests and troughs. The intensity of the sea-floor irregularities reflect the degree of scouring by icebergs. The records are examples from the inner (A), mid (B) and outer (C) continental shelf located in Figure 5.1. The vertical and horizontal scales (metres) are shown. The former is water depth with depth increments of 10 m.

Figure 5.7 (A-C). Parasound records illustrating the acoustic character and irregularity of the sea-floor reflector of sub-units Va and Vb, located in Figure 5.1. (A-C) Sub-unit Va consists of acoustically homogeneous sediment with diffuse sub sea-floor reflectors. (C) Sub-unit Vb consists of acoustically discontinuous to continuous stratified sediment. The intensity of sea-floor reflector irregularities vary between high (A), intermediate (B) and low (C). The irregularities are composed of paired crests and troughs. The intensity of the sea-floor irregularities reflect the degree of scouring by icebergs. The records are examples from the inner (A), mid (B) and outer (C) continental shelf located in Figure 5.1. The vertical and horizontal scales (metres) are shown. The former is water depth with depth increments of 10 m.

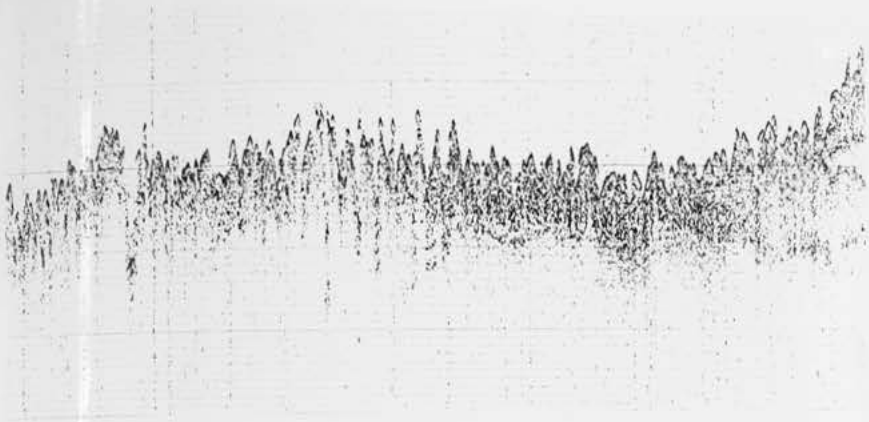

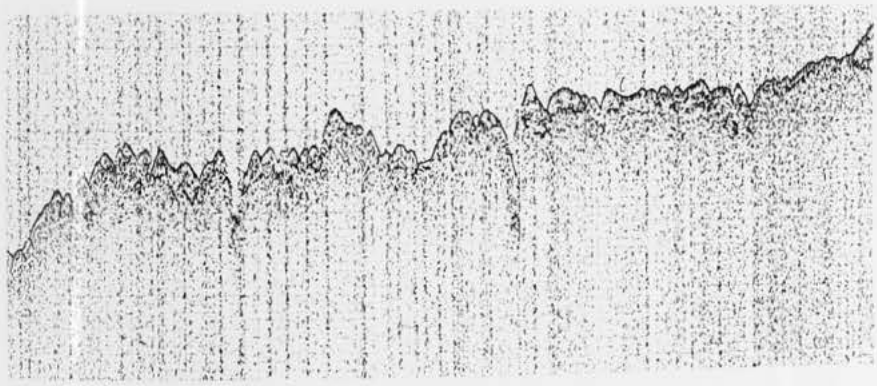

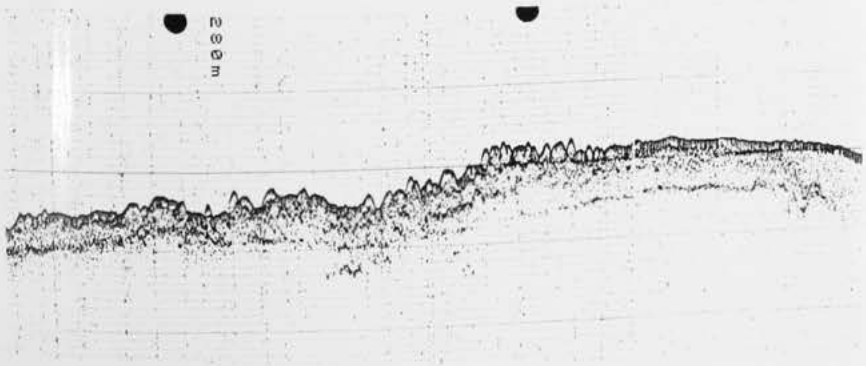
mmm

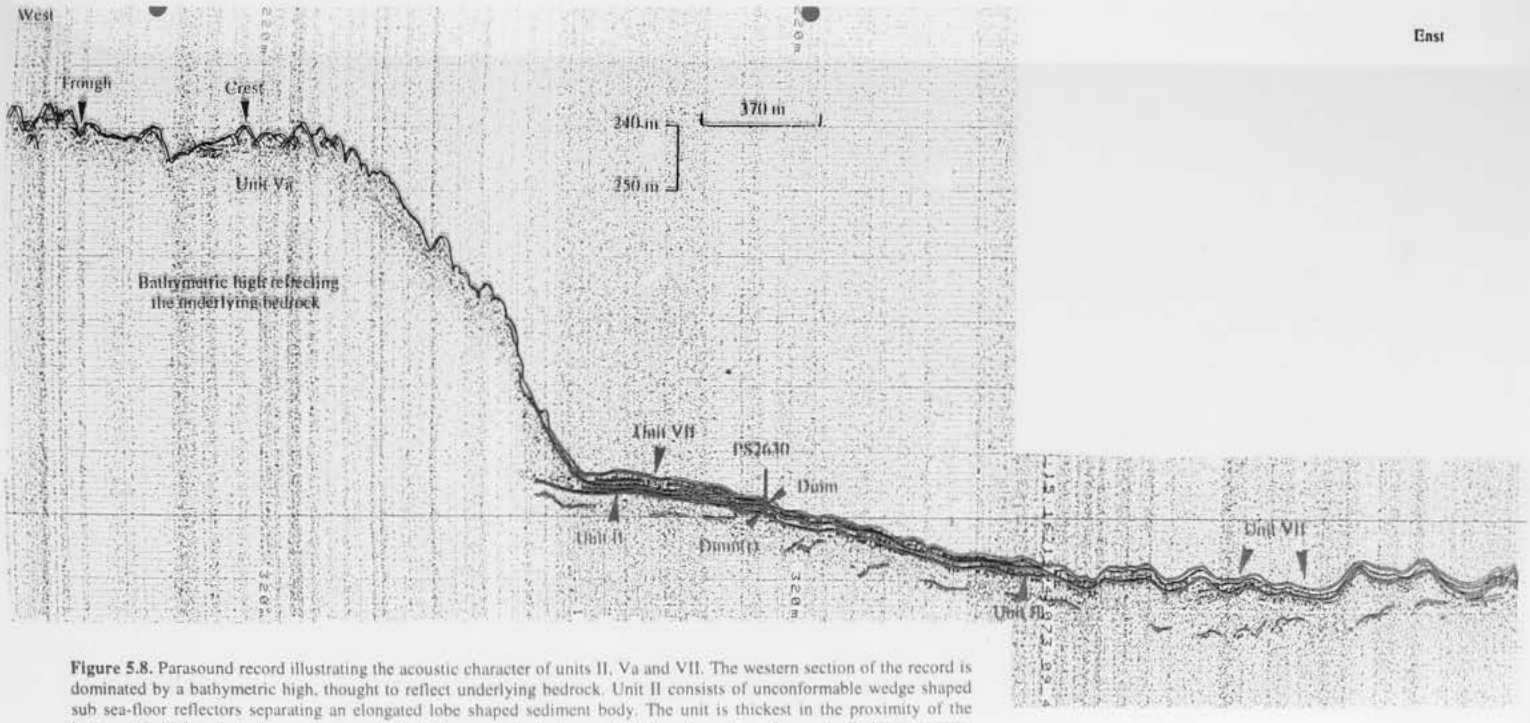

Figure 5.8. Parasound record illustrating the acoustic character of units II, Va and VII. The western section of the record is dominated by a bathymetric high, thought to reflect underlying bedrock. Unit II consists of unconformable wedge shaped sub sea-floor reflectors separating an elongated lobe shaped sediment body. The unit is thickest in the proximity of the bathymetric high and pinches out eastwards. Unit Va covers the bathymetric high, and consists of acoustically homogeneous sediment with diffuse sub sea-floor reflectors. Unit VII consists of parallel, hummocky sea-floor and sub sea-floor reflectors that form a single conformable cover draping bathymetric highs and troughs. Sediment core PS2630 was recovered close to the bathymetric high, and the lithofacies (Table 4.1 and Fig. 4.1) and location are shown. The record is from the mid continental shelf located on Figure 5.1. The vertical and horizontal scales (metres) are shown. The former is water depth with depth increments

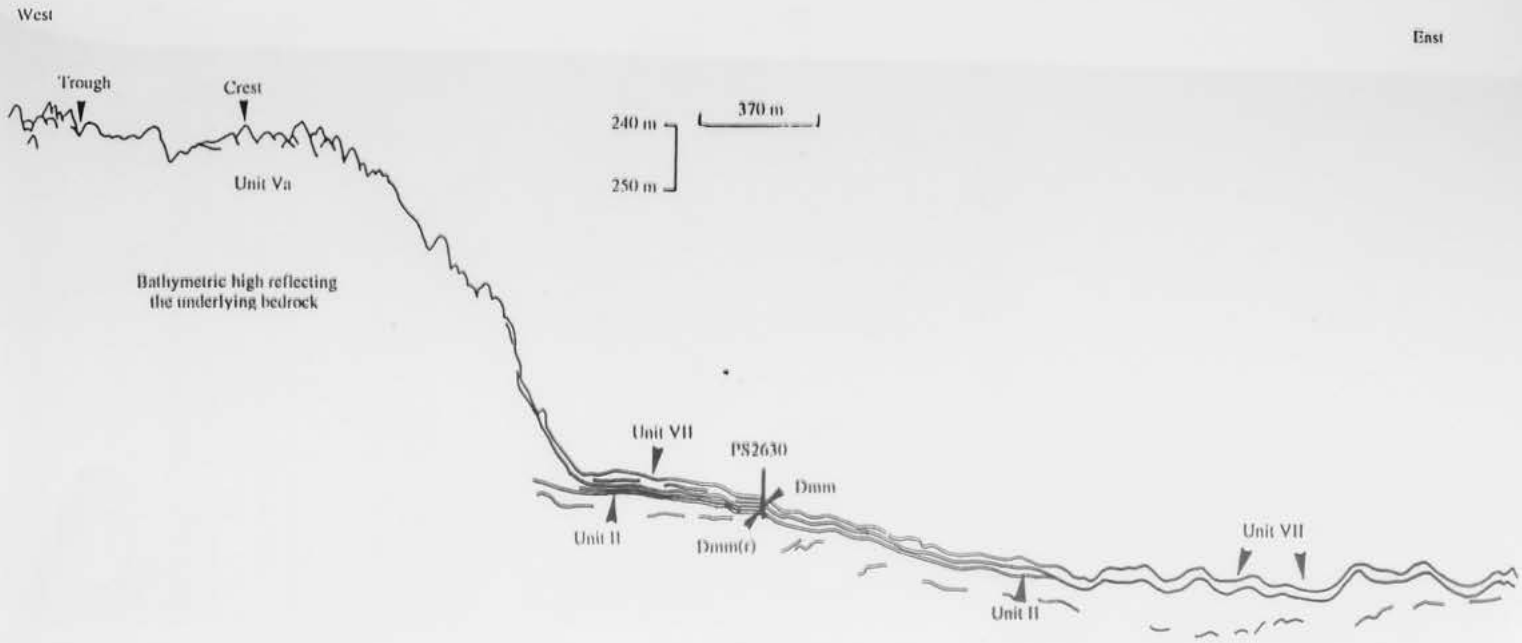

Figure 5.8. Parasound record illustrating the acoustic character of units II, Va and VII. The western section of the record is dominated by a bathymetric high, thought to reflect underlying bedrock. Unit II consists of unconformable wedge shaped sub sea-floor reflectors separating an elongated lobe shaped sediment body. The unit is thickest in the proximity of the bathymetric high and pinches out eastwards. Unit Va covers the bathymetric high, and consists of acoustically homogeneous sediment with diffuse sub sea-floor reflectors. Unit VII consists of parallel, hummocky sea-floor and sub sea-floor reflectors that form a single conformable cover draping bathymetric highs and troughs. Sediment core PS2630 was recovered close to the bathymetric high, and the lithofacies (Table 4.1 and Fig. 4.1) and location are shown. The record is from the mid continental shelf located in Figure 5.1. The vertical and horizontal scales (metres) are shown. The former is water depth with depth increments of 10 m.

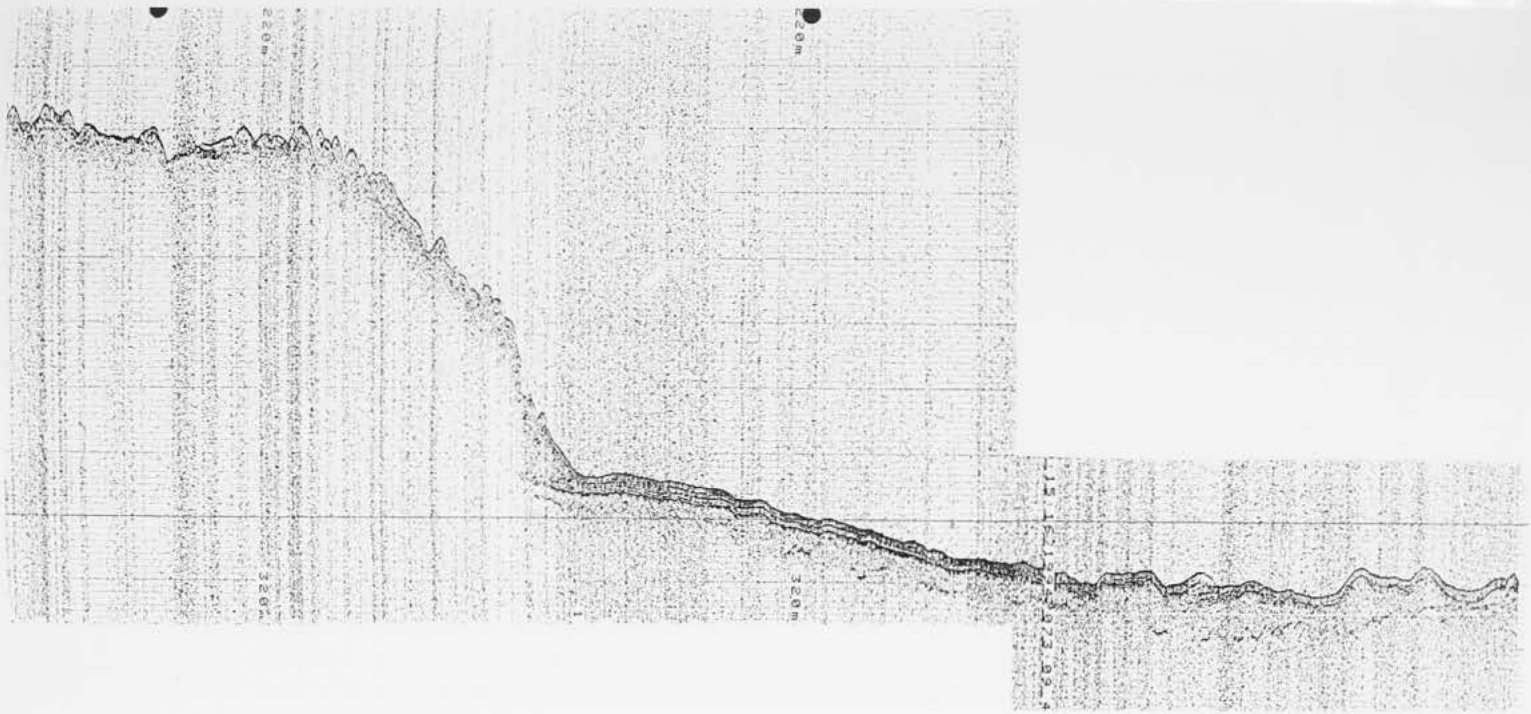
220m
320m
220m
320m

5.4.5 Acoustic unit IV - acoustically stratified sediment exhibiting conformable sea-floor and internal reflectors

The main characteristics of this acoustic unit are summarised in Table 5.1 and illustrated in Figure 5.6. The unit is characterised by a continuous, distinct, sharp sea-floor reflector displaying a planar to mainly hummocky morphology which develops a very occasional degree of surface roughness discussed further in Section 5.3.6. Internal or sub-seafloor reflectors are multiple and parallel, distinct, sharp to diffuse, broad to narrowly spaced (up to several metres thick) and continuous over distances up to ten's of kilometres. Most of the records are acoustically transparent to semi-transparent between reflectors. The sea-floor and internal reflectors are conformable with one another, and over topographic highs and within intervening basins. The hummocky morphology displayed throughout the unit probably reflects topographic variations of the underlying acoustic facies and bedrock even though it is not possible to recognise the bedrock on Parasound records.

5.4.6 Acoustic unit V - acoustically homogeneous and stratified sediment with an irregular sea-floor reflector

The main characteristics of this acoustic unit are summarised in Table 5.1 and illustrated in Figure 5.7(A-C). The unit is characterised by a continuous to discontinuous, distinct and sharp to diffuse irregular sea-floor reflector. The irregular sea-floor reflector is composed of roughness elements comprising crests and troughs of varying intensities. Many have paired crests. In general, the Parasound system is able to resolve the morphology of the crests and troughs but diffraction hyperbolae can occasionally dominate some acoustic sections where changes occur abruptly. The amplitude of the roughness elements reach a maximum of 15 m from crest to trough, and their widths vary from metres to tens of metres. The intensity of the roughness elements can be classified into three types: i) High intensity composing a poorly defined, discontinuous to continuous and highly irregular sea-floor reflector with relatively few flat or planar areas (Fig 5.7A). This acoustic character results from the inability of the small footprint diameter of Parasound to effectively resolve the abrupt changes in sea-floor reflector morphology (Dowdeswell et al. 1993, 1997a), ii) Intermediate intensity composing a more distinct, irregular sea-floor reflector where crest morphology are more rounded and increasingly separated (Fig 5.7B), and iii) Low intensity with a continuous, distinct sea-floor reflector where regions of crest-trough morphology are exhibited and separated by extensive planar regions (Fig 5.7C). The internal acoustic nature of this unit varies in response to the intensity of the surface roughness elements, resulting in two sub-units:

- Sub-unit Va . Homogeneous sediment structure characterised by diffuse signal return associated with regions of high and intermediate surface roughness intensity (Fig 5.7A,B).
- Sub-unit Vb. Homogeneous to stratified sediment which the latter consists of continuous to discontinuous, diffuse, conformable/ponded reflectors, both associated with low surface roughness intensity (Fig 5.7C). The internal acoustic character is interpreted to match that described for units Ia, IV and VII. This unit was not classified as either unit Ia, IV or VII as the roughness of

the sea-floor reflector is the most distinguishing character as opposed to their subordinate acoustic structure which are in general, poorly developed. The nature of the internal acoustic character of this unit in comparison with acoustic units Ia, IV and VII will be distinguished in terms of the distribution in Section 5.5. In contrast, acoustic unit IV (Section 5.4.5) very occasionally exhibits sea-floor reflector roughness of very low intensity, and as a result is accepted as a subordinate character in comparison to the acoustic structure.

5.4.7 Acoustic unit VI - acoustically semi-penetrable sediment with a distinct to semi-prolonged sea-floor reflector

The main characteristics of this acoustic unit are summarised in Table 5.1 and illustrated in Figure 5.4A. The unit is characterised by a continuous, semi-prolonged and planar sea-floor reflector. The unit is acoustically homogeneous, and semi-transparent to opaque. Internal or sub-sea floor reflectors are diffuse and shallow-based, and point diffractions are numerous. Stratified internal reflectors, where present, are generally weak, distinct to diffuse and discontinuous. Along limited sections of both transects, the sea-floor reflector consists of gentle hummocks underlain by poorly defined unconformable reflectors. These may represent acoustically transparent lens shaped sediment bodies of unit II, though the presence of the complete and clear morphology is restricted. The poor seismic coverage over the continental slope, coupled with the low acoustic return, makes it difficult to identify these sediment bodies and determine their spatial distribution.

5.4.8 Acoustic unit VII - acoustically massive sediment forming a conformable unit

The main characteristics of this acoustic unit are summarised in Table 5.1 and illustrated in Figures 5.3, 5.5 and 5.8. The acoustic unit is characterised by a continuous, distinct and sharp sea-floor reflector that displays a planar to hummocky morphology that is underlain by a parallel sub-sea floor reflector of similar characteristics. Both reflectors form a single conformable unit. The unit is acoustically massive and transparent to opaque, though discontinuous internal reflectors can be occasionally traced over short distances on the continental shelf. The unit is conformable over topographic highs and within intervening basins and sea-floor depressions. The acoustic unit thins laterally against and over topographic highs, but does not pinch out. The hummocky to planar morphology probably reflect topographic variations of the underlying bedrock and sedimentary facies, even though it is not possible to recognise the bedrock on Parasound records for the former case.

5.4.9 Acoustic unit VIII - acoustically homogeneous sediment with an irregular-hummocky top-surface, sub-seafloor reflector

The main characteristics of this acoustic unit are summarised in Table 5.1 and illustrated in Figure 5.8. The unit is overlain by a continuous, sharp, distinct, irregular to hummocky top-surface

reflector. The unit is acoustically homogeneous, though discontinuous stratification is occasionally present, and transparent to semi-transparent. It is difficult to assess whether point diffractions are numerous as there is a problem of differentiating these from acoustic noise on Parasound sections. In some acoustic sections, point reflectors appear to be low in number. The bottom-surface reflector of the unit is only present occasionally, and appears discontinuous, irregular and distinct.

5.5 REGIONAL DISTRIBUTION OF ACOUSTIC UNITS

5.5.1 Introduction

The distribution of the acoustic units outlined in the previous section was mapped for the mid-outer region of the Kejser Franz Josephs Fjord, and adjacent continental shelf and slope. The mapping was based on the ship tracks (Fig 5.1a) along which the Parasound records were collected. The distribution of acoustic units within the study area is described in this section, illustrated in the map of Figure 5.9, and summarised in Table 5.1. The full vertical extent and thickness of acoustic units are discussed where the upper and lower surfaces are visible on sections of the Parasound records. In cases of poor seismic return or extensive sediment thicknesses, the lower surfaces of the acoustic units are not visible and, therefore, minimum thicknesses are quoted.

5.5.2 Continental slope

Units Ib and II are recorded on the mid to lower continental slope (Figs 5.4A-C, 5.9). Unit Ib predominates the mid-lower slope region (Fig 5.4B&C, 5.9). Unit II forms concentrated, shallow sub-sea floor bodies in the upper-mid continental slope transitional region (ca. 73° 09' N, 16° 15' W and 73° 10' N, 15° 39' W), and isolated deeper bodies further down the continental slope, both with thicknesses up to 7 m. The former case is only observed along the most northerly of the two profiles taken across the slope (Fig 5.1a). In shallow cases, unit II results in a hummocky sea-floor. Unit VI is observed on the upper continental slope extending from the mid-upper continental slope transitional region to the continental shelf break (Figs 5.4A, 5.9). The upper acoustic layers of unit Ib grades into Unit VI at ca. 73° 09' N, 16° 06' W on the upper continental slope.

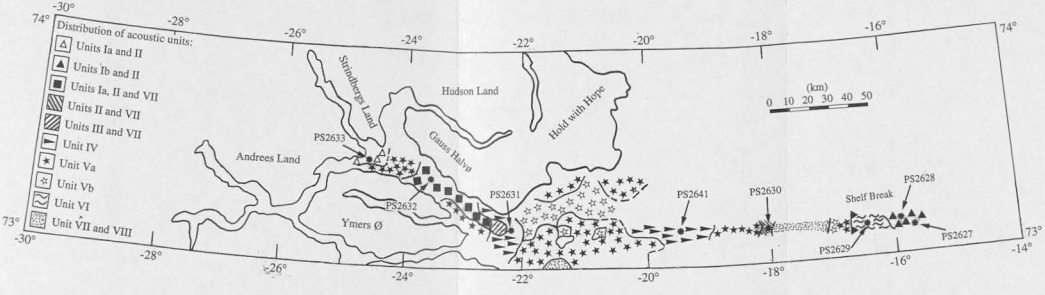

Figure 5.9. Map of Kejser Franz Joseph Fjord and the adjacent continental shelf and slope showing the distribution of acoustic units recognised from Parasound records. The study area in relation to Greenland is shown within the inset of Figure 5.1. A key to the symbols representing the acoustic units is provided. The map scale is indicated. The distribution was based on Parasound records obtained along the ship tracks shown in Figure 5.1. Sediment cores of this study are shown.

5.5.3 Continental shelf and Fosters Bugt

Sub-units Va and Vb form the uppermost acoustic unit on the outer continental shelf between ca. 73° 09' N, 17° 17' W and the continental shelf break (Figs 5.7C, 5.9). Unit Va is most prevalent in the region on, and approaching the continental shelf break (Fig 5.9). Unit V grades laterally into unit VII (<2 m thick) and forms the uppermost unit draping underlying irregularities between the outer and mid continental shelf (Figs 5.8, 5.9). Some sections of sub-unit Vb display a character similar to that of unit VII. In a limited number of regions between the mid and outer continental shelf, units Vb and VII are underlain by unit VIII (Figs 5.8, 5.9). However, this unit is poorly defined due to very weak acoustic return. On the mid continental shelf, unit VII terminates midway up the slope of the eastern margin of the bathymetric high (Figs 5.8, 5.9; Section 5.3.3). In the region adjacent to this margin unit VII is underlain by unit II. Unit II is at its thickest (8.5 m) at the base of the bathymetric high slope and extends eastwards for 2500 m where it pinches out at ca. 73° 09' N, 18° 00' W (Fig 5.8, 5.9). Unit II is underlain by unit VIII (Fig 5.8). The bathymetric high is covered by unit Va which grades laterally into unit IV on the eastern margin of the inner continental shelf basin (Figs 5.6, 5.8, 5.9; Section 5.3.3). Unit IV forms a conformable cover draping the western (<6 m thick) and eastern (<11 m thick) margins of this basin, though the centre of the basin is relatively devoid of significant sediment cover (<2 m thick) (Figs 5.6, 5.9). Sub-units Va and Vb form the only units within Fosters Bugt, and the inner continental shelf between the western margin of the basin and Bontekoe Ø (Figs 5.7A-B, 5.9). Sub-unit Vb characterises the sea floor to the north, north west and north east of Bontekoe Ø, where the sediment displays an acoustic character of mainly unit IV character, and occasionally unit Ia within small-scale depressions.

5.5.4 Mid-Outer Kejser Franz Josephs Fjord

The sea-floor along the southern margin of the outer fjord and over the major sill between the mid and outer fjord (Fig 5.1b) comprises acoustic unit Va (Fig 5.9). However, no acoustic data ~~was~~ were recorded along the northern margin in order to assess the acoustic character of the sea-floor. The mid fjord basin fill comprises predominantly unit Ia and occasional, interdigitating lobed bodies of unit II (Figs 5.2, 5.9). The sediment fill of the innermost sub-basin of the outer fjord (Fig 5.1b) comprises a sequence consistent with units from the lowermost upwards (Figs 5.3, 5.9) of unit Ia (>10 m thick but poorly defined due to weak acoustic return), unit II (<34 m thick), unit Ia (20 m thick) interdigitating with occasional lobed bodies of unit II (<20 m thick), and unit VII (<4 m thick) which is conformable with the underlying acoustic units. Unit VII can only be differentiated from the individual stratified layers of unit Ia when it is underlain by the isolated, interdigitating bodies of unit II (Fig 5.3), restricted to the outer region of the innermost sub-basin. Away from these regions, unit VII is observed to grade laterally into the uppermost acoustic layer of unit Ia where it cannot be differentiated. Therefore, the unit is classified as part of unit Ia. Unit VII is conformable over the adjoining sill and across the adjacent intermediate and outermost sub-basins of the outer fjord (<2 m thick) (Figs 5.1b, 5.3, 5.9). One of the lobed bodies of unit II interdigitating with unit Ia in the

innermost sub-basin can be traced over an adjoining sill and into the intermediate sub-basin (Fig 5.3). This unit continues throughout the length of the sub-basin attaining a thickness of 14 m proximal to the sill, and increases to >30 m down fjord. In the intermediate sub-basin unit II is underlain by unit Ia (>30 m thick) and is mainly ponded within small-scale depressions (Fig 5.3), though this is only evident along occasional parts of the acoustic sections. The inner and central region of the outermost sub-basin comprises predominantly unit III (>60 m thick) overlain by unit VII (<2 m thick) (Figs 5.5, 5.9). Unit II of the intermediate sub-basin is traced into the outer sub-basin in some acoustic sections and terminates abruptly against the steep slope marking the transition into Fosters Bugt (Section 5.3.4). Based on the close proximity and vertical and spatial distribution it is likely unit II grades laterally into unit III. Unit IV characterises the outer and marginal regions of the same basin (>25 m thick) (Fig 5.9). Unit Ia, with interdigitating lobed bodies of unit II, is common within small-scale basins confined by bathymetric highs along the southern margin of the outer fjord, and west and south of Bontekoe Ø.

5.6 CORRELATION OF ACOUSTIC UNITS AND CORE LITHOSTRATIGRAPHY

5.6.1 Introduction and correlation method

The lithostratigraphy and sedimentology of cores provide the ground truthing used in establishing the sedimentary nature and associated processes of deposition of acoustic units recognised from seismic records. This section concentrates on the correlation of the lithostratigraphy of cores PS2627, PS2628, PS2629, PS2630, PS2641, PS2631, PS2632 and PS2633 recovered along the main transect (Chapter 4), with the acoustic units (Sections 5.4, 5.5) of the study area (Figs 1.1, 5.1a). A summary of the correlation between the lithofacies of each core and the corresponding acoustic units at each core site is given in Table 5.2, and the location of the cores in relation to the ship tracks for which Parasound data ~~is~~ are available is shown in Figure 5.1a.

The correct positioning of cores on the acoustic records is necessary for this section and involves several steps. First, a core site is located on the Parasound tracklines (Fig 5.1a) using the latitude and longitude coordinates determined at the time of coring. Second, the core site is located within the Parasound records (Fig 5.1a). This position is determined by matching the coordinates of the core site with those of the trackline logged at discrete intervals on the corresponding section of the Parasound records. However, matching is more difficult if the coordinates of the core site lie between those logged on the Parasound records. A simple technique using water depths was used to overcome this which would not hold true with a horizontal sea-floor. The core site is located by correlating the water depth to the sea-floor recorded at the core site (Table 3.1) to a point with equal water depth along the sea-floor reflector in the relevant section of the Parasound record.

5.6.2 Core sites and acoustic units

5.6.2.1 PS2627, PS2628 and PS2629 (lower to upper continental slope)

Cores PS2627 and PS2628 of the lower and mid continental slope, respectively, penetrated up to 292 cm of acoustic unit Ib (Figs 5.4B&C, 5.9; Sections 5.3.2, 5.5.2). In addition, the lowermost section of core PS2627, below a core depth of 320 cm, intersected an 87 cm section of acoustic unit II (Figs 5.4C, 5.9; Sections 5.3.2, 5.5.2). Core PS2629, on the upper continental slope, penetrated a 244 cm section of acoustic unit VI (Figs 5.4A, 5.9; Sections 5.3.2, 5.5.2).

5.6.2.2 PS2630 and PS2641 (mid to inner continental shelf)

Core PS2630 was recovered ca. 2 km east of the eastern margin of the mid continental shelf bathymetric high (Fig 5.1b, 5.8; Sections 5.3.3, 5.5.3). The upper section of PS2630 (down to a core depth of 174 cm) intersected the entire thickness of acoustic unit VII, and the lower section of the core (between core depths 185-302 cm) penetrated 117 cm of the underlying acoustic unit II (Figs 5.8, 5.9). Core PS2641 penetrated a 700 cm section of acoustic unit IV on the eastern margin of the inner continental shelf basin (Figs 5.1b, 5.6, 5.9; Sections 5.3.3, 5.5.3).

5.6.2.3 PS2631, PS2632 and PS2633 (outer to mid Kejser Franz Josephs fjord)

Core PS2631 penetrated a 725 cm section of acoustic unit IV within the outermost sub-basin of the outer fjord (Figs 5.1b, 5.9; Sections 5.3.4, 5.5.4). Core PS2633 of the shallower, marginal region of the mid fjord basin, and PS2632 of the innermost sub-basin of the outer fjord (Fig 5.1b; Sections 5.3.4, 5.5.4) penetrated 585 cm and 258 cm sections of the uppermost and near-surface acoustic unit Ia, respectively (Fig 5.9; Section 5.5.4). No figures for these core sites are included in this thesis as the general nature of the acoustic units for PS2631, PS2632 and PS2633 is similar to those shown in Figures 5.6, 5.3 and 5.2, respectively. In the case of PS2632, the upper acoustic unit Ia and the overlying unit VII of Figure 5.3 are a continuation of unit Ia (Section 5.5.4) that the core penetrated.

5.6.3 Correlation of core lithofacies and acoustic units

5.6.3.1 PS2627, PS2628 and PS2629 (lower to upper continental slope)

The sequence of lithofacies (Fig 4.1) within PS2627 and PS2628 correlate with the sequence of individual layers within acoustic unit Ib, and the underlying unit, unit II (Table 5.2; Fig 5.4B&C). The lithofacies are presented in Table 5.2, and correlated to the acoustic layers in Figure 5.4B&C. The lower acoustic layers were not penetrated by coring (Fig 5.4B&C). The acoustic layer corresponding to the sandy mud couplet facies (Figs 4.1, 5.4B&C) continues up slope to ca. 73° 09' N, 16° 06' W (Section 5.5.2). The three subfacies of the normally graded gravel-sand-mud facies in PS2627 (Fig 4.1) appear as lens-shaped bodies, and extend short distances either side of the core site (Fig 5.4C). The thinly intercalated sequence of resedimented sandy mud diamicton, massive sandy

mud and massive mud facies in PS2627 and PS2628, and additionally massive sand in PS2627 (Fig 4.1), cannot be resolved into separate acoustic layers (Table 5.2; Fig 5.4B&C). Unit II at core site PS2627 (Fig 5.4C) correlates to the resedimented sandy mud diamicton facies in the lowermost section of PS2627 (Fig 4.1; Table 5.2). This facies originates a short distance upslope of the core site, and extends as a thin lens-shaped body down slope (Fig 5.4C). The majority of PS2629 on the upper slope is composed of sandy mud diamicton (Fig 4.1) and, therefore, corresponds to acoustic unit VI (Table 5.2; Fig 5.4C). The uppermost bioturbated mud facies and the massive sandy mud facies immediately underlying and from lower in the sequence (Fig 4.1), are not differentiated as separate acoustic units from unit VI (Table 5.2; Fig 5.4C).

5.6.3.2 PS2630 and PS2641 (mid to inner continental shelf)

The sequence of lithofacies within PS2630 (Fig 4.1) corresponds to the acoustic stratigraphy at, and bordering the core site (Fig 5.8). Unit VII forming the uppermost/surface acoustic unit correlates to the sandy mud diamicton and sandy diamicton facies (Fig 4.1) in the upper section of PS2630, though both facies are not differentiated (Table 5.2; Fig 5.8). The underlying unit II corresponds to the resedimented sandy mud diamicton facies (Fig 4.1) in the lower section of PS2630 (Table 5.2; Fig 5.8).

The bioturbated mud facies separating the upper and lower diamicton units (Fig 4.1) is too thin to be resolved as a separate acoustic unit, but probably coincides with the boundary between units VII and II (Fig 5.8). The sequence of lithofacies within PS2641 (Fig 4.1) corresponds to the individual acoustic layers within unit IV (Table 5.2; Fig 5.6). The uppermost/surface acoustic layer correlates to a thick sequence of bioturbated mud (Fig 4.1) which forms the majority of the core (Table 5.2; Fig 5.6). This acoustic layer contains numerous conformable but discontinuous internal layers (sub-layers; Fig 5.6) that are not reflected as facies variations within the bioturbated mud. This effect could reflect subtle variations in acoustic properties of the lithofacies and not lithofacies variations. Equally the core could have penetrated a section of the sediment column where stratification was absent. The base of the acoustic sequence comprises two acoustic layers where the upper correlates to the laminated mud and the lower to the sandy mud diamicton (Table 5.2; Figs 4.1, 5.6).

5.6.3.3 PS2631, PS2632 and PS2633 (outer to mid Kejser Franz Josephs Fjord)

The lithofacies of PS2631 correlate with the uppermost sequence of acoustic layers within unit IV. The majority of the core consists of bioturbated mud (Fig 4.1) which corresponds to the uppermost and thickest acoustic layer (Table 5.2). Furthermore, this acoustic layer contains numerous conformable but discontinuous internal layers (sub-layers) similar to those documented for the acoustic records around the core site of PS2641 (Fig 5.6), that are not reflected as facies variations within the bioturbated mud. Again this reflects the two causes cited in Section 5.6.3.2.

Table 5.2. Correlation of core lithofacies (Chapter 4) and acoustic units identified from Parasound records for the Kejser Franz Josephs Fjord - continental shelf - continental slope study area (Fig 1.1). The ordering of the lithofacies/subfacies reflects their downcore sequencing (refer to Fig 4.1 for core depths). In the case of acoustic units Ia/Ib and IV, the individual acoustic layers correlate to the lithofacies/subfacies indicated.

Core	Sequence of Lithofacies/Subfacies (facies code indicated)	Acoustic unit
PS2633 (mid fjord)	a) Massive mud with dropstones - Fm(d-sl) b) Massive sandy mud with dropstones - SFm(d) c) Laminated mud with dropstones - Fl(d)	Unit Ia Unit Ia Unit Ia
PS2632 (outer fjord)	a) Bioturbated mud with dropstones - Fb(d)	Unit Ia
PS2631 (outer fjord)	a) Bioturbated mud with dropstones - Fb(d) b) Laminated mud - Fl c) Laminated mud with dropstones and bioturbation - Fl(b-d)	Unit IV Unit IV Unit IV
PS2641 (inner shelf)	a) Bioturbated mud with dropstones - Fb(d) b) Laminated mud with dropstones - Fl(d) c) Sandy mud diamicton - Dmm	Unit IV Unit IV Unit IV
PS2630 (mid shelf)	a) Sandy diamicton - Dmm b) Sandy mud diamicton - Dmm c) Bioturbated mud with dropstones - Fb(d) d) Resedimented sandy mud diamicton - Dmm(r)	Unit VII Unit VII Not differentiated Unit II
PS2629 (upper slope)	a) Bioturbated mud - Fb b) Massive mud with dropstones - Fm(d) c) Sandy mud diamicton - Dmm d) Massive sandy mud with dropstones - SFm(d) e) Sandy mud diamicton - Dmm	Not differentiated Not differentiated Unit VI Unit VI Unit VI
PS2628 (mid slope)	a) Bioturbated mud with dropstones - Fb(d) b) Massive sandy mud with dropstones - SFm(d) c) Sandy mud couplets - SFc(m-l) d) Resedimented sandy mud diamicton - Dmm(r)/ massive mud with bioturbation and dropstones - Fm(b-d)/ massive sandy mud with dropstones and bioturbation - SFm(b-d)	Unit Ib Unit Ib Unit Ib Unit Ib
PS2627 (mid-lower slope)	a) Bioturbated mud with dropstones - Fb(d) b) Normally graded sandy mud - SFng c) Sandy mud couplets - SFc(m-l) d) Resedimented sandy mud diamicton - Dmm(r)/ massive mud with bioturbation, dropstones and sand lenses - Fm(b-d-sl)/ massive sandy mud with bioturbation and dropstones - SFm(b-d)/ massive sand - Sm e) Normally graded gravelly sand - GSng f) Normally graded muddy sand - FSng g) Resedimented sandy mud diamicton - Dmm(r)	Unit Ib Unit Ib Unit Ib Unit Ib Unit Ib Unit Ib Unit II

The lower boundary of the underlying acoustic layer, which would correpond to the lower boundary of the laminated mud facies not penetrated by coring (Table 5.2), is difficult to identify as

the acoustic record in this section is dominated by discontinuous reflectors. The bioturbated mud facies of PS2632 (Fig 4.1) correlates with the uppermost/surface acoustic layer of unit Ia (Table 5.2). The underlying acoustic layers of unit Ia and the much deeper unit II (Section 5.5.4) are not penetrated by coring. The massive mud, massive sandy mud and laminated mud of PS2633 (Fig 4.1) correlate with the uppermost sequence of acoustic layers within unit Ia (Table 5.2). However, the acoustic layering around the core site is poorly defined and, therefore, it is difficult to correlate the lithofacies precisely with specific acoustic layers.

5.7 INTERPRETATION OF ACOUSTIC UNITS

5.7.1 Introduction

The acoustic units presented in this chapter (Sections 5.4, 5.5) are interpreted in terms of the sediment character, and associated sedimentary environments and processes of sedimentation. These interpretations are based on ground truthing using the lithofacies of cores recovered from the study area (Section 5.6). However, only five out of the eight, and limited sections of some acoustic units and sequences were penetrated by coring. Therefore, further interpretation is based on the acoustic character coupled to known sedimentary facies documented in other work. The processes of sedimentation associated with each acoustic unit are summarised in Table 5.3.

5.7.2 Acoustic unit I - acoustically stratified sediment

The deep acoustic penetration, and multiple, parallel sea-floor and internal reflectors associated with this unit reflects lowly compacted, mainly fine grained and stratified sediments (e.g. Damuth 1978; Kuhn & Weber 1993). The acoustic layers of (i) sub-unit Ia are ponded within the basins of the main fjord and Fosters Bugt, although they can very occasionally be traced over small scale bathymetric highs (e.g. Fig 5.3), and (ii) as continental slope deposits within sub-unit Ib on the mid to lower continental slope. The regional morphology and physiography of sub-unit Ib is not well constrained due to the poor seismic coverage. Therefore, it is not known whether the acoustic layers of the unit form deposits conformable with the slope, or form part of a fan/channelised system. GLORIA data have shown that the continental slope north of 72°N is relatively sediment starved, and no submarine fan systems have developed (Mienert et al. 1993, 1995). This evidence indicates that the acoustic layers are conformable with the continental slope rather than forming part of a fan system.

Even though the cores are spatially limited, they do provide evidence for the sedimentary composition and depositional processes producing the acoustic architecture of sub-units Ia and Ib. Cores PS2628 and PS2627 reveal that sub-unit Ib is composed of mainly fine grained lithofacies, with occasional coarser grained lithofacies (Table 5.2; Section 5.6.3) deposited through a combination of: (i) vertical rain out and suspension settling of sediment particles introduced to the water column from ice-rafting, meltwater/fluvial outflows, biogenic/pelagic activity and resuspension

of sea-floor sediments (Table 4.4; Section 4.7), and (ii) debris flows and low concentration turbidity currents (Table 4.4; Section 4.7). The ponded nature of the acoustic layers within sub-unit Ia from the sub-basins of the fjord and Fosters Bugt, is indicative of basin infill controlled mainly by sediment gravity flows, particularly turbidity currents (Syvitski et al. 1987, 1996; Syvitski 1989; Sexton et al. 1992; Niessen & Whittington 1997a). These sediments were only penetrated by coring in the shallower, marginal regions of the mid fjord basin, where the fine grained sediments of PS2633 (Table 5.2; Section 5.6.4) indicate that sediment derived from meltwater/fluvial outflow and iceberg rafting (Tables 4.4; Section 4.7) are additional processes contributing to sedimentation. These processes would also produce acoustic layers over bathymetric highs surrounding the sub-basins as sedimentation is controlled by the settling of debris through the water column. However, this is mainly not the case and it is probable that subsequent downslope movement removed these acoustic layers. Additional poor acoustic returns associated with the slope may have also contributed to the absence of acoustic layering. The numerous vertically aligned dislocations of the acoustic layering in sub-unit Ia (Section 5.4.2) are interpreted to reflect syn-sedimentary faulting (Niessen & Whittington 1997b).

5.7.3 Acoustic unit II - acoustically homogeneous sediment exhibiting lobed/ elongate morphology

The acoustically homogeneous/transparent architecture, lobed/elongate morphology and irregular surfaces of the sediment bodies of unit II are consistent with debris flow deposits (e.g. Damuth 1978; Nardin et al. 1979; Piper et al. 1985; Yoon et al. 1991; Kuhn & Weber 1993; Laberg & Vorren 1995; Dowdeswell et al. 1996, 1997b; King et al. 1996; Elverhøi et al. 1997; Niessen & Whittington 1997a; Whittington & Niessen 1997). In limited sections, the bodies show lateral thinning away from the base of slopes supportive of this interpretation. The acoustically transparent internal nature (few point reflectors) of the debris lobes reflect strong homogeneity resulting from uniform sediment structure and composition (e.g. Dowdeswell et al. 1996; Elverhøi et al. 1997). The acoustic homogeneity of the debris lobes could be explained by Bingham-type fluid behaviour within the flow, whereby sediment moves downslope as a plug without significant internal deformation and sorting during transport (Elverhøi et al. 1997). For this to occur, the original sediment would have to be soft, clay-rich (>30%) and cohesive (Elverhøi et al. 1997). Unit II was penetrated by coring on the mid shelf (PS2630) and lower slope (PS2627) and consists of sandy mud diamicton with a clay content >33% (Sections 4.3.2.3, 4.7.2.1, 5.6.3.2). Deformational homogenisation during downslope transport could also explain the homogeneity (Nardin et al. 1979). The acoustic homogeneity is reflected within the predominantly homogeneous structure of the diamicton, except for a small imbricated section at the top of the facies in PS2630. The sedimentological nature of the diamicton supports both explanations of homogenisation during downslope transport. It is assumed that this diamictic facies and associated structure, of glacigenic origin, applies to the uncored debris bodies throughout the study area, and is also consistent with debris lobes from other Polar North Atlantic margins (e.g. Laberg & Vorren 1995, 1996; Dowdeswell et al. 1996, 1997b; Elverhøi et al. 1997).

Acoustic Unit	Acoustic Sub-Units	Code	Distribution	Sedimentary processes/environment
Acoustically stratified sediment	Basin infill	Unit Ia	Mid and outer fjord Fosters Bugt	Sub-unit Ia: mainly sediment gravity flows (turbidity currents and debris flows) and additional vertical rain out and suspension settling of sediment particles introduced to the water column through ice rafting, meltwater/fluvial outflow, biogenic/pelagic activity and resuspended sea-floor sediments. Cores only show the presence of stratified sediments deposited through rain out and suspension settling.
	Slope deposits	Unit Ib	Mid/lower continental slope	Sub-unit Ib: combination of turbidity currents, and vertical rain out and suspension settling of sediment particles introduced to the water column through the processes listed for sub-unit Ia. Cores show deeper rain out and suspension settling sediments are more enriched in ice rafted debris than surface deposits. Cores shows a predominantly stratified, fine grained, non compacted sediment nature.
Acoustically homogeneous sediment exhibiting lobed/ elongate morphology		Unit II	Mid/outer fjord, Mid continental shelf, Mid/ lower continental slope	Debris flow emplacement. Cores show that the debris lobes have a diamictic composition. The strong homogeneity of the debris lobes reflect uniform sediment composition and structure produced by (i) the flow behaving as a Bingham type fluid whereby sediment moves downslope as a plug without significant internal deformation and/or sorting, or (ii) deformational homogenisation during downslope transport.
Acoustically heterogeneous sediment with a hummocky top-surface reflector		Unit III	Outer fjord	Mass-flow emplacement. Difficult to elaborate whether the sediment was deposited through sliding/slumping or debris flow as the acoustic characters in parts are consistent with each of these processes. A debris flow origin is supported by the observation that the acoustic unit grades laterally into acoustic unit II. No cores were recovered to support this.
Acoustically stratified sediment with conformable sea-floor and internal reflectors		Unit IV	Outer fjord Inner continental shelf	Vertical rain out and suspension settling of sediment particles introduced to the water column through ice rafting, meltwater/fluvial outflow, pelagic/biogenic activity and resuspended sea-floor sediments. Cores show that the relative dominance of each process with respect to one another results in a range of facies that vary from muds to diamicton. Cores and acoustic character show the sediment to be mainly stratified, fine grained and non compacted.
Acoustically homogeneous to stratified sediment with an irregular sea-floor reflector	Acoustically homogeneous	Unit Va	Mid/outer fjord, Fosters Bugt, Continental shelf	Iceberg scouring and turbation of sea floor sediments. Scouring and turbation results through keel-sea floor contact. Sub-unit Va: iceberg scouring results in total turbation of sea floor sediments.
	Acoustically stratified (weak)	Unit Vb	Fosters Bugt Outer continental shelf	Sub-unit Vb: iceberg scouring results in only part turbation of sea floor sediments where the original acoustic units are consistent with Ia, IV and VII.
Acoustically semi-penetrable sediment with a distinct to semi-prolonged sea-floor reflector		Unit VI	Upper continental slope	Cores show that the original sediment was deposited through vertical rain out and suspension settling of sediment particles introduced to the water column through mainly ice rafting, and part meltwater outflow and pelagic/biogenic activity. The occurrence of similar acoustic units on the continental slope of other high latitude regions was interpreted as the result of proximal mass-flows. However, subsequent mass-flow resedimentation is difficult to assess due to poor acoustic coverage, penetration and return. The latter two result from a combination of the diamictic sediment composition and the steep gradient of the upper continental slope.
Acoustically massive sediment forming a conformable unit		Unit VII	Outer fjord Mid/outer continental shelf	Vertical rain out and suspension settling of sediment particles introduced to the water column through ice rafting, meltwater outflow, pelagic/biogenic activity and resuspended sea-floor sediments. Cores show that ice rafting is the dominating sedimentation process for the acoustic unit on the mid to outer shelf, and meltwater outflow for the fjord.
Acoustically homogeneous sediment with an irregular-hummocky top-surface sub sea-floor reflector		Unit VIII	Mid/outer continental shelf	Similar internal characteristics as acoustic unit II and, therefore, assumed to reflect a diamictic composition. Not related to debris flows as it is not distributed proximal to slopes or have a lobed morphology. Therefore, it is assumed to result from predominantly iceberg rafting, with additional sediment from meltwater outflows, sea ice rafting and resuspended sea-floor sediments. No cores were recovered to support this.

Table 5.3. Summary of the depositional processes of the acoustic units determined from Parasound records obtained along ship tracks from the mid-outer region of the Kejser Franz Josephs Fjord, Fosters Bugt and the adjacent continental shelf and slope (Figure 5.1a). Details include: i) Acoustic units and sub-units, ii) Acoustic unit code, iii) Distribution of the acoustic units, and iv) Processes of deposition indicated by the acoustic units.

5.7.4 Acoustic unit III - acoustically heterogeneous sediment with a hummocky top-surface reflector

The acoustically heterogeneous architecture (chaotic, stratified and massive) of unit III (Section 5.4.4) can be interpreted in two ways. The first is based mainly on the chaotic architecture of the unit which is consistent with similar descriptions from till deposits originating from subglacial processes (e.g. Piper et al. 1985; Sættem et al. 1992; Andersen et al. 1995). The appearance of stratified and massive internal reflections would also suggest till structure. This interpretation is discounted in this study as the unit is covered by a thin veneer of unit VII (<2 m thick), equating to an unrealistically low sedimentation rate for the period of time elapsed since glaciers last occupied this region of the fjord at ca. 10,000 yr BP (Funder & Hansen 1996). Instead, a thicker sediment pile would be expected to accumulate during this time period consistent with other parts of the fjord.

The second, and more likely interpretation is that the internal acoustic architecture, coupled with the hummocky top-surface reflector, are characteristic of mass-flow deposits (e.g. Nardin et al. 1979; Yoon et al. 1991; Laberg & Vorren 1995, 1996). The lateral extent and morphology of the unit is poorly constrained due to the low seismic coverage in this region of the fjord. Therefore, it is not known whether the unit has a debris lobe morphology, or is accompanied by slide/slump scars and/or shear-slip surfaces. This, coupled with a lack of core data, makes it difficult to elaborate whether the sediments of this unit represents deposits from sliding/slumping or debris flow activity. The acoustic characteristics are, in parts, consistent with sediments deposited through both processes (e.g. Nardin et al. 1979; Piper et al. 1985; Dowdeswell et al. 1996, 1997b; Laberg & Vorren 1995, 1996). Debris flow deposition is partially supported by the fact that the unit grades into the debris flow body of unit II (Section 5.7.3) further up fjord. If this is correct then the predominating massive/stratified acoustic internal architecture may represent either the original stratified sediment structure partially preserved through Bingham type flow behaviour (Elverhøi et al. 1997), or represent partial homogenisation. Based on the acoustically heterogeneous architecture, the unit is probably diamictic in composition (e.g. Laberg & Vorren 1995, 1996). This is supported by numerous internal diffractions indicative of high energy backscatter associated with small-scale inhomogeneities such as gravel clasts.

5.7.5 Acoustic unit IV - acoustically stratified sediment exhibiting conformable sea-floor and sub-sea floor reflectors

The acoustic character, and conformity of reflectors within unit IV, with irregularities associated with the underlying bedrock or sedimentary facies, is consistent with sediment drape deposited by the vertical rain out and suspension settling of particles through the water column (e.g. Syvitski et al. 1987; Syvitski 1989; Syvitski & Hein 1991; King et al. 1996; Niessen & Whittington 1997a). The significance of bottom reflector roughness is discussed in Section 5.7.6. The deep acoustic penetration, and multiple, conformable reflectors represents lowly compacted, fine grained and stratified sediments (Kuhn & Weber 1993). Cores recovered from the outer fjord (PS2631) and

on the inner shelf (PS2641) show that the unit consists of a mainly fine grained sediment composition, though coarse grained sediments are occasionally present (Table 5.2; Section 5.6.3, 5.6.4). The acoustically layered sediment results from the settling of particles introduced to the water column through a combination of meltwater/fluvial outflow, ice rafting, biogenic/pelagic activity, and resuspension of sea-floor sediments (Table 4.4; Section 4.7). The range of depositional processes are envisaged for uncored sections of the same unit.

5.7.6 Acoustic unit V - acoustically homogeneous-stratified sediment with an irregular sea-floor reflector

The absolute dimensions and form of the sea-floor reflector irregularities (surface roughness), which consist of a paired crest and trough morphology (roughness elements), coupled with the acoustic nature of the sub-surface (Section 5.4.6), are analogous to the description of Dowdeswell et al. (1993, 1997a) for sea-floor sediments scoured by iceberg through keel-substrate contact. Scouring is exhibited as a series of paired crest (berm) and trough morphology. The acoustic architecture of the unit is characterised by diffuse (sub-unit Va) and stratified (sub-unit Vb) reflectors, indicative of iceberg turbation of sediments, and the degree to which the original sedimentary structure is influenced (cf. Dowdeswell et al. 1993, 1997a). Sub-unit Va reflects total iceberg turbation, and sub-unit Vb only minor surface turbation with the original acoustic structure preserved. The original structure of sub-unit Vb is the same as for units I, IV and VII in Sections 5.7.2, 5.7.5 and 5.7.8, respectively. This interpretation applies to the roughness exhibited in the sea floor reflector of unit IV (Section 5.7.5), though the scouring is of very little significance to influence the internal stratification. The sedimentary composition of the unit is unknown as no cores were recovered. No further interpretation is made of this acoustic unit here, as it is the focus of Section 5.8.

5.7.7 Acoustic unit VI - acoustically semi-penetrable sediment with a distinct to semi-prolonged sea-floor reflector

The shallow based, diffuse internal acoustic character of this unit (Section 5.4.7) is a result of acoustic signal scattering by the steep upper slope and steep gradient associated with the fjord bathymetric highs, which prevents significant acoustic penetration, and subsequent return to the ship (e.g. Kuhn & Weber 1993). The sediments of PS2629, correlating to this unit, are dominated by sandy mud diamicton (Table 5.2; Sections 4.3.2.1, 5.6.3.1). The fine grained veneer covering the diamicton is not differentiated on acoustic records related to the steep gradient of the slope. The semi-prolonged sea-floor reflector and shallow-based diffuse reflections are also a product of the coarse grained nature of the diamicton, which acts to prevent acoustic penetration (e.g. Damuth 1978; Kuhn & Weber 1993; Melles & Kuhn 1993). The multiple point diffractions characterising the diffuse nature of the unit (Section 5.4.7) result from high backscattering of the acoustic signal related to numerous, small-scale inhomogeneities within the diamicton. The sedimentological characteristics of the diamicton show that primary deposition was through predominantly iceberg rafting processes

with additional sedimentation from meltwater/fluvial outflows, sea ice rafting, biogenic activity and resuspension of sea floor sediments (Section 4.7.2.1, 4.7.2.2).

The acoustic unit and associated coarse grained sediment could also be interpreted as proximal mass-flow deposits (Kuhn & Weber 1993; Melles & Kuhn 1993). However, the poor acoustic coverage over the slope, and low penetration and return of the acoustic signal result in relatively little spatial determination of sub sea-floor (internal) features characteristic of mass-flows, such as debris lobes, deformational planes, shear/slip surfaces, and/or slide/slump scars. Based on the evidence available from the acoustic unit, it is difficult to assess whether or not mass-flow processes have contributed to sedimentation on the upper slope through the redistributon of the original sediment. If mass flows did occur, the subsequent retention of the original sediment structure in PS2629 would result if the flow deposit maintains sufficient cohesiveness during transport i.e. moves as a plug flow (e.g. Elverhøi et al. 1997) (Sections 4.7.2.1, 5.7.3). This would occur within slides/slumps where the main undeforming body moves along a deforming plane (Nardin et al. 1979; Pickering et al. 1989; King et al. 1996), or debris flows behaving with Bingham-type fluid properties (Elverhøi et al. 1997).

5.7.8 Acoustic unit VII - acoustically massive sediment forming a conformable unit

The acoustic conformity of unit VII with irregularities associated with the underlying bedrock or sedimentary facies is consistent with sediment drape deposited by the vertical rain out and suspension settling of particles through the water column (e.g. Syvitski et al. 1987; Syvitski 1989; Syvitski & Hein 1991; King et al. 1996; Niessen & Whittington 1997a). Cores recovered from the fjord (PS2632) and on the mid shelf (PS2630) show that the unit consists of a mainly fine grained sediment composition in the former, and coarser grained diamictons in the latter (Table 5.2; Sections 5.6.3, 5.6.4). It must be noted that core PS2632 penetrated the upper acoustic layer of unit Ia in the innermost sub-basin of the outer fjord, but this layer is traced to, and differentiated down-fjord, as unit VII, and is assumed to retain its sedimentary composition. The acoustic unit in the fjord is the result of the sedimentation of debris introduced to the water column through meltwater/fluvial outflows, iceberg rafting, and biogenic activity (Table 4.4; Section 4.7.8.2). The unit on the shelf results from predominantly iceberg rafting, with additional sedimentation from meltwater/fluvial outflows, minor biogenic activity, sea ice rafting and settling of resuspended sea floor sediments (Table 4.4; Section 4.7.2.2), modified in part by current winnowing (Table 4.4; Section 4.7.2.3). These processes are envisaged for uncored sections of the applicable units, provided they can be traced to the acoustic section at the core site.

5.7.9 Acoustic unit VIII - acoustically homogeneous sediment with an irregular-hummocky top-surface, sub-sea floor reflector

The acoustically homogeneous and transparent nature composed of point reflectors is similar to that of unit II. The unit has not been penetrated by coring. Cores show that sediments of unit II are

diamictic in composition. Therefore, based on matching acoustic characteristics, unit VIII is probably of a similar composition. The diamictic composition of the unit is further supported by the presence of point diffractions characteristic of high energy backscattering from small-scale inhomogeneities reflecting coarser grained sediment components. The poor acoustic return, coupled with no sedimentological information, provides uncertainty in the interpretation of the likely process of deposition. The unit is distributed across the shelf away from major slopes, and coupled with a non-lobe morphology it is unlikely to be the result of debris flows. Instead the assumed diamictic composition is probably the result of sediment delivery through mainly iceberg rafting, with additional sedimentation of the range of grain sizes from meltwater outflows and sea ice rafting. An origin from subglacial processes is ruled out as the acoustic character does not display a chaotic internal character expected for subglacial till (see Section 5.7.4).

5.8 ICEBERG SCOURING OF THE SEAFLOOR

5.8.1 Introduction

Acoustic unit V, including sub-units Va and Vb, was interpreted in Section 5.7.6 as a product of iceberg scouring of sea-floor sediments through keel-substrate contact. Scouring through sea ice keel-substrate contact is ruled out as it is largely restricted to water depths of less than about 20 m (Dowdeswell et al. 1993), which only occur along the coastline of the study area. This section will concentrate on presenting additional information supporting iceberg scouring, the pattern of iceberg scouring within the mid to outer Kejser Franz Josephs Fjord and the adjacent shelf and slope, relate scouring to water depth, place ages on the scouring and discuss general implications for iceberg scouring.

5.8.2 Other observations supporting iceberg scouring

Observations on the occurrence and dimensions of modern icebergs within Kejser Franz Josephs Fjord and the adjacent shelf, similar to the study of Dowdeswell et al. (1992), were not undertaken during the *Polarstern* cruise in 1994. Therefore, there are no statistics to assess whether or not icebergs are of sufficient numbers and sizes for their keels to scour the sea bed. However, Reeh (1985) estimates that 8 $km^3\ yr^{-1}$ of ice is discharged from outlet glaciers into the modern day Kejser Franz Josephs Fjord (Fig 1.4; Section 1.2.4.2). Icebergs influencing the shelf of the study area are more likely to be derived from glaciers from further north in East Greenland, which are subsequently transported south in the East Greenland Current (cf. Wadhams 1981). This is supported by the observation of icebergs on the shelf at 75°N, that are assumed to be derived from glaciers terminating in Dove Bugt at 76°N followed by southward transportation along the shelf in the East Greenland Current (Dowdeswell et al. 1993). It follows that icebergs such as these would continue their drift

further south to influence the shelf of the study area. These facts, together with the unquantified visual sightings during the 1994 cruise, show that icebergs actively traverse the fjord. Furthermore, Dowdeswell et al. (1992) show that iceberg drafts of up to 550 m commonly impact the modern day sea bed to produce scours within the nearby Scoresby Sund fjord complex (Fig 1.1). Therefore, it is likely that icebergs impact the sea bed within the study area resulting in the acoustic character of unit V (Section 5.7.6).

5.8.3 Age of iceberg scours

Dowdeswell et al. (1993) has suggested that not all observed scours within Scorseby Sund, and on the adjacent shelf, are the product of very recent iceberg-substrate impact. Rather, the sea-floor is composed of a number of superimposed scours of varying ages dating back to the Late Weichselian. This is related to the fact that scours can survive for long periods of time, as subsequent sedimentation would drape both the scour and the adjacent sea floor, and only act to gradually damp out the morphology. The range of ages suggested by Dowdeswell et al. (1993) is likely to apply for iceberg scours within this investigation.

5.8.4 Intensity of iceberg scouring

Based on the interpretation of acoustic unit V, the high, intermediate and low surface roughness (irregularity) intensity within the sea-floor reflector (Section 5.4.6), indicates corresponding levels of intensity of iceberg scouring of sea-floor sediments (cf Dowdeswell et al 1993). The acoustic character associated with high intensity scouring (Section 5.4.6) reveals a series of intersecting scours with sharp crest morphology and varying depth and direction (Fig 5.7a). No areas of undisturbed sea floor are associated with this intensity. The acoustic character associated with intermediate iceberg scouring (Section 5.4.6), reveal that scours become increasingly more rounded and separated, though undisturbed areas of the sea floor are relatively rare (Fig 5.7b). The acoustic character associated with low intensity scouring (Section 5.4.6), reveal isolated/clustered scours separated by extensive areas of undisturbed sea floor. No iceberg scouring is indicated by a totally undisturbed sea-floor (Fig 5.7c). The acoustically homogeneous internal nature of sub-unit Va (i.e. very diffuse reflections) is associated with high and intermediate intensity scouring, and interpreted to reflect complete iceberg turbation of sea-floor sediments. The sub-surface zone of diffuse reflections disappears within sediments of sub-unit Vb, suggesting low intesnity to absent scouring, and the original acoustic character of units I, IV and VII is partially preserved. This is indicative of only partial iceberg turbation.

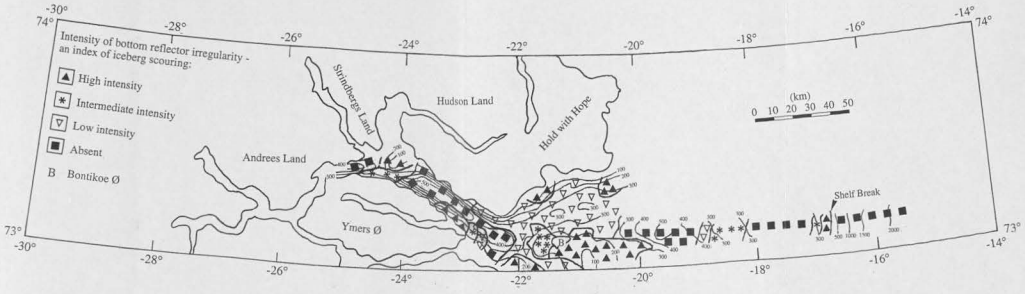

Figure 5.10. Map of Kejser Franz Josephs Fjord and the adjacent continental shelf and slope showing the distribution of seafloor irregularity. Four levels of intensity are recognised: i) High, ii) Intermediate, iii) Low, and iv) Absent. A key to the symbols representing the four levels of intensity is provided. The intensity of irregularity is taken as an index of iceberg scouring. The study area in relation to Greenland is shown within the inset of Figure 5.1. The map scale is indicated. The distribution was based on Parasound records obtained along the ship tracks shown in Figure 5.1. Bathymetric contours are shown and spaced at intervals of 100 metres in the fjord and adjacent continental shelf, and 500 metres on the continental slope.

5.8.5 Pattern of iceberg scouring within the study area

The distribution of acoustic sub-units Va and Vb throughout the study area was discussed in Section 5.5. Where these sub-units were encountered, the intensity of iceberg scouring of the sea floor was mapped as either high, intermediate, low or absent. A map showing the distribution of iceberg scouring of varying intensity is presented in Figure 5.10. The Parasound profiles within the fjord and Fosters Bugt provide a reasonable coverage of the sea floor except along coastal margins (Fig 5.1a). However, there are only two closely spaced profiles running in a narrow transect across the adjcaent continental shelf and slope parallel to ca. 73° N providing a laterally restrictive coverage of the sea floor (Fig 5.1a).

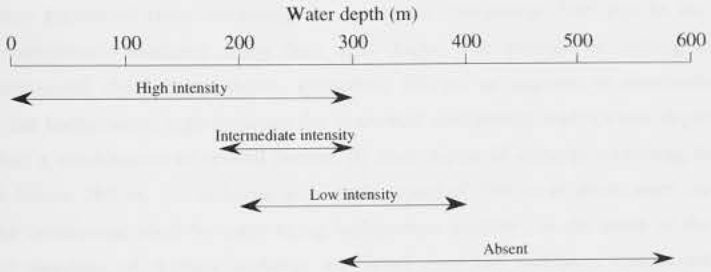

Figure 5.11. Schematic diagram illustrating the relationship of iceberg scouring intensity and water depth within the study area (Fig 5.1a). Iceberg scouring intensity falls within the four classes: (i) high, (ii) intermediate, (iii) low, and (iv) absent. Water depths are in metres (m). A map illustrating the pattern of iceberg scouring intensity within the study area is provided in Figure 5.10.

Several regions of the study area are unscoured at water depths from between 280 m and greater than 380 m, and include the continental slope, the mid-outer continental shelf, the inner continental shelf basin, outer fjord sub-basins, and mid fjord basin (Figs 5.10, 5.11). Sea-floor scours of high intensity occur in water depths of less than 300 m characterising the region immediately at the continental shelf break, west of the inner continental shelf basin, south and east of Bontekoe Ø, along the southern margin of the outer fjord region, and over the mid/outer fjord sill (Figs 5.10, 5.11). Sea-floor scours of intermediate intensity occur in water depths exceeding 180 m and less than 300 m, characterising the region approaching the shelf break, between the mid continental shelf bathymetric high and eastern margin of the inner continental shelf basin, west of Bontekoe Ø, and south of the mid/outer fjord sill (Figs 5.10, 5.11). Sea-floor scours of low intensity occur in water depths exceeding 200 m and less than 380 m, characterising Fosters Bugt to the north and west of Bontekoe Ø, and the northern/eastern margin of the outermost sub-basin of the outer fjord (Figs 5.10, 5.11).

5.8.6 Implications of iceberg scouring and associated distribution

Bathymetry plays a crucial role in the distribution of iceberg scours and scour intensity within the study area. The intensity of iceberg scouring reveals an inverse relatationship with water depth (Fig 5.11). An overlap between the range of water depths for each intensity class (Fig 5.11) is related to both the current-drift tracks of icebergs, and the sub sea-floor topography within local regions of the study area (cf. Dowdeswell et al. 1993).

Scouring is absent in the deeper regions of the study area (fjord basins, inner shelf basin and continental slope) in water depths generally exceeding 380 m. This lowers to 280-320 m between the mid shelf bathymetric high and outer shelf (Fig 5.10). This implies that the draft depth of icebergs traversing the fjord, Fosters Bugt and inner to mid continental shelf must have remained below 380 m, and below 320 m on the mid to outer continental shelf. Icebergs with keels exceeding these depths may have been prevented from traversing the fjord and continental shelf due to the presence of intervening bathymetric shallows along their drift tracks. The absence of iceberg scours on the mid/outer continental shelf (water depths exceeding 280 m) as opposed to intermediate scouring intensity on the bathymetric high between the inner/mid continental shelf (water depths below 275 m), may reflect a combination of several factors: (i) draft depths of icebergs traversing the continental shelf remain below 280 m, (ii) icebergs with draft depths of 280 m or more were prevented from traversing the continental shelf by intervening bathymetric shallows to the north of the profile, and (iii) absolute numbers of drifting icebergs are small over the mid/outer continental shelf. The presence of iceberg scours on the inner/mid continental shelf and at the continental shelf break are significant, as these could not be produced by icebergs discharged from Kejser Franz Josephs Fjord as the southward flowing East Greenland Current would prevent them from reaching these shelf regions. Instead the scouring is more likely to be related to icebergs calved from further north along East/Northeast Greenland e.g. the Dove Bugt region at 76°N (cf. Reeh 1985), where they were subsequently transported south in the East Greenland Current (cf. Dowdeswell et al. 1993).

The highest intensity of scouring (high and intermediate intensity) is found in shallower waters of the study area where iceberg keel-sea floor interaction are far more likely to occur, and of a more frequent nature. Even though water depths are generally less than 340 m in Fosters Bugt, the sea floor is only characterised by low intensity scouring, which reflects the reduced drift of icebergs and/or that only icebergs with insufficient draft depths to contact the sea floor traversed the region. It is more likely to reflect the general configuration of Fosters Bugt. The Bugt could act to protect the sea floor to the north, north west and north east of Bontekoe Ø from the encroachment of icebergs transported south across the shelf in the East Greenland Current, and/or from those traversing the adjacent fjord. This is supported by the high/intermediate intensity scouring to the southwest, west and south of Bontekoe Ø, which is assumed to reflect the main drift of icebergs leaving the fjord along a trajectory to the south of Bontekoe Ø. Bontekoe Ø could also act to protect the sea floor to its east from the encroachment of icebergs discharged from the fjord. As a result, the high intensity scouring of the sea floor is likely to result from icebergs derived from further north, as this area is assumed to be left relatively unprotected from the southward flowing East Greenland Current.

5.9 SEDIMENTATION PATTERNS AND PROCESSES

5.9.1 Introduction

This chapter has so far: (i) discussed the acoustic units recognised within the Parasound records, (ii) described their distribution throughout the study area, (iii) compared the lithostratigraphy of the cores of this study (Chapter 4) with the acoustic units at each core site, and (iv) interpreted the acoustic units in terms of their sedimentary composition and associated processes of deposition. In light of this the lithostratigraphy and associated sedimentary processes and environments of determined for each core in Chapter 4 are placed within a regional context through a discussion of the regional sedimentation patterns and processes observed in both the cores and acoustic records. The following discussion will be related to a preliminary but broad chronology, and to glacial-interglacial climatic fluctuations. The regional sedimentation processes determined from the acoustic and sedimentary records are shown in Figure 5.12.

5.9.2 Sedimentation patterns and processes on the continental slope

5.9.2.1 Introduction

The distribution of intermittant, small-scale and localised acoustic units and core lithofacies consistent with mass-flow resedimentation suggests that the East Greenland continental slope of the study area has been relatively less active during the Late Quaternary than the Western Svalbard-Norwegian continental margin on which mass-wasting events are larger-scale, more frequent and dominant and occur on a regional scale (e.g. Laberg & Vorren 1995, 1996; Dowdeswell et al. 1996, 1997b). The difference probably relates to the lower rate and volume of sediment delivery to the continental slope in this region of East Greenland. This is reflected in the wide distribution of sediments deposited through the rain out and suspension settling of debris. The lower sedimentation activity on the continental slope is supported by evidence from GLORIA side-scan data which shows that the continental slope north of 72°N has been relatively sediment starved throughout the Late Pleistocene, and that no submarine fan or channelised systems have developed (Mienert et al. 1993, 1995; Dowdeswell et al. 1996, 1997b). Therefore, the mass wasting deposits recognised from the acoustic and sedimentary records from the East Greenland continental slope of the study area are produced from unchannelised mass flow events. The mass flow sediments present on the continental slope are characteristic of a high energy sedimentary environment. In comparison, the rain out and suspension settling of debris reflect periods of much lower energy sedimentation. The intermittant relationship of both depositional styles points to a fluctuation in the energy of the sedimentary environment.

5.9.2.2 Sedimentation patterns and processes on the continental slope

The upper continental slope consists solely of acoustically semi-penetrable sediment (acoustic unit VI) reflecting low acoustic penetration and return (Fig 5.4A) in response to the coarse grained composition of sediment and the steep gradient of the continental slope (4.4°; Section 5.7.7). Core PS2629 shows the sediment to have a mainly diamictic composition (Fig 4.1; Table 5.2; Section 5.6.3.1), with sedimentary characteristics reflecting a glacigenic origin through the vertical settling of sediment derived mainly from iceberg rafting, and less so, sea-ice rafting, distal remnants of meltwater outflows, pelagic/biogenic activity and settling of resuspended sea-floor sediments (Fig 5.12; Tables 4.4, 5.3; Sections 4.7.2.2, 5.7.7). The acoustic evidence discussed in Section 5.7.7 showed that it could not be determined whether or not the original sediment deposited on the upper continental slope was influenced by subsequent proximal mass-flows as described for similar sediments and acoustic units on other high latitude continental slopes (e.g. Kuhn & Weber 1993; Laberg & Vorren 1996; Dowdeswell et al. 1996, 1997b). If mass-flows occurred, the original glacigenic sediment would have been resedimented within the same region and further down the continental slope (Fig 5.12). Subsequent preservation of the sedimentary characteristics of the sandy mud diamicton (Table 4.2; Section 4.3.2.1) would only occur provided the mass-flows maintained sufficient cohesiveness during down slope transportation (Sections 4.7.2.2, 5.7.7; e.g. Nardin et al. 1979; Pickering et al. 1989; Elverhøi et al. 1997). If the original glacigenic diamicton underwent some form of downslope cohesive mass wasting, it is possible that its extent across the continental slope may be exaggerated in a downslope direction in comparison to the original extent, which may have been much closer to the very upper continental slope/continental shelf break. As a result the spatial extent to which the significant number of icebergs contributing to the deposition of the diamicton, influence the upper continental slope is more restricted than what is indicated by the diamicton distrbution. However, this argument would not apply if cohesive mass wasting occurred within, and was confined to, the original glacigenic diamicton zone.

Large to small-scale debris flow deposits (acoustic unit II) are distributed close to the sediment surface on the upper/mid continental slope transitional area and further down the continental slope (Figs 5.4C, 5.12). Core PS2627 penetrated one such debris flow deposit on the lower continental slope, and revealed that it is mainly diamictic in composition (resedimented sandy mud diamicton facies; Dmm(r); Fig 4.1; Tables 4.4, 5.2; Section 4.7.2.1, 5.6.3.1). Small-scale debris flow deposits not differentiated on acoustic records are also present in PS2627 and PS2628, and are similarly diamictic in composition (Fig 4.1; Tables 4.4, 5.2; Sections 4.7.2.1, 5.6.3.1). The debris flows are interpreted to have been generated in response to mass-flow events further up slope from the location of the debris flow sediments (e.g. Wright & Anderson 1982; Laberg & Vorren 1995, 1996; Dowdeswell et al. 1996, 1997b). Debris flow deposits distributed on the continental slope of other high latitude regions are commonly interpreted to result from debris flows that have been generated from mass-flow events (slides/slumps) on the upper continental slope with subsequent transformation during the downslope transport (e.g. Hampton 1972; Wright & Anderson 1982; Piper et al. 1985; Kuhn & Weber 1993; Laberg & Vorren 1995, 1996; Dowdeswell et al. 1996, 1997b).

Therefore, the debris flow deposits on the continental slope of the study area may have been deposited through debris flows generated from mass-flow events on the upper continental slope. However, it is not possible to determine whether or not mass-flow events (slides/slumps) based on acoustic records (Section 5.7.7) occurred on the upper continental slope, ascertain the run-out distances of these debris flows, or even correlate between the debris flow and upper continental slope sediments in support of this interpretation, as the acoustic coverage is limited and characterised by very low penetration/return of the acoustic signal. Regardless of the inconclusive nature of the evidence from the acoustic and sedimentary records (Section 5.7.7), the presence and distribution of debris flow deposits on the upper/mid continental slope transitional area supports the occurrence of mass-flow resedimentation on the upper continental slope. The debris flow deposits further down the continental slope may not necessarily have resulted from debris flows generated by resedimentation events on the upper continental slope, but could equally have been initiated from lower regions of the continental slope.

The acoustic layering (acoustic unit Ib) on the mid to lower continental slope (east of ca. 73° 09' N, 16° 06' W; Figs 5.4B,C) and associated cores (PS2627 and PS2628), reveal a mixture of gravity flow, and rain out and suspension settling deposits (Fig 5.12; Table 5.3; Section 5.7.2). The deposition of both units indicates the fluctuation between high and low energy environments reflecting intermittant periods of mass-flow, and rain out and suspension settling sedimentation, respectively. Large sediment bodies produced by turbidity currents occur on the lower continental slope. Core PS2627 penetrated two of these bodies and show that they are mainly normally graded gravel-sand-mud turbidity current deposits (Fig 4.1; Table 4.4, 5.2; Sections 4.7.4, 5.6.3.1). Smaller turbidity current deposits not differentiated on acoustic records are present in PS2627, and are composed mainly of massive sand (Fig 4.1; Tables 4.4, 5.2; Sections 4.7.5, 5.6.3.1). The acoustic layer correlating to the sandy mud couplet facies within PS2627 and PS2628 (Figs 4.1, 5.4B,C; Table 5.2; Sections 4.7.6, 5.6.3.1), deposited through episodic turbidity currents (Table 4.4) can be traced up slope from the lower/mid continental slope to the margin of the upper continental slope sediments of acoustic unit VI (ca. 73° 09' N, 16° 06' W). The acoustic layer can not be differentiated from the upper continental slope sediments (acoustic unit VI) further up slope suggesting that either the two sediment units have merged, or the steep upper continental slope has resulted in very little penetration/ return of the acoustic signal. Regardless of these points, the tracing of the acoustic layer to the upper continental slope clearly indicates that the turbidity currents were generated in this region. It is not possible to trace the larger turbidite bodies such as those in core PS2627 to regions further up slope due to the limited acoustic coverage. In general, the turbidity current activity across the continental slope, similar to other high latitude regions, are interpreted to have been triggered by mass-flows events further upslope with subsequent transformation during downslope transport (e.g. Hampton 1972; Wright & Anderson 1982; Piper et al. 1985; Dowdeswell et al. 1996, 1997b). It is likely that the transformation to turbidity currents is generated through the increased dilution of the preceding flow body by uptake of ambient sea water, and/or turbulence at the head of a debris flow (e.g. Hampton 1972; Piper et al. 1985; Laberg & Vorren 1995, 1996).

Based on the low concentration and intermittant presence of debris flow deposits and turbidites in acoustic and sedimentary records of this study and GLORIA side-scan data (Mienert et al. 1993, 1995), resedimentation across the continental slope as awhole is restricted to intermittant or low frequency, small to large scale events that are interpreted to originate from localised slope regions. It is not possible to determine whether the mass wasting events have a local or regional slopewide or downslope extent by examining the dimensions and run out lengths of these flows, as acoustic data in this study is inconclusive with respect to this, but it is envisaged that both situations are likely to occur.

Surface sediments on the mid-lower continental slope (cores PS2628 and PS2627) were deposited through rain out and suspension settling sedimentation (Figs 4.1, 5.4B,C), derived from meltwater/fluvial outflows escaping East Greenland fjords, ice rafting, settling of resuspended sea-floor sediment, and biogenic/pelagic activity (Tables 4.4, 5.3; Sections 4.7.3, 4.7.8.1). The surface sediments are traced upslope where they cannot be differentiated from the upper slope diamictic sediments in acoustic sections (Fig 5.4A). They are, however, identified within core PS2629 (Fig 4.1). Rain out and suspension settling-related deposits also characterise sediments deeper within the sediment column (Figs 4.1, 5.4B,C), where they commonly punctuate the debris flow and turbidity current deposits of PS2628 and PS2627 on the mid to lower continental slope. These sediments are more enriched in iceberg rafted debris than their surface counterparts (Sections 4.7.3, 4.7.8.1). The intermittant distribution of mass-flow, and rain out and suspension settling-related sediments show that the sedimentary environment fluctuates between high and low energy, respectively.

5.9.2.3 Generation of mass flow events on the continental slope

In general, the mass-flows discussed in Section 5.9.2.3 can be triggered through either: (i) the build-up of excess pore pressure due to rapid sediment accumulation, (ii) build-up of sediment on an unstable and/or steep substrate, (iii) oversteepening of the sediment pile, and/or (iv) iceberg scouring of sea-floor sediments (e.g. Syvitski & Hein 1991; Laberg & Vorren 1995, 1996; Dowdeswell et al. 1996, 1997b; Elverhøi et al. 1997).

5.9.2.4 Preliminary chronology for the sedimentation patterns and processes

The mass-flows indicate a high energy environment, where they are likely to be generated through an increased supply of sediment to the continental slope. The ice distal setting of the continental slope is relatively sediment starved during interglacials. Therefore, the increased and rapid accumulation of sediment needed to generate mass flows is probably derived during the Late Weichselian. Sedimentation during this period is focused on the continental margin in response to the extension of glacier-ice of the Greenland Ice Sheet and invigorated glacimarine processes (iceberg rafting, sea ice rafting and meltwater outflows) capable of delivering large quantities of sediment to the continental slope. Based on the low concentration and intermittant presence of mass flow deposits in acoustic and sedimentary records of this study and GLORIA side-scan data (Mienert et al. 1993,

1995), resedimentation on the continental slope is restricted, and only constrained to localised regions. The composition of sediments deposited through the process of rain out and suspension settling in PS2629, PS2628 and PS2627 indicate that a combination of mainly iceberg rafting and meltwater outflows were processes by which glacigenic sediment was delivered to the continental slope. The distribution of suspension settling sediments between mass-flow deposits, and the high amounts of iceberg rafted debris (particles >2 mm/cm and grain size >63 μm) indicate that they were deposited during the Late Weichselian in response to increased glacial activity.

The distribution of suspension settling-related deposits at or close to the surface of the sediment column on the continental slope are assumed to represent the Holocene. Cores show these sediments to consist of very small volumes of glacial derived components (very low amounts of iceberg rafted debris and no grain size >63 μm) as the glacier-ice margin and associated sedimentation focus are removed from the continental margin to the inner regions of East Greenland fjords with the continental slope becoming an extremely ice distal setting.

5.9.3 Sedimentation patterns and processes on the continental shelf

5.9.3.1 Mid to outer continental shelf

The sediment thickness represented on acoustic records from the mid/outer continental shelf is limited due to the coarse grained composition of the sediment which restricts acoustic penetration (e.g Damuth 1978). The continental shelf between the mid shelf bathymetric high and the shelf break (Section 5.3.3) is covered by a thin, conformably bedded veneer of glacimarine sediment (acoustic unit VII) (Figs 5.8, 5.12; Table 5.3; Section 5.7.8). Core PS2630 shows this veneer to be of a diamictic composition (sandy mud diamicton facies; Fig 4.1; Table 5.2; Section 5.6.3.2) deposited through a combination of mainly ice rafting, and less so, meltwater/fluvial outflow into the marine environment, and biogenic/pelagic activity (Tables 4.4, 5.3; Section 4.7.2.2), with further modification by the East Greenland Current (Table 4.4; Section 4.7.2.3). The diamicton veneer is assumed to have been deposited during the Late Weichselian, and not the Holocene as the surface distribution would suggest. This is because Holocene aged surface facies within Kejser Franz Josephs Fjord and Hochstetter Bugten (Stein et al. 1993; Hubberten et al. 1995) are mainly muds, even though they are more proximal to the source of icebergs calved from tidewater glaciers (Section 5.9.4). Therefore, the Late Weichselian was the last time that icebergs could reach the continental shelf in significant numbers to deposit the diamicton facies. The bioturbated mud facies immediately underlying this sandy mud diamicton facies in PS2630 (Fig 4.1; Table 5.2; Section 5.6.3.2) is not differentiated on acoustic sections and therefore, its distribution across the continental shelf can not be ascertained. The surface veneer of diamicton is directly underlain by acoustic unit VIII in a limited number of regions on the mid to outer continental shelf. No cores penetrated this unit but as discussed in Section 5.7.9 the sediments are probably diamictic in composition deposited mainly as a result of iceberg rafting. As the acoustic facies directly underlies the surface diamicton veneer of acoustic unit VII, it is highly likely that the diamicton was also deposited during the Late Weichselian.

The surface veneer is disturbed by iceberg scouring in the vicinity of the continental shelf break (Fig 5.12) resulting in partial (acoustic unit Vb) to total (acoustic unit Va) turbation of the sediment (Fig 5.7C; Table 5.3). The age of the iceberg scouring can conceivably correspond to a number of dates back to the Late Weichselian (cf. Section 5.8.3) as even during peak Late Weichselian glaciation, it is proposed that glacier-ice did not occupy the mid to outer region of the continental shelf (e.g. Funder 1989; Funder & Hansen 1996). The absence of a surface veneer of fine-grained hemipelagic sediment in both PS2630 and across the mid-outer continental shelf within the acoustic records show that it is possible that the accumulation of Holocene sediments was prevented, and/or subsequently removed through winnowing associated with the East Greenland Current (Section 4.7.8). The latter is commonly observed on other parts of the East Greenland continental margin (e.g. Funder & Larsen 1989; Mienert et al. 1992; Nam 1996), and similarly on the western Svalbard continental margin (e.g. Cadman 1996).

In the immediate vicinity of the eastern margin of the mid continental shelf bathymetric high (Section 5.3.3), a mass-flow deposit (acoustic unit II) underlies the diamicton veneer (Figs 5.8, 5.12; Table 5.3; Section 5.7.3). The deposit is at its thickest at the base of the slope (Fig 5.8), and considered to originate from the resedimentation of debris deposited on or close to the slope surface. The mass-flow deposit extends 2500 m to the east (Fig 5.8). The diamictic composition in core PS2630 (Fig 4.1; Table 5.2; Section 5.6.3.2) shows the sediment to have been deposited by debris flows (Table 4.4, 5.3; Sections 4.7.2.1, 5.7.3). However, the thickening of sediment in the vicinity of the slope is thought to represent slump-related resedimentation. Therefore, a transformation from slumping into debris flow during transport appears to have occurred (e.g. Laberg & Vorren 1996). The sea floor sediment on the bathymetric high and close to its eastern margin are heavily scoured by icebergs (Figs 5.8, 5.12; Sections 5.8.5, 5.8.6). It is interpreted that the action of iceberg scouring, combined with the processes outlined in Section 5.9.2.3, initiated slope instability and downslope resedimentation. The diamictic composition of the mass-flow deposit shows the original sediment to be glacigenic in origin, derived from mainly ice-rafting processes. The mass-flow is assumed to be deposited during the Late Weichselian. The contact between the overlying diamicton veneer and the underlying mass-flow deposit is marked by rain out and suspension settling-related muds not visible on acoustic records (Table 5.2; Figs 4.1, 5.8). A glacimarine deposit thought to be diamictic in composition from ice rafting processes (Section 5.7.9) underlies the debris flow deposit in occasional regions across the mid/outer continental shelf. This is thought to have been deposited during the Late Weichselian.

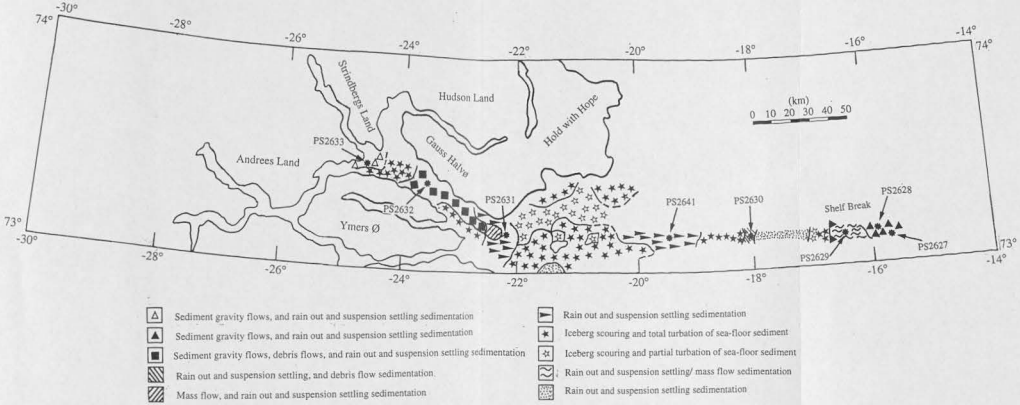

Figure 5.12. Map of Kejser Franz Josephs Fjord and the adjacent continental shelf and slope showing the regional distribution of the main sedimentary processes and environments interpreted from core lithofacies (Chapter 4) and acoustic units recognised from Parasound records. The study area in relation to Greenland is shown within the inset of Figure 5.1. A key to the symbols representing the sedimentary processes and environments is provided. The map scale is indicated. Sediment cores of this study are shown.

5.9.3.2 Mid to inner continental shelf

The inner continental shelf basin comprises conformably, stratified glacimarine sediment (acoustic unit IV) derived from rain out and suspension settling sedimentation (Figs 5.6, 5.12; Table 5.3; Section 5.7.5). Core PS2641 shows the sediment over the eastern margin of the basin to consist mainly of a sequence of bioturbated and laminated mud, and a thin unit of sandy mud diamicton facies at the base (Fig 4.1; Table 5.2; Section 5.6.3.2). The acoustic records show that these facies can be traced along the eastern margin (Fig 5.6). It is not possible to ascertain whether deeper sediment sequences occur below these sediments, as there is no further acoustic penetration possibly relating to either underlying bedrock, or sediment sequences into which the acoustic signal is impenetrable (Fig 5.6). The deepest region of the basin is marked by very low acoustic return representing relating to similar causes (Fig 5.6). The western margin also consists of stratified and conformable bedding style sediments deposited through a similar range of sedimentary processes.

The transition from sandy mud diamicton to laminated mud to bioturbated mud facies is interpreted to represent deposition under increasingly ice-distal conditions (e.g. Svendsen et al. 1992, 1996) associated with the retreat of glacier ice from the outer region of Kejser Franz Josephs Fjord/ inner continental shelf during the last deglaciation (Tables 4.4, 5.3; Sections 4.7.2.1, 4.7.7). The laminated mud and sandy mud diamicton facies represent deglacial sedimentation through sediment ladened meltwater outflows, and iceberg rafting (Tables 4.4, 5.3; Section 4.7). The thick surface bioturbated mud facies with small amounts of iceberg rafted debris represent ice-distal, post glacial, Holocene sedimentation associated with meltwater/fluvial outflows escaping the neighbouring East Greenland fjord systems, settling of sediment resuspended from shallower continental shelf regions by the East Greenland Current, and occasional iceberg rafting (Tables 4.4, 5.3; Section 4.7.8). Whether the sediment sequence was deposited in response to glacier ice retreat during the Late Weichselian deglaciation or post Younger Dryas deglaciation will not be discussed at this point. The interpretation that the sediment and acoustic sequence are deposited in association with a retreating ice margin, and the timing of this ice retreat, will be discussed further in Chapter 7 following the presentation of the chronology of core PS2641 in Chapter 6. The facies sequence of PS2641 occurs right across the eastern margin of the basin, and probably also occur across the western margin. However, no acoustic units could be correlated between the eastern and western margins, and no cores were recovered on the western margin to substantiate this claim. No moraines or subglacial till were found on the inner continental shelf (e.g. Jokat unpub. data; Jokat et al. 1995; Whittington 1995; Hubberten et al. 1995) associated with the proposed location of the glacier-ice margin during the Late Weichselian glaciation (Funder 1989; Funder & Hansen 1996).

The shallower regions of the inner continental shelf and across the bathymetric high on the mid continental shelf is disturbed by iceberg scouring (Fig 5.12) resulting in predominantly total turbation of sea-floor sediments (acoustic unit Va; Fig 5.7; Table 5.3). The age of the iceberg scouring can conceivably correspond to a number of dates back to the Late Weichselian (cf. Section 5.8.3).

5.9.4 Sedimentation patterns and processes in Kejser Franz Josephs Fjord and Fosters Bugt

5.9.4.1 Introduction

It is proposed that glacier ice of the Greenland Ice Sheet, which advanced during the Late Weichselian glaciation, retreated from the outer fjord/Fosters Bugt region at ca. 10,000 yr BP, and reached present day limits at ca. 7,000 yr BP (Hjort 1979; Funder 1989; Funder & Hansen 1996). However, air gun reflection records of Fosters Bugt and the outer fjord have failed to reveal any ice-contact moraines supportive of glacier-ice advance to the outer fjord and inner continental shelf during the Late Weichselian, and its Younger Dryas stillstand position during ice retreat (Jokat unpub. data; Jokat et al. 1995; Whittington 1995; Hubberten et al. 1995). Sea floor sediments in the fjord and Fosters Bugt preceding this glacial phase are assumed to have been removed by grounded ice of the Late Weichselian, in a manner similar to other fjord systems in East Greenland (e.g. Dowdeswell et al. 1994). The removal of glacier ice from the fjord during deglaciation following 10,000 yr BP allows glacimarine sedimentation to re-commence. Therefore, the sedimentary sequences observed within the cores and Parasound records from the fjord are assumed to have accumulated since 10,000 yr BP corresponding to the Holocene. If the 10,000 yr BP was positioned in the outer fjord then glacimarine sedimentation within Fosters Bugt may have re-commenced shortly before 10,000 yr BP in response to the proposed retreat of glacier-ice from the inner continental shelf during the Late Weichselian deglaciation (e.g. Funder 1989; Funder & Hansen 1996).

The acoustic records show that the basins and shallow bathymetric highs of the fjord and Fosters Bugt act as significant sediment traps accompanied by high sedimentation rates. The acoustic units and core lithostratigraphy show that the mid/outer section of the fjord and Fosters Bugt are dominated by a range of depositional styles that are, for the most part, consistent with an ice-distal fjord setting (e.g. Syvitski & Hein 1991; Hein & Syvitski 1992). This is supported within the Parasound records by an absence of subglacial till and moraines that are indicative of direct glacial activity. Sediments result from sediment gravity flows (turbidity currents and debris flows) and rain out and suspension settling of sediment (combination of ice rafting, sediment laden meltwater/fluvial outflows originating from tidewater glaciers and subaerial rivers fed by glacier and snow melt, and settling of resuspended sea-floor sediment) that combine to produce ponded, basin fill and conformable depositional styles (Fig 5.12; e.g. Syvitski & Hein 1991; Hein & Syvitski 1992; Niessen & Whittington 1997a; Whittington & Niessen 1997).

5.9.4.2 Outer Kejser Franz Josephs Ford and Fosters Bugt

A number of the small isolated depressions across Fosters Bugt consist of sediment gravity flow and occasional rain out and suspension settling deposits (acoustic unit Ia; Fig 5.12; Table 5.3; Section 5.7.2), interdigitating with debris flow deposits (acoustic unit II) (Figs 5.2, 5.12; Table 5.3; Section 5.7.3). The marginal regions of the outermost sub-basin in the outer fjord and a number of small depressions in Fosters Bugt, comprise conformably stratified, fine grained glacimarine sediments (acoustic unit IV) deposited through rain out and suspension settling processes (Fig 5.12; Table 5.3; Section 5.7.5). These sediments are derived through processes that consist of iceberg

rafting, meltwater/fluvial outflow and the settling of resuspended sea-floor sediment. The acoustic records from the northern and eastern parts of the outermost sub-basin of the outer fjord consists of acoustically stratified sediment overlain by a surface unit of acoustically massive/coarsely stratified sediment. The sediment sequence in core PS2631 shows that (i) the acoustically massive sediment at the surface comprises bioturbated mud, and (ii) the uppermost section of the underlying acoustically stratified sediment comprises laminated mud (Fig 4.1; Table 5.2; Section 5.6.3.3).

The transition from laminated mud facies/ acoustically stratified sediment to bioturbated mud facies/ acoustically massive sediment is interpreted to represent deposition under increasingly ice-distal conditions (e.g. Svendsen et al. 1992, 1996), and coupled with its position in the outer fjord, is probably associated with the retreat of glacier ice from the outer region of Kejser Franz Josephs Fjord during deglaciation after the Younger Dryas (cf. Hjort 1979; Funder 1989; Funder & Hansen 1996). The fine grained nature of the facies within PS2631 indicates that deposition occurred mainly within an ice-distal, low energy setting that becomes increasingly more so with subsequent deposition of the bioturbated mud facies/ acoustically massive sediment (Section 4.7.7). The underlying uncored acoustically stratified sediments are interpreted to be deposited increasingly more proximal to the glacier-ice margin with increasing depth and, therefore, should become progressively coarser related to the increasingly higher energy of the environment. Deposition is expected to be controlled by continued meltwater outflow with associated sediment production, and/ or subaqueous mass wasting events driven by downslope currents or failure of ice-proximal sediments that become increasingly more proximal to the glacier-ice margin with sediment depth (e.g. Dowdeswell et al. 1994b).

The combined sediment sequence in PS2631 and acoustic facies sequence is interpreted to represent deposition associated with glacier-ice recession during the deglaciation of the outer region of Kejser Franz Josephs Fjord ca. 10,000 yr BP, and the subsequent transition into the post-glacial Holocene. The interpretation that the sediment and acoustic sequence are deposited in association with a retreating ice margin, and the timing of this ice retreat, will be discussed further in Chapter 7 following the presentation of the chronology of core PS2631 in Chapter 6.

5.9.4.3 Mid to Outer Kejser Franz Josephs Fjord

Bathymetric highs (sills) throughout the mid and outer fjord are relatively devoid of sediment. The sediment that is present is heavily turbated through iceberg scouring. The general absence of sediment on bathymetric highs is assumed to result from the downslope resedimentation of any rain out and suspension settling deposits that may have accumulated. This is supported in acoustic sections by sediment thickening at the base of some bathymetric highs such as at the base of the mid fjord sill, interpreted to represent mass-flow related sedimentation. These deposits grade laterally into stratified sediments probably representing the transformation to sediment gravity flows with run out distance (e.g. Laberg & Vorren 1995, 1996). The present day fjord is influenced by the intrusion of shelf water of the East Greenland Current system (Vogt et al. 1995), which probably has been the case for the Holocene period following the recession of glacier-ice through the fjord from its Late Weichselian glaciation extent. Therefore, sediments deposited on bathymetric highs

throughout the Holocene may have undergone resuspension due to the influence of bottom current activity associated with the intrusion of the East Greenland Current into the fjord system (e.g. Marienfeld 1991, 1992b; Syvitski and Hein 1991; Vogt et al. 1995). Subsquent deposition of the resuspended sediment occurs within the deeper and more quiescent basins of the fjord (e.g. Marienfeld 1991, 1991b).

The mid fjord basin consist mainly of sediment gravity flow deposits (acoustic unit Ia) (Fig 5.12; Table 5.3; Section 5.7.2) and occasional interdigitating debris flow deposits (acoustic unit II) (Figs 5.2, 5.12; Table 5.3; Section 5.7.3). The massive and laminated muds of core PS2633 (Table 5.2; Sections 5.6.3.3, 5.7.2) indicate that glacimarine sedimentation within the mid fjord basin also occurs through the rain out and suspension settling of debris derived through iceberg rafting, meltwater/fluvial derived turbid surface plume activity and settling of resuspended sea-floor sediment.

The surface unit within the inner/intermediate/outer sub-basins of the outer fjord consists of a thin veneer of conformably bedded sediment deposited through the vertical rain out and suspension settling of sediment (acoustic unit VII) within a low energy environment (Figs 5.3, 5.5; Table 5.3; Section 5.7.8). Core PS2632 shows this to consist of fine grained glacimarine mud with small amounts of iceberg rafted debris (Fig 4.1; Table 5.2; Section 5.6.3.3). These sediments represent the most recent and quiescent part of the Holocene. Beneath this surface veneer the sedimentary sequence consists solely of basin infill. In the innermost and intermediate sub-basins, the base of the sequence is marked by a weakly stratified sequence (acoustic unit Ia) of sediment deposited by sediment gravity flows, and the rain out and suspension settling of sediment (Fig 5.3; Table 5.3; Section 5.7.2). The upper sediment layers of the unit are continuous over the adjoining sill into the intermediate sub-basin, reflecting either rain out and suspension settling sedimentation or mass wasting events that may have overspilled the sill (Fig 5.3). This sequence in the innermost sub-basin is overlain by a debris flow deposit (acoustic unit II) that runs the entire length of the sub-basin (Fig 5.3; Section 5.7.3), overlain in turn by a thick stratified sequence of ponded sediment derived mainly through sediment gravity flows, and the rain out and suspension settling through the water column (acoustic unit Ia; Fig 5.3; Section 5.7.2), interdigitating with occasional debris flow deposits (acoustic unit II; Fig 5.3; Section 5.7.3). The debris flow deposits are side entry in origin from the margins of the fjord, as reflected in their cross sectional lobe appearance (Fig 5.3). The interdigitised debris flow deposits are interpreted to have been deposited following the emplacement of the stratified sediment gravity flow deposits as they cut through almost the entire thickness of the acoustically stratified unit, and small sections of the stratified sediments are incorporated into the debris flow deposit (Fig 5.3). This illustrates the erosive nature of the debris flow in order to remove, encorporate and redeposit sediment previously deposited (cf. Laberg & Vorren 1995, 1996; Niessen & Whittington 1997a; Whittington & Niessen 1997).

The interdigitating debris flow deposits in the innermost sub-basin proximal to the sill is continuous into the intermediate and outermost sub-basins where it develops an elongate bedding style. In the former case it overlies a stratified sequence of sediment gravity flow, and rain out and suspension settling-related sediments confined to small-scale depressions (Fig 5.3). This would seem

to represent overspill of the debris flow deposit as the intervening sill is small scale and not pronounced (Fig 5.3). The debris flow deposit correlates to acoustic unit III in the deeper regions of the outermost sub-basin (Fig 5.5). A similar interpretation of the sedimentation processes in the outer region of Kejser Franz Josephs Fjord has been made by Niessen & Whittington (1997a) and Whittington & Niessen (1997) based on selected sections from the acoustic records used in this study.

5.9.4.4 Generation of resedimentation events in Kejser Franz Josephs Fjord and Fosters Bugt

The supply of sediment to the mid and outer region of Kejser Franz Josephs Fjord, and Fosters Bugt during the Holocene is assumed to be relatively high due to active transport mechanisms on-land that deliver sediment to the fjord. Sedimentation at the fjord margins can not be investigated from acoustic evidence in this study as acoustic profiling in these regions was not performed during the Polarstern ARK X/2 cruise. Even with the absence of this evidence, it is highly probable that the turbidity current flow and debris flow deposits characterising the basin infill were derived from sediment piles that accumulated on the bathymetric highs (sills) and steep margins of the fjord (e.g. Gilbert 1982; Syvitski & Hein 1991; Hein & Syvitski 1992). An origin from the fjord margins is supported by stratified units of acoustic unit Ia (that in some cases may relate to turbidity current deposits) and debris flow deposits (acoustic unit II) that in general, perpendicularly cut the fjord axis within the sub-basins of the outer fjord. Additionally, the stratified units of acoustic unit Ia and debris flow deposits terminate away from bathymetric highs (e.g. mid fjord sill), particularly in the mid fjord basin and numerous depressions across Fosters Bugt, supporting their origin from these areas.

The steep margins of the fjord and bathymetric highs can be considered as loci for temporary and unstable storage of sediment deposited from the rain out and suspension settling of particles from iceberg, meltwater/fluvial outflow, aeolian and bottom current sources, side entry glaciofluvial/fluvial deltas and fans, and subaerial debris falls and slides (talus cones) (e.g. Gilbert 1982; Syvitski & Hein 1991; Hein & Syvitski 1992). The basinward transport of sediment from the bathymetric highs (sills) and margins of the fjord is a result of episodic unstable sediment accumulation and failure associated with the conditions outlined in Section 5.9.2.3. Aerial photographs and satellite imagery of the present day fjord support iceberg, meltwater/fluvial outflow and side entry delta and fan activities (Section 1.2; Figs 1.2, 1.3). Numerous fluvial systems (the largest being Paralleldal and Badlanddal) fed by snow melt and precipitation drain the land bordering the mid and outer fjord such as Gauss Halvø, Hold with Hope and Gunnar Anderssons Land (Figs 1.1-1.3), and provide major input of sediment to the fjord margins throughout the mid and outer fjord and Fosters Bugt. These point source inputs of sediment could explain the small, debris flow deposits that perpendicularly intersect the axis of the outer fjord sub-basins, as opposed to the more regional slope failures for the more laterally extensive sediment gravity flow deposits. However, this interpretation can not be tested as it is not possible to trace the debris flow deposits from the basins to the margins of the fjord due to the absence of acoustic sections along the fjord margins.

5.9.4.5 Iceberg scouring in Kejser Franz Josephs Fjord and Fosters Bugt

Sediments deposited in shallow regions of the fjord and Fosters Bugt are influenced further by iceberg scouring during the Holocene period following the recession of glacier-ice from its proposed position in the outer fjord/ Fosters Bugt region after ca. 10,000 yr BP (cf. Section 5.8.3; Hjort 1979; Funder 1989; Funder & Hansen 1996; Table 5.3; Fig 5.12; Section 5.8). If glacier-ice did not occupy the Fosters Bugt region at this time then iceberg scouring may have occurred pre-10,000 yr BP following the retreat of ice from its proposed peak Late Weichselian glaciation position on the the inner continental shelf during the Late Weichselian deglaciation (cf. Section 5.8.3; Funder 1989; Funder & Hansen 1996). The variable degree of iceberg scouring results in sea-floor sediments being partially to totally homogenised. This is most marked over the sills, bathymetric highs, and shallow regions within Kejser Franz Josephs Fjord and Fosters Bugt (Fig 5.10, 5.12; Section 5.8).

CHAPTER 6

CHRONOLOGY, STABLE ISOTOPES, SEDIMENTATION AND ACCUMULATION FLUXES, AND PALAEOENVIRONMENTAL IMPLICATIONS

6.1 INTRODUCTION

The development of a detailed chronology is essential to Late Quaternary glacimarine/marine geological investigations in high latitude regions (e.g. Kellogg 1976, 1980; Kellogg et al. 1978; Jones & Keigwin 1988; Stein et al. 1994a,b; Nam et al. 1995). The chronology provides an absolute temporal control on reconstructed environmental history associated with glacial-interglacial fluctuations. Two forms of timescale are adopted in these studies. First, a relative oxygen isotope stratigraphy based on the direct sensitivity of stable oxygen to Late Quaternary glacial-interglacial climatic oscillations (Emiliani 1955; Shackleton 1967). Second, an absolute chronology based on radiocarbon dating, from which the conventional chronostratigraphy of the Late Quaternary (Section 1.3) can be applied to the sediments.

As a result, a timescale comprising a relative stable oxygen isotope stratigraphy coupled with an absolute chronology has been constructed from six of the cores along the Kejser Franz Josephs fjord-shelf-slope transect (Fig 1.1). The chronology addresses three objectives central to this thesis:

- to place the lithostratigraphy (Chapter 4) and acoustic record (Chapter 5), and the reconstructed sedimentary environments within a chronological context.
- to assist in the correlation of lithofacies and associated sedimentological parameters between cores through the construction of time lines in order to differentiate the sedimentary environments of the fjord, shelf, and slope for specific time periods.
- to calculate linear sedimentation (cm kyr^{-1}) and mass accumulation rates (g cm^{-2} kyr^{-1}) in order to quantitatively define the flux of sediments supplied to the fjord, continental shelf, and continental slope of the study area in response to glacial and interglacial climatic fluctuations during the Late Weichselian and Holocene.

The stable oxygen and carbon isotope records also yield important palaeoclimatic and palaeoenvironmental implications for the East Greenland continental margin. These include the determination of (i) marine and terrestrial bioproductivity, (ii) sea-ice cover, (iii) meltwater discharge events associated with the melting of ice masses and the associated salinity changes within seawater, (iv) variations in the exchange of CO_2 between atmosphere and ocean surface waters, and (v) ice sheet volume change associated with fluctuating atmospheric temperatures.

This chapter will:

1. Present the composite timescale constructed for the suite of cores, by outlining the radiocarbon chronology and stable oxygen stratigraphy of each core dating from the Late Weichselian glaciation (Isotopic stage II) through to the Holocene (Isotopic stage I).
2. Discuss the palaeoenvironmental implications of the stable isotope records.
3. Present the linear sedimentation rates (LSRs) and mass accumulation rates (MSRs). Relate the rates to the lithostratigraphy of the study area cores. Discuss the palaeoenvironmental implications of the rates.

6.2 RADIOCARBON CHRONOLOGY

6.2.1 Introduction

AMS radiocarbon (^{14}C) dating provides a means by which the absolute chronology can be obtained. The dates provide an absolute chronological control on the stable oxygen isotope chronostratigraphy (Section 6.3), and palaeoenvironmental implications of the stable oxygen and carbon isotope stratigraphy. The AMS ^{14}C dating procedure is summarised in Section 3.5.4, and a full list of the biogenic species used in the datings, with the corresponding core depths, are provided in Table 3.2. The radiocarbon datings were performed at selected stratigraphic points (based on the amount of mono-carbonate) in cores PS2631, PS2641, PS2630, PS2629, PS2628, and PS2627. No ^{14}C dates were determined from cores PS2633 and PS2632 within the mid-fjord region due to the absence of biogenic carbonate.

6.2.2 Measured AMS and conventional radiocarbon dates

Table 6.1 lists the radiocarbon dates and the corresponding core depths determined on the mono-carbonate from six cores along the Kejser Franz Josephs fjord-shelf-slope transect (PS2631, PS2641, PS2630, PS2629, PS2628 and PS2627). Only the reservoir corrected radiocarbon dates are used in this study (Section 3.5.2). The position of the radiocarbon dates in relation to the lithostratigraphy of each core are presented in Figure 6.1. Based on the stratigraphically sequenced radiocarbon dates, in conjunction with the published chronology of the Late Quaternary (Section 1.3), the composite sedimentary record of cores from the study area extends as far back as 25,800 yr BP (Late Weichselian glaciation through to the Holocene). Three cores, PS2629, PS2628 and PS2627 on the upper to lower continental slope, respectively, yield radiocarbon dates that cover this interval (Table 6.1). The other cores yield ages that correlate to specific periods of time. A significant number of Holocene dates are documented in the sedimentary sequences of PS2641 and PS2631 (Table 6.1). These were measured along a major proportion of the core length and provide a high resolution chronology for the last 10,000 years.

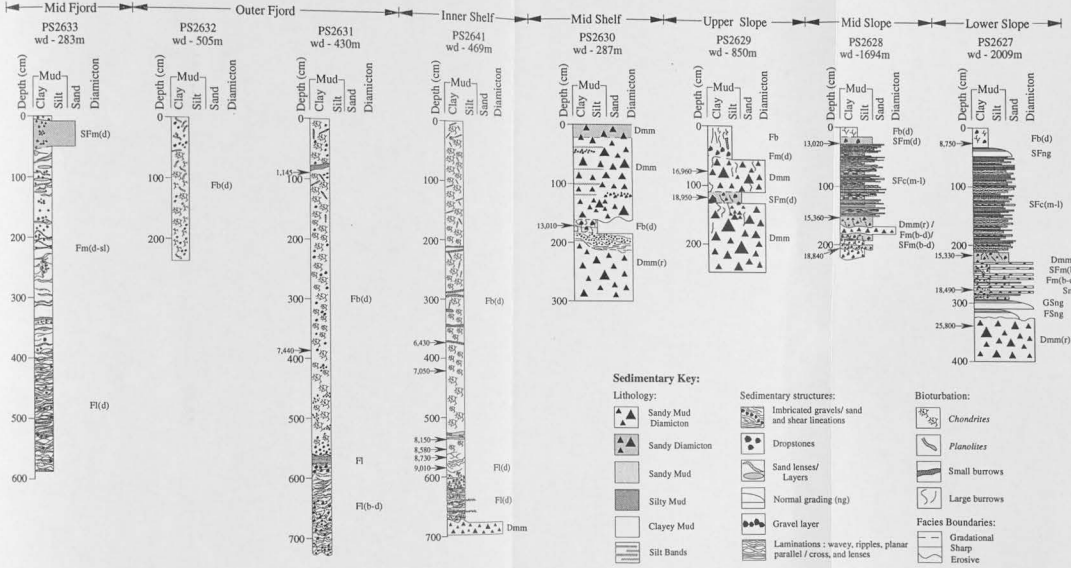

Figure 6.1. AMS radiocarbon datings (yr BP) in relation to the lithostratigraphy of the sedimentary cores of this study. The cores were taken along a west-east transect parallel to 73° N through the mid to outer Kejser Franz Josephs Fjord system and the adjacent continental shelf and slope (refer to Figure 1.1). Water depths (wd) of the recovered cores are indicated. A sedimentary key listing the lithologies and sedimentary characteristics is provided. A key to the lithofacies nomenclature is provided in Table 4.1.

Table 6.1. AMS ^{14}C datings of sediment samples from selected intervals within the cores recovered along the Kejser Franz Josephs fjord-shelf-slope transect (Fig 1.1). The table lists the core number, sample depth below seafloor (cm bsf), and uncorrected and corrected (reservoir effect of 550 years) radiocarbon ages. Measurements were performed at the AMS dating laboratory of the Institute of Physics and Astronomy, Aarhus University, Denmark.

Core	Laboratory No	Depth (cm bsf)	Uncorrected age (years BP)	Reservoir corrected age (years BP)
PS2627	AAR-2432	20	9300 +/- 100	8750 +/- 100
	AAR-2431	220	15880 +/- 120	15330 +/- 120
	AAR-2430	270	19040 +/- 230	18490 +/- 230
	AAR-2429	330	26350 +/- 380	25800 +/- 380
PS2628	AAR-2428	30	13570 +/- 120	13020 +/- 120
	AAR-2427	150	15910 +/- 160	15360 +/- 160
	AAR-2426	210	19390 +/- 190	18840 +/- 190
PS2629	AAR-2425	70 (30)‡	17510 +/- 160	16960 +/- 160
	AAR-2424	130 (90)‡	19500 +/- 210	18950 +/- 210
PS2630	AAR-2423	180	13560 +/- 130	13010 +/- 130
PS2641	AAR-2422	375	6980 +/- 130	6430 +/- 130
	AAR-2688	413	7600 +/- 70	7050 +/- 70
	AAR-2689	535	8700 +/- 75	8150 +/- 75
	AAR-2690	554	9130 +/- 80	8580 +/- 80
	AAR-2691	565	9280 +/- 80	8730 +/- 80
	AAR-2692	585	9560 +/- 120	9010 +/- 120
PS2631	AAR-2686	98 - 100	1695 +/- 55	1145 +/- 55
	AAR-2687	390	7990 +/- 210	7440 +/- 210

‡ Based on the correlation of records of oxygen isotopes and number of particles >2 mm/cm (indicative of iceberg rafted debris - IRD) between the gravity and box cores at location PS2629, it is determined that the topmost 40 cm are missing from the gravity core. Numbers in brackets are uncorrected gravity core depths, and the adjacent number is the corrected depth based on the box core.

6.2.3 Estimated and correlated ages

The AMS ^{14}C radiocarbon ages outlined above are further supplemented by dates correlated from neighbouring cores using recognised lithostratigraphic tie-points. Further dates are interpolated from events recognised in the records of stable oxygen and carbon isotopes (Section 6.3), and the number of particles >2 mm/cm (Fig 4.9; Section 4.5) indicative of iceberg rafted debris (IRD) in non-resedimented lithofacies.

It is assumed, based on a comparison of the sedimentary record of the uppermost sediments of the gravity core and box cores, that the surface sediments of each gravity core (except for PS2630) date at 0 yr BP. A comparison of the records of stable oxygen and carbon isotopes, and the number of particles >2 mm/cm (interpreted as iceberg rafted debris) of both the box core and uppermost section of the gravity core of PS2629, reveal that the latter must be corrected by the addition of 40 cm before the surface can be assumed to date at 0 yr BP.

The surface sediment in PS2630 is interpreted to pre-date the Holocene as it is composed of a sandy mud diamicton containing a very high amount of particles >2 mm/cm representing iceberg rafted debris (Fig 4.9; Sections 4.5, 4.7.2.2), unlikely to have been deposited during the Holocene. A pre-Holocene age is inferred as only small numbers of icebergs are discharged from modern-day outlet glaciers in the north east of Greenland (Reeh 1985), which is assumed to apply throughout the Holocene. Therefore, the significant numbers of icebergs needed to transport the IRD to the ice-distal site of PS2630 are more likely to have occurred during the Late Weichselian. The Holocene-aged, fine-grained sediment facies with low amounts of IRD in cores PS2631 and PS2641 from the outer fjord and inner continental shelf, respectively, and in cores from the fjord and continental shelf of the Hochstetter Bugten region (Stein et al. 1993; Hubberten et al. 1995) support this interpretation (Figs 4.9, 6.1; Section 4.5). If the uppermost diamicton in PS2630 was deposited during the Holocene a stronger IRD signal would be expected in these cores which are more proximal to iceberg producing outlet glaciers. The pre-Holocene interpretation is supported by the observation of a similar sandy mud diamicton close to the Late Weichselian-Holocene boundary in PS2641 (Figs 6.1, 6.2; Section 6.2.5). In light of this discussion the surface sediments are interpreted to date as recent as 10,000 yr BP (Holocene-Late Weichselian boundary). However, the assumed age of 10,000 yr BP must be considered the youngest of a possible range of ages, where the true age could date between 10,000 yr BP and the radiocarbon dated point of 13,010 yr BP at a core depth of 180 cm (Fig 6.1). This can not be resolved further due to poor chronological constraints in this section of PS2630. An age of 10,000 yr BP is estimated for the core depth of 35 cm in PS2629 as the number of particles >2 mm/cm, indicative of iceberg rafted debris (IRD), decreases to zero (Fig 4.9), marking the transition from the Late Weichselian into the Holocene based on the assumptions discussed for the age of the sediment surface in core PS2630.

The depletion of oxygen and carbon isotope records towards light values occurs at a core depth of 100 cm within PS2631, and is radiocarbon dated at 1,145 yr BP (Figs 6.3, 6.4; Section 6.3). A similar trend in the isotopic values is also recognised at a core depth of 125 cm in PS2641 (Figs 6.3, 6.4; Section 6.3). Therefore, the event in PS2641 is assumed to date at 1,145 yr BP. In core PS2628 (mid slope), the boundary between the sandy mud couplet facies and an overlying massive sandy mud facies at a core depth of 31 cm (Section 4.3.5) is AMS radiocarbon dated at 13,020 yr BP (Figs 4.1, 6.1). The sandy mud couplet facies is also recognised in core PS2627 where the upper boundary is observed at a core depth of 38 cm (Figs 4.1, 6.1; Section 4.3.5). This boundary is assumed to also date at 13,020 yr BP, regardless of the fact that the overlying facies consists of normally graded sandy mud rather than massive sandy mud as in PS2627 (Figs 4.1, 6.1).

The boundary separating the Late Weichselian glaciation and the onset of deglaciation is positioned at core depths of 54 cm in PS2629, 140 cm in PS2628 and 214 cm in PS2627 using a balance between the stable oxygen isotope stratigraphy (Fig 6.3; Section 6.3), and the record of particles >2 mm/cm, indicative of iceberg rafted debris (Fig 4.9; Section 4.5). The boundary is ascertained by: (i) the point at which the stable oxygen and carbon isotope records decrease to very light values, marking the onset of Termination Ia (Late Weichselian deglaciation; Section 6.3.5), and (ii) an abrupt decrease in the number of particles >2 mm/cm, indicative of iceberg rafted debris, from maximum values typical of the

Late Weichselian glaciation to lower values of the Late Weichselian deglaciation marking the reduced drift of icebergs. The culmination of the Late Weichselian glaciation and the onset of deglaciation is estimated to date at about 15,250 yr BP in PS2628 and PS2627, using the linear timescale outlined in Section 6.2.5 and Figure 6.2. No radiocarbon dates were determined for the top 54 cm of PS2629 (Fig 6.1; Table 6.1) and, therefore, the timescale between the nearest available dates (0 yr BP at the sediment surface and 16,950 yr BP at a core depth of 70 cm) could not be used with any accuracy for estimating the age of the Late Weichselian glaciation-deglaciation boundary. Instead the estimated age of 15,250 yr BP from PS2628 and PS2627 was applied to the Late Weichselian glaciation-deglaciation boundary in PS2629.

6.2.4 Validity of the AMS radiocarbon chronology

The majority of the radiocarbon dates acquired from the samples from the study area are stratigraphically ordered. This is supported by the fact that all dates were obtained from lithofacies not affected by resedimentation processes. The position of the radiocarbon dates in relation to the lithostratigraphy of each core are presented in Figure 6.1. An AMS radiocarbon date of 25,800 yr BP at a core depth of 330 cm in PS2627 was measured on a sample extracted from a resedimented sandy mud diamicton interpreted to represent a debris flow deposit (Section 4.7.2.1; Figs 4.1, 6.1). The radiocarbon age must post-date the sediment emplacement and, therefore, resedimentation must have occurred post 25,800 yr BP (e.g. Laberg & Vorren 1995).

A further source of error in the radiocarbon dates may result from the bioturbation of the host sediment. Commonly, bioturbation results in the mixing of sediment from different stratigraphic horizons (e.g. Shackleton & Opdyke 1973, 1976). Therefore, carbonate material deposited at different depths within the sediment column could be mixed together resulting in an unrepresentative radiocarbon age for a particular stratigraphic horizon. It is virtually impossible to test for the effects of bioturbation and, therefore, the carbonate used in the datings can only be assumed to be in situ, and that the dates provided are representative.

6.2.5 Construction and implementation of a linear timescale

A linear timescale is constructed for cores PS2631, PS2641, PS2630, PS2629, PS2628 and PS2627 (Fig 1.1). The timescale is constructed using the measured AMS radiocarbon dates (Sections 6.2.2, 6.2.3) and estimated ages (Section 6.2.4). However, the constructed timescale is only as accurate as the resolution of the radiocarbon chronology. The timescale is extrapolated to the lower, undated sections of each core using the linear sedimentation rates calculated between the two nearest dated stratigraphic points (Section 6.4), based on the assumption that the rate of sedimentation remains constant (e.g. Elverhøi et al. 1995). The core depth and the corresponding chronology of each core is plotted in Figure 6.2. The constructed timescales for each core are used in Figures 6.6-6.16.

The linear timescale shows that the sedimentary record extends reliably back to about 22,600 yr BP in PS2629 (upper continental slope), 20,900 yr BP in PS2628 (mid continental slope), and 19,700 yr BP in PS2627 (lower continental slope). However, the age stated for PS2627 is pre- dated by an AMS radiocarbon age of 25,800 yr BP but it is not possible to extend the timescale to this section of the sedimentary record because it is composed of facies deposited through resedimentation processes (Section 6.2.4). For the same reason the timescale is not extended back beyond 13,010 yr BP in PS2630. The timescale constructed for PS2630 (continental shelf) back to the radiocarbon dated point of 13,010 yr BP is probably unreliable, as the age of 10,000 yr BP assumed for the sediment surface is the most recent out of a possible range of ages that extend back to 13,010 yr BP (Section 6.2.3).

In PS2631 (outer fjord), the timescale can only reliably extend back to 7,440 yr BP, corresponding to a core depth of 375 cm. If the timescale is extended beyond this depth to the base of the core, an age of 14,386 yr BP is estimated. The proposed ice margin of the Greenland Ice Sheet was positioned in the outer fjord/inner shelf region as recent as 10,000 yr BP (Funder 1989; Funder & Hansen 1996). Therefore, glacimarine sediments older than 10,000 yr BP could not have accumulated at the core site rendering the timescale below a core depth of 375 cm inaccurate.

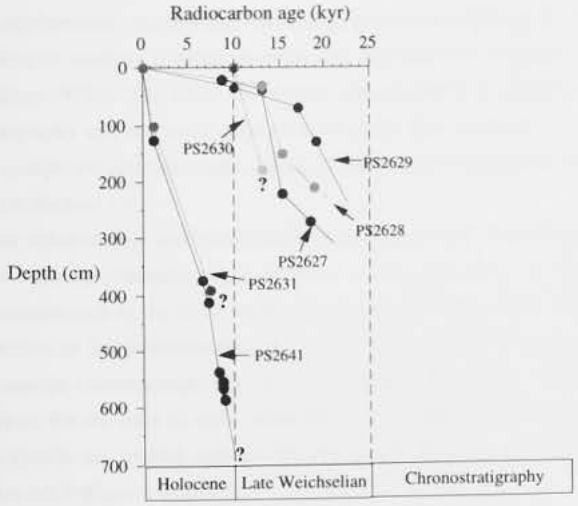

Figure 6.2. Plot of age (kyr) derived from measured and correlated radiocarbon datings against core depth (cm) for cores PS2641, PS2631, PS2630, PS2629, PS2628, and PS2627 recovered along the Kejser Franz Josephs fjord-shelf-slope transect. The closed circles represent AMS/conventional radiocarbon dated samples, and open circles correlated/estimated ages. The question marks refer to core sections in which the timescale is not certain. The chronostratigraphy based on this thesis is indicated.

In PS2641 (inner continental shelf), the timescale can be reliably extended back to 9,540 yr BP, corresponding to a core depth of 623 cm. If the timescale is extended to the base of the core, an age of

10,410 yr BP is estimated. Therefore, the lower section of the core would, in part, correlate to the Younger Dryas Cooling Event dated between 10,000-11,000 yr BP in the region (Marienfeld 1991; Section 1.3). In response, the stable isotopic record would exhibit heavy oxygen and light carbon isotope values characteristic of glacial conditions (e.g. Kennett 1990; Stein et al. 1994a,b; Nam 1996). Instead very light isotopes were recorded in the lower section of PS2641 which is consistent with Termination Ib post dating 10,000 yr BP (Section 6.3.5). Therefore, it is assumed that the base of the core does not pre-date 10,000 yr BP. A date of 10,000 yr BP is applied to the timescale.

6.3 STABLE ISOTOPE STRATIGRAPHY

6.3.1 Introduction

Stable oxygen and carbon analyses were performed on the planktonic foraminifera *Neogloboquadrina pachyderma* (sin.) from seven cores PS2632, PS2631, PS2641, PS2630, PS2629, PS2628, PS2627 (Fig 1.1). The measurement of stable oxygen and carbon isotopes were performed for two associated reasons: (i) The direct sensitivity of stable oxygen to Late Quaternary glacial and interglacial climatic oscillations (Emiliani 1955; Shackleton 1967), enables the construction of a relative chronostratigraphy supplementing the absolute chronology presented in Section 6.2. Carbon isotopes, on the other hand, are directly sensitive to bioproductivity and only indirectly to glacial-interglacial climatic oscillations (Shackleton 1977b). Therefore, the carbon isotopes are used primarily to supplement the oxygen isotope stratigraphy and the correlation between cores, and indirectly as a timescale. (ii) The oxygen and carbon isotopic records bear major palaeoenvironmental implications for the study area that are discussed further in Section 6.4.

Details on the stable isotope method are outlined in Section 3.5.3. In general, most stable isotope records are obtained from the planktonic foraminifera *N. pachyderma* (sin.) as it is a common species within polar water masses such as the Polar North Atlantic (e.g. Kellogg 1976, 1980; Nam et al. 1995; Nam 1996), irrespective of the predominating glacial or interglacial environment. This section will outline the oxygen isotope chronostratigraphy, and the corresponding results of the stable oxygen and carbon isotope analyses for the suite of cores along the Kejser Franz Josephs fjord-shelf-slope profile. The stable isotope results are plotted against the core depth (Figures 6.3, 6.4) and the timescale constructed in Section 6.2.5 (Figures 6.6-6.11).

6.3.2 Oxygen isotope stratigraphy: an overview

The composite oxygen isotope stratigraphy for the study area (Sections 6.2.3 and 6.2.4) represents the isotopic chronology back to Stage II and possibly Stage III (Figs 6.3, 6.4). The transition from Stage II to Stage I (last glacial-present interglacial) corresponds to the last deglaciation referred to, in oxygen isotopic terminology, as Termination I (cf. Broecker & van Donk 1972; Broecker 1984). Termination I is subdivided into Terminations Ia and Ib (cf. Duplessy et al. 1981; Fig 6.3). Termination Ia

corresponds to the first stage of deglaciation following the last glacial, and precedes the Younger Dryas Stadial. Termination Ib corresponds to the second stage of deglaciation following the culmination of the Younger Dryas Stadial at 10,000 yr BP. The Younger Dryas Stadial is only partially observed in the isotope records of PS2627. The position of the Stage I/II boundary in the scientific literature is commonly placed either at the onset or at the culmination of Termination Ia (e.g. Grousset & Duplessy 1983; Zahn et al. 1985; Stein et al. 1994a&b; Nam et al. 1995; Nam 1996; Stein et al. 1996). The Stage I/II boundary is placed at the onset of Termination Ia in this study, and is estimated to date at 15,250 yr BP in PS2629, PS2628 and PS2627 (Figs 6.2-6.4, 6.6-6.7, 6.8).

Oxygen isotope Stages I, II and III, and the corresponding boundaries between stages were established according to published literature (e.g. Martinson et al. 1987; Stein et al. 1994a,b; Nam et al. 1995; Nam 1996). Termination Ia and Ib were similarly identified from other published scientific work (e.g. Duplessy et al. 1981; Zahn et al. 1985; Jones & Keigwin 1988; Jansen & Veum 1990; Andrews et al. 1991, 1993; Sarnthein et al. 1992; Koc & Jansen 1994; Stein et al. 1994a,b; Nam et al. 1995; Nam 1996).

6.3.3 Oxygen isotope stage II / III

The lower sequence from PS2627 on the lower continental slope consist of $\delta^{18}O$ and $\delta^{13}C$ values that range between 3.604 ‰ to 4.105 ‰ and -0.041 ‰ to 0.213 ‰, respectively (Figs 6.3, 6.4). This section is interpreted to represent a reworked and, therefore, a mixed isotopic record that pre-dates early Stage II and encorporates Stage III isotopic values. This interpretation is based on two lines of reasoning: i) the upper section of the sequence (core depth of 330 cm) yields an AMS date of 25,800 yr BP consistent with Stage III, and ii) the entire section corresponds to a sandy mud diamicton facies deposited by debris flow (Chapter 4) which must have been emplaced between the estimated age of 19,700 yr BP and the radiocarbon date of 25,800 yr BP (Sections 6.2.4, 6.2.5).

6.3.4 Oxygen isotope stage II (Late Weichselian glaciation)

Stage II (Late Weichselian glaciation) is only represented in PS2629, PS2628, and PS2627 running from the upper to lower continental slope. The radiocarbon dates (Table 6.1) corresponding to the isotopic units of all three cores yield a timescale consistent with the Last Glacial Maximum of the Late Weichselian and are discussed in Section 6.2. The isotopic record of Stage II comprises heavy $\delta^{18}O$ and light $\delta^{13}C$ values. The composite $\delta^{18}O$ and $\delta^{13}C$ values from the stable isotope records of the three cores vary from 4.555 to 2.949 ‰ and -0.232 to 0.195 ‰, respectively (Figs 6.3, 6.4). The $\delta^{18}O$ and $\delta^{13}C$ records of PS2627 and PS2628 exhibit very little variation. On the other hand, the Stage II record of PS2629 can be divided into two isotopic units characterised by: i) an upper unit between core depths 55-140 cm composed of heavy $\delta^{18}O$ and light $\delta^{13}C$ values that vary from 4.169 to 4.540 ‰ and 0.010 to 0.118 ‰, respectively (Figs 6.3, 6.4), and ii) a lower unit over the remainder of the core of slightly lighter $\delta^{18}O$ and $\delta^{13}C$ values that vary from 4.171 to 2.949 ‰ and -0.232 to 0.113 ‰, respectively (Figs 6.3, 6.4), with the transition occurring at about 18,950 yr BP (Figs 6.1, 6.9).

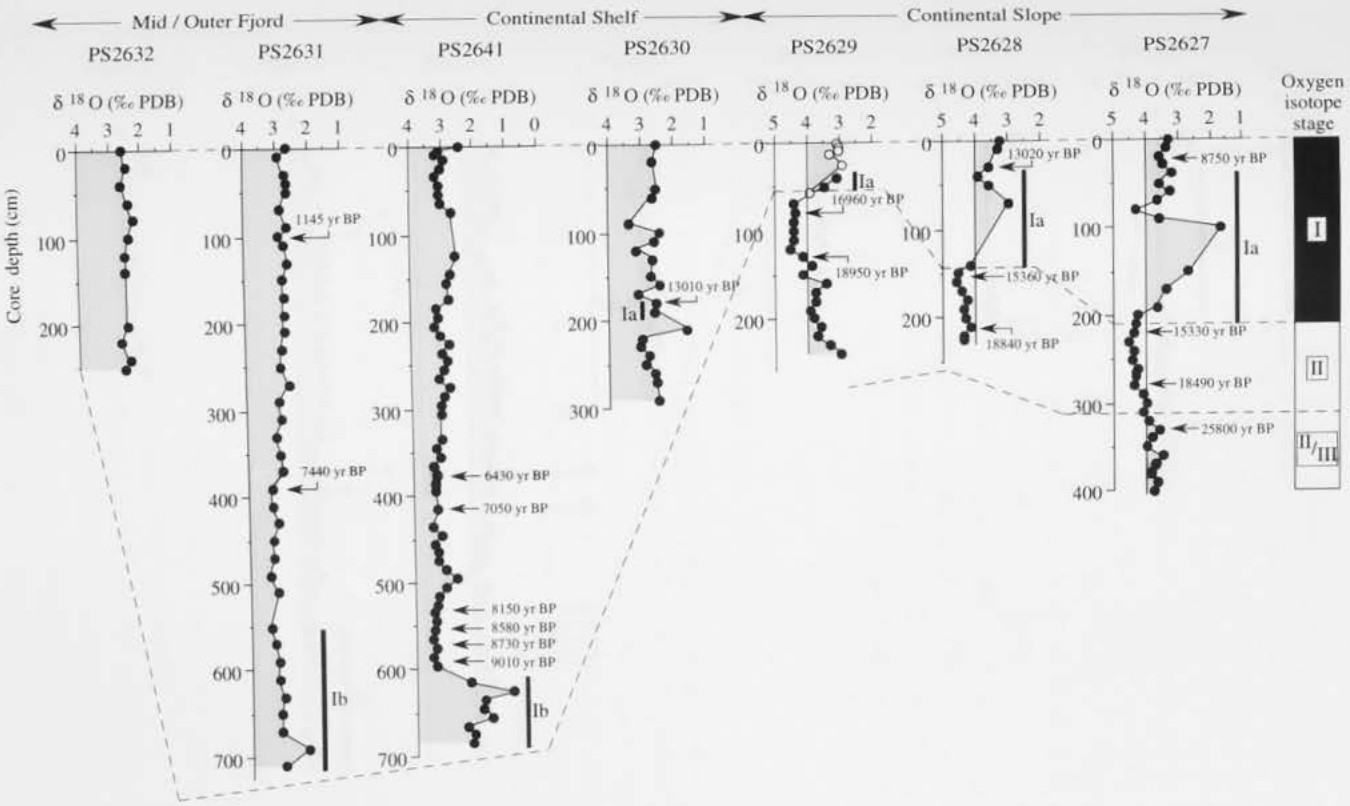

Figure 6.3. Stable oxygen isotope ($\delta^{18}O$) records measured on the planktonic foraminifer *Neogloboquadrina pachyderma* (sin) from cores PS2632, PS2631, PS2641, PS2630, PS2629, PS2628, and PS2627 recovered from the Kejser Franz Josephs Fjord-shelf-slope transect. The oxygen isotopic stage scale is indicated. Dotted lines correlate the oxygen isotopic stratigraphy between the cores. Termination Ia and Ib are shortened to I a and Ib, respectively, and are indicated by a solid black bar. AMS radiocarbon ages are indicated and provide an absolute chronological control on the oxygen isotope stratigraphy. The depth of the gravity core PS2629 is corrected by 40 cm by comparing its isotopic record with that of the box core. The box core record is indicated by the open circles.

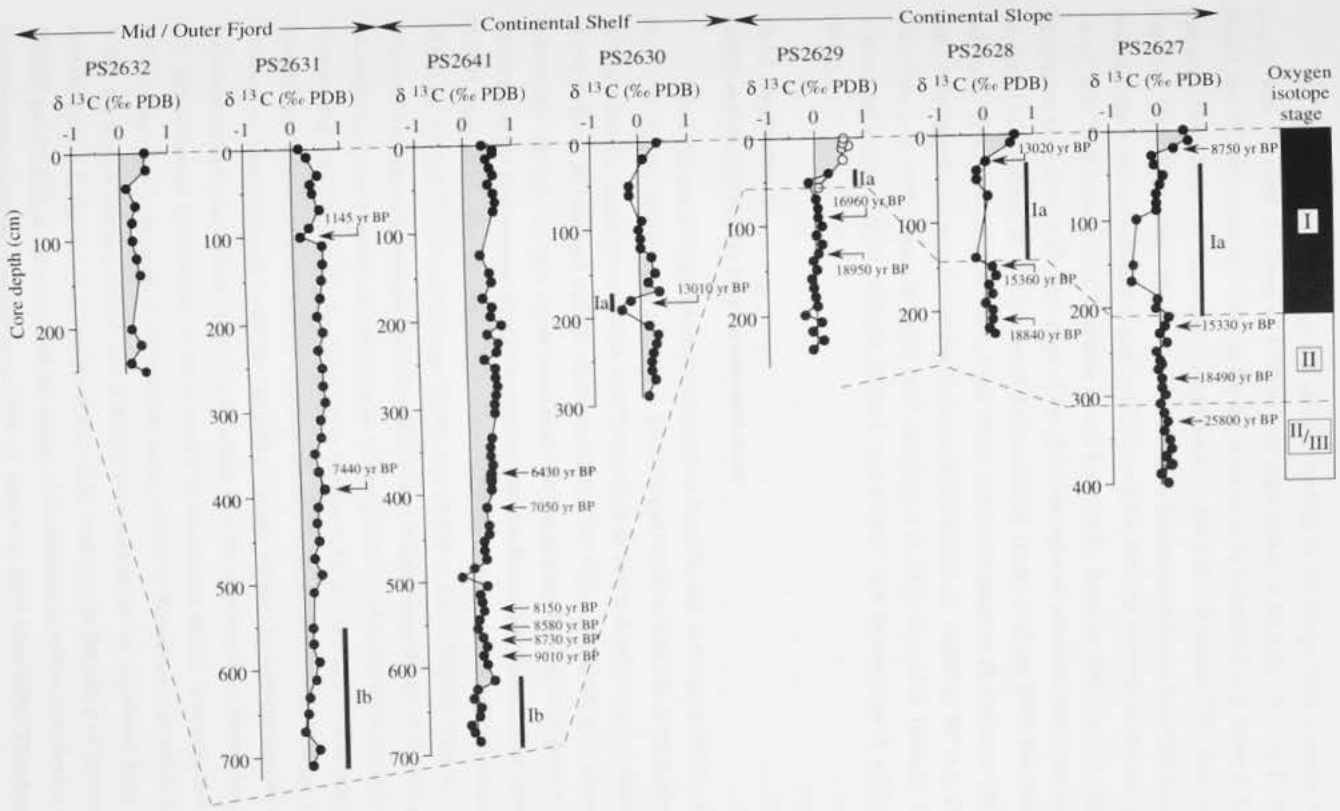

Figure 6.4. Stable carbon isotope ($\delta^{13}C$) records measured on the planktonic foraminifer *Neogloboquadrina pachyderma* (sin) from cores PS2632, PS2631, PS2641, PS2630, PS2629, PS2628, and PS2627 recovered from the Kejser Franz Josephs Fjord-shelf-slope transect. The oxygen isotopic stage scale is indicated. Termination Ia and Ib are shortened to I a and Ib, respectively, and are indicated by a solid black bar. AMS radiocarbon ages are indicated and provide an absolute chronological control on the carbon isotope stratigraphy. The depth of the gravity core PS2629 is corrected by 40 cm by comparing its isotopic record with that of the box core. The box core record is indicated by the open circles.

6.3.5 Termination I (deglaciation)

The transition between Stages II and I is marked by an abrupt 'shift' towards $\delta^{13}C$ minima coupled with the rapid depletion of $\delta^{18}O$ to very light values in PS2627, PS2628, PS2629, PS2630, PS2631 and PS2641, consistent with the last deglaciation or Termination I (e.g. Jones & Keigwin 1988; Bard et al. 1990; Jansen & Veum 1990; Sarnthein et al. 1992; Koc & Jansen 1994; Stein et al. 1994a,b; Nam et al. 1995; Nam 1996). The onset of Termination I corresponds to the Stage II/I boundary and the onset of Stage I, and is estimated to date at 15,250 yr BP in PS2629, PS2628 and PS2627 (Figs 6.2-6.4, 6.6-6.7, 6.8). Termination I (cf. Broecker & van Donk 1972; Broecker 1984) is two staged, where (i) Termination Ia represents the first stage of the glacial-interglacial transition immediately following the last glacial (e.g. Zahn et al. 1985; Jones & Keigwin 1988; Jansen & Veum 1990; Sarnthein et al. 1992; Stein et al. 1994a,b; Nam et al. 1995; Nam 1996), and (ii) Termination Ib represents the second, later stage, following the culmination of the Younger Dryas Stadial ca. 10,000 yr BP (e.g. Duplessy et al. 1981; Zahn et al. 1985; Jansen & Veum 1990; Sarnthein et al. 1992; Stein et al. 1994a,b). Termination Ia is preserved within PS2630, PS2629, PS2628, and PS2627, and Termination Ib within PS2631 and PS2641.

6.3.5.1 Termination Ia

PS2628 and PS2627 (mid to lower continental slope)

The $\delta^{18}O$ and $\delta^{13}C$ values vary from 3.668 to 1.660 ‰ and -0.045 to -0.565 ‰, respectively, in PS2627, to slightly heavier ones of 3.609 to 2.952 ‰ and -0.192 to 0.047 ‰ in PS2628 (Figs 6.3, 6.4). The light isotopic signal is consistent with Termination Ia and is dated to occur between 13,020 and 15,250 yr BP in PS2628 and PS2627 (Sections 6.2.2, 6.2.3; Figs 6.1, 6.2, 6.6, 6.7). Heavy $\delta^{18}O$ values indicate that the light isotopic signal associated with Termination Ia culminates prior to 13,020 yr BP. The timing of the light isotopic signal is consistent with that from other studies in East Greenland (Nam et al. 1995; Nam 1996). The lightest isotopic values correlate to the peak within Termination Ia, and date at 13,800 yrs BP in PS2627 and between 13,800 and 14,434 yr BP in PS2628 (Figs 6.2, 6.6, 6.7). The proposed Termination Ia isotopic record in PS2627 and PS2628 (core depths of 38-214 cm and 31-140 cm, respectively) corresponds to a thick facies of sandy mud couplets deposited through distal turbidity currents (Fig 4.1; Chapter 4). As discussed in Section 4.7.6 it could not be determined whether the foraminifera tests were reworked by turbidity currents or deposited directly through pelagic settling between or concomittantly with the turbidity current events. If resedimentation occurred, the displacement and redeposition of foraminifera tests of older ages may have taken place and would, on first approximation, place doubt on the reliability of the isotopic record. However, the light $\delta^{18}O$ and $\delta^{13}C$ values clearly represent a deglaciation signal related to Termination Ia which lies in-sequence within the overall isotopic record, and is further corroborated by the sequenced dates bracketing this section (Table 6.1; Figs 6.1, 6.2; Sections 6.2.2, 6.2.3). Furthermore, the dating of Termination Ia in both PS2627 and PS2628 is consistent with the timing of Termination Ia within cores further south along the East Greenland continental margin at ca. 72°N (cf. Nam et al. 1995; Nam 1996). Therefore, the light $\delta^{18}O$ and $\delta^{13}C$ values in PS2627 and PS2628 are interpreted as Termination Ia and will be discussed as such

within Section 6.4. The dating of Termination Ia can only be confined to the estimated and radiocarbon ages bracketing this section, and not the estimated dates from within (Figs 6.6, 6.7).

PS2629 (upper continental slope)

A comparison of the isotopic records from the gravity and box cores of PS2629 show that the former needs to be corrected by the addition of 40 cm providing a higher resolution to the uppermost sediment column. The corrected isotopic records between 10,000 and 15,250 yr BP (core depths 35 to 54 cm) are incomplete (Figs 6.3, 6.4, 6.9) due to the absence of the foraminifera *N. pachyderma sin.* Therefore, the isotopic records are inconclusive in support of the occurrence of Termination Ia during this interval. However, a set of moderately light $\delta^{18}O$ and $\delta^{13}C$ values of 3.473 ‰ and -0.154 ‰, respectively, are measured (Figs 6.3, 6.4), and are estimated to date ca. 13,980 yr BP (Fig 6.9). This is consistent with the timing of Termination Ia in PS2628 and PS2627.

PS2630 (continental shelf)

A thin isotopic unit at a core depth of 180-190 cm in PS2630, corresponding to a bioturbated mud facies (Figs 4.1, 6.1), consists of light $\delta^{18}O$ and $\delta^{13}C$ values of 2.527‰ and -0.211‰, respectively (Figs 6.3, 6.4), and has been radiocarbon dated at 13,010 yr BP. This signal relates to Termination Ia, and its timing is consistent with that in PS2628 and PS2627, and from other studies in East Greenland (e.g. Nam et al. 1995; Nam 1996; Stein et al. 1996). In general, the isotopic record post dating 13,010 yr BP is characterised by light $\delta^{18}O$ (2.427 to 3.360‰) and $\delta^{13}C$ (-0.194 to 0.403‰) values (Table 6.2; Figs 6.3, 6.4). The sediment surface in PS2630 is assumed to date at its most recent at 10,000 yr BP (Section 6.2.3). Therefore, it follows that in part, the light isotopic record post dating 13,010 yr BP documents the continuation of Termination Ia, which can conceivably culminate as recent as 11,000 yr BP (the onset of the Younger Dryas). How much of this record, however, relates to Termination Ia is unknown due to: (i) poor chronological constraints associated with the absence of radiocarbon dates after 13,010 yr BP, and (ii) the unreliability of the timescale constructed between 10,000 and 13,010 yr BP, relating to the 10,000 yr BP age adopted for the sediment surface being the most recent of a possible range of ages (cf. Sections 6.2.3, 6.2.5). Therefore, Termination Ia is only indicated for the chronologically fixed point at 13,010 yr BP in Figures 6.3, 6.4 and 6.12 to 6.16.

If the sediment surface does date as recent as 10,000 yr BP (Section 6.2.3), then it would follow that the Younger Dryas cooling event should be reflected within the high resolution isotopic record as heavy $\delta^{18}O$ and light $\delta^{13}C$ values (cf. Duplessy et al. 1981; Kennett 1990; Stein et al. 1994a,b; Nam 1996). A limited shift towards heavy $\delta^{18}O$ (max. 3.34‰) and light $\delta^{13}C$ (min. 0.06‰) values occurs at a number of points in the records, with the most recent at a core depth of 90 cm (Figs 6.3, 6.4), which dates at ca. 11,500 yrs BP in the timescale (Figs 6.2, 6.8; Section 6.2.5). However, the shifts in $\delta^{18}O$ and $\delta^{13}C$ are not convincing for such high resolution isotopic records, and the final shift at 11,500 yr BP does not correlate to the Younger Dryas which occurs between 10-11,000 yr BP. These observations exemplify the unreliability of the timescale. It is conceivable that the remainder of the isotopic record post dating 13,010 yr BP actually pre- dates 11,000 yr BP (onset of the Younger Dryas), and corresponds in its entirety to

Termination Ia. However, this is can not be resolved due to the unreliability of the timescale and poor chronological constraints on the isotopic record post dating 13,010 yr BP.

The isotopic record below a core depth of 190 cm in PS2630 (underlying the Termination Ia isotopic record) corresponds with a resedimented diamicton (Figs 4.1, 6.1; Section 4.7.2.2), and consists of isotopic values uncharacteristic of Termination Ia (see above; Figs 6.3, 6.4). This suggests that resedimentation may have influenced the isotopic record.

6.3.5.2 Termination Ib

Termination Ib is preserved within the isotopic records of PS2641 and PS2631, but not in PS2630, PS2629, PS2628 and PS2627. The Termination I signal within the $\delta^{18}O$ and $\delta^{13}C$ records of PS2641 (inner continental shelf) consists of very light values that vary between 2.365 to 0.910 ‰ and -0.142 to 0.096 ‰, respectively (Figs 6.3, 6.4). An abrupt shift in the $\delta^{18}O$ record towards heavier values typical of Stage I occurs at a core depth of 625 cm, and marks the end of Termination I. The culmination of Termination I, using the timescale of Section 6.2.5, dates at 9,540 yr BP (Fig 6.11), and the very light isotopic signal preceding the transition corresponds to Termination Ib (Section 1.3). The remaining very light isotopic signal of Termination Ib is interpreted to post-date 10,000 yr BP as heavy $\delta^{18}O$ and light $\delta^{13}C$ values typical of the Younger Dryas Cooling Event pre-dating 10,000 yr BP (e.g. Duplessy et al. 1981; Kennett 1990; Stein et al. 1994a,b; Nam 1996) are not observed in this section of the isotope record (Section 6.2.5).

Termination Ib is documented within the lower 150 cm section of PS2631 (outer fjord), providing high resolution $\delta^{18}O$ and $\delta^{13}C$ records that vary between 3.256 to 2.225 ‰ and -0.032 to 0.270 ‰, respectively (Figs 6.3, 6.4). Even though the light isotopic values are not AMS dated, it is assumed that the light isotopic values correspond to Termination Ib as the section is post-dated by a radiocarbon age of 7,440 yr BP at a core depth of 390 cm (Table 6.1; Fig 6.2). The transition from Termination Ib to Stage I occurs at 565 cm and is marked by a more gradual shift in the $\delta^{18}O$ values than that documented in PS2641 (Fig 6.3) reflecting the higher resolution of the Termination Ib record (Fig 6.3). Termination Ib is reflected more strongly in light $\delta^{13}C$ values (Fig 6.4). The strongly bioturbated nature of the mud facies in this section of the core (Chapter 4) may have reduced the amplitude of variation expected within a high resolution isotopic record such as this through vertical mixing of components within the sediment column (e.g. Shackleton & Opdyke 1973, 1976; Hutson 1980; Grobe et al. 1990).

6.3.6 Oxygen isotope stage I (present interglacial)

The Stage II/I boundary is estimated to date at 15,250 yr BP in PS2629, PS2628 and PS2627, and corresponds to the onset of Termination I (Section 6.3.5; Figs 6.2-6.4, 6.6-6.7, 6.8). The Stage I isotopic record corresponding to Terminations Ia and Ib was presented in Section 6.3.5. This section presents the remaining (post Termination I) Stage I isotopic record. A comparison of the near seafloor surface isotopic records from the gravity and box cores of PS2629 (upper continental slope) reveals that the depth needs

to be corrected by the addition of 40 cm, providing a higher resolution record for Stage I. The range and average values for $\delta^{18}O$ and $\delta^{13}C$ from the isotopic records determined for Stage I are listed in Table 6.2.

The Stage I isotopic records between 10,000 and 13,020 yr BP in PS2629, PS2628 and PS2627 are incomplete (Figs 6.3, 6.4, 6.6, 6.7, 6.9), due to the absence of the foraminifera *N. pachyderma* on which isotope measurements of this study were performed, and the limited sedimentary record caused by low sedimentation rates. A shift towards heavy $\delta^{18}O$ and light $\delta^{13}C$ values (Figs 6.3, 6.4, 6.7) occurs at a core depth of 30 cm in PS2627, and is estimated to date ca. 10,500 yr BP. This section of the isotopic record and its timing is consistent with the Younger Dryas Stadial (e.g. Duplessy et al. 1981; Kennett 1990; Stein et al. 1994a,b; Nam 1996), although the $\delta^{18}O$ values are not as heavy as expected for this event.

A complete Stage I isotopic record occurs in all cores following 10,000 yr BP (except PS2630; cf. Section 6.3.5.1), corresponding to the Holocene. As demonstrated by the average $\delta^{18}O$ and $\delta^{13}C$ values, the Stage I Holocene isotopic records in each core (Table 6.2; Figs 6.3, 6.4) become progressively lighter along the transition from the continental slope (PS2627, PS2628, and PS2629) across the continental shelf (PS2641), and into the Kejser Franz Josephs fjord (PS2641 and PS2632). This trend is illustrated in Figure 6.5.

Table 6.2. Summary of Stage I $\delta^{18}O$ and $\delta^{13}C$ records from along the Kejser Franz Josephs Fjord-shelf-slope transect.

Core	$\delta^{18}O$ (‰)	Average $\delta^{18}O$ (‰)	$\delta^{13}C$ (‰)	Average $\delta^{13}C$ (‰)
PS2632	2.244 - 2.653	2.482	0.133 - 0.533	0.319
PS2631	2.584 - 3.396	2.907	0.164 - 0.637	0.431
PS2641	2.537 - 3.466	3.050	0.060 - 0.702	0.407
PS2629	2.880 - 3.264	3.051	0.289 - 0.707	0.566
PS2628	3.213 - 3.319	3.300	0.519 - 0.622	0.571
PS2627	3.295 - 3.580	3.414	0.296 - 0.622	0.477

The Stage I sequences in PS2631 and PS2641 from the outer fjord and inner continental shelf, respectively, correspond with a thick sediment sequence. These provide high resolution isotopic records (Figs 6.3, 6.4) that exhibit discrete fluctuations associated with localised, short-lived events not preserved in the thinner sequences of remaining cores along the transect. However, the high resolution isotopic records of PS2631 and PS2641 appear uncharacteristically smooth where the amplitude of variations are damped (Figs 6.3, 6.4), and interpreted to reflect partial sediment mixing through strong bioturbation (e.g. Shackleton & Opdyke 1973, 1976; Shackleton 1977b; Hutson 1980; Zahn et al. 1986; Grobe et al. 1990). Even though there is a dense network of *Chondrites* type burrows within both cores (Section 4.3) it is commonplace not to encounter complete bioturbation of sediment with this type (Gorsline 1984).

Therefore, the fluctuations within PS2641 to a certain degree may be representative of the true variability within this section of the isotopic record.

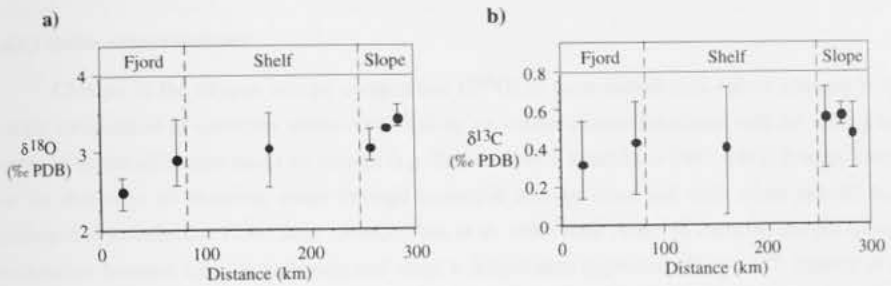

Figure 6.5 a,b. Schematic representation of the Stage I (Holocene) $\delta^{18}O$ and $\delta^{13}C$ records of cores PS2631, PS2641, PS2629, PS2628, and PS2627 with respect to their position along the Kejser Franz Josephs Fjord-shelf-slope transect. The average isotopic values associated with each record are indicated by points and the range of values by the bracketing bars.

In general, the $\delta^{18}O$ and $\delta^{13}C$ records of PS2631 and PS2641 become lighter and heavier, respectively, with progression away from the Stage I-Termination I transition with occasional discrete shifts from this trend (Figs 6.3, 6.4, 6.10, 6.11). This progression is interrupted in PS2641 by an abrupt shift towards light $\delta^{18}O$ and $\delta^{13}C$ values at a core depth of 495 cm, which dates at 7,790 yr BP (Section 6.2.5). A similar shift is observed at a core depth between 85 and 125 cm ($\delta^{18}O$ of 2.537-2.688 ‰ and $\delta^{13}C$ of 0.310-0.490 ‰), and is also recognised in PS2631 at 100 cm ($\delta^{18}O$ of 2.618-2.912 ‰ and $\delta^{13}C$ of 0.178-0.360 ‰). An AMS age in PS2631 reveals the shift to date at 1,145 yr BP and is correlated to PS2641. Furthermore, several additional smaller shifts in the isotopic record to slightly lighter values are observed in PS2641 (between 150-300 cm) and PS2631. However, the shifts are less obvious in the PS2631 (only observed in the $\delta^{18}O$ record) probably as a result of the light record in general.

6.4 PALAEOENVIRONMENTAL IMPLICATIONS OF STABLE ISOTOPE RECORDS

6.4.1 Introduction and background

The stable oxygen and carbon isotopic composition of planktonic foraminifera carbonate tests are in equilibrium with the isotopic composition of ocean/sea surface waters (e.g. Charles & Fairbanks 1990). The fractionation of oxygen and carbon isotopes within ocean/sea surface water is controlled by a number of environmental conditions that change with glacial/interglacial fluctuations. The controls on the fractionation of oxygen and carbon within ocean/sea surface water are discussed in this section. Based on these controls, the $\delta^{18}O$ and $\delta^{13}C$ records presented in Section 6.3 can be used to reconstruct the

palaeoenvironmental changes associated with the transition from the last glacial of Stage II through the ensuing deglaciation of Termination I (last deglaciation) and into the current interglacial of Stage I.

6.4.1.1 Stable oxygen isotopes

Changes in the oxygen isotope composition ($\delta^{18}O$) of foraminifera tests reflect changes in the isotopic composition of ocean/sea waters controlled by ice volume change associated with the waxing and waning of terrestrial/marine based ice masses (e.g. Emiliani 1955; Shackleton 1967, 1987; Bradley 1985), and the discharge of meteoric water through terrestrial derived river and melt water run-off (e.g. Spielhagen & Erlenkeuser 1994; Stein 1994a,b; Nam et al. 1995; Nam 1996). In addition, oxygen isotope fractionation between calcium carbonate and water is temperature dependent (Urey 1947; Epstein et al. 1953). Therefore, the oxygen isotope composition of planktonic foraminifera tests, is also controlled by the temperature of surface waters coupled to atmospheric temperature, reflecting glacial-interglacial oscillations (Emiliani 1955; Shackleton 1967).

The vapour pressure of H_2O^{16} is higher than that for H_2O^{18}. Therefore, H_2O^{16} evaporates preferentially from the ocean waters (Emiliani 1955). A significant amount of evaporation occurs in the tropical and sub-tropical evaporation belts of the oceans, where this water vapour (meteoric water) becomes increasingly depleted in ^{18}O during poleward migration (Emiliani 1955; Bradley 1985). Meteoric waters precipitated (snow and rain) over high latitude regions are enriched in O^{16}, which subsequently produces ^{16}O enriched, low-saline glacier ice and melt/river water run-off discharged into the oceans (light $\delta^{18}O$ ca. -26 to -31‰; e.g. Emiliani 1955; Bradley 1985; Spielhagen & Erlenkeuser 1994).

During glacials (e.g. Late Weichselian glaciation), the H_2O^{16} precipitated over high latitude regions becomes locked up in expanding ice masses which results in a concomittant enrichment of ^{18}O and therefore, heavy $\delta^{18}O$ within oceanic waters (e.g. Emiliani 1955). During the transition into full interglacial conditions (e.g. present interglacial) and the retreat of ice masses, the H_2O^{16} locked up in glacier ice is released into the oceans via meltwaters, producing a sudden dilution of the ^{18}O content and therefore, rapid depletion of $\delta^{18}O$ within ocean waters (e.g. Ruddiman & McIntyre 1981a,b; Jones & Keigwin 1988). During the following interglacial, the H_2O^{16} precipitated over high latitude regions is not locked up in ice masses, but is returned to the oceans via meltwater/river and iceberg discharge, maintaining the relative enrichment of ^{16}O and therefore, relatively light $\delta^{18}O$ within ocean waters (e.g. Emiliani 1955). In more marginal marine regions near meltwater and riverine input, and melting glacier ice and icebergs, the $\delta^{18}O$ may deviate from average ocean water (Emiliani 1955).

6.4.1.2 Stable carbon isotopes

Changes in the carbon isotope composition ($\delta^{13}C$) of foraminifera tests is only indirectly controlled by the temperatures of fjord/ocean surface water and the atmosphere (e.g. Shackleton 1977a). Instead, changes in the carbon isotope composition of foram tests reflect changes in the $\delta^{13}C$ composition of fjord/ocean surface water ΣCO_2 (i.e. total dissolved carbon: $CO_2 + HCO_3^- + CO_3^{2-}$), controlled

directly by: (i) the ventilation of fjord/ocean surface waters and the associated extent of CO_2 exchange with the atmosphere, (ii) continent and fjord/ocean surface water biological productivity, (iii) ocean nutrient levels and cycles, and/or (iv) supply and/or mixing of water masses of different isotopic composition (e.g. Kroopnick 1974, 1980; Kroopnick et al. 1977; Shackleton 1977a; Labeyrie & Duplessy 1985; Siegenthaler & Eicher 1986; Curry et al. 1988; Charles & Fairbanks 1990; Spielhagen & Erlenkeuser 1994).

Photosynthesis associated with fjord/ocean surface water biological productivity preferentially assimilates and fixes ^{12}C within organic matter (light $\delta^{13}C$ ca. -20 to -25‰; Shackleton 1977a; Charles & Fairbanks 1990), leaving fjord/ocean surface water enriched in ^{13}C and, therefore, $\delta^{13}C$ more positive or heavier (Labeyrie & Duplessy 1985; Siegenthaler & Eicher 1986; Curry et al. 1988; Charles & Fairbanks 1990). Similarly, photosynthesis associated with the continental biomass (mainly tropical rainforests and temperate forests) also preferentially assimilates and fixes ^{12}C within organic matter (light $\delta^{13}C$ ca. -20 to -25‰; e.g. Shackleton 1977a; Labeyrie & Duplessy 1985). The continental biomass assimilates ^{12}C from atmospheric CO_2 which is regulated by the oceans (oceans contain 90% of the global exchangeable carbon) and, therefore, the ^{13}C content of the fjord/ocean carbon reservoir becomes enriched, with $\delta^{13}C$ higher or more positive in response (e.g. Shackleton 1977a; Kroopnick et al. 1977; Labeyrie & Duplessy 1985). During glacials, the continental biosphere (tropical rainforests and temperate forests) reduces in response to the expansion of glacier ice and lower atmospheric temperatures; in high latitude fjords and oceans, surface water bioproductivity decreases due to increased sea ice cover, which acts to attenuate the light needed for photosynthesis (e.g. Shackleton 1977a; Kroopnick et al. 1977; Spielhagen & Erlenkeuser 1994; Nam et al. 1995; Nam 1996). Therefore, carbon (in particular ^{12}C) is transferred between the biosphere and the ocean reservoir, leading to a lighter $\delta^{13}C$ composition in the oceans (e.g. Shackleton 1977a; Kroopnick et al. 1977). During interglacials continental and ocean surface water bioproductivity (and hence, photosynthesis) is enhanced in response to the retreat of glacier ice, higher atmospheric temperatures and reduced sea ice cover conditions. Large amounts of ^{12}C are accumulated within the biosphere, and in response $\delta^{13}C$ in the ocean carbon reservoir becomes heavier or more positive (Shackleton 1977a; Labyerie & Duplessy 1985).

Under sufficient time and conditions, atmospheric CO_2 can reach isotopic equilibrium with the ΣCO_2 of fjord/ocean surface water (e.g. Labeyrie & Duplessy 1985). During equilibration, atmosphere-ocean exchange of CO_2 leaves fjord/ocean surface water enriched in ^{13}C, where $\delta^{13}C$ is more positive or heavier (Shackleton 1977a; Siegenthaler & Eicher 1986; Charles & Fairbanks 1990; Spielhagen & Erlenkeuser 1994). If equilibrium is attained $\delta^{13}C$ within fjord/ocean surface waters reach values of between +1 to +2‰ (e.g. Labeyrie & Duplessy 1985; Siegenthaler & Eicher 1986). In some high latitude regions such as the Arctic Ocean and the East Greenland continental margin, the presence of sea ice, and the production of a melt/river water induced cap or stratification across fjord/ocean surface waters suppresses the ventilation and associated exchange of CO_2 between fjord/ocean waters and the atmosphere, preventing full equilibrium conditions (e.g. Stein et al. 1994a,b; Spielhagen & Erlenkeuser 1994; Nam et al. 1995; Nam 1996). Ventilation of fjord/ocean surface waters and the associated exchange of CO_2 with the atmosphere is restricted to seasonal, temporary or permanent ice free regions (e.g.

Spielhagen & Erlenkeuser 1994; Stein et al. 1994a,b; Nam et al. 1995; Nam 1996). The ventilation of fjord/ocean surface waters and the exchange of CO_2 with the atmosphere is greatly reduced during glacial periods when sea ice cover is more extensive, resulting in light $\delta^{13}C$ values (e.g. Stein et al. 1994a,b; Nam et al. 1995; Nam 1996).

The supply of light $\delta^{13}C$ within river waters (ca. -5 to -15‰; Siegenthaler & Eicher 1986; Spielhagen & Erlenkeuser 1994) may dilute and lower the $\delta^{13}C$ composition of fjord and ocean (particularly along the continental margin) waters (e.g. Spielhagen & Erlenkeuser 1994). The dilution of the $\delta^{13}C$ composition of fjord and ocean waters by river water is considered important in the Arctic Ocean (Spielhagen & Erlenkeuser 1994). The influence of meltwaters, derived from subglacial drainage of tidewater glaciers and glacifluvial systems, on the $\delta^{13}C$ composition of fjord and ocean waters can not be properly ascertained, as there has been virtually no reports on the $\delta^{13}C$ composition of glacier ice and meltwaters, and its associated influence on fjord/ocean waters in the scientific literature. Limited information is available based on Svalbard and Alpine glacier systems, revealing that modern-day glacier-related meltwaters in these regions have a $\delta^{13}C$ composition that ranges between ca. -1‰ to -9‰ (Tranter pers. comm.). Therefore, if the $\delta^{13}C$ compositional range of these meltwaters are representative analogues for meltwaters in general (i.e. in terms of the geographical location of the glacier system, and time), then it is likely that the light $\delta^{13}C$ composition of meltwaters could dilute the $\delta^{13}C$ composition of fjord and ocean waters. The residence time of these melt/river waters in the fjord/ocean is important as they will become progressively equilibrated with the atmosphere over time, affecting their $\delta^{13}C$ composition (e.g. Spielhagen & Erlenkeuser 1994).

6.4.2 Stage II (Late Weichselian glaciation)

The heavy $\delta^{18}O$ values (>+4‰) and $\delta^{13}C$ minima (ca. 0‰) (Figs 6.3, 6.4), between 15,250 and 22,600 yr BP during glacial Stage II (Late Weichselian glaciation) within PS2629, PS2628 and PS2627 from the continental slope cores are a product of a number of factors.

The heavy $\delta^{18}O$ values of Stage II reflect the expansion of high latitude ice sheets, such as the Greenland Ice Sheet, and lower sea surface temperatures coupled to low atmospheric temperatures (cf. Section 6.4.1.1; e.g. Stein et al. 1994a,b; Nam et al. 1995; Nam 1996), both in response to glacial conditions. The extension of terrestrial and marine based ice sheets act as a reservoir for the ^{16}O precipitated within meteoric waters (H_2O^{16}) in high latitude regions, leaving oceanic waters more enriched in ^{18}O and, therefore, heavy $\delta^{18}O$ values (e.g. Emiliani 1955).

The $\delta^{13}C$ minima of glacial Stage II reflect the greatly suppressed ventilation of ocean surface water and associated reduction in the exchange of CO_2 between the ocean and atmosphere, caused by an extended and more permanent sea ice cover (cf. Section 6.4.1.2; e.g. Spielhagen & Erlenkeuser 1994; Stein et al. 1994a,b; Nam et al. 1995; Nam 1996). A reduction in the continent and ocean surface water bioproductivity, in response to decreased atmospheric temperatures and extended sea ice cover, may have also contributed to the $\delta^{13}C$ minima (cf. Section 6.4.1.2; e.g.Shackleton 1977a; Kroopnick et al. 1977; Labeyrie & Duplessy 1985; Stein et al. 1994a,b; Nam et al. 1995; Nam 1996). A reduction in surface

water bioproductivity is expected during glacial Stage II, as this is recorded in other studies from the East Greenland continental margin (e.g. Nam et al. 1995; Nam 1996). However, a reduction in surface water bioproductivity can not be confirmed in this study as the marine organic carbon and biogenic carbonate content have not been determined, and neither have biogenic particles been identified, from sea-floor sediments.

Although the sea ice cover is extended, it is possible that there were at least some seasonally ice free (open waters) conditions in the study area. Other regions of the East Greenland continental margin (16,000-21,000 yr BP) and in the Fram Strait (between 14,500-19,500 yr BP and pre-22,500 yr BP) experienced some seasonally ice free (open waters) conditions during the Late Weichselian glaciation (Hebbeln et al. 1994; Nam et al. 1995; Nam 1996; Hebbeln & Wefer 1997). The presence of planktonic foraminifers and nannofossils within sea-floor sediments on the continental slope of the study area supports at least some seasonally sea ice free conditions during the last glacial (cf. Sections 4.3.7, 4.7.8).

The $\delta^{18}O$ (<+4‰) and $\delta^{13}C$ (<0‰) records decrease to lighter values pre- dating 18,950 yr BP on the upper continental slope (PS2629) (Figs 6.3, 6.4). The $\delta^{18}O$ record suggest that a major incursion of low-saline, ^{16}O enriched meltwater discharged from the melting of ^{16}O enriched glacier ice of the Greenland Ice Sheet, and/or discharged icebergs may have occurred pre-18,950 yr BP (e.g. Baumann et al. 1993; Nam 1996).

6.4.3 Termination I (deglaciation)

The transition between Stages II and I is marked by an abrupt 'shift' towards $\delta^{13}C$ minima coupled with the rapid depletion of $\delta^{18}O$ to very light values (Figs. 6.3, 6.4) representative of the last deglaciation or Termination I (e.g. Zahn et al. 1985; Jones & Keigwin 1988; Sarnthein et al. 1992; Koc & Jansen 1994; Stein et al. 1994a,b; Nam et al. 1995; Nam 1996). The onset of Termination I corresponds with the onset of Stage I and the Stage II/I boundary. The deglacial transition is two stepped, consisting of the first and early part Termination Ia, and a second later part Termination Ib (e.g. Duplessy et al. 1981; Jansen & Erlenkeuser 1985; Jansen & Veum 1990; Stein et al. 1994a,b; Nam 1996).

The first step of deglaciation, Termination Ia, began after 15,250 yr BP in PS2628 and PS2627, culminating in both cores before 13,020 yr BP. The distinct depletion of $\delta^{18}O$ of >2.4‰ exceeds the 1.3‰ attributed to changes in glacial-interglacial ice volume (e.g. Chappell & Shackleton 1986; Labeyrie et al. 1987; Mix 1987; Ruddiman 1987; Jones & Keigwin 1988; Jansen & Veum 1990). As present day surface water temperatures in the region are mostly near freezing point (<-1°C; Hopkins 1991), lower temperatures during the peak glaciation of the Late Weichselian (Last Glacial Maximum; Stage II) are unrealistic. Therefore, the depletion of the $\delta^{18}O$ above that for the ice-volume effect is not due to a temperature increase. Rather, as the $\delta^{18}O$ composition of sea water is linearly related to salinity (Fairbanks et al. 1992; Speilhagen & Erlenkeuser 1994), the depletion of $\delta^{18}O$ above that of the ice volume effect reflects a decrease in surface water salinity resulting from increased low-saline, ^{16}O enriched meltwater (freshwater) discharge associated with the last deglaciation or Termination I (e.g. Jones & Keigwin 1988; Fairbanks 1989; Jansen & Veum 1990; Sarnthein et al. 1992; Stein et al. 1994a,b;

Nam 1996). Using the correlation factor of 1.01 for the relationship between salinity and $\delta^{18}O$ in the Greenland Sea (Fairbanks et al. 1992), a decrease in salinity exceeding 2.4 ‰ from modern-day values of 34.4 ‰ (Section 1.2), is predicted for surface waters during Termination I.

The meltwater pulse associated with the first stage of deglaciation culminates before about 13,020 yr BP consistent with other meltwater signals in the Polar North Atlantic (e.g. Jones & Keigwin 1988; Sarnthein et al. 1992; Koc & Jansen 1994; Dokken et al. 1996; Hald et al. 1996; Hebbeln et al. 1998). The low-saline, ^{16}O enriched meltwaters are interpreted to result from the early disintegration and retreat of glacier ice of the Greenland Ice Sheet from its position during the peak glaciation of the Late Weichselian (Last Glacial Maximum) and the associated melting of discharged icebergs. The $\partial^{13}C$ minima associated with the meltwater signal probably resulted from the widespread capping or stratification of ocean surface water by the meltwaters, which would have greatly suppressed the ventilation of ocean waters and the associated exchange of CO_2 with the atmosphere (cf. Section 6.4.1.2; e.g. Stein et al. 1994a,b; Nam et al. 1995; Nam 1996). The $\partial^{13}C$ minima could also reflect the $\partial^{13}C$ composition of the meltwater, in part or as a whole, provided the $\partial^{13}C$ records determined from modern-day glacier-related meltwaters of the Svalbard and Alpine regions are representative analogues for meltwaters in general (cf. Section 6.4.1.2).

The meltwater signal may also be contributed through an increased supply of low-saline Arctic waters in the East Greenland Current (e.g. Stein et al. 1994a,b; Nam et al. 1995; Nam 1996). The low-saline Arctic waters are derived from the disintegration of the Eurasian Arctic ice sheets and the large Siberian rivers which discharged large volumes of freshwater (enriched in light $\delta^{18}O$; cf. Spielhagen & Erlenkeuser 1994) into the Eurasian Basin of the Arctic Ocean during the last deglaciation, following 15,700 yr BP (Stein et al. 1994a,b). The low-saline waters were subsequently transported via the Transpolar Drift System to the Fram Strait and along the East Greenland continental margin in the East Greenland Current (Stein et al. 1994a,b).

Low saline meltwaters produced from the melting of icebergs calved into the Fram Strait from the western margin of the Barents Sea Ice Sheet during the onset of its decay after ca. 15,000 yr BP (Jones & Keigwin 1988), may have also contributed to the meltwater signal of this study, following encorporation and transportation in the East Greenland Current. The earlier timing for the onset of meltwater production from the Greenland Ice Sheet suggests that it began to decay before the Barents Sea Ice Sheet. The onset of deglaciation further south along the East Greenland continental margin is dated between 15,300 - 15,800 yr BP (Nam et al. 1995; Nam 1996; Stein et al. 1996) which, in some cases, is 700 yr older than that documented in this study. Therefore, the Greenland Ice Sheet may have began to decay in different locations at different times.

The light $\delta^{18}O$ value at 13,010 yr BP in PS2630 on the continental shelf also relates to the low-saline, ^{16}O enriched meltwater pulse of Termination Ia documented in PS2627 and PS2628. Furthermore, the light $\delta^{18}O$ record post- dating 13,010 yr BP marks the continuation of the meltwater event associated with Termination Ia. The occasional fluctuations in the $\delta^{18}O$ record to slightly heavier values (Fig 6.3, 6.4) may indicate fluctuations in the production and influence of meltwater. The subsequent capping or stratification of ocean surface waters in response to the meltwater discharge also fluctuates and is not well

developed, as the moderately heavy $\delta^{13}C$ values indicate some degree of exchange of CO_2 with the atmosphere (e.g Stein et al. 1994a,b; Nam et al. 1995; Nam 1996). The timing of the culmination of this meltwater signal is not ascertained due to the poor chronological constraints in this section of the record and the unreliability of the associated timescale (Section 6.3.5.1). Meltwater signals in PS2629, PS2628 and PS2627 from the continental slope are not observed following 13,020 yr BP. This could be an artefact of the incomplete nature of the isotopic records occurring between 10,000 and 13,020 yr BP in these cores (cf. Section 6.3.6; Figs 6.3, 6.4, 6.6, 6.7, 6.9). However, heavy $\delta^{18}O$ isotopic values show that the meltwater signal associated with Termination Ia culminates before 13,020 yr BP in PS2629, PS2628 and PS2627 (see above; cf. Section 6.3.5.1; Figs 6.3, 6.4, 6.6, 6.7, 6.9). Therefore, the absence of a meltwater event associated with Termination Ia after 13,020 yr BP on the continental slope, may indicate its increasingly distal location with respect to the Greenland ice sheet, whose ice margin was probably retreating from the peak Late Weichselian glaciation position on the inner continental shelf at this time (cf. Funder 1989; Funder & Hansen 1996). In response, the influence of meltwaters would become increasingly more diminished and confined to ice proximal locations such as the continental shelf, producing the post 13,010 yr BP Termination Ia meltwater signal in PS2630.

The $\delta^{13}C$ minima coupled with the depleted $\delta^{18}O$ record pre- dating 9,540 yr BP in PS2641 (inner continental shelf) and pre- dating 7440 yr BP in PS2631 (outer fjord) and post dating 10,000 yr BP in both cores represent the second stage of deglaciation, Termination Ib (e.g. Duplessy et al. 1981; Jansen & Erlenkeuser 1985; Jansen & Veum 1990; Stein 1994a,b). Termination Ib corresponds to the final retreat of the Greenland Ice Sheet following the Younger Dryas Stadial. The depleted $\delta^{18}O$ record occurs in response to major, but localised, discharge of low saline, ^{16}O enriched meltwaters from the retreating Greenland Ice Sheet, and the melting of any discharged icebergs. The $\partial^{13}C$ minima associated with the meltwater signal probably resulted from the widespread capping or stratification of fjord/ocean surface water by the meltwaters, which would have greatly suppressed the ventilation of ocean waters and the associated exchange of CO_2 with the atmosphere (cf. Section 6.4.1.2; e.g. Stein et al. 1994a,b; Nam et al. 1995; Nam 1996). The $\partial^{13}C$ minima could also reflect the $\partial^{13}C$ composition of the meltwaters, in part or as a whole (cf. Section 6.4.1.2). Termination Ib culminates on the inner shelf at 9,540 yr BP marked by the abrupt 'shift' of $\delta^{18}O$ and $\delta^{13}C$ to Holocene Stage I values (Figs 6.3, 6.4). In PS2631, the culmination can only be dated at best as pre- 7,440 yr BP. The fjord transgressive nature of the Termination Ib culmination age indicates the progressive retreat of the Greenland Ice Sheet from the inner continental shelf into Kejser Franz Josephs Fjord during the early Holocene. A $\delta^{13}C$ minima coupled with a depleted $\delta^{18}O$ value at 7,790 yr BP in PS2641 could be linked to a meltwater pulse originating within the inner fjord, marking the very final retreat of the Greenland Ice Sheet. The $\delta^{13}C$ minima reflects the stratification and reduced ventilation of ocean/sea surface waters. Termination Ib is not documented in cores of the slope showing that the meltwaters discharged from the Greenland Ice Sheet during the final stages of decay did not influence the ice distal location of the continental slope.

6.4.4 Stage I (present interglacial)

Following the culmination of Termination I (Figs 6.3, 6.4; Sections 6.3.6, 6.4.3), the remaining Stage I isotopic record can be distinguished as light $\delta^{18}O$ values (<+4‰) and $\delta^{13}C$ maxima (ca. >+0.3‰) (Figs 6.3, 6.4). This Stage I isotopic record occurs after ca. 13,020 yr BP in PS2629, PS2628 and PS2627 and 9,540 yr BP in PS2641, and shortly before 7,440 yr BP in PS2631 (Figs 6.6-6.11). In PS2629, PS2628 and PS2627 the Stage I record pre- dating 10,000 yr BP is incomplete (cf. Section 6.3.6). The isotopic record of PS2629 shows that the pre- 10,000 yr BP period is one of gradual transition to Holocene $\delta^{18}O$ and $\delta^{13}C$ values and the establishment of Holocene environments. In PS2627 the transition is disrupted at 10,500 yr BP by a shift in the isotopic records to heavy $\delta^{18}O$ and light $\delta^{13}C$ values (Figs 6.3, 6.4, 6.7) consistent with the Younger Dryas Stadial (e.g. Duplessy et al. 1981; Kennett 1990; Stein et al. 1994a,b; Nam 1996), although the $\delta^{18}O$ values are not as heavy as expected for this event. The shift to heavy $\delta^{18}O$ values indicate cold conditions, and the $\delta^{13}C$ minima reduced CO_2 exchange between the ocean and atmosphere caused by extended sea-ice (reduced open-water) conditions, both associated with the renewed cooling during the Younger Dryas Stadial (e.g. Stein et al. 1994a,b; Nam 1996).

The lightest $\delta^{18}O$ values and $\delta^{13}C$ maxima, closest to modern-day values, occur during the Holocene following 10,000 yr BP (Figs 6.6-6.11). The $\delta^{18}O$ values reflect increased atmospheric temperatures of the Holocene, and the subsequent stabilisation of the Greenland Ice Sheet at a position similar to the present day with the ^{16}O locked up in the extended glacial ice mass returned to the oceans (cf. Section 6.4.1.1). The corresponding $\delta^{13}C$ maxima of the Holocene (Figs 6.6-6.11) reflect increased ventilation of fjord/ocean surface waters and associated exchange of CO_2 between the ocean and atmosphere, caused by a greatly reduced sea-ice cover and more open water conditions (seasonal sea ice cover) compared to the extended sea ice cover of the last glacial (cf. Section 6.4.1.2; e.g. Shackleton 1977a; Spielhagen & Erlenkeuser 1994; Stein et al. 1994a,b; Nam et al. 1995; Nam 1996). Additionally, increased continent and fjord/ocean surface water bioproductivity (in response to increased atmospheric temperatures and reduced sea ice cover) may have contributed to the $\delta^{13}C$ maxima (cf. Section 6.4.1.2; e.g.Shackleton 1977a; Stein et al. 1994a,b; Nam et al. 1995; Nam 1996). An increase in surface water bioproductivity is expected during Stage I, as this is recorded in other studies from the East Greenland fjords and continental margin (e.g. Marienfeld 1991, 1992a,b; Williams 1993; Williams et al. 1995; Nam et al. 1995; Nam 1996). However, an increase in surface water bioproductivity can not be confirmed in this study as the marine organic carbon and biogenic carbonate content have not been determined, and neither have biogenic particles been identified, from sea-floor sediments. The $\delta^{13}C$ maxima are somewhat below true equilibrium values (ca. +1 to +2‰ e.g. Labeyrie & Duplessy 1985), showing that equilibrium between the ocean and atmosphere during the Holocene has not been fully attained (cf. Section 6.4.1.2).

The modern day setting in the Kejser Franz Josephs Fjord and along the adjacent East Greenland continental margin is dominated by a seasonal sea ice cover that breaks up or retreats northwards during the summer season (Section 1.2.2.3), a situation which has applied throughout the Holocene (e.g. Baumann et al. 1993; Stein et al. 1993; Nam et al. 1995; Nam 1996). Therefore, the ventilation of surface waters and associated exchange of CO_2 between the ocean and atmosphere in the Kejser Franz Josephs

Fjord and across the adjacent East Greenland continental margin is probably limited to the summer season when sea ice breaks up. This period of time may not be enough for equilibrium conditions to be attained between the ocean and atmosphere.

As demonstrated by the average $\delta^{18}O$ and $\delta^{13}C$ values, the isotopic records of Stage I in each core become progressively lighter along the transect from the lower East Greenland continental slope (PS2627) to the mid region of Kejser Franz Josephs Fjord (PS2632) (Section 6.3.6; Table 6.3; Figure 6.5). The general trend is interpreted to reflect the stronger influence of relatively ^{16}O enriched meltwaters associated with the freshwater drainage of glacimarine, glacifluvial, and fluvial systems with increased proximity to the East Greenland continent. The enriched ^{16}O meltwaters reflect the high ^{16}O composition of glacier ice of the Greenland Ice Sheet, snow melt and river run-off due to the preferential fractionation of ^{16}O within meteoric water precipitated over high latitude regions ($\delta^{18}O$ ca. -26 to -31‰; Section 6.4.1.1; e.g. Emiliani 1955).

The progressive decrease in the $\delta^{13}C$ records from the East Greenland continental margin towards Kejser Franz Josephs Fjord are interpreted to result from one or a combination of three possible factors:

First, numerous river systems currently drain into Kejser Franz Josephs Fjord and Fosters Bugt, and have probably done so throughout the Holocene. It is interpreted that these systems have supplied light $\delta^{13}C$ enriched waters ($\delta^{13}C$ exceeds -10‰; e.g. Siengenthaler & Eicher 1986; Spielhagen & Erlenkeuser 1994) to the study area during this time. These waters would probably act to dilute and lower the $\delta^{13}C$ composition of the residual waters of the fjord and continental margin (e.g. Spielhagen & Erlenkeuser 1994). The influence of these waters is greatest in the fjord but becomes increasingly less so with progressive distance across the continental margin away from river water efflux points, resulting in the observed trend within the $\delta^{13}C$ records. The influence of meltwaters, derived from subglacial drainage of tidewater glaciers and glacifluvial systems, on the $\delta^{13}C$ composition of fjord and ocean waters can not be properly ascertained, as there has been virtually no reports on the $\delta^{13}C$ composition of glacier ice and meltwaters, and its associated influence on fjord/ocean waters in the scientific literature. The light $\delta^{13}C$ composition of modern-day meltwaters (ca. -1‰ to -9‰; Tranter pers. comm.) determined from Svalbard and Alpine glacier systems could be representative analogues for meltwaters in the study area throughout the Holocene period. If this is the case, then it is likely that the light $\delta^{13}C$ composition of meltwaters could dilute the $\delta^{13}C$ composition of fjord and ocean waters in a manner similar to river waters, resulting in an identical trend in the $\delta^{13}C$ composition of fjord/ocean surface waters with progressive distance away from the fjord system.

Second, melt/river water capping or stratification of fjord/ocean surface waters are known to influence the modern day Kejser Franz Josephs Fjord and the adjacent inner continental shelf (Section 1.2.3; Vogt et al. 1995), and have probably done so throughout the Holocene. The melt/river water capping or stratification effect probably results in the reduced ventilation and CO_2 exchange between the residual surface waters of the fjord/inner continental shelf and the atmosphere. This effect becomes increasingly less influential across the continental shelf with distance away from melt/river water efflux points in the fjord as the

capping or stratification of surface waters becomes progressively less well formed, with their eventual cessation beyond the inner continental shelf (cf. Section 6.4.1.1).

Third, surface water bioproductivity may vary between the fjord, continental shelf and continental slope in response to different environmental conditions (e.g. such as unfavourable hydrographic conditions of the fjord; cf Section 2.2.5), influencing the $\delta^{13}C$ record. However, systematic fluctuations in surface water bioproductivity within the fjord and across the continental margin can not be confirmed in this study as the marine organic carbon and biogenic carbonate content have not been determined, and neither have biogenic particles been identified, from sea-floor sediments. Therefore, it is not possible to determine whether the $\delta^{13}C$ trend is in response to bioproductivity variations.

The 'shifts' in the high resolution isotopic records to light values centred around 1,145 yr BP in PS2631 and PS2641, similar to those of Termination I, are interpreted to reflect short-lived meltwater pulses in response to small-scale climatic warming and the proximity of the cores to the fjord system and freshwater sources associated with glacimarine, glacifluvial, and fluvial systems.

6.5 LITHOSTRATIGRAPHICAL CHRONOLOGY

6.5.1 Introduction

The linear timescale (constructed from radiocarbon and estimated dates, and sedimentation rates), and the stable oxygen isotope chronology outlined in Sections 6.2 and 6.3 are used to date the lithofacies within each core of this study. The lithofacies in each core and their corresponding chronology are illustrated in Figures 6.6-6.11.

6.5.2 Late Weichselian 15,250-22,600 yr BP (Isotope stage II)

In PS2629, sandy mud diamicton (Dmm) facies dates between ca. 15,250 and 22,600 yr BP, and is separated into two units by massive sandy mud (with dropstones) facies (SF[d]) dating ca. 18,950 yr BP (Figs 6.1, 6.9). In PS2628, the sedimentary record dates between ca. 15,250 and 20,900 yr BP, consisting of massive sandy mud to mud (both with dropstones; SFm[b-d]/Fm[b-d]), intercalated with occasional resedimented sandy mud diamicton (Dmm[r]) facies (Figs 6.1, 6.6). In PS2627, the sedimentary record dates between ca. 15,250 and 19,700 yr BP, consisting of massive sandy mud to mud (both with dropstones; SFm[b-d]/Fm[b-d-sl]), closely intercalated with resedimented sandy mud diamicton (Dmm[r]) and massive sand (Sm) facies (Figs 6.1, 6.7). Normally graded muddy sand (FSng) and gravelly sand (GSng) facies, and resedimented sandy mud diamicton pre- date 19,700 yr BP with their deposition occurring sometime after 25,800 yr BP (Section 6.2.4; Figs 6.1, 6.7).

6.5.3 Late Weichselian 10,000-15,250 yr BP (Isotope stage I and Termination Ia)

In PS2628 and PS2627, sandy mud couplet (SFc[m-l]) facies dates between ca. 13,020 and 15,250 yr BP, corresponding to the meltwater event associated with Termination Ia (Figs 6.1, 6.6, 6.7). The period following 13,020 yr BP consists of massive sandy mud (with dropstones; SFm[d]) facies in PS2628, and bioturbated mud (with dropstones; Fb[d]) facies in PS2627 (Figs 6.1, 6.6, 6.7). In PS2629, massive mud facies (with dropstones; Fm[d]) dates between 10,000 and 15,250 yr BP, corresponding in part to the meltwater event of Termination Ia before 13,020 yr BP (Figs 6.1, 6.9). In PS2630, resedimented sandy mud diamicton (Dmm[r]) facies pre- dates 13,010 yr BP, with bioturbated mud (with dropstones; Fb[d]) facies dating at 13,010 yr BP, and sandy to sandy mud diamicton (Dmm) facies post-dating 13,010 yr BP with the sediment surface dating as recent as 10,000 yr BP (Section 6.2.3; Figs 6.1, 6.8). The bioturbated mud facies of PS2630 corresponds to the meltwater event of Termination Ia. The diamicton facies in part, if not in its entirety, may also correspond to the meltwater event of Termination Ia, but how much is unknown due to poor chronological constraints in the upper sedimentary record of PS2630.

6.5.4 Holocene 0-10,000 yr BP (Isotope stage I and Termination Ib)

The Holocene sedimentary record consists of sandy mud (with dropstones; SFm[d]) facies between ca. 8,500 and 10,000 yr BP, and bioturbated mud (with dropstones; Fb[d]) facies following 8,500 yr BP in PS2628 (Figs 6.1, 6.6). In PS2629 and PS2627, the Holocene sedimentary record consists of bioturbated mud (with dropstones; Fb[d]) facies (Figs 6.1, 6.7, 6.9). No Holocene sedimentary record occurs in PS2630 (Fig 6.8). In PS2641, sandy mud diamicton (Dmm) and laminated mud (with dropstones; Fl[d]) facies dating between 9,540 and 10,000 yr BP (Section 6.2.4), corresponding to the meltwater event associated with Termination Ib (Figs 6.1, 6.11). Following 9,540 yr BP in PS2641, the Holocene sedimentary record consist of bioturbated mud (with dropstones; Fb[d]) facies (Figs 6.1, 6.11). In PS2631, laminated mud (with dropstones; Fl[b-d]) facies overlain by bioturbated mud (with dropstones; Fb[d]) facies pre- dates 7,440 yr BP, and is interpreted to post- date 10,000 yr BP (Section 6.2.4; Figs 6.1, 6.10). The laminated mud facies corresponds to the meltwater event associated with Termination Ib. The bioturbated mud facies continues up to the recent (Figs 6.1, 6.10).

6.6 LINEAR SEDIMENTATION RATES

6.6.1 Introduction

Linear sedimentation rates (LSRs) are calculated in this study for two important reasons: i) to determine the flux of sediments (with water content and porosity included) delivered to the fjord, continental shelf and continental slope in response to glacial-deglacial-interglacial environments and associated processes, and ii) to develop a detailed linear timescale in order to determine the chronology of

events interpreted from the lithostratigraphy (Chapter 4) and stable isotope stratigraphy (Section 6.3) investigations of this study. The linear timescale was presented in Section 6.2.5. The sedimentation rates were calculated based on the method outlined in Section 3.6 using the measured and estimated radiocarbon dates presented in Table 6.1 and discussed in Section 6.2. The calculated linear sedimentation rates are presented in Table 6.3 and Figures 6.6-6.16, and are discussed for the Late Weichselian and Holocene in the following section.

6.6.2 Late Weichselian linear sedimentation rates (LSRs)

6.6.2.1 Late Weichselian 15,250-22,600 yrsBP

Linear sedimentation rates are only calculated for the period between 15,250 and 22,600 yr BP in the cores from the continental slope (Table 6.4; Figs 6.6, 6.7, 6.9, 6.12). In general, the linear sedimentation rates decrease downslope from 30.2 cm kyr^{-1} in PS2629 (upper continental slope) to 17.2 cm kyr^{-1} in PS2628 (mid continental slope) to 15.8 cm kyr^{-1} in PS2627 (lower continental slope). These sedimentation rates are applied to the undated lower sections in PS2629, PS2628 and PS2627, based on the assumption that the rates remain constant (Table 6.3). The sedimentation rate in PS2629 decreases to 9.0 cm kyr^{-1} between 15,250-16,960 yr BP. The sedimentation rates calculated in PS2627 and PS2628 must be considered as averages for their respective periods as they were determined from radiocarbon datings corresponding with sandy mud/massive mud facies enriched in dropstones, between which, reworked facies (resedimented sandy mud diamicton and massive sand) are present (Figs 6.1, 6.6-6.11; Chapter 4). Therefore, the sedimentation rates should in fact be lower as resedimentation would act to inflate the rate of sediment flux. No sedimentation rate was determined pre- dating 19,700 yr BP in PS2627 as the lowermost date of 25,800 yr BP is unreliable as it corresponds to a resedimented diamicton (Chapter 4; Section 6.2.3), and the sedimentary record in this section of the core consists of facies deposited through resedimentation processes.

6.6.2.2 Late Weichselian 10,000-15,250 yr BP

On the mid continental shelf the sedimentation rate reaches a value of at least 60 cm kyr^{-1} associated with a sandy to sandy mud diamicton facies (Table 6.3; Figs 6.8, 6.12). This sedimentation rate should be regarded as a minimum because, i) surface sediment (sandy diamicton facies) have been intensively winnowed of the fine grained component by the East Greenland Current (Section 4.7.2.3) probably reducing the original sediment unit thickness, and ii) the sediment surface is estimated to date as recent as 10,000 yr BP, but a range of ages back to the radiocarbon dated point of 13,010 yr BP are possible (Sections 6.2.3, 6.2.5). However, no rate is calculated pre- dating 13010 yr BP as this correlates to a resedimented sandy mud diamicton facies (Chapter 4; Section 6.2.3).

In PS2629 (upper continental slope), the sedimentation rate between the estimated ages of 10,000 and 15,250 yr BP (Section 6.2.3) is 3.8 cm kyr^{-1}, and is associated with a sandy mud facies with dropstones (Table 6.3; Figs 6.9, 6.12). In PS2628 and PS2627 rates reach 2.3 cm kyr^{-1} and 4.2 cm kyr^{-1}, respectively, between 10,000 and 13,020 yr BP (Table 6.3; Figs 6.6, 6.7, 6.12). Sedimentation rates pre-

dating 13,020 yr BP reach values of 51 cm kyr^{-1} in PS2628, and 79 cm kyr^{-1} in PS2627 (Table 6.3; Figs 6.6, 6.7, 6.12). These rates correspond for the most part to a sandy mud couplet facies (Figs 6.1, 6.6, 6.7, 6.12) deposited by turbidity currents (Chapter 4) and, therefore, should be considered averages for this section of the core.

6.6.3 Holocene linear sedimentation rates (LSRs) 0-10,000 yr BP

Holocene (Stage I) LSRs have been calculated from throughout the Kejser Franz Josephs Fjord-shelf-slope transect (Table 6.3; Figs 6.6-6.12). No Holocene sediments were deposited in PS2630 from the mid continental shelf. The high temporal resolution of PS2631 and PS2641 from the outer fjord and inner continental shelf, respectively, yields detailed linear sedimentation rates (Table 6.3; Figs 6.6-6.8, 6.12). The sedimentation rates calculated for these cores vary from 44 cm kyr^{-1} to 111 cm kyr^{-1}, and are associated with a bioturbated mud facies (Figs 6.10, 6.11). An estimated sedimentation rate is determined for the early Holocene (9,540-10,000 yr BP) in PS2641 (inner continental shelf). The assumptions outlined in Section 6.2.5 dictate that the rate is a minimum value. It follows that a minimum rate of 120 cm kyr^{-1} can be considered likely to have occurred during this period, and is associated with a laminated mud facies (Fig 6.11). On the continental slope, sedimentation rates attain very low values that decrease from 3.5 cm kyr^{-1} in PS2629 (upper slope), to 2.3 cm kyr^{-1} in PS2628 and 2.3 cm kyr^{-1} in PS2627 further down the slope. All rates are associated with bioturbated mud facies.

Core	Depth (cmbsf)	Interpolated and reservoir corrected radiocarbon age (yrs BP)	Linear Sedimentation Rate (cm kyr^{-1})	Bulk accumulation rate (g cm^{-2} kyr^{-1})			Terrigenous fraction (>500µm) accum. rate (g cm^{-2} kyr^{-1})			Coarse (> 63µm) fraction accumulation rate (g cm^{-2} kyr^{-1})			Fine (< 63µm) fraction accumulation rate (g cm^{-2} kyr^{-1})		
				Min	Max	Av	Min	Max	Av	Min	Max	Av	Min	Max	Av
PS2627	0	0													
	20	8750 +/- 100	2.3	1.9	2.3	2.1	0.02	0.02	0.02	0.2	0.2	0.2	1.7	1.7	1.7
	38	13020 +/- 120	4.2	5.2	5.2	5.2	0.02	0.02	0.02	0.9	0.9	0.9	4.24	4.2	4.2
	220	15330 +/- 120	79.2	68.2	98.4	76.3	0.0	0.0	0.0	0.0	9.1	2.8	72.8	90.7	81.5
	270	18490 +/- 230	15.8	↓	↓	↓	↓	↓	↓	↓	↓	↓	↓	↓	↓
	290	*19753*		15.8	23.4	17.9	0.1	3.1	0.9	0.3	9.5	3.3	9.8	17.1	14.8
	*330	*25800 +/- 380			Not Calc			Not Calc			Not Calc			Not Calc	
PS2628	0	0													
	30	13020 +/- 120	2.3	2.4	3.2	2.8	0.01	0.1	0.03	0.3	0.4	0.3	2.7	2.8	2.8
	150	15360 +/- 160	51.3	41.2	54.6	47.3	0.0	0.0	0.0	0.2	0.6	0.3	42.3	54.2	47.7
	210	18840 +/- 190	17.2	↓	↓	↓	↓	↓	↓	↓	↓	↓	↓	↓	↓
	235	*20870*		15.7	24.3	18.3	0.1	1.4	0.7	1.4	3.4	2.7	7.6	20.9	15.2
PS2629	0	0													
	35	*10000*	3.5	2.2	2.8	2.6		No data			No data			No data	
	55	*15250*	3.8	3.4	4.4	3.9	0.1	0.1	0.1	0.0	0.3	0.3	3.2	3.2	3.2
	70 (30)	16960 +/- 160	9.0	12.9	13.6	13.3	0.9	0.9	0.9	0.0	4.6	4.6	8.3	8.3	8.3
	130 (90)	18950 +/- 210	30.2	↓	↓	↓	↓	↓	↓	↓	↓	↓	↓	↓	↓
	240	*22598*		28.9	64.6	49.5	0.0	7.5	4.2	0.0	29.3	18.5	24.8	36.3	31.2
PS2630	0	*10000*													
	180	13010 +/- 130	59.8	72.0	130.5	93.7	0.1	32.4	9.6	6.4	81.9	34.7	30.1	69.4	58.9
PS2641	0	0													
	125	*1145*	108.7	71.5	103.8	89.1	0.0	0.0	0.0	1.8	2.6	2.2	69.7	94.7	82.2
	375	6430 +/- 130	48.8	42.6	51.0	47.2	0.0	0.0	0.0	1.1	2.1	1.6	44.4	46.6	45.5
	413	7050 +/- 70	61.3	57.5	63.2	60.2	0.0	0.0	0.0	1.4	1.4	1.4	56.0	56.0	56.0
	535	8150 +/- 75	110.9	103.9	117.6	112.7	0.0	0.0	0.0	1.2	1.2	1.2	114.9	114.9	114.9
	554	8580 +/- 80	44.2	45.4	46.4	45.9	0.1	0.1	0.1	1.3	1.3	1.3	45.0	45.0	45.0
	565	8730 +/- 80	73.3	72.9	73.0	73.0		No data			No data			No data	
	585	9010 +/- 120	71.4	↓	↓	↓		No data			No data			No data	
	623	*9540*		68.8	88.5	75.4	0.1	0.9	0.4	0.3	4.8	2.4	33.9	72.7	69.5
	685	*10000*	120.0	104.7	182.8	134.1	0.2	8.9	3.0	0.4	37.1	12.5	104.7	136.5	123.0
PS2631	0	0													
	100	1145 +/- 55	87.3	58.3	69.4	63.9	0.1	0.1	0.1	0.6	0.8	0.8	57.5	57.5	57.5
	390	7440 +/- 210	46.1	32.4	44.9	40.0	0.0	0.0	0.0	0.6	1.5	0.9	31.9	42.7	37.1

Table 6.3. Linear sedimentation and mass accumulation rates calculated for cores recovered along the Kejser Franz Josephs fjord- shelf - slope. Mass accumulation rates include i) Bulk - BARs, ii) Terrigenous fraction - TARs (>500 µm), iii) Coarse fraction - CARs (>63µm), and iv) Fine fraction - FARs (<63µm). The rates listed are minimum, maximum, and average values calculated for the period between the corresponding and previous radiocarbon ages. Numbers in ***italics*** are: i) estimated/correlated ages discussed in the text, and ii) age of undated lower section of each core determined from the linear timescale (Figure 6.2). ‡ In PS2629, and based on correlation of the oxygen isotope and IRD records between the gravity and box cores, it is determined that the topmost 40 cm are missing from the gravity core and depths are corrected by 40 cm. Numbers in brackets are uncorrected gravity core depths, and the adjacent number is the corrected depth. * No sedimentation rate is calculated between 18,490-25,800 yr BP in PS2627 as the latter AMS date was determined on a debris flow unit; at best the rate calculated between 15,330 and 18,490 yr BP is extended to a core depth of 290 cm (i.e. 19753 yr BP) immediately overlying the resedimented section of the core (turbidites and debris flow deposit; Fig 6.1).

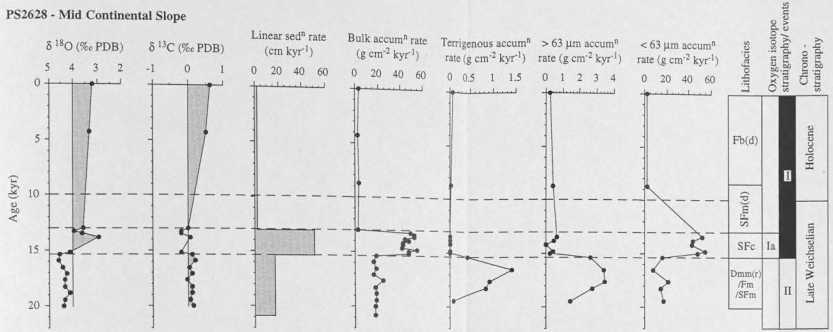

Figure 6.6. Time (kyr) variant mass accumulation rates (g cm^{-2} kyr^{-1}) and stable oxygen and carbon isotope stratigraphy of PS2628 from the mid continental slope. Oxygen isotopic and chronostratigraphical scales are indicated where Termination Ia is shortened to Ia. The lithostratigraphy of PS2628 is shown, and the lithofacies code is provided in Table 4.1. Fm(b-d) is shortened to Fm, SFm(b-d) to SFm, and SFc(m-l) to SFc.

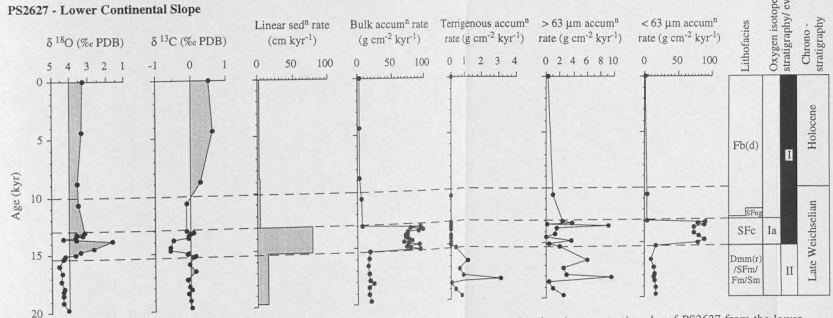

Figure 6.7. Time (kyr) variant mass accumulation rates (g cm^{-2} kyr^{-1}) and stable oxygen and carbon isotope stratigraphy of PS2627 from the lower continental slope. Oxygen isotopic and chronostratigraphical scales are indicated where Termination Ia is shortened to Ia. The lithostratigraphy of PS2627 is shown, and the lithofacies code is provided in Table 4.1. SFc(m-l) is shortened to SFc, SFm(b-d) to SFm, and Fm(b-d-sl) to Fm.

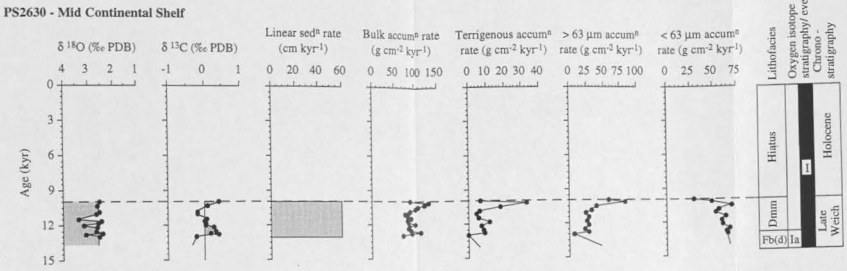

Figure 6.8. Time (kyr) variant mass accumulation rates (g cm^{-2} kyr^{-1}) and stable oxygen and carbon isotope stratigraphy of PS2630 from the mid continental shelf. A hiatus is present in PS2630 between 0 and 10,000 yr BP. Oxygen isotopic and chronostratigraphical scales are indicated where Termination Ia is shortened to Ia, and the Late Weichselian to Late Weich. Rates must be considered minima. The time scale should be used with caution (refer to text for details). The lithostratigraphy of PS2630 is shown, and the lithofacies code is provided in Table 4.1.

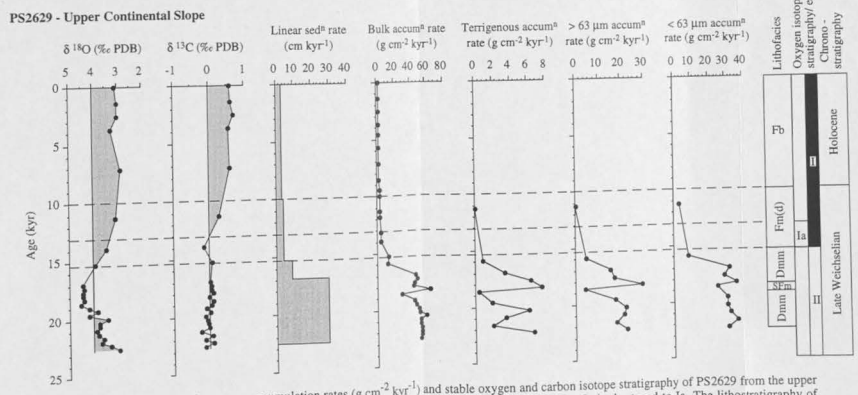

Figure 6.9. Time (kyr) variant mass accumulation rates (g cm^{-2} kyr^{-1}) and stable oxygen and carbon isotope stratigraphy of PS2629 from the upper continental slope. Oxygen isotopic and chronostratigraphical scales are indicated where Termination Ia is shortened to Ia. The lithostratigraphy of PS2629 is shown, and the lithofacies code is provided in Table 4.1.

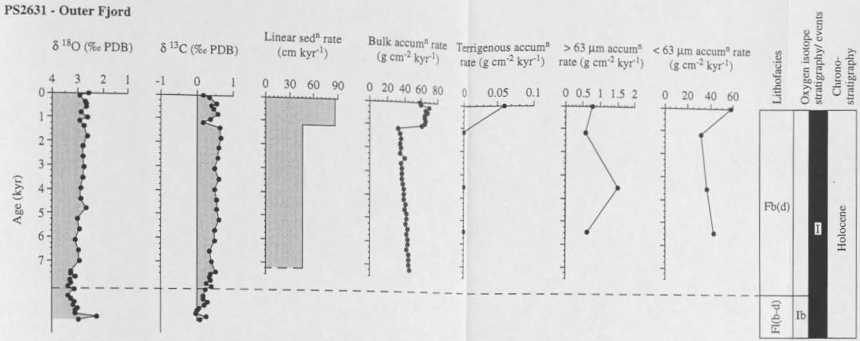

Figure 6.10. Time (kyr) variant mass accumulation rates (g cm^{-2} kyr^{-1}) and stable oxygen and carbon isotope stratigraphy of PS2631 from the outer region of Kejser Franz Josephs Fjord. Oxygen isotopic and chronostratigraphical scales are indicated where Termination Ib is shortened to Ib. The timescale is not extended below 7,440 yr BP due to poor chronological constraints. The lithostratigraphy of PS2631 is shown, and the lithofacies code is provided in Table 4.1.

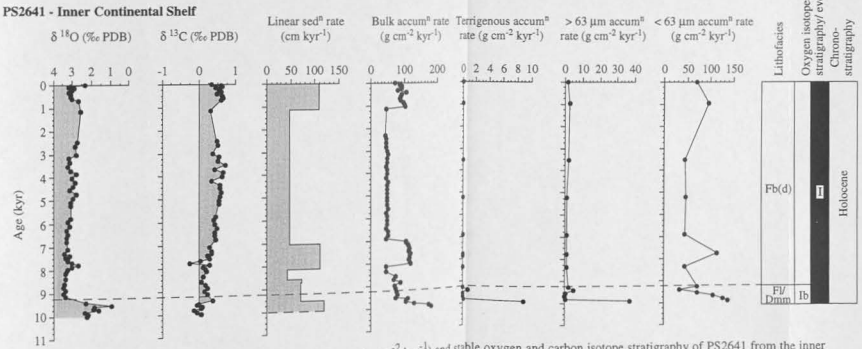

Figure 6.11. Time (kyr) variant mass accumulation rates (g cm^{-2} kyr^{-1}) and stable oxygen and carbon isotope stratigraphy of PS2641 from the inner continental shelf. Oxygen isotopic and chronostratigraphical scales are indicated where Termination Ib is shortened to Ib. The lithostratigraphy of PS2641 is shown, and the lithofacies code is provided in Table 4.1.

6.7 MASS ACCUMULATION RATES (MARs)

6.7.1 Introduction

Mass accumulation rates (MARs; g cm^{-2} kyr^{-1}) are calculated in this study. They differ to linear sedimentation rates in that the effects of water content and porosity are removed, providing a gauge on the flux of sediment grains alone. As with linear sedimentation rates, mass accumulation rates are calculated in order to determine and contrast the flux of bulk sediments and individual components supplied to the fjord, continental shelf and continental slope in response to changes in the sedimentary environment associated with the Late Weichselian and Holocene. Therefore, a number of mass accumulation rates were calculated with the specific aim of gauging these changes and include: i) bulk sediment accumulation rates (BARs), ii) terrigenous component (>500 µm) accumulation rates (TARs), iii) coarse fraction (>63 µm) accumulation rates (CARs), and iv) fine fraction (<63 µm) accumulation rates (FARs). The individual MARs are plotted as absolute (maximum and minimum) values in Figures 6.6-6.11 and 6.13-6.15 where these and the averages for particular time periods are tabulated in Table 6.3.

6.7.2 Derivation of mass accumulation rates

Mass accumulation rates were calculated based on the method outlined in Section 3.6. The MARs reflect the linear sedimentation rates (Section 6.5; Table 6.3) and, therefore, are only as accurate as those calculated using the radiocarbon and estimated ages (Table 6.1; Section 6.2). In general, MARs were determined for each sample taken from the cores. However, the calculation of terrigenous, coarse and fine fraction accumulation rates was based on a limited data set as grain size distribution (%) was only determined on a small number of samples related to the uniformity of the sedimentary facies (Chapter 4).

The MARs calculated for intercalated sedimentary facies e.g. sandy mud couplet facies of PS2627 and PS2628, and laminated mud facies of PS2641 and PS2631 (Chapter 4) must be considered as averages for the range of laminations and intercalations. Not enough material was available for determination of the grain size distribution and water content for each laminae necessary for calculation of the MARs. Therefore, composite samples were taken and the resulting MARs averaged to take account of the sampling enforced variations.

6.7.3 Late Weichselian mass accumulation rates (MARs)

6.7.3.1 Late Weichselian 15,250-22,600 yr BP

Mass accumulation rates (MAR) are only calculated for the period between 15,250 and 22,600 yr BP in the cores from the continental slope (PS2629, PS2628, and PS2627). The range of MARs calculated are presented in Table 6.3, and Figures 6.6, 6.7, 6.9 and 6.13-6.16. In general, averaged MARs decrease down the continental slope from maximum values in PS2629 to minimum values in PS2627; where BARs (av) decrease from 49.5 to 17.9 g cm^{-2} kyr^{-1}, TARs (av) from 4.2 to 0.7 g cm^{-2} kyr^{-1}, CARs (av) from 18.5 to 2.7 g cm^{-2} kyr^{-1}, and FARs (av) from 31.2 to 8.3 g cm^{2} kyr^{-1}. However, the lowest

averaged MARs are calculated for the period 15,250-16,960 yr BP in PS2629. The MARs calculated for PS2628 and PS2627 should be lower as the sedimentation rates on which they are based have been inflated above their true values by resedimentation events (Section 6.6.2.1).

In PS2629, minimum absolute MARs (BAR of 28.9 g cm^{-2} kyr^{-1}, TAR of 0 g cm^{-2} kyr^{-1}, CAR of 0 g cm^{-2} kyr^{-1}, and FAR of 24.8 g cm^{-2} kyr^{-1}) are attained at 18,950 yr BP, and are associated with a sandy mud facies (Fig 6.9; Chapter 4). Maximum absolute rates occur at 18,290 yr BP (BAR of 64.6 g cm^{-2} kyr^{-1}, TAR of 7.5 g cm^{-2} kyr^{-1}, CAR of 29.3 g cm^{-2} kyr^{-1}, and FAR of 36.3 g cm^{-2} kyr^{-1}), and are associated with a sandy mud diamicton facies (Fig 6.9; Chapter 4). A prominant but slightly lower peak is recorded at 20,610 yr BP (Figs 6.9, 6.13-6.16). An additional abrupt decrease in absolute values occurs for TARs (2.0 g cm^{-2} kyr^{-1}), and less so CARs (17.7 g cm^{2} kyr^{-1}) with a corresponding increase in FARs (36.3 g cm^{-2} kyr^{-1}) at 21,935 yr BP (Figs 6.9, 6.13-6.16). Both peaks at 20,610 and 21,935 yr BP correspond to a sandy mud diamicton facies (Fig 6.9; Chapter 4).

In both PS2627 and PS2628, the BARs and FARs (Table 6.3 for average rates) remain relatively constant throughout the period, and are associated with a range of facies from sandy mud/ massive mud enriched in dropstones, sand and resedimented sandy mud diamicton facies. However, maximum values in TARs (up to 1.4 g cm^{-2} kyr^{-1}) and CARs (up to 3.4 g cm^{-2} kyr^{-1}) of PS2628 are restricted to the period post-dating 18,200 yr BP, and are associated with both sandy mud and resedimented sandy mud diamicton facies (Figs 6.6, 6.14, 6.16). Similarly, in PS2627, a prominent peak in TARs (1.5 g cm^{-2} kyr^{-1}) and CARs (6.0 g cm^{-2} kyr^{-1}) occurs at 15,810 yr BP, and is associated with a sandy mud facies (Figs 6.7, 6.14, 6.16). In PS2627, the maximum absolute MAR (Table 6.3) occurs at 18,110 yr BP and corresponds to a resedimented sandy mud diamicton facies (Fig 6.7; Chapter 4). The MARs corresponding to the reworked facies are in reality only minima based on the average linear sedimentation rates used, and would have probably been higher if detailed radiocarbon datings bracketed the facies.

6.7.3.2 Late Weichselian 10,000-15,250 yr BP

In PS2630, the MARs calculated for the period post- dating 13,010 yr BP can only be considered minimums as: i) the surface sediment (sandy diamicton facies) has been intensively winnowed of the fine grained component by the East Greenland Current (Section 4.7.2.3) probably reducing the original sediment unit thickness, resulting in the calculation of lower sedimentation rates, and ii) the sediment surface is estimated to date as recent as 10,000 yr BP, but a range of ages back to the radiocarbon dated point of 13,010 yr BP are possible (Sections 6.2.3, 6.2.5). Absolute BARs attain minimum values of 72.0-130.5 g cm^{-2} kyr^{-1}, TARs of 0.1-32.4 g cm^{-2} kyr^{-1}, CARs of 6.4-81.9 g cm^{-2} kyr^{-1}, and FARs of 30.1-69.4 g cm^{-2} kyr^{-1}, and are associated with a sandy mud diamicton facies (Figs 6.8, 6.13-6.16). The maximum absolute MARs are calculated in the uppermost 20 cm of the sediment column associated with a sandy diamicton facies (Fig 6.8). Minimum MARs occur at 13,010 yr BP associated with a bioturbated mud facies (Fig 6.8).

In PS2629 average MARs between the estimated ages of 10,000 yr BP and 15,250 yr BP (Section 6.2.3) show little variation (Figs 6.9, 6.13-6.16). BARs attain average values of 3.9 g cm^{-2} kyr^{-1}, TARs of 0.1 g cm^{-2} kyr^{-1}, CARs of 0.3 g cm^{-2} kyr^{-1}, and FARs of 3.2 g cm^{-2} kyr^{-1}. The MARs correspond with a

sandy mud facies with dropstones (Fig 6.9). In PS2628 and PS2627 average MARs reveal very little fluctuation between 10,000 and 13,020 yr BP (Figs 6.6-6.7, 6.13-6.16). Average BARs are <5.2 g cm^{-2} kyr^{-1}, TARs <0.03 g cm^{-2} kyr^{-1}, CARs <0.9 g cm^{-2} kyr^{-1}, and FARs <4.2 g cm^{-2} kyr^{-1}, although the average ratescalculated for PS2628 are based on pre- and post- Late Weichselian-Holocene boundary radiocarbon dates.

The MARs pre- dating 13,020 yr BP reach average values of 47.3 and 76.3 g cm^{-2} kyr^{-1} for BARs, 0.3 and 2.8 g cm^{-2} kyr^{-1} for CARs, 47.7 and 81.5 g cm^{-2} kyr^{-1} for FARs are attained in PS2628 and PS2627, respectively. The TARs are zero in both cores (Figs 6.6-6.7, 6.13-6.16). The MARs correspond for the most part to sandy mud couplet facies in both cores (Fig 6.6, 6.7). The absolute values reveal high frequency fluctuations that probably reflect the composite sampling of coarse/fine grained units composing the sandy mud couplet facies (Figs 6.6, 6.7; Section 6.7.2). Therefore, average MARs are calculated to obtain a general value for the MARs.

6.7.4 Holocene mass accumulation rates 10,000-0 yr BP

Mass accumulation rates are calculated for most cores along the sample transect but no Holocene material is preserved in PS2630 on the mid shelf (Table 6.3, Figs 6.6-6.16). The numerous dated stratigraphic points provide detailed absolute records for BARs of 1.9-117.6 g cm^{-2} kyr^{-1}, TARs <0.9 g cm^{-2} kyr^{-1}, CARs < 4.8 g cm^{-2} kyr^{-1}, and FARs of 1.7-114.9 g cm^{-2} kyr^{-1}. The MARs correspond to bioturbated mud facies (Figs 6.6-6.11). The high chronological resolution of PS2631 and PS2641 provide detailed records where maximum MARs occur between 0-1,145 yr BP in both PS2641 and PS2631, and 7,050-8,150 yr BP and pre-dating 8,580 yr BP in PS2641. All are associated with a bioturbated mud facies (Fig 6.11). Between 7,440 and 1,145 yr BP a gradual decrease is observed in the absolute BARs (44.9 to 32.4 g cm^{-2} kyr^{-1}) and FARs (42.7 to 31.9 g cm^{-2} kyr^{-1}). MARs were estimated for the early Holocene (9,540-10,000 yr BP) in PS2641 (inner shelf). However, the assumptions made in Section 6.2.5 dictate that these rates are minimum values. In more detail, the MARs attain minimum values >104.7 g cm^{-2} kyr^{-1} for BARs, >0.2 g cm^{-2} kyr^{-1} for TARs, and >0.4 and >104.7 g cm^{2} kyr^{-1} for CARs and FARs, respectively, (Figs 6.11, 6.13-6.16). The rates correspond to a laminated mud facies (Fig 6.11).

Average MARs show that values are highest in PS2631 and PS2641 from the outer fjord and on the inner shelf, respectively, where the BARs vary between 40-112.7 g cm^{-2} kyr^{-1}, CARs from 0.8-2.4 g cm^{-2} kyr^{-1}, and FARs from 37.1-114.9 g cm^{-2} kyr^{-1}. The MARs of the slope decrease to values <2.8 g cm^{-2} kyr^{-1} for BARs, <0.1 g cm^{-2} kyr^{-1} for TARs, <0.3 g cm^{-2} kyr^{-1} for CARs, and <3.2 g cm^{-2} kyr^{-1} for FARs. No discernable difference is observed in the TARs along the profile.

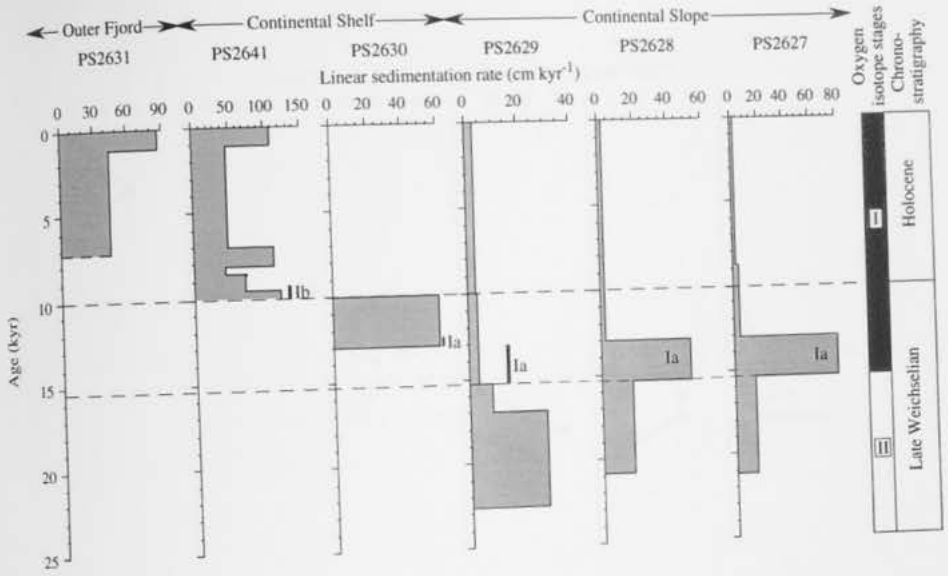

Figure 6.12. Linear sedimentation rates (cm kyr^{-1}) calculated for specific periods in the last 25 kyr for cores along the Kejser Franz Josephs Fjord (PS2631) continental shelf (PS2641 and PS2630) continental slope (PS2629, PS2628, and PS2627) transect parallel to approximately 73° N. Termination Ia and Ib are shortened to Ia and Ib, respectively, in the oxygen isotope and chronostratigraphical scales. Note the linear sedimentation rates axis (x-axis) are not to the same scales.

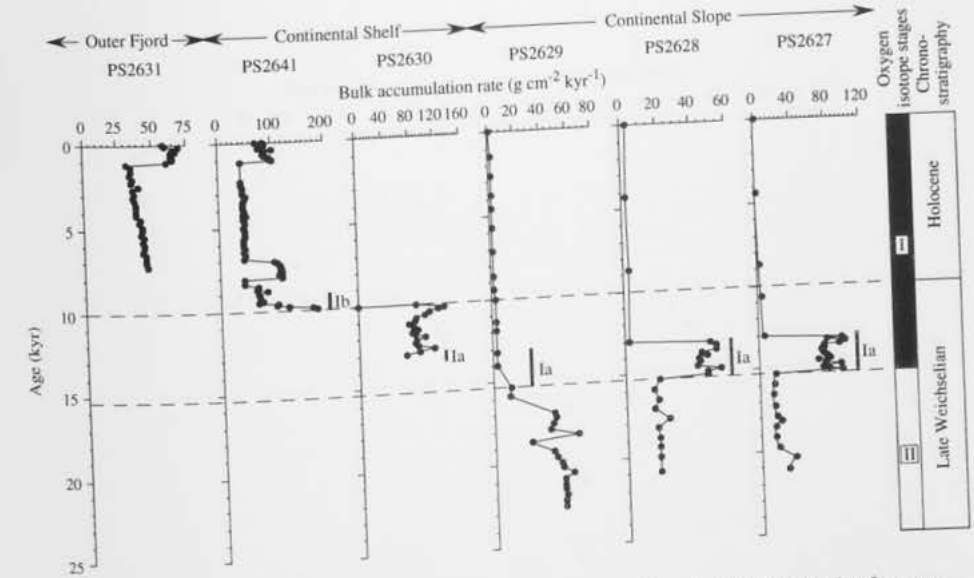

Figure 6.13. Bulk accumulation rates (g cm^{-2} kyr^{-1}) calculated for specific periods in the last 25 kyr for cores along the Kejser Franz Josephs Fjord (PS2631) continental shelf (PS2641 and PS2630) continental slope (PS2629, PS2628, and PS2627) transect parallel to approximately 73° N. Termination Ia and Ib are shortened to Ia and Ib, respectively, in the oxygen isotope and chronostratigraphical scales. Note the bulk accumulation rates axis (x-axis) are not to the same scales.

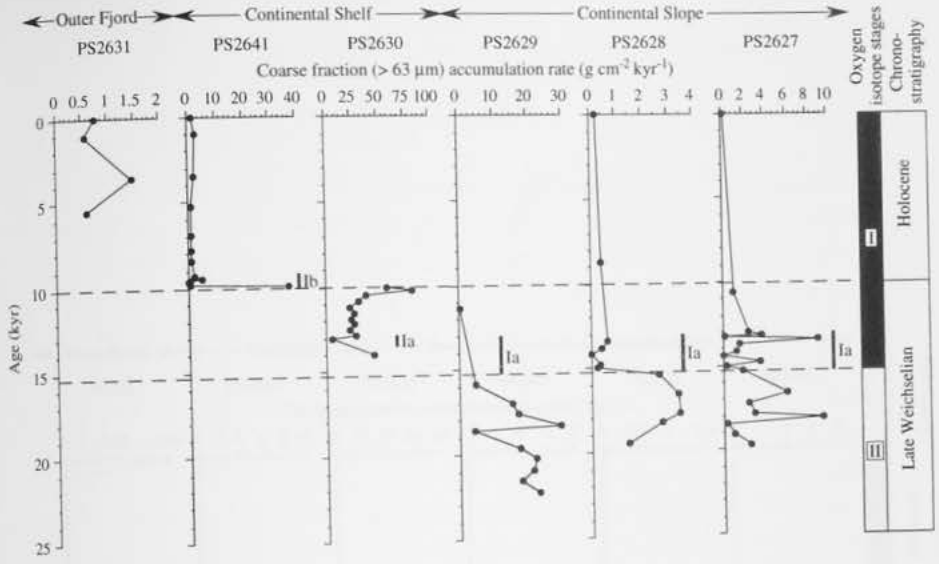

Figure 6.14. Coarse fraction (>63 µm) accumulation rates (g cm^{-2} kyr^{-1}) calculated for specific periods in the last 25 kyr for cores along the Kejser Franz Josephs Fjord (PS2631) continental shelf (PS2641 and PS2630) continental slope (PS2629, PS2628, and PS2627) transect parallel to approximately 73° N. Termination Ia and Ib are shortened to Ia and Ib, respectively, in the oxygen isotope and chronostratigraphical scales. Note the coarse accumulation rate axis (x-axis) are not to the same scales.

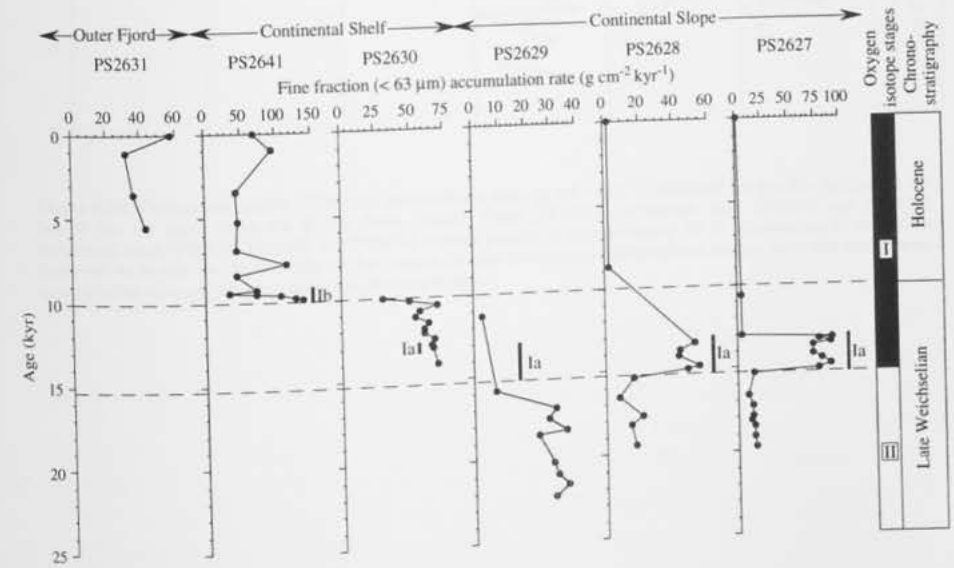

Figure 6.15. Fine fraction (>63 µm) accumulation rates (g cm^{-2} kyr^{-1}) calculated for specific periods in the last 25 kyr for cores along the Kejser Franz Josephs Fjord (PS2631) continental shelf (PS2641 and PS2630) continental slope (PS2629, PS2628, and PS2627) transect parallel to approximately 73° N. Termination Ia and Ib are shortened to Ia and Ib, respectively, in the oxygen isotope and chronostratigraphical scales. Note the coarse accumulation rate axis (x-axis) are not to the same scales.

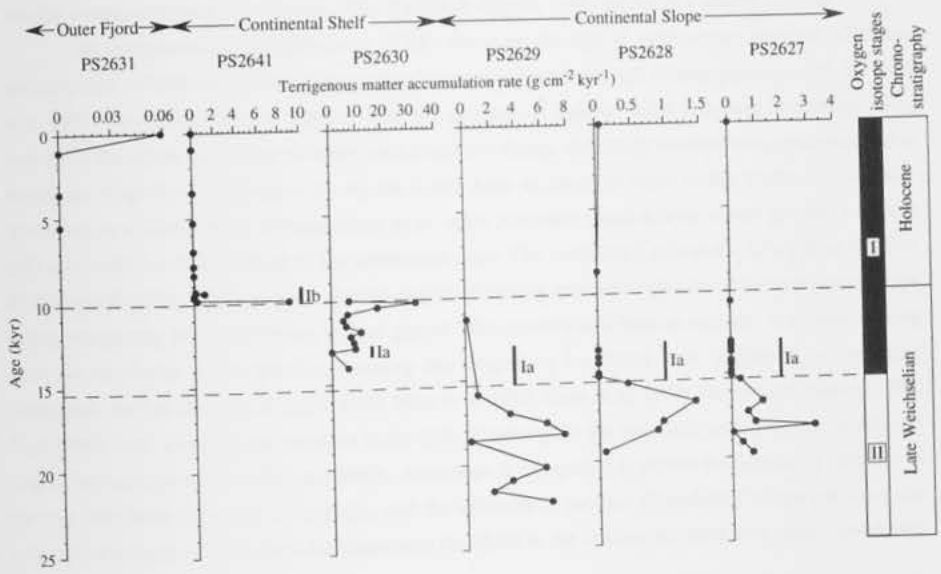

Figure 6.16. Terrigenous matter (>500 µm) accumulation rates (g cm^{-2} kyr^{-1}) calculated for specific periods in the last 25 kyr for cores along the Kejser Franz Josephs Fjord (PS2631) continental shelf (PS2641 and PS2630) continental slope (PS2629, PS2628, and PS2627) transect parallel to approximately 73° N. Termination Ia and Ib are shortened to Ia and Ib, respectively, in the oxygen isotope and chronostratigraphical scales. Note the terrigenous accumulation rates axis (x-axis) are not to the same scales.

6.8 PALAEOENVIRONMENTAL IMPLICATIONS OF LINEAR SEDIMENTATION AND MASS ACCUMULATION RATES

6.8.1 Late Weichselian 15,250-22,600 yr BP

During the last glacial of the Late Weichselian the LSRs and MARs reveal increased values on the ice distal setting of the continental slope (PS2629, PS2628, and PS2627). The enhanced LSRs and MARs reflect the focusing of sedimentation on the continental margin, and the increased supply of sediment through invigorated glacier linked processes, both in response to the expansion of glacier ice onto the continental shelf (e.g. Funder 1989; Funder & Hansen 1996) during this glacial interval.

The terrigenous accumulation rate (TAR) document the flux of sedimentary material >500 µm, and represents an index of terrestrial derived sediment transported through iceberg processes (cf. Elverhoi et al. 1995; Nam 1996). This is supported by the presence of iceberg rafted sediment in corresponding sections of the cores, consisting of sandy mud diamicton facies, and sandy mud/massive mud enriched in dropstones (Figs 6.6-6.9; Chapter 4). As the CARs have an identical trend to the TARs they are also interpreted to reflect iceberg sedimentation as no other processes could deliver coarse grained sediment (>63 µm) to the ice-distal setting of the continental slope. The increased TARs and CARs within PS2629, PS2628 and PS2627 clearly indicate that the supply of iceberg sediment to the ice-distal continental slope setting was greatly increased during the last glacial. This would result from an increase in iceberg calving from the expanded outlet glaciers draining the Greenland Ice Sheet ,that impinged on the inner continental shelf at this time (Funder 1989; Nam et al. 1995; Stein et al. 1996; Funder and Hansen 1996; Nam 1996), with a subsequent increase in the drift of icebergs to the ice-distal setting of the continental slope. The decrease in the LSRs and MARs downslope is interpreted to reflect the increasing distance of the core sites from the source of icebergs, and the influence of the East Greenland Current confining the majority of icebergs calved from the Greenland Ice Sheet to the continental shelf and upper continental slope.

The CARs, TARs and FARs calculated from the upper continental slope (PS2629) probably do not reflect their true rates, as sedimentological evidence discussed in Section 4.7.2.2 suggest that bottom current winnowing of the fine grained component of the sandy mud diamicton may have occurred. The enhanced FARs of the last glacial, corresponding with sandy mud and massive mud facies (Figs 6.6, 6.7; Sections 4.7.3, 4.7.8.1), are interpreted to reflect the increased supply of fine-grained sediment through more invigorated glacial meltwater outflow activity, extended sea-ice and pelagic debris (Sections 4.7.3, 4.7.8.1). Furthermore, as iceberg sediment comprise a mixture of fine and coarse grain sizes (Drewry 1986; Dowdeswell et al. 1994), the enhanced FARs also indicate the increased supply of fine-grained sediment through iceberg activity. An enhancement of the BARs, CARs, and TARs associated with a sandy mud diamicton facies occurs at 18,290 and 20,610 yr BP on the upper continental slope (PS2629), and reflects either a greater supply of iceberg sediment, or the winnowing of the finer grained component through current activity associated with the East Greenland Current system (Section 4.7.2.2).

Maximum MARs post dating 18,200 yr BP occur lower down the continental slope (PS2628 and PS2627). An abrupt decrease in the BARs, CARs, and TARs occurs at 18,950 yr BP on the upper

continental slope (PS2629) associated with a sandy mud facies (Fig 6.9), and reflects the decreased supply of iceberg rafted sediment. A corresponding increase in the FARs indicate the dominance of fine grained sedimentation interpreted to be derived mainly from meltwater outflow activity, sea-ice and pelagic settling (Section 4.7.3).

6.8.2 Late Weichselian 10,000-15,250 yr BP

On the mid (PS2628) to lower (PS2627) continental slope, respectively, the LSRs, BARs and FARs pre- dating 13,020 yr BP are very high. This corresponding section of the cores are dominated by a sequence of sandy mud couplets and normally graded sandy mud deposited through turbidity currents, and representative of a high energy environment (Figs 6.6, 6.7; Section 4.7.6). The high FARs reflect the fine grained nature of sediments deposited by the turbidity currents. The rates are higher on the lower continental slope (PS2627) than on the mid continental slope (PS2628), probably reflecting that the turbidity currents are centred over the core site of PS2627, and that the core site of PS2628 is marginal to the currents. The zero TARs and CARs reflect the absence of iceberg rafted sediment and hence, absence of icebergs over the core site, during this period. The MARs and LSRs are much lower on the upper continental slope (PS2629) during this time, reflecting a low supply of sediment during the first period of deglaciation (Section 6.5.2) and the associated decay of the Greenland Ice Sheet.

At 13,010 yr BP on the mid continental shelf (PS2630), the TARs, CARs, and BARs are reduced and the FARs enhanced. These rates correspond to a bioturbated mud facies, and interpreted to reflect the suppression of iceberg sedimentation and an increase in glacier-derived meltwater outflow and sea ice sediments, and pelagic debris (Fig 6.8; Section 4.7.8.2). A meltwater supply of sediment is thought likely, as deglaciation is interpreted to occur at this time, based on stable isotope records (cf. Sections 6.3.5.1, 6.4.3). In contrast, the period post-dating 13,010 yr BP in PS2630, is dominated by very high MARs and LSRs associated with sandy to sandy mud diamicton facies (Fig 6.8). These rates reflect the significant supply of glacial-derived sediment in response to continued deglaciation. The increased TARs and CARs associated with the diamicton, indicate that a major proportion of the sediment is delivered through icebergs (Sections 4.7.2.2, 4.7.2.3) calved from the decaying Greenland Ice Sheet during this period of deglaciation. Furthermore, the correspondingly high FARs indicate that ice rafting and meltwater outflows deliver a significant amount of fine grained sediment (Section 4.7.2.2) associated with this period of deglaciation. The higher TARs and CARs and lower FARs at the very top of PS2630, corresponding to a sandy diamicton facies (Fig 6.8), are thought likely to be a product of the erosive East Greenland Current which has winnowed a significant proportion of the fine-grained sediment component of the original sediment facies.

Increased LSRs, but of a much lower magnitude, are observed in PS2629 between 10,000-15,250 yr BP associated with a sandy mud facies. MARs and LSRs are low between 10,000-13,020 yr BP in PS2628 and PS2627, although no MARs were calculated in PS2628. An abrupt decrease in LSRs and MARs in the continental slope cores PS2629, PS2628 and PS2627 in comparison to the high values in the continental shelf core PS2630 can be explained by (i) the more proximal position of PS2630 to the

retreating Greenland Ice Sheet and the supply of glacial sediment, and (ii) the East Greenland Current confining icebergs and meltwater outflows predominantly to the continental shelf.

6.8.3 Holocene (0-10,000 yr BP)

The MARs and LSRs remain relatively high between 9,540-10,000 yr BP in PS2641. The TARs, CARs, and FARs are particularly high, associated with laminated mud and sandy mud diamicton facies (Fig 6.11). The rates reflect sedimentation from glacier-derived meltwater outflow and icebergs in response to the continued retreat of the Greenland Ice Sheet into the fjord system during deglaciation following the Younger Dryas Stadial (Sections 6.3.5.1, 6.4.3).

The LSRs and MARs of the continental slope cores (PS2629, PS2628 and PS2627) decrease abruptly to low values during the Holocene. In contrast, the LSRs, BARs, and FARs associated with the bioturbated mud facies (Figs 6.10, 6.11) of the outer fjord core PS2631, and inner continental shelf core PS2641 are very high. The high rates reflect the proximity of the cores to the Greenland continent, and the supply of large volumes of fine grained (<63 µm) terrestrial-derived sediment from glacial and snow melt-fed meltwaters and fluvial systems, draining the land surrounding the fjord and Fosters Bugt (Fig 1.1; Section 4.7.8.2). This seems to have been intensified over the last 1,200 years as MARs and LSRs reach their Holocene maximum during this period. Additionally, the fine grained sediment in PS2641 are derived partly from the redeposition of sediments resuspended from the sea-floor of other regions of the continental shelf, and transported to the inner continental shelf basin, by the East Greenland Current (Section 4.7.8.2). The resuspended sediments transported by the East Greenland Current, and those derived from meltwater and fluvial systems become ponded within the inner continental shelf basin (Section 5.3.3), and allowed to settle relatively unhindered from further current activity.

The very low LSRs and MARs of the slope reflect the markedly reduced supply of terrestrial derived sediment during the Holocene. The low rates mark the return to more quiescent, marine-dominated sedimentation in response to the ice-distal setting of the continental slope and the low energy glacier driven processes of the Holocene. This is reflected in the corresponding bioturbated mud facies (Figs 6.6, 6.7), which is derived mainly from pelagic sedimentation, and partly from the distal remnants of meltwater systems (Section 4.7.8.2). The very low TARs and CARs indicate that iceberg sedimentation is almost absent related to the very low drift of icebergs in response to the ice-distal setting of the continental slope and reduced glacier-driven processes of the Holocene. In contrast, the TARs and CARs are higher in PS2631 and PS2641 reflecting the larger supply of iceberg sediments. This supply occurs in response to the more proximal setting of the outer Kejser Franz Josephs Fjord and inner continental shelf to the outlet glaciers of the Greenland Ice Sheet that actively calve icebergs. The LSRs and MARs of PS2631 and PS2641 intensify over the last 1,200 years showing that processes of sedimentation discussed in this section for the fjord and inner continental shelf are most active during this period.

6.9 SUMMARY

This chapter has presented a chronostratigraphy for the cores of the Kejser Franz Josephs fjord-continental shelf-continental slope transect of the study area. The timescale is composed of an AMS radiocarbon chronology and an oxygen isotope stratigraphy. The chronology was used to calculate linear sedimentation and mass accumulation rates. The chapter can be summarised as follows:

- The absolute chronology dates from the Late Weichselian glaciation through the ensuing deglaciation and into the Holocene. The oxygen isotope stratigraphy agrees with the absolute chronology and extends from the last glacial of Stage II, through the ensuing Termination I, representative of deglaciation, and into the current interglacial of Stage I.
- Deglaciation - Termination I, is recognised by a rapid depletion of $\delta^{18}O$ to light values and $\delta^{13}C$ minima. Termination I is two staged consisting of Termination Ia and Ib. Termination Ia is documented on the continental slope and shelf. The onset of Late Weichselian deglaciation, Termination Ia, began after 15,250 yr BP, and culminated before 13,020 yr BP (PS2627, PS2628 and PS2629). In PS2630 the event is dated at 13,010 yr BP, and probably extends into the post-13,010 yr BP period, although this cannot be chronologically constrained. Termination Ib is only documented on the inner continental shelf (PS2641) and outer fjord (PS2631), and pre- dates 9,540 yr BP in PS2641 and pre- dates 7,440 yr BP in PS2631 (Termination Ib post dates 10,000 yr BP in both cores). A meltwater signal at 7,790 yr BP in PS2641 may correlate to Termination Ib.
- The stable isotope records have several palaeoenvironmental implications:
  - *Stage II (Last Glacial)* - increased ice volume through the maximum extension of high latitude ice sheets in response to colder atmospheric temperatues, and an extended sea ice cover (possibly at least some seasonally ice free conditions) restricting the ventilation of ocean surface waters and exchange of CO_2 between ocean and atmosphere. A reduction in the bioproductivity of ocean surface waters and the continental biosphere (in response to an extended sea ice cover, reduced atmospheric temperatures and expanded continent ice sheets) may have occurred, contributing to the $\delta^{13}C$ minima. Major meltwater signal pre- dating 18,950 yr BP is documented in PS2629.
  - *Termination I (deglaciation)* - massive influx of low-saline, ^{16}O enriched meltwater through: i) local and regional events associated mainly with the disintegration and retreat of glacier-ice of the Greenland Ice Sheet and possibly the Barents Sea Ice Sheet, with associated melting of icebergs, and possibly ii) influx of low-saline Arctic water masses via the East Greenland Current derived from the Russian Arctic region. $\delta^{13}C$ minima produced from either meltwater capping or stratification of fjord/ocean surface waters, resulting in reduced ventilation of fjord/ocean waters and the associated exchange of CO_2 between ocean and atmosphere, and/or the $\delta^{13}C$ composition of meltwaters.
  - *Stage I (present interglacial)* - Stage I record pre- dating 10,000 yr BP is incomplete but the isotopic record of PS2629 shows that the pre- 10,000 yr BP period is one of gradual transition to Holocene $\delta^{18}O$ and $\delta^{13}C$ values. Younger Dryas Stadial is recorded in PS2627 at 10,500 yr BP by a shift in the isotopic records to heavy $\delta^{18}O$ and light $\delta^{13}C$ values, indicating renewed cold conditions, and reduced CO_2 exchange between the ocean and atmosphere caused by an extended sea-ice cover.

Lightest $\delta^{18}O$ values and $\delta^{13}C$ maxima, closest to modern-day values, occur during the Holocene following 10,000 yr BP. $\delta^{18}O$ records indicate a return to interglacial conditions and reduced ice volume where the Greenland Ice Sheet stabilises at its present day extent. $\delta^{13}C$ maxima indicate a return to a reduced and more seasonal sea ice cover, which allows increased ventilation of fjord/ocean surface waters and the associated exchange of CO_2 between ocean and atmosphere. An increase in the continental and fjord/ocean surface water bioproductivity may have occurred, contributing to the $\delta^{13}C$ maxima. $\delta^{18}O$ and $\delta^{13}C$ records become progressively heavier towards the continental slope, reflecting (i) a decreasing influence of melt/river waters with progressive distance from their source within the fjord, and (ii) possible increase in bioproductivity. Occasional localised meltwater influx from the Greenland hinterland is most intense at 1,145 yr BP.

- Linear sedimentation and mass accumulation rates show distinct patterns in response to the transition from the Last Glacial of the Late Weichselian through to the Holocene.

  - *Late Weichselian (Last Glacial)* is characterised by increased LSRs and MARs reflecting an enhanced supply of terrestrial sediment through invigorated glacier related processes. The enhanced TARs and CARs indicate that the supply of coarser sediments through icebergs is a significant process on the slope reflecting an enhanced rate of calving and drifting. On the upper continental slope iceberg sedimentation remains constant throughout the glacial period but decreases abruptly at ca. 18,950 yr BP with a corresponding increase in the FARs reflecting the dominance of melwater and pelagic sedimentation. The TARs and CARs fluctuate more further down the slope, reaching maximum values following 18,200 yr BP. This reflects the more sporadic and a lower supply of icebergs.

  - *Late Weichselian deglaciation* is characterised by variable LSRs and MARs. On the continental slope the rates decrease, reflecting the reduced supply of glacial sediments in response to the retreat of the Greenland Ice Sheet and the confinement of icebergs to the continental shelf and upper slope by the East Greenland Current. Pelagic sedimentation is subsequently re-established. However, the MARs and LSRs are very high before 13,020 yr BP on the mid to lower continental slope, reflecting resedimentation processes. On the continental shelf between 10,000-13,010 yr BP the MARs and LSRs are high and TARs and CARs reflect a significant supply of coarse sediments through iceberg processes in response to continued decay of the Greenland Ice Sheet.

- - *Holocene* is characterised by greatly reduced LSRs and MARs on the continental slope reflecting the return of marine-dominated sedimentation in response to the ice-distal setting and low energy glacier related processes of the present interglacial. No Holocene material is recovered on the mid continental shelf, reflecting the winnowing associated with the East Greenland Current. The LSRs and MARs, (except the TARs and CARs), are very high on the inner continental shelf and outer fjord reflecting the proximity of the Greenland continent and the supply of fine grained sediments mainly through melt and river water systems. BARs and LSRs are high on the inner continental shelf in response to the presence of a basin that prevents winnowing of sea-floor sediments by the East Greenland Current. TARs and CARs are very low, indicating very low iceberg supply (highest in the fjord but decreases across the continental margin).

CHAPTER 7

THE LATE WEICHSELIAN AND HOLOCENE IN KEJSER FRANZ JOSEPHS FJORD, AND ON THE ADJACENT EAST GREENLAND CONTINENTAL MARGIN

7.1 INTRODUCTION

This chapter discusses the Late Weichselian and Holocene environmental history of the Kejser Franz Josephs Fjord and adjacent East Greenland continental margin. The discussion will be based on the data and interpretations of Chapters 4, 5 and 6.

Chapter 4 presented the lithofacies and sedimentological data (water content, porosity, particles >2mm/cm and grain size distribution) of the cores recovered from the study area, with a subsequent interpretation of their associated sedimentary processes of deposition. Chapter 5 presented the sedimentation patterns and processes of the study area using both the acoustic and sedimentary records, and discussed the implications for the distribution of iceberg scouring of the sea-floor. Chapter 6 presented: (i) the chronology of the sediments of the study area using radiocarbon datings and oxygen isotope stratigraphy of cored sediments, (ii) the oxygen and carbon records of cored sediments with a subsequent discussion of the environmental implications of these records, and (iii) the flux of sediment to the fjord, continental shelf and continental slope study during the Late Weichselian and Holocene with the associated environmental implications discussed.

This chapter will bring the various data and interpretations of Chapter 4, 5 and 6 together, and discuss the environmental history of Kejser Franz Josephs Fjord and East Greenland continental margin during the Late Weichselian and Holocene.

7.2 LATE WEICHSELIAN GLACIATION

7.2.1 Onset of glaciation

The onset of glaciation during the Late Weichselian is not evident within the sedimentary and acoustic records from the study area . Therefore, the timing, nature and mechanism for the expansion and advance of glacier-ice of the Greenland Ice Sheet to Late Weichselian glacial maximum conditions and the corresponding sedimentation patterns and processes, and environmental change across the East Greenland continental margin can not be ascertained based on the sediments of the

study area. In the absence of evidence from this study the onset of glaciation is assumed to be synchronous to that outlined in other work. However, the onset of glaciation is poorly constrained in this work but the data available suggests that the onset of glaciation and the associated advance of glacier-ice of the Greenland Ice Sheet began at ca. 25-28,000 yr BP, and reached the inner continental shelf by the peak glaciation of the Last Glacial Maximum at ca. 16-21,000 yr BP (Nam 1996; Stein et al. 1996; Funder & Hansen 1996).

7.2.2 Late Weichselian glaciation ice extent and records from Kejser Franz Josephs Fjord and the adjacent East Greenland continental shelf

The sedimentary and acoustic records of this study offer no evidence on the sedimentation patterns and processes and environmental history for the Kejser Franz Josephs Fjord and adjacent East Greenland continental shelf during the Late Weichselian glaciation (Chapters 4, 5, 6). The absence of a Late Weichselian glaciation sedimentary record from the fjord is not surprising as the fjords of East Greenland were full of glacier-ice at this time (e.g. Hjort 1979, 1981; Funder 1989; Dowdeswell et al. 1994b; Funder & Hansen 1996) preventing glacimarine sedimentation. Sediments deposited within the fjord before the advance of glacier-ice of the Greenland Ice Sheet onto the inner continental shelf are assumed to have been removed by grounded glacier-ice similar to that interpreted for the Scoresby Sund fjord system (e.g. Dowdeswell et al. 1994b). Deposition within the fjord under full glacial conditions would probably have been in the form of subglacial till but this type of facies is not identified from the sedimentary or acoustic records in this study (Chapters 4, 5).

Glacier-ice of the Greenland Ice Sheet is proposed to have advanced approximately onto the inner continental shelf in this region of East Greenland during peak glaciation associated with the Late Weichselian glacial maximum (Funder 1989; Funder & Hansen 1996). However, no direct evidence of this glacier-ice advance in the form of terminal moraines or subglacial till is present in the sedimentary and acoustic records of the fjord and continental shelf of this study (Chapters 4, 5), or from acoustic records of lower resolution air-gun reflection profiles performed in Fosters Bugt and on the inner continental shelf (Jokat unpub. data; Jokat et al. 1995; Hubberten et al. 1995). Therefore, the position of the shelfward extent of the glacier-ice margin during the Late Weichselian glacial maximum can not be ascertained let alone constrained to an exact location based on the sedimentary and acoustic records of this study.

The sedimentary and acoustic records of this study offer no evidence for the sedimentation patterns and processes, and environmental history on the continental shelf in what would have been proximal to distal settings with respect to the advancing and proposed peak glaciation glacier-ice margin during the Late Weichselian. No work has been performed on the air-gun reflection acoustic sections collected from the inner continental shelf and Fosters Bugt (Jokat unpub. data; Jokat et al. 1995) in order to provide possible evidence for the sedimentation and environmental history of the inner continental shelf with respect to the advancing and proposed peak glaciation glacier-ice margin during the Late Weichselian.

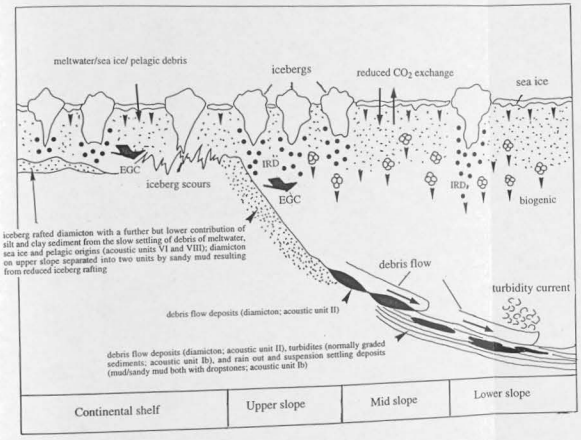

Figure 7.1. Sedimentation and environmental model for the East Greenland continental margin adjacent to Kejser Franz Josephs Fjord during the Late Weichselian glaciation. EGC is short for East Greenland Current, and IRD for iceberg rafted debris.

- Greenland Ice Sheet impinges on the inner continental shelf (after Funder & Hansen 1996).
- $\delta^{13}C$ minima reflect extended sea ice cover (generally considered to experience at least some seasonally ice free conditions in East and Northeast Greenland e.g. Hebbeln et al. 1994; Nam et al. 1995; Nam 1996) that reduced CO_2 exchange between the atmosphere and ocean surface water.

  Reduced continental and surface water bioproductivity (in response to colder atmospheric temperatures and extended sea ice cover) may have also contributed to the $\delta^{13}C$ minima, although marine organic carbon and carbonate content have not been determined in support of this interpretation.
- Sedimentation and accumulation rates are high on the ice-distal continental slope due to the focusing of sedimentation on the continental margin associated with the expansion of the Greenland Ice Sheet, and the subsequent invigoration of glacimarine processes delivering sediment to the slope. Average rates are the highest on the upper continental slope and decrease downslope. This indicates that: i) sedimentation is most active on the upper continental slope, controlled primarily by icebergs, and ii) resedimentation events active downslope are not significant enough to inflate average sedimentation rates.
- Upper continental slope is dominated by rapid rain out and suspension settling sedimentation (up to *c.*30 cm kyr^{-1}) in which contribution from icebergs dominate, with additional fine-grained sediment are probably supplied through ice rafting, remnant meltwater outflows and resuspended sea-floor sediments. This scenario may also apply to the continental shelf, although acoustic evidence is inconclusive. The East Greenland Current may have modified the deposits on both the continental shelf and slope.

  Resedimentation on some areas of the upper continental slope (intermittent and occurring from localised regions of the slope) probably followed due to the rapid build-up of unstable sediment piles that subsequently generated the debris flow and turbidity current activity further downslope, although this activity may also have been generated through resedimentation events lower down on the continental slope.
- Mid to lower continental slope is characterised by intermitent, restricted and local/regional large and small-scale debris flow and turbidity current activity concomitant with rain out and suspension settling sedimentation (derived from ice-rafting, remnant meltwater outflows, biogenic activity and resuspended sea-floor sediment). Average sedimentation rates are typically up to *c.* 17 cm kyr^{-1}.
- The lithofacies distribution indicate that a significant number of icebergs influenced the upper continental slope, and that greatly reduced numbers influenced the mid to lower continental slope. This is probably in response to the activity of the southward flowing East Greenland Current confining the majority of icebergs to the continental shelf and upper continental slope.

7.2.3 Evidence for the Late Weichselian glaciation (isotopic stage II) on the East Greenland continental slope of the study area

The sedimentation patterns and processes, and environmental history associated with the Late Weichselian glaciation can be discerned for the continental slope based on the sedimentary and acoustic records from this study. The continental slope is considered an ice-distal setting with respect to the proposed glacier-ice margin on the inner continental shelf during peak glaciation of the Late Weichselian (cf. Fig 2.7; e.g. Funder 1989; Funder & Hansen 1996).

The Late Weichselian glaciation is documented within the lower sections of the continental slope cores PS2629 (below a core depth of 59 cm), PS2628 (below a core depth of 150 cm) and PS2627 (below a core depth of 220 cm) by: (i) the coarser grained nature of lithofacies (Chapter 4; Figs 4.1, 4.5-4.9, 6.1), (ii) increased amounts of particles >2 mm/cm and grain size distribution >500 µm and in some cases >63 µm, interpreted to reflect iceberg rafted debris (IRD) within lithofacies not influenced by resedimentation. Although the particles in resedimented lithofacies would have originally been derived by iceberg rafting (Chapter 4; Figs 4.1, 4.5-4.9, 6.1), (iii) resedimentation-related lithofacies (Chapters 4, 5; Fig 4.1), (iv) high sedimentation and accumulation rates (Sections 6.5, 6.6, 6.7), and (v) heavy $d^{18}O$ and light $d^{13}C$ values within isotopic records (Sections 6.3, 6.4).

The chronology based on radiocarbon dates and oxygen isotope stratigraphy from the corresponding sections of cores PS2629, PS2628 and PS2627 indicate the timing of the Late Weichselian glaciation or isotopic stage II (Sections 6.2, 6.3). The timing is consistent with the Late Weichselian glaciation in studies from other regions of the Polar North Atlantic (e.g. Elverhøi et al. 1995; Nam et al. 1995; Andersen et al. 1995; Nam 1996; Stein et al. 1996).

Sedimentation during the Late Weichselian glaciation (isotopic stage II) is made up of: (i) sandy mud diamicton back to an estimated age of 22,600 yr BP separated into two units by sandy mud with dropstones radiocarbon dated at 18,950 yr BP in PS2629 (Section 4.3; Figs 4.1, 6.1), (ii) the closely associated and interbedded resedimented sandy mud diamicton, massive mud and sandy mud with dropstones, massive sand in PS2627 and PS2628 back to estimated ages of 19,736 and 20,870 yr BP, respectively, and (iii) normally graded gravel-sand-mud and resedimented sandy mud diamicton in PS2627 deposited before 19,736 yr BP (Sections 4.3; Figs 4.1, 6.1).

Acoustic units II, VI and some stratified layers of acoustic unit Ib corresponding to these lithofacies, and in general, other uncored and related acoustic units representing resedimentation events close to the sediment surface on the continental slope also indicate sedimentation during the Late Weichselian glaciation (Section 5.9.2.2). The acoustic units corresponding to mass wasting sedimentation events (debris flows and turbidity currents) are interpreted to have been emplaced during the Late Weichselian glaciation for several reasons: (i) the acoustic units are distributed close to the sediment surface i.e. sea-floor, (ii) mass wasting deposits within cores are dated to occur during the Late Weichselian glaciation, and (iii) close association of acoustic units with dated sedimentary units deposited during the Late Weichselian glaciation, and (iv) the invigorated processes needed to transport sediments to the continental slope in order to generate downslope mass wasting would occur during the Late Weichselian glaciation. The features within the sedimentary and acoustic record are

interpreted to reflect an increase in glacial activity associated with the expansion of ice masses during the Late Weichselian glaciation, and the increased transportation of sediment and coarser grain sizes to the continental slope.

7.2.4 Sedimentation patterns and processes during the Late Weichselian glaciation on the East Greenland continental slope of the study area

7.2.4.1 Upper continental slope

During the Late Weichselian glaciation sedimentation is focused on the East Greenland continental margin in response to the advance of glacier ice to the inner continental shelf. However, as the ice masses terminated on the inner continental shelf the increased flux of sediment delivered to the continental slope were through glacimarine processes (icebergs, meltwater outflow, sea-ice) as opposed to direct glacier ice activity.

The upper continental slope during the Late Weichselian glaciation between 15,250 to 22,500 yr BP is characterised sandy mud diamicton predominantly composed of high amounts of iceberg rafted debris (sediment fraction >500 µm) (Section 4.7.2.2). This indicates that a significant number of debris-rich icebergs influenced the upper continental slope produced from extended glacier-ice that impinged on the inner continental shelf of East and Northeast Greenland. This resulted in the sedimentation of the sandy mud diamicton composed of high amounts of iceberg rafted debris (sediment fraction >500 µm) (Section 4.7.2.2). Acoustic unit VI shows that the diamicton is distributed across the upper continental slope (Sections 5.5.2, 5.7.7, 5.9.2.2) reflecting the full extent of iceberg sedimentation. However, this record cannot be extended to the period pre-dating 22,500 yr BP as the acoustic records from the upper continental slope are inconclusive and incomplete due to poor acoustic penetration and return associated with the gradient of the continental slope and coarse sediment composition. Sedimentation was generally controlled by the quasi-instantaneous dumping of sediment during iceberg overturn, and the continual melt/rain-out of debris during iceberg melting. Icebergs supply heterogeneous glacier-derived sediment and is the only mechanism by which sediment >63 µm could be delivered to the ice-distal setting of the continental slope, and fine grained sediment <63 µm could also be delivered during this process. Sea-ice rafting is thought unlikely as a source of coarse sediment (>63 µm) as modern day studies show that the sediment is predominantly fine grained in relation to the entrainment mechanisms of freezing of turbid sea water and aeolian action (<63 µm; Pfirman et al. 1989, 1990; Wollenburg 1991; Nürnberg et al. 1994). The same studies show that sea ice do supply a limited quantity of coarse grained sediment (>63 µm).

It is difficult, if not impossible, to sedimentologically differentiate between the fine grained sediments supplied by icebergs from those of sea ice and meltwater outflows (cf. Chapter 2). Therefore, additional fine grained sediment is probably derived through the slow suspension settling of sediment carried in surface turbid meltwater plumes, or that introduced to the water column from the dispersed remnants of meltwater outflows reaching the continental slope after discharging from the extended glacier-ice margin on the inner continental shelf of East and Northeast Greenland. This

is expected as present day and Holocene sedimentation of fine grained sediments on the continental margin of the Barents Sea are supplied through distal remnants of meltwater outflows (e.g. Elverhøi & Solheim 1983). The supply of the fine grained component of the sediment is also derived from sea-ice rafting. Sedimentation from sea ice will only occur on break up when any entrained sediment is released through melting or ice floe fragmentation. Even though the sea level was ca. 120 m below present day values (e.g. Fairbanks 1989; Funder & Hansen 1996) the majority of the East and Northeast Greenland continental margin would have been far too deep for sea-floor sediments to become entrained within sea-ice during formation (Section 4.7.2.2). However, sea-ice entrainment of sediment would have occurred in the very shallow shelf regions. More regions of the continental shelf would have been shallow enough for sea ice entrainment of sea floor sediment than in comparison to the present day as sea-level was much lower. Additional sediment is likely to be rafted in the sea ice that is transported from the Eurasian Arctic Ocean to the East Greenland continental margin (via the Fram Strait) in the Transpolar Drift and East Greenland Current systems following sediment entrainment over the shallower Russian shelf region (cf. Chapter 2; e.g. Pfirman et al. 1989, 1990; Wollenburg 1993; Nürnberg et al. 1994; Hebbeln et al. 1998; Dowdeswell et al. 1998).

The sedimentation of pelagic debris is low as the flux of terrigenous sediment is much greater in comparison, reflected in the low content of foraminifera (<1 grain-%). The supply of pelagic/biogenic debris increases (foraminifera content 25 grain-%) around 18,950 yr BP coinciding with a sudden decrease in iceberg rafted debris (sediment >63µm) and the deposition of sandy mud (with dropstones) facies (Section 4.3.4). The lower supply of terrigenous debris enables the pelagic sedimentation to become more noticable.

The high sand and gravel content (>30%) in the sandy mud diamicton may indicate current winnowing of the finer grained component associated with the East Greenland Current. This is interpreted as similar observations are made for the East Greenland continental margin at 65°N (Mienert et al. 1992). Lowered sea levels of 120 m (cf. Fairbanks 1989; Funder & Hansen 1996) would have enabled lower regions on the continental slope to influenced by the East Greenland Current which in the present-day extends down to around 800 m. The higher amount of iceberg rafted debris within sediments deposited following 18,950 yr BP indicates greater iceberg activity and probably increased calving from parent glacier-ice. This relationship may be associated with peak glaciation and ice extent during the Last Glacial Maximum. During this period a greater volume of icebergs are calved from parent glacier-ice which subsequently drift across the continental slope in association with the maximum extent of glacier-ice in East Greenland. If this is the case then peak glacial conditions associated with the Last Glacial Maximum is dated to occur between 15,250 and 18,950 yr BP in the study area.

It is not clear whether the original diamicton facies deposited on the upper continental slope was influenced by subsequent proximal mass-flows as described for other high latitude continental slopes (e.g. Kuhn & Weber 1993; Laberg & Vorren 1996; Dowdeswell et al. 1996, 1997b). If mass-flows occurred, the glacigenic sandy mud diamicton would have been resedimented within the same region and further down the continental slope. Subsequent preservation of the sedimentary

characteristics of the sandy mud diamicton (Chapter 4, 5) would only occur provided the mass-flows maintained sufficient cohesiveness during down slope transportation (Sections 4.7.2.2, 5.7.7; e.g. Nardin et al. 1979; Pickering et al. 1989; Elverhøi et al. 1997). The presence of debris flow deposits on the mid/upper continental slope transitional area suggests that upper continental slope mass wasting probably occurred.

7.2.4.2 Mid to lower continental slope

Sedimentation on the mid to lower continental slope are derived from a combination of rain out and suspension settling and mass wasting, resulting in an interbedded mixture of massive sandy mud to mud with dropstones facies, graded sand-mud facies and resedimented sandy mud diamicton facies (Chapter 4, 5). Rain out and suspension settling sediments are generally derived through distal remnants of meltwater plumes escaping the ice front of the Greenland Ice Sheet, resuspended sea floor sediments, sea ice rafting and iceberg rafting, although the numbers of icebergs contributing to sedimentation is much smaller than in comparison to those influencing the upper continental slope (Chapters 4, 5; Section 7.2.4.1). A broader and applicable discussion on these processes is provided in Section 7.2.4.1 and the reader is directed to this. Sediment gravity flows include turbidity currents and debris flows that vary from small to large scale. The distribution of sediment gravity flows within core sections and in acoustic records indicate that related-deposits are not widespread indicating that the flows were intermittant, and dated to occur throughout the Late Weichselian glaciation. One notable large scale debris flow is dated to occur before ca.19,736 yr BP. This indicates that the sedimentary environment on the mid to lower continental slope fluctuates between high and low energy where it is characterised by background rain out and suspension settling sedimentation intermittantly punctuated by small to large scale sediment gravity flows.

7.2.5 Iceberg influence on the East Greenland continental slope

The distribution of iceberg rafted debris (>63µm) across the continental slope varies from high on the upper continental slope to much lower on the mid to lower continental slope. This is reflected in facies variations where the higher IRD content coincides with sandy mud diamicton on the upper continental slope, and lower IRD content with sandy mud to mud (with dropstones) facies. This distribution is interpreted to reflect an abrupt decrease in the supply of IRD downslope associated with a corresponding reduction in the number of icebergs that drift over lower continental slope regions. The much reduced supply of icebergs across lower continental slope regions is probably related to the southward flowing East Greenland Current that confined a significant number of icebergs calved from the Greenland Ice Sheet in East and Northeast Greenland to the continental shelf and upper continental slope. Only a small number of icebergs reached across lower continental slope regions. The sandy mud diamicton on the upper continental slope may have underwent some form of downslope cohesive mass wasting (the flow would have to be cohesive if the original

depositional characters are preserved). Therefore, it is possible that the extent of the diamicton across the continental slope may be exaggerated in a downslope direction in comparison to the original extent, which may have been much closer to the very upper continental slope/continental shelf break. If this is the case, the spatial extent to which the significant number of icebergs influencing the upper continental slope is more restricted than what is indicated by the diamicton distrbution, suggesting that the East Greenland Current confined icebergs much closer to the continental shelf than what the distribution leads us to believe. However, this argument would not apply if cohesive mass wasting occurred within, and was confined to, the original glacigenic diamicton zone.

7.2.6 Mass wasting on the East Greenland continental slope of the study area

Based on the low concentration and intermittant presence of debris flow deposits and turbidites in acoustic and sedimentary records of this study and GLORIA side-scan data (Mienert et al. 1993, 1995), resedimentation across the continental slope as awhole is restricted to intermittant or low frequency, small to large scale events that are interpreted to originate from localised slope regions. It is not possible to determine whether the mass wasting events have a local or regional slopewide or downslope extent by examining the dimensions and run out lengths of these flows, as acoustic data in this study is inconclusive with respect to this, but it is envisaged that both situations are likely to occur. Mass wasting is interpreted to be derived from the downslope transport of unstable sediment piles rapidly built up on the upper continental slope by the large flux of iceberg rafted and other glacigenic sediments (Section 7.2.1, 7.2.7).

Large scale debris flows, determined from deposits distributed close to the sediment surface influenced sedimentation on the upper/mid continental slope transitional area with additional small and large scale debris flows further down on the mid to lower continental slope (Chapter 5). The debris flows are interpreted to have been generated in response to mass-flow events further up slope from the location of the debris flow sediments (e.g. Wright & Anderson 1982; Laberg & Vorren 1995, 1996; Dowdeswell et al. 1996, 1997b). Debris flow deposits distributed on the continental slope of other high latitude regions are commonly interpreted to result from debris flows that have been generated from mass-flow events (slides/slumps) on the upper continental slope with subsequent transformation during the downslope transport (e.g. Hampton 1972; Wright & Anderson 1982; Piper et al. 1985; Kuhn & Weber 1993; Laberg & Vorren 1995, 1996; Dowdeswell et al. 1996, 1997b). It is not possible to determine whether or not mass-flow events (slides/slumps) based on acoustic records (Section 5.7.7) occurred on the upper continental slope, ascertain the run-out distances of these debris flows, or even correlate between the debris flow and upper continental slope sediments in support of this interpretation, as the acoustic coverage is limited and characterised by very low penetration/return of the acoustic signal. Regardless of the inconclusive nature of the evidence from the acoustic and sedimentary records (Section 5.7.7), the presence and distribution of debris flow deposits on the upper/mid continental slope transitional area supports the occurrence of mass-flow resedimentation on the upper continental slope. The debris flow deposits further down the continental

slope may not necessarily have resulted from debris flows generated by resedimentation events on the upper continental slope, but could equally have been initiated from lower regions of the continental slope.

Large and small scale turbidity currents occurred intermittantly across the mid to lower lower continental slope. The turbidity current activity across the continental slope, similar to other high latitude regions, are interpreted to have been triggered by mass-flows events further upslope with subsequent transformation during downslope transport (e.g. Hampton 1972; Wright & Anderson 1982; Piper et al. 1985; Dowdeswell et al. 1996, 1997b). It is likely that the transformation to turbidity currents is generated through the increased dilution of the preceding flow body by uptake of ambient sea water, and/or turbulence at the head of a debris flow (e.g. Hampton 1972; Piper et al. 1985; Laberg & Vorren 1995, 1996).

7.2.7 Sediment flux during the Late Weichselian glaciation on the East Greenland continental slope

Sedimentation rates are very rapid on the upper continental slope and vary between 9.0-30.2 cm kyr^{-1} but on the whole are 30.2 cm kyr^{-1}. Accumulation rates reach average values of 49.5 g cm^{-2} kyr^{-1} between 16,960 and 22,500 yr BP decreasing to lower rates of 13.3 g cm^{-2} kyr^{-1} (BAR) following 16,960 yr BP. Sedimentation and accumulation rates are much lower on the mid to lower continental slope (15.8-17.2cm kyr^{-1} and 17.9-18.3 g cm^{-2} kyr^{-1}, respectively). The high sedimentation and accumulation rates across the ice distal setting of the continental slope reflect the focusing of sedimentation on the continental margin, and the increased supply of sediment through invigorated glacier linked processes, both in response to the expansion of glacier ice onto the continental shelf (e.g. Funder 1989; Funder & Hansen 1996) during this glacial interval. The decrease in sedimentation and accumulation rates downslope are probably a product of two things: i) the continental slope becomes increasingly ice distal downslope with a subsequent reduction in the amount of glacier-derived sediments , and ii) the rates are sensitive to the amount of iceberg derived sediment whose content within sediment facies decreases downslope due to the influence of the East Greenland Current (Section 7.2.5). Accumulation rates fluctuate throughout the Late Weichselian glaciation and probably relate to variations in the supply of iceberg rafted debris to the sea floor in response to variation in the number of icebergs drifting across the continental slope.

7.2.8 Sea ice cover and environmental implications during the Late Weichselian glaciation on the East Greenland continental slope

A major incursion of low-saline, ^{16}O enriched meltwater discharged from the melting of ^{16}O enriched glacier ice of the Greenland Ice Sheet, and/or discharged icebergs is thought to have influenced the upper continental slope during the period pre-dating 18,950 yr BP (Chapter 6). The $\delta^{13}C$ minima charcteristic of the Late Weichselian glaciation (Stage II) reflect the greatly suppressed ventilation of ocean surface water and associated reduction in the exchange of CO_2 between the ocean and atmosphere, caused by an extended and more permanent sea ice cover (e.g. Spielhagen &

Erlenkeuser 1994; Stein et al. 1994a,b; Nam et al. 1995; Nam 1996). A reduction in the continent and ocean surface water bioproductivity, in response to decreased atmospheric temperatures and extended sea ice cover, may have also contributed to the $\delta^{13}C$ minima (e.g.Shackleton 1977a; Kroopnick et al. 1977; Labeyrie & Duplessy 1985; Stein et al. 1994a,b; Nam et al. 1995; Nam 1996), although a reduction in surface water bioproductivity can not be confirmed in this study. A reduction in surface water bioproductivity is expected during glacial Stage II, as this is recorded in other studies from the East Greenland continental margin (e.g. Nam et al. 1995; Nam 1996). Although the sea ice cover is extended, it is possible that there were at least some seasonally ice free (open waters) conditions in the study area. Other regions of the East Greenland continental margin (16,000-21,000 yr BP) and in the Fram Strait (between 14,500-19,500 yr BP and pre-22,500 yr BP) experienced some seasonally ice free (open waters) conditions during the Late Weichselian glaciation (Hebbeln et al. 1994; Nam et al. 1995; Nam 1996; Hebbeln & Wefer 1997). The presence of planktonic foraminifers and nannofossils within sea-floor sediments on the continental slope of the study area supports at least some seasonally sea ice free conditions during the last glacial (Sections 4.3.7, 4.7.8).

7.3 LATE WEICHSELIAN DEGLACIATION

7.3.1 Introduction

The proposed model of the retreat of the Greenland Ice Sheet in East Greenland has the ice margin retreating from its maximum Late Weichselian glaciation extent on the inner continental shelf to its stillstand position in the outer region of the Kejser Franz Josephs Fjord by the onset of the Younger Dryas (Hjort 1979; Funder 1989; Funder & Hansen 1996). The exact mechansim of ice loss during this retreat is thought to be through iceberg calving (Funder & Hansen 1996). The nature of the ice retreat is unclear as dated or even undated, ice contact moraines and tills and ice proximal glacimarine sediments have not been recognised across the East Greenland continental margin. Therefore, it is uncertain whether the nature of ice retreat was gradual or punctuated between the culmination of the Late Weichselian glaciation and the onset of the Younger Dryas. Figure 7.2 illustrate the sedimentation processes and patterns and environments within the study area during deglaciation following the Younger Dryas and should be referred to throughout the following section.

7.3.2 Onset of deglaciation, mechanism of ice retreat and meltwater production

The onset of the Late Weichselian deglaciation (first step of deglaciation i.e. Termination Ia) began after 15,250 yr BP. The deglaciation is marked by a distinct depletion of $\delta^{18}O$ exceeding 2.4‰ within ocean surface waters indicative of a major pulse of low saline, ^{16}O enriched meltwater (freshwater) discharged to the western margin of the Greenland Sea. The meltwater pulse culminated

before 13,020 yr BP consistent with other meltwater signals in the Polar North Atlantic (e.g. Jones & Keigwin 1988; Dokken et al. 1996; Hald et al. 1996; Hebbeln et al. 1998). The low-saline, ^{16}O enriched meltwaters are interpreted to result from the early disintegration and retreat of glacier ice of the Greenland Ice Sheet from its inner continental shelf position.

The presence of high amounts of iceberg rafted debris across the continental shelf in sandy mud diamicton facies dated between 10,000-13,010 yr BP, together with what is interpreted to be iceberg rafted diamicton facies pre-dating 13,010 yr BP on acoustic sections (Chapter 5), indicates that mass loss of ice from decaying and retreating glacier-ice of the Greenland Ice Sheet is through iceberg calving. Therefore, the production of meltwater during this period is probably the result of melting of the discharged icebergs. Further meltwater production from the ice sheet itself could occur but cannot be determined based on the evidence in this study.

The meltwater signal may also be contributed through an increased supply of low-saline Arctic waters in the East Greenland Current (e.g. Stein et al. 1994a,b; Nam et al. 1995; Nam 1996). The low-saline Arctic waters are derived from the disintegration of the Eurasian Arctic ice sheets and the large Siberian rivers which discharged large volumes of freshwater (enriched in light $d^{18}O$; cf. Spielhagen & Erlenkeuser 1994) into the Eurasian Basin of the Arctic Ocean during the last deglaciation, following 15,700 yr BP (Stein et al. 1994a,b). The low-saline waters were subsequently transported via the Transpolar Drift System to the Fram Strait and along the East Greenland continental margin in the East Greenland Current (Stein et al. 1994a,b).

Low saline meltwaters produced from the melting of icebergs calved into the Fram Strait from the western margin of the Barents Sea Ice Sheet during the onset of its decay after ca. 15,000 yr BP (Jones & Keigwin 1988), may have also contributed to the meltwater signal of this study, following encorporation and transportation in the East Greenland Current. The earlier timing for the onset of meltwater production from the Greenland Ice Sheet suggests that it began to decay before the Barents Sea Ice Sheet. The onset of deglaciation further south along the East Greenland continental margin is dated between 15,300 - 15,800 yr BP (Nam et al. 1995; Nam 1996; Stein et al. 1996) which, in some cases, is 700 yr older than that documented in this study. Therefore, the Greenland Ice Sheet may have began to decay in different locations at different times.

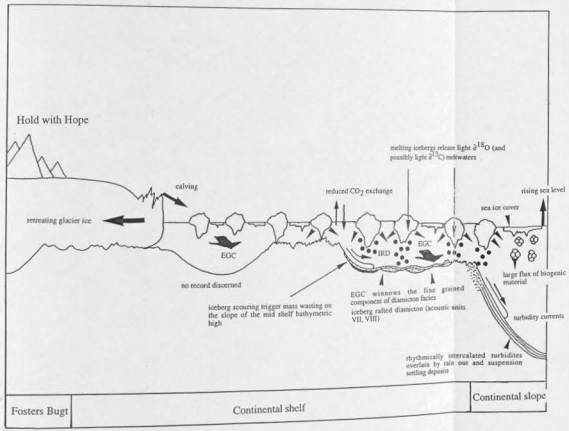

Figure 7.2. Sedimentation and environmental model for the East Greenland continental margin adjacent to Kejser Franz Josephs Fjord during the Late Weichselian deglaciation (Termination Ia) of the continental margin. EGC is short for East Greenland Current, and IRD for iceberg rafted debris.

- Onset of deglaciation began following 15,250 yr BP.
- Presence of iceberg rafted diamicton on the continental shelf indicates that mass loss of ice from the decaying Greenland Ice Sheet was through iceberg calving, although additional meltwater flux cannot be discounted.
- Major influx of low saline, light $\partial^{18}O$ meltwater occurred between 13,010-15,250 yr BP on the continental slope and may have extended to the period post-dating 13,010 yr BP on the continental shelf. Meltwaters are probably derived from either the melting of icebergs derived from the decay of the Greenland Ice Sheet in eastern and northeastern Greenland and possibly the Barents Sea Ice Sheet, and/or influx of a low saline, light $\partial^{18}O$ Arctic water mass sourced from the melting of Eurasian Arctic ice masses in the Russian Arctic region, and transported via the East Greenland Current to the East Greenland continental margin.
- Meltwaters lead to intense stratification of ocean surface waters with a subsequent reduction in the ventilation of ocean waters and associated exchange of CO_2 between the ocean and atmosphere.
- Acoustic evidence suggests that iceberg sedimentation occurs across the mid to outer continental shelf pre-13,010 yr BP. Localised mass wasting occurs close to the mid continental shelf bathymetric high just prior to 13,010 yr BP, triggered from the rapid and unstable build-up of sediment and iceberg scouring of the sea-floor over the bathymetric high. Following 13,010 yr BP the continental shelf is dominated by rain out and suspension settling sedimentation in which a significant contribution from icebergs dominates. The East Greenland Current was probably active modifying sea-floor deposits.
- The sea-floor is actively scoured by icebergs, particularly in the shallowest regions.
- Repetitive turbidity current activity on the mid to lower continental slope between 13,200 and 15,250 yr BP generated through mass wasting on the upper continental slope. Mass wasting probably generated in response to rapid and unstable sediment build-up on the upper continental slope in response to invigorated glacimarine processes associated with deglaciation. Mass wasting terminates at 13,200 yr BP and suspension settling sedimentation dominates, suggesting that sediment accumulation becomes less rapid and much more stable. Contribution from iceberg rafting is minor.

  Upper continental slope dominated by rain out and suspension settling sedimentation with a small but significant contribution by icebergs. The nature of sediments and iceberg contribution may differ further up on the upper continental slope than what is suggested from available geological evidence.
- Lithofacies distribution indicate that i) significant numbers of icebergs influenced the continental shelf, ii) greatly reduced numbers of icebergs in comparison influenced the upper continental slope, although this observation is based on geological evidence from the lower region of the upper slope which may differ markedly further upslope, and iii) virtually no icebergs influenced the mid to lower continental slope. This is probably in response to the southward flowing East Greenland Current that confined the majority of icebergs to the continental shelf.

7.3.3 The initiation and nature of ice retreat during the Late Weichselian deglaciation

The initiation of ice retreat of the Greenland Ice Sheet is related to a small sea level rise of ca. 8-10 m (Fairbanks 1989), which resulted in the sudden increase in icebergs calved from the ice margin. With continued iceberg calving controlled ice mass loss the ice sheet began to decay and retreat fjordwards. However, it is uncertain whether mass loss of ice also occurred through ablation either during the early period of deglaciation or later. The exact nature of the retreat of glacier-ice of the Greenland Ice Sheet during the Late Weichselian deglaciation is uncertain as the geological evidence presented in this study is inconclusive (Chapter 4, 5). Therefore, it remains unclear whether ice retreat in East Greenland was gradual, punctuated by stillstands or was very rapid reaching its Younger Dryas stillstand position sometime before the onset of the Younger Dryas Stadial. The absence of moraines on the inner continental shelf suggests that retreat was gradual and not punctuated by stillstands, but this cannot unequivocally be stated with any certainty.

7.3.4 Sedimentation on the continental shelf and continental slope during the Late Weichselian deglaciation

On the mid to lower continental slope the early period of deglaciation between 15,250-13,020 yr BP coincides with repetitive/episodic turbidity current activity with the deposition of sandy mud couplet facies. Sedimentation and accumulation rates are rapid and typically ca. 51-79 cm kyr^{-1} and 47-76 g cm^{-2} kyr^{-1}. The sandy mud couplet facies is traced up slope to the margin of the upper continental slope indicating that the turbidity currents were generated on the upper continental slope. This suggests that mass wasting on the upper continental slope may have triggered the turbidity currents. The iceberg rafted debris content of the sandy mud couplet facies is virtually absent indicating that little in the way of icebergs drift over the mid to lower continental slope. Sediments from the upper continental slope during this interval are not well constrained in this study due to inconclusive acoustic records and low resolution and restricted core record. Sedimentary records that do exist indicate that this interval is characterised by the deposition of rain out and suspension settling sediments with a low but significant iceberg rafted debris content, indicating that a number of icebergs drift across the upper continental slope. Iceberg rafted diamicton facies pre-dating 13,010 yr BP on acoustic sections are recognised from the mid to outer continental shelf (Chapter 5), indicating that icebergs drifted across the continental shelf in significant numbers in response to the decaying glacier ice of the Greenland Ice Sheet.

Just prior to 13,010 yr BP a mass wasting event was generated from the mid continental shelf bathymetric high (Section 5.3.3), originating from the resedimentation of debris deposited on or close to the slope surface. The diamictic composition indicates the sediment to have been deposited by debris flows having transformed from a slump during downslope transport. The presence of intense scouring of sea floor sediment on the bathymetric high coupled with rapid sedimentation probably initiated slope instability and downslope resedimentation. The diamictic composition of the

mass-flow deposit shows the original sediment to be glacigenic in origin, derived from mainly iceberg rafting before the emplacement of the debris flow (pre-13,010 yr BP).

The mid to outer continental shelf between 10,000-13,010 yr BP is dominated by the drift of a significant number of icebergs resulting in the rapid supply of a large volume of iceberg rafted debris and the depostion of sandy mud diamicton facies (sedimentation and accumulation rates typically ca. 60 cm kyr^{-1} and 94 g cm^{-2} kyr^{-1}). Sedimentation is also contributed from meltwater outflows escaping from the ice margin, and biogenic/pelagic activity, with further modification by the East Greenland Current (Chapters 4, 5). The significant numbers of icebergs are derived in response to the decay of the Greenland Ice Sheet in East Greenland. In contrast sedimentation on the continental slope is dominated by rain out and suspension settling of debris in which iceberg rafted debris form only a small fraction, although the IRD content is greatest across the upper continental slope. The large difference in the IRD content within sediments between the continental shelf and continental slope indicates that the southward flowing East Greenland Current confined the majority of icebergs to the continental shelf where most iceberg sedimentation occurred.

7.3.5 Sea ice, meltwater production and environmental implications during the Late Weichselian deglaciation

The distinct depletion of $\delta^{18}O$ exceeding 2.4‰ is greater than the 1.3‰ attributed to changes in glacial-interglacial ice volume (e.g. Chappell & Shackleton 1986; Labeyrie et al. 1987; Mix 1987; Ruddiman 1987; Jones & Keigwin 1988; Jansen & Veum 1990). As present day surface water temperatures in the region are mostly near freezing point (<-1°C; Hopkins 1991) the depletion of the $\delta^{18}O$ above that for the ice-volume effect is not due to an increase in temperature, but rather a decrease in surface water salinity resulting from increased low-saline, ^{16}O enriched meltwater discharge (Fairbanks et al. 1992; Speilhagen & Erlenkeuser 1994; Stein et al. 1994a,b; Nam 1996). A decrease in salinity exceeding 2.4 ‰ from modern-day values of 34.4 ‰ (Section 1.2), is predicted for surface waters between 15,250-13,020 yr BP across the continental slope based on the correlation factor between salinity and $\delta^{18}O$ in the Greenland Sea (cf. Fairbanks et al. 1992).

Widespread capping or stratification of ocean surface water by the meltwaters probably occurred between 15,250-13,020 yr BP across the continental slope, greatly suppressing the ventilation of ocean waters and the associated exchange of CO_2 with the atmosphere (e.g. Stein et al. 1994a,b; Nam et al. 1995; Nam 1996). Additionally, the $\partial^{13}C$ minima could also reflect the $\partial^{13}C$ composition of the meltwater, in part or as a whole, provided the $\partial^{13}C$ records determined from modern-day glacier-related meltwaters of the Svalbard and Alpine regions are representative analogues for meltwaters in general (cf. Section 6.4.1.2).

Meltwater influence continues across the continental shelf following 13,010 yr BP. The occasional fluctuations in the $\delta^{18}O$ record to slightly heavier values (Fig 6.3, 6.4) may indicate fluctuations in the production and influence of meltwater. The subsequent capping or stratification of ocean surface waters in response to the meltwater discharge also fluctuates and is not well developed, as the moderately heavy $\delta^{13}C$ values indicate some degree of exchange of CO_2 with the atmosphere

(e.g Stein et al. 1994a,b; Nam et al. 1995; Nam 1996). The timing of the culmination of this meltwater signal is not ascertained due to the poor chronological constraints in this section of the record and the unreliability of the associated timescale (Section 6.3.5.1). Meltwater signals from the continental slope are not observed following 13,020 yr BP, indicating that the meltwater pulse culminates before 13,020 yr BP on the continental slope (see above; cf. Section 6.3.5.1; Figs 6.3, 6.4, 6.6, 6.7, 6.9). Therefore, the absence of a meltwater event associated with Termination Ia after 13,020 yr BP on the continental slope, may indicate its increasingly distal location with respect to the Greenland ice sheet, whose ice margin was probably retreating from the peak Late Weichselian glaciation position on the inner continental shelf at this time (cf. Funder 1989; Funder & Hansen 1996). In response, the influence of meltwaters would become increasingly more diminished and confined to ice proximal locations such as the continental shelf, producing the post 13,010 yr BP Termination Ia meltwater signal on the continental shelf.

7.4 YOUNGER DRYAS STADIAL

7.4.1 Ice extent during the Younger Dryas

The sedimentary and acoustic records of this study offers relatively little evidence on the sedimentation patterns and processes and environmental history for the Kejser Franz Josephs Fjord and adjacent East Greenland continental shelf and slope during the Younger Dryas Stadial (Chapters 4, 5, 6). Glacier-ice of the Greenland Ice Sheet is proposed to have retreated to a topographically favourable stillstand position approximately in the outer region of Kejser Franz Josephs Fjord by the onset of the Younger Dryas Stadial (Hjort 1979; Funder 1989; Funder & Hansen 1996). However, no direct evidence of this glacier-ice stillstand position in the form of terminal moraines or subglacial till is present in the sedimentary and acoustic records of the fjord and continental shelf of this study (Chapters 4, 5), or from acoustic records of lower resolution air-gun reflection profiles performed in Fosters Bugt and on the inner continental shelf (Jokat unpub. data; Jokat et al. 1995; Hubberten et al. 1995).

A sediment depocentre is identified within the outer fjord, and based on the transition from laminated to massive cored mud facies and acoustically stratified to massive sediments the sequence represents deglaciation and the gradual transition from ice proximal to ice distal conditions as glacier ice retreats from the outer fjord (cf. Sections 5.9.4.2, 7.5). However, it is uncertain whether the deeper uncored part of the glacimarine sequence represents ice-proximal deposition from glacier-ice at its Younger Dryas stillstand position. Therefore, the position of the the glacier-ice margin during the Younger Dryas Stadial can not be ascertained let alone constrained to an exact location based on the sedimentary and acoustic records of this study.

7.4.2 Sea ice cover and environmental implications during the Younger Dryas

Evidence of the Younger Dryas in the sediment cores of this study are limited relating to the low resolution of the sediment cores of this study, probably due to low sedimentation rates across the corresponding cored interval, and the short duration of the Younger Dryas event (ca. 1,000 yrs). The Younger Dryas is preserved in a limited extent on the lower continental slope. On the lower continental slope at ca. 10,500 yr BP heavy $\delta^{18}O$ and light $\delta^{13}C$ values (Chapter 6; Figs 6.3, 6.4, 6.7) are consistent with the Younger Dryas Stadial (e.g. Duplessy et al. 1981; Kennett 1990; Stein et al. 1994a,b; Nam 1996). The heavy $\delta^{18}O$ values indicate cold conditions, and the $\delta^{13}C$ minima reduced CO_2 exchange between the ocean and atmosphere caused by extended sea-ice (reduced open-water) conditions, both associated with the renewed cooling during the Younger Dryas Stadial (e.g. Stein et al. 1994a,b; Nam 1996).

7.4.3 Sedimentation during the Younger Dryas

On the continental slope sediments across this interval consist of suspension settling mud facies with very minor iceberg rafted debris. The absence of iceberg rafted debris may be a product of the low sedimentation and accumulation rates (23-4.2 cm kyr^{-1}; 3.8 g cm^{-2} kyr^{-1}). The low rates are thought to be in response to the increased distance of the continental slope from the retreated glacier-ice, where sedimentation is now focused much closer to the fjord system. The low IRD content within slope mud facies may reflect the extended sea ice cover occurring during this period. The extended sea ice cover could act to suppress the drift of icebergs through the outer fjord systems of East Greenland following their discharge from glacier-ice (e.g. Marienfeld 1991, 1992a,b; Dowdeswell et al. 1993, 1994a,b), and therefore, reducing the number of icebergs reaching the slope environment. In response suspension settling of sediments derived from distal remnants of sea-ice (only in cases where the sea ice cover can break up), meltwater outflows, pelagic/biogenic debris and resuspended sea floor sediments are more pronounced.

7.5 POST YOUNGER DRYAS STADIAL - EARLY HOLOCENE DEGLACIATION

7.3.1 Introduction

The proposed model of ice retreat of the Greenland Ice Sheet in East Greenland has the ice margin retreating from its stillstand position in the outer region of the Kejser Franz Josephs Fjord following the culmination of the Younger Dryas Stadial (Hjort 1979; Funder 1989; Funder & Hansen 1996). This phase of deglaciation marks the final phase of in the retreat of glacier-ice of the Greenland Ice Sheet to current day positions by around ca. 7-8,000 yr BP (Funder 1989; Funder & Hansen 1996). The exact mechansim of ice loss during this retreat is thought to be through both ablation and iceberg calving driven by increased insolation (COHMAP 1988; Funder & Hansen

1996). No evidence (in the form of terminal moraines or subglacial till is present) exists in the sedimentary and acoustic records of the fjord and continental shelf of this study (Chapters 4, 5), or from acoustic records of lower resolution air-gun reflection profiles performed in Fosters Bugt and on the inner continental shelf (Jokat unpub. data; Jokat et al. 1995; Hubberten et al. 1995) concerning the exact position from which glacier-ice of the Greenland Ice Sheet retreated at the onset of Early Holocene deglaciation. Figures 7.3 and 7.4 illustrate the sedimentation processes and patterns and environments within the study area during deglaciation following the Younger Dryas and should be referred to throughout the following section.

7.3.2 Onset of deglaciation, mechanism of ice retreat and meltwater production

The onset of the post Younger Dryas (Early Holocene) deglaciation (second step of deglaciation i.e. Termination Ib) began soon after 10,000 yr BP. The deglaciation is marked by a distinct depletion of $\delta^{18}O$ within ocean surface waters indicative of a second major pulse of low saline, ^{16}O enriched meltwater (freshwater) discharged to the fjord and inner continental shelf. The meltwater pulse culminated before 9,540 yr BP on the inner continental shelf adjacent to Kejser Franz Josephs Fjord, and sometime before 7,440 yr BP in the outer region of Kejser Franz Josephs Fjord. The fjord transgressive nature of the meltwater culmination age indicates the progressive retreat of the Greenland Ice Sheet through Kejser Franz Josephs Fjord and the subsequent decrease in the influence of meltwaters in ice distal regions. However, the influence of meltwater and its culmination age during continued deglaciation of the remainder of the fjord system is not evident from the sedimentary records of this study. The low-saline, ^{16}O enriched meltwaters are interpreted to result from the last phase in the disintegration and retreat of glacier ice of the Greenland Ice Sheet. This phase is thought to be localised as the meltwater pulse is not documented within records from the continental slope.

The presence of both laminated mud facies and variable quantities of iceberg rafted debris across the inner continental shelf and in the outer region of Kejser Franz Josephs Fjord, indicates that mass loss of ice from decaying and retreating glacier-ice of the Greenland Ice Sheet is through ablation and iceberg calving.

7.3.3 Sedimentation on the continental shelf and continental slope during the Late Weichselian deglaciation

Sedimentation across the mid to outer continental shelf during this interval was prevented by the East Greenland Current which tends to winnow any sediment that may have accumulated on the sea floor or prevents deposition. On the continental slope sedimentation was relatively unaffected by glacier-ice retreat, and comprises rain out and suspension settling. Sedimentation and accumulation rates are typically 2.3-3.5 cm kyr^{-1} and 2.1-2.8 g cm^{-2} kyr^{-1}, respectively.

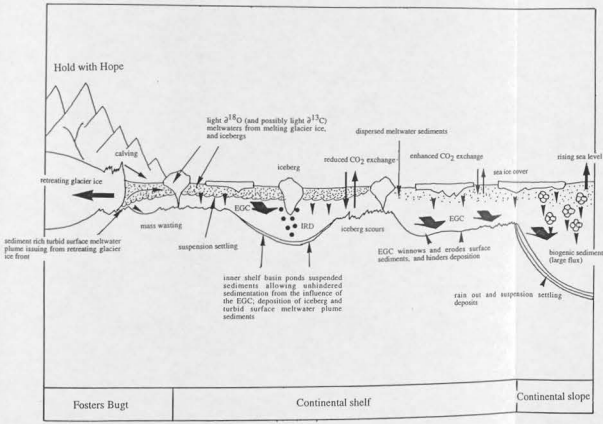

Figure 7.3. Sedimentation and environmental model for the outer Kejser Franz Josephs Fjord, Fosters Bugt and adjacent East Greenland continental margin during Early Holocene deglaciation of the Kejser Franz Josephs Fjord system (Termination Ib). EGC is short for East Greenland Current, and IRD for iceberg rafted debris.

- Deglaciation continued following the culmination of the Younger Dryas cooling event at *c.*10,000 yr BP. Glacier-ice begins to recede into Kejser Franz Josephs fjord from its proposed Younger Dryas extent in the outer fjord-Fosters Bugt region (cf. Funder & Hansen 1996).
- Presence of meltwater and iceberg rafted sediment in the outer fjord and on the continental shelf indicates that the decay of the Greenland Ice Sheet was through ablation (production of meltwater) and iceberg calving.
- Major influx of low saline, light $\partial^{18}O$ meltwater is dated to occur post-10,000 yr BP, and terminating before 9,540 yr BP on the inner continental shelf and before 7,440 yr BP in the outer fjord. Low-saline waters are derived from the discharge of meltwaters and the melting of calved icebergs associated with the decay and recession of glacier-ice of the Greenland Ice Sheet into Kejser Franz Josephs Fjord.
- On the inner to mid continental shelf meltwaters lead to intense stratification of ocean surface waters with a subsequent reduction in the ventilation of ocean waters and associated exchange of CO_2 between the ocean and atmosphere. In contrast, meltwater influence on the outer continental shelf and continental slope is much reduced leading to greater ventilation of ocean waters and associated exchange of CO_2 between the ocean and atmosphere.
- The East Greenland Current is active across the continental shelf winnowing and eroding surface sediments, and hindering further deposition.
- The sea-floor is actively scoured by icebergs, particularly in the shallowest regions.
- The continental slope is dominated by rain out and suspension settling sedimentation with only a very minor contribution from icebergs.
- Sediment rich turbid surface meltwater plumes deposit sediment in the inner continental shelf basin (and possibly other basins in Fosters Bugt), with additional significant sediment supply through iceberg rafting resulting in laminated mud and diamicton facies. The basin is thought to act as a pond allowing unhindered sedimentation from the influence of the East Greenland Current. With retreat of glacier-ice the inner continental shelf becomes more ice-distal resulting in massive mud facies. Any deposition in the shallower regions outside the inner continental shelf basin were probably either hindered by the East Greenland Current or scoured by icebergs.
- Sedimentation and accumulation rates are very high (*c.*>120 $cmkyr^{-1}$; *c.*134 g $cm^{-2}kyr^{-1}$) in association with deglaciation and deposition of the laminated mud and diamicton facies. Rates decrease (44-73 $cmkyr^{-1}$; 45-75 g cm^{-2} kyr^{-1}) in association with deposition of the overlying increasingly more ice-distal massive muds.

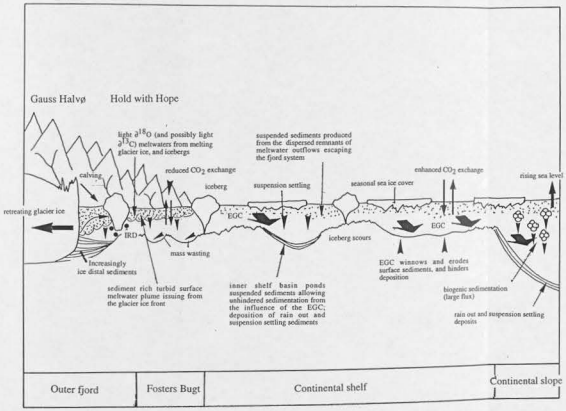

Figure 7.4. Sedimentation and environmental model for the outer Kejser Franz Josephs Fjord, Fosters Bugt and adjacent East Greenland continental margin associated with the continued deglaciation (Termination Ib) of the Kejser Franz Josephs Fjord system during the Early Holocene. EGC is short for East Greenland Current, and IRD for iceberg rafted debris.

- Deglaciation of Kejser Franz Josephs Fjord continued during the Early Holocene. Glacier-ice continued to recede through Kejser Franz Josephs fjord from its proposed Younger Dryas extent in the outer fjord-Fosters Bugt region (cf. Funder & Hansen 1996).
- Presence of meltwater and iceberg rafted sediment in the outer fjord indicates that the continued decay of the Greenland Ice Sheet was through ablation (production of meltwater) and iceberg calving.
- Major influx of low saline, light $\partial^{18}O$ meltwater is dated to occur before 7,440 yr BP in the outer fjord. Low-saline waters are derived mainly from the discharge of meltwaters and less so the melting of calved icebergs associated with the continued decay and recession of glacier-ice of the Greenland Ice Sheet through Kejser Franz Josephs Fjord.
- In the outer fjord and on the inner continental shelf meltwaters lead to intense stratification of ocean surface waters with a subsequent reduction in the ventilation of ocean waters and associated exchange of CO_2 between the ocean and atmosphere. In contrast, meltwater influence on the remaining continental shelf and continental slope is much reduced leading to greater ventilation of ocean waters and associated exchange of CO_2 between the ocean and atmosphere.
- Seasonal sea ice cover.
- The East Greenland Current is active across the continental shelf winnowing and eroding surface sediments, and hindering further deposition.
- The sea-floor is actively scoured by icebergs, particularly in the shallowest regions.
- The continental slope is dominated by rain out and suspension settling sedimentation with only a very minor contribution from icebergs.
- Deglacial sequence recognised in the outer fjord. Similar sequences may also occur in the basins of Fosters Bugt. The sedimentary sequence in the outer fjord is consistent with glacier-ice retreat from more ice-proximal to more ice-distal conditions. However, ice contact sequences (till or moraines) are not observed. Cored sections show a transition from laminated to massive mud consistent with increasingly ice-distal conditions where sedimentation is from sediment rich turbid surface meltwater plumes with additional sediment supply through iceberg rafting. The iceberg component is overwhelmed by the high rate of sedimentation from meltwater-plumes. The uncored underlying sequence is assumed to represent increasingly more ice-proximal conditions with increasing depth. Sedimentation is assumed to be derived from sediment rich turbid surface meltwater plumes, icebergs and possibly mass wasting.
- In the inner continental shelf basin massive mud deposition occurs derived from the suspension settling of sediment produced from the dispersed remnants of meltwater outflows escaping Kejser Franz Josephs Fjord. The basin acts as a pond allowing unhindered sedimentation from the influence of the East Greenland Current. Deposition also probably occurred in other regions of the inner continental shelf and Fosters Bugt, particularly in the basins. Any deposition in the shallower regions outside the inner continental shelf basin were probably either hindered by the East Greenland Current or scoured by icebergs.

The transition from sandy mud diamicton to laminated mud to bioturbated mud facies on the inner continental shelf is interpreted to represent deposition under increasingly ice-distal conditions (e.g. Svendsen et al. 1992, 1996) associated with the retreat of glacier ice of the Greenland Ice Sheet from the outer region of Kejser Franz Josephs Fjord/ inner continental shelf following 10,000 yr BP (Chapters 4, 5, 6). Sedimentation and accumulation rates are high typically 120 cm kyr^{-1} and 134 g cm^{-2} kyr^{-1}, respectively, relating to the invigorated glacier driven processes of the deglaciation period that are capable of delivering large volumes of sediment. The laminated mud and sandy mud diamicton facies represent deglacial sedimentation through sediment ladened meltwater outflows, and iceberg rafting (Tables 4.4, 5.3; Section 4.7). The supply of meltwater-derived sediments occurs at a rate that is insufficient to overwhelm the supply of iceberg rafted debris. The deposition of both facies occurs between 9,540-10,000 yr BP coinciding with the major pulse of low saline meltwater. There is little evidence from this study to position the exact glacier-ice margin at the onset of deglaciation during the Early Holocene. The fine-grained nature of the laminated mud facies and the generally thin extent of the complete deglacial sequence supports an ice-distal setting for the inner continental shelf at the onset, and during deglaciation. This would support the proposed position of the ice margin in the outer region of Kejser Franz Josephs Fjord (e.g. Hjort 1979; Funder 1989; Funder & Hansen 1996). The inner continental shelf becomes increasingly ice distal with continued retreat of glacier-ice into Kejser Franz Josephs Fjord. This retreat is marked by the transition from the laminated mud and sandy mud diamicton into thick bioturbated mud facies with small amounts of iceberg rafted debris.

Similarly, a deglaciation sequence is recognised from the outer region of Kejser Franz Josephs Fjord. The transition from laminated mud facies/ acoustically stratified sediment to bioturbated mud facies/ acoustically massive sediment is interpreted to represent deposition under increasingly ice-distal conditions (e.g. Svendsen et al. 1992, 1996), associated with the retreat of glacier ice through Kejser Franz Josephs Fjord. The deposition of the laminated mud facies occurs sometime before 7,440 yr BP coinciding with the major pulse of low saline meltwater. The fine grained nature of the facies within PS2631 indicates that deposition occurred mainly within an ice-distal, low energy setting that becomes increasingly more so with subsequent deposition of the bioturbated mud facies/ acoustically massive sediment. The supply of meltwater sediments overwhelms that supplied by icebergs resulting in a low iceberg rafted debris content. The underlying uncored acoustically stratified sediments are interpreted to be deposited increasingly more proximal to the glacier-ice margin with increasing depth and, therefore, should become progressively coarser related to the increasingly higher energy of the environment. Deposition is expected to be controlled by continued meltwater outflow with associated sediment production, and/ or subaqueous mass wasting events driven by downslope currents or failure of ice-proximal sediments that become increasingly more proximal to the glacier-ice margin with sediment depth (e.g. Dowdeswell et al. 1994b).

7.3.4 Sea ice, meltwater production and environmental implications during the Late Weichselian deglaciation

Widespread capping or stratification of surface waters in Kejser Franz Josephs Fjord and across the inner continental shelf by the meltwaters greatly suppresses the ventilation of ocean waters and the associated exchange of CO_2 with the atmosphere (Section 6.4.1.2; e.g. Stein et al. 1994a,b; Nam et al. 1995; Nam 1996). This influence does not extend to the continental slope where records show a distinct recovery to true Holocene conditions where surface waters are well ventilated with increased exchange of CO_2 with the atmosphere. The influence of meltwater capping or stratification ceases soon after 9,540 yr BP across the inner continental shelf and sometime before 7,440 yr BP in Kejser Franz Josephs Fjord, leading to increased exchange of CO_2 with the atmosphere.

7.6 HOLOCENE

7.6.1 Introduction

Figures 7.5 and 7.6 illustrate the sedimentation processes and patterns and environments within the study area during the Holocene and should be referred to throughout the following section.

7.6.2 Sedimentation in Kejser Franz Josephs Fjord and Fosters Bugt during the Holocene

It is proposed that the glacier ice of the Greenland Ice Sheet that retreated from the outer region of Kejser Franz Josephs Fjord/Fosters Bugt region following the culmination of the Younger Dryas at ca. 10,000 yr BP, reached present day limits at ca. 7,000 yr BP (Hjort 1979; Funder 1989; Funder & Hansen 1996). The removal of glacier ice from the fjord allowed glacimarine sedimentation to re-commence. Therefore, the sedimentary sequences within the fjord determined from cored and acoustic sections in this study are assumed to have accumulated since 10,000 yr BP. The numerous radiocarbon ages and stable isotope chronology confirm this. A postglacial Holocene age is further supported within the acoustic records by the absence of subglacial till and moraines that are indicative of direct glacial activity, indicating that deposition is ice-distal. If the glacier-ice stillstand position at 10,000 yr BP was positioned in the outer fjord then glacimarine sedimentation within Fosters Bugt would have re-commenced shortly before 10,000 yr BP in response to the proposed retreat of glacier-ice from the inner continental shelf during the Late Weichselian deglaciation (e.g. Funder 1989; Funder & Hansen 1996).

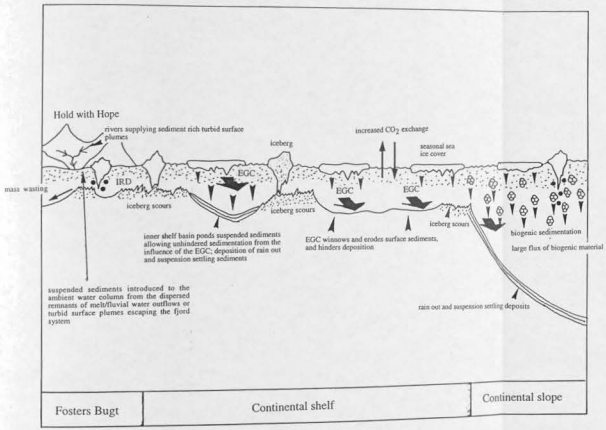

Figure 7.5. Sedimentation and environmental model for the East Greenland continental margin adjacent to Kejser Franz Josephs Fjord during the Holocene. EGC is short for East Greenland Current, and IRD for iceberg rafted debris.

- Glacier-ice of the Greenland Ice Sheet have retreated to current positions by the Early Holocene (e.g., Funder & Hansen 1996).

- $\partial^{18}O$ records become progressively lighter from the continental slope to the continental shelf/ Fosters Bugt reflecting the progressively stronger influence of low-saline, light-$\partial^{18}O$ melt/fluvial waters (glacimarine, glacifluvial and fluvial drainage systems) escaping the East Greenland fjord systems with increased proximity to the East Greenland continent.

- Seasonal sea ice cover leading to increased ventilation of ocean surface waters and the associated CO_2 exchange between the atmosphere and ocean. Ventilation of ocean surface waters across the continental margin are expected to occur during summer months when the seasonal sea ice cover breaks up.

- Increased continent and ocean surface water bioproductivity may have contributed to heavier $\partial^{13}C$ records (in response to warmer atmospheric temperatures and reduced sea ice conditions), although marine organic carbon and carbonate content have not been determined in support of this interpretation.

  $\partial^{13}C$ records become progressively lighter from the continental slope to the continental shelf/Fosters Bugt reflecting the progressively stronger influence of melt/ fluvial waters escaping the East Greenland fjord systems with increasing proximity to the East Greenland continent that lead to: i) increased stratification of ocean surface waters with a subsequent decrease in the ventilation and associated exchange of CO_2 between the atmosphere and ocean, ii) a decrease in surface water bioproductivity, although marine organic carbon and carbonate content have not been determined in support of this interpretation, and iii) introduction of light $\partial^{13}C$ melt/fluvial waters into the ocean, although this is only a tentative interpretation.

- The East Greenland Current is active across the continental shelf winnowing and eroding surface sediments, and hindering further deposition.

- The sea-floor in the shallowest regions is actively scoured by icebergs. The sea-floor of deeper regions, particularly the inner shelf basin, are left unscoured.

- The continental slope is dominated by rain out and suspension settling sedimentation with only a very minor contribution from icebergs. Suspended sediments are thought to be derived partly from the dispersed remnants of melt/fluvial water outflows escaping the fjord systems of East Greenland. Large flux of biogenic material.

- In the inner continental shelf basin massive mud deposition occurs derived from the suspension settling of sediment produced from the dispersed remnants of melt/fluvial water outflows escaping Kejser Franz Josephs Fjord, and possibly other East Greenland fjords to the north. The basin ponds sediment allowing unhindered sedimentation from the influence of the East Greenland Current. Any deposition in the shallower regions outside the inner continental shelf basin were probably either hindered by the East Greenland Current or scoured by icebergs.

  Deposition also occurs in other regions of the inner continental shelf and Fosters Bugt, particularly in the numerous small basins. Deposition from sediment gravity flows (turbidity currents and debris flows) are also evident in the basins of Fosters Bugt, derived from the bathymetric highs surrounding the basin.

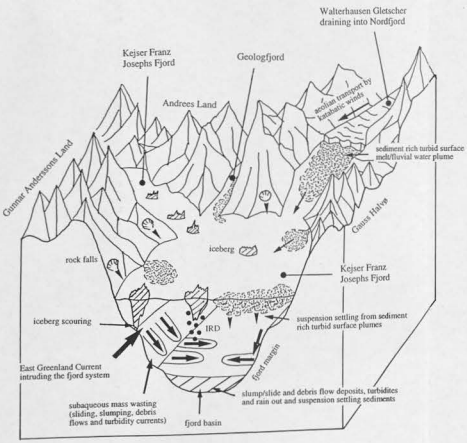

Figure 7.6. Sedimentation and environmental model for the mid to outer region of Kejser Franz Josephs Fjord during the Holocene period following the deglaciation of the fjord system. IRD is short for iceberg rafted debris.

- Glacier-ice of the Greenland Ice Sheet have retreated to current positions by the Early Holocene (e.g., Funder & Hansen 1996).

- $\partial^{18}O$ records become progressively lighter from the outer fjord to the mid fjord reflecting the progressively stronger influence of low-saline, light-$\partial^{18}O$ melt/fluvial waters with increased proximity to the inner fjord and glaciomarine, glacifluvial and fluvial drainage systems.

- Seasonal sea ice cover allows increased ventilation of fjord surface waters and the associated CO_2 exchange between the atmosphere and fjord waters. Ventilation of fjord surface waters in the fjord are expected to occur during summer months when the seasonal sea ice cover breaks up.

- Increased continent and ocean surface water bioproductivity may have contributed to heavier $\partial^{13}C$ records (in response to warmer atmospheric temperatures and reduced sea ice conditions), although marine organic carbon and carbonate content have not been determined in support of this interpretation.

  $\partial^{13}C$ records become progressively lighter from the outer fjord to the mid fjord reflecting the progressively stronger influence of melt/ fluvial waters with increasing proximity to the inner fjord that lead to: i) increased stratification of fjord surface waters with a subsequent decrease in the ventilation and associated exchange of CO_2 between the atmosphere and ocean, ii) a decrease in surface water bioproductivity, although marine organic carbon and carbonate content have not been determined in support of this interpretation, and iii) introduction of light $\partial^{13}C$ melt/fluvial waters into the fjord, although this is only a tentative interpretation.

- The East Greenland Current may intrude the fjord system winnowing and eroding sediments on fjord bathymetric highs.

- The sea-floor on the shallow bathymetric highs and fjord margins is actively scoured by icebergs. The sea-floor of the deeper fjord basins are unscoured.

- The steep margins of the fjord and bathymetric highs are loci for temporary and unstable storage of sediment deposited from rain out and suspension settling processes (iceberg rafting, meltwater/fluvial outflow, aeolian and resuspended sea-floor sediments), side entry glacifluvial/fluvial deltas and fans, and subaerial debris falls and slides.

  Sediments on the margins of the fjord and bathymetric highs undergo episodic failure resulting in the basinward transport of sediment by subaqueous mass wasting (debris flows, turbidity currents, sliding and slumping). In response the mid to outer fjord basins are infilled with small and large scale debris flow and turbidity current deposits, and sliding and slumping deposits proximal to slopes of bathymetric highs. These deposits are typically ponded within the fjord basins although some overspill occurs between basins. Debris flows in some cases erode and entrain pre-existing deposits. Rain out and suspension settling sediments (bioturbated mud with drop stones) are also deposited within the fjord basins and drape the flanking bathymetric highs derived mainly from sediment rich turbid surface melt/fluvial water plumes and the distal remnants of such plumes, iceberg rafting, resuspended sea-floor sediments, and aeolian transport.

  The iceberg rafted component within fjord sediments increases towards the mid fjord related to the increasing proximity of iceberg producing tidewater glaciers at the heads of the tributary fjords in the Kejser Franz Josephs Fjord system.

Aerial photographs and satellite imagery of the present day fjord indicate that icebergs, meltwater/fluvial outflow and side entry delta and fan activities are the main contributors supplying sediment to the fjord (Section 1.2; Figs 1.2, 1.3). Numerous fluvial systems (the largest being Paralleldal and Badlanddal) fed by snow melt and precipitation drain the land bordering the mid and outer fjord such as Gauss Halvø, Hold with Hope and Gunnar Anderssons Land (Figs 1.1-1.3), and provide major input of sediment to the fjord margins throughout the mid and outer fjord and Fosters Bugt. Turbid surface meltwater plumes escape from the fjord margins to influence offshore regions. Such plumes commonly develop into distal remnants that introduce sediments into the water column in more offshore regions distal to both fluvial and meltwater outlets.

Two broad sedimentation processes are recognised from the mid to outer fjord and the basins of Fosters Bugt, comprising sediment gravity flows (debris flow and turbidity current) and rain out and suspension settling (combination of ice rafting, sediment laden meltwater/fluvial outflows originating from tidewater glaciers and subaerial rivers fed by glacier and snow melt, and settling of resuspended sea-floor sediment). These processes combine to produce ponded, basin fill and conformable sediment drapes. It is probable based on the mainly ponded architecture of fjord sediments that sediment gravity flows contribute by far the greatest volume of sediment to the fjord basins. Suspension settling sedimentation is concomittant with sediment gravity flows.

Sediments deposited through rain out and suspension settling are typically bioturbated mud facies with variable amounts of iceberg rafted debris which currently dominate the most recent sedimentation within the basins of the outer fjord and over the bathymtric highs (Chapters 4, 5). The muds are deposited through a number of processes. The iceberg rafted debris content increases within the mud facies with distance up-fjord related to the increasing proximity of tidewater glaciers and the origin of icebergs (Chapter 4).

Bathymetric highs (sills) throughout the mid and outer fjord are relatively devoid of sediment. The sediment that is present is heavily turbated through iceberg scouring. The general absence of sediment on bathymetric highs is assumed to result from the downslope resedimentation of any rain out and suspension settling deposits that may have accumulated. The present day fjord is influenced by the intrusion of shelf water of the East Greenland Current system (Vogt et al. 1995), which probably has been the case for the Holocene period following the recession of glacier-ice through the fjord. Therefore, sediments deposited on bathymetric highs throughout the Holocene may have undergone resuspension due to the influence of bottom current activity associated with the intrusion of the East Greenland Current into the fjord system (e.g. Marienfeld 1991, 1992b; Syvitski and Hein 1991; Vogt et al. 1995). It is envisaged that subsquent deposition of the resuspended sediment occurs within the deeper and more quiescent basins of the fjord (e.g. Marienfeld 1991, 1991b).

The supply of sediment to the mid and outer region of Kejser Franz Josephs Fjord, and Fosters Bugt during the Holocene is assumed to be relatively high due to active transport mechanisms on-land that deliver sediment to the fjord. Sedimentation and accumulation rates of rain out and suspension settling facies within the fjord are in the range of 46-87 cm kyr^{-1} and 40-64 g cm^{-2} kyr^{-1},

respectively. The steep margins of the fjord and bathymetric highs can be considered as loci for temporary and unstable storage of sediment deposited from the rain out and suspension settling of particles from icebergs, meltwater/fluvial outflow, aeolian and bottom current sources, side entry glaciofluvial/fluvial deltas and fans, and subaerial debris falls and slides (talus cones) (e.g. Gilbert 1982; Syvitski & Hein 1991; Hein & Syvitski 1992). The basinward transport of sediment from the bathymetric highs and margins of the fjord is a result of episodic unstable sediment accumulation and failure.

Sediments deposited in shallow regions of the fjord and Fosters Bugt are influenced further by iceberg scouring during the Holocene period following the recession of glacier-ice during the Early Holocene (Section 5.8, 5.9.4.5; Hjort 1979; Funder 1989; Funder & Hansen 1996; Table 5.3; Fig 5.12). If glacier-ice did not occupy the Fosters Bugt region at this time then iceberg scouring may have occurred pre-10,000 yr BP following the retreat of ice from its proposed peak Late Weichselian glaciation position on the the inner continental shelf during the Late Weichselian deglaciation (Section 5.8.3; Funder 1989; Funder & Hansen 1996). Iceberg scouring leads to the partial or total homogenisation of sediment over the sills, bathymetric highs, and shallowest regions of Kejser Franz Josephs Fjord and Fosters Bugt (Fig 5.10, 5.12; Section 5.8).

7.6.3 Sedimentation on the continental shelf during the Holocene

Sedimentation on the continental shelf is composed of rain out and suspension settling, resulting in bioturbated mud facies, consistent with an ice-distal setting. Processes include the settling of resuspended sea floor sediments, occasional rain out of iceberg rafted debris and settling of sediment derived from the distal remnants of meltwater/fluvial outflows escaping the neighbouring East Greenland fjords. Sedimentation is mainly confined to the basins or topographic depressions of the continental shelf protected from the influence of the southward flowing East Greenland Current. The mud facies are derived partly from the redeposition of sediments resuspended from the sea-floor of other regions of the continental shelf, and transported to the inner continental shelf basin, by the East Greenland Current (Chapter 4). The resuspended sediments transported by the East Greenland Current, and those derived from meltwater/fluvial outflows escaping the neighbouring East Greenland fjord systems become ponded within the inner continental shelf basin (Section 5.3.3), and allowed to settle relatively unhindered from further current activity. Sedimentation and accumulation rates are typically ca. 44-109 cm kyr^{-1} and 46-113 g cm^{-2} kyr^{-1}.

The absence of a surface veneer of fine-grained rain out and suspension settling sediment across the mid-outer continental shelf (Chapter 5) indicates that the accumulation of Holocene sediments was prevented, and/or subsequently removed through winnowing associated with the East Greenland Current (Section 4.7.8). The latter is commonly observed on other parts of the East Greenland continental margin (e.g. Funder & Larsen 1989; Mienert et al. 1992; Nam 1996), and similarly on the western Svalbard continental margin (e.g. Cadman 1996). The surface sediment is

composed of sandy diamicton facies consisting of a high gravel and sand content, supporting intense winnowing of fine-grained sediments within facies on the sea floor by the East Greenland Current.

Sea floor sediments across the shallower regions of the continental shelf (over bathymetric highs and at the continental shelf break) are partially to totally disturbed by iceberg scouring (Chapter 5). The icebergs producing these scours are probably derived from further north along East and Northeast Greenland and transported south in the East Greenland Current (Chapter 5).

7.6.4 Sedimentation on the continental slope during the Holocene

Sedimentation on the continental slope is composed of rain out and suspension settling, resulting in mud facies. The rate of sedimentation and accumulation are very low (2.3-3.5 cm kyr^{-1} and 2.1-2.8 g cm^{-2} kyr^{-1}, respectively) due to more quiescent, marine-dominated sedimentation in response to the ice-distal setting of the continental slope and the low energy glacier driven processes of the Holocene. It is envisaged that sediment is derived through a number of processes that include the distal remnants of meltwater/fluvial outflows escaping East Greenland fjords, ice rafting, settling of resuspended sea-floor sediment, and biogenic/pelagic activity (Chapters 4, 5). The high biogenic content (indicated by foraminifera >50 grain-%) indicates that pelagic sedimentation is probably the biggest contributor. Sedimentation from meltwater/fluvial outflow is realistic for the continental slope as present day and Holocene sedimentation of fine grained sediments on the continental margin of the Barents Sea are supplied through distal remnants of meltwater outflows (e.g. Elverhøi & Solheim 1983). A contribution from iceberg sedimentation is negligible related to the very low drift of icebergs in response to the ice-distal setting of the continental slope and reduced glacier-driven processes of the Holocene.

7.6.5 Sea ice cover, oceanography and environmental implications during the Holocene

The Holocene (heavy $\delta^{18}O$) is characterised by increased atmospheric temperatures, and the subsequent stabilisation of the Greenland Ice Sheet at a position similar to the present day with the ^{16}O locked up in the extended glacial ice mass returned to the oceans (Sections 6.4.1.1, 6.4.4). Additionally, increased ventilation of fjord/ocean surface waters and associated exchange of CO_2 between the ocean and atmosphere occurred during the Holocene (reflected in $\delta^{13}C$ maxima), indicating a greatly reduced sea-ice cover and more open water conditions (seasonal sea ice cover) (Sections 6.4.1.2, 6.4.4; e.g. Shackleton 1977a; Spielhagen & Erlenkeuser 1994; Stein et al. 1994a,b; Nam et al. 1995; Nam 1996). Increased continent and fjord/ocean surface water bioproductivity (in response to increased atmospheric temperatures and reduced sea ice cover) may have also contributed to the $\delta^{13}C$ maxima (Sections 6.4.1.2, 6.4.4; e.g.Shackleton 1977a; Stein et al. 1994a,b; Nam et al. 1995; Nam 1996), but an increase in surface water bioproductivity can not be confirmed in this study (Section 6.4.4). The ventilation of surface waters and associated exchange of CO_2 between the ocean and atmosphere in the Kejser Franz Josephs Fjord and across the adjacent East

Greenland continental margin is probably limited to the summer season when sea ice breaks up (a situation common in the modern day setting (Section 1.2.2.3), similar to observations in other parts of East Greenland (e.g. Baumann et al. 1993; Stein et al. 1993; Nam et al. 1995; Nam 1996). However, the seasonal break up of sea ice may not provide enough for equilibrium conditions to be attained between the ocean and atmosphere, explaining why the $\delta^{13}C$ maxima are somewhat below true equilibrium values (ca. +1 to +2‰ e.g. Labeyrie & Duplessy 1985).

The isotopic records ($\delta^{18}O$ and $\delta^{13}C$) of Stage I become progressively lighter along the transect from the lower East Greenland continental slope to the mid region of Kejser Franz Josephs Fjord (Sections 6.3.6, 6.4.4; Figs 6.5, 7.6). The general trend reflects the stronger influence of relatively ^{16}O enriched meltwaters associated with the freshwater drainage of glacimarine, glacifluvial, and fluvial systems with increased proximity to the East Greenland continent. The enriched ^{16}O meltwaters reflect the high ^{16}O composition of glacier ice of the Greenland Ice Sheet, snow melt and river run-off due to the preferential fractionation of ^{16}O within meteoric water precipitated over high latitude regions (Sections 6.4.1.1, 6.4.4; e.g. Emiliani 1955).

The progressive decrease in the $\delta^{13}C$ records from the East Greenland continental margin towards Kejser Franz Josephs Fjord may result result from one or a combination of three possible factors:

First, numerous river systems currently drain into Kejser Franz Josephs Fjord and Fosters Bugt, and it is interpreted that these systems have supplied light $\delta^{13}C$ enriched waters ($\delta^{13}C$ exceeds -10‰; e.g. Siengenthaler & Eicher 1986; Spielhagen & Erlenkeuser 1994) to the study area during the postglacial Holocene. These waters would probably act to dilute and lower the $\delta^{13}C$ composition of the residual waters of the fjord and continental margin (e.g. Spielhagen & Erlenkeuser 1994). The influence of these waters is greatest in the fjord but becomes increasingly less so with progressive distance across the continental margin away from river water efflux points.

Second, melt/river water capping or stratification of fjord/ocean surface waters are known to influence the modern day Kejser Franz Josephs Fjord and the adjacent inner continental shelf (Section 1.2.3; Vogt et al. 1995), and have probably done so throughout the Holocene. It is interpreted that the melt/river water capping or stratification effect probably results in the reduced ventilation and CO_2 exchange between the residual surface waters of the fjord/inner continental shelf and the atmosphere. This effect becomes increasingly less influential across the continental shelf with distance away from melt/river water efflux points in the fjord as the capping or stratification of surface waters becomes progressively less well formed, with their eventual cessation beyond the inner continental shelf (Section 6.4.1.1).

Third, surface water bioproductivity may vary between the fjord, continental shelf and continental slope in response to different environmental conditions (e.g. such as unfavourable hydrographic conditions of the fjord; Section 2.2.5), although systematic fluctuations in surface water bioproductivity within the fjord and across the continental margin can not be confirmed in this study (Section 6.4.4).

CHAPTER 8

CONCLUSIONS

8.1 INTRODUCTION

This study has set out to investigate the glacimarine/marine sedimentary record, and its relationship to glacial and interglacial environmental change associated with the Late Weichselian and Holocene, is investigated in the mid to outer Kejser Franz Josephs Fjord, and adjacent continental shelf and slope region, East Greenland (73°N). This chapter outlines the main findings of the study.

8.2 LATE WEICHSELIAN GLACIATION

- The timing, nature and mechanism for the expansion and advance of glacier-ice of the Greenland Ice Sheet to Late Weichselian glacial maximum conditions and the corresponding sedimentation patterns and processes, and environmental change can not be ascertained based on the sediments of the study area. Additionally, the position of the shelfward extent of the glacier-ice margin during the Late Weichselian glacial maximum can not be ascertained let alone constrained to an exact location based on the sedimentary and acoustic records of this study.
- $\partial^{13}C$ minima reflect extended sea ice cover (although at least some seasonally sea ice cover is experienced) that restricts ventilation between the atmosphere and the ocean, reducing the CO_2 exchange between the atmosphere and ocean surface water. Reduced continental and surface water bioproductivity (in response to colder atmospheric temperatures and extended sea ice cover) may have also contributed to the $\partial^{13}C$ minima, although marine organic carbon and carbonate content have not been determined in support of this interpretation.
- Sedimentation and accumulation rates are high on the ice-distal continental slope due to the focusing of sedimentation on the continental margin associated with the expansion of the Greenland Ice Sheet onto the continental shelf, and the subsequent invigoration of glacimarine processes delivering sediment to the slope. Average rates are the highest on the upper continental slope and decrease downslope. This indicates that: i) sedimentation is most active on the upper

continental slope, controlled primarily by icebergs, and ii) resedimentation events active downslope are not significant enough to inflate average sedimentation rates.

- Upper continental slope is dominated by rapid rain out and suspension settling sedimentation (up to *c.*30 cm kyr^{-1}) in which contribution from icebergs dominate. Additional fine-grained sediment are supplied through ice rafting, distal remnants of sediment laden meltwater outflows and resuspended sea-floor sediments. This scenario may also apply to the continental shelf, although acoustic evidence is inconclusive. The East Greenland Current may have modified the deposits on both the continental shelf and slope. Resedimentation on some areas of the upper continental slope occurs but is generally intermittent occurring from localised regions of the slope probably in response followed to the rapid build-up of unstable sediment piles that subsequently generated the debris flow and turbidity current activity further downslope, although this activity may also have been generated through resedimentation events lower down on the continental slope.

- Mid to lower continental slope is characterised by intermittent, restricted and local/regional large and small-scale debris flow and turbidity current activity concomitant with rain out and suspension settling sedimentation (derived from ice-rafting, remnant meltwater outflows, biogenic activity and resuspended sea-floor sediment). Debris flows and turbidity currents are generated from further upslope and may have undergone transformation during downslope transport. Average sedimentation rates are typically up to *c.*17 cm kyr^{-1}.

- The lithofacies distribution indicate that a significant number of icebergs influenced the upper continental slope, and that greatly reduced numbers influenced the mid to lower continental slope. This is probably in response to the activity of the southward flowing East Greenland Current confining the majority of icebergs to the continental shelf and upper continental slope.

8.3 LATE WEICHSELIAN DEGLACIATION

- Onset of deglaciation began following 15,250 yr BP. The exact nature of the retreat of glacier-ice of the Greenland Ice Sheet during the Late Weichselian deglaciation is uncertain as the geological evidence presented in this study is inconclusive. Therefore, it remains unclear whether ice retreat in East Greenland was gradual, punctuated by stillstands or was very rapid reaching its Younger Dryas stillstand position sometime before the onset of the Younger Dryas Stadial.

- Presence of iceberg rafted diamicton on the continental shelf indicates that mass loss of ice from the decaying Greenland Ice Sheet was through iceberg calving, although additional meltwater flux cannot be discounted.

- Major influx of low saline, light $\partial^{18}O$ meltwater occurred between 13,010-15,250 yr BP on the continental slope and may have extended to the period post-dating 13,010 yr BP on the continental shelf. Meltwaters are probably derived from either the melting of icebergs derived from the decay of the Greenland Ice Sheet in eastern and northeastern Greenland and possibly

the Barents Sea Ice Sheet, and/or influx of a low saline, light $\partial^{18}O$ Arctic water mass sourced from the melting of Eurasian Arctic ice masses in the Russian Arctic region, and transported via the East Greenland Current to the East Greenland continental margin.

- Meltwaters lead to intense stratification of ocean surface waters with a subsequent reduction in the ventilation of ocean waters and associated exchange of CO_2 between the ocean and atmosphere.
- Repetitive turbidity current activity on the mid to lower continental slope between 13,200 and 15,250 yr BP generated through mass wasting on the upper continental slope (51-79 cm kyr^{-1}). Mass wasting probably generated in response to rapid and unstable sediment build-up on the upper continental slope in response to invigorated glacimarine processes associated with deglaciation. Mass wasting terminates at 13,200 yr BP and suspension settling sedimentation dominates, suggesting that sediment accumulation becomes less rapid and much more stable. Contribution from iceberg rafting is minor. Upper continental slope dominated by rain out and suspension settling sedimentation with a small but significant contribution by icebergs. The nature of sediments and iceberg contribution may differ further up on the upper continental slope than what is suggested from available geological evidence.
- Acoustic evidence suggests that iceberg sedimentation occurs across the mid to outer continental shelf pre-13,010 yr BP. Localised mass wasting occurs close to the mid continental shelf bathymetric high just prior to 13,010 yr BP, triggered from the rapid and unstable build-up of sediment and iceberg scouring of the sea-floor over the bathymetric high. Following 13,010 yr BP the continental shelf is dominated by rain out and suspension settling sedimentation in which a significant contribution is derived from icebergs. Sedimentation is ver rapid (60 cm kyr^{-1}). The East Greenland Current was active winnowing the fine-grained component of sea-floor deposits.
- The sea-floor is actively scoured by icebergs, particularly in the shallowest regions.
- Lithofacies distribution indicate that i) significant numbers of icebergs influenced the continental shelf, ii) greatly reduced numbers of icebergs in comparison influenced the upper continental slope, although this observation is based on geological evidence from the lower region of the upper slope which may differ markedly further upslope, and iii) virtually no icebergs influenced the mid to lower continental slope. This is probably in response to the southward flowing East Greenland Current that confined the majority of icebergs to the continental shelf.

8.4 YOUNGER DRYAS STADIAL

- The sedimentary and acoustic records of this study offers relatively little evidence on the sedimentation patterns and processes and environmental history for the Kejser Franz Josephs Fjord and adjacent East Greenland continental shelf and slope. No direct evidence of a glacier-ice stillstand position (terminal moraines or subglacial till) in the outer region of Kejser Franz Josephs Fjord or in Fosters Bugt.

- $\delta^{18}O$ records indicate cold conditions. $\delta^{13}C$ records indicate reduced CO_2 exchange between the ocean and atmosphere caused by extended sea-ice (reduced open-water) conditions.

8.5 POST YOUNGER DRYAS (EARLY HOLOCENE) DEGLACIATION

- Second phase of deglaciation continued following the culmination of the Younger Dryas cooling event at *c.*10,000 yr BP. Glacier-ice recedes through Kejser Franz Josephs Fjord from its proposed Younger Dryas extent in the outer fjord-Fosters Bugt region.
- Presence of meltwater and iceberg rafted sediment in the outer fjord and on the continental shelf indicates that the decay of the Greenland Ice Sheet was through ablation (production of meltwater) and iceberg calving.
- Major influx of low saline, light $\partial^{18}O$ meltwater is dated to occur 9,540-10,000 yr BP on the inner continental shelf and sometime before 7,440 yr BP in the outer fjord. Low-saline waters are derived from the discharge of meltwaters and the melting of calved icebergs associated with the decay and recession of glacier-ice of the Greenland Ice Sheet into Kejser Franz Josephs Fjord.
- On the inner to mid continental shelf meltwaters lead to intense stratification of ocean surface waters with a subsequent reduction in the ventilation of ocean waters and associated exchange of CO_2 between the ocean and atmosphere. In contrast, meltwater influence on the outer continental shelf and continental slope is much reduced leading to greater ventilation of ocean waters and associated exchange of CO_2 between the ocean and atmosphere.
- The East Greenland Current is active across the continental shelf winnowing and eroding surface sediments, and hindering further deposition.
- The sea-floor is actively scoured by icebergs, particularly in the shallowest regions.
- The continental slope is dominated by rain out and suspension settling sedimentation with only a very minor contribution from icebergs.
- Sediment rich turbid surface meltwater plumes deposit sediment in the inner continental shelf basin (and possibly other basins in Fosters Bugt), with additional significant sediment supply through iceberg rafting resulting in laminated mud and diamicton facies. The basin is thought to act as a pond allowing sedimentation unhindered from the influence of the East Greenland Current. With retreat of glacier-ice the inner continental shelf becomes more ice-distal resulting in massive mud facies. Any deposition in the shallower regions outside the inner continental shelf basin ~~were~~ was probably either hindered by the East Greenland Current or scoured by icebergs.
- Sedimentation and accumulation rates are very high (*c.* 120 $cmkyr^{-1}$; *c.*134 g cm^{-2} kyr^{-1}) in association with deglaciation and deposition of the laminated mud and diamicton facies. Rates decrease (44-73 $cmkyr^{-1}$; 45-75 g cm^{-2} kyr^{-1}) in association with deposition of the overlying increasingly more ice-distal massive muds.

- Deglacial sequence recognised in the outer fjord. Similar sequences may also occur in the basins of Fosters Bugt. The sedimentary sequence in the outer fjord is consistent with glacier-ice retreat from more ice-proximal to more ice-distal conditions. However, ice contact sequences (till or moraines) are not observed. Cored sections show a transition from laminated to massive mud consistent with increasingly ice-distal conditions where sedimentation is from sediment rich turbid surface meltwater plumes with additional sediment supply through iceberg rafting. The iceberg component is overwhelmed by the high rate of sedimentation from meltwater-plumes. The uncored underlying sequence is assumed to represent increasingly more ice-proximal conditions with increasing depth. Sedimentation is assumed to be derived from sediment rich turbid surface meltwater plumes, icebergs and possibly mass wasting.
- In the inner continental shelf basin massive mud deposition occurs derived from the suspension settling of sediment produced from the dispersed remnants of meltwater outflows escaping Kejser Franz Josephs Fjord. The basin acts as a pond allowing unhindered sedimentation from the influence of the East Greenland Current. Deposition also probably occurred in other regions of the inner continental shelf and Fosters Bugt, particularly in the basins. Any deposition in the shallower regions outside the inner continental shelf basin were probably either hindered by the East Greenland Current or scoured by icebergs.

8.6 HOLOCENE

- There is no evidence on the timing of the retreat of glacier-ice of the Greenland Ice Sheet to present day positions in this study.
- $\partial^{18}O$ records become progressively lighter from the continental slope to the mid fjord reflecting the progressively stronger influence of low-saline, light-$\partial^{18}O$ melt/fluvial waters (glacimarine, glacifluvial and fluvial drainage systems) escaping the East Greenland fjord systems with increased proximity to the East Greenland continent.
- Seasonal sea ice cover leading to increased ventilation of ocean/fjord surface waters and the associated CO_2 exchange between the atmosphere and ocean/fjord. Ventilation of ocean/fjord surface waters across the continental margin are expected to occur during summer months when the seasonal sea ice cover breaks up.
- Increased continent and ocean/fjord surface water bioproductivity may have contributed to heavier $\partial^{13}C$ records (in response to warmer atmospheric temperatures and reduced sea ice conditions), although marine organic carbon and carbonate content have not been determined in support of this interpretation. $\partial^{13}C$ records become progressively lighter from the continental slope to the mid fjord reflecting the progressively stronger influence of melt/ fluvial waters escaping the East Greenland fjord systems with increasing proximity to the East Greenland continent that lead to: i) increased stratification of ocean surface waters with a subsequent

decrease in the ventilation and associated exchange of CO_2 between the atmosphere and ocean/fjord, ii) a decrease in surface water bioproductivity, although marine organic carbon and carbonate content have not been determined in support of this interpretation, and iii) introduction of light $\partial^{13}C$ melt/fluvial waters into the ocean, although this is only a tentative interpretation.

- The East Greenland Current is active across the continental shelf winnowing and eroding surface sediments, and hindering further deposition.
- The sea-floor in the shallowest regions is actively scoured by icebergs, including the shallow bathymetric highs and fjord margins. The sea-floor of the deeper fjord and inner continental shelf basins are unscoured.
- The continental slope is dominated by rain out and suspension settling sedimentation with only a very minor contribution from icebergs. Suspended sediments are thought to be derived partly from the dispersed remnants of melt/fluvial water outflows escaping the fjord systems of East Greenland. Large flux of biogenic material. Sedimentation and accumulation rates are low (2.3-3.5 cm kyr^{-1} and 2.1-2.8 g cm^{-2} kyr^{-1}) related to the focus of sedimentation returning to the fjord.
- In the inner continental shelf basin massive mud deposition occurs derived from the suspension settling of sediment produced from the dispersed remnants of melt/fluvial water outflows escaping Kejser Franz Josephs Fjord, and possibly other East Greenland fjords to the north. The basin ponds sediment allowing unhindered sedimentation from the influence of the East Greenland Current. Any deposition in the shallower regions outside the inner continental shelf basin were probably either hindered by the East Greenland Current or scoured by icebergs. Sedimentation rates are high inresponse (44-109 cm kyr^{-1}). Deposition also occurs in other regions of the inner continental shelf and Fosters Bugt, particularly in the numerous small basins. Deposition from sediment gravity flows (turbidity currents and debris flows) are also evident in the basins of Fosters Bugt, derived from the bathymetric highs surrounding the basin.
- The steep margins of the fjord and bathymetric highs are loci for temporary and unstable storage of sediment deposited from rain out and suspension settling processes (iceberg rafting, meltwater/fluvial outflow, aeolian and resuspended sea-floor sediments), side entry glacifluvial/fluvial deltas and fans, and subaerial debris falls and slides. Sediments on the margins of the fjord and bathymetric highs undergo episodic failure resulting in the basinward transport of sediment by subaqueous mass wasting (debris flows, turbidity currents, sliding and slumping). In response the mid to outer fjord basins are infilled with small and large scale debris flow and turbidity current deposits, and sliding and slumping deposits proximal to slopes of bathymetric highs. These deposits are typically ponded within the fjord basins although some overspill occurs between basins. Debris flows in some cases erode and entrain pre-existing deposits. Rain out and suspension settling sediments (bioturbated mud with dropstones) are also deposited within the fjord basins and drape the flanking bathymetric highs derived mainly from sediment rich turbid surface melt/fluvial water plumes and the distal remnants of such plumes, iceberg rafting,

resuspended sea-floor sediments, and aeolian transport. The iceberg rafted component within fjord sediments increases towards the mid fjord related to the increasing proximity of iceberg producing tidewater glaciers at the heads of the tributary fjords in the Kejser Franz Josephs Fjord system.

8.7 FUTURE WORK

This study has demonstrated the use a broad number of techniques in order to produce a composite model of the sedimentation patterns and processes and environments occurring within glacier-influenced fjord, continental shelf and continental slope settings. However, the techniques used do not, by any means, provide the complete answer to the problems arising from this investigation. A number of outstanding issues have arisen from this study which would need careful consideration in any future investigation within the East Greenland region.

The timing and nature of the onset of the Late Weichselian glaciation within the Kejser Franz Josephs Fjord region, similar to East Greenland in general, is only poorly constrained. High resolution and dated sedimentary sequences preferably from the continental slope covering this interval would go further to establishing the early history of the onset of full glacial conditions.

Resedimentation on the continental slope of the study area provided a number of unanswered questions. Although mass wasting deposits were identified from acoustic and sediment core records the general scale, downslope run-out lengths and the connectivity of mass wasting deposits on the upper and lower continental slope could not be determined. Furthermore, it could not be determined with any certainty whether or not the upper continental slope was influenced by cohesive mass flows following deposition. The presence of debris flows at the transition between the upper and mid continental slope suggested mass flows took place on the upper continental slope. However, the acoustic records could not be used to trace the run out distances of such debris flow deposits, or even determine or characterise the extent to which mass wasting influenced the upper slope. Further coring and acoustic profiling (high and low resolution seismics and GLORIA sidescan sonar) of the continental slope is suggested. A greater area of the continental slope must be covered in order to develop a better understanding and characterisation of the resedimentation processes active on a continental margin in response to glacimarine sedimentation derived from glacier-ice that was positioned on the inner continental shelf.

The nature of the retreat of glacier ice of the Greenland Ice Sheet during the Late Weichselian deglaciation following 15,250 yr BP is not well understood based on the low resolution and spatially limited sedimentary record of this investigation. A more detailed array of cores and acoustic profiles are required from across the continental shelf and slope. These would provide more spatially-detailed and hopefully higher resolution sedimentary records for this investigation. Additionally, the retreat of glacier-ice through the fjord during the Early Holocene could be constrained more by detailed acoustic investigations but concentrating on the marginal areas of the fjord. This work would also enable the sediment gravity flow deposits within the basins of Kejser Franz Josephs Fjord to be traced to their source.

REFERENCES

Aagaard, K. and Coachman, L.K., 1968. The East Greenland current north of Denmark Strait., Part 1. *Arctic*, **21**, 181 - 200.

Alley, R.B., Blankenship, D.D., Rooney, S.T. and Bentley, C.R., 1989. Sedimentation beneath ice shelves - the view from Ice Stream B. *Marine Geology*, **85**, 101 - 120.

Andersen, J.B., Brake, c., Domack, E., Myers, N. and Wright, R., 1983. Development of a polar glacial-marine sedimentation model from Antartic Quaternary deposits and glaciological information. From Molnia, B.F. (ed), *Glacial-Marine Sedimentation*, Plenum Press, New York, 233 - 264.

Andersen, E.S., Østmo, S.R., Forsberg, C.F. and Lehman, S.J., 1995. Late- and post-glacial depositional environments in the Norwegian Trench, northern North Sea. *Boreas*, **24**, 47 - 64.

Andersen, E.S., Dokken, T.M., Elverhøi, A., Solheim, A. and Fossen, I., 1996. Late Quaternary sedimentation and glacial history of the western Svalbard continental margin. *Marine Geology*, **133**, 123 - 156.

Andrews, J.T., and Matsch, C.L. 1983. Glacial marine sediments and sedimentation: annotated bibliography. *Geo Abstracts*, Norwich, pp227.

Andrews, J.T., Erlenkeuser, H., Evans, L.W., Briggs, W.M., and Jull, A.J.T., 1991. Meltwater and deglaciation, SE Baffin Shelf (NE margin Laurentide Ice Sheet) between 13.5 and 7 ka: From O and C stable isotopic data. *Paleoceanography*, **6** (5), 621 - 637.

Andrews, J.T. and Tedesco, K., 1992. Detrital carbonate-rich sediments, northwestern Labrador Sea: implications for ice-sheet dynamics and iceberg rafting (Heinrich) events in the North Atlantic. *Geology*, **20**, 1087 - 1090.

Andrews, J.T., Dyke, A.S., Tedesco, K. and White, J.W., 1993. Meltwater along the Arctic margin of the Laurentide Ice Sheet (8 - 12 ka): stable isotopic evidence and implications for past salinity anomalies. *Geology*, **21**, 881 - 884.

Andrews, J.T., Milliman, J.D., Jennings, A.E., Rynes, N. and Dwyer, J., 1994. Sediment thicknesses and Holocene glacial marine sedimentation rates in three East Greenland fjords (ca. 68°N). *The Journal of Geology*, **102**, 669 - 683.

Bard, E., Labeyrie, L.D., Pichon, J.-J., Labracherie, M., Arnold, M., Duprat, J., Moyes, J., and Duplessy, J.-C., 1990. The last deglaciation in the southern and northern hemispheres: a comparison based on oxygen isotope, sea surface temperature estimates, and accelerator ^{14}C dating from deep-sea sediments. From Bleil, U., and Thiede, J. (eds), *Gelogical History of the Polar Oceans: Arctic versus Antarctic*, NATO ASI Series C, Kluwer Academic Publishers, Dordrecht, 405 - 415.

Barnes, P.W., Reimnitz, E. and Fox, D., 1982. Ice rafting of fine-grained sediment. A sorting and transport mechanism, Beaufort Sea, Alaska. *Journal of Sedimentary Petrology*, **52** (2), 493 - 502.

Barry, R.G., 1989. The present climate of the Arctic Ocean and possible past and future states. From Herman, Y. (ed), *The Arctic Seas: Climatology, Oceanography, Geology and Biology*. Van Nostrand Reinhold, New York, 1 - 46.

Baumann, K.-H., Lackschewitz, K.S., Erlenkeuser, H., Henrich, R. and Jünger, B., 1993. Late Quaternary calcium carbonate sedimentation and terrigenous input along the East Greenland continental margin. *Marine Geology*, **114**, 13 - 36.

Berner, H. and Wefer, G., 1990. Physiographic and biological factors controlling surface sediment distribution in the Fram Stait. From Bleil, U. and Thiede, J. (eds), *Geological History of the Polar Oceans: Arctic Versus Antarctic*, Kluwer Academic Publishers, Netherlands, 317 - 335.

Björck, S., Bennike, O., Ingolfsson, O., Barnekow, L. and Penney, D.N., 1994a. Lake Boksehandsken's earliest postglacial sediments and their palaeoenvironmental implications, Jameson Land, East Greenland. *Boreas*, **23**, 459 - 472.

Björck, S., Wohlfarth, B., Bennike, O., Hjort, C. and Persson, T., 1994b. Revision of the Early Holocene lake sediment based chronology and event stratigraphy on Hochstetter Forland, NE Greenland. *Boreas*, **23**, 513 - 523.

Bond, G., Heinrich, H., Broecker, W., Labeyrie, L., McManus, J., Andrews, J., Huon, S., Jantschik, R., Clasen, S., Simet, C., Tedesco, K., Klas, M., Bonani, G. and Ivy, S., 1992. Evidence for massive discharges of icebergs into the North Atlantic ocean during the last glacial period. *Nature*, **360**, 245 - 248.

Bond, G., and Lotti, R., 1995. Iceberg discharges into the North Atlantic on millennial time scales during the last glaciation. *Science*, **267**, 1005 - 1010.

Bouma, A.H., 1962. *Sedimentology of flysch deposits. A graphic approach to facies interpretation.* Elsevier, pp168.

Bourke, R.H., Newton, J.L., Paquette, R.G. and Tunnicliffe, M.D., 1987. Circulation and water masses of the East Greenland Shelf. *Journal of Geophysical Research*, **92**, 6729 -6740.

Bradley, R.S., 1985. *Quaternary Paleoclimatology. Methods of Paleoclimatic Reconstruction*. Chapman and Hall, London, pp472.

Broecker, W.S., 1984. Terminations. From Berger, A.L. *et al.* (eds), *Milankovitch and Climate, Part 2*, D. Reidel Publishing Company, 687 - 698.

Broecker, W.S. and van Donk, J., 1970. Insolation changes, ice voulumes, and the ^{18}O record in deep-sea cores. *Rev. Geophys. and Space Phys.* **8**, 169 - 197.

Bromley, R.G. and Ekdale, A.A., 1984. Chondrites. A trace fossil indicator of anoxia in sediments. *Science*, **224**, 872 - 874.

C.I.A. (Central Intelligence Agency), 1978. *Polar Regions Atlas*. C.I.A., Washington.

Cadman, V.M., 1996. *Glacimarine Sedimentation and Environments during the Late Weichselian and Holocene in the Bellsund Trough and Van Keulenfjord, Svalbard*. PhD Thesis, University of Cambridge.

Chappell, J. and Shackleton, N.J., 1986. Oxygen isotopes and sea level. *Nature*, **324**, 137 - 140.

Charles, C.D. and Fairbanks, R.G., 1990. Glacial to interglacial changes in the isotopic gradients of southern ocean surface water. From Bleil,U. and Thiede, J. (eds), *Geological History of the Polar Oceans: Arctic Versus Antarctic*, Kluwer Academic Publishers, Netherlands, 519 - 538.

CLIMAP project members, 1976. The surface of the ice age earth. *Science*, **191**, 416 - 419.

COHMAP members, 1988. Climatic changes of the last 18,000 years: observations and model simulations. *Science*, **241**, 1043 - 1052.

Cook, H.E., 1979. Ancient continental slope sequences and their value in understanding modern slope development. From Doyle, L.J. and Pilkey, O.H. (eds) *Geology of Continental Slopes*, Society of Economic Paleontologists and Mineralogists (SEPM) Special Publication, **27**, 287 - 305.

Cowan, E.A., Cai, J., Powell, R.D., Clark, J.D. and Pitcher, J.N., 1997. Temperate glacimarine varves: An example from Disenchantment Bay, Southern Alaska. *Journal of Sedimentary Research*, **67** (3), 536 - 549.

Cowan, E.A. and Powell, R.D., 1990. Suspended sediment transport and deposition of cyclically interlaminated sediment in a temperate glacial fjord, Alaska, U.S.A. From Dowdeswell. J.A. and Scourse, J.D. (eds) *Glacimarine Environments: Processes and Sediments*. Geological Society Special Publication, **53**, 75 -89.

Craig, H., 1957. Isotopic standards for carbon and oxygen and correction factors for mass-spectrometric analysis of carbon dioxide.. *Geochim. Cosmochim. Acta*, **12**, 133 - 149.

Curry, W.B., Duplessy, J.-C.. Labeyrie, L.D., Oppo, D. and Kallel, N., 1988. Quaternary deep-water circulation changes in the distribution of $\delta^{13}C$ of deep water ΣCO_2 between the last glaciation and the Holocene. *Paleooceanography*, **3**, 317 - 342.

Damon, P.E., Lerman, J.C. and Long, A., 1978. Temporal fluctuations of atmospheric ^{14}C: causal factors and implications. *Annual Review of Earth and Planetary Science*, **6**, 457 - 494.

Damuth, J.E., 1978. Echo character of the Norwegian-Greenland Sea: relationship to Quaternary sedimentation. *Marine Geology*, **28**, 1 - 36.

Dansgaard, W., Johnsen, S.J., Clausen, H.B., Dahl-Jensen, D., Grundestrup, N.S., Hammer, C.U., Steffensen, J.P., Sveinbjornsdottir, A.E., Jouzel, J. and Bond, G., 1993. Evidence for general instability of past climate from a 250-kyr ice-core record. *Nature*, **364**, 218 - 220.

Dokken, T.M., Andersen, E.S., Hald, M. and Hebbeln, D., 1996. Palaeoceanographic changes and sediment distribution along the Svalbard margin during the last 30,000 years. *Marine Geology*, 30pp.

Dowdeswell, J.A., 1987. Processes of glacimarine sedimentation. *Progress in Physical Geography*, **11**, 52 - 90.

Dowdeswell, J.A., 1989. On the nature of Svalbard icebergs. *Journal of Glaciology*, **35** (120), 224 - 234.

Dowdeswell, J.A., and Dowdeswell, E.K., 1989. Debris in icebergs and rates of glacimarine sedimentation: observations from Spitsbergen and a simple model. *Journal of Geology*, **97**, 221 - 231.

Dowdeswell, J.A. and Murray, T., 1990. Modelling rates of sedimentation from icebergs. From Dowdeswell, J.A. and Scourse, J.D. (eds), *Glacimarine Environments: Processes and Sediments*. Geological Society Special Publication, **53**, 121 - 137.

Dowdeswell, J.A. and Cromack, M., 1991. Behavior of a glacier-derived suspended sediment plume in a small arctic inlet. *Journal of Geology*, **99**, 111-123.

Dowdeswell, J.A., Whittington, R.J. and Hodgkins, R., 1992. The sizes, frequencies, and freeboards of East Greenland icebergs observed using ship radar and sextant. *Journal of Geophysical Research*, **97** (C3),3315 -3528.

Dowdeswell, J.A., Villinger, H., Whittington, R.J. and Marienfeld, P., 1993. Iceberg scouring in Scoresby Sund and on the East Greenland continental shelf. *Marine Geology*, **111**, 37 - 53.

Dowdeswell, J.A., Whittington, R.J. and Marienfeld, P., 1994a. The origin of massive diamicton facies by iceberg rafting and scouring, Scoresby Sund, East Greenland. *Sedimentology*, **41**, 21 - 35.

Dowedeswell, J.A., Uenzelmann-Neben, G., Whittington, R.J. and Marienfeld, P., 1994b. The Late Quaternary sedimentary record in Scoresby Sund, East Greenland. *Boreas*, **23**, 294 - 310.

Dowdeswell, J.A., Maslin, M.A., Andrews, J.T. and McCave, I.N., 1995. Iceberg production, debris rafting, and the extent and thickness of Heinrich layers (H-1, H-2) in North Atlantic sediments. *Geology*, **23**, 301 - 304.

Dowdeswell, J.A., Kenyon, N.H., Elverhøi, A., Laberg, J.S., Hollender, F.-J., Mienert, J. and Siegert, M.J., 1996. Large-scale sedimentation on the glacier-influenced polar North Atlantic margins: long-range side-scan sonar evidence. *Geophysical Research Letters*, **23** (24), 3535 - 3538.

Dowdeswell, J.A., Whittington, R.J. and Villinger, H., 1997a. Iceberg scours: records from broad and narrow-beam acoustic systems. From Davies, T.A., Bell, T., Cooper, A.K., Josenhans, H., Polyak, L., Solheim, A., Stoker, M.S. and Stravers, J.A., *Glaciated Continental Margins: An Atlas of Acoustic Images*, Chapman and Hall, London, 27 - 29.

Dowdeswell, J.A., Kenyon, N.H. and Laberg, J.S., 1997b. The glacier-influenced Scoresby Sund Fan, East Greenland continental margin: evidence from GLORIA and 3.5 kHz records. *Marine Geology*, **143**, 207 - 221.

Dowdeswell, J.A., Elverhøi, A. and Spielhagen, R., 1998. Glacimarine sedimentary processes and facies on the polar North Atlantic margins. From Elverhøi *et al.* (eds), *Glacial and oceanic history of the polar North Atlantic margins*. Quaternary Science Reviews.

Drewry, D. and Cooper, A.P.R., 1981. Processes and models of Antarctic glacimarine sedimentation. *Annals of Glaciology*, **2**, 117 - 122.

Drewry, D., 1986. *Glacial Geologic Processes*. Edward Arnold, pp276.

Duplessy, J-C., Delibrias, G., Turon, J.L., Pujol, C. and Duprat, J., 1981. Deglacial warming of the Northeastern Atlantic Ocean: correlation with the palaeoclimatic evolution of the European continent. *Palaeogeography, Palaeoclimatology, Palaeoecology*, **35**, 121-144.

Eckdale, A.A., Bromley, R.G. and Pemberton, S.G., 1984. *Ichnology: the use of trace fossils in sedimentology and stratigraphy*. Soc. Eon. Paleo. and Min., Tulsa, Short Course, **15**, pp317

Elverhøi, A., Liestøl, O. and Nagy, J., 1980. Glacial erosion, sedimentation and microfauna in the inner part of Kongsfjorden, Spitsbergen. *Norsk Polarinstitutt Skrifter*, **172**, 33 - 58.

Elverhøi, A., Lonne, O. and Seland, R., 1983. Glacimarine sedimentation in a modern fjord environment. *Polar Research*, **1 (2)**, 127 - 149.

Elverhøi, A. and Solheim, A., 1983. The Barents Sea ice sheet - a sedimentological discussion. *Polar Research*, **1**, 23 -42.

Elverhøi, A., Andersen, E.S., Dokken, T.M., Hebbeln, D., Spielhagen, R., Svendsen, J.L., Sorflaten, M., Rornes, A., Hald, M. and Forsberg, C.F., 1995. The growth and decay of the Late Weichselian Ice Sheet in Western Svalbard and adjacent areas based on provenance studies of marine sediments. *Quaternary Research*, **44**, 303 - 316.

Elverhøi, A., Norem, H., Andersen, E.S., Dowdeswell, J.A., Fossen, I., Haflidaxon, H., Kenyon, N.H., Laberg, J.S., King, E.L., Sejrup, H.P., Solheim, A. and Vorren, T., 1997. On the origin and flow behavior of submarine slaides on deep-sea fans along the Norwegian-Barents Sea continental margin. *Geo-Marine Letters*, **17**, 119 - 125.

Emiliani, C., 1955. Pleistocene temperatures. *Journal of Geology*, **63**, 538 - 578.

Epstein, S., Buchsbaum, R., Lowenstam, H.A., and Urey, H.C., 1953. Revised carbonate-water isotopic temperature scale. *Geological Society of America Bulletin*, **64**, 1315 - 1326.

Escher, A. and Watt, W.S. (eds), 1976. *Geology of Greenland*. Publication of the Geological Survey of Greenland, pp603.

Eyles, N., Eyles, C.H. and Miall, A.D., 1983. Lithfacies types and vertical profile models; an alternative approach to the description and environmental interpretation of glacial diamict and diamictite sequences. *Sedimentology*, **30** (3), 393 - 410.

Eyles, C.H., Eyles, N. and Miall, A.D., 1985. Models of glaciomarine sedimentation and their application to the interpretation of ancient glacial sequences. *Palaeogeography, Palaeoclimatology, Palaeoecology*, **51** (1-4), 15 - 84.

Eyles, N., Vossler, S.M., and Lagoe, M.B., 1992. Ichnology of a glacially-influenced continental shelf and slope; the Late Cenozoic Gulf of Alaska (Yakataga Formation). *Palaeogeography, Palaeoclimatology, Palaeoecology*, **94**, 193 - 221.

Fairbanks, R.G., 1989. A 17,000-year glacio-eustatic sea level record: influence of glacial melting rates on the Younger Dryas Event and deep-ocean circulation. *Nature*, **342**, 637 - 642.

Fairbanks, R.G., Charles, C.D. and Wright, J.D., 1992. Origin of global meltwater pulses. From Taylor, R.E., Long, A. and Kra, R.S. (eds) 1992. *Radiocarbon after four decades: an interdisciplinary perspective*. Springer-Verlag, pp596.

Folk, R.L., 1954. The distinction between grain-size and mineral composition in sedimentary rock nomenclature. *Journal of Geology*, **62**, 344 - 359.

Folk, R.L. and Ward, W.C., 1957. Brazos river bar, a study in the significance of grain size parameters. *Journal of Sedimentary Petrology*, **27**, 34 - 59.

Frey, R.W. and Pemberton, S.G., 1985. Biogenic structures in outcrops and cores. 1. Approaches to ichnology. *Bulletin of Canadian Petroleum Geology*, **33** (1), 72 - 115.

Funder, S., 1972a. Remarks on the Quaternary geology of Jameson Land and adjacent areas, Scoresby Sund, East Greenland. *Gronlands geologiske Undersogeise*, **48**, 93 -98.

Funder, S., 1972b. Deglaciation of the Scoresby Sund fjord region, north-east Greenland. *Institute of British Geographers, Special Publications*, **4**, 33 - 42.

Funder, S., 1978. Holocene stratigraphy and vegetation history in the Scoresby Sund area, East Greenland. *Gronlands geologiske Undersogeise*, Bulletin **129**, pp66.

Funder, S., 1989. Quaternary geology of the ice-free areas and adjacent shelves of Greenland. From Fulton, R. J. (ed), *Quaternary Geology of Canada and Greenland*. Geological Survey of Canada, Geology of Canada, **1**, 743 - 792.

Funder, S. and Hjort, C., 1973. Aspects of the Weichselian chronology in central East Greenland. *Boreas*, **2**, 69 - 84.

Funder, S. and Larsen, H.C., 1989. Quaternary geology of the shelves adjacent to Greenland. From Fulton, R. J. (ed), *Quaternary Geology of Canada and Greenland*. Geological Survey of Canada, Geology of Canada, **1**, 769 - 772.

Funder, S. and Fredskild, B., 1989. Paleofaunas and floras (Greenland). From Fulton, R. J., (ed), *Quaternary Geology of Canada and Greenland*. Geological Survey of Canada, Geology of Canada, **1**, 775 - 783.

Funder, S., Hjort, C. and Landvik, J.Y., 1994. The last glacial cycles in East Greenland, an overview. *Boreas*, **23**, 283 - 293.

Funder, S. and Hansen, L., 1996. The Greenland Ice Sheet - a model for its culmination and decay during and after the last glacial maximum. *Bulletin of the Geological Society of Denmark*, **42**, 137 - 152.

Gealy, E.L., 1971. Saturated bulk density, grain density, and porosity of sediment cores from the Western Equatorial Pacific: Leg 7, Glomar Challenger. From Winterer, E.L. *et al.* (eds), *Initial Reports DSDP*, **7**, Washington (US Govt. Printing Office), 1081 - 1104.

Geyh, M.A. and Schleicher, H., 1990. *Absolute age determination: physical and chemical dating methods and their application*. Springer-Verlag, Berlin, pp503.

Gilbert, R., 1982. Contemporary sedimentary environments on Baffin Island, N.W.T., Canada: glaciomarine processes in fiords of Easter Cumberland Peninsula. *Arctic and Alpine Research*, **14** (1), 1 - 12.

Gilbert, R., 1983. Sedimentary processes of Canadian Arctic fjords. *Sedimentary Geology*, **36**, 147 - 175.

Gilbert, R., 1990. Rafting in glacimarine environments. From Dowdeswell, J.A. and Scourse, J.D. (eds), *Glacimarine Environments: Processes and Sediments*. Geological Society Special Publication, **53**, 105 - 120.

Goldhaber, M..B. and Kaplan, R., 1974. The sulfur cycle. From Goldberg, E.D. (ed), *The Sea 2*, Wiley, New York, 596 - 656.

Goldschmidt, P.M., Pfirman, S.L., Wollenburg, I. and Henrich, R., 1992. Origin of sediment pellets from the Arctic seafloor: sea ice or icebergs? *Deep-Sea Research*, **39** Supplt.2, S539 - S565.

Goldschmidt, P.M., 1994. *The ice rafting history in the Norwegian-Greenland Sea for the last two glacial / interglacial cycles*. Berichte SFB 313, Universität Kiel, **50**, pp103.

Gorsline, D. S., 1984. A review of fine-grained sediment origins, characteristics, transport and deposition. From Stow, D.A.V. and Piper, D.J.W. (eds), *Fine-grained Sediments: Deep Sea Processes and Facies*. Geological Society Special Publication, **15**, 17 - 34.

Gove, H.E., Litherland, A.E. and Elmore, D., 1987. Accelerator mass spectrometry. *Nucl. Instrum. Methods Phys. Res.*, B29 (1, 2), pp455. North-Holland, Amsterdam.

Görlich, K., Weslawski, J.M. and Zajaczkowski, M., 1987. Suspension settling effect on macrobenthos biomass distribution in the Hornsund Fjord, Spitsbergen. *Polar Research*, **5**, 175 - 192.

Grant, J.A. and Schreiber, R., 1990. Modern swath sounding and sub-bottom profiling technology for research applications: The Atlas Hydrosweep and Parasound system. *Marine Geophysical Researches*, **12**, 9 - 19.

Grobe, H., 1987. A simple method for the determination of ice rafted debris in sediment cores. *Polarforschung*, **57**, (3), 123 - 126.

Grobe, H., Mackensen, A., Hubberten, H.-W., Spiess, V. and Fütterer, D.K., 1990. Stable isotope record and Late Quaternary sedimentation rates at the Antarctic continental margin. From Bleil, U. and Thiede, J. (eds), 1990, *Geological History of the Polar Oceans: Arctic versus Antarctic*, NATO ASI Series C, Kluwer Academic Publishers, Dordrecht, 539 - 572.

Grousset, F.E., and Duplessy, J.C., 1983. Early deglaciation of the Greenland Sea during the last glacial to interglacial transition. *Marine Geology*, **52**, 11 - 17.

Hald, M., Dokken, T., and Hagen, S., 1996. Palaeoceanography of the European Arctic margin during the last deglaciation. From Andrews, J.T., Austin, W.E.N., Bergsten, H. and Jennings, A.E. (eds), 1996, *Late Quaternary Palaeoceanography of the North Atlantic Margins*, Geol. Soc. Sp. Publ., no. 111, 275 - 288.

Haller, J., 1971. *Geology of the East Greenland Caledomides*. Wiley, London, pp413.

Hamblin, W.K., 1962. X-ray radiography in the study of structures in homogeneous sediments. *Journal of Sedimentology Petrology*, **32**, 201 - 210.

Hambrey, M., 1994. *Glacial Environments*, UCL Press, London, pp296.

Hamilton, E.L., 1971. Prediction of in situ acoustic and elastic properties of marine sediments. *Geophysics*, **36**, 266 - 284.

Hampton, M.A., 1972. The role of subaqueous debris flow in generating turbidity currents. *Journal of Sedimentary Petrology*, **42**, 775 - 793.

Hansen, L.A., Jørgensen, M.E., Houmark-Nielsen, M., and Kronborg, C., 1994. Late Pleistocene stratigraphy and depositional environments of the Fynselv area, Jameson Land, East Greenland. *Boreas*, **23**, 385 - 397.

Hantzchel, W., 1975. Trace fossils and problematica. From Teichert, C. (ed), *Treatise on Invertebrate Palaeontology, Part W*, pp289.

Hebbeln, D. and Wefer, G., 1991. Effects of ice coverage and ice-rafted material on sedimentation in the Fram Strait. *Nature*, **350**, 409 - 411.

Hebbeln, D., Dokken, T., Andersen, E.S., Hald, M., and Elverhøi, A., 1994. Moisture supply for northern ice-sheet growth during the Last Glacial Maximum. *Nature*, **370**, 357 - 360.

Hebbeln, D. and Wefer, G., 1997. Late Quaternary paleoceanography in the Fram Strait. *Paleoceanography*, **12** (1), 65 - 78.

Hebbeln, D., Henrich, R. and Baumann, K.-H., In Prep. Paleoceanography of the last interglacial/glacial cycle in the polar North Atlantic. From Elverhøi *et al.* (eds), *Glacial and oceanic history of the polar North Atlantic Margins*. Quaternary Science Reviews.

Hedges, R.E.M., 1981. Radiocarbon dating with an accelerator: Review and preview. *Archaeometry*, **23** (1), 3 - 18.

Hein, F.J., van Wagoner, N.A. and Mudie, P.J., 1990. Sedimentary facies and processes of deposition: ice island cores, Axel Heiberg Shelf, Canadian Polar Continental Margin. *Marine Geology*, **93**, 243 - 265.

Hein, F.A. and Syvitski, J.P.M., 1992. Sedimentary environments and facies in an Arctic basin, Itirbilung Fiord, Baffin Island, Canada. *Sedimentary Geology*, **81**, 17 - 45.

Heinrich, H., 1988. Origin and consequences of cyclic ice rafting in the Northeast Atlantic Ocean during the past 130,000 years. *Quat. Res.*, **29**, 142 - 152.

Henrich, R., Kassens, H., Voglesang, E. and Thiede, J., 1989. Sedimentary facies of glacial-interglacial cycles in the Norwegian Sea during the last 350 ka. *Marine Geology*, **86**, 283 - 319.

Henrich, R., 1990. Cycles, rhythms and events in Quaternary Arctic and Antarctic glaciomarine deposits. From Bleil, U. and Thiede, J. (eds), *Geological History of the Polar Oceans: Arctic Versus Antarctic*, Kluwer Academic Publishers, Netherlands, 213 - 244.

Hesse, R. and Chough, S.K., 1980. The Northwest Atlantic Mid-Ocean Channel of the Labrador Sea:11. Deposition of parallel laminated levee-muds from the viscous sublayer of low density turbidity currents. *Sedimentology*, **27**, 697 - 711.

Hill, P.R., 1984. Sedimentary facies of the Nova Scotian upper and middle continental slope, offshore eastern Canada. *Sedimentology*, **31**, 293 - 309.

Hjort, C., 1973. A sea correction for East Greenland, *Geologiska Forenungen i Stockholm Forhandlungar*, **95**, 132 - 134.

Hjort, C., 1979. Glaciation in northern East Greenland during the Late Weichselian and Early Flanderian. *Boreas*, **8**, 281 - 296.

Hjort, C., 1981. A glacial chronology for northern East Greenland. *Boreas*, **10**, 259 - 274.

Holdsworth, G. and Glynn, J.E., 1978. Iceberg calving from floating glaciers by a vibration mechanism. *Nature*, **274** (5670), 464 to 466.

Holdsworth, G., 1985. Some effects of ocean currents and wave motion on the dynamics of floating glacier tongues. In Jacobs, S.S., (ed), *Oceanology of the Antarctic continental shelf*. American Geophysical Union, Washington D.C., 253 - 271.

Hopkins, T.S., 1991. The GIN Sea - A synthesis of its physical oceanography and literature reviews 1972 - 1985. *Earth Science Reviews*, **30**, 175 - 318.

Hubberten, H.-W., 1995. *The expedition ARKTIS-X/2 of R.V."Polarstern" in 1994*. Berichte zur Polarforschung, **174**, pp186.

Hubberten, H.-W., Grobe, H., Jokat, W., Melles, M., Niessen, F. and Stein, R., 1995. Glacial History of East Greenland Explored. *Eos, Transactions, American GeophysicalUnion*, **76** (36), 353 - 356.

Hughes, T.J., 1989. Calving ice walls. *Annals of Glaciology*, **12**, 74 - 80.

Hutson, W.H., 1980. Bioturbation of deep-sea sediments: oxygen isotopes and stratigraphic uncertainty. *Geology*, **8**, 127 - 130.

Ingolfsson, O., Lyså, A., Funder, S., Moller, P. and Bjorck, S., 1994. Late Quaternary glacial history of the central west coast of Jameson Land, East Greenland. *Boreas*, **23**, 447 - 458.

Israelson, C., Funder, S., and Kelly, M., 1994. The Aucellaelv stade at Aucellaelv, the first Weichselian ice advance in Scoresby Sund. *Boreas*, **23**, 424 - 431.

Jansen, E. and Veum, T., 1990. Evidence for two-step deglaciation and its impact on North Atlantic deep-water circulation. *Nature*, **343**, 612 - 616.

Jansen, E. and Erlenkeuser, H., 1985. Ocean circulation in the Norwegian Sea during the last deglaciation: isotopic evidence. *Palaeogeography, Palaeoclimatology, Palaeoecology*, **49** (3-4), 189 - 206.

Jokat, W., Alberts, P., Fechner, N., Fischbeck, H., Gödde, K., Kopsch, K., Kunsch, B., Lensch, N., Martens, H., Moorfeld, K., Schlindwein, V., Studinger, M., Sylvester, D., and Whittington, R., 1995. Seismic reflection. From Hubberten, H.-W. (ed) *The expedition ARKTIS-X/2 of R.V."Polarstern" in 1994*. Berichte zur Polarforschung, **174,** 22 - 29.

Jones, G.A. and Keigwin, L.D., 1988. Evidence from Fram Strait (78°N) for early deglaciation. *Nature*, **336**, 56 - 59.

Jones, K.P.N., McCave, I.N. and Patel, P.D., 1988. A computer-interfaced sedigraph for modal size analysis of fine-grained sediment. *Sedimentology*, **35**, 163 - 172.

Keller, G.H., Lambert, D.N. and Bennett, R.H., 1979. Geotechnical properties of continental slope deposits - Cape Hatteras to Hydrographer Canyon. From Doyle, L.J. and Pilkey, O.H. (eds) *Geology of Continental Slopes*, Society of Economic Paleontologists and Mineralogists (SEPM) Special Publication, **27**, 131 - 151.

Kellogg, T.B., 1976. Late Quaternary climatic changes: evidence from deep-sea cores of the Norwegian and Greenland Seas. From Cline, R.M., and Hays, J.D., (eds), *Investigation of Late Quaternary Paleoceanography and Paleoclimatology*. Geol. Soc. Amer. Memoir, **145**, 77 - 110.

Kellogg, T.B., 1977. Paleoclimatology and paleoceanography of the Norwegian and Greenland Seas: The last 450,000 years. *Marine Micropalaeontology*, **2**, 235 - 249.

Kellogg, T.B., 1980. Paleoclimatology and paleoceanography of the Norwegian and Greenland Seas: Glacial-interglacial contrasts. *Boreas*, **9**, 115 - 137.

Kellogg, T.B., Duplessy, J.-C. and Shackleton, N.J., 1978. Planktonic foraminiferal and oxygen isotopic stratigraphy and paleoclimatology of Norwegian Sea deep-sea cores. *Boreas*, **7**, 61 -73.

Kempema, E.W., Reimnitz, E. and Barnes, P.W., 1989. Sea ice sediment entrainment and rafting in the Arctic. *Journal of Sedimentary Petrology*, **59** (2), 308 - 317.

Kennett, J.P., 1990. The Younger Dryas Cooling Event: An introduction. *Palaeoceanography*, **5** (6), 891 - 895.

King, E.L., Sejrup, H.P., Haflidason, H., Elverhøi, A. and Aarseth, I., 1996. Quaternary seismic stratigraphy of the North Sea Fan: glacially-fed gravity flow aprons, hemipelagic sediments, and large submarine slides. *Marine Geology*, **130**, 293 - 315.

Klein, J., Lerman, J.C., Damon, P.E. and Ralph, E.K., 1982. Calibration of radiocarbon dates. *Radiocarbon*, **24**, 103 - 150.

Koc Karpuz, N. and Jansen, E., 1992. A high-resolution diatom record of the last deglaciation from the SE Norwegian Sea: documentation of rapid climatic changes. *Paleoceanography*, **7** (4), 499 - 520.

Koc Karpuz, N. and Jansen, E., 1994. Response of the high-latitude Northern Hemisphere to orbital climate forcing: evidence from the Nordic Seas. *Geology*, **22**, 523 - 526.

Koch, L., 1945. The East Greenland ice. *Meddelelser om Gronland*, **130**, 1 - 373.

Koch, L. and Haller, J., 1971. Geological map of East Greenland 72° - 76°N Latitude (1:250,000). *Meddr. Grønland*, **183**, pp26, 13 map sheets in portfolio.

Kovacs, A. and Mellor, M., 1974. Sea ice morphology and ice as a geologic agent in the southern Beaufort Sea. In Reed, J.C., and Sater, J.E., (eds), 1974; The coast and shelf of the Beaufort Sea. *Proc. of symposium on Beaufort Sea coast and shelf research - Arctic Institute of North America*, p.113 to 161.

Kroopnick P., 1974. Correlations between ^{13}C and ΣCO_2 in surface waters and atmospheric CO_2. *Earth and Planetary Science Letters*, **22**, 397 - 403.

Kroopnick, P.M., 1980. The distribution of ^{13}C in the Atlantic Ocean. *Earth and Planetary Science Letters*, **49**, 469 - 484.

Kroopnick, P.M., Margolis, S.V., and Wong, C.S., 1977. $\delta^{13}C$ variations in marine carbonate sediments as indicators of the CO_2 balance between the atmosphere and oceans. From Andersen. N.R. and Malahoff, A. (eds) *The Fate of Fossil Fuel CO_2 in the Oceans*, Plenum Press, 295 - 319.

Kuhn, G. and Weber, M.E., 1993. Acoustical characterization of sediments by *Parasound* and 3.5 kHz systems: related sedimentary processes on the southeastern Weddell Sea continental slope, Antarctica. *Marine Geology*, **113**, 201 - 217.

Laberg, J.S. and Vorren, T.O., 1995. Late Weichselian submarine debris flow deposits on the Bear Island Trough Mouth Fan. *Marine Geology*, **127**, 45 - 72.

Laberg, J.S. and Vorren, T.O., 1996. The middle and late Pleistocene evolution of the Bear Island Trough Mouth Fan. *Global and Planetary Change*, **12**, 309 - 330.

Labeyrie, L.D., and Duplessy, J.-C., 1985. Changes in the oceanic $^{13}C/^{12}C$ ratio during the last 140,000 years: high latitude surface water records. *Palaeogeography, Palaeoclimatology, Palaeoecology*, **50**, 217 - 240.

Labeyrie, L.D., Duplessy, J.-C. and Blanc, P.L., 1987. Variations in mode of formation and temperature of oceanic deep waters over the past 125,000 years. *Nature*, **327**, 477 - 482.

Lamb, H.H. and Woodroffe, A., 1970. Atmospheric circulation during the last ice age. *Quaternary Research*, **1**, 29 - 58.

Landvik, J.Y., Lysa, A., Funder, S. and Kelly, M., 1994. The Eemian and Weichselian stratigraphy of the Langelandselv area, Jameson Land, East Greenland. *Boreas*, **23**, 412 - 423.

Lehman, S.J., Jones, G.A., Keigwin, L.D., Andersen, E.S., Butenko, G., and Østmo, S.R., 1991. Initiation of Fennoscandian ice sheet retreat during the last deglaciation. *Nature*, **349**, 513 - 516.

Lyså, A., and Landvik, J., 1994. The lower Jyllandselv succession: evidence for three Weichselian glacier advances over coastal Jameson Land, East Greenland. *Boreas*, **23**, 432 - 446.

Mackiewicz, N.E., Powell, R.D., Carlson, P.R. and Molnia, B.F., 1984. Interlaminated ice-proximal glacimarine sediments in Muir Inlet, Alaska. *Marine Geology*, **57**, 113 -147.

Mangerud, J., Andersen, S.T., Berglund, B.E. and Donner, J.J., 1974. Quaternary stratigraphy of Norden, a proposal for terminology and classification. *Boreas*, **3**, 109 - 128.

Mangerud, J. and Berglund, B.E., 1978. The subdivision of the Quaternary of Norden: a discussion. *Boreas*, **7**, 179 - 181.

Mangerud, J. and Funder, S., 1994. The interglacial-glacial record at the mouth of Scoresby Sund, East Greenland. *Boreas*, **23**, 349 - 358.

Mangerud, J., Jansen, E. and Landvik, J.Y., 1996. Late Cenozoic history of the Scandinavian and Barents Sea ice sheets. *Global and Planetary Change*, **12**, 11 - 26.

Marienfeld, P., 1991a. Holozäne sedimentationsentwicklung im Scoresby Sund, Ost-Grönland. *Berichte zur Polarforschung*, **96,** Alfred Wegener Institut, Bremerhaven, p166.

Marienfeld, P., 1991b. ^{14}C dates of glaciomarine sediments from Scoresby Sund, East Greenland. From Möller, P., Hjort, C. and Ingolfsson, O. (eds), *The Last Interglacial-Glacial Cycle: Jameson Land and Scoresby Sund, East Greenland. Lundqua Report Series*, **33**, 165 - 167.

Marienfeld, P., 1992a. Postglacial sedimentary history of Scoresby Sund, East Greenland. *Polarforschung*, **60**, 181 - 195.

Marienfeld, P., 1992b. Recent sedimentary processes in Scoresby Sund, East Greenland. *Boreas*, **21**, 169 - 186.

Martinson, D.G., Pisias, N.G., Hays, J.D., Imbrie, J., Moore, T.C. and Shackleton, N.J., 1987. Age dating and the orbital theory of ice ages: development of high resolution 0 to 300,000-year chronostratigraphy. *Quaternary Research*, **27**, 1 - 29.

McCave, I.N., 1985. Sedimentology and stratigraphy of Box cores from the HEBBLE site on the Nova Scotian Continental Rise. *Marine Geology*, **66**, 59 - 89.

Melles, M. and Kuhn, G., 1993. Sub-bottom profiling and sedimentological studies in the southern Weddell Sea, Antarctica: evidence for large-scale erosional/depositional processes. *Deep-Sea Research*, **40** (4), 739 - 760.

Micromeritics, 1984. *Instruction Manual, SediGraph 5000ET, Particle Size Analyzer*. Micromeritics Co., Georgia, U.S.A., pp92.

Middleton, G.V. and Hampton, M.A., 1976. Subaqueous sediment transport and deposition by sediment gravity flows. From Stanley, D.J. and Swift, D.J.P. (eds), *Marine sediment transport and environmental management*, John Wiley, New York, 197 - 218.

Midttum, L., 1985. Formation of dense bottom water in the Barents Sea. *Deep-Sea Research*, **32**, 1233 - 1241.

Mienert, J., Andrews, J.T. and Milliman, J.D., 1992. The East Greenland continental margin (65°N) since the last deglaciation: changes in seafloor properties and ocean circulation. *Marine Geology*, **106**, 217 - 238.

Mienert, J., Kenyon, N.H., Thiede, J. and Hollender, F.J., 1993. Polar continental margins: studies off East Greenland. *EOS*, **74** (20), 225,234,236.

Mienert, J., Hollender, F.J. and Kenyon, N.H., 1995. GLORIA survey of the East Greenland margin: 70°N to 80°N. From Crane, K. and Solheim, A. (Eds.), *Seafloor Atlas of the Northern Norwegian-Greenland Sea*. Norsk Polarinstitut Medd. **137**, 150 - 151.

Mix, A.C., 1987. The oxygen-isotope record of glaciation. From Ruddiman, W.F., and Wright, H.E., Jr., (eds), *North America and adjacent oceans during the last deglaciation*, Boulder, Colorado, Geological Society of America, The Geology of North America, K-3, 111 - 135.

Molnia, B.F., 1983. *Glacial-Marine Sedimentation*. Plenum Press, New York, pp844.

Mook, W.G. and Grootes, P.M., 1973. The measuring procedure and corrections for the high-precision mass-spectrometric analyses of isotopic abundance ratios. *Int. Jour. Mass. Spectrom. Ion Physics*, **12**, 273 - 298.

Mook, W.G., 1984. Archaeological and geological interest in applying ^{14}C AMS to small samples. *Nucl. Instrum. Methods*, **233** (B5), 297 - 302.

Munsell Colour Co., 1954. *Munsell Soil Colour Charts*. Munsell Colour Co., Inc., Baltimore, p23.

Myhre, A.M. and Thiede, J., 1995. North Atlantic-Arctic Gateways. *Proceedings of the Ocean Drilling Program, Initial Reports*. **151**, 5 - 26.

Nam, S.-I., 1996. *Late Quaternary glacial history and palaeoceanographic reconstructions along the East Greenland continental margin: Evidence from high resolution records of stable isotopes and ice rafted debris*. PhD thesis, University of Bremen, pp158.

Nam, S.-I., Stein, R., Grobe, H. and Hubberten, H.-W., 1995. Late Quaternary glacial/interglacial changes in sediment composition at the East Greenland continental margin and their palaeoceanographic implications. *Marine Geology*, **122**, 243 - 262.

Nardin, T.R., Hein, F.J., Gorsline, D.S. and Edwards, B.D., 1979. A review of mass movement processes, sediment and acoustic characteristics, and contrasts in slope and base-of-slope systems versus canyon-fan-basin floor systems. From Doyle, L.J. and Pilkey, O.H. (eds), *Geology of Continental Slopes*, Society of Economic Paleontologists and Mineralogists (SEPM) Special Publication, **27**, 61 - 73.

Nielsen, S.H., Conradsen, K., Hanemeier, J., Knudsen, K., Nielsen, H.L., Rud, N. and Sveinbjornsdottir, A.E., 1995. Radiocarbon dating of shells and foraminifera from the Skagen core, Denmark: evidence of reworking. From Cook, G.T., Harkness, D.D., Miller, B.F., and Scott, E.M., (eds), *Proceedings of the 15th International Conference. Radiocarbon*, **37**, 2, 119 - 130.

Niessen, F. and Whittington, R., 1995. Marine sediment echosounding using *Parasound*. From Hubberten, H.-W. (ed) *The expedition ARKTIS-X/2 of R.V."Polarstern" in 1994*. Berichte zur Polarforschung, **174**, 62 - 68.

Niessen, F. and Whittington, R.J., 1997a. Typical sections along a transect of a fjord in East Greenland.. From Davies, T.A., Bell, T., Cooper, A.K., Josenhans, H., Polyak, L., Solheim, A., Stoker, M.S. and Stravers, J.A., *Glaciated Continental Margins: An Atlas of Acoustic Images*, Chapman and Hall, London, 182 - 186.

Niessen, F. and Whitttington, R.J., 1997b. Syn-sedimentary faulting in an East Greenland Fjord. From Davies, T.A., Bell, T., Cooper, A.K., Josenhans, H., Polyak, L., Solheim, A., Stoker, M.S. and Stravers, J.A., *Glaciated Continental Margins: An Atlas of Acoustic Images*, Chapman and Hall, London, 130 - 132.

Nürnberg, D., Wollenburg, I., Dethleff, D., Eicken, H., Kassens, H., Letzig, T., Reimnitz, E. and Thiede, J., 1994. Sediments in Arctic sea ice: implications for entrainment, transport and release. *Marine Geology*, **119**, 185 - 214.

Nuttall, A.-M., 1993. *Glaciological Investigations in East Greenland Using Digital Landsat Imagery*. M.phil thesis, University of Cambridge.

Nuttall, A.-M. and Dowdeswell, J.A., In prep. Drainage basins and balance velocities of tidewater glaciers in East Greenland. *Journal to be decided*.

Ohmura, A. and Reeh, N., 1991. New precipitation and accumulation maps for Greenland. *Journal of Glaciology*, **37** (125), 140 - 148.

Osterkamp, T.E. and Gosink, J.P., 1984. Observations and analyses of sediment-laden sea ice. From Barnes, P.W., Schell, D.M. and Reimnitz, E. (eds), *The Alaskan Beaufort Sea: Ecosystems and Environments*. Academic Press, 73 - 93.

Ovenshine, A.T., 1970. Observations of iceberg rafting in Glacier Bay, Alaska, and the identification of ancient ice rafted deposits. *Geological Society of America Bulletin*, **81** (3), 891 to 894.

Parker, G., 1982. Conditions for the ignition of catastrophically erosive trubidity currents. *Marine Geology*, **46**, 307 - 327.

Pelto, M.S. and Warren, C.R., 1991. Relationship between tidewater glacier calving velocity and water depth at the calving front. *Annals of Glaciology*, **15**, 115 - 124.

Pemberton, S.G. and Frey, R.W., 1982. Trace fossil nomenclature and the planolites - palaeophycus dilemma. *Journal of Paleontology*, **56** (4), 843 - 881.

Perry, 1986. Bathymetry. From Hurdle, B.G. (ed), *The Nordic Seas*, Springer, New York,

Pfirman, S.L., and Solheim, A., 1989. Subglacial meltwater discharge in the open-marine tidewater glacier environment: observations from Nordaustlandet, Svalbard archipelago. *Marine Geology*, **86**, 265 - 281.

Pfirman, S.L., Wollenburg, I., Thiede, J. and Lange, M.A., 1989. Lithogenic sediment on Arctic pack ice: potential aeolian flux and contribution to deep-sea sediments. From Leinen, M., and Sarnthein, M., (eds), *Palaeoclimatology and Palaeometeorology: Modern and Past Patterns of Global Atmospheric Transport*. NATO ASI Series C 282, Kluwer, Dordrecht, 463 - 493.

Pfirman, S.L., Lange, M.A., Wollenburg, I. and Schlosser, P., 1990. Sea ice characteristics and the role of sediment inclusion in deep-sea deposition: Arctic-Antarctic comparisons. From Bleil, U. and Thiede, J. (eds), *Geological History of the Polar Oceans: Arctic Versus Antarctic*, Kluwer Academic Publishers, Netherlands, 187 - 211.

Pickering, K.T., Hiscott, R.N. and Hein, F.J., 1989. *Deep Marine Environments*. Unwin Hyman, London.

Piper, D.J.W., 1978. Turbidite muds and silts on deep-sea fans and abyssal plains. From Stanley, D.J. and Kelling, G. (eds) *Sedimentation in Submarine Canyons, Fans, and Trenches*, 163 -176.

Piper, D.J.W., Farre, J.A. and Shor, A., 1985. Late Quaternary slumps and debris flows on the Scotian Slope. *Geological Society of America Bulletin*, **96**, 1508 - 1517.

Powell, R.D., 1981. A model for sedimentation by tidewater glaciers. *Annals of Glaciology*, **2**, 129 - 134.

Powell, R.D., 1983. Glacial-marine sedimentation processes and lithofacies of temperate tidewater glaciers, Glacier Bay, Alaska. From Molnia, B.F. (ed), *Glacial-Marine Sedimentation*. Plenum, 185 - 232.

Powell, R.D., 1984. Glacimarine processes and inductive lithofacies modelling of ice shelf and tidewater glacier sediments based on Quaternary examples. *Marine Geology*, **57**, 1 - 52.

Powell, R.D., 1990. Glacimarine processes at grounding-line fans and their growth to ice-contact deltas. From Dowdeswell, J.A. and Scourse, J.D. (eds), *Glacimarine Environments: Processes and Sediments*, Geological Society Special Publication, **53**, 53 -73.

Powell, R.D. and Molnia, B.F., 1989. Glacimarine sedimentary processes, facies and morphology of the south-southeast Alaska shelf and fjords. *Marine Geology*, **85**, 359 - 390.

Reading, H.G. and Levell, B.K., 1996. Controls on the sedimentary rock record. From Reading, H.G. (ed), *Sedimentary Environments: Processes, Facies and Stratigraphy*, Blackwell Scientific Publications, Oxford, 3rd edition, Chapter 2, pp688.

Rearic, D.M., Barnes, P.W. and Reimnitz, E., 1990. Bulldozing and resuspension of shallow shelf sediment by ice keels: implications for Arctic sediment transport trajectories. *Marine Geology*, **91** (1 - 2), 133 - 147.

Reeh, N., 1968. On the calving of ice from floating glaciers and ice shelves. *Journal of Glaciology*, **7**, 215 - 232.

Reeh, N., 1985. Greenland Ice-Sheet mass balance and sea-level change. From Report DOE/EV/60235-1 *Glaciers, Ice Sheets and Sea Level: Effect of a CO_2-induced Climatic Change.*, U.S. Department of Energy, Washington, DC, 155 - 171

Reeh, N., 1989. Dynamic and climatic history of the Greenland Ice Sheet. From Fulton, R. J., (ed), *Quaternary Geology of Canada and Greenland*. Geological Survey of Canada, Geology of Canada, **1**, 795 - 822.

Ruddiman, W.F., 1987. Synthesis; The ocean ice/sheet record. From Ruddiman, W.F., and Wright, H.E., Jr., (eds), *North America and adjacent oceans during the last deglaciation*, Boulder, Colorado, Geological Society of America, The Geology of North America, K-3, 463 - 478.

Ruddiman, W.F. and McIntyre, A., 1981a. The mode and mechanism of the last deglaciation: oceanic evidence. *Quaternary Research*, **16**, 125 - 134.

Ruddiman, W.F. and McIntyre, A., 1981b. The North Atlantic Ocean during the last deglaciation. *Palaeogeography, palaeoclimatology, Palaeoecology*, **35**, 145 - 214.

Sættem, J., Poole, D.A.R., Ellungsen, L. and Sejrup, H.P., 1992. Glacial geology of outer Bjørnøyrenna, southwestern Barents Sea. *Marine Geology*, **103**, 15 -51.

Sarnthein, M., Jansen, E., Arnold, M., Duplessy, J.-C., Erlenkeuser, H., Flatoy, A., Veum, T., Vogelsang, E. and Weinelt, M.S., 1992. $\delta^{18}O$ time-slice reconstructions of meltwater anomalies at Termination I in the North Atlantic between 50 and 80 N. From Bard, E., and Broecker, W.S., (eds), *The Last Deglaciation: Absolute and Radiocarbon Chronologies*, NATO ASI Series, **I2**, 184 - 200, Springer-Verlag Berlin Heidelberg.

Savin, S.M. and Douglas, R.G., 1973. Stable isotope and magnesium geochemistry of recent planktonic foraminifera from the South Pacific. *Geol. Soc. Am. Bull.*, **84**, 2327 - 2342.

Sexton, D.J., Dowdeswell, J.A., Solheim, A. and Elverhøi, A., 1992. Seismic architecture and sedimentation in northwest Spitsbergen fjords. *Marine Geology*, **103**, 53 - 68.

Shackleton, N.J., 1967. Oxygen isotope analyses and paleotemperatures re-assessed. *Nature*, **215**, 15 - 17.

Shackleton, N.J., 1977a. Carbon-13 in Uvigerina: Tropical rainforest history and the equatorial pacific carbonate dissolution cycles. From Andersen. N.R. and Malahoff, A. (eds) *The Fate of Fossil Fuel CO_2 in the Oceans*, Plenum Press, pp749.

Shackleton, N.J., 1977b. The oxygen isotope stratigraphic record of the Late Pleistocene. *Phil. Trans. R. Soc. Lond.*, B. **280**, 169 - 182.

Shackleton, N.J., 1987. Oxygen isotopes, ice volume and sea level. *Quaternary Science Reviews*, **6**, 183 - 190.

Shackleton, N.J. and Opdyke, N.D., 1973. Oxygen-isotope and palaeomagnetic stratigraphy of equatorial Pacific core V28-238: Oxygen isotope temperatures and ice volumes on a 10^5 and 10^6 year scale. *Quaternary Research*, **3**, 39 - 55.

Shackleton, N.J. and Opdyke, N.D., 1976. Oxygen-isotope and paleomagnetic stratigraphy of Pacific core V28-239: Late Pliocene to Latest Pleistocene. *Geol. Soc. of Am.*, memoir **145**, 449 - 464.

Siegenthaler, U. and Eicher, U., 1986. Stable oxygen and carbon isotope analyses. From Berglund, B. E., (ed), *Handbook of Holocene Palaeoecology and Palaeohydrology*, John Wiley and Sons Ltd., 407 - 422.

Simpson, S., 1957. On the trace fossil Chondrites. Geological Society of London Quarterly Journal, **112**, 475 - 499.

Spielhagen, R.F. and Erlenkeuser, H., 1994. Stable oxygen and carbon isotopes in planktic foraminifers from Arctic Ocean surface sediments: Reflection of the low salinity surface water layer. *Marine Geology*, **119**, 227 - 250.

Stein, R., 1985. Rapid grain-size analyses of clay and silt fraction by SediGraph 5000D: Comparison with Coulter and Atterberg methods. *Journal of Sedimentary Petrology*, **55** (4), 590 - 593.

Stein, R., Grobe, H., Hubberten, H.-W., Marienfeld, P. and Nam, S.-I., 1993. Latest Pleistocene to Holocene changes in glaciomarine sedimentation in Scoresby Sund and along the East Greenland continental margin: Preliminary results. *Geo-Marine Letters*, **13**, 9 - 16.

Stein, R., Nam, S.-I., Schubert, C., Vogt, C., Fütterer, D. and Heinemeier, J., 1994a. The last deglaciation event in the Eastern Central Arctic Ocean. *Science*, **264**, 692 - 695.

Stein, R., Schubert, C., Vogt, C. and Fütterer, D., 1994b. Stable isotope stratigraphy, sedimentation rates, and salinity changes in the latest Pleistocene to the Holocene eastern central Arctic Ocean. *Marine Geology*, **119**, 333 - 355.

Stein, R., Nam, S.-I., Grobe, H. and Hubberten, H.-W., 1996. Late Quaternary glacial history and short term ice rafted debris fluctuations along the East Greenland continental margin. From Andrews, J.T., Austin, W.E.N., Bergsten, H. and Jennings, A.E. (eds), 1996, *Late Quaternary Palaeoceanography of the North Atlantic Margins*, Geol. Soc. Sp. Publ., no. 111, 135 - 151.

Stewart, T.G., 1991. Glacial marine sedimentation from tidewater glaciers in the Canadian High Arctic. *Geological Society of America*, **special paper 261**, 95 - 104.

Stow, D.A.V., 1979. Distinguishing between fine-grained turbidites and contourites on the Nova Scotia deep water margin. *Sedimentology*, **26**, 371 - 387.

Stow, D.A.V., 1992. Facies characteristics: overview and commentary. From Stow, D.A.V. (ed) *Deep-Water Turbidite Systems*, Reprint Series **3**, International Association of Sedimentologists, Blackwell Scientific Publications.

Stow, D.A.V. and Lovell, J.P.B., 1979. Contourites: their recognition in modern and ancient sediments. *Earth Science Review*, **14**, 251 - 291.

Stow, D.A.V. and Bowen J.B., 1980a. A physical model for the transport and sorting of fine-grained sediment by turbidity currents. *Sedimentology*, **27**, 31 - 46.

Stow, D.A.V. and Shanmugam, G., 1980b. Sequence of structures in fine-grained turbidites: comparison of recent deep-sea and ancient flysch sediments. *Sedimentary Geology*, **25**, 23 - 42.

Stow, D.A.V. and Piper, D.J.W., 1984a. Fine-grained sediments: deep sea sediments: deep sea processes and facies. *Geological Society Special Publication*, **15**.

Stow, D.A.V. and Holbrook, J.A., 1984b. North Atlantic contourites: an overview. From Stow, D.A.V. and Piper, D.J.W. (eds), *Fine-grained Sediments: Deep Sea Processes and Facies*. Geological Society Special Publication, **15**, 245 - 255.

Stuiver, M. and Polach, H.A., 1977. Discussion reporting of ^{14}C data. *Radiocarbon*, **19** (3), 355 - 363.

Stuiver, M., Long, A. and Kra, R.S. (eds), 1993a. *Calibration 1993*. Radiocarbon, **35** (1), 215 - 230.

Stuiver, M. and Reimer, P.J., 1993b. Extended data base and revised CALIB 3.0 age calibration program. In Stuiver, M., Long, A. and Kra, R.S. (eds), Calibration 1993. *Radiocarbon*, **35** (1), 215 - 230.

Svendsen, J.I., Mangerud, J., Elverhøi, A., Solheim, A. and Schutterhelm, R.T.E., 1992. The Late Weichselian glacial maximum on western Spitsbergen inferred from offshore sediment cores. *Marine Geology*, **104**, 1 - 17.

Svendsen, J.I., Elverhøi, A. and Mangerud, J., 1996. The retreat of the Barents Sea Ice Sheet on the western Svalbard margin. *Boreas*, **25**, 244 - 256.

Swift, J.H., 1986. The Arctic Water. From Hurdle, B.G. (ed), *The Nordic Seas*, Springer, New York,

Syvitski, J., 1989. On the deposition of sediment within glacier-influenced fjords: oceanographic controls. *Marine Geology*, **85**, 301 - 329.

Syvitski, J.P.M., Burrell, D.C. and Skei, J.M., 1987. *Fjords: Processes and Products*, Springer-Verlag, New York, pp379.

Syvitski, J.P.M. and Hein, F.J., 1991. Sedimentology of an Arctic Basin: Itirbilung Fiord, Baffin Island, Northwest Territories, *Geological Survey of Canada*, Paper **91 - 11**, pp67.

Syvitski, J.P.M., Andrews, J.T. and Dowdeswell, J.A., 1996. Sediment depostion in an iceberg-dominated glacimarine environment, East Greenland: basin fill implications. *Global and Planetary Change*, **12**, 251 - 270.

Thomsen, E., and Vorren, T.O., 1984. Pyritization of tubes and burrows from Late Pleistocene continental shelf sediments off North Norway. *Sedimentology*, **31**, 481 - 492.

Tucker, M.E., 1988. *Techniques in Sedimentology*, Blackwells, Oxford, pp394.

Tveranger, J., Houmark-Nielsen, M., Lovberg, K. and Mangerud, J., 1994. Eemian-Weichselian stratigraphy of the Flakkerhuk ridge, southern Jameson Land, East Greenland. *Boreas*, **23**, 359 - 384.

Urey, H.C., 1947. The thermodynamic properties of isotopic substances. *Journal of Chemistry Society*, 169 - 182.

van Andel, T.H., Heath, G.R. and Moore, T.C., 1975. Cenozoic history and palaeoceanography of the central equatorial Pacific. *Mem. Geol. Soc. Amer.*, **143**, p134.

Vanneste, K., Uenzelmann-Neben, G. and Miller, H., 1995. Seismic evidence for long-term history of glaciation on central East Greenland shelf south of Scoresby Sund. *Geo-Marine Letters*, **15**, 63 - 70.

Vinge, T.E., 1977. Sea ice conditions in European sector of the marginal seas of the Arctic 1966 - 1975. *Norsk Polarinstitutt Årbok 1975*, 163 - 174.

Vogt. C., Matthiessen, J., Hubberten, H.-W. and Monk, J., 1995. Water column investigations: Hydrography. From Hubberten, H.-W. (ed) *The expedition ARKTIS-X/2 of R.V."Polarstern" in 1994*. Berichte zur Polarforschung, **174,** 89 - 94.

Wadhams, P., 1981. The ice cover in the Greenland and Norwegian Seas. *Reviews of Geophysics and Space Physics*, **19** (3), 345 - 393.

Wadhams, P., 1986. The sea ice cover. From Hurdle, B.G. (ed), *The Nordic Seas*. Springer, New York, 21 - 84.

Warren, C.R., 1992. Iceberg calving and the glacioclimatic record. *Progress in Physical Geography*, **16** (3), 253 -282.

Weinelt, M.S., Sarnthein, M., Vogelsang, E., and Erlenkeuser, H., 1991. Early decay of the Barents Shelf Ice Sheet - spread of stable isotope signals across the Norwegian Sea. *Norsk Geol. Tidsskr.*, **71**, 137 - 140.

Whittington, R.J., 1995. Seismic reflection: first results. From Hubberten, H.-W. (ed) *The expedition ARKTIS-X/2 of R.V."Polarstern" in 1994*. Berichte zur Polarforschung, **174,** 24 - 26.

Whittington, R.J. and Niessen, F., 1997. A cross-section of a fjord debris flow, East Greenland. From Davies, T.A., Bell, T., Cooper, A.K., Josenhans, H., Polyak, L., Solheim, A., Stoker, M.S. and Stravers, J.A., *Glaciated Continental Margins: An Atlas of Acoustic Images*, Chapman and Hall, London, 128 - 130.

Williams, K.M., 1993. Ice sheet and ocean interactions, margin of the East Greenland ice sheet (14 Ka to present): diatom evidence. *Paleoceanography*, **8** (1), 69 - 83.

Williams, K.M., Andrews, J.T., Weiner, N.J. and Mudie, P.J., 1995. Late Quaternary Paleoceanography of the Mid- to Outer Continental Shelf, East Greenland. *Arctic and Alpine Research*, **27** (4), 352 -363.

Wollenburg, I., 1993. Sedimenttransport durch das arktische Meereis: die rezente lithogene und biogene Materialfracht. *Berichte zur Polarforschung*, **127**, 1 - 159.

Wright, R. and Anderson, J.B., 1982. The importance of sediment gravity flow to sediment transport and sorting in a glacial marine environment: East Weddell Sea, Antarctica. *Geological Society of America Bulletin*, **93**, 951 - 963.

Wright, R., Anderson J.B. and Fisco, P.B., 1983. Distribution and association of sediment gravity flow deposits and glacial/glacial-marine sediments around the continental margin of Antarctica. From Molnia, B.F. (ed), *Glacial-Marine Sedimentation*. Plenum, 265 - 298.

Yoon, S.H., Chough, S.K., Thiede, J. and Werner, F., 1991. Late Pleistocene sedimentation on the Norwegian continental slope between 67° and 71° N. *Marine Geology*, **99**, 187 - 207.

Yoon, S.H. and Chough, S.K., 1993. Sedimentary characteristics of Late Pleistocene bottom-current deposits, Barents Sea slope off northern Norway, *Sedimentary Geology*, **82**, 33 - 45.

Zahn, R., Markussen, B. and Thiede, J., 1985. Stable isotope data and depositional environments in the Late Quaternary Arctic Ocean. *Nature*, **314**, 433 - 435.

Zahn, R., Winn, K. and Sarnthein, M., 1986. Benthic foraminiferal $\delta^{13}C$ and accumulation rates of organic carbon: Uvigerina peregrina group and Cibicidoides wuellerstorfi. *Palaeoceanography*, **1**, 27 - 42.